Ninth International Workshop on Laser Ranging Instrumentation

incorporating a

Symposium on Western Pacific Laser Ranging Network

WPLS '94

Canberra 1994

VOLUME 2

Compiled and edited by John McK. Luck
with assistance from Georgina R. Luck, Mark J. Elphick, Robbie Horn

Australian Government Publishing Service
Canberra

ISBN 0 644 47425 4 (Vol. 2)
ISBN 0 644 47427 0 (Set)

The Ninth International Workshop on Laser Ranging Instrumentation, incorporating WPLS '94, was held at Becker House, Canberra, Australia, from 7 to 11 November 1994.

Workshop sponsors: Auslig, EOS, Qantas

Symposium sponsor: STA, Japan

Papers compiled and edited by:
John McK. Luck
Orroral Geodetic Observatory
Australian Surveying and Land Information Group
Canberra ACT, Australia

Cover photograph: Orroral Observatory, Australia
Photographer: Anthony Willing

Produced by the Australian Government Publishing Service

TABLE OF CONTENTS

VOLUME 2

VOLUME 1

New Fixed Stations—Yang Fumin

Timing Devices and Calibration—Hiroo Kunimori

Lunar Laser Ranging—Peter Shelus

Eyesafe Systems—John Luck

Data Analysis and Models—Giuseppe Bianco

VOLUME 3

SYMPOSIUM on Western Pacific Laser Ranging Network (WPLS'94)
Convenor: Hiroo Kunimori

Papers presented during Workshop sessions are noted by (W) in Table of Contents for Volumes 1 & 2.

Viewgraph Presentations

Future Science Applications—Christian Veillet

Target Signatures and Biases—Andrew Sinclair

New Mobile Stations—Erik Vermaat

New Fixed Stations—Yang Fumin

Timing Devices and Calibration—Hiroo Kunimori

Eyesafe Systems—John Luck

Data Analysis and Models—Giuseppe Bianco

Laser Technology Development—Karel Hamal

Streak Camera Systems—Ivan Prochazka

Presentations Not Recorded in the Proceedings

Invited Paper: *25 Years of LLR,* C. Alley

ZIMLAT: The New Zimmerwald Laser and Astrographic Telescope, W. Gurtner, E. Pop, T. Schildknecht, J. Utzinger, U Wild

Transmit/Receive Electronics for SLR 2000, T. Varghese, R. Eichinger, C. Steggerda, H. Donovan, J. Degnan

Development of an Automated Q/C Model for NASA SLR Data, J. Horvath, V. Husson

Automatic and Remote Control of SLR Systems, B. Greene, T. May, J. Luck, H. Kunimori

DETECTORS AND SPECTRAL FILTERS

Chairperson : Ulrich Schreiber

Installing / Testing an Avalanche Photodiode Detector at MLRS

by
J. R. Wiant and P. J. Shelus
McDonald Observatory, Ft. Davis, Texas 79734

Abstract

In a cooperative effort with the personnel at the Wettzell Laser Ranging Station, a newly designed avalanche photodiode detector system is being installed and tested at MLRS. The unit is currently installed and operational. Initial testing has just begun.

Introduction

It is claimed that avalanche photodiode (APD) detectors offer more gain, more ruggedness to bright light and provide narrower output pulses when compared with standard photomultiplier tubes. An important goal at the MLRS is to increase lunar data output. Therefore we are highly motivated to investigate the advantages of using an APD. The higher gain of the APD would increase data yield. Its ruggedness to bright light would greatly reduce the worry of cloud reflections. The narrower output pulse would enhance the data quality.

Installing the APD

As the initial step, two simple commercial power supplies were purchased to provide the gate voltage and the high voltage. Due to critical space limitations at MLRS, OEM power supplies without meters were purchased, instead of the much larger bench-type models that come with a myriad of knobs and meters. These two power supplies were mounted on a flat plate, and two LCD voltmeters, together with two LCD ammeters, were mounted on a perpendicular front plate. A third, standard bench-type power supply was purchased to be the APD's peltier current source.

As an equipment safety precaution, a small four-pin bulkhead connector was installed on the APD housing to connect the gate voltage (+45.3 v) and high voltage (-145 v) sources. This eliminates using BNC connectors for "unfriendly" voltages.

The mounting flange on the APD housing was drilled and tapped to match the MLRS detector package flange. At first, the APD housing was mounted with the two radial vernier stems at a right angle and parallel to the floor, respectively. However, it was soon discovered that both the upward pointing and sideways pointing vernier stems were in the operator's way for other alignment tasks in the detector package area. Also, gravity worked against the interal X-Y stage springs, causing the APD stage to stick considerably during vernier adjustments. The APD housing was then rotated 120 degrees and mounted with both of the vernier stems now pointing at a downward angle. Both stems are now out of the operator's way and gravity now helps reduce the X-Y stage sticking. For identification purposes, felt-tip pens were used to color one vernier red and the other vernier blue. The axial vernier was left uncolored, giving us a fine patriotic red, white, and blue color scheme.

Using Ulrich Schreiber's circuit design, an IR detector for the YAG laser oscillator was constructed. A simple, miniature X-Y mount was also built to hold the detector which sees the oscillator energy through the first turning mirror.

It is important for thermal noise characteristics that an APD be used in a thermally cooled environment. Initial experiments were performed to see how much cooling could be accomplished using a non-pumped coolant flowing through the peltier inside the APD housing and a much larger external peltier. The results were not encouraging. We then added a coolant circulating pump driven by a DC motor and the external peltier was replaced by a small refrigerator. The coldest temperature attained while supplying 3 amps to the internal peltier was -6.1 ° C. Presently, however, for an as yet unexplained reason, -2.4° C is the coldest we can attain. This is in spite of increasing the length the tubing inside the refrigerator, changing the coolant flow rate, reducing the peltier current, and changing the coolant from water to isopropyl alcohol. Even though changing from water to alcohol gave the same results, the coolant does not now freeze even when the circulating pump is stopped.

Initial Results

As an initial test, a series of noise counts versus detector temperature was taken on the APD with the following results.

+5.1 °C	189 counts
+1.5 °C	173 counts
-0.3 °C	164 counts
-1.1 °C	75 counts
-1.2 °C	3 counts
-1.3 °C	no counts

It is interesting to note that the noise counts at +10.3 °C and +21.1°C were not appreciably different from the +5.1 °C count.

MLRS uses a continuously self-calibrating internal calibration system/technique that automatically accounts for timing changes that might occur whenever a cable, detector, etc. is changed for any of the usual reasons. Therefore it is of no concern, yet understandable to observe that the APD has several nanoseconds less propagation delay than our present Varian photomultiplier tube with its amplifier. This is easily observed in the raw plotted calibration-K histogram. As predicted, the Tennelec discriminator can be set anywhere between -0.5v and -8.3v (monitor voltages) with no change whatsoever in the quality or quantity of the calibration Ks.

At the time that this report is being written, laser ranging to various targets using the APD has just begun. The LAGEOS pair of satellites were used to obtain system alignments. Initial ranging to the GPS-3535 target with the multi-channel photomultiplier (MCP), the Varian photomultiplier and the APD has shown that the Varian has more gain than the APD and that the APD has more gain than the MCP. These results are based on only a handful (less than 5) passes taken with the APD. Lunar attempts have been made but the weather was always marginal. More thought, tweaking, and attempts will have to be applied to the APD before a final assessment has been made.

APPENDIX

Present support equipment for the MLRS APD:

Gate Voltage power supply: Lambda model LMS-3120, 0-120V, 0.25A
High Voltage power supply: Lambda model LMS-4300, 0-300V, 0.14A
Liquid crystal display meters, four each: Jewell model 590 032039, with various shunts.
Peltier power supply: Kepco model MSK10-10M, 1-10V, 0-10A
Micro Pump pump #040-000-200, 0.316 millilters per revolution, 10,000 max r.p.m.
Micro Pump motor #000-331-000, 0-12V, 0-7 amps
Pump motor power supply: Trygon model SHR40-1.5, 0-40V, 0-1.5A
Refrigerator: Abscold Corp. model AR021M615R, 1.7 cubic feet
Tygon tubing, 1/4 inch, 18 feet
Copper tubing, 1/4 inch, 50 feet

Field experience with various detector types at SLR - Station 7836 Potsdam

Ludwig Grunwaldt, Harald Fischer
GeoForschungsZentrum Potsdam
Dept. I: Recent Kinematics and Dynamics of the Earth
Telegrafenberg A 17
D-14473 Potsdam, Germany

ABSTRACT:

Experience with 3 different detector types (RCA-APD, 100 µm SPAD and HAMAMATSU H 5023 photo-multiplier) used for satellite laser ranging under the usual working conditions at an SLR-station is described with respect to timing jitter and signal dependent time shift. Special attention is given to the performance of the
H 5023 photomultiplier to separate the observed signal dependent time shift into different effects as laser pulse width and amplitude dependent discriminator behaviour.
The effect of virtual double pulses observed under critical choice of discriminator parameters is described as well.

The use of a detector matched to the laser pulsewidth and the proper choice of its operational parameters is essential to gain both precise measurements and good calibration stability. Under the conditions of a routinely operated SLR-station, the detector performance obtained in „clean" laboratory experiments is usually not accessible. Electrical noise (mainly from the laser) can be suppressed only to a certain level and often a compromise has to be chosen between minimum timing jitter and minimum signal dependent time walk. Some experience with various detectors used at the Potsdam station since the beginning of its operation in 1992 is described here.
The following detectors were tested:

Detector type	Sensitive area	QE @ 532 nm	QE @ 1064 nm	Timing jitter	Thermal noise
RCA C 30902 S-TC (@T= 0°C)	small (500 µm)	30 %	2 %	medium (150 ps)	very low (< 100 Hz)
SPAD 100 µm (@ T=20°C)	very small (100 µm)	20 %	1 %	very low (30 ps)	high (>100 kHz)
PMT H 5023	very large (>1 cm)	8 %	-	low (60 ps)	low (< 2 kHz)

1. Avalanche diodes RCA C 30902 S-TC and SPAD (100 µm)

The RCA avalanche diode with an integrated single-stage Peltier cooler and the well-known C 30902 S chip offers interesting features as high quantum efficiency and low thermal noise, but suffers from a higher timing jitter, a considerable walk effect with increasing signal strength (see below) and a pronounced asymmetric distribution of ranging residuals. Laboratory experiments show that the timing jitter can be further reduced to 100 ps by cooling the chip down to about -60°C also obtaining a certain decrease in the asymmetry of the distribution, but the additional effort to do this is probably higher than the improvement in detector performance. The built-in cooler can achieve a maximum temperature difference between the outer shell and the chip of about 25 degrees only, and an additional outer cooler raises problems like removal of condensation on the entrance window. It should also be mentioned that the threshold of self-breakdown is strongly temperature-dependent for this diode (about -1 V/deg.), and with the detector package mounted outside with no special climatisation (as it is the case at our station) one can expect problems in the long-term stability of calibration. For all these reasons, the
C 30902 S-TC is now mainly used as a spare detector or in case of a demand for very high quantum efficiency (for example tracking of GPS - satellites).

The uncooled 100 µm SPAD is only by a factor of 1.5 less sensitive at the Nd:YAG-SHG wavelength . The high thermal noise is not a major problem because of the drastically improved quality of satellite orbital predictions, and the change of parameters with temperature is much less than for the RCA diode. The main reason not to use this detector as a routine one for the Potsdam station is the limited field of view due to the small sensitive area . This causes a problem at the present state of the mount quality at our station, mainly the strong wobble of the transmit-receive switches makes it difficult to „hit" the diode by the received signal. Some measures to improve the T/R mechanics are underway, but up to now the 100 µm SPAD was used only for targetting tests with the T/R switches in fixed position.

Experiments to measure the signal dependent time walk for both receivers were carried out using the full SLR system with a a single cube corner reflector at a fixed position in front of the telescope and neutral density filters in front of the detector to vary the signal strength. The average photoelectron number was derived for low return rates by statistical means, for higher values from the change in filter factors. The result is given below:

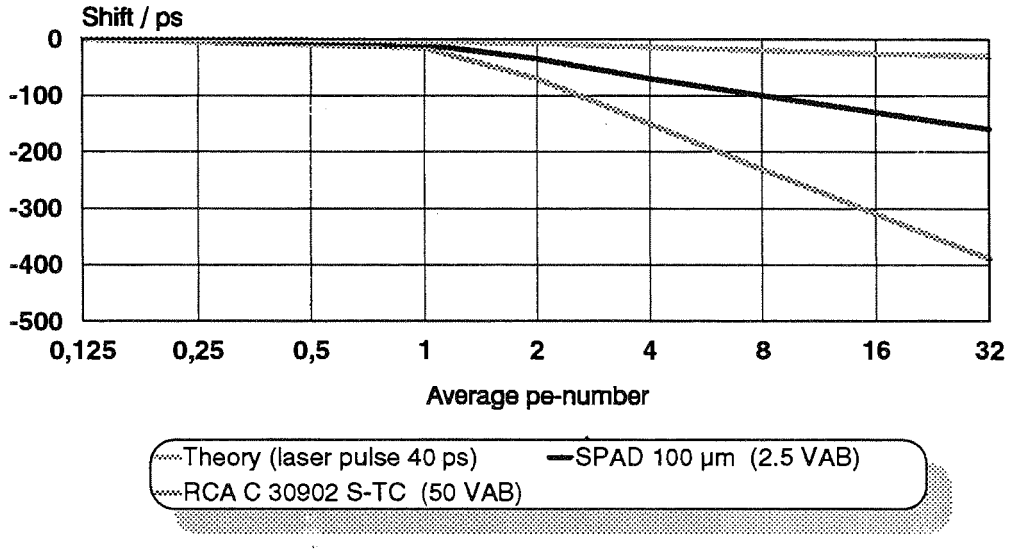

Both walk curves are compared with the theoretical values to be expected for a given laser pulse width which was repeatedly determined by streak records to be about 35...40 ps /1/. It is obvious that the laser pulse shape can explain the observed time walk up to about one average photoelectron quite well, but beyond this level there are different effects in action which exceed the influence of the laser pulse shape by far. Probably these effects are related to the process of avalanche triggering inside the detectors. This assumption is also supported by the fact that the two detectors show a fully different behaviour for the same signal level: the slope for the SPAD is in the order of -100 ps/decade for pe-numbers >2, the one for the RCA diode shows about -250 ps/decade. Due to the uniform output signal of both receivers independent on the number of incident photons discriminator effects can play no role; discriminators are usually not applied for APD's.
The observed time walk for target calibrations could be verified for the C 30902 S-TC in real satellite ranging as well /1/. The general recommendation to be derived from this experience is to keep the return signal well below 1 average photoelectron to avoid walk effects.

2. Photomultiplier HAMAMATSU H 5023

The 10-stage hybrid PMT H 5023 (rise time 600 ps, transit time spread 160 ps FWHM) offers an interesting alternative to avalanche diodes especially due to its large field of view in combination with low timing jitter and thermal noise. Different from the APD's, a matched pre-amplifier (H 4267) and a TC 454 constant fraction discriminator have to be used as well. The comments made below about the H 5023 should always be considered to be valid for the complex system PMT + preamplifier + discriminator. The main reason to test the H 5023 at the Potsdam station was to achieve fully blind tracking (day + night) even in the case of insufficient pointing accuracy + T/R-switch wobble as mentioned above, but it soon turned out that this PMT offers some other interesting feature: its distribution of ranging residuals is nearly symmetric and very narrow thus making it a good candidate for satellite signature experiments (see the histogram below which was obtained from 1000 returns at the single-pe level). After a test period in mid 1993, the H 5023 is used as standard detector at Potsdam station since the beginning of 1994 thus resulting in an average RMS of 9...10 mm for returns from the flat calibration target or a single cube corner.

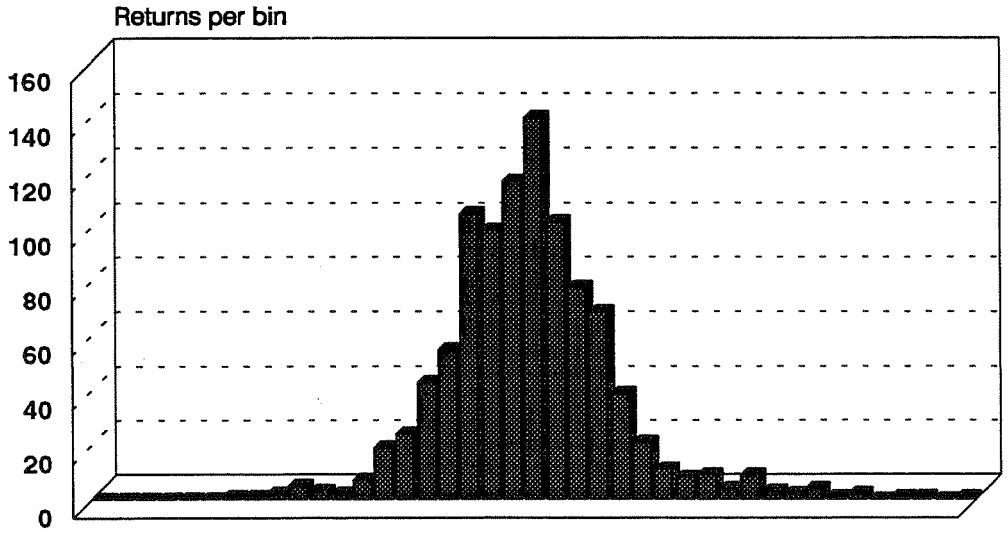

To test for a possible signal-dependent time shift, the same experimental procedure as for the avalanche diodes using a single cube corner and neutral density filters was carried out for the system PMT + preamplifier + TC 454. Additionally, a selfmade pulse height indicator was used in the stop channel with 3 bit resolution and a dynamical range from 100 ... 800 mV. For each return the pulse height was registered in the range from 1 ... 8 photoelectrons. Typical series of target returns for an average pe-level between 0.125 and 16.6 showed the following composition:

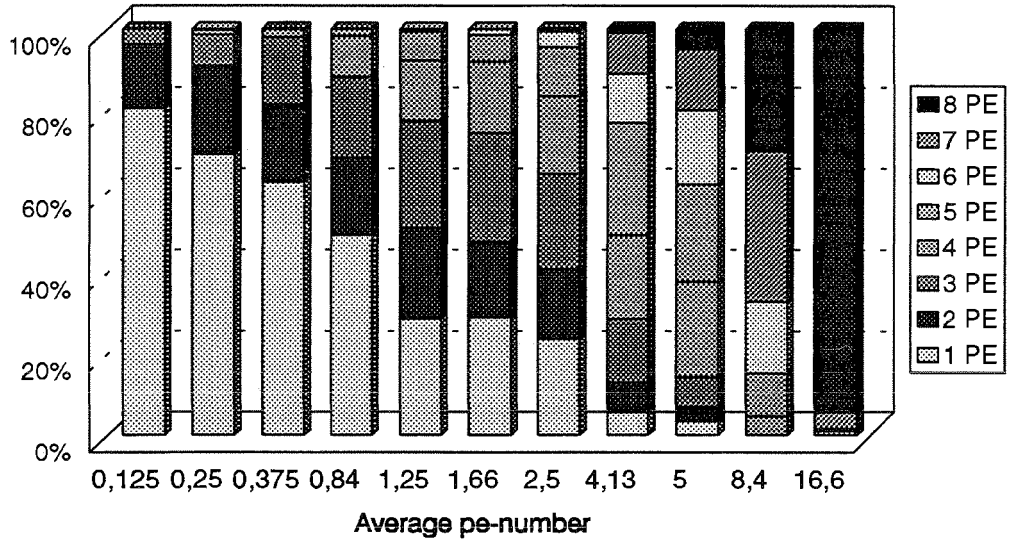

It is clearly seen that with increasing signal strength the number of single-pe pulses reduces considerably while the multi-pe returns increase. For a perfectly matched discriminator, this should be no problem; one would expect only a very small time walk dependent on the pulse height, but this seems not to be the case here.
The graph below was obtained by averaging the time-of -flight times of all pulses found in channel 1, 2, 3, ... 8, respectively. This procedure seemes justified because the spread in these TOF values for a given channel is low compared with the difference in the absolute TOF values between neighboured channels. With increasing pulse height, a considerable time shift becomes visible.

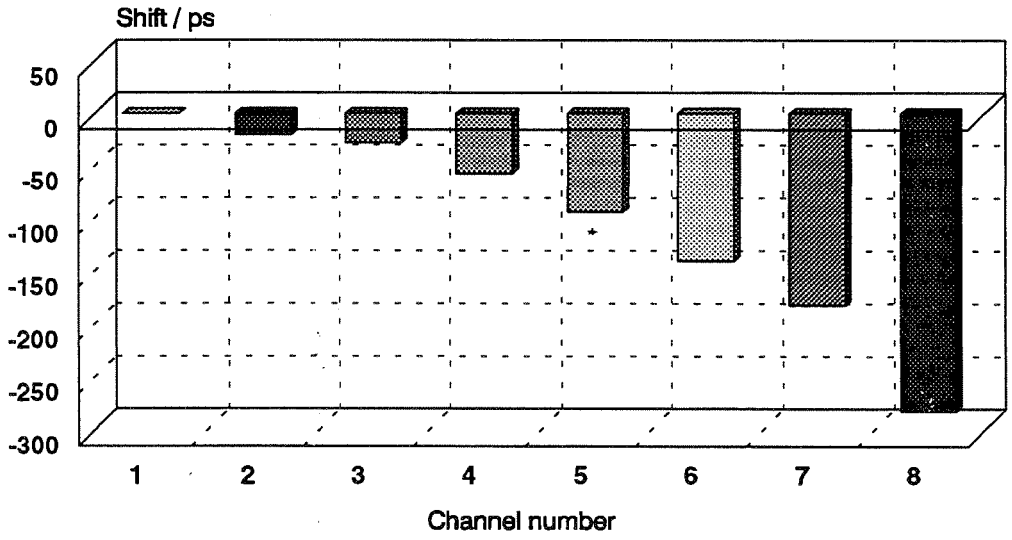

The reason for this unexpectedly large effect is somewhat unclear, but it seems that not fully proper setting of the discriminator parameters and/or possible changes in the pulse shape with increasing amplitude play the main role.
In the next graph, both the observed time walk and the „synthetic" walk based upon the known pulse height composition of the returns and the average time shift for each pulse height (as derived from the former graph) is shown in comparison with the expected time walk due to the laser pulsewidth alone. Again, it is clearly visible that the effect of the laser pulsewidth explains the observed shift for an average signal level up to about 1 pe reasonably. For higher signal levels, the pulse height dependent discriminator effects are considerably higher.

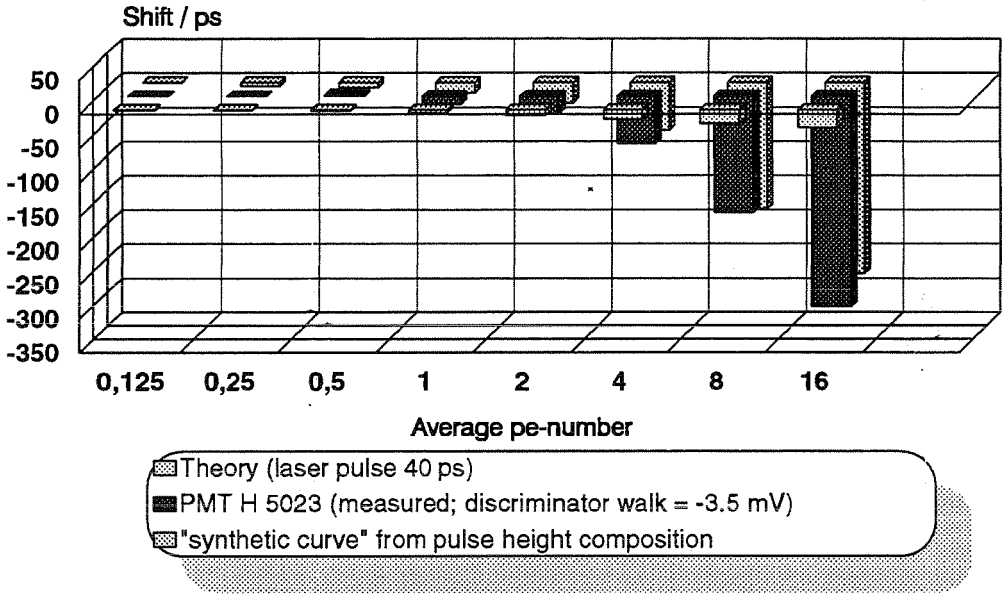

Also for the H 5023 the recommendation can be given to keep the signal level during satellite ranging below 1 pe to avoid the above mentioned time walk effects.

An additional effect should be pointed out here: with a setting of the discriminator walk very close to zero and a certain level of HF-noise from the laser present in the stop channel, virtual double pulses with a considerably higher pulsewidth than usual were observed as shown in the graph below. The difference between the maxima of both pulses was about 1.6 ns. For this reason, the discriminator walk should be set not too close to zero even if this results in a slightly higher timing jitter of the system.

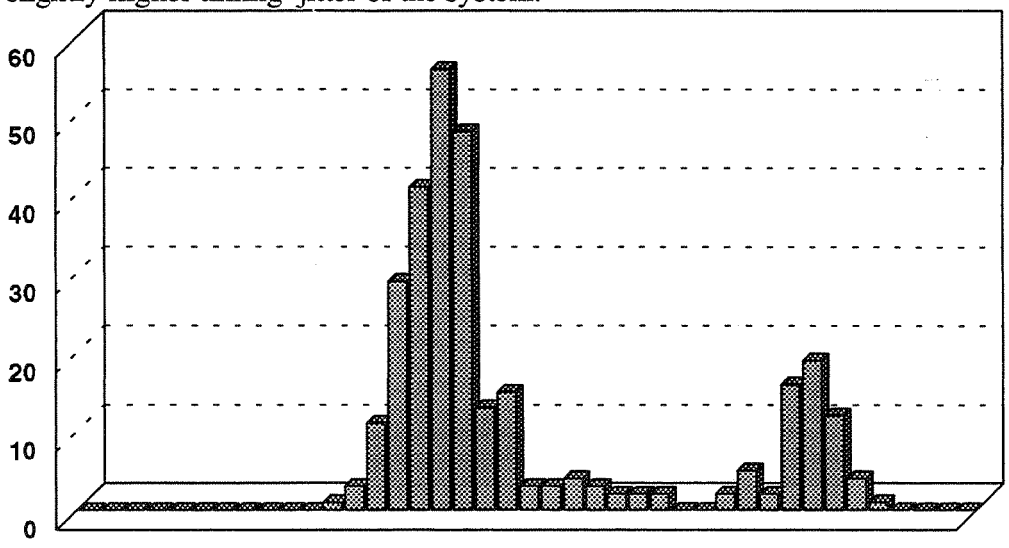

Bin width = 100 ps
Virtual double-pulses observed with discriminator walk ≈ 0

3. Future perspectives

The question arises how far the ranging accuracy can be improved by the detectors presently in use. Is the full capability with respect to time resolution already achieved or not?
To test this, both the PMT H 5023 and the 100 µm SPAD were illuminated by SHG pulses from a Ti:Sapphire laser (pulsewidth 1.3 ps @ 402 nm) in combination with an ORTEC time-to-amplitude converter. The resulting distributions are shown below.

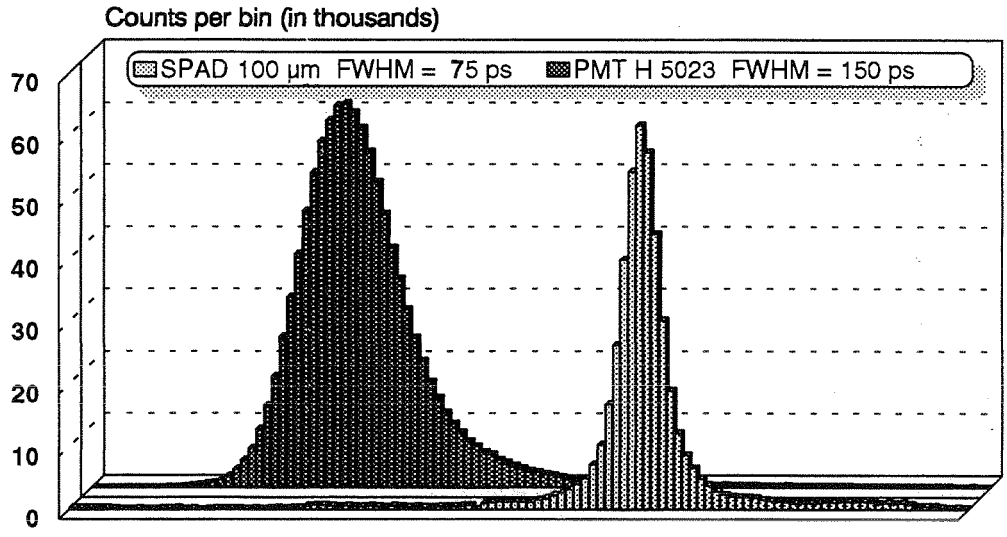

Bin width = 13.2 ps
PMT H 5023 and 100 µm SPAD response to ultrashort Ti:Sapphire pulses

It turns out that for the H 5023 the obtained timing jitter of about 60 ps is already the limit while the timing distribution for the SPAD is much narrower so that one would expect a value of 30 ps or a little less for a negligible laser pulse width. Even with laser pulses having a duration of 35 ... 40 ps a RMS below 50 ps could be expected. Obviously this value could not yet be obtained in our target rangings (see below), the standard value is now 51 ps.

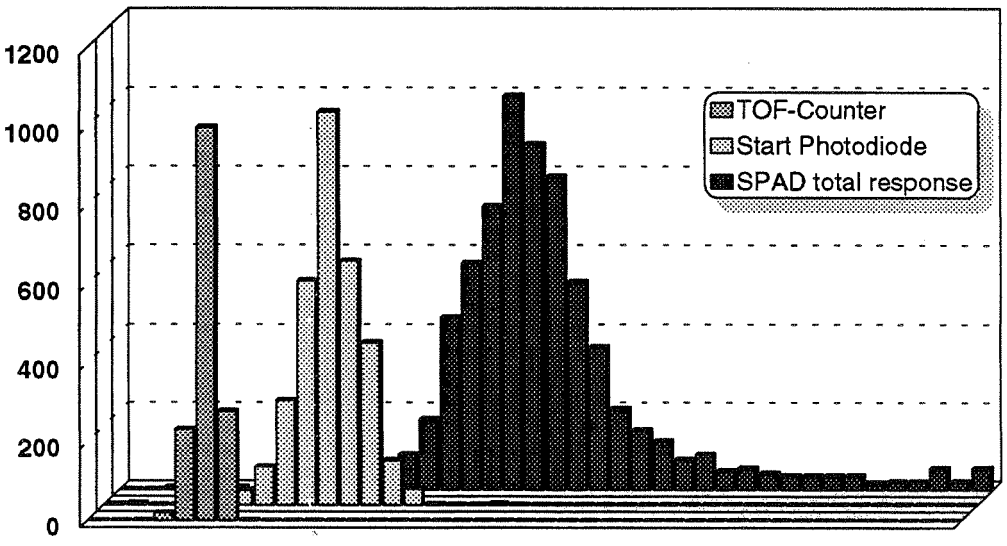

Bin width = 20 ps
Contributions to SPAD total response (Nd:YAG SHG, laser 40 ps)

In the graph above the residual distribution for 1000 returns split into the contributions of the single components of the system is displayed. The values for time-of-flight counter and start diode are too small to explain the full response of the SPAD. A possible reason is the presence of electrical noise in the stop channel. In this case it is expected to improve the performance of the SPAD detector with respect to timing jitter in near future by further reduction of this electrical noise level.

With respect to the H 5023 photomultiplier, improved setting of the discriminator parameters should result in a drastical reduction of the observed signal dependent walk effects.

We believe the combined detector system H 5023 + SPAD to be an optimum choice for our SLR system operated routinely at the single-photoelectron level.

Reference

/1/ R. Neubert: Analytical model for spherical satellites, these proceedings

Tests and Developments at the MTLRS-1 Receiving System

P. Sperber, R. Motz, P. Schötz
Institut für Angewandte Geodäsie
Fundamentalstation Wettzell
93444 Kötzting

M. Maberry, R. Zane
Institute for Astronomy
University of Hawaii
P.O. Box 209
Kula, Maui
HI 96790, USA

Abstract

During the last years different receiver configurations where tested at the German "Modular Transportable Laser Ranging System" MTLRS-1. In this paper the ranging experiences with two different Photomultipliers and two different Avalanche Photodiodes are summarized. In cooperation with the University of Hawaii a new discriminator for PMT and MCP with better time walk, compared to standard constant fraction discriminators, was developed. This experiments result in an optimum configuration for the MTLRS-1 receiving system using two receivers to combine best accuracy with high system sensitivity.

1. Introduction

In current SLR Systems the single photon detector has the main influence to system sensitivity, accuracy and noise level. Two types of detectors - Micro Channel Plate Photomultiplier and Single Photon Avalanche Diodes - are used in one-cm-accuracy-systems. The shape and amplitude of the signal from Avalanche Diodes is independent from the number of received photons, the amplitude of the PMT signal is linearly dependend on the signal strength, therefore a discriminator is necessary to prepare a pulse for the time interval counters. For this purpose standard constant fraction discriminators are used in most systems. This discriminators are not optimized for Satellite Laser Ranging, there is no possibility to adapt the electronics to new detectors with short pulsewidth or high dynamic range.

To find an optimum configuration of receivers for the new TIGO SLR-module and for MTLRS-1 we tested different detectors and a prototype of a new discriminator.

2. Testconfiguration

All receiver tests, described in this paper are made with MTLRS-1 in the following configuration:

- Nd:YAG Laser, 532 nm, 30 ps pulseduration, 10 mJ pulseenergy, 10 Hz repetition rate
- Start diode: optoswitch diode, 25 ps R.M.S.
- Ranging to internal target, single photon mode due to filters in transmission path
- Counter: HP 5370A, used in timeintervall-mode or in event timing mode (stop channels connected to 10 MHz signal from Caesium clock)
- Receiving filter: two echelle grating in complementary order, two detector parts.

3. Detectortests

The output of the receiving package (parallel beam, 8 mm diameter) was focused (3 cm focal length) on the following detectors:

- Avalanche Photodiode RCA C30902ST (cooled to -20° C)
- Single Photon Avalanche Diode (SPAD) from the group of Prof. Hamal, Czech Technical University in Prague
- Photomultiplier RCA 8850
- Photomultiplier Hamamatsu H 5023.

The results of this test are summarized in Table 1.

For high accuracy measurements the SPAD and the H5023 PMT are useable. The SPAD had the disadvantage of a very small active area and high noise level; the PMT has a low quantum efficiency and can be used only to low flying satellites or Lageos at extremely clear sky.

The disadvantages of the SPAD are probably solved with the new version TE cooled, 0.2 mm diameter SPAD.

The detector with the best quantum efficiency was the RCA APD.

Therefore it was decided, that the best combination of detectors at the two MTLRS-1 detector parts is:

- RCA C30902 ST APD for high flying satellites or bad weather conditions

- SPAD or H5023 PMT for high accuracy measurements.

4. Discriminator Developments

Photomultiplier and Microchannelplates are linear detectors, the amplitude of the electrical signal is dependend on the number of detected photons. Discriminators are used to transform this signal into a standard signal, which can be used for the input of counters.

This discriminators should give an output signal which is strictly time correlated to the input signal and which is independend to the amplitude of this input signal.

Up to now standard constant fraction discriminators are used for this purpose. This components are quite old fashioned and have a bandwidth far below the bandwidth, which can be realized with modern components. They have also problems with the short pulses at the output of modern detectors. Therefore it was decided to develop a new type of discriminator using state-of-the-art techniques, optimized for our detectors.

The idea and first design was developed at the SLR observatory in Maui, Hawaii, the final design and realization was done at the Fundamentalstation in Wettzell.

In difference to the constant fraction discriminators, in which a delayed inverted pulse of half amplitude is compared to the original pulse, the new type is designed as nanosecond delayed symmetry discriminator (NDSD). Here the pulse is compared to a delayed pulse of equal amplitude. The principle of operation and a block diagram is shown in Fig. 1, the electrical design of the trigger and discriminator part is shown in Fig. 2a/b. The greater differential slope at the discrimination point is more steep which a definite advantage of the NDSD and gives a higher resolution and a better time walk characteristic.

An other advantage is the easy adjustement of the time walk bias Voltage to get a zero timewalk over a high dynamic range of input signals. Fig. 3 shows the result of a measurement made at the Hollas Observatory in Maui, the time walk slope in fs per received energy meter readout versus time walk bias. The result shows a linear coherence, therefore only two measurements are necessary to find the zero time walk Voltage.

Using state-of-the-art electronical components a bandwidth of 600MHz was achieved. This in combination with the easy adjustement of the delay cables to the FWHM of the pulse allows the discrimination of the short pulses (some 100 ps) with the new detectors. The printed circuit boards of a two channel NDSD are now ready, the prototype will be tested at the MTLRS-1, MTLRS-2 and Hollas SLR systems.

5. Conclusion

This paper presents the testresults of four single photon detectors and of a prototype of a new discriminator. To optimize the system performance of MTLRS-1 in data quality and quantity a combination of two detectors will be used. The RCA C30902 APD will provide high sensitivity and good accuracy for high flying satellites and relatively poor weather conditions. The H5023 PMT or the SPAD with lower quantum efficiency will be employed for high accurate measurement under good conditions. The standard discriminator for linear detec tors with short output pulses (PMT, MCP) will be the new nanosecond delayed symmetry discriminator (NDSD).

Table 1: Results of the MTLRS-1 Detector Tests

	APD RCA C30902S	APD SPAD	PMT RCA 8850	PMT Hamamatsu H5023
Accuracy (RMS)	2.0 - 2.5 cm	1.0 - 1.5 cm	3 cm	1.2 - 1.5 cm
Quantum efficiency	20% - 40 %	10% - 20%	14%	8%
Noise	< kHz	100 kHz - 1 MHz	< kHz	100 Hz
Active area	0.5 mm	0.1 (0.2) mm	8 mm	10 mm
Supply Voltage	200 V, 60 V	< 50 V	2000 V	2000 V
Gating	20 microsec	2 microsec	no	no

Figure 1: Principle of Operation- and Block-Diagram of CFD and NDSD

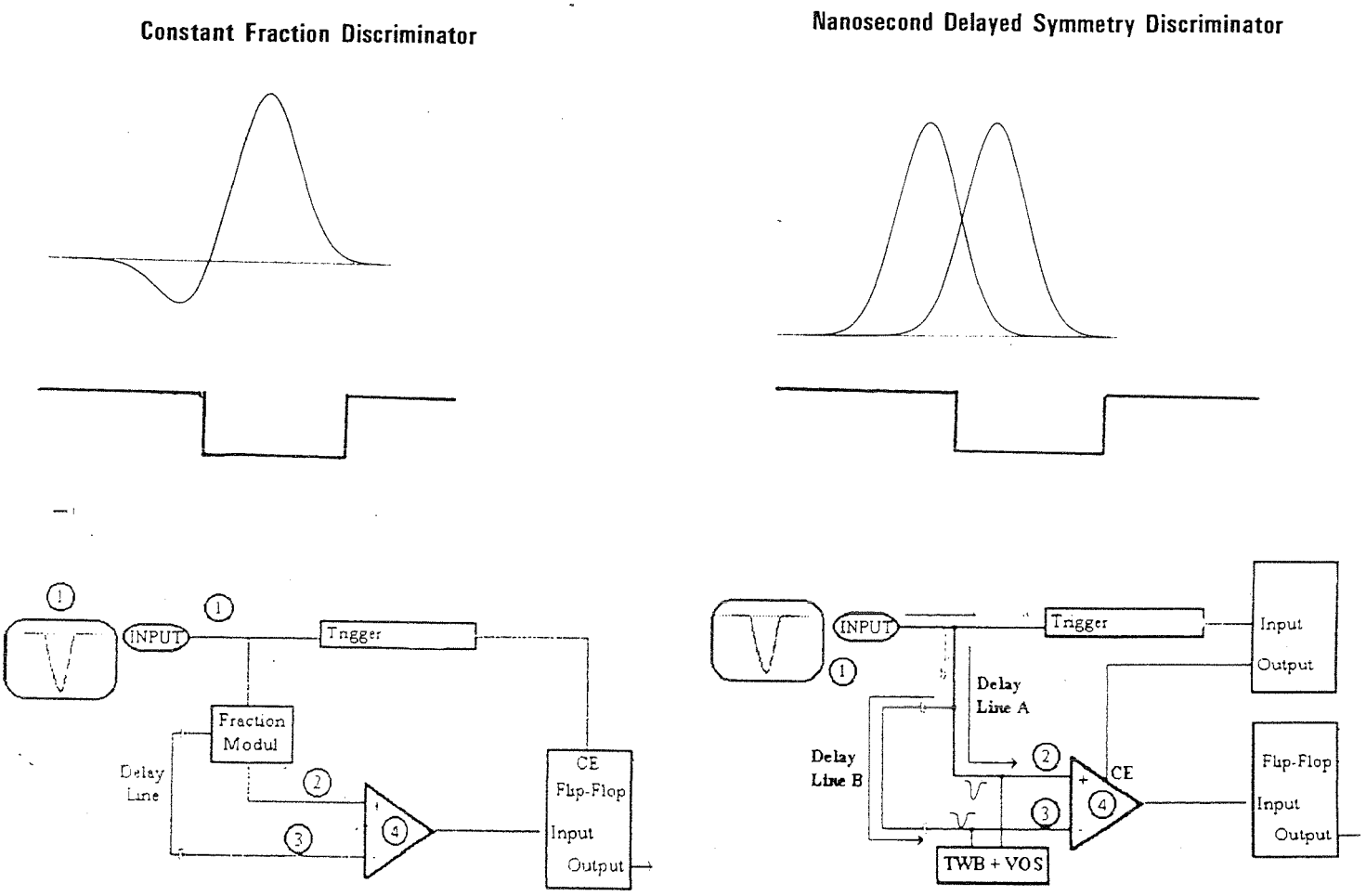

Figure 2a: NDSD Threshold Discriminator, Gating

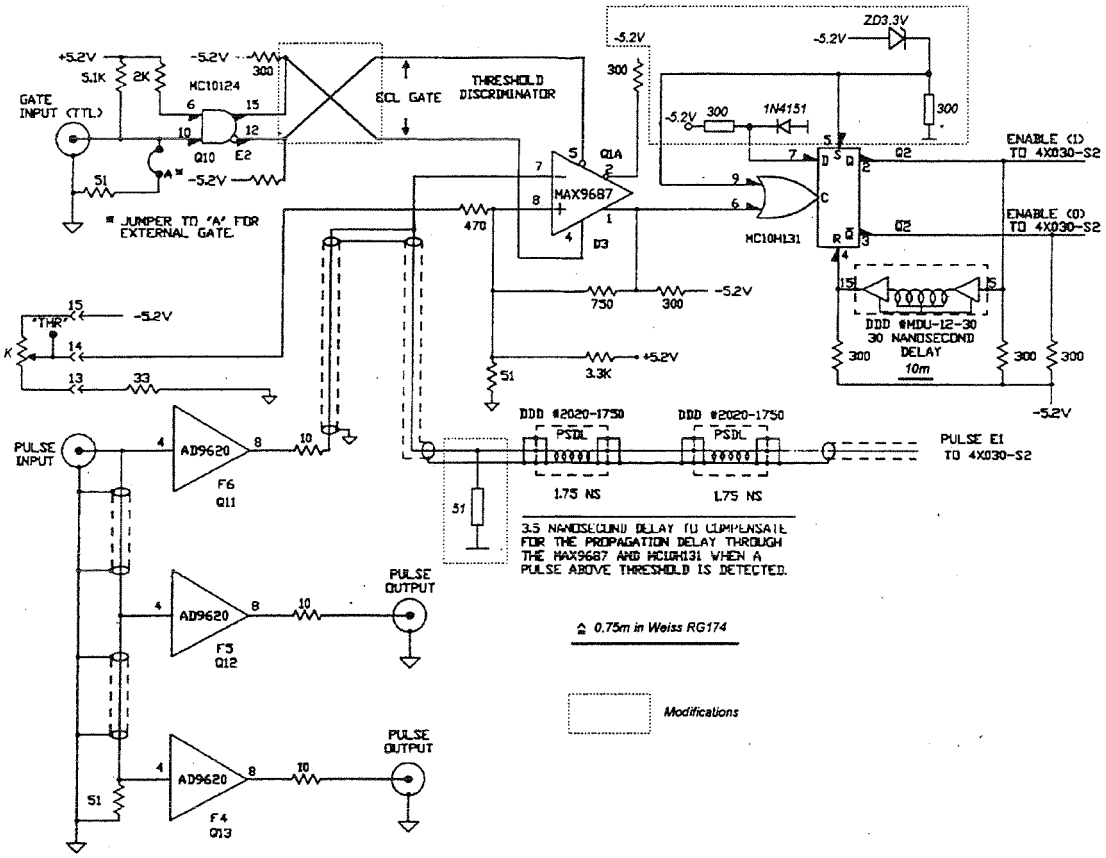

Figure 2b: NDSD Discrimainator part

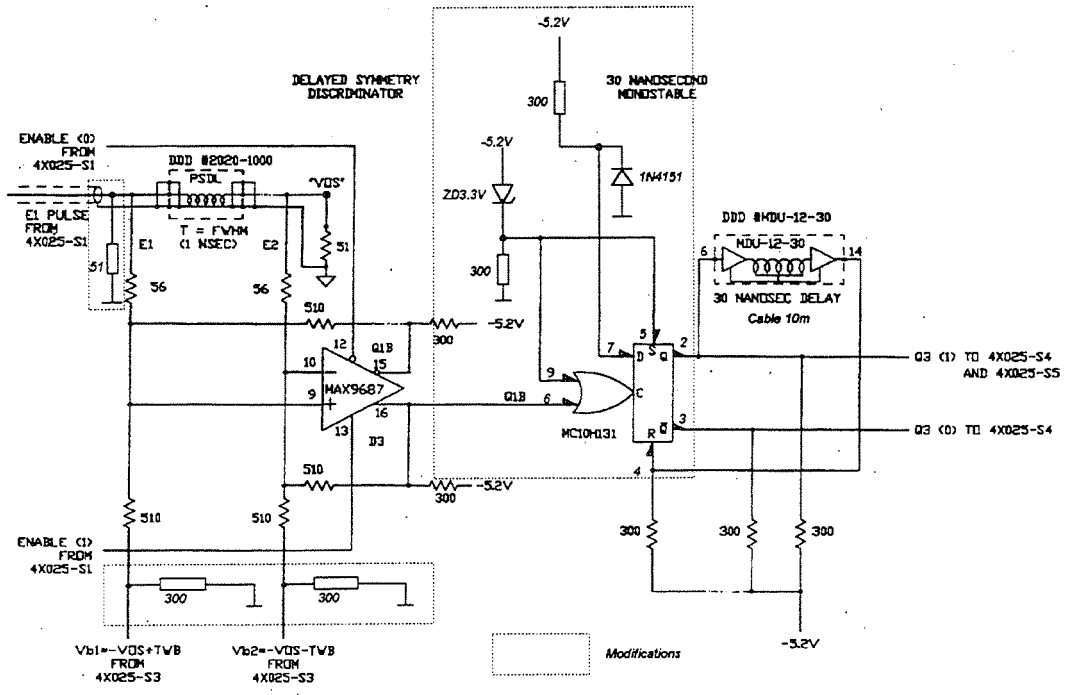

Figure 3: Time Walk Slope versus Time Walk Bias of the NDSD

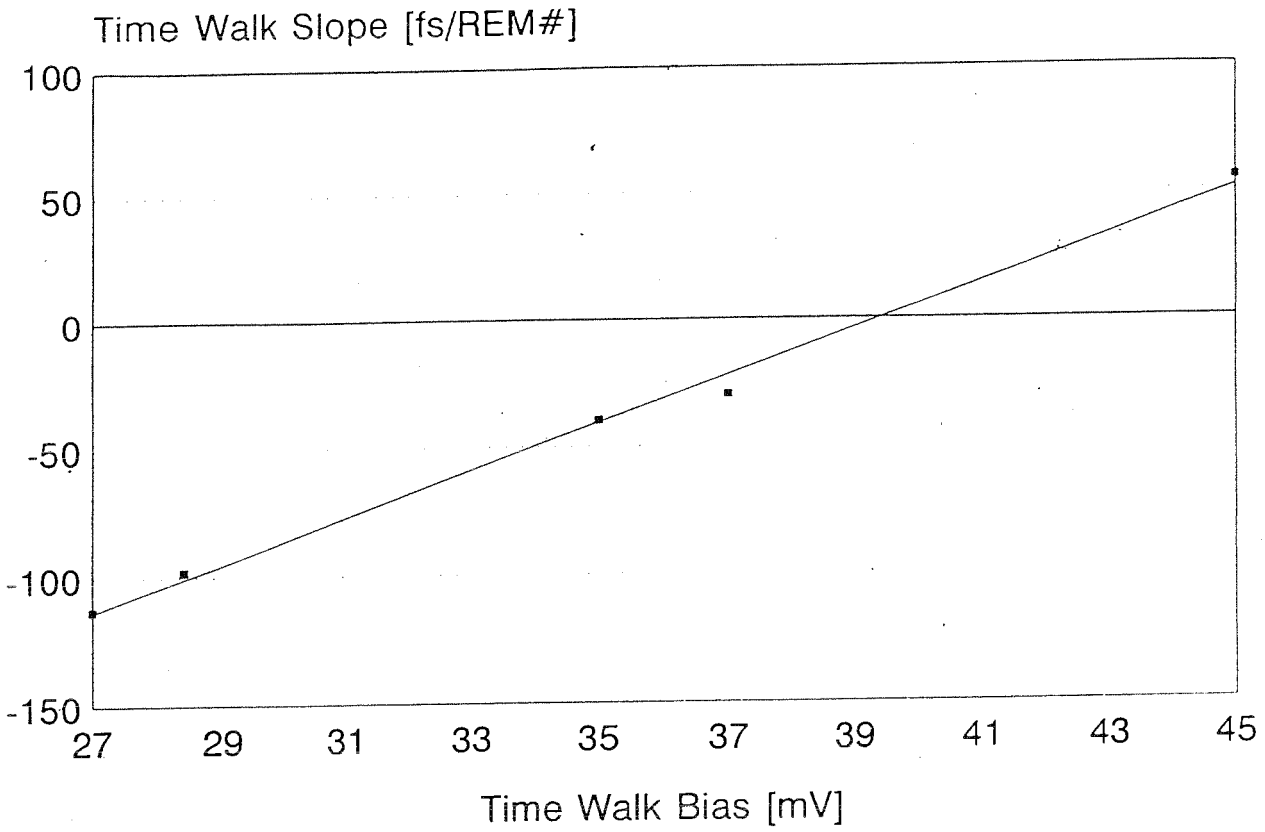

Transmit / receive two-colour optical unit for TIGO

H.W.T. Braakman, M.R. van der Kraan, H. Visser, B.A. van der Zwan
TNO Institute of Applied Physics (TNO-TPD)
2600 AD Delft, The Netherlands
P. Sperber
IfAG, Fundamentalstation für Satellitengeodäsie
Wettzell, 93444 Kötzting, Germany

Abstract

For the German TIGO project a new, dedicated transmit/receive optical unit has been designed that acts as the optical interface between the two-colour Ti-Sapphire pulse laser, the telescope mount and the detectors of the TIGO-SLR system. In fact the detectors are part of this optical unit.
This unit also has most of the built-in alignment tools for the optical alignment of the entire SLR system, and it has an internal calibration stability check over an optical fiber.
A general system overview of the new two-colour transportable TIGO-SLR system is presented in the "New Mobile Stations" session of this workshop.

1. Introduction

The TIGO-SLR optical system configuration consists of the following main parts:
- a telescope
- a two-colour Ti-Sapphire laser (847 nm + 423.5 nm)
- a transmit/receive optical unit that interfaces with the laser, the telescope and the detectors.

Of these three major optical units only the telescope is located outside in the open air as indicated in figure 1. The laser and the transmit/receive unit are built in an air-conditioned cabin.

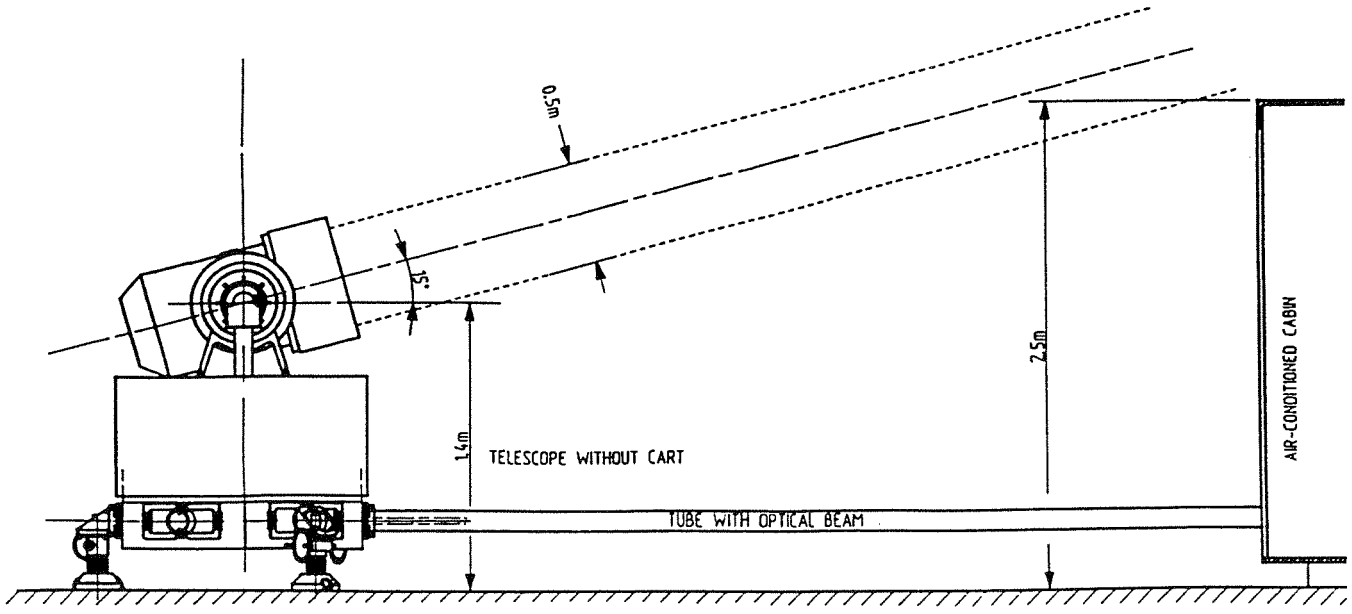

Figure 1 General TIGO-SLR system configuration

2. Main tasks

For the here described transmit/receive optical unit the following main tasks can be distinguished:

- spectral separation of an adequate telescope field of view and wavelength range for visual guidance and alignment purposes (eyepiece or camera).
- spatial separation of the transmitted pulse laser beam and the received optical beam at the laser wavelengths (847 nm and 423.5 nm)
- divergence setting of the transmitted laser beam over an adequate range for all targets
- collection of the received optical signal from an adjustable field of view at the sky
- narrow band spectral filtering of the received energy at the laser wavelengths to enable day-time operations
- collection of the filtered optical receiver signal at the "stop" detectors
- providing a simultaneous calibration stability check (during satellite ranging) over a fixed, internal lightpath (a single mode optical fiber, used at the 847 nm laser wavelength).

In figure 2 is shown how the most important input beams and output beams of the transmit/receive optical unit are separated.

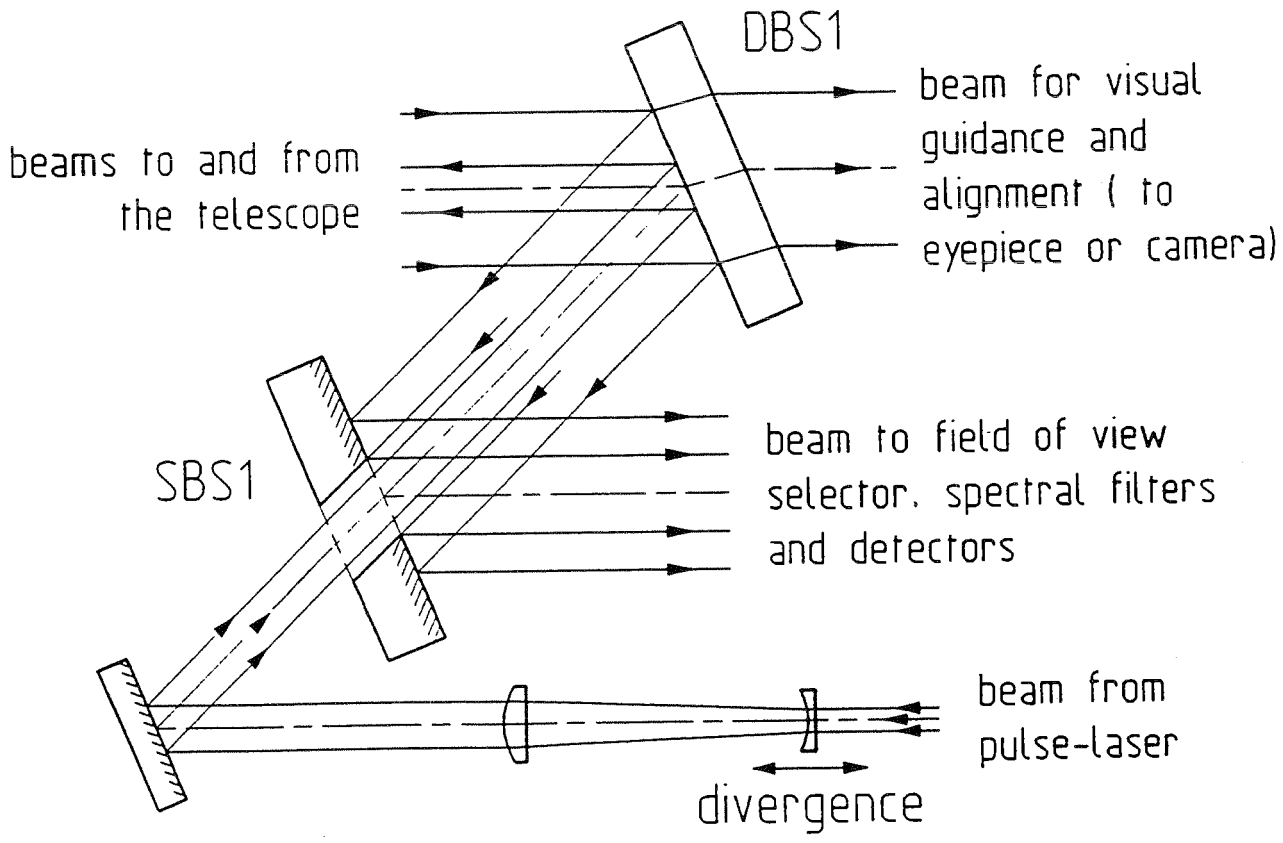

Figure 2 Beam separating optical configuration.

DBS1 = dichroic beam splitter (R_{laser} > 99%; T_{eye} > 80%)
SBS1 = spatial beam splitter

3. Laser beam incoupling

Along the optical path from the pulse laser to the divergence setting optics (as indicated in figure 2) there are a number of not yet mentioned optical subsystems. These optical subsystems are schematically shown in figure 3, inclusive of the already presented divergence setting optics.

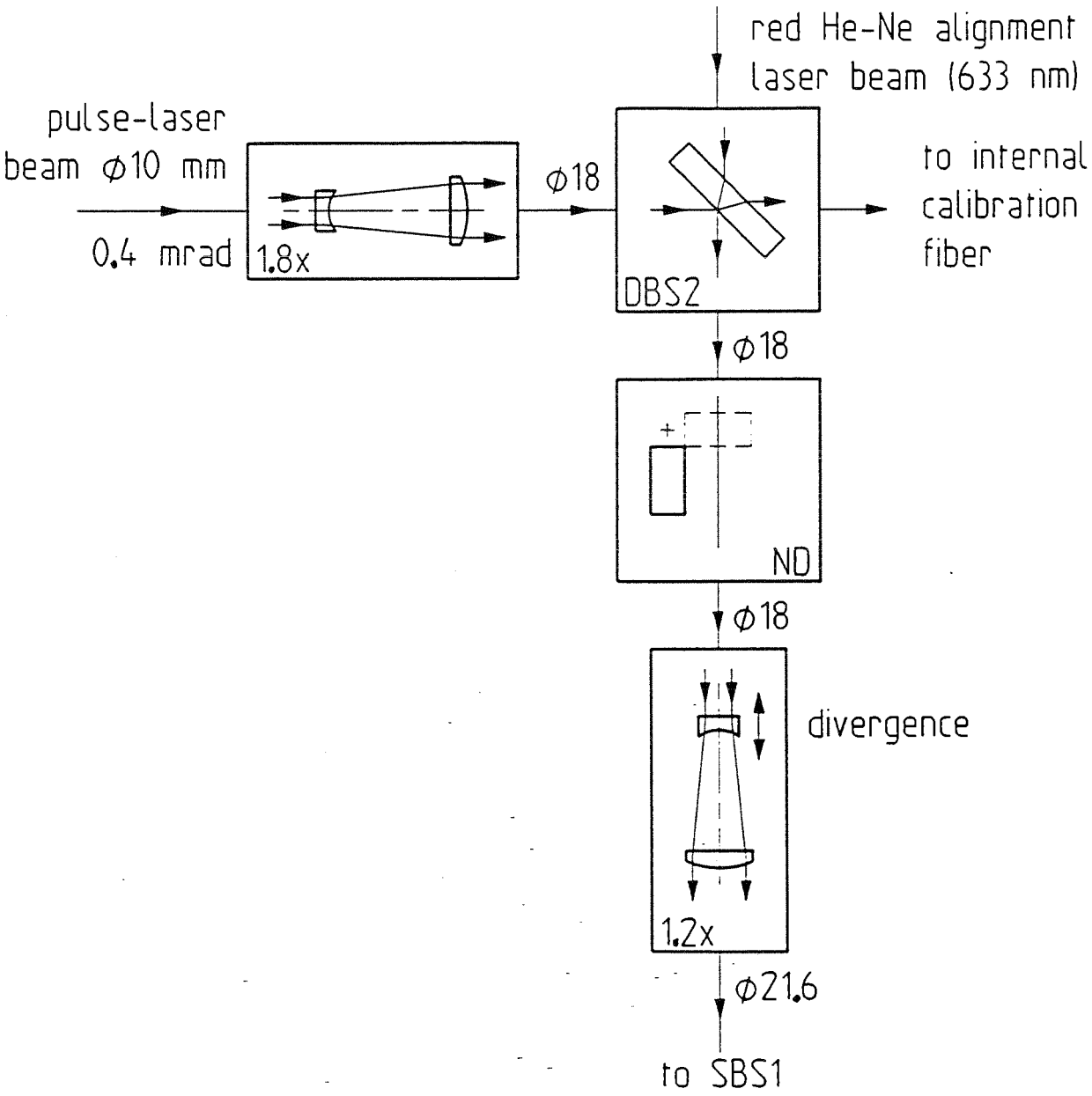

Figure 3 Optics along the optical train from the pulse laser to spatial beamsplitter SBS1

The incoming pulse laser beam has a specified diameter of 10 mm and a specified collimation of 0.4 mrad (= 82 arcsec.).
With the optics of figure 3 this beam is first enlarged in diameter to 18 mm by an 1.8 times telescope system. This improves the laser damage resistance of the following optics along the optical train.
At dichroic beamsplitter DBS2 the pulse laser wavelengths (847 nm and 423.5 nm) are both reflected with an efficiency of more than 99%. A very small fraction of the energy (at 847 nm), that is transmitted through DBS2, is used as input of an internal calibration lightpath over a single mode optical fiber (e.g. 100 m long).
A red (633 nm) He-Ne alignment laser beam is transmitted through DBS2.
For calibration purposes and for ranging to terrestrial targets a neutral density (ND) filter unit has been added to the optical train. In this filter unit 7 ND filters can individually be rotated in or out of the beam. With combinations of the 7 filters the transmitted laser energy can be attenuated in steps of about ND = 0.5 (factor of $\sqrt{10} \approx 3$) from ND = 0 (no attenuation) upto ND = 16 (factor of 10^{16}).
Finally the already mentioned divergence setting optics in the form of an 1.2 times telescope system enlarges the transmitted beam diameter at the spatial beamsplitter SBS1 to 21.6 mm. By the indicated movement of the negative lens the divergence of the transmitted beam can be adjusted from best collimation (for the specified laser characteristics this is about 40 arcsec at SBS1, or about 5 arcsec at the sky, with a transmitted beam diameter of about 0.18 m at the telescope front lens), upto a divergence that corresponds to about 1 arcmin at the sky (8.3 arcmin at SBS1).

As can be seen in figure 2 the transmitted laserbeam is directed to the telescope through a central hole in a mirror (spatial beamsplitter SBS1). This hole in the mirror (that reflects the beam to the detectors) reduces the effectively used collecting area of the telescope as a receiver of the "stop" signals, to about 84% ($1 - (24/60)^2 = 0.84$, where 24 mm is the diameter of the hole in SBS1 and 60 mm is the diameter of the on-axis coudé beam as it comes from the telescope mount).
As a result of this optical transmit/receive configuration the TIGO-SLR system can routinely be operated without a (rotating) transmit/receive optical switch, so that there is also no limitation to the shortest measurable distance.

With the use of an optional transmit/receive switch in the form of a rotating lens assembly at the telescope mount, the collimation of the transmitted beam can be improved to about 2 arcsec at the sky (for the specified pulse laser of 0.4 mrad at 10 mm diameter beam). This option may be useful for measurements to very distant satellites (e.g. in geostationary orbit).
In figure 4 the location of this optional T/R switch at the telescope mount is shown. The rotating pair of lenses has a very long focal length of about 10 m to accommodate for the distance between the telescope mount and the air-conditioned cabin in which the transmit/receive optical interface unit is housed. By using the T/R switch the transmitted beam diameter at the telescope front lens is enlarged to about 0.4 m.
Note in figure 4 also some of the built-in alignment and calibration facilities of the telescope mount.

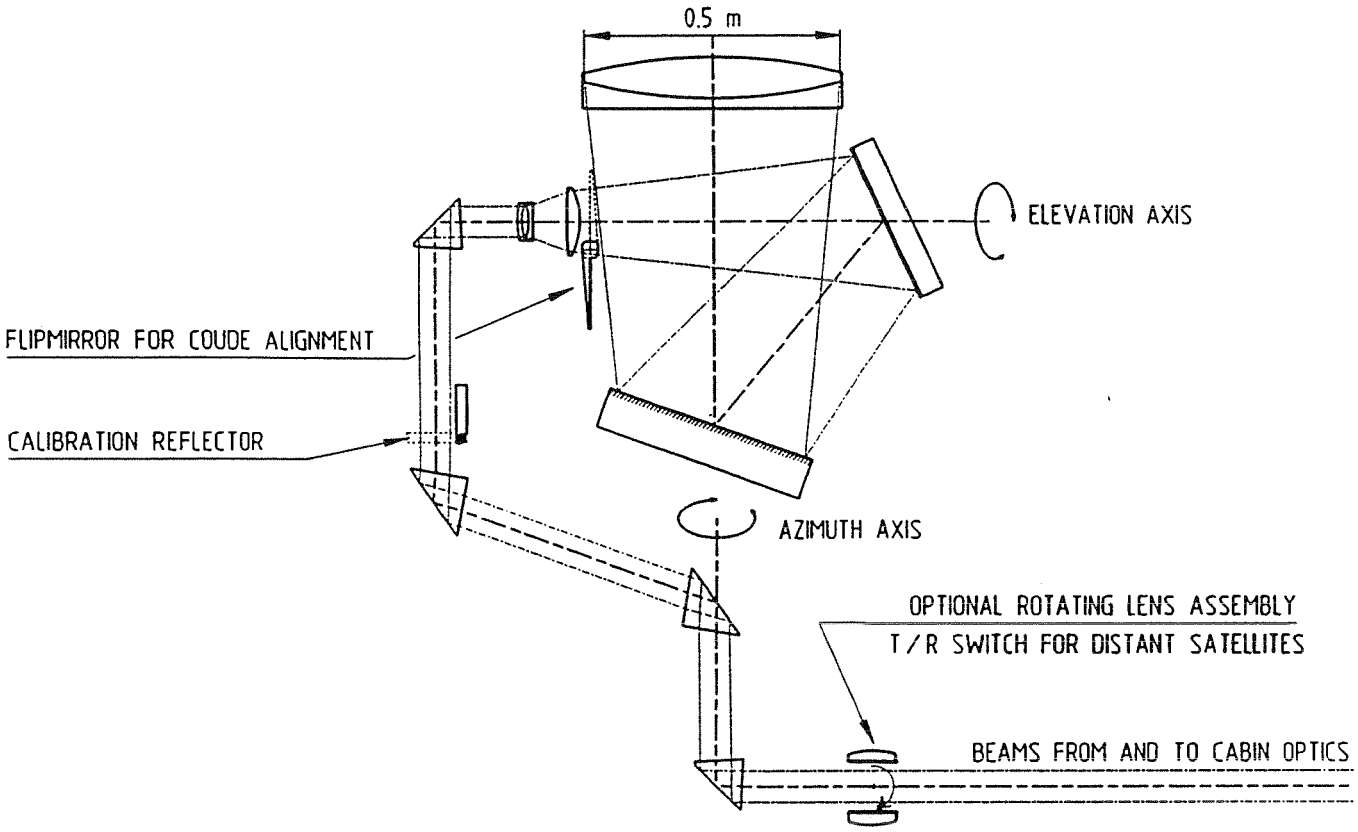

Figure 4 Telescope mount optics

4. The optical train from SBS1 to the detectors

In figure 5 the receiver optical train, from spatial beamsplitter SBS1 upto the "stop" detectors, is presented schematically. The received collimated beam, as reflected by SBS1, is first imaged by lens L_1 into an adjustable Field of View (FOV) opening (via a reflection at flat folding mirror M).
Just in front of the adjustable FOV opening a rotating shutter (RS) is shown in figure 5. The function of this rotating shutter is to be able to protect the detectors from excessive straylight. This straylight may come from the optical elements (also in the telescope) when the laser is firing at full power. The rotating shutter is designed so that, for all satellites, the lightpath to the detectors is closed when the laser fires, and is open at the moment that the reflected signal from the satellite is expected. For calibration and ranging to terrestrial targets the rotating shutter is open when the laser fires, but in that situation the laser power can be reduced by the previously described ND filter unit (as shown in figure 3). The adjustable FOV opening can continuously be adjusted at any desired FOV value, ranging from zero (closed FOV opening) upto about 1.5 arcmin at the sky.

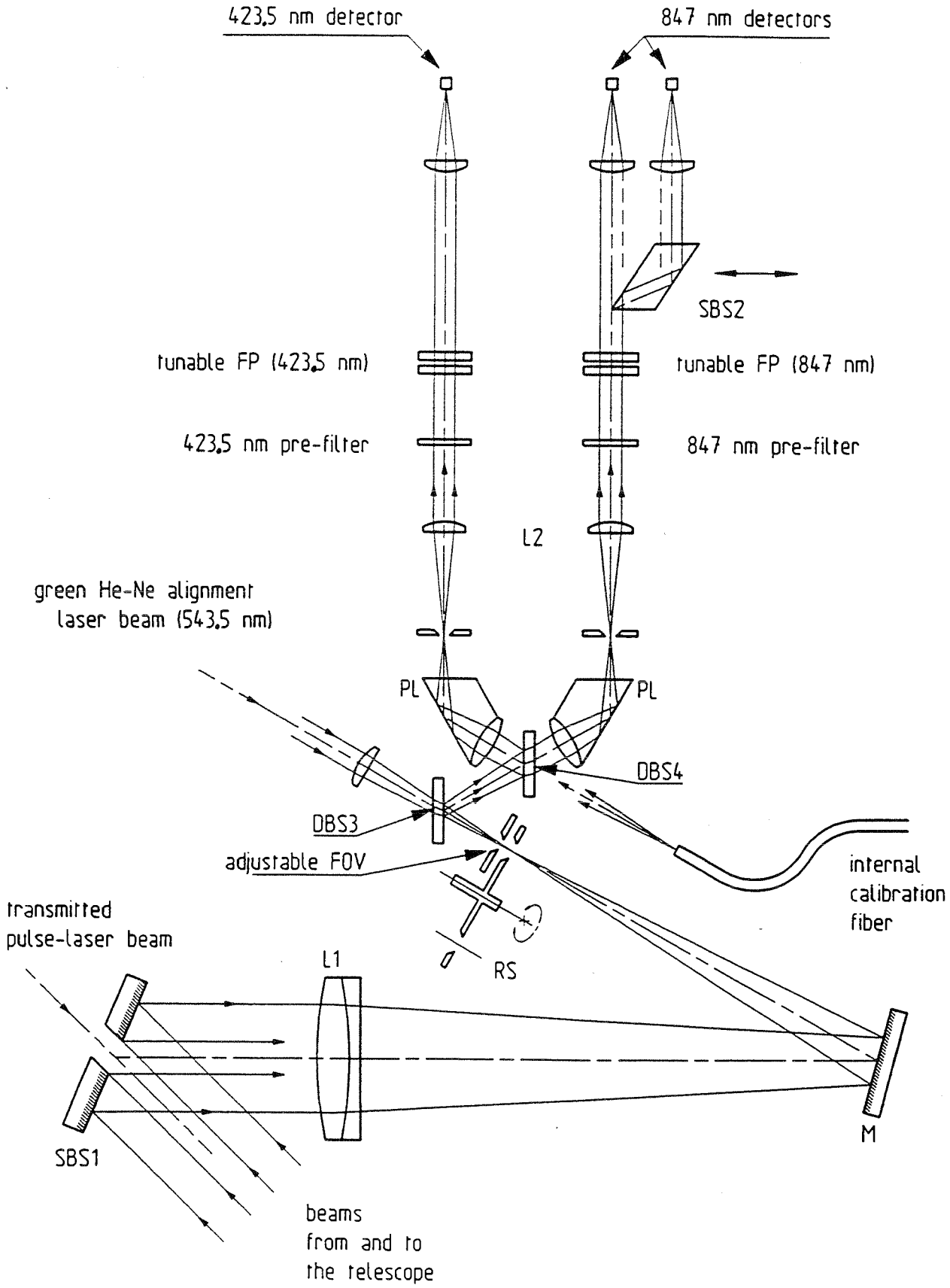

Figure 5 Receive optical train to the detectors

Following the adjustable FOV opening both laser wavelengths are reflected at dichroic beamsplitter DBS3 towards dichroic beamsplitter DBS4. At DBS4 the 847 nm laser wavelength is transmitted and then refocused by one of the two prism-lens assemblies PL. The blue laser wavelength (423.5 nm) is reflected at DBS4 and then also refocused by the other prism-lens assembly PL.

Both beams are recollimated by the lenses L_2 at a diameter of about 13 mm and then spectrally filtered, first by relatively broadband high efficiency interference filters (the so-called pre-filters) and secondly by tunable narrow band Fabry-Perot filters (FP). The pre-filter function is to select the proper Fabry-Perot filter order.
Because of the not very narrow bandwidth of the Ti-Sapphire laser (0.2 nm at 847 nm) the tunable Fabry-Perot filters are not very narrow bandwidth either. For the 847 nm FP-filter a bandwidth of 0.6 nm (full width at half maximum) has been specified and for the 423.5 nm FP-filter a bandwidth of 0.3 nm has been specified. Both FP-filters have a high efficiency (> 80%), an airgap of 12 µm and a relatively low finesse (50 for the 847 nm filter and 25 for the 423.5 nm filter). The free spectral range of the 847 nm filter is about 30 nm and of the 423.5 nm filter about 7.5 nm. Wavelength tuning of the FP-filters is achieved by deliberately ordering the FP-filters at a somewhat (0.3 - 0.6 nm) shorter wavelength and by putting each of the two filters individually in a small pressure chamber. By changing the air pressure inside the small pressure chambers the wavelength of the filters can be tuned to the pulse laser wavelengths. Per bar the wavelength of the FP-filters changes with about 0.028% of the wavelength (0.12 nm per bar for the 423.5 nm filter and 0.23 nm per bar for the 847 nm filter).

At 847 nm the signal is divided over two detectors, as indicated in figure 5, by the spatial beamsplitter SBS2 in the form of a moveable prism. Any distribution of received signal over the two 847 nm detectors is possible in this way (100% to detector 1, 100% to detector 2, or any ratio inbetween).
The 423.5 nm beam has just one detector in the present design. The project team is still discussing the to be implemented detector types for the TIGO-SLR system (SPAD, MCP-PMT, or other type). The detectors are at an easily accessible place on the table top of the transmit/receive optical unit, with sufficient space to accommodate all envisaged detector possibilities. Detectors can also easily be exchanged in a later stage.

At DBS4 a small fraction of the output of the internal calibration fiber is reflected into the 847 nm receiver optics (only a small fraction because most of the 847 nm output of the fiber is transmitted through DBS4 and "lost" in the 423.5 nm receiver optics). This small fraction of the fiber output provides a possibility of an internal, simultaneous calibration stability check during satellite ranging.

Indicated in figure 5 is also that from the "other side" of DBS3 a green He-Ne alignment laser beam can be transmitted into the optical system. Together with the red He-Ne alignment laser beam as indicated in figure 3, the alignment facilities in the telescope mount, and some other not shown alignment facilities, a powerful and complete set of built-in alignment tools is part of the TIGO-SLR optical configuration.

5. Visual guidance

For visual guidance and alignment purposes a visual wavelength range is transmitted through DBS1, as indicated in figure 2. This beam is focused by a lens system in the focal plane of an eyepiece at a convenient location at the transmit/receive optical unit, or it can be directed to a camera system. A 2-position mechanism will make switching from eyepiece to camera easy.

In front of the eyepiece/camera switch a 6-position filter wheel offers the possibility to limit the transmitted wavelength range (e.g. to 520 - 600 nm) to reduce the chromatic rest aberrations of the telescope and to reject the pulse laser wavelengths to levels that are safe for the eye (and camera), also during firing of the pulse laser at full power.

Because of the large distance between the telescope mount (outside) and the eyepiece/ camera (inside the air-conditioned cabin) the telescope field of view that is transmitted to the eyepiece/camera is limited to about 0.1 degrees at the sky. This is sufficient for alignment purposes, star observations and visual tracking of satellites.

6. Mechanical structure of the transmit/receive unit

The mechanical support of the components of the transmit/receive optical unit is supplied by an aluminium table (table top are 1.2 x 0.6 m^2) and a box like aluminium structure underneath the table top (1.0 x 0.5 x 0.8 m^3).

The laser beam incoupling (upto the ND filter unit), the tunable Fabry-Perot filters, the detectors, the He-Ne alignment lasers, eyepiece and camera are mounted on the table top area. These components are easily accessible. The space underneath the table top is used for the beam separating optics, additional optical alignment aids, the divergence setting optics of the transmitted laser beam (remote control), the ND filter unit (remote control), the rotating shutter, the internal calibration fiber and the receiver field of view adjustment (remote control).

The entire transmit/receive optical unit is directly supported by the TIGO platform (supporting feet through the cabin floor) and can be adjusted over the two relevant angles. A CAD presentation of the mechanical structure of the transmit/receive optical unit is shown in figure 6. Through the opening in the side wall at the right the optical beams to and from the telescope are transmitted. The openings in the table top are for transmitting of the pulse laser and the alignment laser beams, and for the received beams to the detectors and to the eyepiece or camera. In figure 7 an inside view of the structure is presented, inclusive of many (but not all) of the opto-mechanical elements. On the table top only the routing of the transmitted laser beam is shown.

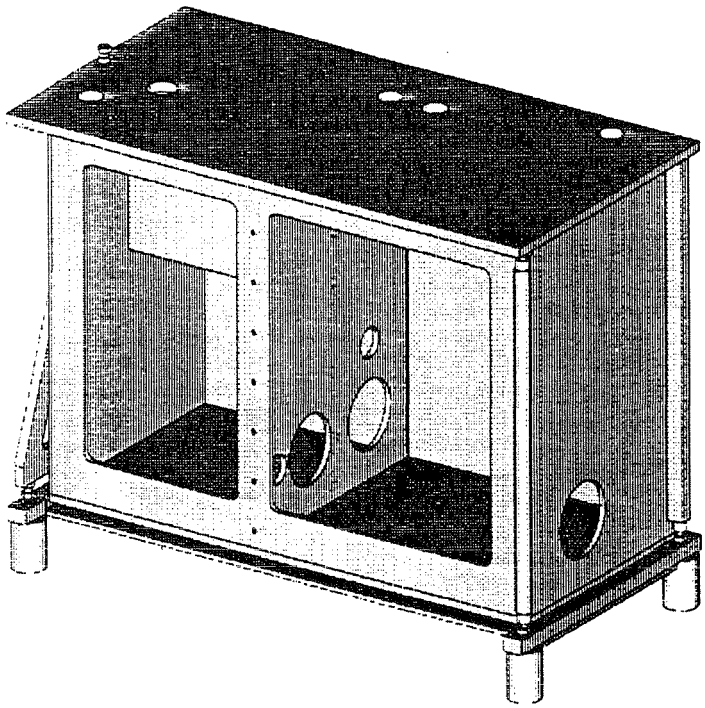

Figure 6 Mechanical structure of the transmit/receive optical unit.

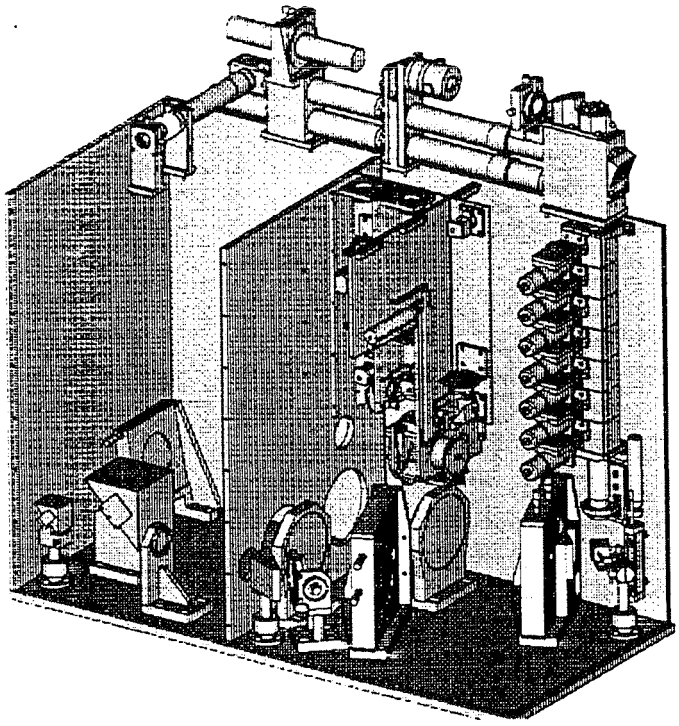

Figure 7 Inside view on opto-mechanical elements.

Improved TeO_2 and Te Acoustooptic Spectrometer-Imaging System

Dominique Souilhac and Dominique Billerey

Institut National Polytechnique de Lorraine
Laboratoire d'Electricité et de Mécanique Théorique et Appliquée
2 Avenue de la Forêt de Haye, 54516 Vandoeuvre)lès-Nancy, France
FAX: 83 44 07 63

ABSTRACT

An improved TeO_2 and Te infrared acoustooptic tunable spectrometer has been developed by Infrared Fiber Incorporated, using infrared fibers, a high speed frequency synthesizer and optimized algorithms. A comparison is made with the next best AOTF materials, Tl_3AsSe_3, Hg_2Cl_2 and $PbBr_2$.

Following our previously reported design study of the TeO_2 and Te acoustooptic imaging spectrometer for operation in the two thermal bands using a HgCdTe focal plane array cooled at 77°K, we illustrate and discuss briefly, more applications of the AOTF using telescope coupling for the visible, mid-infrared and far infrared wavelength regions . A high performance infrared spectral-imager typical test result that can be obtained with the high performance spectral analyser from Minirad Systems Incorporated or with the infrared acoustooptic imaging spectrometer from Diversified Optical Limited is shown.

Finally we indicate by comparison with existing visible-near infrared spectrometry instrumentation, that simultaneous spectroscopy at every pixel with the TEO_2 AO imaging spectrometer can display spectras at every pixel in times of a millisecond instead of a hundred of second required for fast Fourier Transform computation.

1. INTRODUCTION

1.1. Types of Spectrometers and Comparisons.

The acoustooptic tunable filter (AOTF) is a birefringent crystal which acts as an electronically tunable narrowband filter. Ref.[6] analyses in detail this very important optoacoustic device. In the visible region, a typical bandpass is about 2 angstroms and about 100 Å ($20cm^{-1}$) in the infrared.The AOTF compared with a grating or Fourier

Transform Infrared Spectrometer (FTIR) include no moving parts, small size, high speed and random wavelength selectivity. Its size of typically 10x10mm, improves the coupling to fiber bundles, and makes possible spectral imaging (Section 4). These advantages are especially important for chemical analysis in remote, hazardous or confined locations found in many industrial, medical or aerospace applications. Although the AOTF is more expensive than bandpass filters, it offers random access to a large number of wavelengths which is limited only by the computer and electronic design. Also the AOTF offers n times more throughput where n is the refractive index, than a 30° blazed reflection grating having the same resolution and losses.

A historical list of AOTF publications is listed in Ref.[1-8].

1.2. AOTF Design and Trade-Offs.

The acoustooptic tunable filter which exhibits a wide angular aperture operates by virtue of anisotropic AO diffraction, and among the optically anisotropic materials, uniaxial crystals have been most widely used in their implementation. In light of our formulation the operation of the device can be explained based on the schematics shown in Fig.1. When the transducer is driven by an R.F. amplifier it launches an acoustic wave with wavevector K_a which propagates inside the crystal along the x_1 axis, the orientation of the axes x_1,x_2,x_3 with respect to the crystalline axes x,y,z is specified by the Euler angles $\phi\ \Theta\ \psi$ [9]. The acoustic wave interacts with a broadband incident optical wave, this wave has one spectral component, with wavevector k_i lying in the x_1x_2 AO interaction plane, which propagates inside the crystal. Θ_I is the incident Bragg angle, the angle between the optical wavevector k_i and the normal to the acoustic wavevector, x_2 axis. We choose k_i extraordinary polarized and k_d ordinary polarized. (See Fig.1). As the optical wavelength of the incident optical wave is changed the phase-matching requirement is no longer satisfied, the intensity of the diffracted beam decreases and the diffracted beam exhibits a passband type behaviour with respect to the incident optical wavelength and hence the AOTF acts as a bandpass filter. This method is based on the compensation of momentum mismatch due to the angular change of incident light by the angular change of birefringence of the extraordinary wave. As shown in Fig.1b, the acoustic K-vector is chosen so that the tangents to the incident and diffracted light wavector loci are paralell. Thus, for a change in incident light direction, the momentum matching is still approximately maintained[6].

Using the equations of Ref.[6 7] the exact variations of Θ_I, the tuning curves and

also the resolution curves for the TeO_2 (mid-infrared) and Te (infrared) AOTF are obtained (Fig.2,3,4,5,6,7). In Fig.8, we note that the effective bandpass of the AOTF is broadened if the focal ratio number of the input beam is smaller than the AOTF. Thus, the effective numerical aperture (NA) of the AOTF is an important design parameter. The design goals and tradeoffs for the AOTF consists of i) Achieve optimum optical properties consistent with electronic limitations and cost, ii) Choose center wavelength of tuning range, this will determine the impedance matching and electronic requirements (rf frequency) and power . iii) Tradeoff a higher N.A. and shorter crystal for a higher rf drive power (a high and low N.A. increases and decreases respectively the power requirement).

In order to improve the SNR and reject stray light, a modulation scheme and lock-in technique is often used. The diffracted wavelength is modulated usually at 15KHz, which rejects stray light. Note that for the non-collinear filter, the angular change of birefringence compensates the phase-mismatch due to the angular variation of light incidence. Thus collimated light is not necessary and the AOTF can have a large angular aperture. On contrary for collinear AOTF collimated light is required.

Characteristics of the TeO_2 (mid-IR) and Te (IR) AOTF, the best next mid-IR and IR AOTF materials like Tl_3AsSe_3, Hg_2Cl_2 and $PbBr_2$ AOTF materials and the AOTF design equations are given in Tables I,II,III, respectively.

1.3. Discussion with next best IR AOTF materials: Tl_3AsSe_3, Hg_2Cl_2, $PbBr_2$ [10]

From Tables I,II,III, for AOTF spectrometry applications where a high acoustooptic figure of merit, a narrow spectral bandpass and a moderate bandwidth are required, the Tellurium crystal is the best AOTF material due to its high AO figure of merit, very high birefringence and moderate acoustic attenuation for longitudinal sound and good transmission with diamond like carbon AR coating, for the use in the spectral range 5-20μm. (The transmission can be increased from 26% to 80% with diamond like carbon AR coating of 1.1μm thickness).

Hg_2Cl_2 is the most promising future AOTF material because of its very wide transparency range (0.35-20μm), high acoustooptic figure of merit, moderate acoustic attenuation and hence moderate rf bandwidth and may be preferred to TeO_2 and Tl_3AsSe_3, but is different of Te in the infrared because of its smaller birefringence and hence spectral bandpass. Finally, Tl_3AsSe_3 is the best AOTF material for the mid-IR and IR waveband due to its high AO figure of merit and moderate acoustic attenuation ,

but for spectrometry applications where a narrow spectral bandpass is required, the very small value of its birefingence makes Hg_2Cl_2 and Te superior AOTF materials for such applications.

$PbBr_2$ is an excellent candidate IR AOTF material for the mid- to far-infrared region, due to its high acoustooptic figure of merit and moderate acoustic attenuation, especially where it is useful to have transmission in the visible but its birefringence is much too small for high resolution AOTF spectrometry.

For rapid spectrum scanning TeO_2 is the fastest and Hg_2Cl_2 the slowest AO crystal:

The spectral resolution of the AOTF is also limited by the speed with which the optical spectrum may be scanned. Since the acoustic beam takes a finite time to cross the optical beam the filtered light contains a band of optical λ for a band of Δf_{acous}.

2. DESIGN OF AOTF SPECTROMETERS.[11]

2.1. Introduction and Block Diagram.

Although TeO_2 transmits from .35 to 5μm, the optimum wavelength range of a given device depends on the thickness of the acoustic transducer. For example, the device can operate from .37 to .9μm, which covers the UV and visible region, or from 2.5 to 5μm in the infrared.

We have analysed theoretically and experimentally optimized impedance matching circuit to extend the operational wavelength range of any given device, and to minimize the reflected rf power to improve the efficiency of the device . A mid-infrared AOTF spectrometer using a TeO_2 crystal and operating in the wavelength range from 2-4.7μm, having a resolution of $20cm^{-1}$ has been previously fabricated with a shift in the wavelength with a change of temperature of about .1%/°C and can be reduced to under 0.1nm by placing the crystal in a temperature stabilized oven[11].

2.2. Block Diagram and Optics.

2.2.1. Optical Layout.

Based on the work of Ref.[11] a diagram of a fiber-coupled AOTF spectrometer is shown in Fig. 9 . The light is focused through the AOTF crystal, and into the fiber. Hollow waveguides are not chosen here because of the large curvature.[12] The light is either transmitted through or reflected off the sample and returned by a second fiber to the photodetector. Fiber optics allow remote sensing from the U.V. to infrared. The detector consists of either a silicon photodiode for the visible, or

thermoelectric cooled PbSe or InSb for the infrared. Another detector we have used is a HgCdTe detector cooled at 77°K.

2.2.2. Fiber Optics.

A zirconium fluorideglass fiber transmits from about 400nm in the ultraviolet to 5μm in the infrared. The range of lowest attenuation is between 1 and 4μm, with a loss minimum of about 50dB/km at 2.5μm (Fig. 10, 11, 12). To increase the optical throughput of the fibers, their numerical aperture can be increased from .2 to .30 and the core/clad ratio can be increased from 80% to 90%. These fibers have already been fabricated into cables and bundles of various configurations and used to obtain remote spectra of gases and liquids[12]. Recently it has been developed an extended wavelength fluoride fiber[11]. The minimum bend radius for this fiber is shown in Fig. 10. For transmission in the infrared region, chalcogenide glass fibers can be used (Fig. 12).[12]

2.3. Electronics (Hardware and Software).

Fig. 13 shows more details of the electronics and computer which are often used to control the AOTF[11]. The signal is amplified by a lock-in amplifier and processed by a microprocessor. The computer normalizes, averages and analyses the data before displaying the result on the monitor. The AOTF is driven by an rf amplifier and digital frequency synthesizer. The high speed 16 bit synthesizer is used to control the rf frequency, and can tune more than 10000 points in a single scan, with a random access time of 30 microseconds per point. The rf power level is typically around 2 Watts average and is sinusoidally modulated to allow lock-in detection. The frequency response for the rf amplifier should be between 10 and 200MHz, with about 10 Watts of power output. For higher speed, the modulation can be eliminated and the detector signal passes directly into the computer. Because the crystal's impedance changes with frequency, an impedance matching circuit is used to match the crystal to 50 ohms. This system can have two basic modes of operation. In the spectral scan mode, the user enters the start and stop wavelengths into the computer, the total number of wavelengths points to be obtained during the scan, and the time between wavelengths points. The synthesizer then generates the appropriate frequencies to scan the wavelength over the desired range. A reference scan can be run to normalize the sample scan, and repetitive scans can be obtained for signal averaging using a high speed A/D converter, the time between wavelength points can be as short as 50 microseconds. Another mode of operation is the random access, or "hopping" mode. The

user specifies discrete wavelengths and the synthesizer will jump between these wavelengths. This mode is useful for monitoring the change in concentration of specific samples as a function of time, when the peak wavelength of each sample is known in advance. The computer then displays the concentration for each sample separately on a windowed display. Fig.14,15 show details of the software chart.

3. APPLICATIONS AND TEST RESULTS.[11]

Applications of the AOTF spectrometer include chemical process control, medical diagnostics, scientific research and spectral imaging. It can be divided into six applications fields:

1-Transmission and reflectance spectroscopy (Chemical process control (food,plastics,petrochemical,etc.), combustion control, toxic gas and liquid monitor (waste sites, methane leaks, etc.), rocket plume analysis, medical diagnostics (airway gas, blood gas, angioplasty, etc.)).

2-Fluorescence spectroscopy (biochemistry, medical diagnostics).

3-Spectral radiometry (fire detection, gas temperature, ceramic temperatures and aerospace vehicles).

4- Spectral imaging (aerospace, medical diagnostics, planetary and Earth studies).

5-Laser line tunability and Acoustooptic filtering of Lidar (Dials) signals.

6-Wavelength division multiplexing in high data rate fiber optic system.

The concentration of CO_2 mixed with air can be monitored using the peak absorption wavelength at 4.25μ. This signal is normalized to a reference signal at 3.39μm in order to compensate for background drift. The AOTF hops between these two wavelengths rapidly to reduce the effect of drift. A change in CO_2 concentration from 5% to 8% is indicated. The length of the sample cell was 5cm and the length of the fiber cable was 8 inches. (Fig.18).

The AOTF spectrometer can also be used for reflectance spectroscopy. A thin layer of vacuum pump oil on a metal substrate was used as the sample. The fiber probe could be used to monitor oil contamination inside of metal vacuum tubing, for example.

If a mixture contains several unknown samples from a list of many possible samples, the AOTF can be programmed to hop to many wavelengths and an algorithm is used to determine the composition and concentration of the unknown mixture, assuming

the spectra of the pure samples are known in advance. One algorithm, for example, involves solving simultaneous linear equations, which can be done at high speed using digital signal processing. The advantage of the AOTF in this case is that the set of wavelengths can be changed to optimize the algorithm, depending on which samples are present. For example, a rough estimate of the composition can first be done to narrow down the composition to a few samples. Then, the wavelengths can be changed in real time to obtain better accuracy for the actual samples present in the mixture. This real time change of the wavelengths increases the signal-to-noise ratio by eliminating unecessary wavelengths and signal averaging at only the important wavelengths. Furthermore, the time between hops can be programmed in order to optimize this signal averaging routine. For example, if certain wavelengths are especially important or are noisy, then the AOTF will sit and average for a longer time at that particular wavelength.

Other applications of the AOTF include telescope coupling to obtain remote, high speed spectra of rocket engine plumes. Currently, detector arrays are used to obtain these spectra, however large arrays do not operate beyond 5μm , because the technology is still not mature enough for absolute temperature measurement from measured calibrated radiants[14]. Interesting combustion gases such as water vapor and carbon dioxide could be monitored using the AOTF. See Fig.20,21,22,23 Ref[13] and Table IV.

In addition, the imaging capability could be used to obtain spectral images of the engine exhaust plume. Monitoring the temperature of this exhaust or of other materials such as ceramics where the emissivity is unknown could be done using spectral radiometry. The AOTF could scan the emitted infrared radiation and determine the true temperature from the shape of the blackbody radiation curve. Emission lines superimposed on a blackbody curve can be used to distinguish flashes from hot objects in infrared fiber-optic fire sensor applications.[19]

The effective temperature of the target and its effective area can be obtained through the use of the ratio method. This method is based on equating the ratio between to signatures (Watt/str), that were measured in two spectral bands, to the expression of the corresponding ratio ,of the spectral radiances (Planck's function) (Watt/cm^2.str.μm) integrated over the two bands.[17]

Fig.23,24 show a high resolution spectra obtained with a high performance spectral analyser. The AOTF in this case can replace the filter wheel and display the spectra in time of a millisecond, in each visible, mid and far infrared spectral regions. Experimentally we measured the target temperature with the ratio method.

Remote sensing technology has become an advanced tool in the search for minerals for mining. For example, four images can be captured with the TeO_2 AOTF tuned to 450, 492, 582 and 646nm. The image resolution is greater than 100lines/mm as measured with a tungstene-halogen source [15] [16].

The TeO_2 AO spectrometer using a telephoto lens and a CCD camera may be used in the 0.4-1μm band. The weight, the size of the imaging spectrometer shown in Fig.25 can be reduced , and the fast Fourier computing time typically required of 115 seconds to display a spectra at every pixel can be reduced to a millisecond.

Diversified Optical Limited (DIOD), (Suffolk, U.K.), fabricates a 3-5 & 8-12μm AO imaging spectrometer and creates a spectral line overlay on the thermal image using acoustic modulator selection.

In these test examples, each spectral image may be displayed as a pseudo color image including a spectral display of any pixel, moving a cursor on the screen. As explained in the previous section, each spectral signature can be stored and compared to archived spectral data for identification of differences in the various spectral signatures between material and stuctures identifying subtle changes in pollution or environmental hazards.

4. CONCLUSION.

An improved TeO_2 mid-infrared acoustooptical tunable spectrometer has been developed by Infrared Fiber Inc., using infrared fibers, a high speed frequency synthesizer, and optimized algorithms. This system performs well in the mid-infrared spectral region with many applications in chemical process control, medical diagnostics aerospace and earth studies.

The development of a visible-near infrared AO imaging spectrometer can be readily accomplished from existing technology and an infrared acoustooptic imaging spectrometer is now fabricated, but the development of a far-infrared AO imaging spectrometer is still some way in the future depending on the fabrication of much larger HgCdTe focal plane arrays cooled at 77°K.Indeed the technology is still not mature enough for absolute temperature measurement from measured calibrated radians.

5. APPENDIX A

The Infrared Electronically Scanned Array (MESA) (P.N.J.Dennis, Sira Communications Ltd, Chislehurst, Kent, U.K., Course Notes). (See Table IV).

Cadmium Mercury Telluride (CMT/Si) hybrid stucture technology produces IR detectors with high quantum efficiency. The CMT array interfaced to a silicon CCD in which the photocurrent is injected into the CCD for a period known as the stare time t_s. The charge packets are then clocked out and multiplexed onto a single output line. The performance of these arrays can be expressed as a fraction of the frame time for which the device is staring and this is determined by the incident photon flux, the charge capacity of each CCD pixel and the output data rate. Consequently the stare efficiency can be very high, typically between 50 and 90%, in the 3-5μm band . However for the longer waveband these stare efficiencies are much more difficult to acheive due to the very much larger photon fluxes emitted in the 8-12 micron band from a 300K ambient scene, which causes the CCD wells to fill up and saturate rapidly. In addition, to acheive a high injection efficiency into the CCD the photodiode slope resistance must be greater than the CCD input impedance and this becomes progresively more difficult to acheive as the wavelength is increased, as the energy gap of the infrared detector is reduced. Consequently two dimensional close packed CCD arrays have currently been restricted to the 3-5 micron band or to cut-off wavelengths out to approximately 9.5 microns.

For operation at longer wavelengths an alternative readout technique has been developed in which each photodiode detector in the array is connected to a silicon MOS switch. Each line of elements is addressed through a decoder or shift registerand the signal integrated off the focal plane on a set of integrating amplifiers [15]. Consequently these arrays have a much greater dynamic range than that acheived with the CCD as there is no limit to the amount of charge that can be stored on the integrator off of the focal plane thus permitting their operation at very long wavelengths. In addition the photodiodes can have a much lower IR product than that required for a direct inject circuit such as the CCD. However at present the performance of any system using these arrays is limited to one line equivalent output. Also it is necessary to take a large number of leads carrying the photocurrent from the dewar. A logical extension of this coordinate addressing technique matrix is to incorporate the integration and multiplexing circuits on the focal plane. Fig. 24 shows schematically how this can be achieved by adding additional circuitry to the basic coordinate addressing matrix of the line scanned array. The resulting Multiplexed Electronically Scanned Array (MESA) consists of a linear array of direct injection transistors to transfer photocharge from the infrared diodes to

the storage capacitors. The capacitors are precharged to a voltage using a reset transistor and are then discharged by the photocurrent for a fixed integration time. At the end of each period the residual capacitor voltages are sampled by a sample and hold circuit and then sequentially multiplexed to a single voltage output. Consequently there is only a single signal lead coming off of the focal plane and thus a simple dewar may be used for these arrays.

Sophisticated digital electronics working at least 10 bits accuracy is required for the non-uniformity correction of these arrays. The output from 2 elements in the array have a variation in both offset and gain or responsivity as a function of scene temperature. These non-uniformities of the imager can be referenced to two uniform temperatures set to the maximum and minimum values of the scene at switch on. These coefficients are then stored and used to correct in realtime the detector outputs.Any dead element in the array can be concealed in the video using simple nearest neighbour averaging.

One difficulty which can arise with a staring array system is due to the discrete sampling which occurs and thus in the limitation in the high frequency spatial performance. This can result in dramatic aliasing affects in which high frequency scene detail is obscured in the image and appears at lower spatial frequencies with a confusing result.

The modulation function can be calculated from the ratio of the image contrast to the object contrast. Furthermore imaging systems exhibit phasing effects between the detector elements and the target resulting in a deformation of the MTF curve towards lower values.
Also the MTF curve shows a spectral fold back above the Nyquist frequency (highest spatial frequency apparent at the output is equal to half the sampling frequency). The spatial spectrum of the system is modified by aliasing effects.

In order to reduce these effects a microscan has been adopted in which the image scene has been displaced by some fraction of a pixel with respect to the detector array. (One third of a pixel). Aliasing effects are significantly reduced by this technique. Image formats of 128x128 and 192x192 pixels can be produced from a 64x64 array.

Although the technology of the two dimensional staring array is new. many applications can already be identified with the types of array now being produced. In particular this include missile homing heads and possibly with the microscan mechanism which employs a simple plain mirror actuated by piezo-ceramic transducers, a man-portable surveillance camera and a wide field surveillance system is still some way in the future depending on the development of much larger 2D infrared matrix arrays.

A typical value of the dynamic range obtained with such IR array(with background) scene substraction) is of the order of 10^5.

6. ACKNOWLEDGMENTS.

We are grateful to the Acoustic Research Group at McGill University, Sira Communications Ltd (Chislehurst, Kent, U.K.), Dr K.H.Levin of Infrared Fiber Inc., Brimrose Corporation of America, CI Systems Inc., Minirad Systems Inc., Diversified Optical Ltd, U.K., Amber Engineering, Professor A.D.Devir, Technion R&D Foundation for their support in the field of Acoustooptic Imaging Spectrometry and finally to Dr Ulrich Schreiber,Wettzell Observatory and Dr J.McK.Luck Orroral Observatory.

7. REFERENCES.

1-I.C.Chang, "Analysis of the NonCollinear Acoustooptic Filter", Electronic Letters, Vol.11, pp.617-618, 1975.

2-J.B.Houston, M.Gottlieb, S.K.Kao, I.C.Chang, J.Tracy, L.M.Smithline and G.J.Wolga, 'The Potential for Acoustooptics in Instrumentation: An Overview for the 1980's, Opt. Engr., Vol.20, pp.712-720, 1981.

3-D.J.Taylor, S.E.Harris, S.T.K.Nieh, and T.W.Hansch, "Electronic Tuning of a Dye Laser Using the Acoustooptic Filter", Appl. Phys. Lett., Vol.19, pp.269-270, 1971.

4-I.C.Chang, "Noncollinear Acoustooptic Filter with Large Angular Aperture", Appl. Phys. Lett., Vol.19, pp.370-372, 1982.

5-A.Sivanayagan and D.Findlay, "High Resolution NonCollinear Acoustooptic Filter with Variable Passband Characteristics Design", Appl. Optics, Vol.23 (24), pp.4601-4608, 1984.

6-J.E.B.Oliveira and E.L.Adler, "An Analytical Method for Dersigning Acoustooptic Tunable Filter", IEEE Ultrasonics Symposium, pp.505-510, 1987

7-J.E.B.Oliveira, C.K.Jen and E.L.Adler, "GHz Acoustooptic Tunable Filter Configuration in Uniaxial Crystals", IEEE Ultrasonics Symposium, pp.441-445, 1988.

8-C.S.Tsai, "Integrated Acoustooptic Circuits for Communications, Signal Processing and Computing", SPIE Proceedings, Advances in Optical Information Processing, pp.182-

194, 1992.

9-D.Souilhac, D.Billerey and A.Gundjian, "Photoelastic Tensor of Tellurium", Appl. Opt., Vol.15 (9), pp.2250-2258, 1976.

10-M.Gottlieb, A.P.Goutzoulis, N.B.Singh, "High Performance Acoustooptic Materials: Hg_2Cl_2 and $PbBr_2$", Opt. Engr., Vol.31, pp.2210-2117, 1992.

11-K.H.Levin, "Acoustooptic Tunable Filter Spectroscopy", Course Notes, SPIE OE/LASE 1990, Los Angeles.

12-J.A.Harrington and G.H.Sigel, "Infrared Optics", Course Notes, SPIE OE/LASE 1990, Los Angeles.

13-D.Souilhac and D.Billerey, "TeO_2 and Te Acoustooptic Spectrometer-Imaging System", In Europto SPIE Proceedings,, Rome, October 1994.

14-J.M.Arias, J.G.Pasko, M.Zandjian, L.J.Kozlowski, R.E.DeWames, "Molecular Beam Epitaxy HgCdTe Infrared Detectors", Opt. Engr., Vol.35 (5), pp.1422-1428, 1994.

15-W.G.Egan, "Photometry and Polarization in Remote Sensing", Editor Elseweir, New York York, Amsterdam, Oxford.

16-Thomas M.Lillesand and Ralph W.Kiefer, "Remote Sensing and Image Interpretation", Second Edition, Editor John Wiley and Sons, New York, Chichester, Brisbane, Toronto, Singapore.

17-A.D.Devir, "Remote Sensing and Object Plane Radiometry" SPIE Course Notes, O/E Aerospace Sensing, Orlando 1993.

18-L.A.Stockum and M.K.Masten, "Precision Stabilization, Tracking and Laser Pointing Systems Design and Development", SPIE course Notes, O/E Aerospace Sensing, Orlando 1993.

19- Paul J.Thomas, Allan B. Hollinger, R.H. Wiens, "Adaptive Infrared Forest Fire Sensor", SPIE Proceedings, Vol. 1969, pp.370-381, Orlando 1993.

20 -William J.Parrish, "Advanced Topics in Infrared Focal Plane Electronics" SPIE Course Notes, O/E Aerospace Sensing, Orlando, 1993.

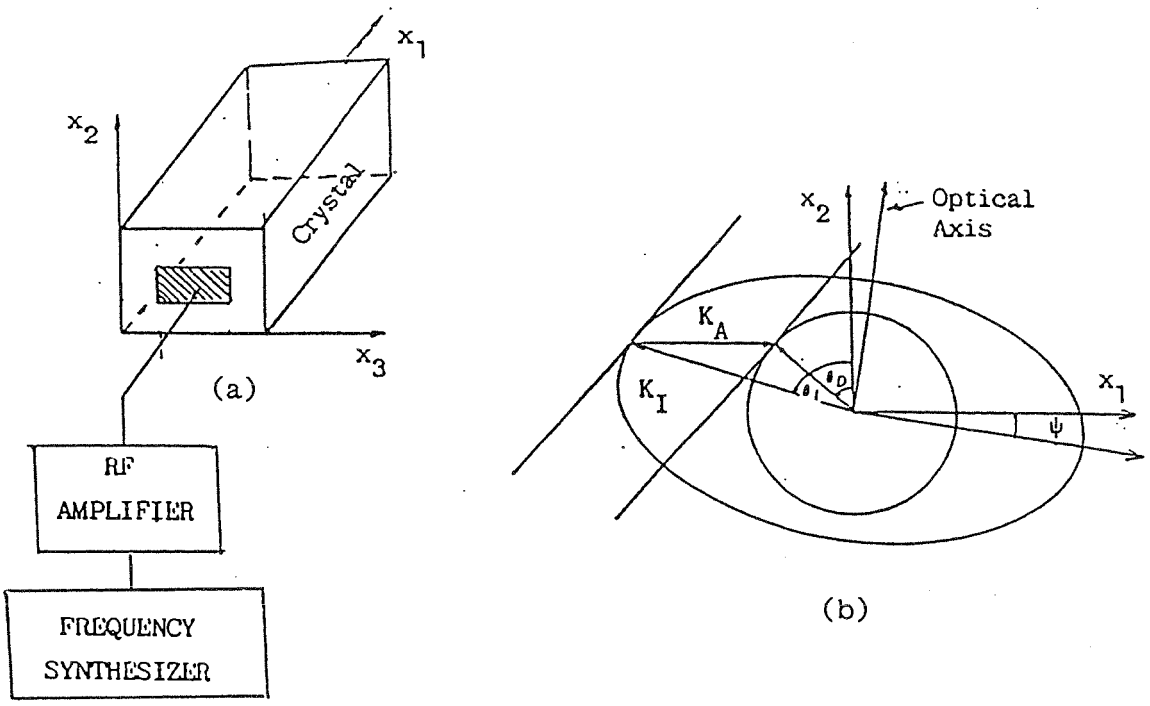

Figure 1: Schematic of an AOTF (a) indicates a crystal sample with a transducer bonded to its x_2x_3 face. x_1, x_2, x_3 are the rotated axes from the crystalline axes x,y,z by the three Euler angles ϕ θ ψ . The orientations of the acoustic wave (wavevector K_A) and the incident optic wave (wavevector K_I) are indicated in (b) illustrating the orientation of the incident and diffracted optic waves for an AOTF Configuration, (the optical axis must lý in the AO Interaction plane, see Ref.[6])

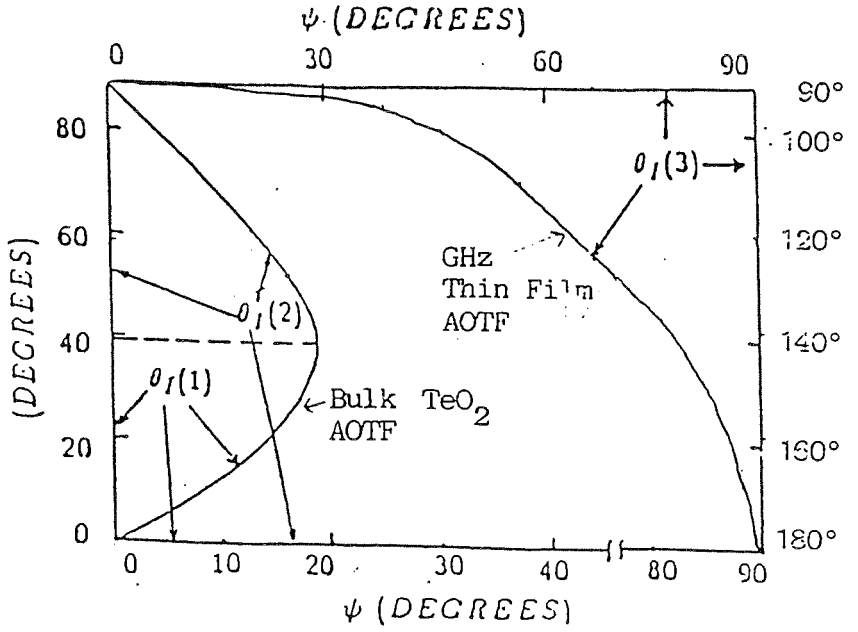

Figure 2: Typical variations of $\theta_I(1)$, $\theta_I(2)$, $\theta_I(3)$ in TeO_2 at 3μm

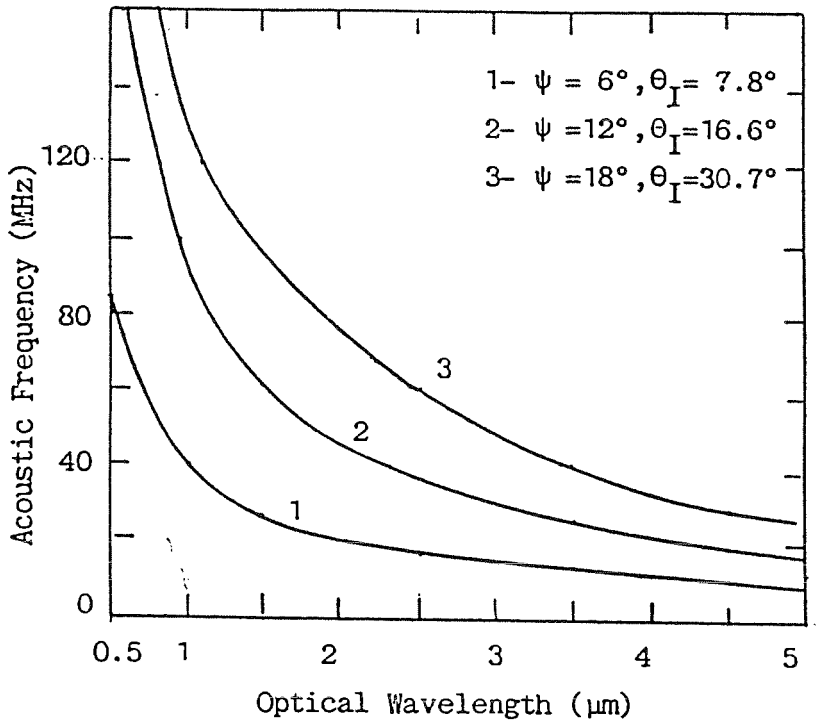

Figure 3: Tuning curve for AOTF configurations which involve slow-shear and quasilongitudinal acoustic waves propagating in the plane normal to the ($\bar{1}10$) axis in TeO_2.

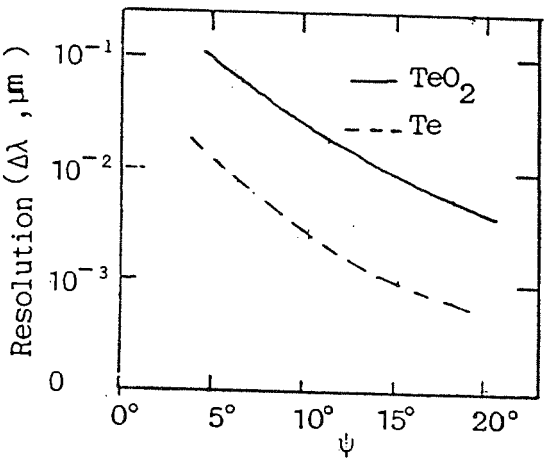

Figure 4: AOTF resolution in TeO_2 crystal, λ_o = 4μm, , L=5cm.
Te crystal: λ_o = 5 μm , L= 5cm

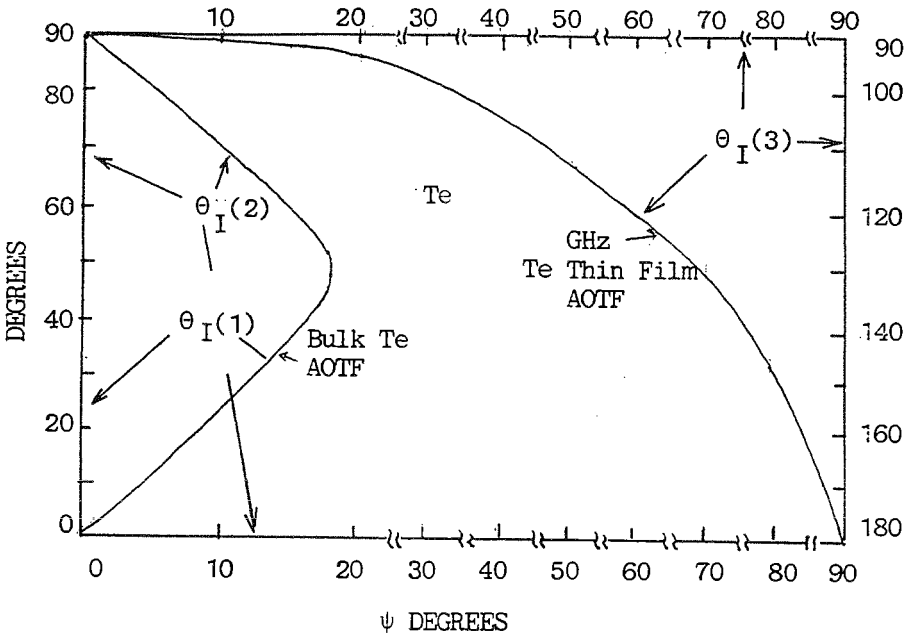

Figure 5.: Typical variations of $\theta_I(1), \theta_I(2), \theta_I(3)$ in Te at 10.6μm.

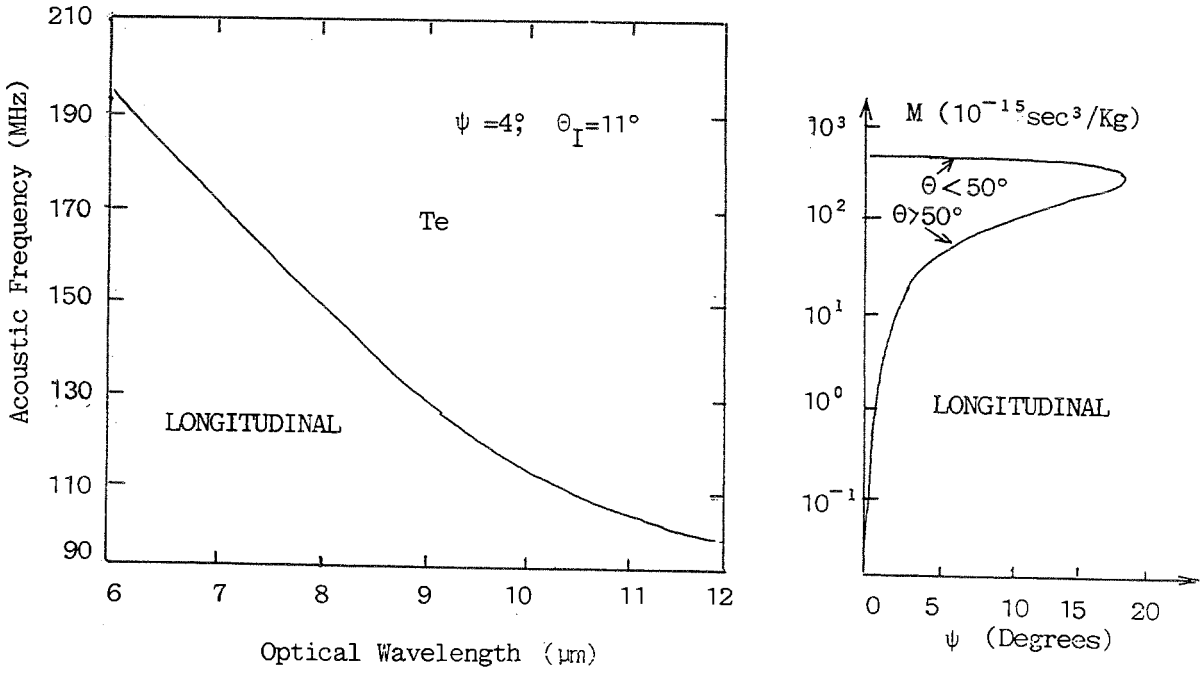

Figure 6a) Tuning curve for AOTF configurations which involve longitudinal acoustic wave propagating in Te at 4° off the (001) axis in the prinipal plane (XOZ) of the crystal. (V_p=2445m/s). (See Text).

b)Acoustooptic Figure of Merit versus ψ(Longitudinal)

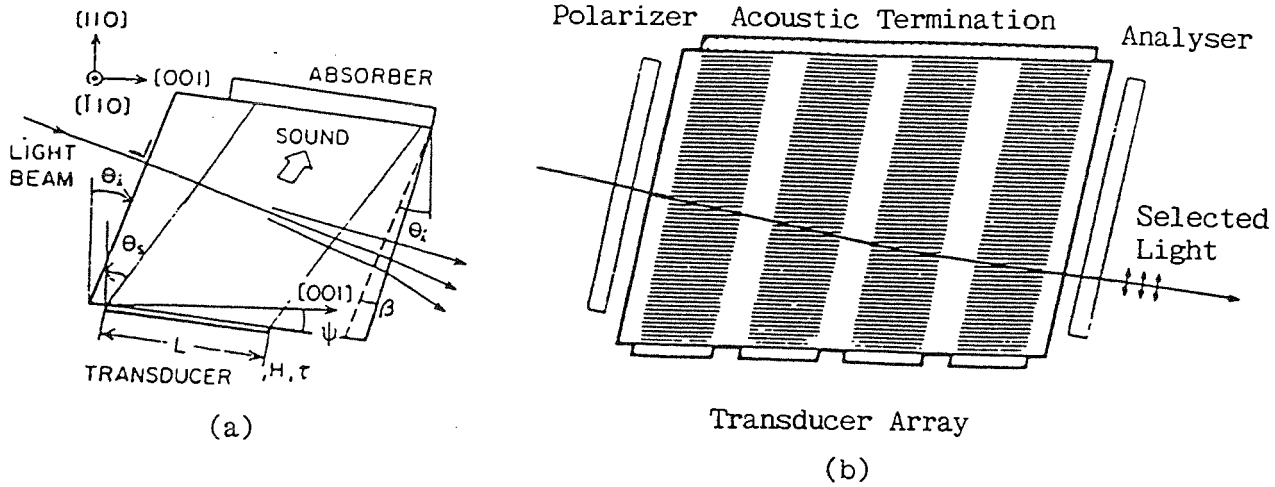

Figure 7: (a) (b) A tilt configuration of TeO_2 and Te noncollinear Tunable Acoustooptic Filter.

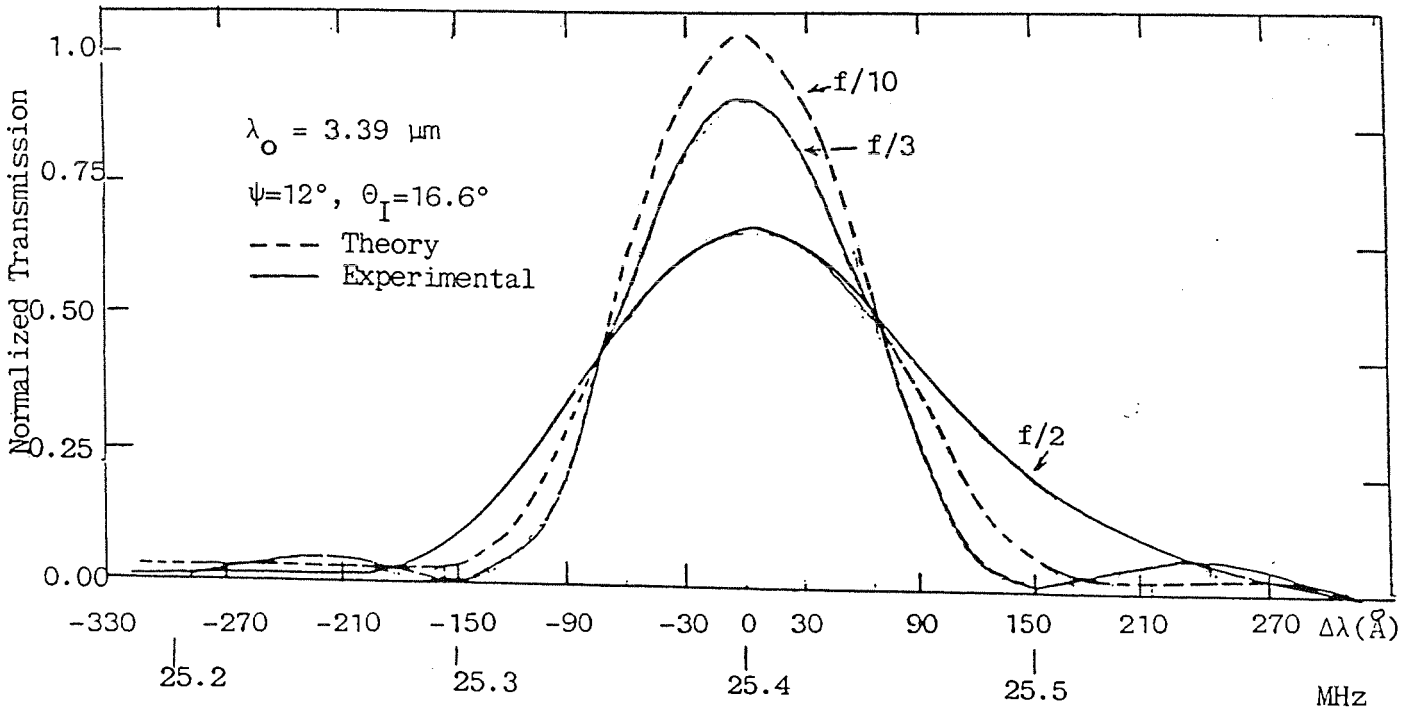

Figure 8 : Bandpass Characteristics of TeO_2 AOTF. (3.4μm Scan of He-Ne Laser)(After Ref.[11])

Table I : Characterestics of the TeO_2 AOTF. (High Resolution).
(Courtesy of Brimrose Corporation of America)

Item	Units	1	2	3	4
Substrate	-	TeO_2	TeO_2	TeO_2	Te
Spectral Range	nm	1500 - 2400	2400 - 3200	3200 - 4500	5-12μm
Corresponding Drive Frequency	MHz	64 - 39	39 - 29	29 - 20	90–190MHz
Optical Aperture	mm	5.0 x 5.0	5.0 x 5.0	6.0 x 6.0	10x10
Acceptance Angle	deg	5.0	5.0	5.0	7°
Spectral Resolution	Å @ nm	80 @ 1500	140 @ 2400	200 @ 3200	200–1200
Drive Power	Watts	2 - 3	2 - 4	2 - 4	25
Diffraction Efficiency	% @ nm	30 @ 1500	40 @ 2400	30 @ 3390	30 (10μm)

Table II CHARACTERISTICS OF BEST MID-IR, IR AOTF MATERIALS: [10]

Material	λ	n	Symmetry Group	Velocity (m/s)	Density (Kg/m³)	Direction Mode	*α (dB/cm-GHz²)	x 10^{-15} M (sec³/Kg)	TBWP†
Te	5–20μm	4.7939	32	2445	6210	L(100)	420	500	473
		6.2433		1439		S(010)	1300	2300	770
TeO_2	0.35–5μm	2.2515	422	616	5990	S(110)	290	1060	1900
		2.4112		4210		L(001)	10	230	
Hg_2Cl_2	0.35–20 μm	1.90	4/mmm	347	7180	S(110)	230.5	640	3335
		2.45		1622		L(100)		540	
$PbBr_2$	0.36–30μm	2.47 2.52 2.55	mmm	2310	6620	L(010)	52	550	500–1000
Tl_3AsSe_3	2–12μm	3.152	3m	1050	6200	S(100)	314	2800	1100
		3.339							
$PbMoO_4$	0.4–5.5μm	2.39	Orthorhombic	3630	6950	L(001)	14.6	36	2000

*α (dB/μsec-GHz²): Acoustic Attenuation

† TBWP: Time-Bandwidth Product (For Te, TeO_2, Hg_2Cl_2 and Tl_3AsSe_3, due to high acoustic attenuation at low acoustic velocities, these materials provide moderate bandwith (100 to 150MHz at a center frequency of the order of 100MHz) with moderate TBWPs of the order of 500– 3000)

Table III: DESIGN EQUATIONS FOR AOTF (NON-COLLINEAR) [1,4,6]

1- Transmission:

$$T \cong T_o \sin^2 \frac{\lambda-\lambda_o}{\Delta\lambda} \quad \text{(1)}$$

Low AO Diffraction

where T = Transmission, T_o = Peak Transmission, λ = Wavelength, λ_o = Center Wavelength, $\Delta\lambda$ = Full Width Half Maximum (FWHM is the Bandpass or Spectral Resolution)

For High AO Diffraction (Ref. 13)

2-Spectral Resolution:

$$\Delta\lambda \approx \frac{0.9\,\lambda_o^2 \cos(\theta_D-\delta_a)}{\Delta n L \sin^2(\theta_I+\psi)} \quad \text{(2)}$$

where L = Interaction Length, θ_I = Incident Light Angle, $\Delta n = n_o - n_e$ (Birefringence = 0.14 for TeO_2)

3- Angular Aperture:

$$\Delta\theta \approx 2n \left[\frac{\lambda_o}{\Delta n L F}\right]^{1/2}$$

where $\Delta\theta$ = Angular Aperture (for incident light cone: N.A.), n = Index (=2.2585 ordinary for TeO_2), F = $1+\cos^2\theta_I$ (azimuth); F = $2\cot^2\theta_I - 1$ (polar)

4- Sellmeir Equation for TeO_2 (Indices of Refraction):

$$n_o^2 = 1 + \frac{2.5844\lambda^2}{\lambda^2 - (0.1342)^2} + \frac{1.1557\lambda^2}{\lambda^2 - (0.2638)^2} \quad \text{(4a)}$$

$$n_e^2 = 1 + \frac{2.8525\lambda^2}{\lambda^2 - (0.1342)^2} + \frac{1.5141\lambda^2}{\lambda^2 - (0.2631)^2} \quad \text{(4b)}$$

5- Tuning Curve:

$$\lambda_o = \frac{V_a}{f_a} n_o \left[\frac{n_e \sin\theta_I - [n_e^2 \sin^2\theta_I - (n_e^2 - n_o^2)\sin^2(\theta_I+\psi)]^{1/2}}{[n_o^2 + (n_e^2 - n_o^2)\cos^2(\theta_I+\psi)]^{1/2}} \right]$$

Where V_a = Acoustic Velocity , f_a = Acoustic Frequency (20-160MHz)

6- Peak Transmission:

$$T_o = \sin^2(P/P_o)^{1/2} \quad \text{(6)}$$

where P = Acoustic Power, P_o = Constant (See Ref.12 for the general expression)

6- Angle Between Incident and Diffracted Beam ($\Delta\theta$):

$$\Delta\theta \approx \Delta n \sin\theta_I / n_o \tan(\theta_I - \psi) \quad \text{(7)}$$

7-The Sellmeir Equations for Tellurium can be obtained from the Infrared Hanbook, ed. by W. Wolfe and G. Zissis, 1978.

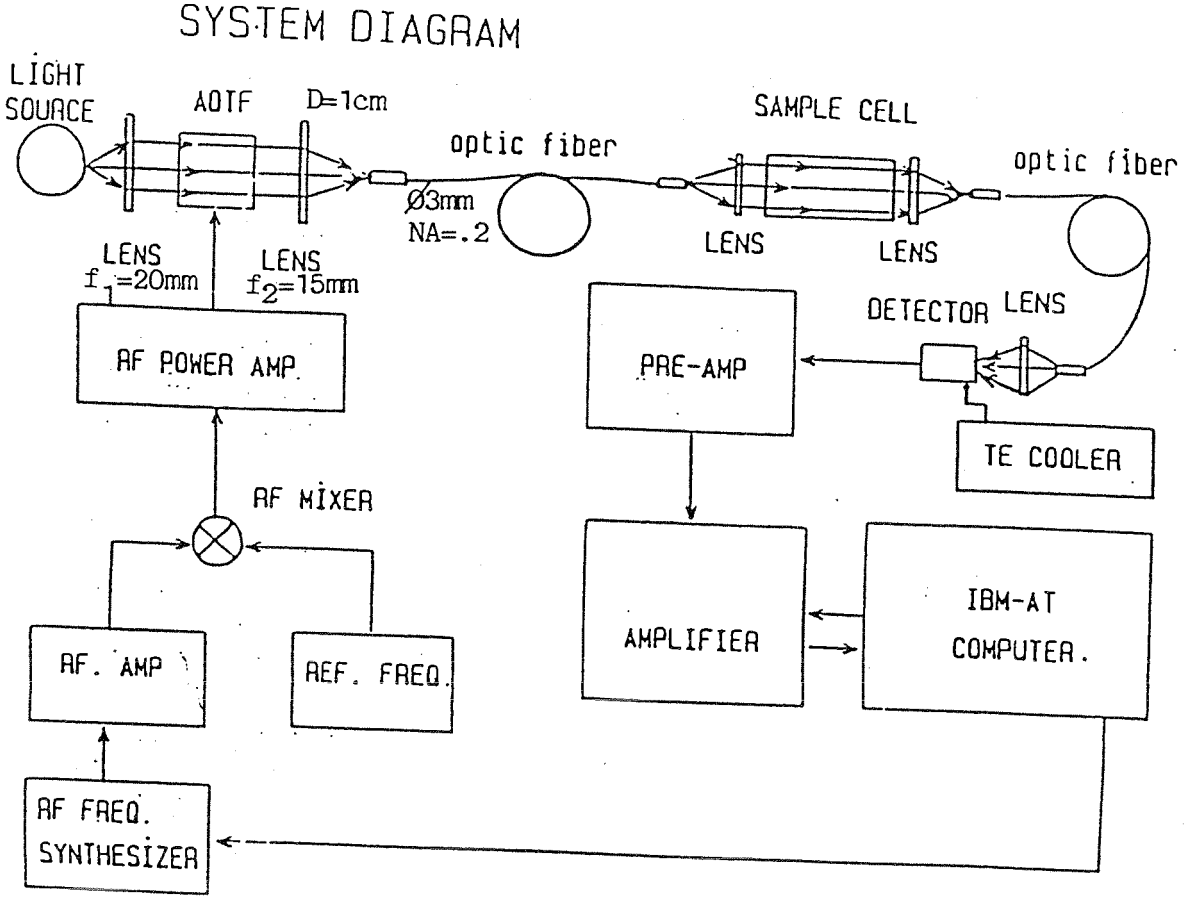

Figure 9 : Block Diagram of the Fiber-Coupled AOTF Spectrometer.(Ref.[11])

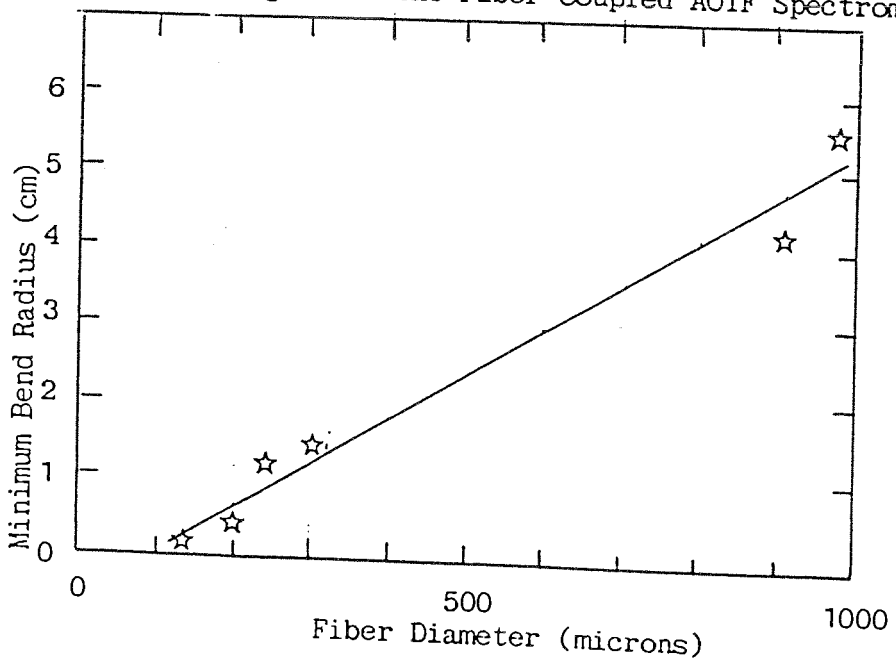

Figure10.: Zirconium Fluoride Glass Fiber , Minimum Bend Radius (at breakage) vs. Fiber Diameter. (Ref.[11])

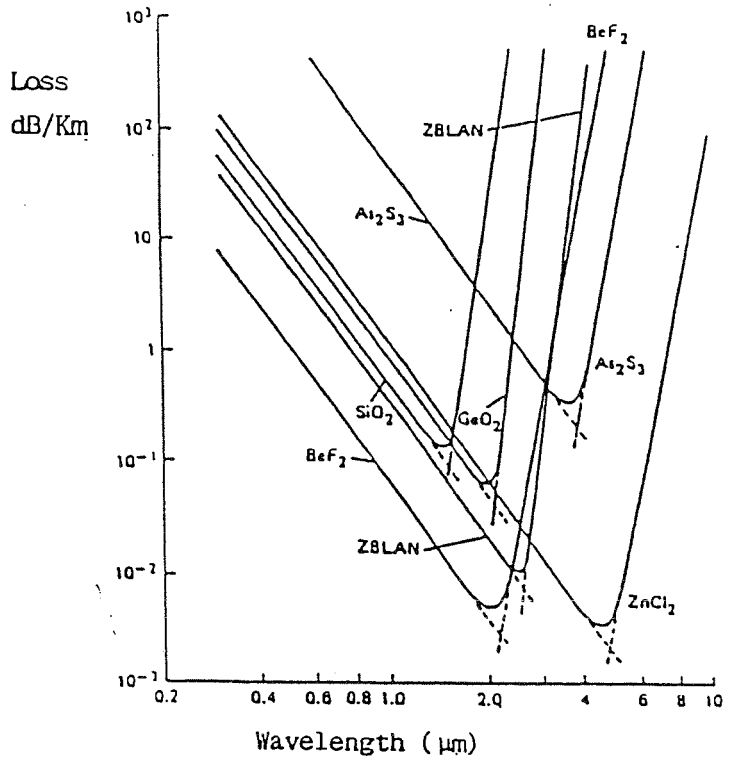

Figure 11: Intrinsic Losses of Fibers (theoretical)[12]

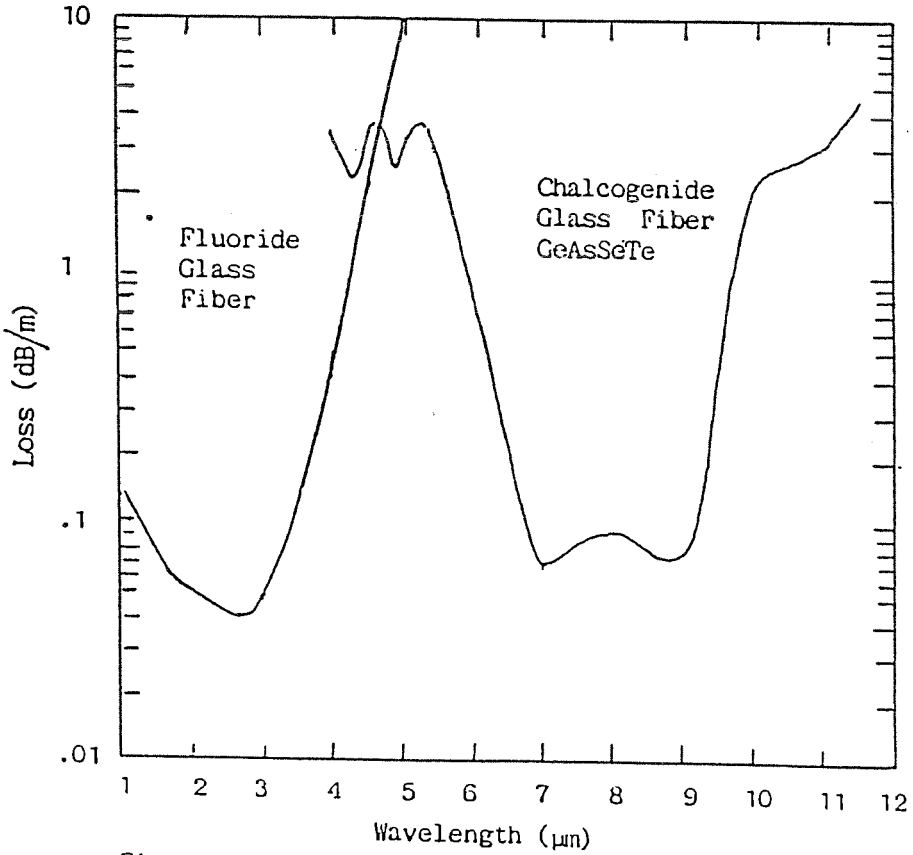

Figure 12: Spectral Loss Curve Fluoride Glass Fiber and Chalcogenide Glass Fiber.[12]

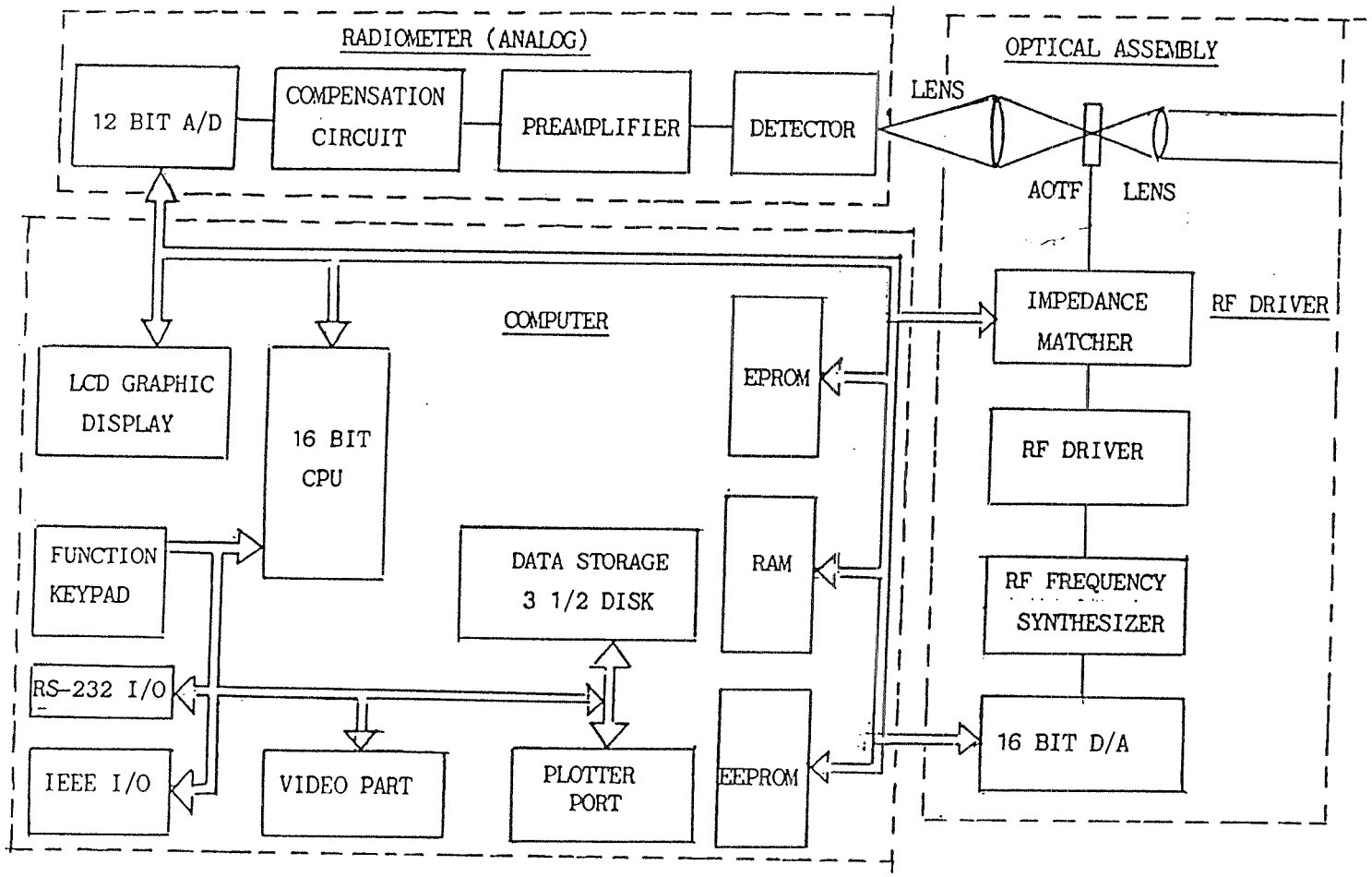

Figure 13: AOTF High Speed Spectrometer (Electronics and Computer).[11]

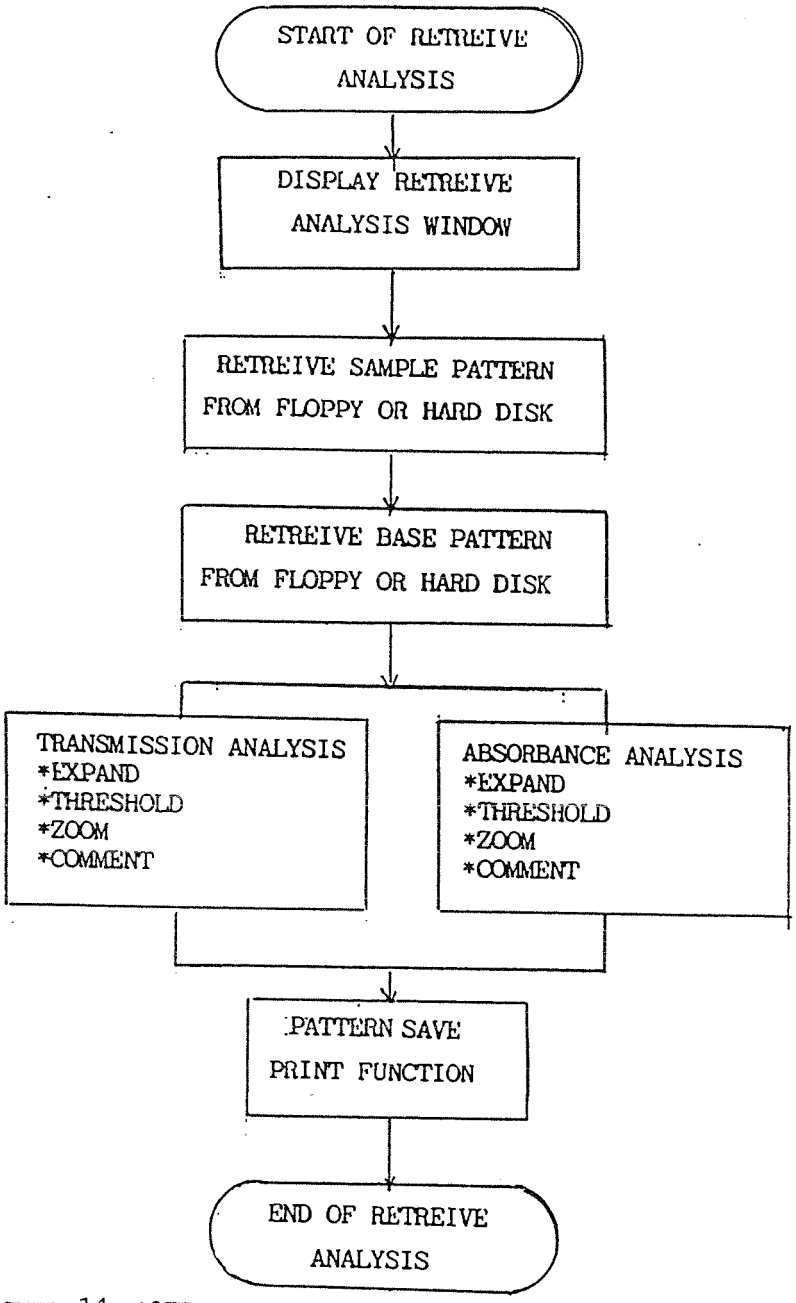

Figure 14: AOTF Retreive Analysis Function Software Chart.[11]

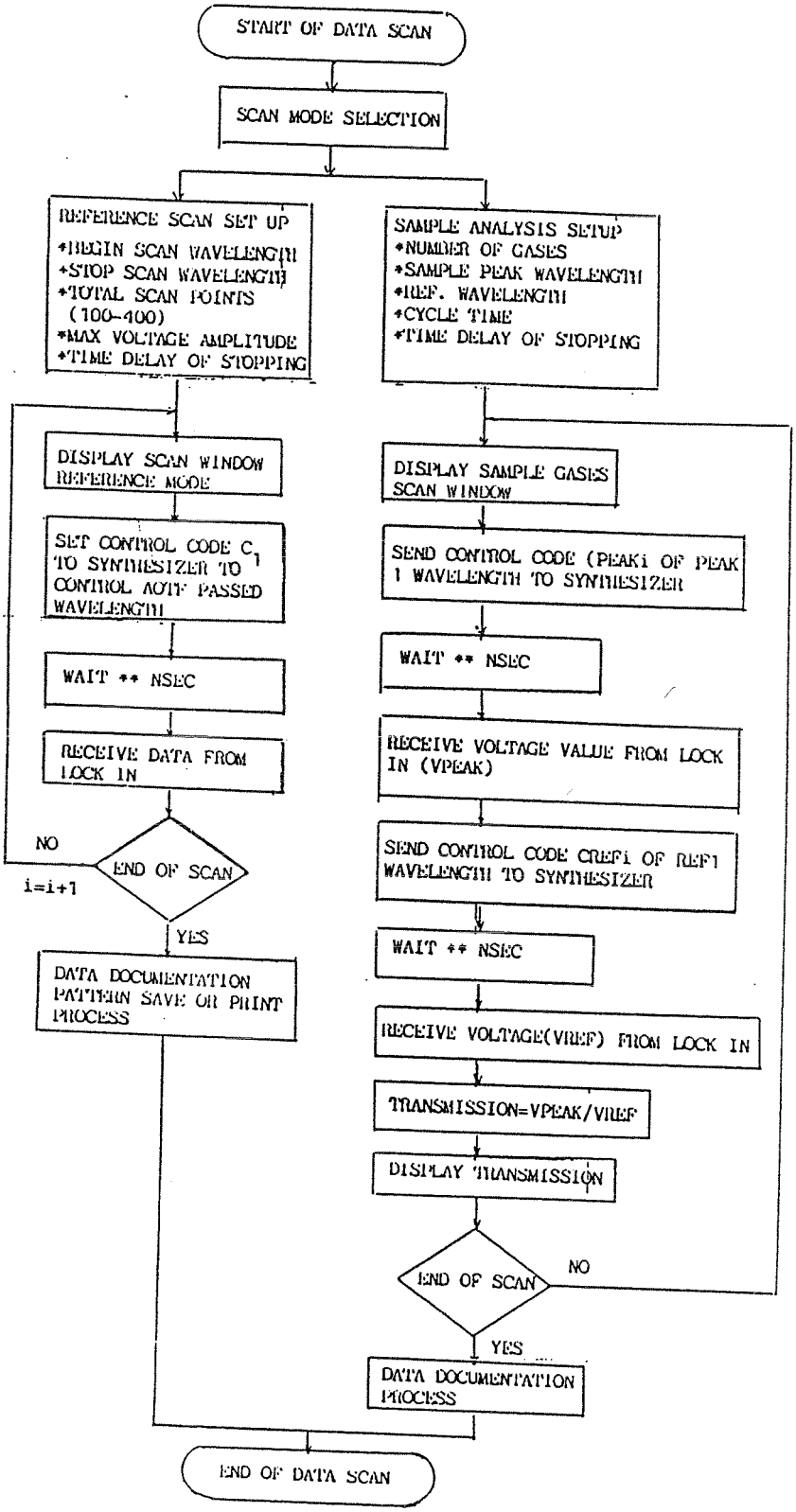

Figure 15: Data Scan Function Software Chart[11]

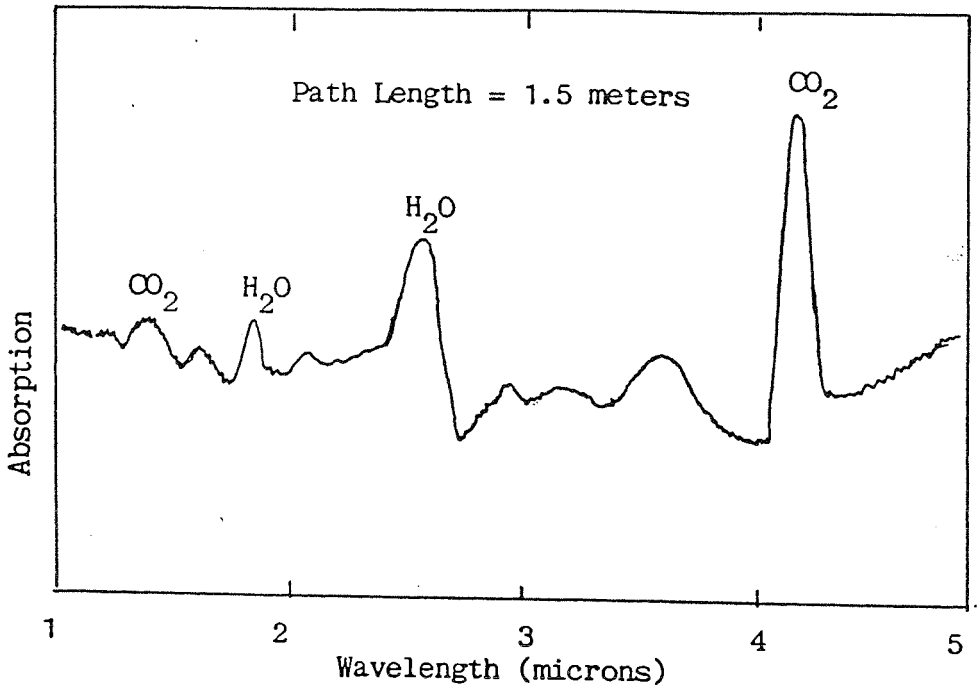

Figure 16: Atmospheric Absorption Measured Using Infrared Fiber AOTF Spectrometer.(Ref.[11])

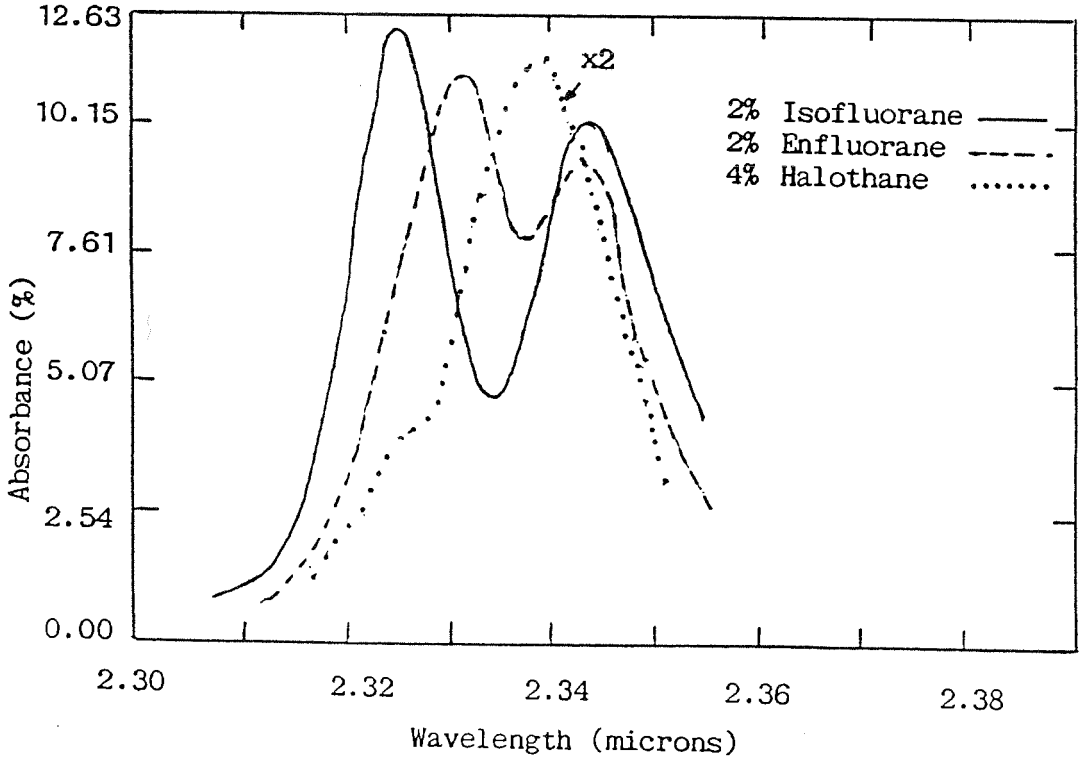

Figure 17 : Patterns Retreive Analysis from AOTF. (Voltage 450μV) .(Ref.[11])

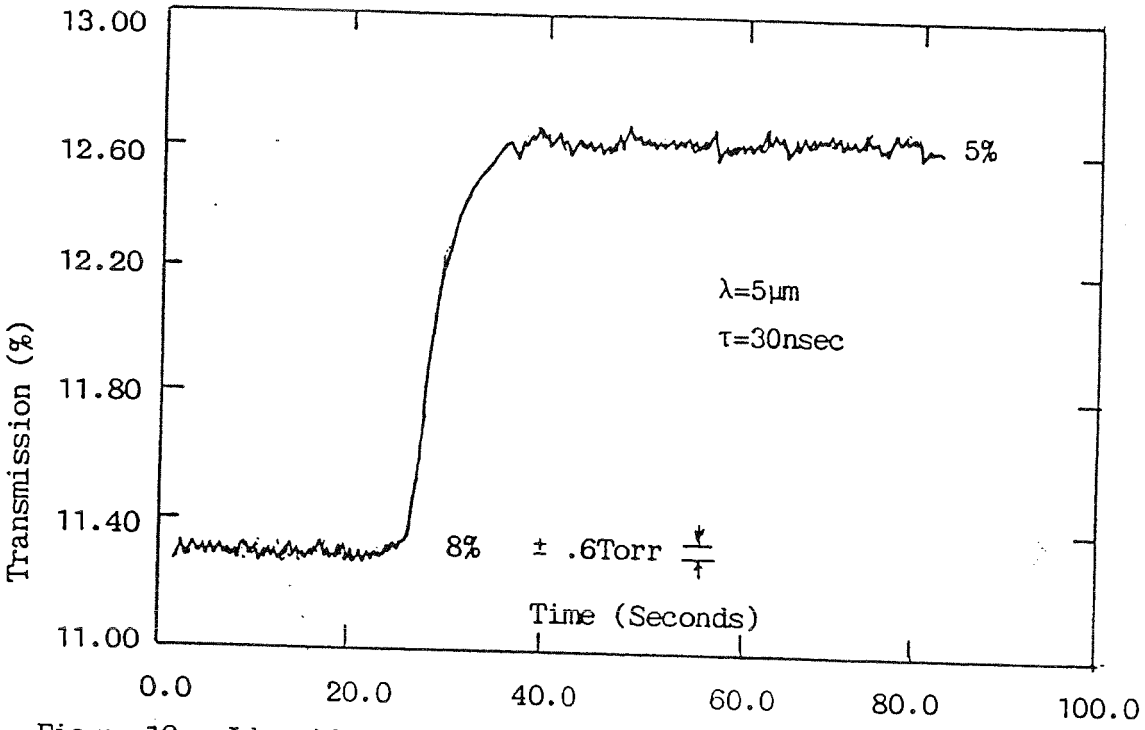

Figure 18 : Identification of CO_2 using the AOTF. (Ref.[11])

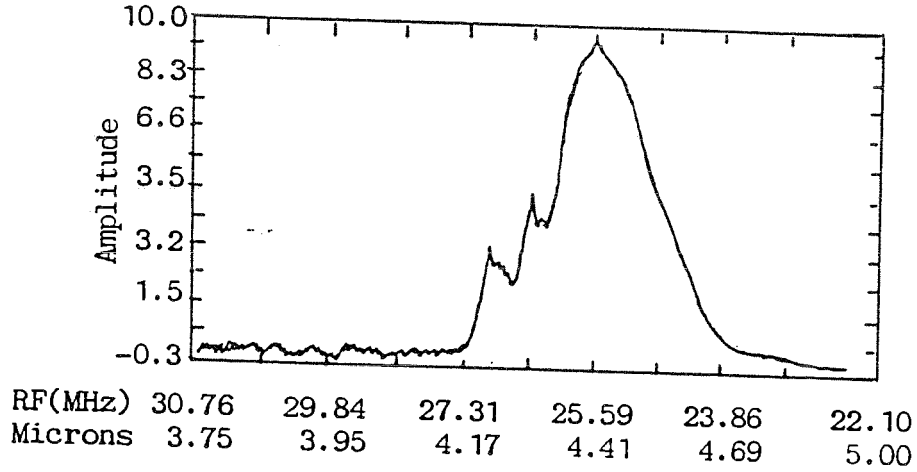

Figure 19 : Infrared Spectra of a Propane Flame. (Ref.[11])

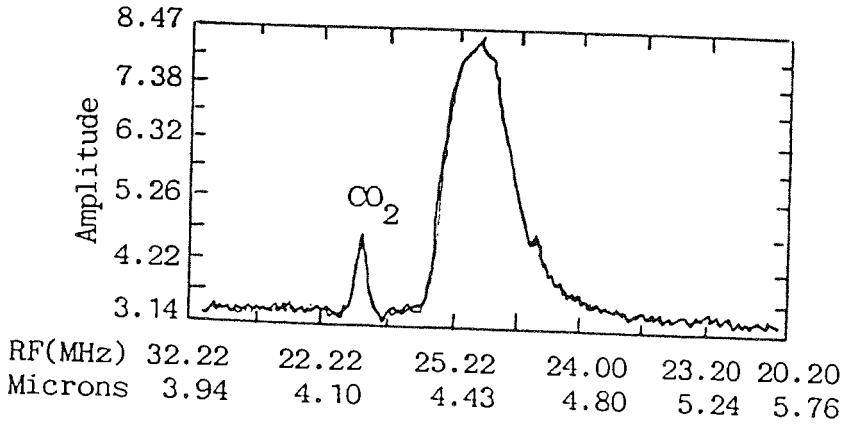

Figure 20 : Rocket Engine Plume Spectra. (Ref.[11])

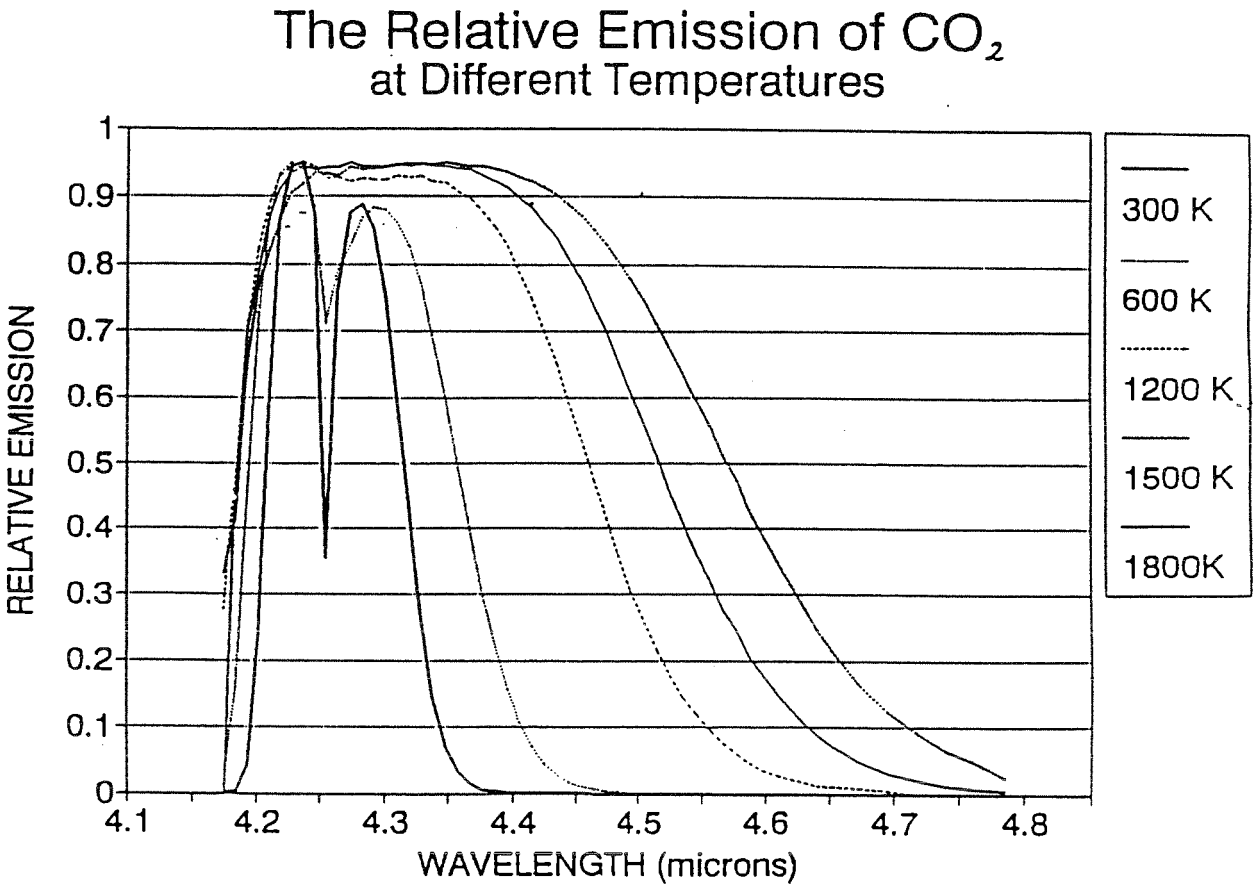

Figure 21: High resolution spectras are necessary for remote sensing of CO_2 rocket combustion gases.

From the distance between the maximum of the P and Q branches of the rotational-vibrational lines of the CO_2 gas, knowing the constants of the rotational-vibrational CO_2 molecule, from quantum mechanics you can calculate the temperature of the gas

You need a high spectral resolution Fourier radiometer or a high resolution acoustooptic spectrometer (increased opto-acoustic interaction length).[5]

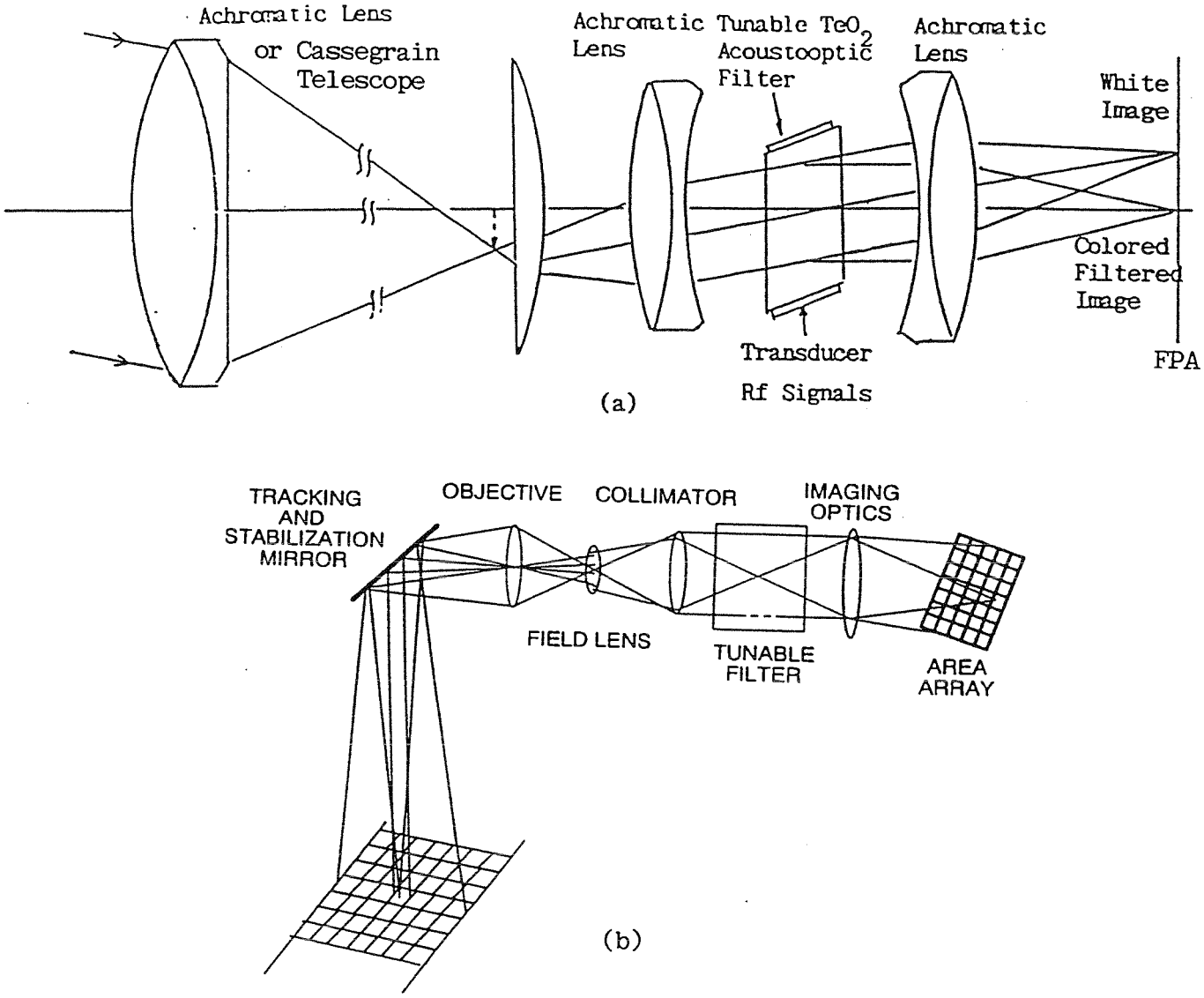

Figure 21: Spectral Imaging with the TeO_2 acoustooptic deflector:

(a) A (1x5cm) TeO_2 AOTF was placed in front of a tungsten-wire halogen source and the image of the filament was recorded with a 35mm camera. Four images were captured with the TeO_2 AOTF tuned to 450,492,582 and 646nm.[11]

(b)For remote sensing applications the focal lens is 108cm, the instantaneous field of view (IFOV) = 20x20m on the ground if the diode size is 25μm and the orbit altitude 831km.
Trade-offs between cross-track field of view,spectral resolution and étendue drive the optimum field lens size.Geometric calibration,ground positioning, tracking, stabilization of the mirror and of the platform inertial navigation system and radiometric calibration of the in-flight imaging spectrometer are described in Ref.[16 17 18]

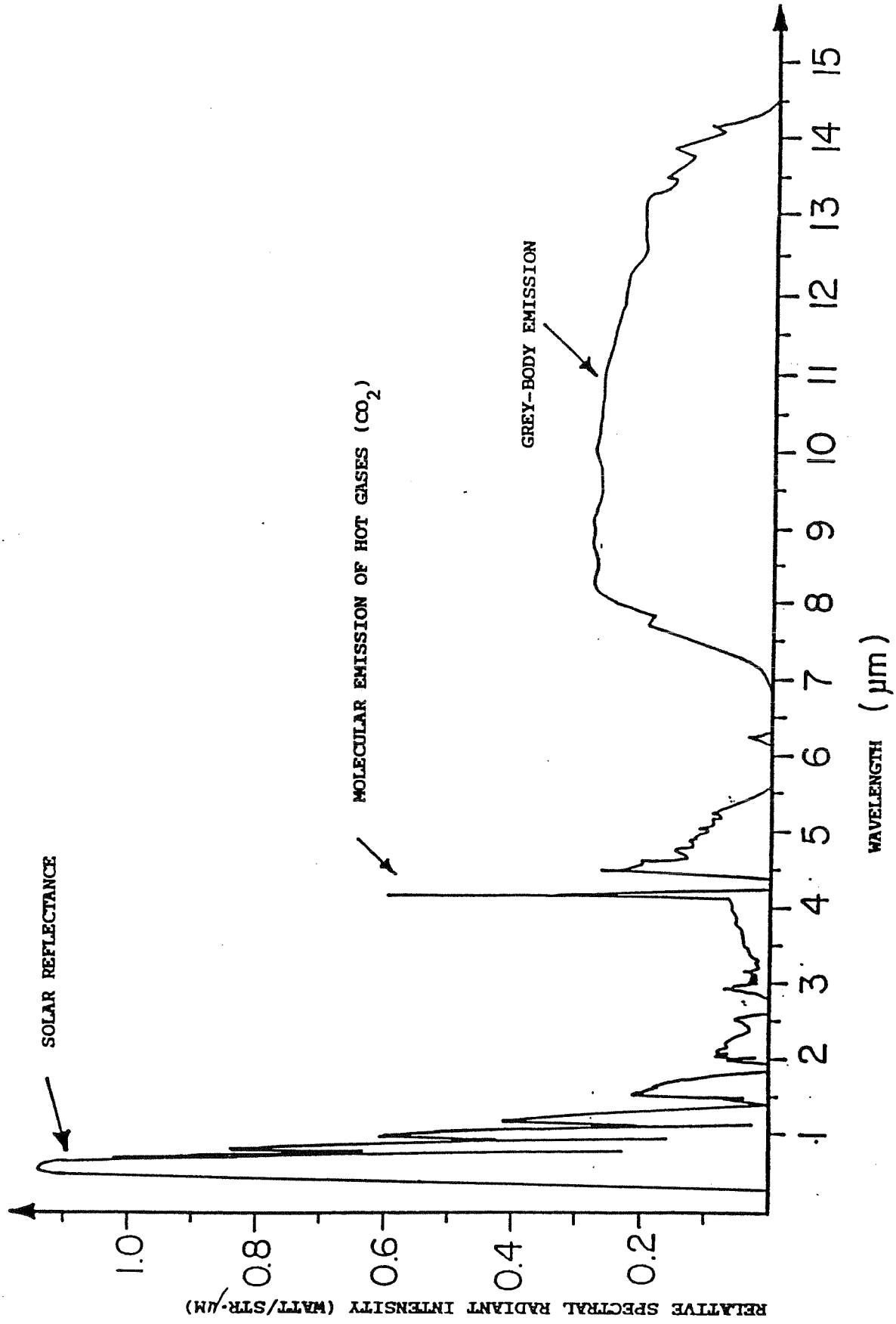

Figure 22: Relative spectral radiant intensity obtained with a high performance spectral analyser [17]

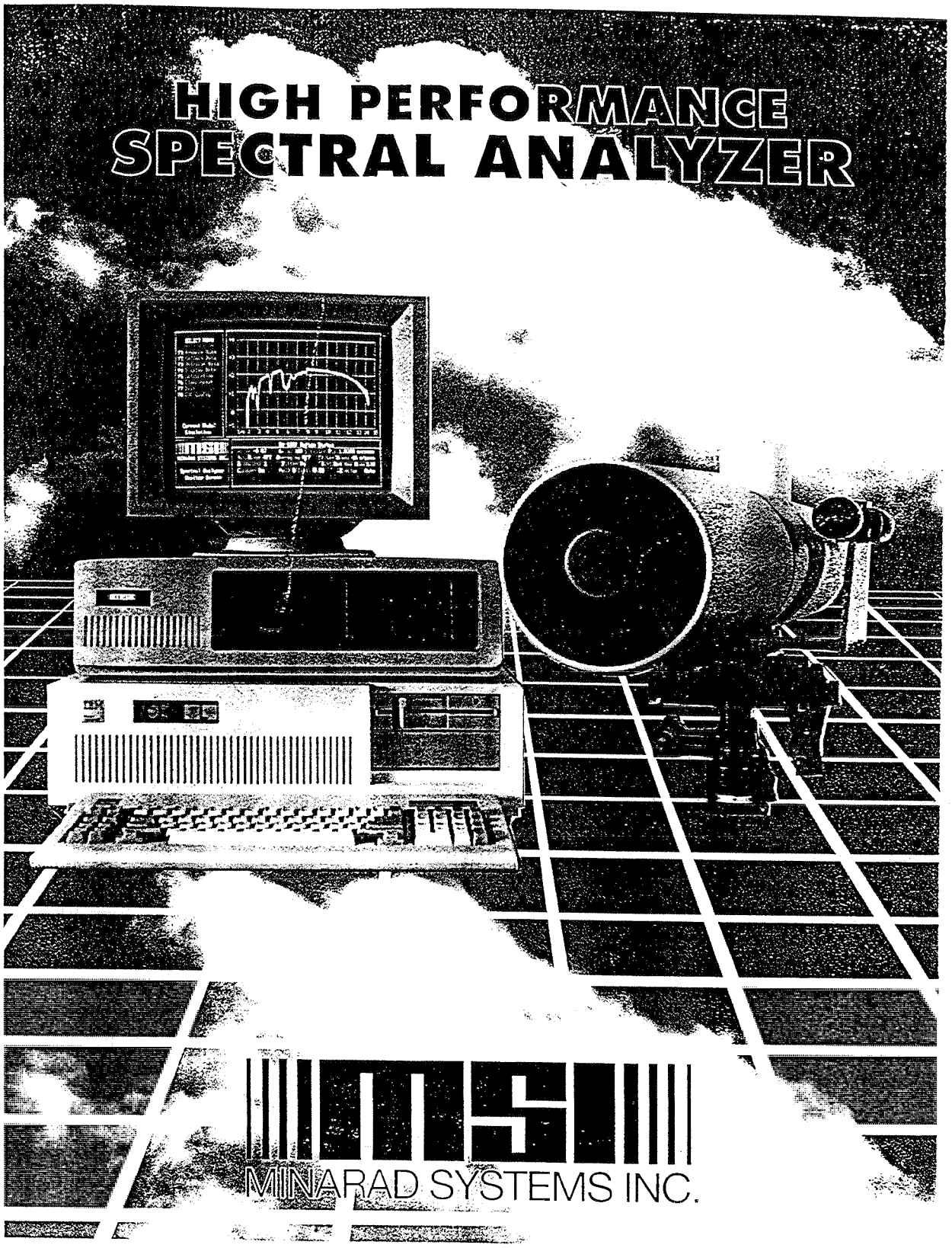

Figure 23.(Specifications are available at Minirad Systems Inc; 1525 Kings Highway East, Fairfield, CT 06430, USA)

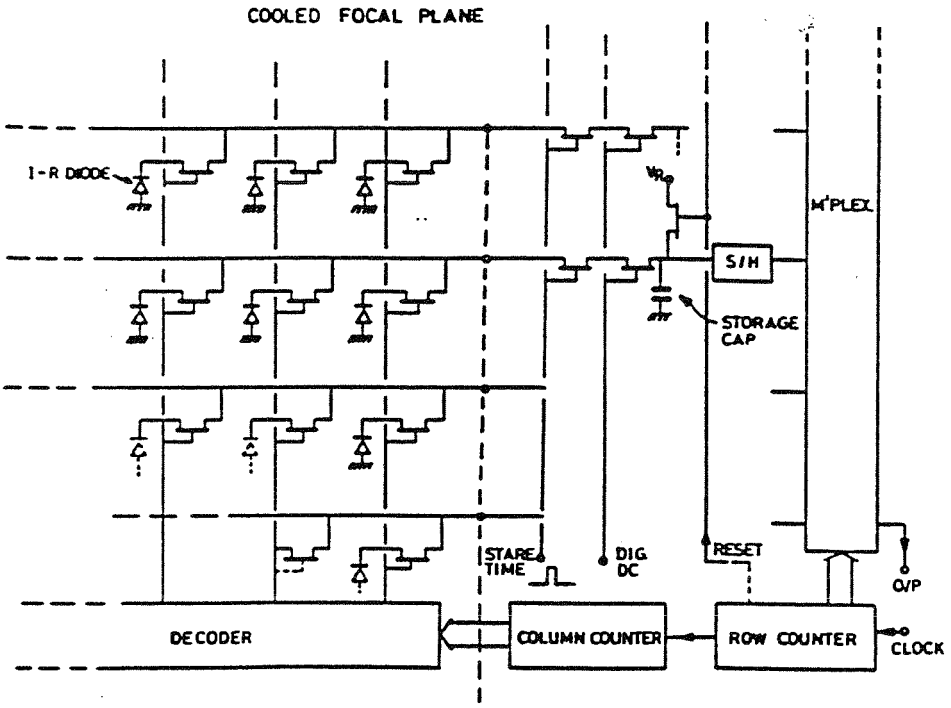

Figure 24: Muliplexed Infrared Electronically Scanned Array (MESA) (Ref.[15])

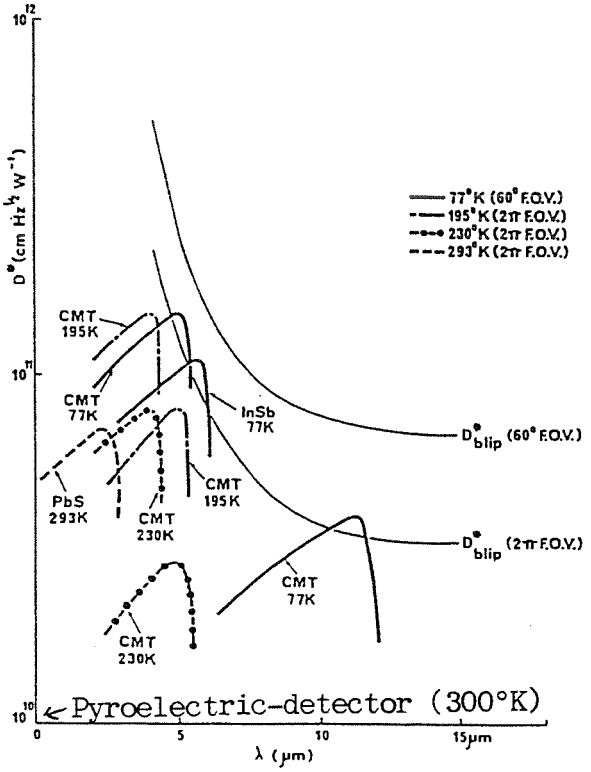

Figure 25: Typical Detector Responses (Courtesy F D Morten)

Table IV (Long and Medium HgCdTe Infrared Scanning Staring Array-Design Example (After Ref.[14-20])

-Staring Focal Plane Arrary (FPA) Design Example (Medium Wavelength Infrared Array (MWIR))

System Specifications	
Detector Technology	p on n HgCdTe photodiode
Readout Technology	Silicon CCD
Number of Elements	64x64
Spectral Sensitivity	3-5μm
Frame Rate	100 Frames/sec
Cooling	Liquid Nitrogen
Image Display	4096 Colors out of a Palette of 1600000
FPA Performance	
Detector Type	Photovoltaic p on HgCdTe
Number of Detectors	4096
Detector Size	50x50μm
Detector Capacitance	0.8pF
Q_{Signal}	less than $2x10^{14}$ ph/cm^{2}sec
$Q_{Background}$	10^{12}-10^{14} ph/cm^{2}sec
Storage Capacity	$4x10^{12}$ charges/cm^2
Quantum Efficiency	60%
R_oA	$10^5\Omega cm^2$
Detectivity	See Figure 25,(50% BLIP at $Q_B=10^{14}$ph/cm^{2}sec)
Power Dissipation	44.9mW
Output Noise	286μV_{rms}

-High Performance scanned 200x4 LWIR HgCdTE Focal Plane Array (FPA).

Detectors	FPA
p on n HgCdTe	$Q = 2x10^{15} - 10^{17}$ ph/cm^{2}sec (Signal)
λ_c = 11μm	$Q_{B\ Nom} = 10^{16}$ph/cm^{2}sec (Background Flux)
R_oA = 50Ωcm^2	T_{INT} = 10μs (Integration Time)
Temp = 70K	T_{LINE} = 20μs
A_D = 35x45μm (Area of Detector)	N° of outputs = 4
η =0.6 (Quantum Efficiency)	$f_{Readout}$ = 5MHz/output (MOS Readout)

Table V: TeO_2 Acoustooptic Imaging Spectrometer (Fig.9 and 21), (0.4–1μm band). (CCD Camera and Data Processing Design Specifications Example).

CCD Camera (After Ref.[18]) (Photodiode coupled to MOS readout card array plus optics)

Noise Electrons (read)	N_e=100/pixel	Camera lens:	
Full well capacity	$N_{sat}=10^6$/pixel	Aperture	D=100mm
Gate Size	l=30μm/pixel	Focal length	f=108cm
Integration Time	t_i=10msec	Transmission	τ_o=0.5
Quantum Efficiency	η=0.8	CCD Focal Plane Array (MOS):	
Wavelength	λ=0.4–1μm	Total Dark Output	51.6mV
Number of Pixels	1024 (Size 25μm)	Total Read Noise	10mV
Signal	$202064e^-$/pixel	Signal to Noise	7000
Shot Noise	$\sqrt{202064} = 450e^-$/pixel	Dynamic Range	16000
Radiant Responsivity	250mA/W (at 600nm)	Saturation Exposure	$120x10^{-9}J/cm^2$

Imaging Spectrometer Design Specifications Example: (After CI Systems, Inc,CA)

Spectral Characteristics:

Spectral Range	0.4 to 1μm	Spectral Resolution	180 and $1400cm^{-1}$
		Best Resolution	3nm at 0.4μm

Optical Characteristics:

Spatial Resolution 640x640 pixels Focusing depending on fore-optics Zoom

Spectral Sampling Modes:

Each sample is an average of KxK pixels (K=1-8), up to 30000 samples ($180–360cm^{-1}$)

Data Acquisition:

Data Acquisition Time 3 sec for 200x200 pixels; A/D Dynamic Range 8 bits

Data Processing:

Fast Fourier Transform Calculation; Processing Time 115sec for 100x100 pixels

Software:

Pseudo-Color Map superimposed on the monochrome prechosen spectral signature
Spectrum Display and Storage of any pixel in the region of interest
Image Display during Data Acquisition, adjustable rectangular window to select size
Averaging Spectra of adjacent pixels to reduce noise(decrease of spatial resolution)
3-D display of spectra (such as row or column of the image)
Spectral library archiving and comparison algorithm (256 spectras can be archived)
Menu driven, user friendly

Standard Computer Configuration:

IBM compatible 486,66 MHz,VGA screen with 32000 colors,200MB hard Disk,64MB memory
600 MB erasable optical disk .Weight: Optical Head and Scanner (expected 5Kg)

Detector studies for millemetric Lunar Laser Ranging at OCA

E. Samain
JF. Mangin

Cerga / OCA
Av. Copernic
06130 Grasse FRANCE

Abstract.

A study of the detectors has been achieved in order to upgrade the accuracy of Lunar Laser Ranging at OCA. This work allowed us to perfect a start pulse detection device with a temporal dispersion of 5 ps, and a return pulse detection device with a temporal dispersion in single photon mode of 35 ps. A new method has been developed allowing temporal measurements with a resolution below 1 ps. This method has been used to study the start detector. A comparative evaluation of several return detectors has been performed.

I. Introduction.

Major upgrades at the OCA Lunar Laser Ranging (Grasse, France [1]) are undertaken in order to measure the Earth-Moon distance with an instrumental accuracy better than 3 millimeters for a normal point, i.e. 20 ps. The atmosphere will then be the accuracy limiting factor. A LLR normal point is computed from about 25 echoes. Each of them has then to be timed with a precision of about 70 ps. The precision of these normal points is the quadratic sum of several instrumental dispersions which can be assessed as following :

timer :	10 ps
start detector:	10 ps
return detector :	60 ps
laser :	30 ps.

The goal of this paper is to present the studies made for two of these errors sources : the start and return detectors. Each of them has to work in very different conditions, as the light pulse returning from the Moon contains rarely more than one photon, when the start detector can use as much light as required. Two different experimental setups have then been established for the measurement of the characteristics of these detectors, in order to allow the choice of the best devices to be used at the LLR station.

II. Study of the start detector

II.1 Introduction

It is necessary to determine with a great exactitude the dispersion and the time walk of a detector. The experimental principle is to measure the delay between two signals coming from two distinct detectors to be studied. This delay is measured with some logic electronics and a delay line. The measurement could be achieved with one perfect detector (no dispersion and no variation of the time walk) and a second one unknown. It can also be performed with two similar unknown detectors. In the latter case, which is used here, the dispersion of one

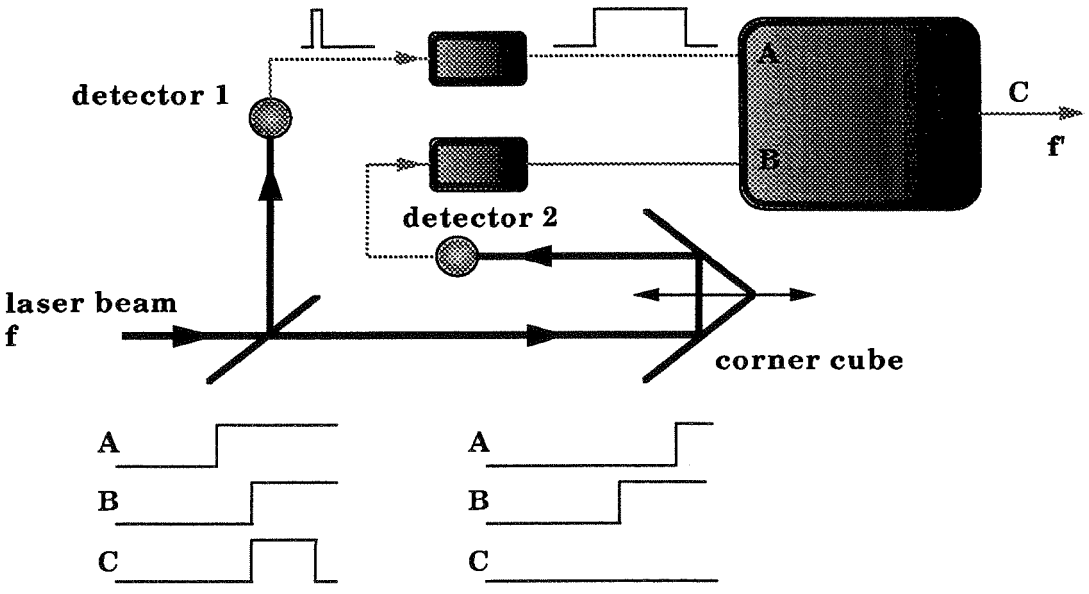

figure 1

of the detectors will be computed from the dispersion of the two detectors, InGaAs pin photodiodes

II.2 The experimental setup

It is described in figure 1. A laser light pulse is divided in two parts with a beam splitter. One of them is sent directly onto a detector N°1, and the other is sent through a delay line onto a detector N°2. These two detectors are identical. The electrical pulses (1 from detector 1, 2 from detector 2) are sent in a very simple electronic device : Pulse 1 arrives on input A, and pulse 2 on input B. A signal will be emitted through output C only if pulse 1 arrives before pulse 2. The time interval between these two signals can be adjusted by changing the length of the delay line. The laser pulses are emitted at a rate f. The observed rate f ' of the output C is a function of the delay line length (d') and of the dispersions of the two detectors. If the detectors have no dispersion, the rate f ' will be equal to f for a given delay d' and equal to zero for any different value d'+δd' (fig. 2). On the other hand, if the detectors have a non-zero dispersion, we will then observe a curve as shown in figure 3, which represents the probability to have a time interval between the signals 1 and 2 of any value larger than zero. To extract the dispersion of the two diodes from this last curve, we need one more step, shown on figure 4. The x-axis is still a distance (or a time) and the y-axis is the probability that the time interval between the two signals is included between ΔT - δT and ΔT + δT. This new curve represents the time distribution of the two detectors. This picture is computed from the following formulae :

$$N_i = f'_{i-1} - f'_i$$

$$d_i = (d'_{i-1} + d'_i)/2$$

II.3 Experimental results

A distribution curve is shown on figure 5.

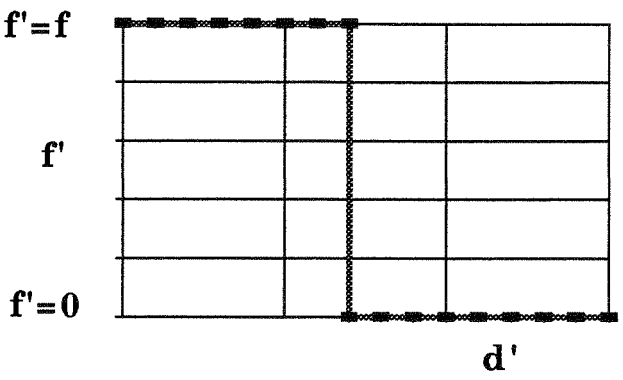

figure 2.

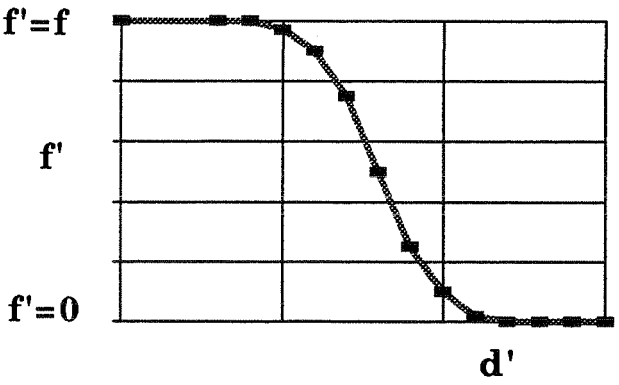

figure 3.

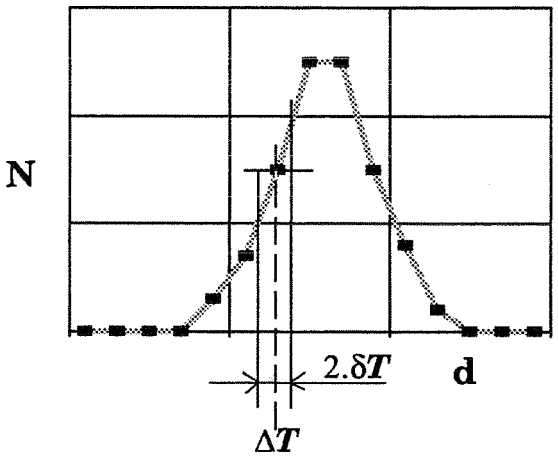

figure 4.

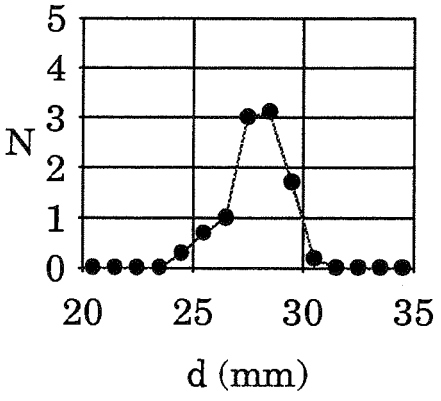

figure 5.

The characteristics of the tested diodes are :

InGaAs (Fermionics FD 80)
diameter : 80 µm
$\eta_{1.06} = 0.8$
bias voltage : 9V
output voltage : 3 V

The light pulse, generated by a BMI laser, is as following :

25 ps width
10 Hz rate
532 nm wavelength

The electronics device is made from ECL III chips.

The total time dispersion observed in this experiment is : σ = 8ps. It includes several dispersions coming from :

- the two diodes . The dispersion of one of them is the dispersion of the two divided by $\sqrt{2}$.
- the shape of the laser pulse. A rising edge variation of the laser pulse may imply a rising time time variation of the electrical pulse. The laser pulse length is also able to modify the timing if it is shorter than the rising time of the electrical pulse.
-the electronics device dispersion.

The same experiment is performed at different levels of light. It allows to measure the variation of the time walk between many experiments with a great precision. The time walk changes only by 800 fs ($8 .10^{-13}$ s) with a factor 2 change of the light level on one of the diodes. The number of photons necessary to reach such small dispersions and variations of the time walk is the one that gives a level of 1 Volt at the output of the diode with a bias voltage of 9 Volts. All these considerations demonstrate that such a detector is suitable for the timing of any light pulse providing a sufficient number of photons.

III. Study of the return detector

III.1 Introduction

The return detector must be able to detect single photons. Photomultipliers, Micro Channel Plate and avalanche photodiodes operating in Geiger mode [3] are detectors commonly used in the laser ranging community. Price, lifetime and efficiency led us to the latter type. The dispersion of such diodes is relatively larger in single photon mode than in mutli-photon mode. A classical timer like the Stanford interval counter (SR 620) can then be used for the study of this detector (dispersion, time walk, quantum efficiency).

III.2 Geiger mode

A negative bias voltage a few volts below the breakdown is applied via a 10 MΩ load resistor. A gate pulse of variable voltage HT (10-250V) is superimposed via a capacitor for a few hundreds of nanoseconds. During this period the total voltage applied to the diode is above the breakdown voltage and a single photon can be detected.

III.3 Dispersion, time walk, noise

III.3.1 Introduction

The aim of this first study is to determine the dispersion and the variations of the time walk of several avalanche photo-diodes in Geiger mode.

The following notation will be used :

- t the time interval between the light pulse and the electrical pulse. t caracterizes the time walk of the detector.
- σ the dispersion of t
- Noise : events in advance of the light events
- HT : Geiger voltage

The following quantities will be determined :

- t and σ versus bias and geiger pulse voltages
- t versus delay between geiger pulse and light event
- σ versus Geiger voltage
- σ versus the number of photons N
- t versus Geiger voltage
- t versus N
- t versus temperature T
- Noise versus total voltage

III.3.2 Experimental setup

A laser light pulse (λ=532nm) is sent through a fiber optic. Its width, 25ps, has been measured with a Hamamatsu streak camera at the output of the laser. The same measurement made at the end of 30 meters of fiber optic gave exactly the same laser pulse lenght (this fiber optic is monomode at 1.06µm). The laser pulse is divided in two parts with a beam splitter (fig.6). One of them is sent onto a pin detector (InGaAs). The light level is sufficient to have a good synchronisation between the laser pulse and the electrical pulse. This electrical signal is sent to the stop of the counter. The other light pulse goes onto the

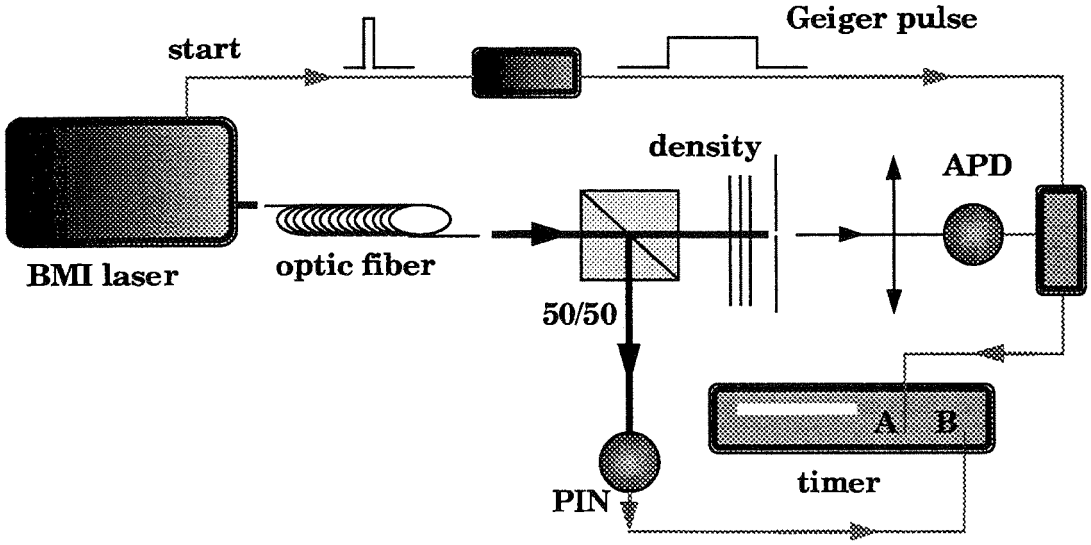

figure 6

avalanche photodiode to be measured. The adjustment of the level of light is made with neutral densities. A start signal is produced inside the laser in order to generate a Geiger pulse in advance of the light pulse which has to travel through nearly 30 meters of fiber optic. The electrical pulse provided by the avalanche photo-diode is used to trigger the counter.

The laser rate is 10 Hz. The determination of the dispersion and the time walk of a detector requires more than 200 detected events for good statistics. A detection probability of 2% insures the single photon mode, and the duration of each measurement will then be 10000 seconds. Every single measurement is recorded and processed on a computer. We can then obtain a histogram representing the probability to have an event versus the transit time of the signal in the diode (fig. 7). The dispersion of the detector and the time walk can also be computed by eliminating values which have a probability lower than 5% of the highest probability of the distribution. In general it corresponds to a filtering at +/- 3 sigma.

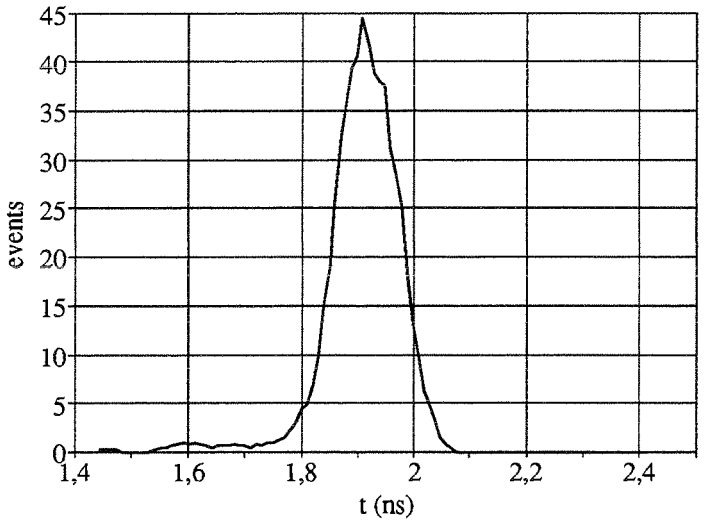

figure 7

III.3.3 Experimental results

t and σ versus bias voltage and Geiger pulse

The mean value of the time walk t and the dispersion σ of the diode depend only on the total voltage applied to the diode.

The measurements have been made with the diodes RCA C 30-902s and Hamatsu s2381.

t versus delay between Geiger pulse and light event

A variation of the transit time t versus the delay between Geiger pulse and light events is observed. It seems to be a function of the voltage applied to the diode, which is itself varying with time when it is close to the start of the Geiger pulse. The measurements have been made on the diodes S2381 and SSO-AD230, using a Geiger pulse with a rising edge of 10 Volts/ns. The Geiger pulse used for the other measures has a rising edge of about 100 Volts/ns.

dispersion versus number of real photons and Geiger voltage

The variation of the dispersion versus the Geiger voltage and versus the real number of photons can be fitted by an logarithmic law, illustrated in figures 8.

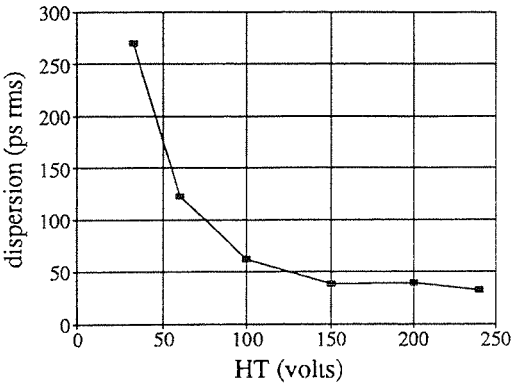

diode : SS0-AD230
single photon detection
bias voltage : 160 V
T = -40°C

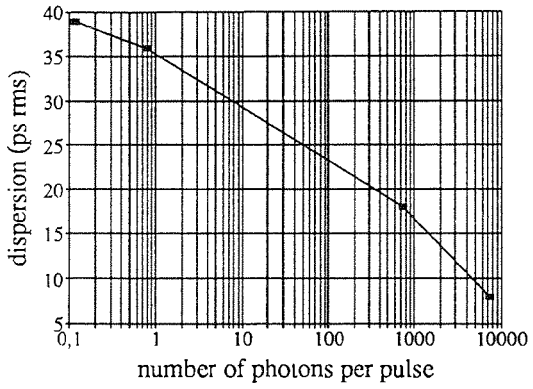

diode : SS0-AD230
bias voltage : 160 V
geiger pulse voltage : HT=200 V
T = -40°C

figures 8

the time walk t versus number of real photons N

The variation of the time walk t versus the real nomber of photons can be fitted by a logarithmic law as soon as the number of photons is greater than 2, as shown in figures 9.

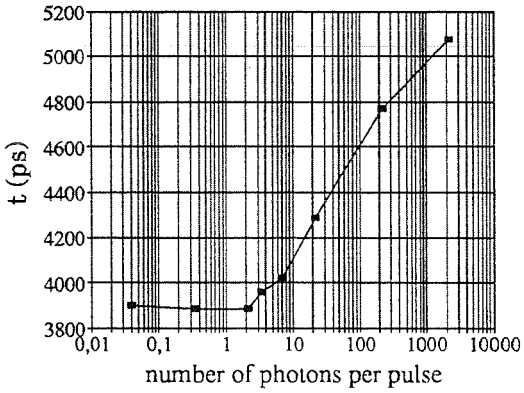

diode : C30-902S
bias voltage : 160 V
geiger pulse voltage : HT=200 V
T = 20°C

figure 9

Noise effects

An example of the variation of noise versus the Geiger voltage is shown in figure 10 at two different temperatures.

The noise increases and the time dispersion decreases when increasing the voltage applied to the diode. The dispersion σ_{wn} of a white noise inside a gate of width ΔT is $\sigma_{wn} = \Delta T/3.46$. One can consider a ditribution with noise :

- n_T is the total number of event
- k is the proportion of the noise : k = number of noise event / n_T
- σ_T is the total dispersion of the distribution.

- σ_{no} is the dispersion of the noise : $\sigma_{no} = \Delta T / 3.46$
- σ is the real dispersion of the distribution.

$$\sigma = \sqrt{\frac{\sigma_T{}^2 - k.\sigma_{no}{}^2}{1-k}}$$

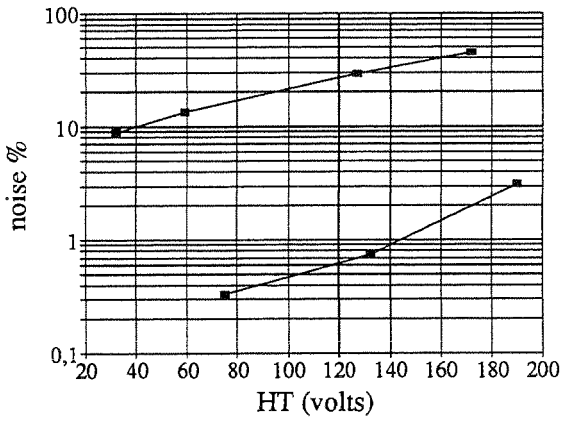

diode : SS0-AD230
no light
bias voltage : 160 V
T= 20°C and -40°C

figure 10

This effect degrades the dispersion of the diode when this dispersion is small and when the noise increases. It occurs when the voltage applied onto the diode is too high, and when the temperature is not low enough. The curves in figure 11 show the dispersion of an avalanche photodiode at room temperature. On one of them the noise has been subtracted. It has been evaluated by assessing the white noise outside the distribution.

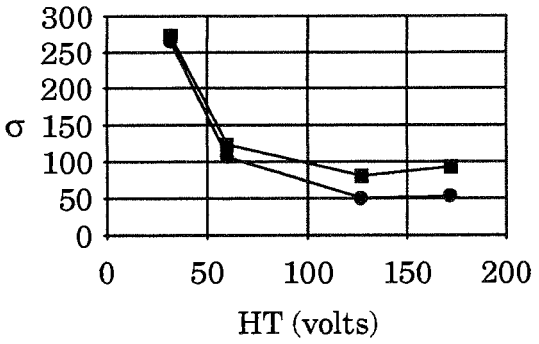

diode : SS0-AD230
single photon detection
bias voltage : 190 V
T = 20°C

figure 11

III.4 Quantum efficiency

The study of the quantum efficiency is made in comparison with a standard diode : the RCA C30-902S diode already measured by Bowman [4] using a method proposed by D.N. Klyshko [5]. Its quantum efficiency is $\eta_{902S} = 0.25$. To compare the efficiency of one diode in comparison with the 902S, the experimental setup shown in figure 12 is used : The two light

pulses contain the same number of photons. The two diodes work in single photon detection. The real number of photons N sent onto the diodes is computed from the detection probability

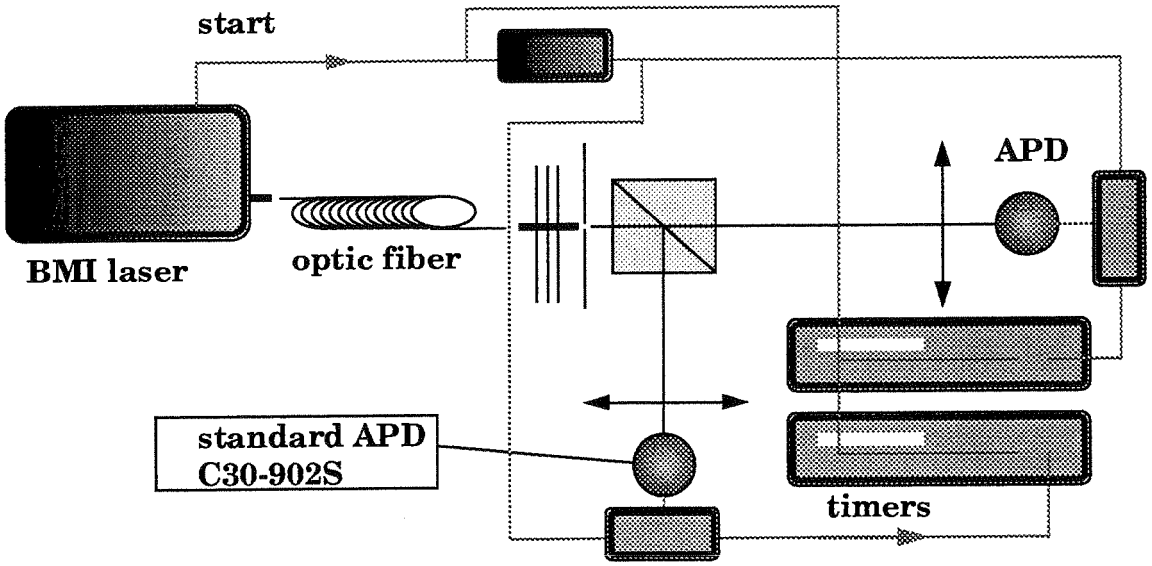

figure 12

P_{902S} of the 902S diode .

$$N = -\ln(1-P_{902S})/\eta_{902S}$$

The quantum efficiency η_{dio} of the diode is then :

$$\eta_{dio} = \eta_{902S} \cdot \ln(1 - P_{dio}) / \ln(1 - P_{902S})$$

The variation of the quantum efficiency versus Geiger voltage is shown in figure 13.

IV. Summary results

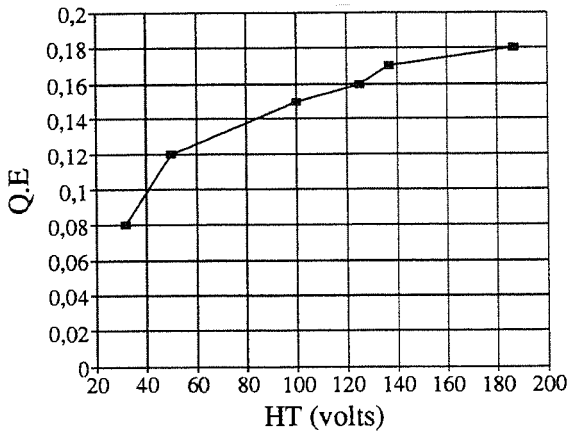

diode : S2381
single photon detection
bias voltage : 160 V
T = -40°C

figure 13

All the measurements described before have been performed on various avalanche photodiodes. They are summarized in table 1.

diode	σ (ps)	η	Vb (V)	dt/dT (ps/°C)	dt/dN (ps/dec)	no=b.a^{HT} (% 100ns)	no (% 100ns)	id (µA)	η_{532}	ϕ (µm)
	note 1	note 2	note3	note 4	note 5	note 6	note7	note8	note9	
SP 114 cool	140	0,15	148	20	180	1.01; 13	60			230
C30-902S	170	0,25	236		500		0,1	0,02	0,46	500
sso ad-230 9	35	0,2	199	6	250	1.02; 0,07	1,4	0,06	0,65	230
sso ad-230 13	60	0,2	87	6,5	180	1,01; 4,9	21	1	0,65	230
S 2381	80	0,18	110	3,5	300	1,03; 0,01	0,9	0	0,35	200
sd 0127062541	85	0,17	170		330			0	0,2	330
SP 114	55	0,13	210		180					230

table 1

Notes :

note 1. σ : Minimum dispersion of the detector in single photon mode.

note2. η : Quantum efficiency in single photon mode with a 150 Volt Geiger pulse.

note 3. V_b : Breakdown voltage given at 20°C.

note 4. dt/dT : Variation of the time walk versus the temperature in single photon mode.

note 5. dt/dN : Variation of the time walk versus the real number of photons sent onto the diode. It is expressed in picoseconds per decade, and computed as soon as the number of photons is greater than 5.

note 6. no = b.a^{HT} : number of events detected in advance of the light events for 100 Geiger pulses. The delay between the start of the Geiger pulse and the light events is 100 ns. The table gives the two coefficients a and b of the exponential law. The temperature is -40°C.

note 7. no: Noise defined as in note 6 computed with a Geiger voltage of 150 Volts.

note 8. id : dark current is the gain mode in µA. The temperature is 20°C (data given by the constructor).

note 9. η_{532} : Quantum efficiency in the gain mode with λ = 532 nm (data given by the

constructor).

manufacturer :
C30 902S : RCA
SP 114 & sso ad 230 : Silicon Sensor
S 2381 : Hamamatsu
sd 0127062541 : Advanced Photonix
The diodes SP 114 and sso ad 230 are respectively an old fabrication and a new fabrication, but their design could be identical (provided by U. Schreiber, WLRS).

V. Conclusion.

Two experimental setups have been developed and successfully used for the characterization of various detectors, mainly the time walk and its dispersion.

The InGaAs pin photodiode FD 80 built by Fermionics allows the timing of a light pulse (multi-photon mode) with a dispersion less than 5 ps and a very small time walk. This detector can be used for the laser start time measurement.

In single photon mode, the best avalanche photodiode measured is the sso ad 230 built by Silicon Sensor (150V breakdown, 0.05 µA dark current in gain mode). The destruction of the diode occurs when the total voltage applied on the diode for 100ns is greater than 400 Volts. As it seems reasonable to work 100 Volts below this limit, a geiger voltage of 150 Volts can be applied onto the diode. The diode must be cooled at -40°C in order to minimize the noise. In these conditions, a temporal dispersion of about 40 ps in single photon detection and a quantum efficiency of 0.2 can be achieved.

These two devices should be implemented at the OCA LLR in 1995 for the completion of the millimetric development phase.

Acknowledgement.

The authors thank Dr U. Schreiber, Satellitenbachtungstation Wettzell for supplying the sp114 photodiodes.

References.

1. Veillet C. Image de la physique CNRS, 92-103, 1992.
2.Veillet et al. LLR at OCA on the way to millimetric accuracy (*These proceedings*).
3. PA. Ekstrom, Triggered avalanche detectionof optical photons, J.appl. phys. 52,6974, 1981.
4. Bowman S. The design, construction, and testing of high precision LLRS. PhD dissetation, Faculty of the graduate school of the university of Maryland, 1986.
5. D.N. Klyshko, Use of two-photon light for absolute calibration of photoelectric detectors, *Sov.J. Quantum Electron*, 1980.

CIRCUITS FOR EXPLOITING THE TIME RESOLUTION OF AVAILABLE HIGH-QUANTUM-EFFICIENCY HIGH-VOLTAGE SPAD

S.Cova*, M.Ghioni*, C.Samori*, M. Locatelli*, D.Bonaccini°

* Politecnico di Milano, Dipartimento di Elettronica e Informazione, Milano , Italy
°Osservatorio Astrofisico di Arcetri, Firenze, Italy

Abstract

Avalanche photodiodes known as Single Photon Avalanche Diodes SPADs detect single-photons when operated in Geiger-mode, at bias voltage higher than the breakdown level. Silicon SPADs having high quantum detection efficiency (up to 80% at 800 nm wavelength) and sensitive area with a few hundred micron diameter are industrially produced. The main features and the intrinsic performance of recently developed SPAD devices are illustrated and discussed. It is shown that their intrinsic time resolution is better than 100ps rms. These devices are commercially available in compact electronic modules, that require only a low voltage supply and include all the bias and quenching circuitry, but have 200ps rms specified resolution in photon-timing. A new compact active quenching circuit has been specifically designed for extracting at best the time information in the avalanche pulse, with high counting rate and gated operation capability. Experimental results confirm the expected performance and demonstrate that these silicon SPADs offer a combination of detection efficiency and timing resolution of high interest for laser ranging.

1. Introduction: high efficiency SPAD detectors

Silicon avalanche photodiodes working in Geiger-mode, biased at voltage higher than the breakdown level, detect single optical photons. They are therefore called Single-Photon Avalanche Diodes SPADs and, in comparison to photomultiplier tubes (PMT), they provide remarkably higher quantum detection efficiency and mark the photon arrival time with comparable or better resolution [1]. SPADs are gaining wide acceptance in laser ranging applications and have open new perspectives in various other applications of photon-counting and photon-timing measurements. As concerns industrially produced devices, the situation for SPADs is different from that of ordinary avalanche photodiodes (APD), which exploit the avalanche for amplifying linearly the photoinduced current signal. Silicon APDs providing good performance in analog applications are available from various sources, but only a few of these devices can be employed as SPADs with good performance. The group led by R.J.McIntyre at the former RCA Electrooptics laboratories, now EG&G Optoelectronics Canada, has carried out a pioneering role in this field, developing and progressively improving in the last two decades silicon APD devices with high photon detection efficiency, fairly large

sensitive area (150 to 500 micron diameter) and capability of working as SPADs [2]. Since various years the C30902S and C30921S types are specified for photon counting: they have breakdown voltage of about 250V, detection efficiency of about 50% at 633 nm wavelength and it has been verified [3] that they can attain time resolution around 150ps rms (root-mean square).

More recently, a new improved APD has been developed [4] by refining the device structure design and the fabrication technology. This EG&G device, called Slik^{TM} , was originally devised as analog amplifying avalanche photodiode with very low multiplicaton noise. As outlined in Fig.1, the field profile in the p-n junction has been redesigned [4] for minimizing the value of the effective k ratio (a weighted ratio of the ionization coefficients of holes to that of electrons) for a given thickness of the active volume of the device. In fact, the name Slik stays for "super-low k".

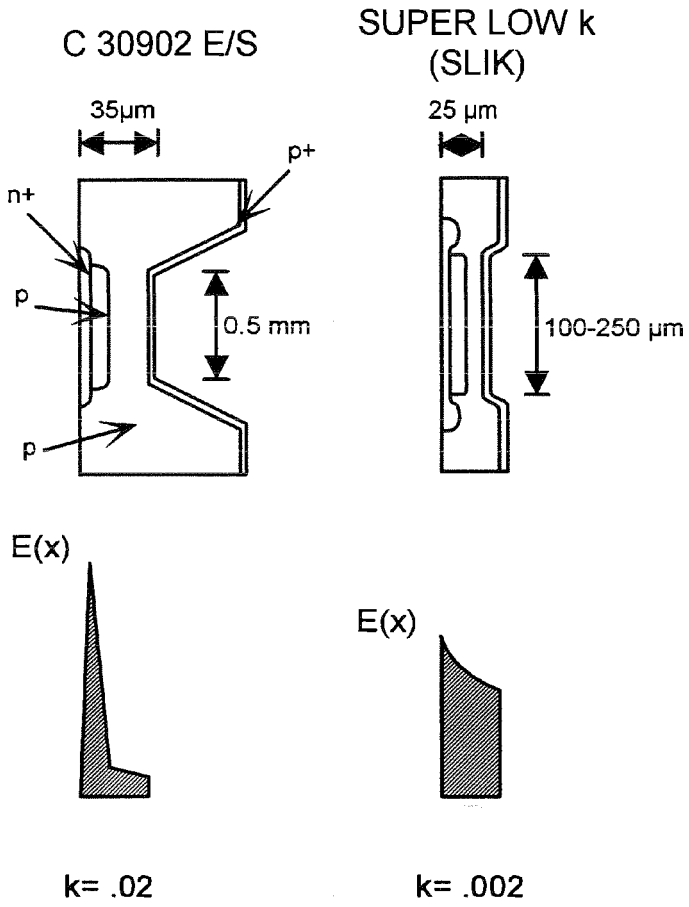

Fig.1 Schematic cross section and electric field profile of silicon avalanche photodiodes suitable as SPADs: the new Slik is compared to the C30902S.

Because of the smooth field distribution, the Slik has breakdown voltage V_B remarkably higher than that of the C30902S, about 440V at room temperature. The design approach adopted, however, also leads to improve the operation in Geiger mode, making of the Slik a high performance SPAD.

As illustrated in Fig.2, the probability that the primary generated electron-hole pair initiates an avalanche is significantly higher [4]. As shown in Fig.3, the probability of detecting a single photon, that is, the quantum detection efficiency is correspondingly enhanced.

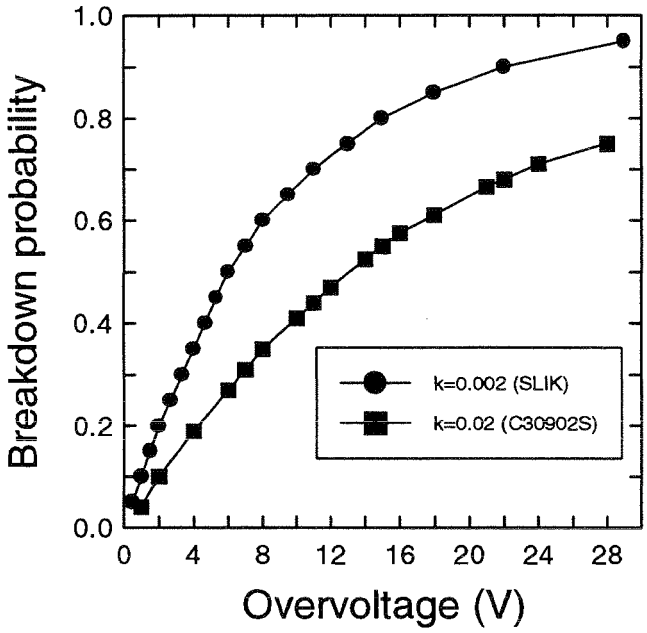

Fig.2 Avalanche-triggering probability versus excess bias voltage above the breakdown level for different photodiode structures. The performance of the new Slik is compared to the previous C30902S type.

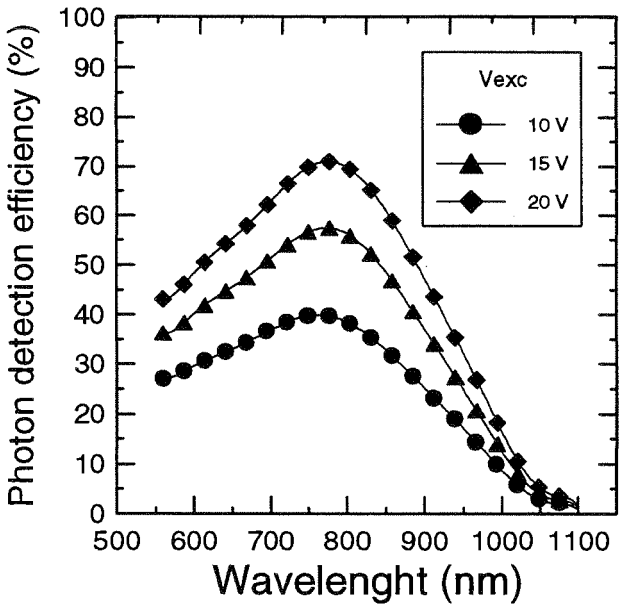

Fig.3 Quantum detection efficiency of the new Slik avalanche photodiode versus photon wavelength, at different excess bias voltage above the breakdown level.

The single-photon detection efficiency of the Slik is significantly better than that of the previous C30902S over most of the spectral range covered with silicon SPAD detectors. A peak efficiency of about 70 % is measured at 820nm, consistent with the presence of an anti reflection (AR) coating centered at this wavelength. With a different AR coating and a slightly modified structure, a quantum efficiency in excess of 80% at 500 nm has been verified [4]. As shown in Fig. 3, a photon detection efficiency of about 3% is measured at 1064 nm.

The thermal generation of carriers within the active junction volume (that gives rise to the primary dark counting rate) is reduced to very low level, a few thousand per second or less at room temperature. After each avalanche pulse, the carrier trapping and delayed release phenomena (that produce afterpulsing effect enhancing the total dark-counting rate) are reduced to rare events (probability of a few percent) occurring within a short time (a few tens of nanoseconds). As shown in Fig.4, this brings down to very low level the intrinsic noise of the detector. The total dark counting rate is only a few 1000 counts per second at room temperature and can be dramatically reduced (down to a few counts/s) by lowering the detector temperature to -40 C, a level that can be easily attained by using a double stage thermoelectric peltier cooler.

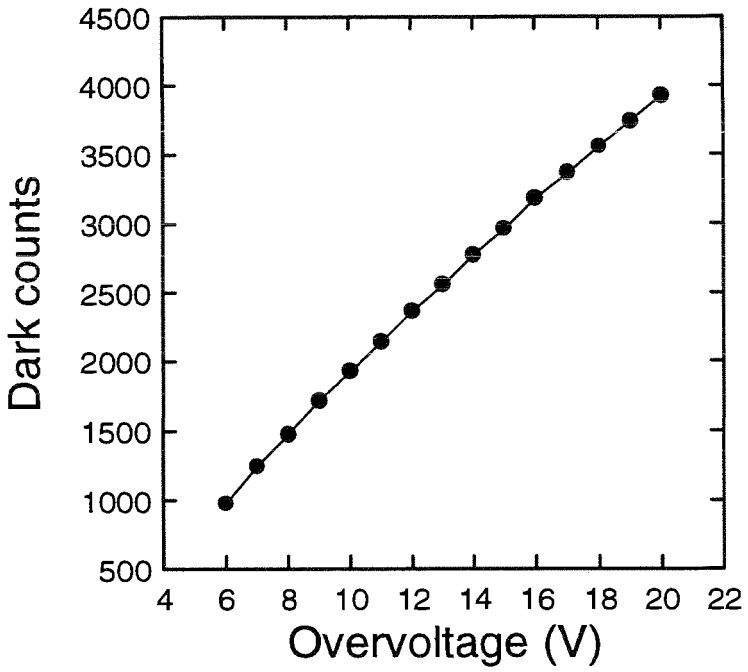

Fig.4 Dark-counting rate at room temperature versus excess bias voltage above the breakdown level for a Slik avalanche photodiode having active area with 250 μm diameter.

In order to facilitate the application and avoid practical drawbacks due to the fairly high breakdown voltage, Slik detectors are commercially available in compact electronic modules (SPCM series) requiring only a 5V voltage supply and including all the necessary front-end circuitry, that is, the high voltage supply and the quenching circuitry, with passive and active quenching versions [4].

2. Timing performance of high efficiency SPADs and limitations due to quenching circuits

Theoretical analysis of the physical phenomena involved in the avalanche build-up and in the propagation over all the active area, supported by computer simulations that take into account the detailed structure of Slik photodiodes, point out that the inherent detector resolution is significantly better than 100 ps rms [1,5-7]. Experimental data supporting the theoretical predictions have been reported, obtained in measurements performed with the Slik device working in a simple passive quenching circuit, deriving a fast output signal directly from the fast avalanche current pulse and processing it with external fast amplifying and timing circuits [8]. With the available SPCM active-quenching module, however, resolution values limited to about 200 ps rms are specified. Other circuits developed in our laboratory for astronomical applications, that primarily required high counting rate capability and compact circuit structure [9], showed equivalent performance in photon timing. We estimated that a significant limitation to the performance had to be ascribed to the design approach adopted in these quenching circuits, aiming to high counting rate rather than high resolution timing [4,9]. In fact, a basic limitation of these circuits can be ascribed to the configuration employed for taking out the avalanche signal and for extracting the time information from it. A schematic diagram of the circuit described in Ref.4 is shown in Fig.5.

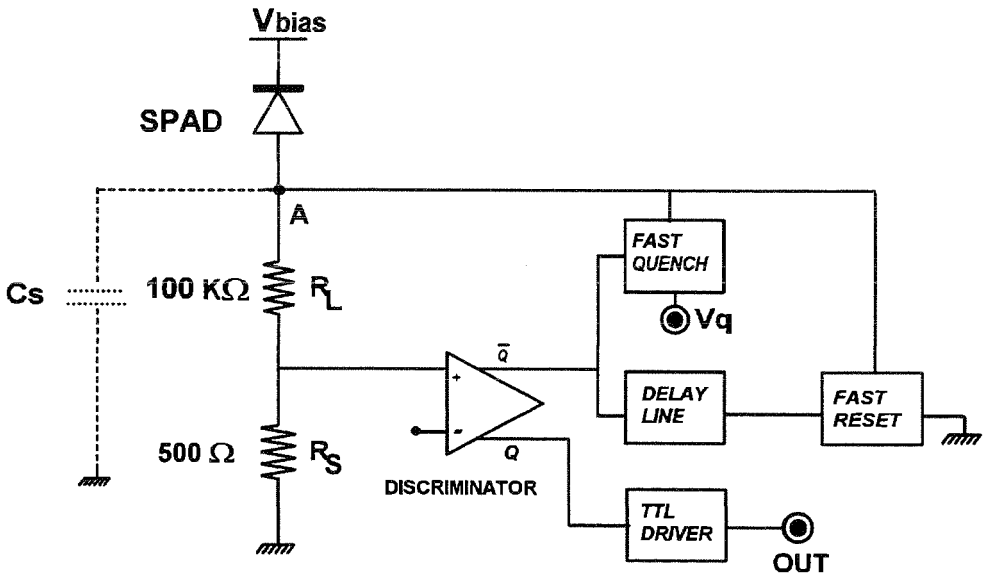

Fig.5 Simplified diagram of the compact active quenching circuit employed in the SPCM modules and described in Ref.4.

When a photon triggers an avalanche, the current flows in the 100KΩ resistor, providing a voltage signal to the threshold discriminator. The photon arrival time is marked by the switching of the discriminator. Since a stray capacitance C_S of a few pF between the node A and ground is unavoidable, the voltage pulse on the discriminator input is actually affected by a low-pass filter with non negligible time constant $R_L C_S$. It has been foreseen in theoretical analysis and verified in experiments that such a filtering has a detrimental influence on the photon-timing accuracy, which can be only in part compensated by employing a very low threshold level in the timing circuit [7,10].

3. New compact active quenching circuit for high-resolution photon-timing

We have specifically developed a compact active quenching circuits for extracting at best the time information in the avalanche pulse, maintaining the capability of gated operation and of working at high counting rate. A schematic diagram of the circuit is shown in Fig.6. It represents an evolution of the above mentioned design approach [9] ; the essential new feature is the addition of circuitry that exploits the very first part of the avalanche current signal for generating a timing signal.

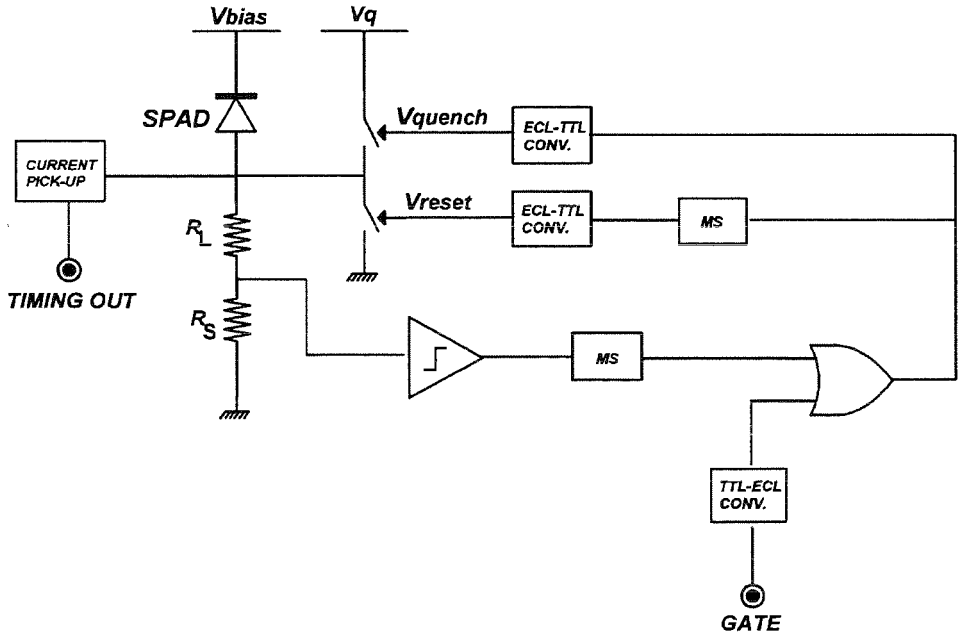

Fig.6 Simplified diagram of the compact active quenching circuit developed for high resolution photon-timing with SPADs having high breakdown voltage.

The current pick-up stage has a variable impedance input. In the quiescent state the impedance is low, so that the SPAD terminal is connected to a low impedance load. When the SPAD is triggered, the onset of the avalanche current pulse flows into this low impedance input. A waveform with the fast risetime of the avalanche current (about one ns or less) is therefore supplied by the current pick-up stage to a timing circuit, which can thus exploit at best the detector performance. As soon as the avalanche current exceeds 1mA the variable impedance is switched to a high value, so that the current is diverted to the load resistor R_L . It thus develops a voltage signal at the input of the threshold discriminator, which controls the quenching and reset circuitry. Fast ECL comparator and monostables are employed for minimizing the delay between the onset of the avalanche and the application of the quenching pulse to the SPAD. The quenching and reset switches are implemented by using fast DMOS FET transistors (Siliconix SST215), which can be employed with a maximum excess bias voltage of about 25V. ECL to TTL level converters provide the proper driving signal to these switches and generate a standard TTL output pulses. An external TTL gate-off signal acts on the quenching switch through an OR circuit. Gate-off pulses with duration ranging from 10ns to minutes can be employed.

A mixed passive-active quenching scheme is adopted in the circuit [10]. A fairly high passive load (R_L+R_S) provides a prompt passive quenching or at least a quasi-quenching, reducing the avalanche current to very low value. With a short delay (typically 10 ns), quenching is confirmed by the active loop formed by the discriminator, the monostable and the quenching switch. The active loop drives the voltage well below (by about 4V) of the nominal breakdown voltage V_B, avoiding reignition due to nonuniformity of V_B over the APD active area [4]. The mixed passive-active quenching is advantageous for minimizing the avalanche charge and the related afterpulsing effect due to carrier trapping [10]. Furthermore, this approach turns out to be in practice almost mandatory for minimizing the power dissipation of SPADs with high breakdown voltage V_B working at high excess bias voltage. In these devices the power dissipation attains various Watts and, without an effective limitation of the pulse charge, it would lead to excessive heating of the detector at high pulse repetition rate. The various phases in the operation cycle can be identified in the voltage waveform at the SPAD terminals, as shown in Fig.7. After the passive quenching phase (A) the quenching switch is activated (B); the SPAD is then held below the breakdown voltage during the hold-off time (C); finally, the reset switch is activated (D) and makes the SPAD ready again to detect another incoming photon. The capability of working at remarkably high counting rate is illustrated by Fig.8. The fast quenching and reset circuitry enables to work with an overall deadtime for counting below 40 ns, corresponding to a counting rate exceeding 25 Mcounts/s.

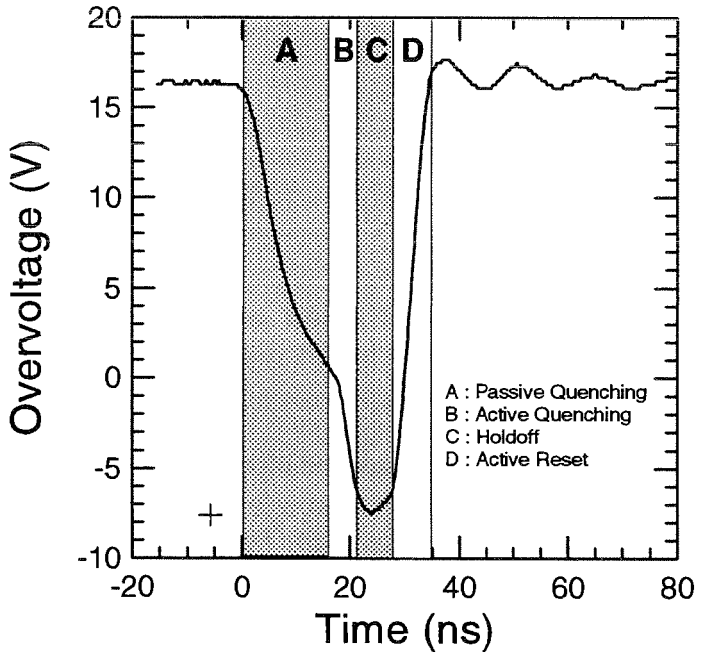

Fig.7 Voltage waveform at the terminals of a SPAD working in the circuit of Fig.6. The various phases in the quenching-holdoff-reset cycle are pointed out in the figure.

The resolution in single photon timing of the Slik working in the new active quenching circuit was tested in a conventional time-correlated single-photon counting setup. A gain switched laser diode emitting pulses with pulse duration 20 ps full-width at half maximum (FWHM) at 820 nm wavelength was employed. The detector was operated at room temperature, biased 20 V above the breakdown voltage.

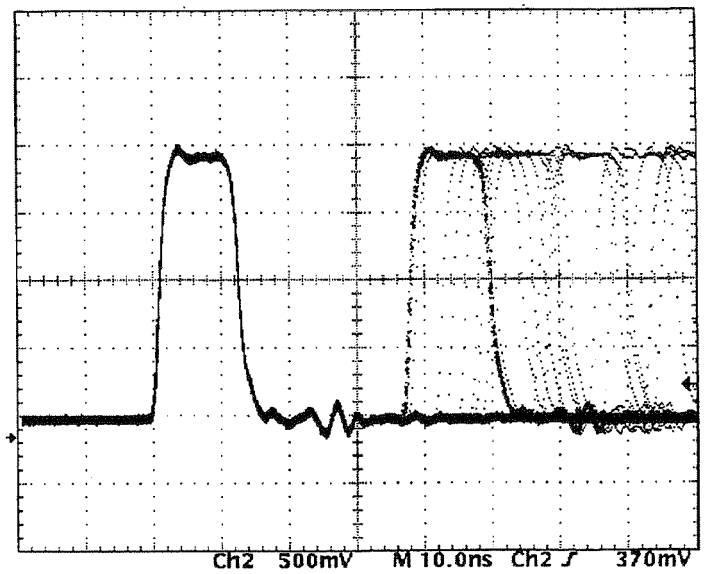

Fig.8 Output voltage waveform of the circuit in Fig.6, showing that the deadtime is shorter than 40ns (horizontal scale 10 ns/div; vertical scale 0.5 V/div).

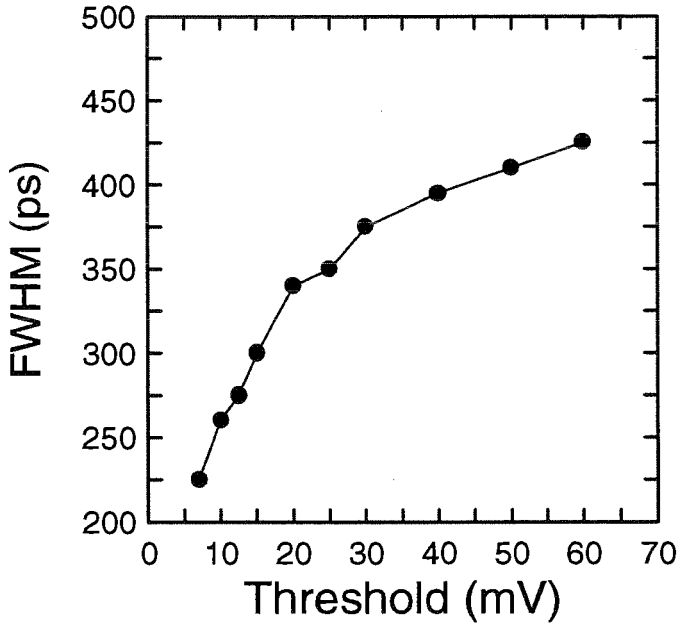

Fig.9 Time resolution of the Slik detector as a function of the threshold level of the timing discriminator. The detector is biased 20 V above the breakdown voltage.

Fig.9 shows how the time resolution of the Slik detector depends on the threshold level of the timing discriminator. A minimum value of about 220 ps FWHM (~ 100 ps rms) was measured with a threshold of 8 mV, corresponding to an avalanche current level of 160μA . These results are in agreement with the data reported by Li and Davis: in tests performed employing laser pulses at 584 nm wavelength and a Slik at 20V excess bias voltage, cooled at -45 C and

operating with a simple passive quenching circuit, they obtained 168 ps FWHM time resolution at low repetition rate of the avalanche pulses [8].

4. Conclusion

In conclusion, we have demonstrated that the intrinsic performance of the new Slik silicon avalanche photodiodes can be fully exploited working with suitably designed compact quenching circuits. It is thus possible and practical to work in laser ranging applications with a single-photon detector that, over a wide spectral range extending up to 1064nm, offers an unprecedented combination of the highest available quantum detection efficiency and a very good time resolution. Among the available single-photon semiconductor detectors, this resolution is inferior only to that of the ultrafast SPADs, having structure optimized for timing at the cost of remarkably lower quantum efficiency [1].

Acknowledgements

This work was supported in part by ASI (Italian Space Agency) and by MURST (Italian Ministry of University and Research).

References

1. A.Lacaita, M.Ghioni, F.Zappa, G.Ripamonti, and S.Cova, *"Recent advances in the detection of optical photons with silicon photodiodes"*, Nucl.Instr. and Meth. **A326**, 290-294 (1993)
2. A.W. Lightstone and R.J. McIntyre, *"Photon counting silicon avalanche photodiodes for photon correlation spectroscopy"*, in Photon Correlation techniques and applications, Vol.1, of OSA Proceedings Series (Optical Society of America, Washington, DC, 1988) pp.183-191
3. M.Ghioni and G.Ripamonti, *"Improving the performance of commercially-available Geiger-mode avalanche photodiodes"*, Rev.Sci.Instrum. **62**, 163-167 (1991)
4. H. Dautet, P. Deschampes, B. Dion, A.D. MacGregor, D. MacSween, R.J. McIntyre, C. Trottier, and P. Webb, *"Photon Counting techniques with silicon avalanche photodiodes"*, Appl.Opt. **32**, 3894-3900 (1993) and SPCM-AQ Single-photon Counting Module Data Sheet, EG&G Optoelectronics Canada Ltd., Vaudreuil, Quebec, Canada
5. A.Lacaita, S.Cova, A.Spinelli, and F.Zappa, *"Photon-assisted avalanche spreading in reach-through photodiodes"*, Appl. Phys. Lett., **62**, 606-608 (1993)
6. A.Lacaita, S.Longhi, and A.Spinelli, *"Limits to the timing performance of single photon avalanche diodes"*, Proc. ICAPT94 Int.Conf. on Applications of Photonic Technology, Toronto, Canada, June 21-23, 1994
7. A.Lacaita et al (personal communication, to be published 1994).
8. Li-Quiang Li and L.M. Davis *"Single photon avalanche diode for single molecule detection"*, Rev.Sci.Instrum. **64**, 1524-1529 (1993)
9. D. Bonaccini, S. Cova, M. Ghioni, R. Gheser, S. Esposito, and G. Brusa, *"Novel avalanche photodiode for adaptive optics"* SPIE Proc. Vol 2198, pp , D.Crawford and E.Craine eds, 1994 - SPIE Topical meeting on Adaptive Optics, Kona-Hawai, March 1994
10. S. Cova, M. Ghioni, A. Lacaita, and C. Samori, "*Active, Passive and Gated Quenching Circuits for Single-Photon Avalanche Diodes*", to be published.

RECENT ACHIEVEMENTS IN SOLID STATE DETECTOR TECHNOLOGY FOR LASER RANGING

I.Procházka, K.Hamal

Faculty of Nuclear Science and Physical Engineering
Czech Technical University
Brehova 7, 115 19 Prague 1, Czech Republic
ph +42 2 85762246, fax +42 2 85762252, prochazk@earn.cvut.cz

General

The solid state detector technology is becoming widely applied within the satellite laser ranging community. The Single Photon Avalanche Diodes (SPADs) are alternatives to the fast photomultipliers; their timing resolution, quantum efficiency, simplicity and ruggedness of the solid state detector package are the most attractive features. The single photon ranging technique in connection with SPAD demonstrated its capability of multiple wavelength subcentimeter satellite laser ranging (Graz), daylight ranging to the high orbiting satellites like Etalon (Herstmonceux) and millimeter ranging biases and picosecond long term stability (SALRO). The references may be found in this Proceedings.

Improving the SPAD detector package and considering the field experience within the last three years we did focus on the dark count rate reduction, manufacturing of larger active area detectors. Simultaneously, we did investigate the timing properties of the device.

SPAD timing performance

In an indoor calibration facility [1] we measured the timing resolution, Fig.1. Please note, the SPAD active area diameter 200 micrometer and no focussing. As the same timing performance has been measured for SPAD samples with the diameter of 20 micrometers only, one can conclude that no position sensitivity can be detected. The gate speed response is on Figure 2, no measurable time dependence has been found after 50 nanoseconds after "gate on". Detector time walk and jitter within the range of 1 to 100 photons/shot are plotted on Figures 3 and 4. Note the dependence on the voltage above the break, for higher voltage above, the signal strength dependence is more flat. The break voltage of the diode was 26.0 Volts. It is worth to mention, that the time walk is caused by two effects : finite laser pulse leading edge and the time walk of the detection chip itself.

For multiple wavelength ranging on SPAD purpose the timing resolution dependence on the wavelength has been repeatedly remeasured at the Graz station. In contrast to the results we published in Annapolis, no difference of the timing resolution has been found within the range 355 to 1064 nanometers (third harmonic and fundamental of NdYAG, respectively).

Operating the SPAD package in the Herstmonceux, RGO the temperature dependence of the detection delay has been measured to be 6-7 picoseconds per Kelvin. The detector built in comparator has been found to be responsible for this dependence. The comparator manufacturer is claiming the same value for the

comparator itself, the experience gained at SALRO is supporting this idea. The temperature induced drift can be slightly reduced by proper selection of the comparator exemplar and/or by reducing temperature drifts of the detector package.

Dark count reduction

The SPAD detection chip dark count rate was reduced by two ways : tuning the chip manufacturing technology and lowering the chip temperature. The latest technology is permitting to manufacture SPAD structures of diameter of 0.2 millimeter and acceptable dark count rate. The dark count rate can be further decreased by cooling. The experience from Graz [2] and MTLRS-1 [3] with the thermoelectrical cooling of the conventional SPAD structure showed the complexity of such a solution. To simplify the cooled SPAD application, we did develop the new chip sealed housing with the thermoelectrical cooling built in. The protective internal atmosphere or vacuum inside the housing is avoiding any condensation problems. Thanks to low mass to be cooled and low heat transfer, a low electric power is needed for the thermoelectrical element. As the housing window is connected to the "hot" side of the cooling element, there is no water condensation problem in this setup.

On Figure 5a. there is a plot of 100 micrometer SPAD chip effective dark count rate versus voltage above the break. The total cooling power needed is about 300 milliWatts only. The typical dark count rate reduction is 10x in comparison to the uncooled version. The effective dark count rates of 200 micrometers chips cooled by single, two and three stage thermoelectrical coolers is on Figure 5b. The curves for the maximal permitted and recommended cooling current are plotted. The housing of the cooled SPAD detector packages are on Figure 6.

Conclusion

The available SPAD technology is permitting to manufacture a selfconsistent single photon solid state detector package with an active area 0.2 millimeter in diameter, timing resolution better than 25 picoseconds RMS. The data distribution nonsymetry due to the SPAD is detectable, but lower than the nonsymetry caused by the satellite retro array geometry. The effective dark count rate is bellow 10 kHz. This fact not only simplifies the acquisition of satellites with poor prediction quality, but also permits to use range gate width up to 100 microseconds. Thus no more problems with gating the detector for short path internal calibration, the gate signal may be simply related to the laser trigger signal.

[1] I.Prochazka, J.Blazej, Target characterization using single photon ranging on SPAD, in this Proceedings
[2] G.Kirchner, F.Koidl, Graz, private communication, 1991-93
[3] P.Sperber, MTLRS-1, Germany, private communication, 1992

SPAD detector package

TIMING RESOLUTION

200um chip,NO focus, 3V above break
laser 32 psec/0.8um, electronics 30 psec

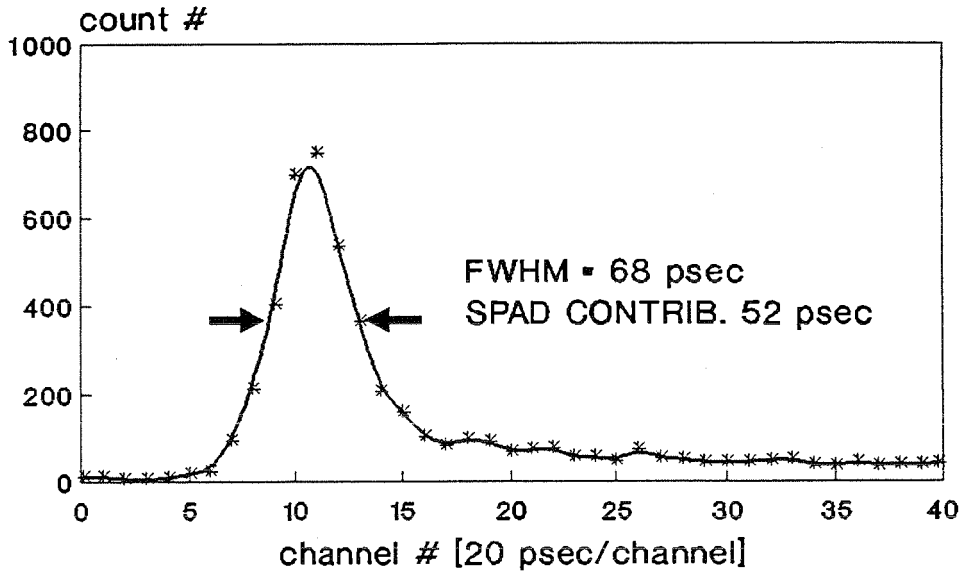

Fig.1

SPAD gate ON response

HCT board,100um chip,no focus,2.5V above
Laser 0.8um/32psec,timing el.30psec FWHM

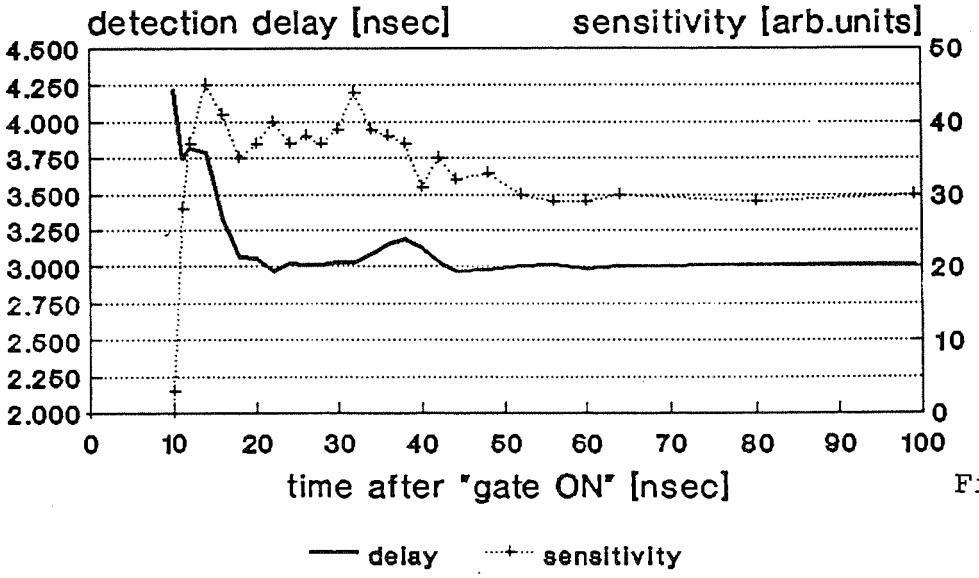

Fig. 2

I.Prochazka, September 1992

SPAD upgrade package for RGO

100um,LN selected chip,HCT board

32ps/0.8um laser diode, 30 ps electronic

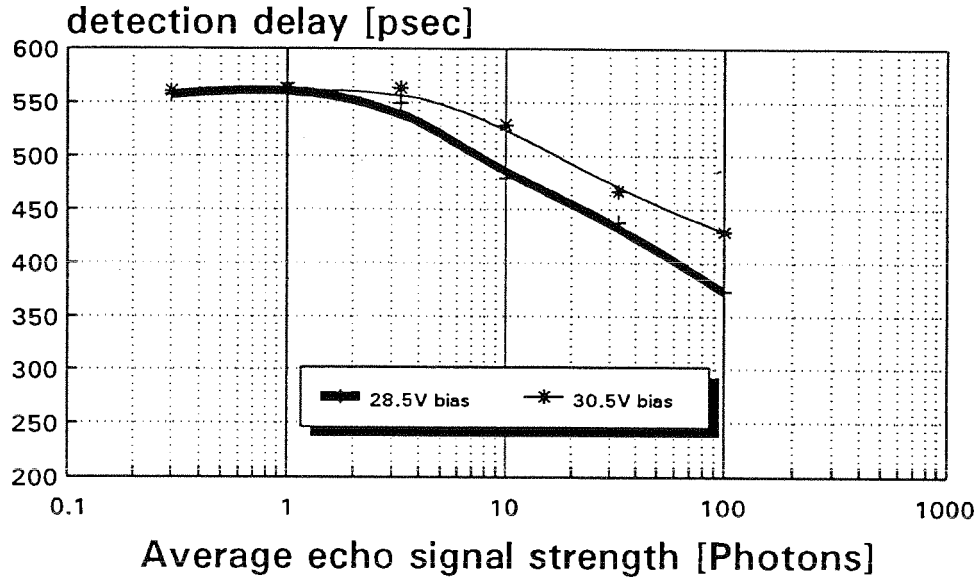

I.Prochazka, July 23,1993

Fig.3

SPAD upgrade package for RGO

100um,LN selected chip,HCT board

32ps/0.8um laser diode, 30 ps electronic

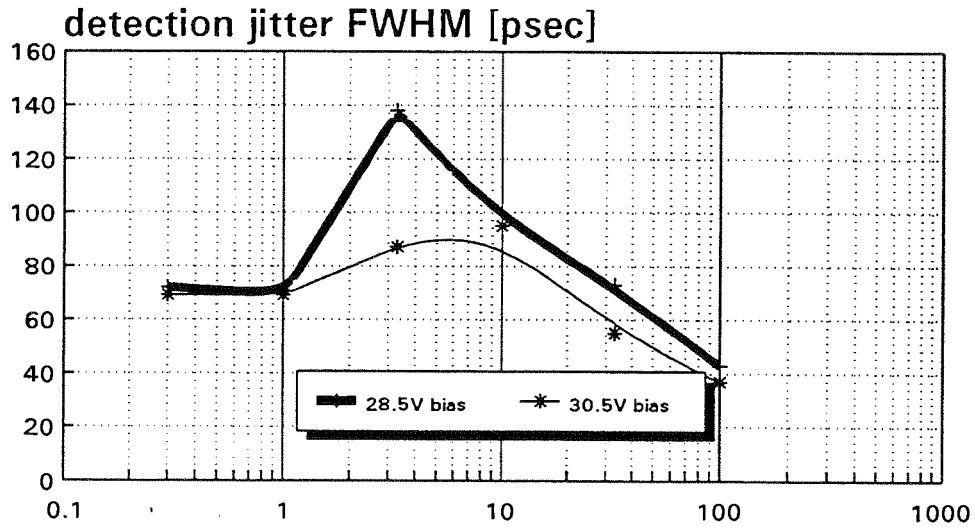

I.Prochazka, July 23,1993

Fig.4

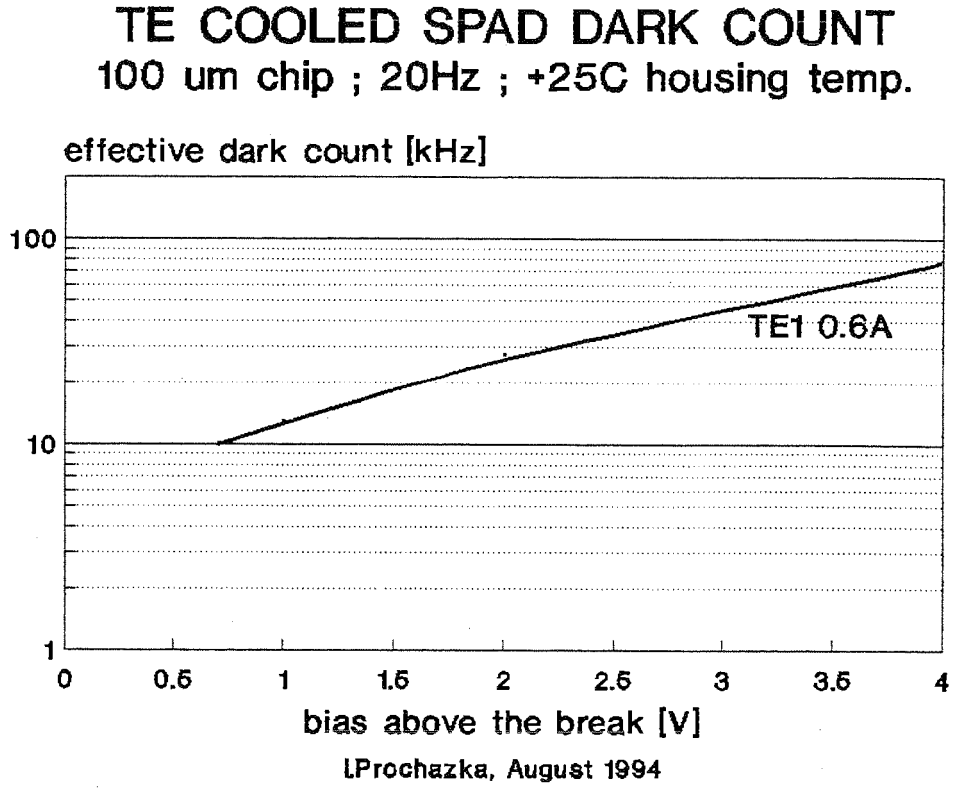
TE COOLED SPAD DARK COUNT
100 um chip ; 20Hz ; +25C housing temp.
effective dark count [kHz]
100
10
1
0
0.5
1
1.5
2
2.5
3
3.5
4
TE1 0.6A
bias above the break [V]
LProchazka, August 1994

Fig.5a

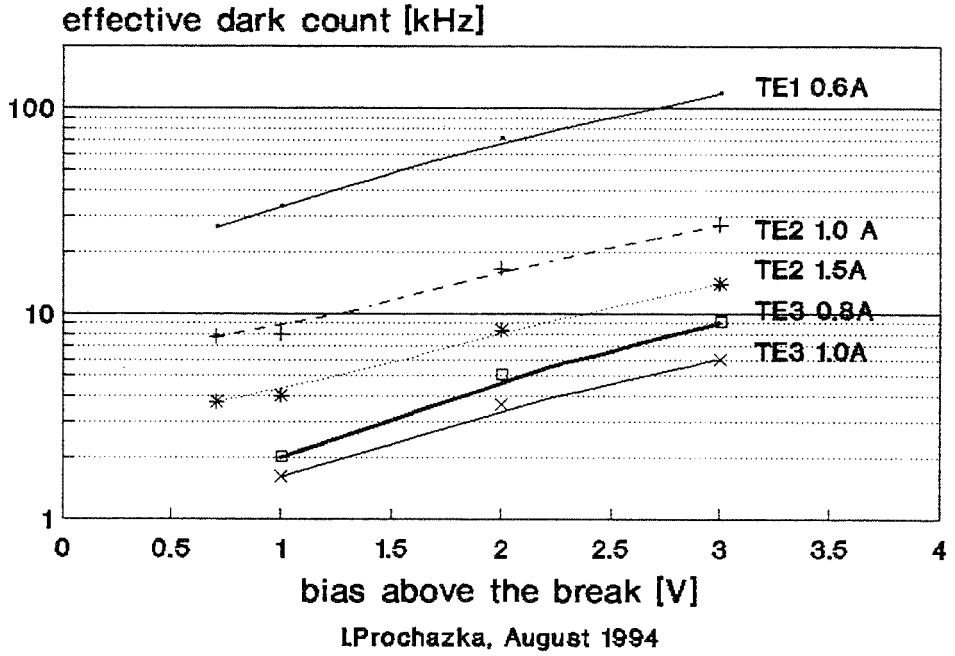
TE COOLED SPAD DARK COUNT
200 um chip ; 20Hz ; air blow
effective dark count [kHz]
100
10
1
0
0.5
1
1.5
2
2.5
3
3.5
4
TE1 0.6A
TE2 1.0 A
TE2 1.5A
TE3 0.8A
TE3 1.0A
bias above the break [V]
LProchazka, August 1994

Fig.5b

Single Photon Avalanche Diode
Detector package versions

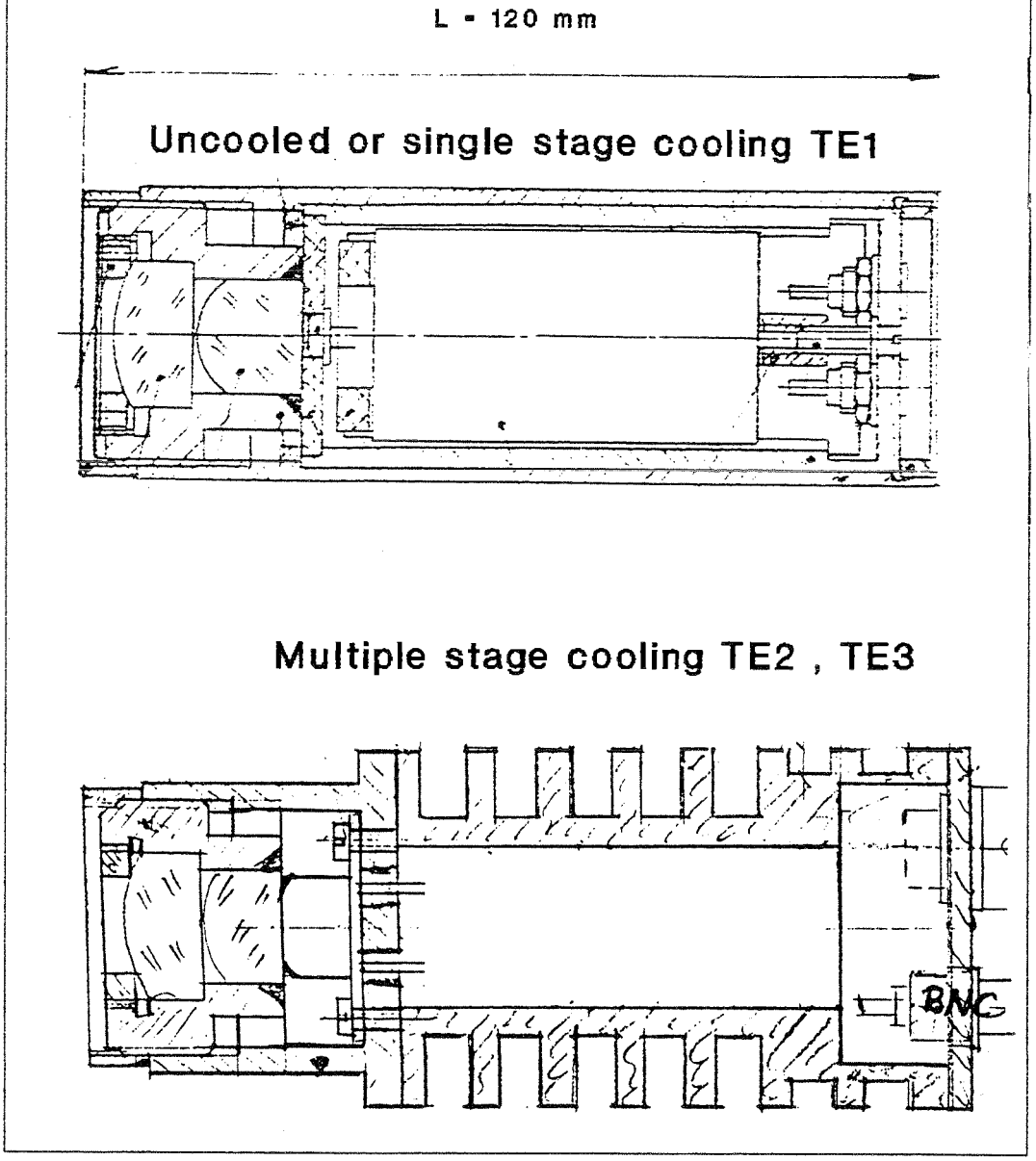

Fig. 6

I.Prochazka, October 1994

PERFORMANCE OF NEAR-INFRARED SINGLE-PHOTON DETECTORS IN LASER RANGING MEASUREMENTS.

S. Cova, A. Lacaita, P. Lovati and F. Zappa

Politecnico di Milano, Dipartimento di Elettronica e Informazione and CNR-CEQSE
Piazza Leonardo da Vinci, 32 - 20133 Milano (Italy)

Phone: +39(2)23996149 FAX: +39(2)2367604 E-mail: cova@elet.polimi.it

Abstract

We investigate the performances of various Ge and InGaAs APDs working biased above breakdown and cooled to 77K. In gated operation the Ge samples can detect single photons with a time resolution of 35ps rms and NEP of $5 \cdot 10^{-16}$ W/Hz$^{1/2}$ *in the wavelength range 0.8-1.45μm. InGaAs devices are instead sensitive up to 1.6 μm, with better NEP (* $2.7 \cdot 10^{-16}$ W/Hz$^{1/2}$ *) but with a time resolution of 82 ps rms. The results make Geiger-mode APD's suitable for laser-ranging application in the 1-1.6 μm wavelength range, where there is high atmospheric transmission and eye-safe operation.*

1. Introduction

Silicon Avalanche Photodiodes (APD's) biased above the breakdown voltage V_B are able to detect single photons in the 0.5-1.1μm wavelength range with excellent timing performance [1]. These devices find applications in photon correlation spectroscopy, velocimetry, Optical Time-Domain Reflectometry, Laser Ranging. However, the need of fast and more sensitive photodetectors working beyond 1μm is increasingly required in many fields of science and technology, not to mention all applications related to optical communications aiming to careful testing of optical components and networks at 1.3μm and 1.55μm. This is the reason why we have carried out an extensive investigation of the performance of commercially available germanium and III-V APD's when operated in Geiger-mode [2,3]. In this paper we highlight the results achievable with some commercially available devices when employed in laser ranging measurements at 1.06μm wavelength and beyond, closer to the 2μm atmospheric transmission window. The figures of merit of a single photon detector are i) the

precision in the measurement of the photon arrival time, which is usually referred to as time resolution and ii) the detection efficiency, η. For a Geiger mode APD both of these figures improve as the excess bias increases. However, also the dark count rate, R, steeply rises with the bias, thus impairing the detector sensitivity. Therefore, in order to quote the detector sensitivity it is better to use the Noise Equivalent Power, defined as the signal power required to attain a unity signal to noise ratio over a bandwidth of 1Hz:

$$NEP=\frac{h\nu}{\eta}\sqrt{2R}$$

Reach-through silicon devices (SLIK) commercially available from the EG&G Canada, cooled at -40°C reach an η value of 1% at 1.06μm with a dark count rate of 1 pulse per second [5]. This corresponds to an ultimate NEP of 2 $10^{-17}W/Hz^{1/2}$. However, in laser-ranging application, the background photons give a rate R significantly higher than 1pps, therefore the achievable (signal-limited) NEP is at least an order of magnitude higher.

2. State of the technology and gated operation

The fabrication technology of both germanium and III-V detectors is still far from the reliability and the cleanness of silicon technology. Breakdown voltage is not uniform over the device area, therefore the sensitive area is always smaller than the nominal junction area and its actual value depends on the bias. In particular the tested III-V samples exhibit a sensitive area which is to 1/4 of the device area, at 5V above V_B. The dark count rate is remarkably higher than that of silicon devices and is essentially due to afterpulses (Fig.1).

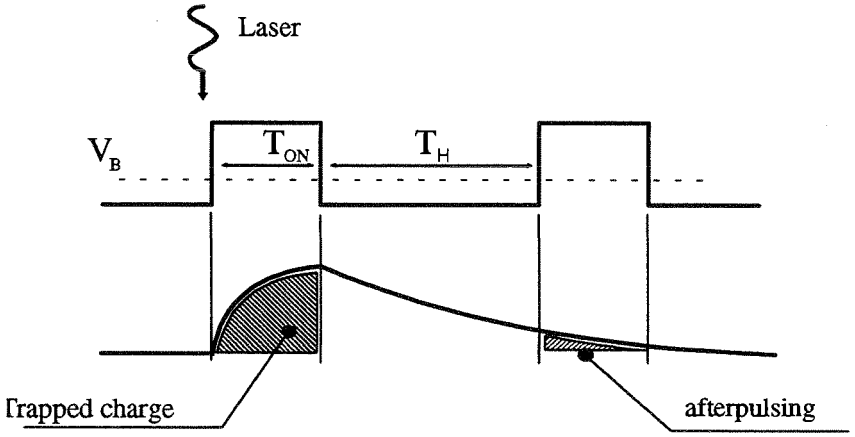

Fig.1 Afterpulses are due to the avalanches triggered by carrier trapped during T_{ON} and released after dead time T_H. Upper trace represents bias voltage, the lower one trap population.

This effect is caused by carriers, trapped in a previous avalanche pulse, which are released when the bias is again above V_B, thus triggering the avalanche again. The higher the density of trapping centers located in the junction, the higher is the contribution of afterpulses to the dark counts. Improvement of the fabrication technology, and the

design of suitable detector structures should make possible to reduce the gap between the performance of these infrared detectors and that of silicon APD's.

While in most of the applications the sensitivity degradation due to the afterpulses is severe, this is not the case of laser ranging. In these measurements the detector is operated gated, biased above V_B only in a short time window, synchronous with the arrival of back scattered photons (Fig.1). The bias is then lowered below the breakdown and held at the stand-by level for milliseconds, until the subsequent gating pulse. Due to this peculiar operation most of the carriers that get trapped during an avalanche pulse have the time to be released before the detector bias is raised again above V_B. Therefore the dark count rate within each gate interval is remarkably lower than the value measured with the detector operated in free-running. These residual dark counts are only due to thermal generation, tunneling effects [4] and trapping centers with lifetimes in the millisecond range.

3. Germanium samples

We have studied the performance of germanium APD's from different suppliers: the Fujitsu FPD13R31 with a 30μm-diameter (#Ge-F), the Judson J16A with a 100μm-diameter (#Ge-J) and a few developmental devices from Siemens with a 50μm-diameter, all with $V_B \approx 32V$ at room temperature. The devices were operated cooled at 77K in order to avoid the thermal contribution to the dark count rate. At this temperature the sensitivity cut-off of germanium occurs at 1.45μm wavelength.

The dark count rate of the devices was measured with an experimental set-up which drives the detector with a pair of voltage pulses as shown in Fig.1. A waveform generator provided voltage pulses of 5μs duration, that raised the APD bias above V_B. A laser diode emits a light shot synchronous whith first voltage pulse, triggering an avalanche in this time window. The bias was then lowered below V_B for a hold-off time, T_H, until the second voltage pulse restored the APD bias above V_B. In the window defined by the second voltage pulse, we measured the time delay, T_d, between the rise of the bias and the onset of the avalanche. This measurement was performed with a Time to Pulse Height Converter. The detector bias was then held below V_B for 5 ms in order to make possible the emission of all the trapped carriers, and the pulse sequence was then repeated. A Multichannel Analyzer stored the results of many measurements. The average counting rate in the second gating interval is given by $1/\langle T_d \rangle$, where $\langle T_d \rangle$ is the average of the measured time delays.

Fig.2 shows the dark-count rate of a #Ge-F APD, biased at stand-by only 0.2V below V_B. During the gate interval the bias was raised 0.5V above V_B Note that the dark counts steeply increases as T_H is reduced below 25μs: This means that most of the trapping centers have a lifetime shorter than 25μs. For very long T_H, which is the case of laser ranging measurements, the dark count rate approaches an asymptotic value which is essentially due to carrier tunneling. Since tunneling is weakly dependent on temperature, it is not worth to further cool the detector. Instead it is important to point out that a significant increase of the dark counts occurs if a stand by of many volts below V_B is adopted [3].

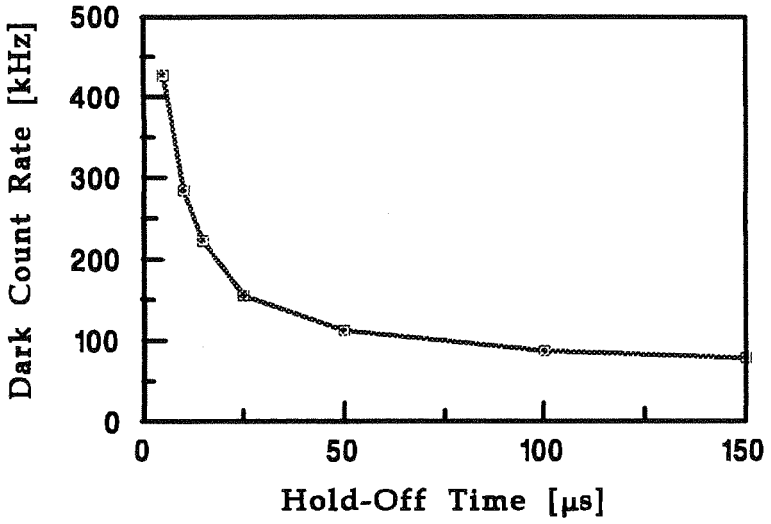

Fig.2 Dark count rate versus Th. The decrease in dark counts with hold off time is due to afterpulsing. Excess bias is 0.5 V and the stand by voltage is only 0.2V below V_B

Fig.3 shows the *NEP* expected in laser ranging measurements at 1.06μm with the #Ge-F samples. The *NEP* value is almost constant at a value of about $5 \cdot 10^{-16} W/Hz^{1/2}$. Note that about the same value is achievable in the wavelength range up to 1.4μm, while at wavelength higher than 1.06μm the use of silicon devices is out of question.

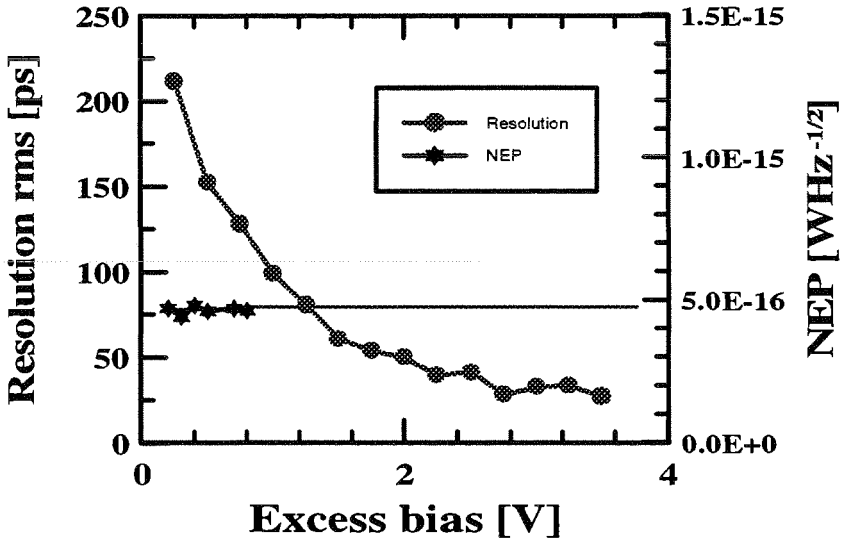

Fig.3 Time resolution and NEP performances obtained with 30 μm diameter Fujitsu Ge APD's. Points are experimental data at 1.3μm and 77K. The same values can be found at 1.06 μm because of the very small difference in the germanium absorption coefficient at the two wavelengths.

Since the Judsons's germanium APD have a sensitive area 10 times larger, their dark count rate is 10 times higher and the corresponding NEP is three times higher. The NEP values reported here are already sufficient to perform laser ranging measurements, however at 1.06μm the adoption of commercially available germanium detectors is not expected to lead to performance better than that achievable with SLIK silicon detectors. In order to be fair, it should be noted that the NEP value obtained are not the ultimate figures achievable with Germanium devices. The tunneling rate can be reduced by designing the APD with a larger depletion layer thickness, thus lowering the electric field at the junction.

The precision in the measurement of the photon arrival time was measured in a conventional Time Correlated Photon Timing set-up [6]. A Multichannel Analyzer collected the histogram of the time delay between the emission of a laser pulse (25ps rms at 1.3μm wavelength) and the avalanche pulse. The measurements were performed with a laser diode at 1.3μm, and there is no reason by which the performance at 1.06μm should be worse. The #Ge-F devices reach the best 85ps FWHM (35ps rms) time resolution (Fig.4) at 3V above breakdown. The second peak in Fig.4 is due to the shape of the optical pulse, while the 105 ps FWHM is due to the quadratic composition of laser and detector response.

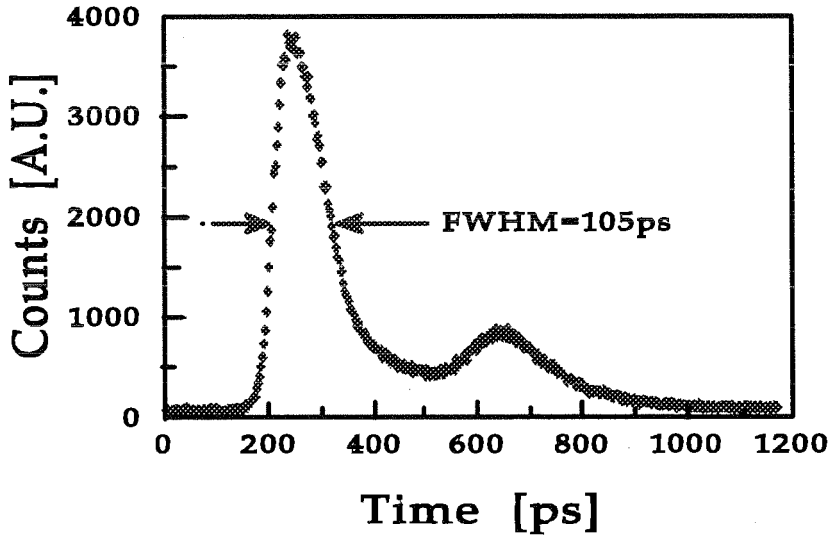

Fig.4 Best time resolution of #Ge-F APD at 1.3 μm, 3V above breakdown and 77K.

4. III-V photodiodes

In order to measure signals beyond 1.45μm other semiconductor devices must be employed. We tested some developmental InGaAs/InP APD's from EG&G (#InP-E) with 50μm-diameter, and commercially available Fujitsu FPD15R31 (#InP-F) with 30μm diameter and $V_B \approx 60$V at room temperature.

The schematic band diagram of these devices is reported in Fig.5. Photons in the 1.0-1.6μm wavelength range are only absorbed within the InGaAs layer. The photogenerated holes can pile-up at the InGaAs/InP-heterointerface and may recombine before jumping across the step by thermoionic emission and triggering the avalanche in the InP layer. In order to make easier for the holes to jump across the energy discontinuity, a layer of InGaAsP with intermediate energy gap is inserted between the InP and the InGaAs layer. This layer was 500nm thick in the Fujitsu's samples and 50nm thick in the EG&G devices.

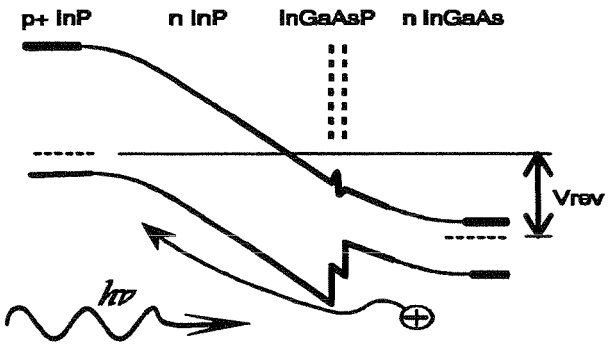

Fig.5 Schematic band structure of a InGaAs/InP Separate Absorption Grading and Multiplication APD. The grading layer of InGaAsP is 50 nm thick in #InP-E, while is 500 nm in #InP-F devices

The dark count rate of these detectors is extremely high and they must be operated at low temperature. Fig.6 shows the NEP and the time resolution of the Fujitsu's samples at 77K as a function of the excess bias.

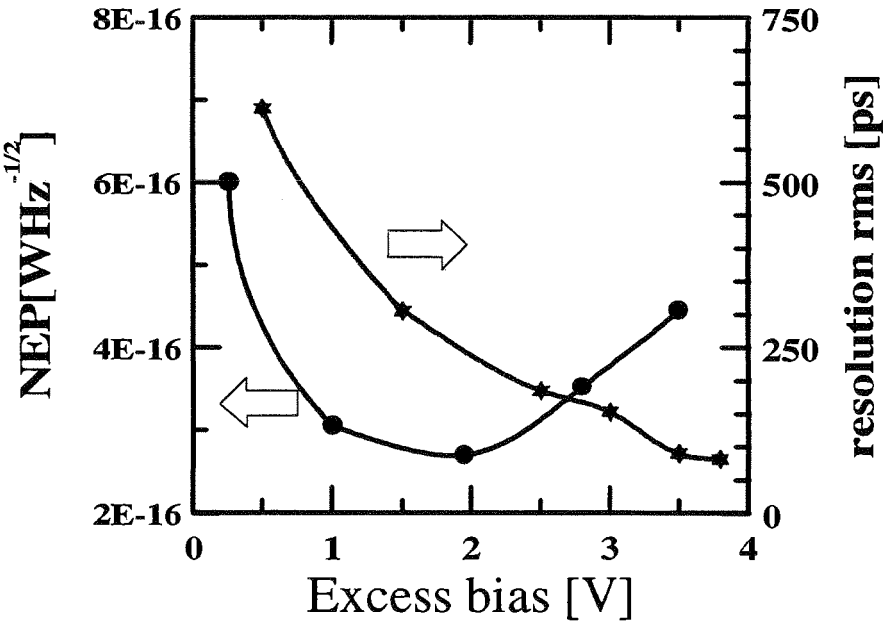

Fig.6 Time resolution and NEP of #InP-F devices versus $V-V_B$

The optimum NEP of $2.7 \cdot 10^{-16} W/Hz^{1/2}$ is reached at 1.9V of excess bias. At lower bias the NEP increases due to the decrease of the detection efficiency, while the increasing dark counts impairs the detector sensitivity at larger excess bias. The time resolution steadily improves as the bias increases, reaching 82ps rms at 3.8V. Fig.7 shows the best time response of a Fujitsu-InGaAs/InP APD at 77K.

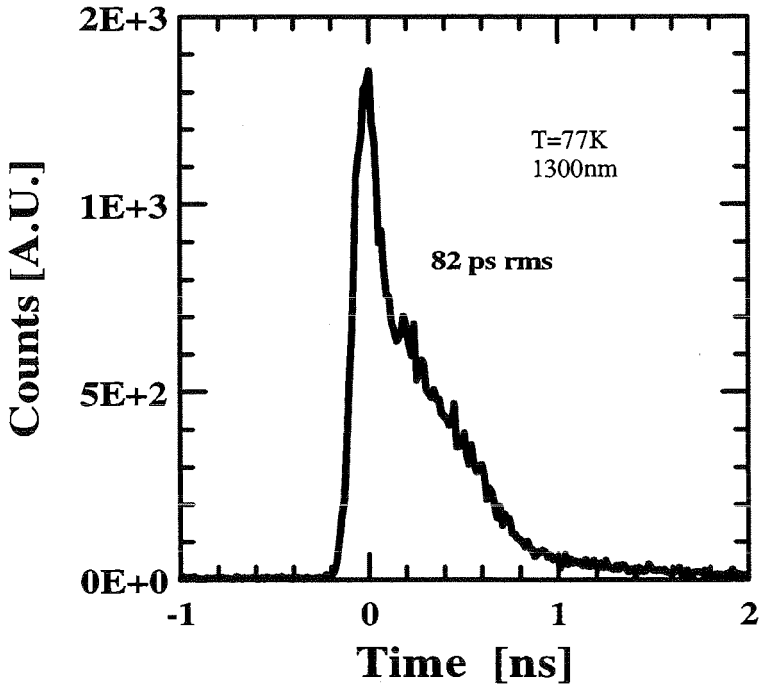

Fig.7 Best time resolution of #InP-F devices at 3.8V of excess bias

These devices work well also at 150K. The best time resolution achieved with a Fujitsu's sample at this temperature is 186ps rms. For comparison, note that the EG&G devices in the same operating conditions reaches 350ps rms.

5. Conclusions and perspectives

We have carried out extensive measurements on commercially available germanium and InGaAs APD's in order to assess their performance as single photon detectors in the near-infrared wavelength range. Even if the sensitivity of presently available devices is impaired by afterpulses, in laser ranging measurements this limitation can be overcome due to the peculiar gated operation with milliseconds time intervals between subsequent activations of the detector. The Fujistu's samples, both in germanium and in InP/InGaAs, show the best performance in terms of achievable NEP and time resolution. Further improvements can be expected if the device structure will be optimized for Geiger-mode operation.

Acknowledgements

Work support in part by ASI (Italian Space Agency) and by MURST (Italian Ministry of University and Research). The authors wish to thank Rino Micheloni who carried out some of the measurements here reported.

References

1. S. Cova, A. Lacaita, M. Ghioni, G. Ripamonti, T.A. Louis,
"20 ps timing resolution with single-photon avalanche diodes"
Rev. Sci. Instrum., **60**, 1104-1110 (1989).

2. F: Zappa,A. Lacaita, S. Cova, P.Webb
"Nanosecond single-photon timing with InGaAs/InP photodiodes"
Opt. Lett., **19**, 846-848 (1994)

3. A. Lacaita, P.A. Francese, F. Zappa and S. Cova,
"Single Photon Detection Beyond 1μm: Performance of Commercially Available Germanium Photodiodes"
Appl. Opt., **33**, 6902-6918 (1994)

4. W. Haecker, O. Groezinger and M. H. Pilkuhn,
"Infrared Photon Counting by Ge Avalanche Diodes"
App. Phys. Lett., **19**, 113-115 (1971)

5. H. Dautet, P. Deschamps, B. Dion,
"Photon Counting Techniques with Silicon Avalanche Photodiodes"
Appl. Opt., **32**, 3894-3900, (1993)

6. D.V. O'Connor and D. Phillips,
Time Correlated Single Photon Counting
Academic Press, New York 1983

A narrow bandpass filter for ATLID

Ludwig Meier, Gebhard Kühn, Peter Köhler

Carl Zeiss Jena GmbH, Tatzendpromenade 1a, Jena 07745

INTRODUCTION

For ATLID, a filter featuring a narrow transmission band of less than 0.2 nm and a high transmission of greater than 50% is required. The Fabry-Perot etalon is a possible variant to achieve these specifications. The present paper will analyse how the required specifications are met by means of a birefringent filter.

1. THE TWO FAMILIAR BASIC BIREFRINGENT FILTER DESIGNS

All familiar birefringent filters have more or less been derived from two basic designs, the Lyot and the Solc filter design (Fig. 1). Both designs feature plates made of birefringent material whose entrance and exit surfaces are arranged parallel to the crystal axis. In the Lyot filter, each plate is located between polarizers and their thicknesses follow a geometric series. In the Solc filter, a number of plates of equal thicknesses is arranged between two polarizers. Fig. 2 shows the typical spectral transmission curve of such a filter.

2. DERIVATION OF THE CONCEPT FOR AN OPTIMUM FILTER DESIGN

2.1 Series of maxima

Both the typical curve (Fig. 2) and the analytic expressions (Fig. 3) of the spectral transmission feature periodicity, i. e. a series of principal maxima. From this results the first requirement to be considered for the filter design, i. e. the necessary use of a blocking filter for blocking a single maximum out of the series of maxima.

1st decision for the filter concept: Use of a blocking filter

2.2 Peak transmission

The two most important parameters to be considered for the ATLID filter are the peak transmission and the full width at half maximum. When using a birefringent filter, the peak transmission value depends on the following influences:

- value of filter function for required wavelength,
- transmission of all birefringent plates
- transmission of prefilter
- transmission of all polarizers employed
- transmission of all media between the plates (cement, coatings)
- transmission loss due to light transition from one medium to another

The above influences have to be minimized. Polarizing sheets normally used for birefringent filters are not suitable, because their transmittance is too low. The comparison between cement and coatings leads to another recommendation, namely to use cement if there are not any objections of other kind.

2nd decision for the filter concept: Use of high-transmission crystal polarizers

2.3 Required full width at half maximum

The possibilities of finding a material and plate thickness meeting the demands placed on the full width at half maximum are limited, because there is a defined dependence between the required full width at half maximum and the total thickness of the material:

$$FWHM = c \cdot \frac{\lambda^2}{L \cdot \mu}$$

where μ is the difference between the refraction indices and L is the total thickness of the birefringent material; c is a constant which has a value of about 0.87 in both Lyot and Šolc filters. From this results, that for the required full width at half maximum of 0.2 nm and the wavelength of 1064 nm the value of $L \cdot \mu$ should be about 5 mm.

The selection of the material is further limited by the permissible overall length of the filter. If $L \cdot \mu$ is 5 mm, the total thickness of the below-mentioned common birefringent materials is the following:

Calcite: L = 31 mm
ADP: L = 120 mm
Quartz: L = 573 mm.

Hence it follows that calcite should be used. There is, however, a further possibility, i.e. the use of two different materials. This requires to consider another aspect which will be dealt with in 2.4.

3rd decision for the filter concept: Use of calcite is necessary

2.4 Required useful spectral range

The distance between two maxima of a spectrum is expressed by the following relation:

$$\Delta\lambda = \frac{\lambda^2}{d \cdot \mu}$$

where d is the thickness of the thinnest plate of the filter. This (thinnest) thickness is influenced by the manufacturing processes and by the spectral transmission of the prefilter. It can be assumed that, when using high-transmission prefilters, transmission at a distance of about 15 nm from the central wavelength is sufficiently low for blocking out the adjacent maximum. According to the above formula, the smallest plate thicknesses of the already mentioned materials are:

Calcite: d = 0.46 mm
ADP: d = 1.81 mm
Quartz: d = 8.66 mm.

Calcite plates of 0.46 mm thickness are difficult to work; they split easily. Since calcite has to be used in any case, the problem has be solved by using two materials. To this end, the filter has to be divided into two stages, in a high- and a low-resolution stage. In this conjunction, it should be mentioned that all the above considerations refer to both Lyot and Šolc filters.

4th decision for the the filter concept: Division of the filter into a high-resolution stage made of calcite and a low-resolution stage made of quartz

2.5 Comparison of Lyot filter with Šolc filter

Advantages of the Šolc filter:
- All plates have the same thickness
- Only two polarizers are needed.
- The spectral properties of the filter may be influenced by varying the plate orientations.

Advantages of the Lyot filter:
The effect of deviations from the required plate thicknesses is slightly smaller than with the Šolc filter.

This leads to the
5th decision for the filter concept: Preference is given to the Šolc design

2.6 Required number of plates and plate thicknesses

From the requirements 2.3 to 2.5 the following equation is valid with regard to the two filter stages:

$$5\ \text{mm} = n_c\, d_c\, \mu_c + n_q\, d_q\, \mu_q ,$$

where the index indicates the kind of material used (calcite or quartz), n is the number of plates of the Šolc filter, d is the plate thickness and μ is the difference between the refraction indices (see 2.3). Variation is still possible with regard to the number and thicknesses of the plates. They are defined by two further requirements: Due to the multiple-beam interference taking place in the Šolc filter the required accuracy of the plate thicknesses increases together with the plate number. Considering the manufacturing possibilities, the number of calcite plates should not be higher than 8. Since the quartz stage is a kind of prefilter for the calcite stage, the first minimum of the quartz stage must be located at the point of the first adjacent principal maximum of the calcite stage. Considering both requirements, stages of eight plates having a value of approximately 9 for the ratio $d_c\, \mu_c / d_q\, \mu_q$ appear reasonable. This also defines the required thicknesses for the calcite and quartz plates.
6th decision for the filter concept: Use of two Šolc filters of eight plates each

2.7 Variation of plate orientations in the Šolc filter

The next decision results from the requirement for a small equivalent bandwidth. In the Šolc filter, it is possible to determine permissible modifications in the position of the crystal axis relative to the polarizing direction by leaving the height of the principal maximum unchanged while largely reducing the heights of the parasitic secondary transmissions. The reduction of the heights of the parasitic secondary transmissions, however, entails a slight increase in the full width at half maximum (Fig. 4). This involves the solution of an extreme value problem, in which the determination of the minimum area below the spectral transmission curve has to be determined. In other words, it is necessary to find the degree of reduction of the secondary maxima, at which the equivalent bandwidth reaches its minimum. The solution of this task supplies the optimum orientations for the crystal axes in the filter.
7th decision for the filter concept: Determination of the plate orientations from
the minimum of the equivalent bandwidth

2.8 Size of field of view

The influence of beam tilt has not been considered so far. Perhaps it will be necessary to apply any of the familiar plate division methods for increasing the field of view. This would greatly influence the design. In the Šolc filter, a deviation from the perpendicular incidence of the beam does not cause a change of the form of the spectral transmission curve but a shift of the curve in the spectrum. Considering the definition of the useful field of view, (namely the shift of all rays inside this field should not exceed one tenth of the full width at half maximum), the field of view resulting for the dominating calcite stage at a full width at half maximum of 0.2 nm is approximately 10 mrd. Since the required value for the useful field of view is 5.3 mrd, the non-split Šolc filter variant can be used.
8th decision for the filter concept: Use of the non-split Šolc filter variant

3. SELECTED FILTER DESIGN

The considerations described in Section 2 lead to a filter concept based on birefringent material which optimally meets the requirements of ATLID (Fig 5).

The first filter stage is a prefilter consisting of dielectric multiple layers and a coloured glass filter. The next stage is an eight-step Solc filter consisting of calcite plates of 3.7 mm thickness. This is followed by a thin-film polarizer. The next stage is an eight-step Solc filter made of quartz plates 7 mm thick. The filter is completed by another thin-film polarizer. In the calcite plates, the crystal axes are aligned relative to the assumed perpendicular polarizing direction of the incident light at the angles 4.13 -5.13 6.13 -7.13 7.13 -6.13 5.13 -4.13 degrees. For the quartz plates the angular values are 4.88 -5.38 5.88 -6.38 6.38 -5.88 5.38 -4.88 degrees. The oscillation direction of the first polarizer is crossed and that of the second polarizer is parallel to that of the incident light.

The optical components are cemented. The surfaces contacting the air are provided with an antireflection coating. The filter unit is accommodated in a metal mount equipped with a thermostat. Temperature sensors are provided directly on the crystal plates. The thermostat has a constancy of better than 0.1 K.

The theoretic effect of the filter design, leaving error influences out of account, is illustrated in the figures 6 to 9. Fig. 6 shows the effect of the calcite stage, Fig. 7 shows the quartz stage, Fig. 8 shows the combined effect, and Fig. 9 shows the function of the complete filter.

4. COMPARISON OF THE FILTER PARAMETERS WITH THE ATLID REQUIREMENTS

The shown curves already give a qualitative impression of the the effect of filtering. Concerning the various parameters, the following values are achieved (error influences not considered).

Full width at half maximum
The computation yields a value of 0.19 nm for the complete filter unit. The required value is $<= 0.2$ nm.

Peak transmission
Considering all influences mentioned in 2.2, peak transmission is expected to be 0.60. The required peak transmission is > 0.50.

Field of view
The amount of shift of the transmission curve in the spectrum depends on the azimuth of beam tilt. At the maximum, its value is 0.0058 nm for a tilt of 5.3 mrd. This is only about 3% of the full width at half maximum compared with the 10% according to the definition of an useful field of view.

Equivalent bandwidth
The equivalent bandwidth largely depends upon the design of the prefilter. The value for the vicinity of the maximum can be determined by computation. Within the range from 1056 to 1072 it lies at 0.25 nm. The required total value is smaller than 0.28 nm.

Centre wavelength
The centre wavelength is defined by the plate thickness and the operating temperature. The required centre wavelength stability is, therefore, a demand concerning the manufacturing tolerances.

5. ERROR INFLUENCES

The most essential error influences are inhomogeneities in the birefringent materials (especially in calcite), manufacturing errors in the plate thickness, and instabilities in the operating temperature.

5.1 Inhomogeneities

The influence of inhomogeneities in the crystals is minimized by appropriate material selection. In case of remaining unacceptable values, the surface retouching method has to be tried.

5.2 Thickness error

The influence of thickness deviations is of complex nature. An essential error portion results from the deviation of the mean value d_m of all thicknesses produced in manufacture from the nominal value d_0. The difference $d_m - d_0$ leads to a shift of the centre wavelength. And because this shift should be less than one tenth of the full width at half maximum a very high thickness accuracy in the case of calcite plates is required. But the shift of the centre wavelength, caused by these thickness errors, can be compensated by changing the operating temperature. Compensation is, however, limited by the achievable temperature stability. For this reason and because of the other error influences, the thickness tolerance of calcite is about 0.2 μm.

5.3. Thermomodels

The temperature influences the position of the centre wavelength. The required temperature stability determines the requirements with regard to the thermostat. Normally a temperature gradient resulting from the difference between operating and outside temperature has to be expected. The Šolc filter offers the important advantage that deviations in the form of a "balance model" produce no effect. "Balance model" means that the temperature remains constant in the centre of a Šolc filter stage and deviates towards both directions to the same degree but with opposite sign. Deviations of this kind are compensated by the filter. Only the influences of other irregularities remain.

5.4 Other influences

There are a number of other influences of less important effect. For example the influences of errors in the plate orientations become only noticeable when the amounts exceed several tenths of a degree.

6. SUMMARY

The computations of birefringent filters show that a combination of a calcite and a quartz Šolc filter stage seems to be appropriate to meet the requirements of ATLID. In the filter design, high demands are placed on the homogeneity and the thickness accuracy of the calcite plates.

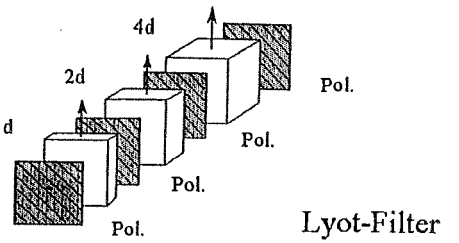

Lyot-Filter

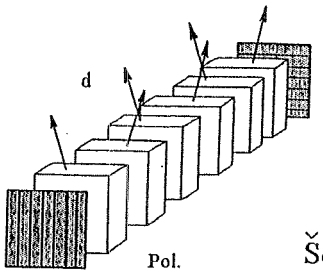

Šolc-Filter

Fig. 1

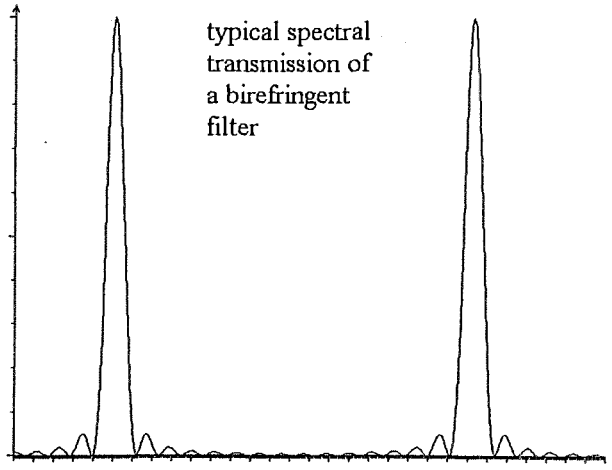

Fig. 2

Spectral transmission

analytical expression for a Lyot-Filter

$$T(\lambda) = \prod_{i=1}^{n} \cos^2 \frac{\pi d_i \mu}{\lambda}$$

and for a Standard-Šolc-Filter

$$T(\lambda) = \frac{\sin^2 n\chi}{\sin^2 \chi} \cdot \cos^2 \chi \cdot \tan^2 \alpha$$

$$\cos\chi = \cos\left(\frac{\pi d_i \mu}{\lambda} - \frac{\pi}{2}\right) \cdot \cos\alpha \quad , \quad n\alpha = \frac{\pi}{2}$$

μ : difference of refraction indices
d_i : thickness of plates
α : orientation of plates

Fig. 3

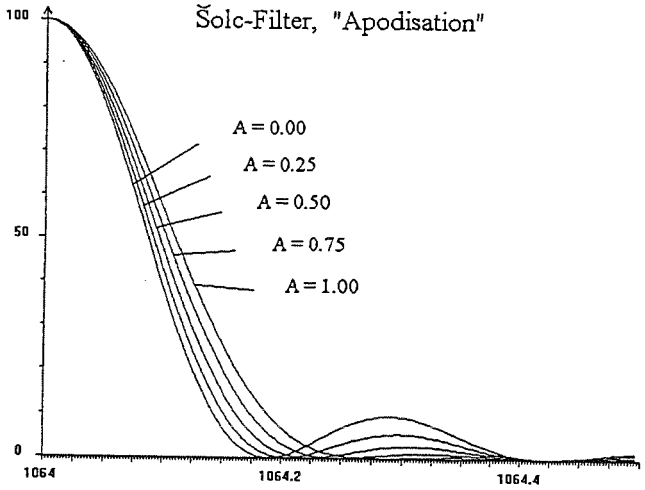
Šolc-Filter, "Apodisation"
100
50
0
A = 0.00
A = 0.25
A = 0.50
A = 0.75
A = 1.00
1064
1064.2
1064.4

Fig. 4

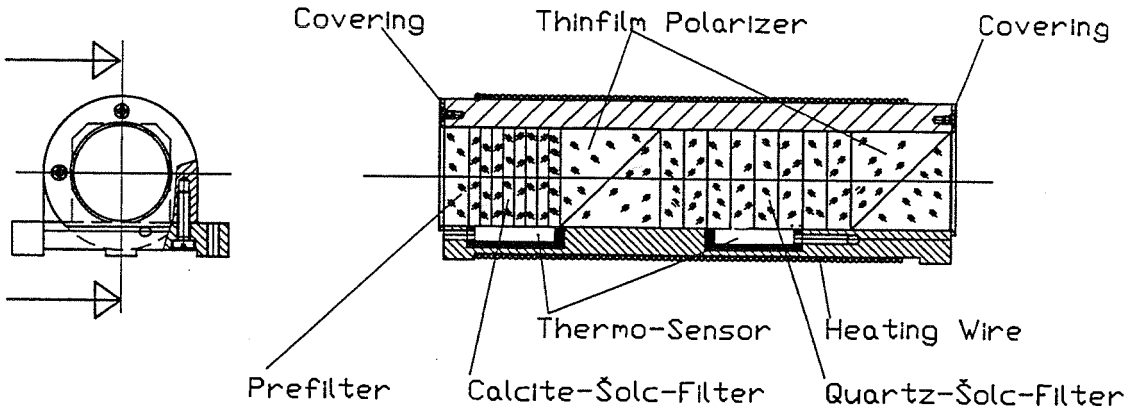
Covering
Thinfilm Polarizer
Covering
Thermo-Sensor
Heating Wire
Prefilter
Calcite-Šolc-Filter
Quartz-Šolc-Filter

Fig. 5

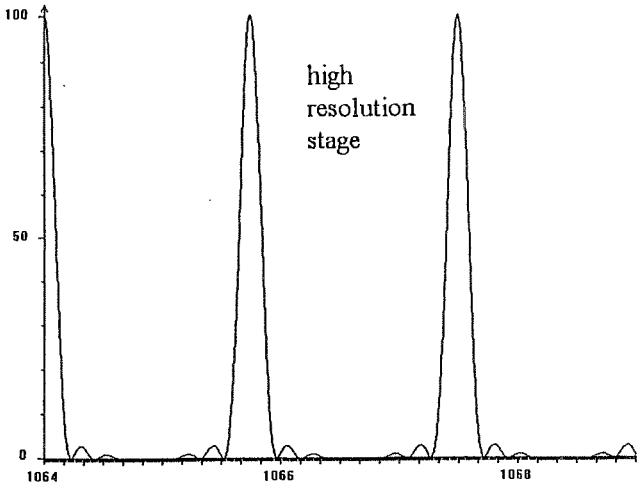

Fig. 6

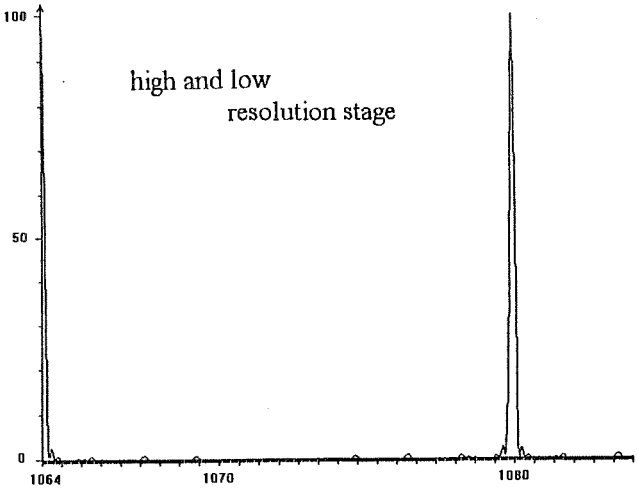

Fig. 8

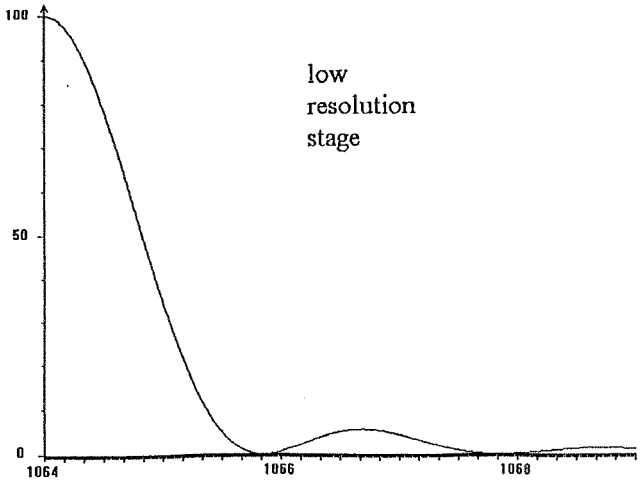

Fig. 7

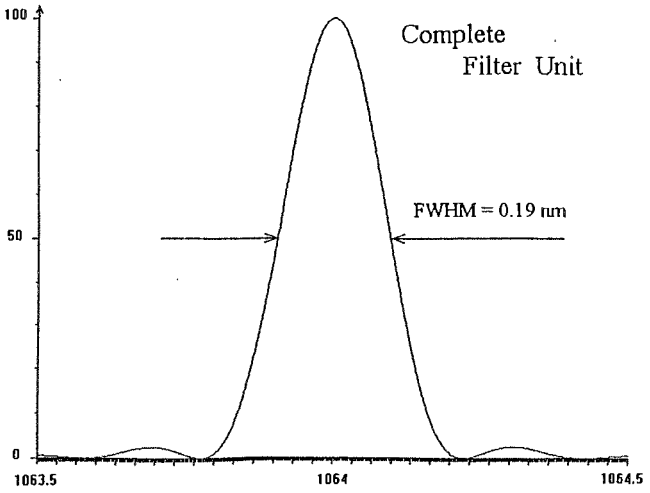

Fig. 9

LASER TECHNOLOGY DEVELOPMENT

Chairperson : Karel Hamal

LASER FOR TWO COLORS LASER RANGING

J. Gaignebet, J.L. Hatat, C. Lucchini
OCA/CERGA Ave N. Copernic F. 06130 GRASSE - France
Tel. (33) 93405337 Fax (33) 93405333

We are implementing a two color laser ranging equipment where the differential flight time between the two colors is determined by the use of a streak camera.
In the process of developing this station new concepts of streak camera use and laser pulse handling were conceived.
This paper will explain our ultimate ideas for the optimization of laser pulses, needed in two color laser ranging using a streak camera.

STREAK CAMERA EQUATION

$$\sigma_D^2 = \frac{(0,15)^2}{N}\left[\sigma_M^2 + A^2\left(\frac{\sigma_{0\lambda_1}^2 + \sigma_{\lambda_1}^2}{n_1 Q_e \lambda_1} + \frac{\sigma_{0\lambda_2}^2 + \sigma_{\lambda_2}^2}{n_1 Q_e \lambda_2} + \sigma_S^2\right)\right]$$

Where :

σ_D is the rms error of the corrected distance in mm
N is the of measurements averaged (N = 1 in our case)
O.15 = c/2 in mm ps^{-1}
σ_M is the rms error of the round trip flight time measurement in picoseconds.
A is the sensitivity of the two color measurement (varies from 10 to 50 and is determined by the couple of wavelengths adopted)
$\sigma o\, \lambda_i$ is the intrinsic streak camera limit at λ_i(two ps with our SC)
λ_i is the contribution of the laser pulsewidth at λ_i (0.4247 FWHM)
n_i is the number of photons reaching the photocathode at λ_i
$Qe\lambda_i$ is the quantum efficiency of the streak camera photocathode at λ_i
σ_S is the rms residual error of the streak camera due to non linearities and calibration uncertainties.

For given A, N $\sigma o \lambda_i$ we could compute the number of photons n_i to be collected in order to reach a projected accuracy.

This number is increasing almost as the square of the pulsewidth when they are larger than 3 ps. For pulses shorter the decrease slows down and is negligible for pulsewidth under 2 ps (FWHM). With such pulses n_i is minimized to the level imposed by the $\sigma_O \lambda_i$ of the streak camera resolution.

The generation of picosecond pulses is technically possible but two main limitations limit their utility :

a) the pulse is broadened by its travel through the atmosphere.

b) energy per pulse is limited to avoid optical damage.

PULSE BROADENING

The spectral bandwidth of a short pulse could be expressed by the following relation :

$$\Delta\lambda = \frac{c\Delta\nu}{\nu_0^2 - \frac{\Delta\nu^2}{4}} = \frac{c\Delta\nu}{\frac{c^2}{\lambda_0^2} - \frac{\Delta\nu^2}{4}}$$

At the Fourier limit $\Delta\nu \cdot \tau \cong 1$

$$\Delta\lambda = \frac{\frac{c}{\tau}}{\frac{c^2}{\lambda_0^2} - \frac{1}{4\tau^2}} = \frac{c}{\tau\left[\frac{c^2}{\lambda_0^2} - \frac{1}{4\tau^2}\right]}$$

where

$\Delta\lambda$ is the spectral bandwidth
υo is the central frequency
$\Delta\upsilon$ is the frequency bandwidth
τ is the pulsewidth
λo s the central wavelength

The Fourier limit $\Delta\nu \cdot \tau \cong 1$ is difficult to reach in practice because it means the full use of the crystal bandwidth and mode locking of all the longitudinal modes. In practice most of the lasers reach a merit figure of $\Delta\nu \cdot \tau \cong 3$.

In this case the formulae is :

$$\Delta\lambda = \frac{3c}{\tau\left[\left(\frac{c}{\lambda_0}\right)^2 - \frac{9}{4\tau^2}\right]}$$

The broadening is given by the equation :

$$\Delta\tau = R_\lambda\left(\lambda_0 - \frac{\Delta\lambda}{2}\right) - R_\lambda\left(\lambda_0 + \frac{\Delta\lambda}{2}\right)$$

with :

$$R_\lambda = \int_0^r \frac{n_2 - 1}{c} dz$$

where :

$\Delta\tau$ is the pulse broadening
R is the delay given by the atmosphere
r is the range

At the end :

$$\theta = \sqrt{\tau^2 + \Delta\tau^2}$$

where θ is the returning pulsewidth.

These curves 1 to 6 are giving the pulsewidth received for a given emitted one, for three different wavelengths, (YAP fundamental, doubled and doubled Raman downshifted in hydrogen) for $\Delta\nu \cdot \tau = 1$ and $\Delta\nu \cdot \tau = 3$ for a double crossing of the atmosphere.

Three regimes are studied thereafter :

a) pulse in the 10 ps width

The broadening is negligible and the number of photons rather high (several hundreds)

b) pulses giving the minimum return pulsewidth.

In this case the emitted pulsewidth has to be around 2 ps at the Fourier limit and 3 to 3.5 ps for $\Delta\nu \cdot \tau \cong 3$.The number of photon decreases to several tens. No pulse processing is necessary but the emitted energy is already limited.

c) pulses emitted in the picosecond regime

the broadening is important and the number of photons needed is at the level reached by the 10 ps pulses. This limit could be turned out by pulse compression.

PULSE COMPRESSION

The pulse broadening could be corrected by pulse compression techniques at the receiver end. This could be done by two gratings for example.

This way opens a new possibility. The emitted pulse could be chirped, rather long and compressible at the picosecond level. In this case the recompression handles both the chirp and the broadening.
This allows very short pulses at the level of the streak camera (ps) with rather long emitted pulses (ns) and a reduced optical damage for a given emitted energy.

Furthermore the compression done by hardware has to be monitored for different pointing elevations.(variations of the atmosphere path). Hybrid compression partially hardware (mean correction) and software by a spectral dispersion of the returning light on the streak camera's slit overcome this suggestion.

The slope of the image of the slit is a representation of the residual broadening and could be corrected in the processing of the streak camera measure of the differential times of flights.

Time width at the reception

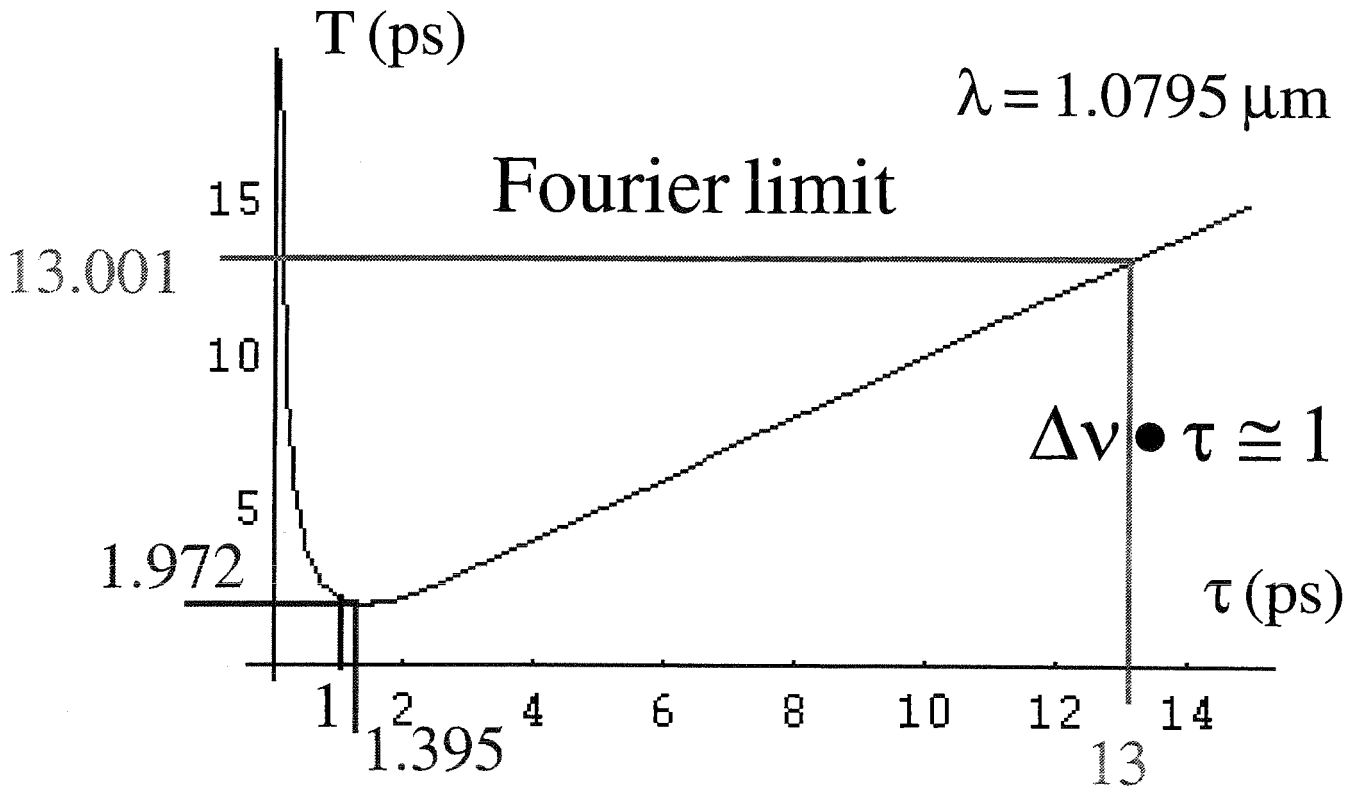

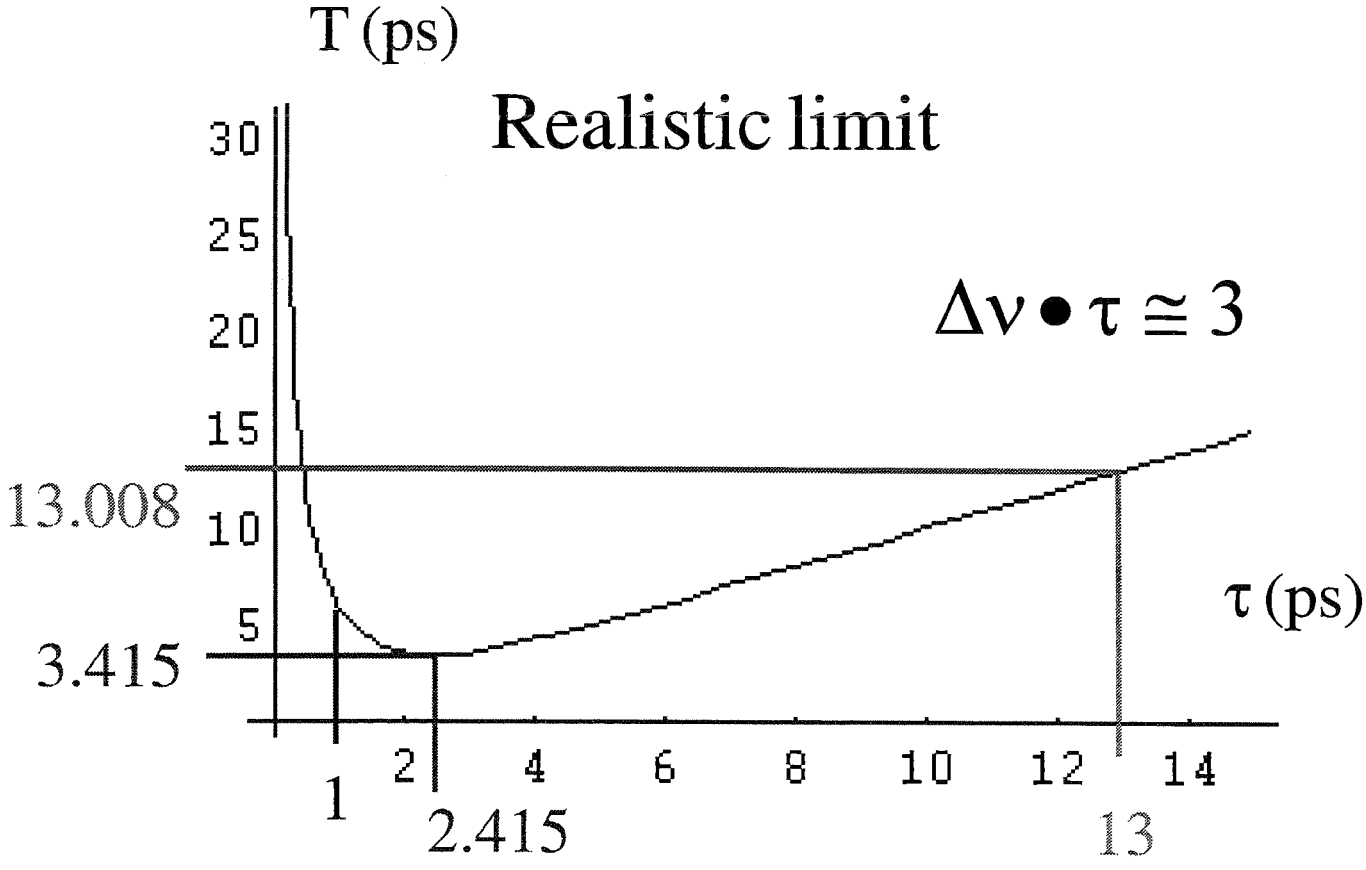

Time width at the reception

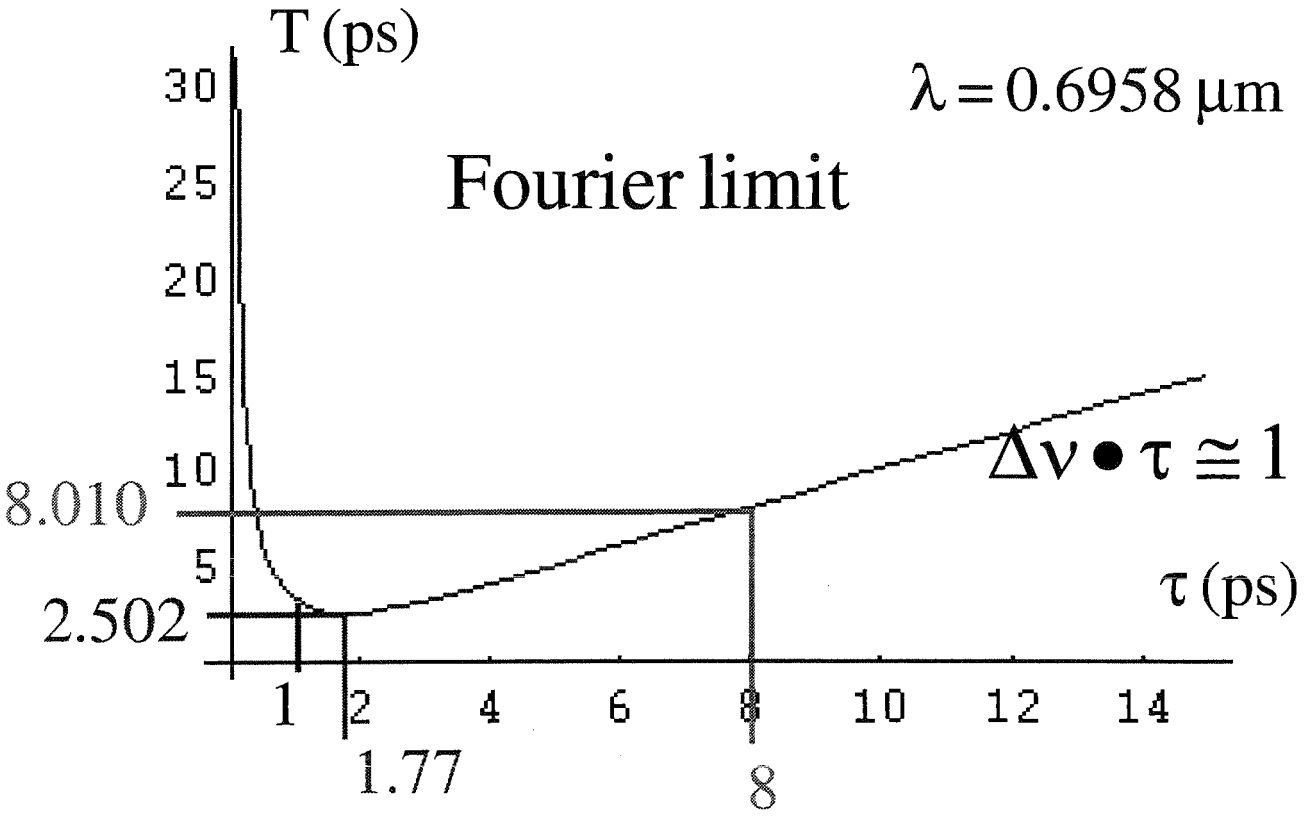

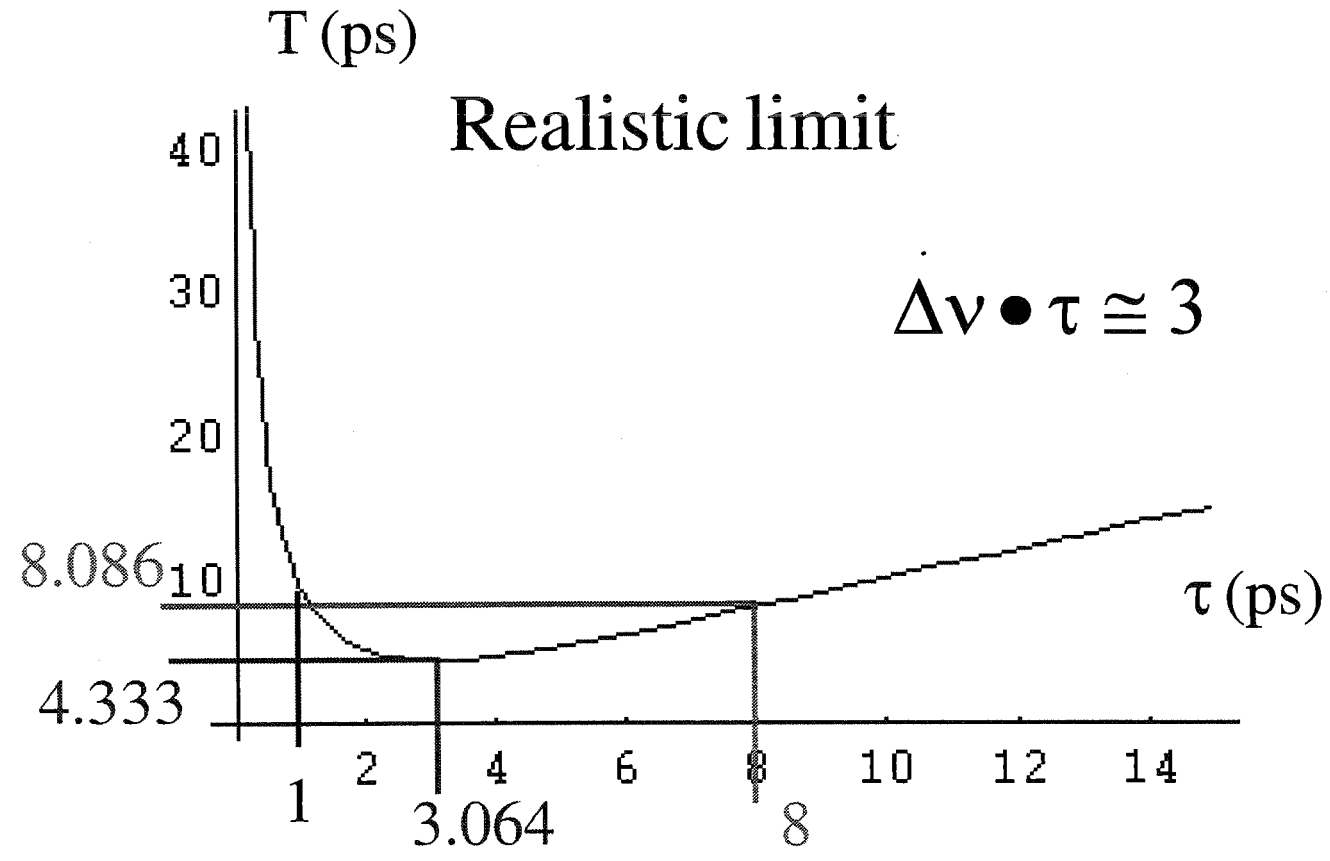

Time width at the reception

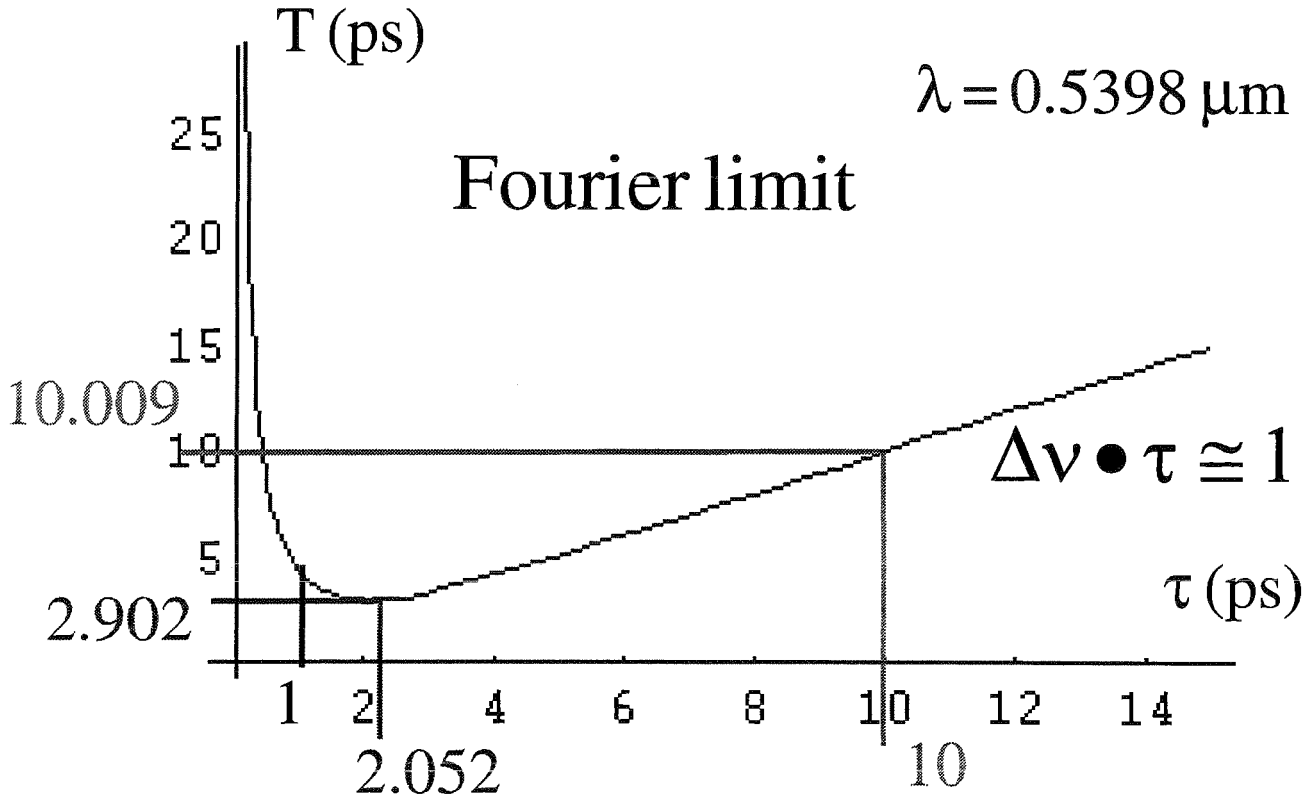

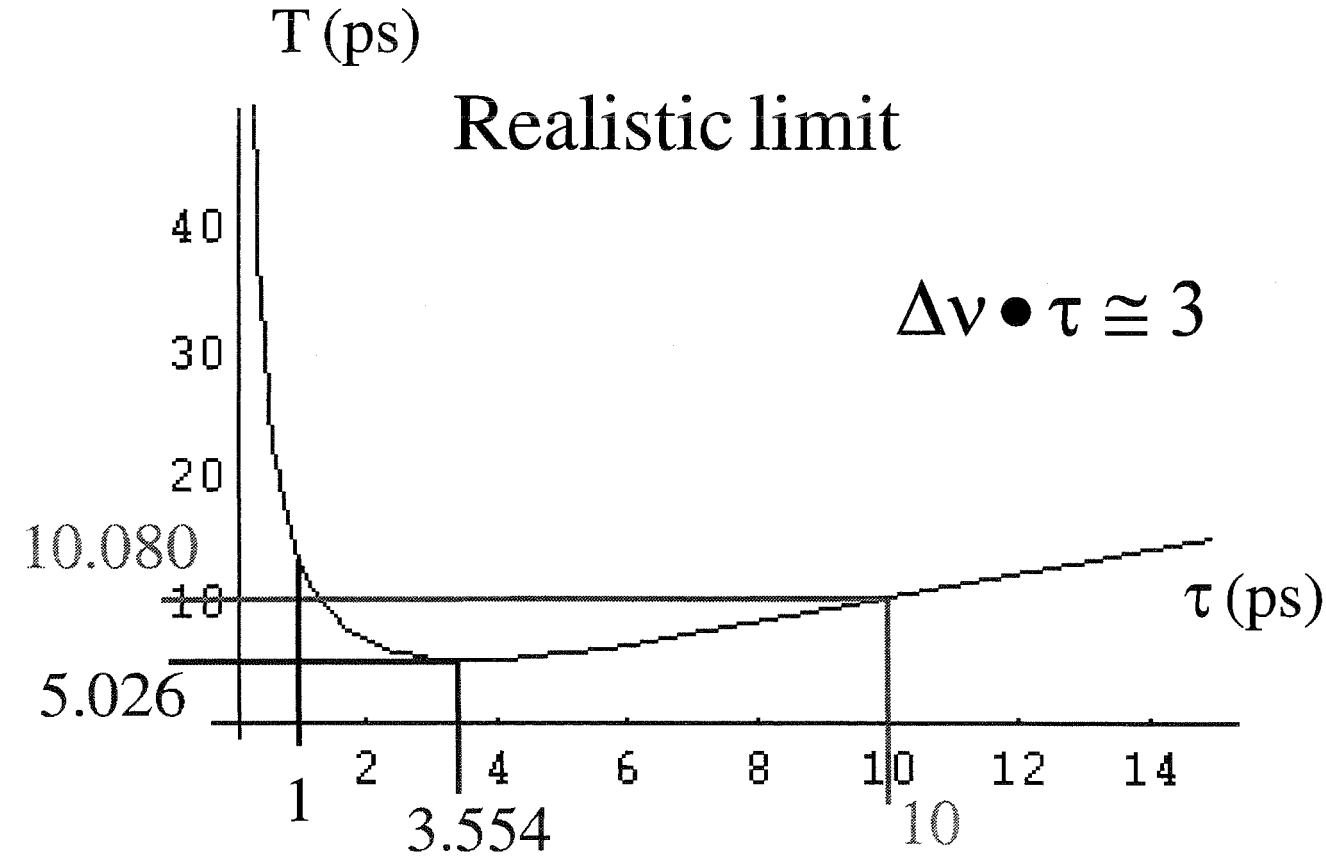

TWO WAVELENGTHS SOLID STATE LASER FOR MOBILE SATELLITE LASER RANGING STATION

A. Ferrario, C. Malvicini, F. Vannutelli
QUANTA SYSTEM Srl - Milano

P. Sperber
INSTITUT FUR ANGEWANDTE GEODASIE - D-93444 Kotzting

SUMMARY

Accuracy in the ground-to-satellite distance measurements are mainly limited by the laser performances.

The recent developments on Tunable Solid State lasers have opened the possibility to improve laser specifications in terms of peak power, pulse width, wavelength emission and repetition rate.

These improved laser performances are obtained with high efficiency allowing the construction of compact and low power consumption lasers as required for mobile stations.

In this paper we are reporting the design, the realization and the preliminary characterization of a Ti:Sapphire laser pumped by Nd:YAG laser developed under a Contract between Institut fur Angewandte Geodasie and Quanta System Srl to be utilized in the new mobile station.

A new mobile satellite ranging station is under construction at Institut fur Angewandte Geodasie.

This station is based on the utilization of a solid state laser with the specifications reported in Table I.

To meet the required specifications we have designed a laser system consisting of:

- a ps diode laser low power oscillator
- a Ti:Sapphire regenerative pre-amplifier pumped by Q-switched Nd:YAG laser
- two Ti:Sapphire amplifier stages pumped by Q-switched Nd:YAG laser
- a Second Harmonic Generator

The laser will be mounted in a container with the dimensions shown in Fig. 1.

This design is based on the following considerations:

- Laser crystals

  Only two laser crystals can be used for obtaining the required output wavelengths: Cr:LiSaF and Ti:Al2O3.

  Cr:LiSaF crystal could be a good choice because has a maximum gain at 850 nm and has a sufficient long upper laser level lifetime to be pumped by flashlamps but its thermomechanical characteristics rule out the possibility to utilize LiSaF crystal for this application requiring an high repetition rate laser.

- Oscillator

Cw Mode-Locked laser is the best solution for obtaining transform limited pulses in ps time domain. Ti:Sapphire mode-locked lasers are very well developed sources, but requiring a green (Argon or Nd:YAG doubled laser) laser for pumping. This solution is not viable due to its large dimension and power consumption. CW mode-locked Cr:LiSaF laser pumped by red diode laser could be a very interesting solution for this application. Very recently fs mode-locked Cr:LiSaF lasers pumped by 1 W diode laser have been developed, using Kerr-lens mode-locking effect. This solution is not useful for obtaining ps pulses because the pump laser power required is too high and not achievable with the present diode laser technology.

On the other hand, are now available AlGaAs ps diode lasers emitting pulses as short as 10 ps.

The other measured specifications of this device are reported in the Table II.

The pulses emitted by ps diode lasers are not transform limited, exhibiting a bandwidth of about 5 nm (FWHM). To reduce the emitted bandwidth we have used an interferential filter with 2 A of bandwidth peaked at 847 nm.

The peak power after the interferential filter is about 200 mW.

- Regenerative pre-amplifier

For obtaining peak power of few GW and reaching an amplification factor of 10^10 the only approach available is to use a regenerative pre-amplifier scheme with a gain of 10^8 and power amplifier stages. The optical layout of the regenerative amplifier is shown in Fig. 2.

The laser pulse emitted by the diode laser oscillator and filtered by the interferential filter is injected in the regenerative pre-amplifier stage using a thin film polarizer.

A two lenses beam expander is used for matching the ps diode laser mode to the regenerative amplifier mode cavity. A 60 dB isolator is used to avoid back reflection to the diode laser. The laser pulse amplified by regenerative amplifier is exctracted, rotating the beam polarization by a Pockels cell.

The exctracted beam with an energy of 1 mJ is then amplified by two three-passes amplifier.

The Ti:Al2O3 crystal is pumped by the Second Harmonic of the Nd:YAG laser (Figg. 3 and 4) with a fluence of 2 J/cm² and a repetition rate of 15 Hz. The total gain is 10^8 and the output energy at 847 nm is 1 mJ and the pulseiwdth is 15 ps as measured by an optical autocorrelator.

The mechanical layout of the regenerative amplifier stage is shown in Fig. 5.

- Amplifier stages

Two Ti:Al203 aplifier stages pumped by Nd:YAG Q-switched laser are used to obtain a total amplification factor of 60. The Ti:Al203 crystals (dimensions 10x10x25 mm3) are pumped at a fluence of 3 J/cm² and to exctract the stored energy we have used three passes amplifier configuration as shown in Fig. 6.

The output energy at 847 nm wavelength is 60 mJ per pulse and the pulse duration is 20 ps.

Then the output beam is sent into a type I phase-matching BBO crystal 10x10x5 mm3 of dimensions converting 50% of the input pulse in the Second Harmonic Frequency (423.5 nm).

The laser specifications as preliminary measured are shown in Table III.

Further work is in progress for testing the final specifications.

TABLE I

Solid State Laser Specifications

- Wavelength emission	: 847 nm and 423.5 nm
- Linewidth	: 0.2 nm
- Pulsewidth	: ≤ 25 ps
- Energy/pulse	: ≥ 30 mJ at 847 nm ≥ 30 mJ at 423.5 nm
- Energy stability	: 8% rms
- Repetition rate	: 15 Hz fixed
- Transverse Mode	: $M^2 \leq 1.5$
- Beam diameter	: 10 mm
- Beam divergence	: ≤ 0.4 mrad
- Beam pointing stability	: ≤ 0.2 mrad
- Laser Dimensions	: optical bench 1600 x 1000 mm^2
- Electrical consumption	: ≤ 7 KW

TABLE II

Ps Diode Laser Specifications

Peak power	: ≥ 5 W
Pulsewidth	: < 10 ps (FWHM)
Linewidth	: ≤ 5 nm
Repetition rate	: up to 100 KHz
Beam diameter after the collimation lens)	: 2 mm
Beam divergence	: 2 mrad

TABLE III

PS Ti:Al2O3 laser

Preliminary Specifications

- Output wavelengths	: 847 nm and 423.5 nm
- Linewidth	: 0.4 nm
- Pulsewidth	: 20 ps
- Energy/pulse	: 30 mJ at 847 nm 30 mJ at 423.5 nm
- Energy stability	: ± 10% at 847 nm ± 15% at 423.5 nm
- Repetition rate	: 15 Hz
- Beam diameter	: 8 mm
- Beam divergence	: 1 mrad
- Beam pointing stability (1°C temperature stabilization)	: ± 100 µrad
- Laser Dimensions	: 1600 x 1000 mm²
- Electrical services	: 380 V, 3 phases, 5 KVA

STREAK CAMERA SYSTEMS

Chairperson : Ivan Prochazka

RESULTS of THE STREAK-CAMERA-BASED-RANGE-FINDER and NEWLY DEVELOPED STREAK CAMERAS

Hitoshi Suzuki, Hamamatsu Photonics K. K., 812 Jokocho, Hamamatsu city, Japan

Tel:+81 53 435 1214, Fax:+81 53 433 7957, E-mail: PXI10622@niftyserve.or.jp

1.Introduction

There has never been a laser range finder to measure long distance of from a several tens km to around 100km with the resolution of 10^{-7}.This sort of ranging system has been needed to measure geodetic movement.To realize such a ranging system it had been decided to employ two picosecond streak cameras, a modelocked Q-switched Nd:YAG laser producing three different wavelengths and an optical clock as a time marker. Three years had been spent in designing, constrncting and checking the laser range finder.After that the measurement in the area of Suruga Bay had started.

2. System Design

As a pulsed light sourse we have employed a CW modelocked Q-switched Nd: YAG laser(Quantronix Model 416) with an SHG, a THG crystals and a single pulse selector. One of the reasons why it was chosen is that it delivers power level of not only being enough for the measurement but also being safe to naked eye at target sites.All three wavelength pulses, 1064nm, 532nm and 355nm, emerge simultaneously at the repetition rate of 500Hz and have pulse width of around or less than 100ps and have peak power of 100, 100 and 50 kw respectively.A block diagram of this system is shown in Fig.1. A portion of 532nm optical pulse is delivered to streak camera A thorugh the optical fiber. Its photoelectrons together with those of optical clock light pulse are swept in time and displayed on the phosphorscreen of streak camera A.The displayed streak image is read by an SIT camera and then stored into a frame memory of image processor A.

The telescope system consists of a sending telescope and a receiving telescope. The sending telescope emploies a 15cm-diameter Newtonian mirror with F number of 5.0.The receiving one emploies a 40cm-diameter Cassegrainian mirror with F number of 3.35. A

computer controlled beam-steering mirror is used to act as a periscope so that this system measures a several baselines and keep the hight of the beams higher than those of staffs. The returning optical pulses are collected by the receiving telescope and delivered to a 60 degree prism, where three wavelength pulses are spatially dispersed by it and then positioned at the input slit of streak camera B together with the optical clock pulse. The temperature stabilized quartz crystal is tuned to 10MHz with a short term stability of 10^{-9} . The output is split and delivered to a frequency synthesizer for making the laser modelocked and Q-switched, to another frequency synthesizer for feeding the optical clock pulse generater on 1GHz electrical clock signal and to a time synthesizer for it to send out a trigger signals to each of the two streak cameras.

In Fig.2 the measurement principle of this system is shown.Time difference between the optical clock pulse and outgoing pulse is measured by streak camera A.Time differences of the optical clock pulse and the returning pulses are measured by streak camera B.From stored streak image in each of the image processors, the exact instants of each signals peak are calculated by a personal computer based on the center of gravity method applied to temporal profiles corresponding to each wavelength.Also sweep nonlinearity in a streak image is corrected carefully.When streak sweep speed of 1.5ns full scale is used, timing resolution of 10ps corresponding to a distance accuracy of 3mm has obtained for 33seconds integration, i.e.16500 shots integration of laser pulses.

3. Results

The three color correction method had been proposed because the method doesn't have to take atmospheric parameters such as temperature, pressure and water vapor into consideration. However owing to the large correction coefficients, which multiply the time difference between the arrival timing of optical pulses having different wavelength each other, even small measurement errors had brought multiplied large errors, accordingly deteriorating the overall resolution.The correction coefficients in typical condition are 168 and 78 for a wavelength set of 1064nm, 532nm and 355nm.

Due to the above mentioned reason alternative method had been discussed and the single color method was adapted sinse measurement accuracy of $3\times$ 10-7 was thought to be attainable with the condition that temperature, pressure and humidity fluctuations are limited to within 0.35℃ , 1.3hPa and 32% respectively.In order to achiev these conditions, the following meteorological consideration was made.

The observatory and three target sites had been chosen to be close to the shoreline and to provide an altitude of a several hundred meter . Suruga Bay has a depth of deeper than 1500m so that it provides a huge heat capacity.According to the study [1] as long as a sea breeze is present, the isothermal contour plane above the deep bay can be treated as uniform and flat. To analyze the altitude dependence of the temperature, the pressure and the water vapor a model is made, in which all three atmospheric parameters are treated to be decresed exponentialy as shown in below.

$$T=T_0\exp(-K_TZ),\ p=p_0\exp(-K_pZ),\ w=w_0\exp(-K_wZ)$$

where K is the lapse rate and Z is altitude. To find those lapse rates in the arguments much of meteorological measurement was done. Finally it was found that at the sunset time when temperatures of different altitudes invert each other moderately, the temperature lapse rate becomes adiabatic and is safely extrapolated over the entire altitude range along the ray trajectory.Kp was also found and Kw is determined by the vapor pressure table.

In Fig.3 typical results obtained by single color method at 1064nm is shown.Before August of 1989 the adiabatic correction was not made thoroughly, so the accuracy was poor.As a whole, the change in the baseline AB and AC is much smaller than the expected change of less than 0.5cm per year.The measurement is still underway.

4.Modified two color ranging method[2]

When measuring some distance, say a round trip of 100km , with an accuracy of $\pm 1 \times 10^{-7}$, the allowable fluctuations of atmospheric parameters for the single color ranging method are limited to ± 0.1℃ for temperature, ± 0.3hPa for pressure and $\pm 12\%$ for humidity. This makes time and area to be measured very limited.While the three color ranging method requires quite precise accuracy in measuring the arrival timing differences among three pulses. It is ± 0.1ps for a wavelength set of 1064nm, 532nm and 355nm.

The modified two color ranging method has been proposed to bring more practical one . With this method three atmospheric patameters of temperature, pressure and humidity must be measured but with more moderate accuracy.Instead the difference of arrival timing of two pulses must be measured also with more moderate accuracy. To measure a round trip of 100km with an accuracy of $\pm 1 \times 10^{-7}$, the accuracies of ± 1.4 ℃ for temperature, ± 80 hPa for pressure, $\pm 5\%$ for humidity and ± 0.9ps for a spacing of two peaks of light pulses of 1064nm and 532nm are required. A formula which gives measured

distance D with the method follows.

$$D = \{ti + Aij\ (\rho s, \rho w)\ \cdot \delta tji\}\ \cdot C$$

$$Aij(\rho s, \rho w) = (\alpha i + \beta i \cdot \rho w/\rho s)/\ \{(\alpha i + \beta i \cdot \rho w/\rho s) - (\alpha j + \beta j \cdot \rho w/\rho s)\}$$

where C : the speed of light in vacuum, ti : propagating time of light pulse of wavelength i ρ s: dry air density, ρ w: water vapor density, α i and β i : coefficients depending only wavelength, δ tji : propagating time difference of two light pulses having different wavelength i and j each other.This method is now in use. However it would take some time to obtain a certain result.

5. Newly developed streak cameras

5-1.Universal streak camera

When a streak camera is used it is usually coupled with a readout camera to capture streak image with short lifetime on a phosphorscreen and its output is sent to a computer where streak image is stored and analyzed.Through the measurement mentioned earlier many things that should be improved has been made clear concerning not only a streak camera itself but also a readout system.Newly developed streak camera named C5680 and its readout system have been designed based on more advanced technologies compared to those used for the former Hamamatsu made streak cameras.

Non-linearity of streak sweep speed, which originates from non-linearity of deflection voltage and geometric distortion of a readout camera, makes the measuring accuracy of spacing between pulse peaks worse.Sinse the deflection sensitivity of streak tube has been improved to be twice as goog as that of a former streak tube, it has brought more simplified sweep circuit and shortening of wiring, resulting in decreasing sweep speed non-linearity. The employment of a CCD camera, because it has no geometric distortion, has contributed to decrease overall non-linearity of sweep speed also.With a former streak camera system

a sweep speed non-linearity was within $\pm$ 3 percent, it has now become much easier to have that of within $\pm$ 0.5 percent for C5680.

Triggering jitter should be considered when streak sweep is done many times in a measuring period to integrate streak images either on a phosphorscreen or on a frame memory to have a streak image with better S/N ratio.Trigger circuit of C5680, with which triggering timing is determined by variable threshold voltage level, emploies less elements

and a faster IC than those of the former models.Owing to it jitter in FWHM has been improved from 10 to 15 ps of the former models to better than 4.5ps.

For a readout system two types of camera have been developed. The one emploies a non-cooled CCD chip with a tapered fiber for coupling it with the phosphorscreen.This camera outputs video signal and is suitable for a streak camera operating in synchroscaning mode.The another, named C4880, emploies a cooled CCD chip with 1000 times 1018 pixels. This is coupled with a phosphorscreen via lenses.Because it has very low dark current noise and readout noise and because its dynamic range is much wider than non-cooled CCD camera or SIT camera, it gives the streak camera system photon-counting level detectability and wider dynamic range.For reference dynamic range of C5680 is 6bits to 10 bits, very much depending on sweep speed, and those of non-cooled CCD camera , SIT camera and C4880 are 8bits, 7bits and 12 bits or more respectively.As a computer for storing and analyzing streak image, both Macintosh based and IBM compatible PC based system are available, having a 16 bits depth frame memory.

To use a streak tube with a two-stage MCP gives a streak camera system better photon-counting detectability.Even with a streak tube having a single stage MCP photon-counting is possible. However it takes much longer time before getting a streak image of same S/N ratio as that of obtained by a streak camera system with the two-stabe MCP streak tube, because the probability of appearance of a bright spot orignated from an incident photon on a phosphorscreen becomes larger by using a two-stage MCP.The streak tube has been available on request even for the former models.

Time resolution of C5680 in single sweep mode hasn't been improved, remainimg same 2ps as those of the former models.Because to realize better than 1ps time resolution needs much more advanced streak tube and sweep circuit, it has resulted in a streak camera qualified to use of shorter than a several hundreds picoseconds of full scale region.

5-2.Femtosecond streak camera

A femtosecond streak camera has been developed, whose time resolution is better than 200 fs.In order to realize a streak camera having time resolution in the order of 100 fs, a completely new streak tube and a deflection circuit have been designed and realized.

A key to let a streak tube have better time resolution is how to minimize the temporal broadening of a photoelectron bunch in the streak tube, which is generated by an incident photon bunch at a photocathode. Accelerating the photoelectrons in a period as short as

possible to top speed brings minimized broadening of the bunch.To do so a high voltage pulse of -5kV is added to a photocathode biased at -9kV, while voltage of an acceleration mesh is kept at 0V.With this method the electric field just behind the photocathode is achieved to 8.75kV/mm.Sinse the -5kV pulse is added only when the streak camera is triggered, the probability of discharge between the photocathode and the mesh to occur and increase of dark current noise due to the very strong electric field is quite low. Another key is to employ a Meander type traveling wave deflector. Due to its wide bandwidth up to 900MHz high speed deflection voltage can be applied and it shows the deflection sensitivity of 58mm/kV.Transmission speed of applied deflection voltage on the deflector with respect to a direction of the tube axis is designed to be same as that of photoelectron bunch.This makes brodening of the bunch with respect to a direction perpendicular to the tube axis minimum, thus resulting in less temporal broadening on a phosphorscreen compared to that produced by a conventional deflector.

An impeadance matched deflection circuit has been developed, which consists of an avalanche pulser, gaussian filters, coaxial switches and a push-pull transformer. In order to minmize jitter of the avalanche pulser, avalanche transistors are carefully classified according to each breakdown voltage and trigger delay time and chosen.This deflection circuit provides sweep speed of 8.76 times 10^8 m/sec on a phosphorscreen with the jitter of around 5ps in FWHM.

In Fig.4 a temporal profile of light pulses from a modelocked CPM ring dye laser is shown.It should be noted that the jitter of a timing electronics of a pulsed laser ranging system would be required to be at least less than 20ps if this type of ultrafast streak camera is adapted to the system, because this streak camera named FESCA-200 has a full scale of 20ps at the fastest speed.

6.Conclusion

A sreak camera based range finder had been built and the measurement to monitor geodetic movement is now underway. The method used is the single color ranging method with careful meteorological correction. A relative resolution of 3×10^{-7} has been confirmed.The modified two color ranging method has been proposed and the measurement using the method is also underway.

The author is grateful to the staffs of a project especially to Mr.Y.Warashina, Mr.A.Takeshima and Mr. I.Ogawa. In the project all of the jobs on the range finder has

been carried out. It should be made clear that this report was made based on the papers 3 and 4 in the following references.

7. References

1.F. Fujibe and T. Asai, "A detailed analysis of the land and sea breeze in the Sagami Bay area in summer", J. Meteorol. Soc. Jpn. 62, 534-550 (1984)

2.I.Ogawa, Y.Warashina, A.Takeshima, M.Takeichi, K.Ichie and Y. Mizushima, "Modified multicolor correction method for a long-range laser measurement with 10^{-7} accuracy", Appl. Opt. (to be published)

3.M.Takeichi, Y.Warashina, A.Takeshima, I.Ogawa, K.Ichie and Y. Mizushima, "Streak-camera-based long-distance range finder with 10^{-7} resolution., Appl. Opt., vol. 33, NO. 13 , 2502-2510, May 1994

4.Akira Takahashi , et al, "New Femtosecond Streak Camera with Temporal Resolution of 180fs", SPIE vol. 2116, 275-284

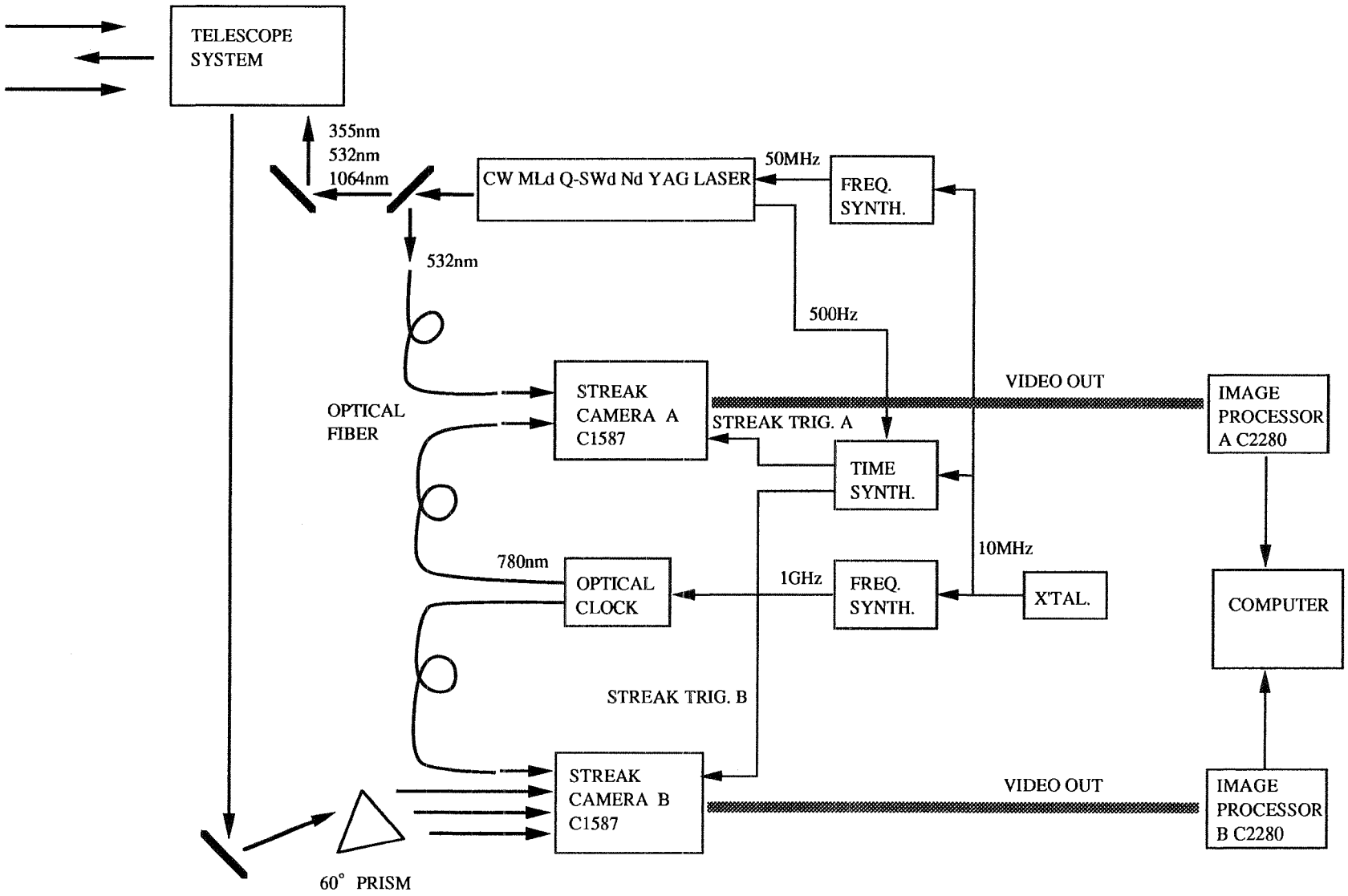

FIG.1 Simplified Block Diagram of The Streak Camera Based Range Finder

STREAK IMAGES OF SENDING AND RETURNING PULSES

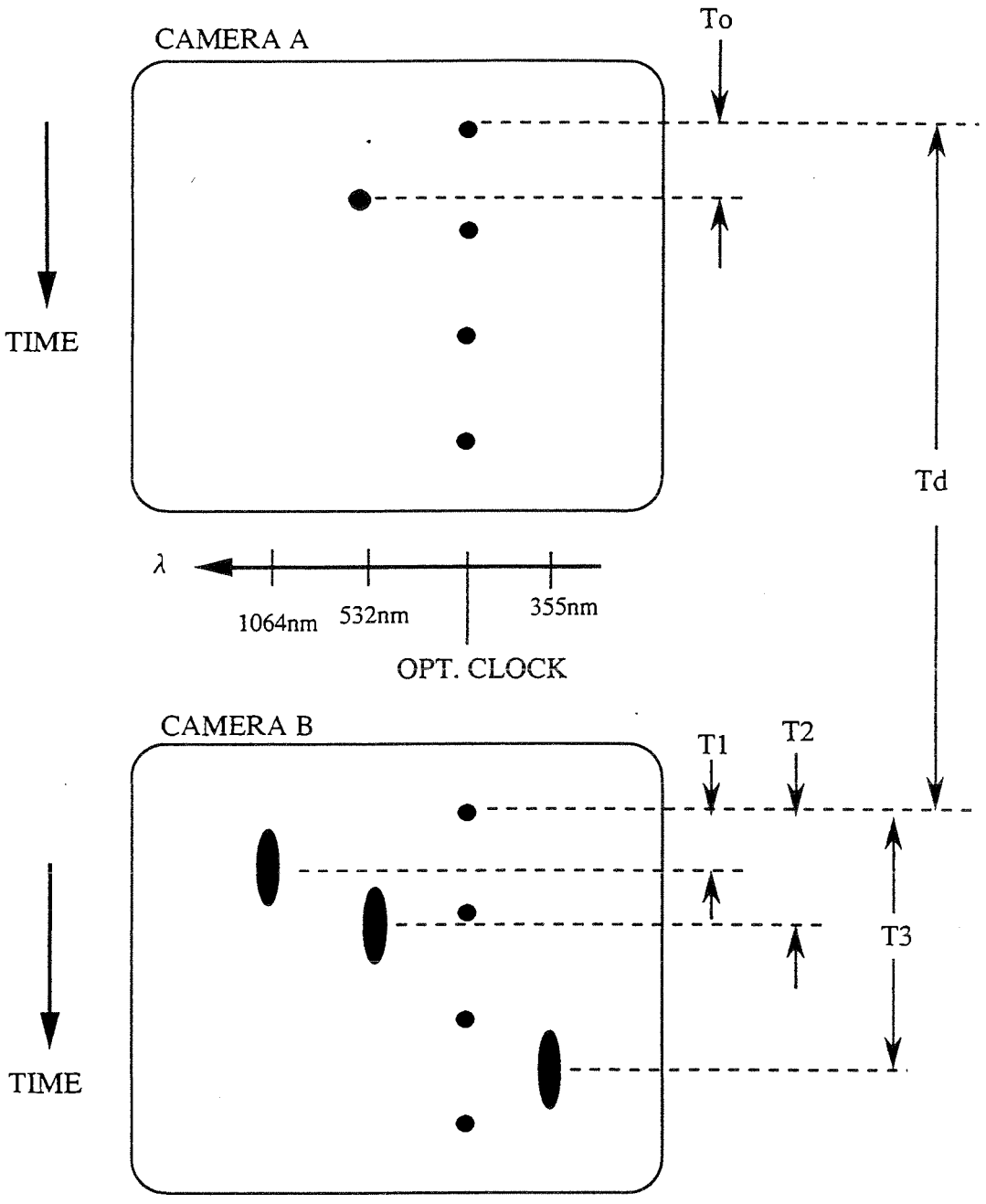

$$Tpi = Td - To + Ti \qquad \begin{array}{l} i=1 \text{ for } 1064nm \\ 2 \text{ for } 532nm \\ 3 \text{ for } 355nm \end{array}$$

FIG. 2 MEASUREMENT PRINCIPLE

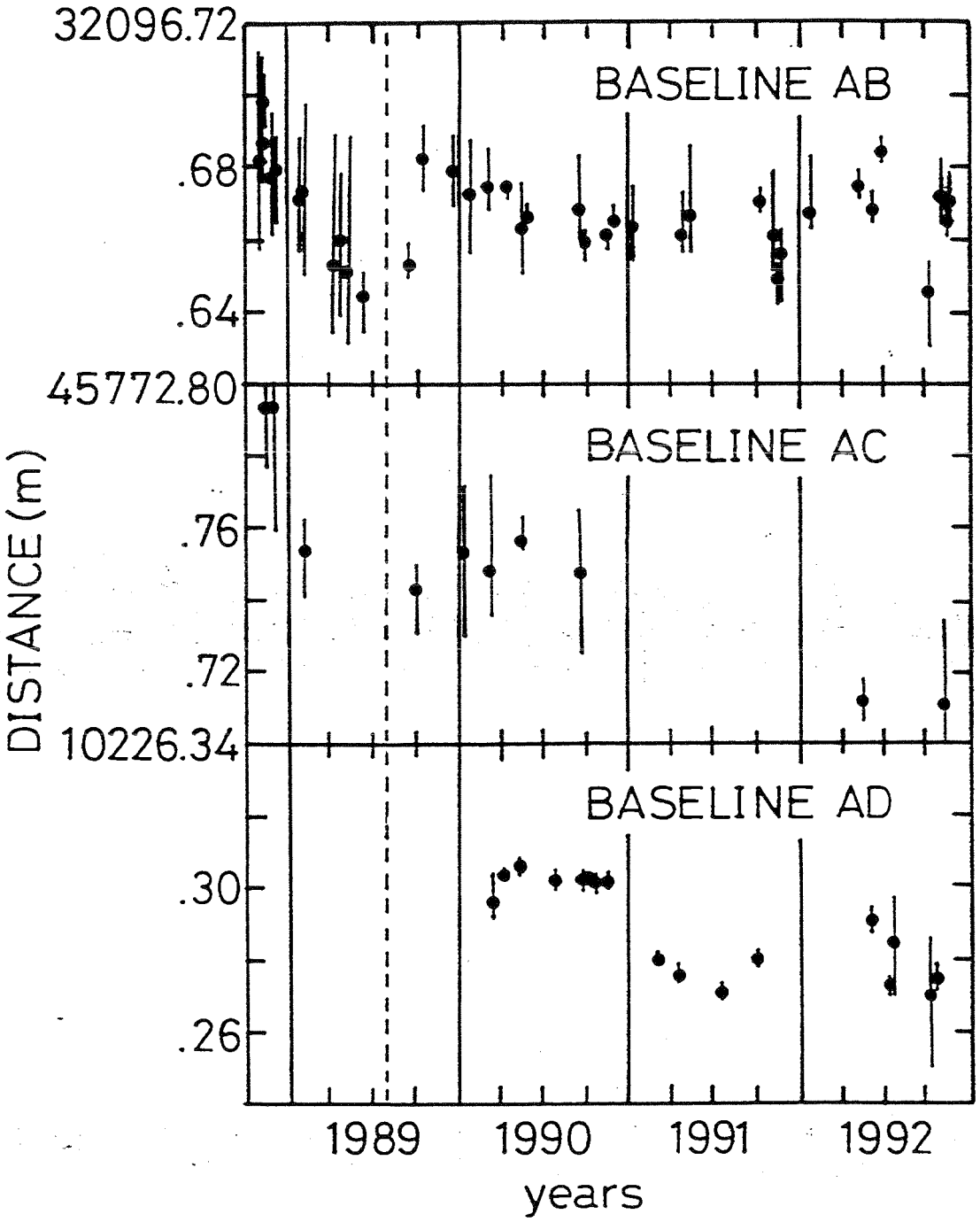

Fig.3 Typical changes in baselines AB, AC and AD over 4 years.

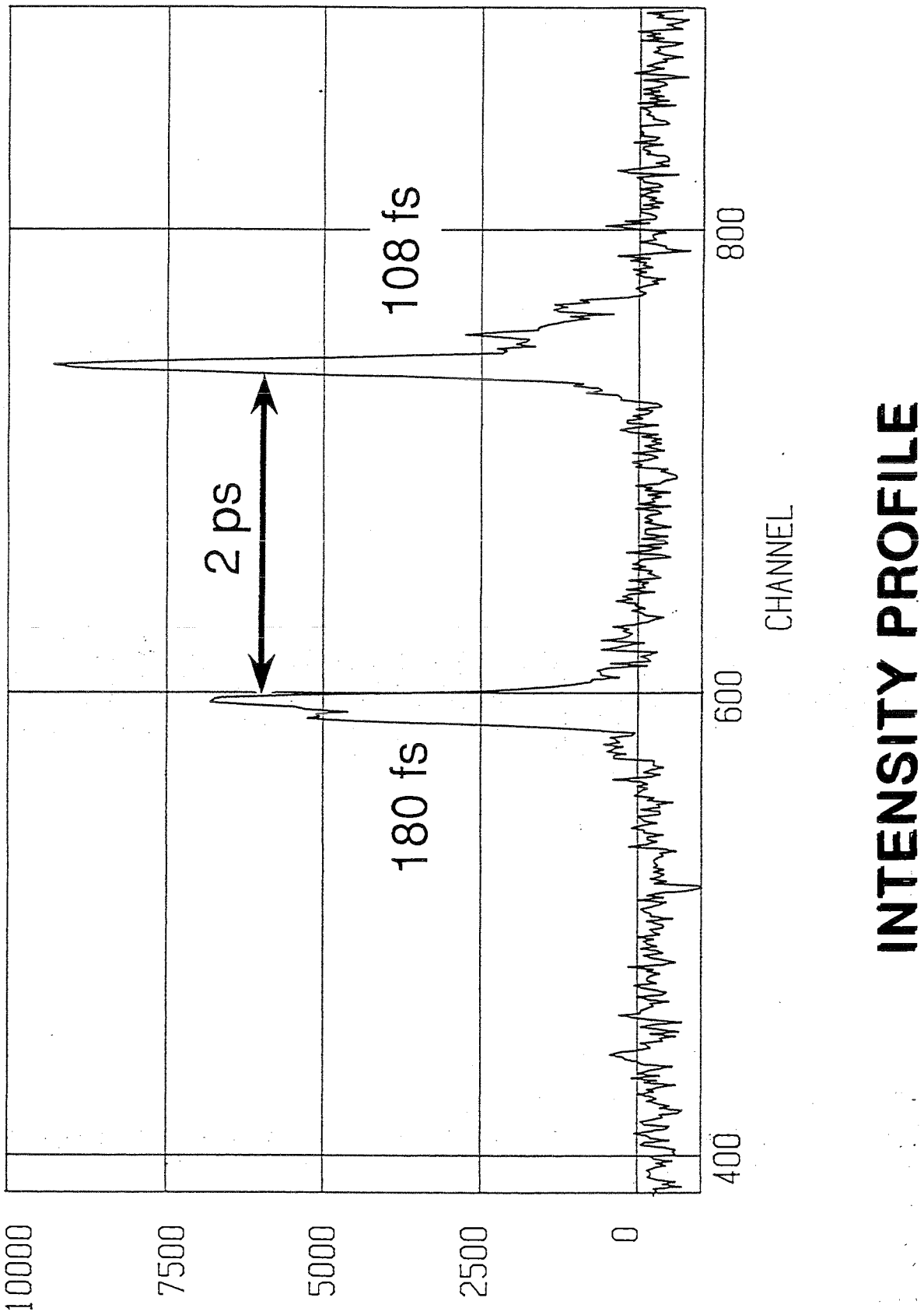

Fig.4 Temporal profile showing better than 200fs resolution

STREAK CAMERA

Calibration, distortions corrections, measurements

C. Lucchini, J. Gaignebet, J.L. Hatat
Equipe de Recherches Electro-optiques OCA-CERGA
Av. Copernic 06130 Grasse France
tel. : (33) 93.40.53.53, fax : (33) 93.40.53.33

We developed a system calibrating and correcting images from a streak camera for two color laser ranging. With the same system we make measurements of differential flight time between the two wavelengths (without and with spectral dispersion along the slit of the beams).

1. Calibration of the streak camera

Fig. : calibration experiment.

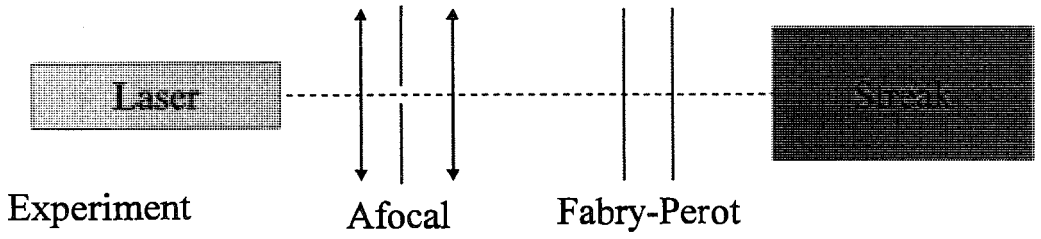

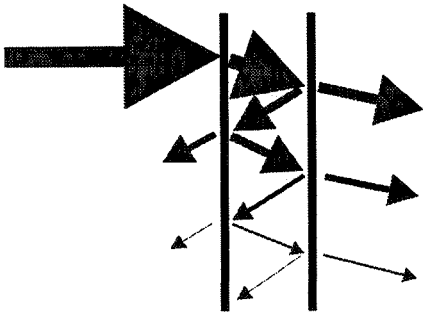

Light in Fabry-Perot

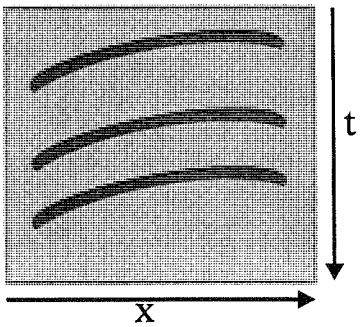

Typical image on the screen of the streak camera

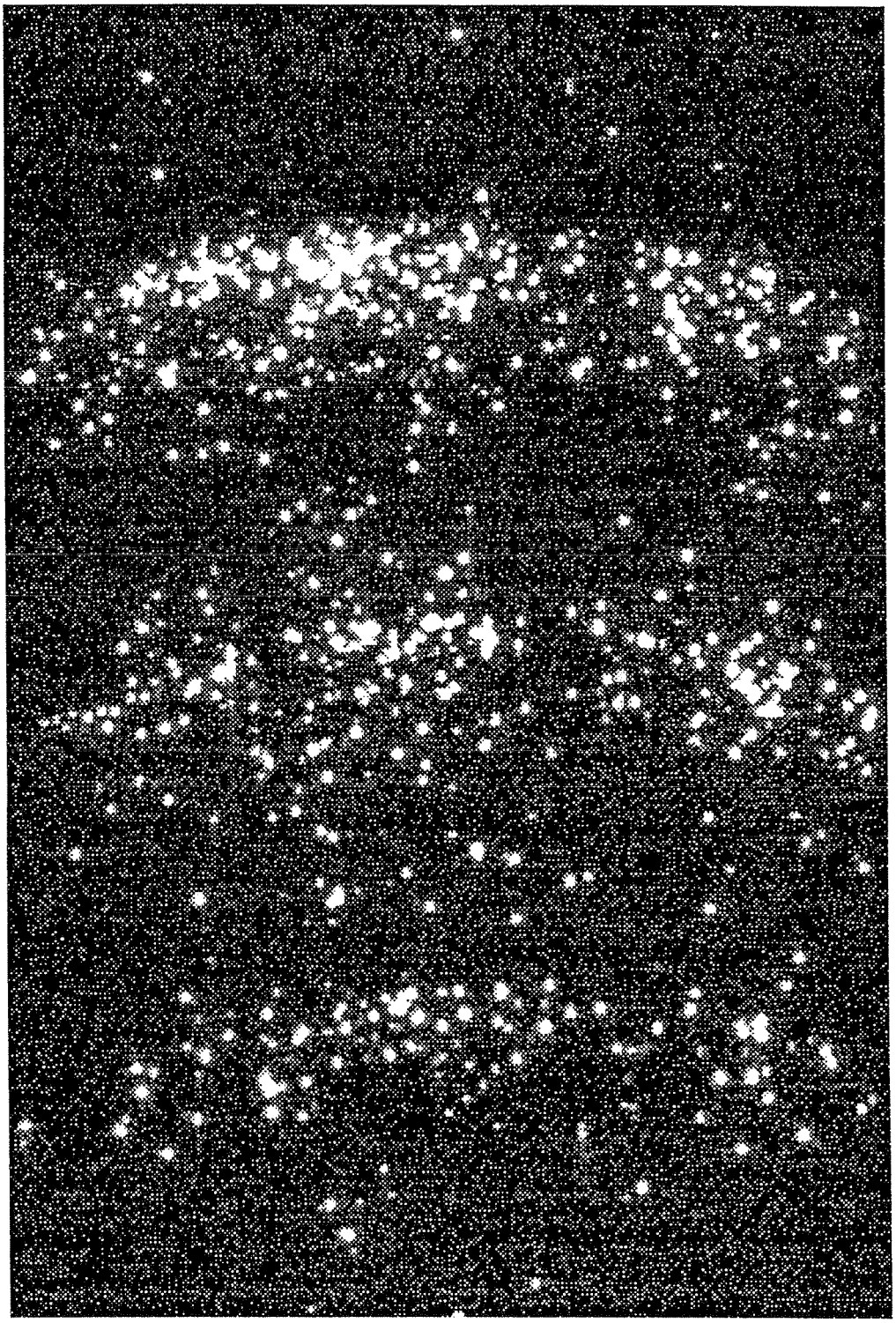

On the image (see previous page for a typical calibration image) there are three defects :

- non linearity

the streak is non-linear in time.

- curvature of the image

the transfer times of the photo-electrons are different in the middle and on the edges of the screen..

- tilt of the image

the slit is not perpendicular to the streak and the CCD camera coupled to the streak camera is not parallel to the slit.

2. Corrections

The first step before correcting is to determine the number of the stripes and to evaluate their position. Then we can start the corrections.

2.1. Curvature of the image

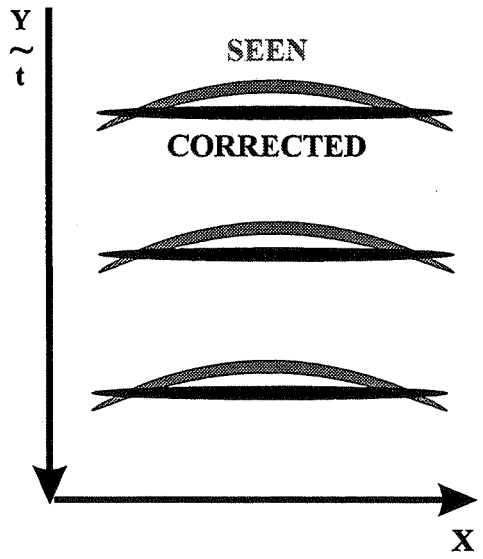

For each ray, we try to determine the best curve (a parabola) with the form like this : $y = ax^2 + b$, which fits the cloud of points and we measure the evolution of curvature in time by comparing with the others clouds and evaluating the third order polynomial which describe this evolution

Then, our software straights out the clouds using these equations

2.2. Tilt of the image

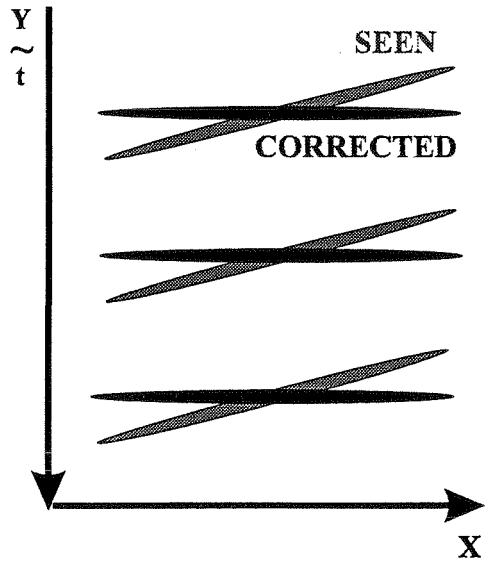

For each cloud, we measure the inclination with regard to the temporal axis and we evaluate the polynomial $y = px + b$ which fits this inclination.

We try to adjust the orientation of the slit and the CCD with respect to the streak direction to have p equals to zero.

2.3. Streak non linearity

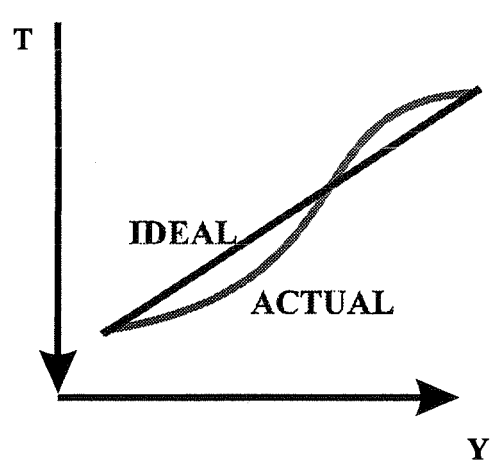

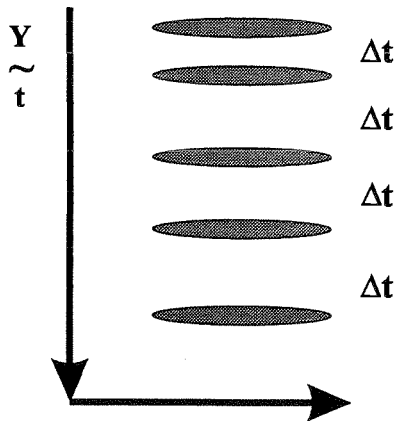

Δt = Thickness of a Fabry-Perot = 50 or 100 ps.

To correct this problem, we evaluate the third order polynomial that fits the evolution on the time axis.

Now we can calibrate the vertical axis Y in time knowing the thickness of the Fabry-Perot. After all these corrections, the screen is calibrated and we can do measurements.

3. Measurements

Now, dividing the screen in two parts (right and left) for each wavelength, we could measure the differential flight times by evaluating the distances between the two clouds corresponding to the two wavelengths, after a laser shot.

We could not only divide the screen in two parts but also spread spectrally each wavelength on its half slit using a grating. So we will see not straight images of the photo-electrons but tilted narrow pictures.

The reason is that : spreading the wavelengths (not totally monochromatic) in λ, we spread them in time on the streak camera, so now the clouds are very thin.

To make measurements, we have to evaluate the slope of these thin clouds and to measure distance between barycenters.

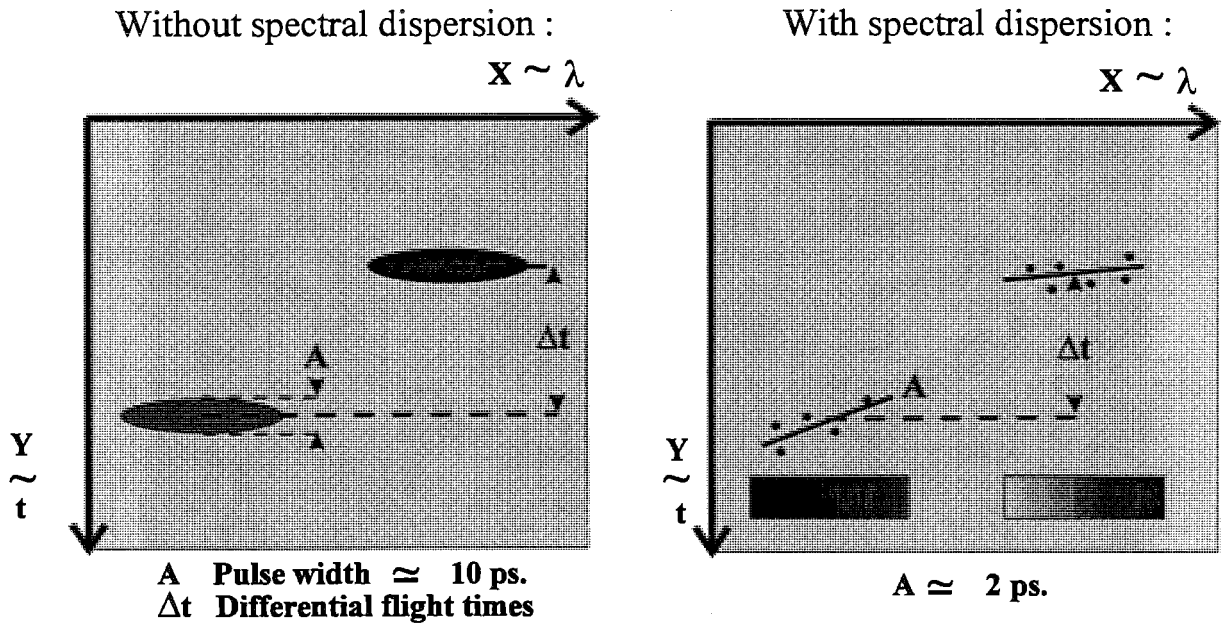

Fig. : theoretical images on the screen without and with spectral dispersion.

(See next page for a typical image not corrected without spectral dispersion).

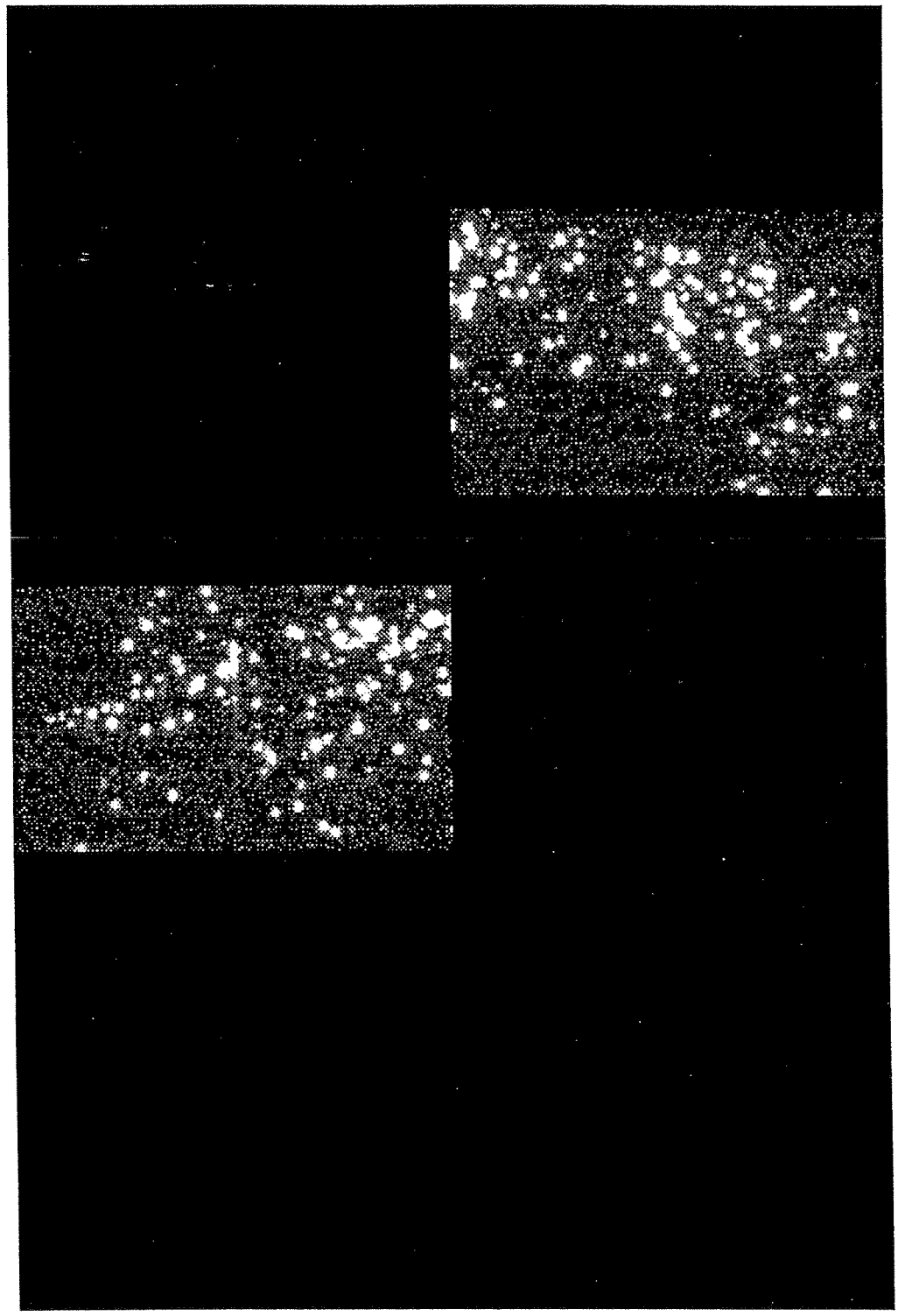

4. Conclusion

These operations enhance the streak camera resolution by reducing the biais on the measurement on the screen. The following formula shows the repartition of the error in the corrected distance measurement :

$$\sigma_D^2 = \frac{(0.15)^2}{N} \cdot A^2 \cdot \left[\frac{\sigma_0^2 + \sigma_{\lambda_1}^2}{n_{\lambda_1} Q_{e\lambda_1}} + \frac{\sigma_0^2 + \sigma_{\lambda_2}^2}{n_{\lambda_2} Q_{e\lambda_2}} + \sigma_S^2 \right]$$

with :

σ_D (mm) = rms error on corrected distance
$\sigma_{\lambda i}$ (ps) = 0.4247 * FWHM at λ_i
σ_0 (ps) = intrinsic resolution of the streak camera (2 ps)
$n_{\lambda i}$ = number of detector incident at λ_i
$Q_{e\lambda i}$ = quantum efficiency of the streak camera at λ_i
N = number of measurements (shots)
σ_s = unaccountable biais of the streak camera
A = sensibility factor of the two colors measurement

Our software permits to reduce σ_s near zero.

We have implemented this system on a PC (Compaq 486/50). We calibrate the streak camera in 11s and we can make a measurement on the differential flight times in 8s approximately.

This speed is too slow to work in real time on satellite but it demonstrates that the system works. Now we plan to enhance the speed using DSP systems.

References :

- J. Gaignebet : Streak camera; Geoscience Laser Ranging System, Phase B Final Report Volume 2 July 1990 Mc Donnell Douglas, Aerospatiale, Electro Optic Systems.
- C. Lucchini : rapport d'avancement #1 des travaux de thèse : télémétrie laser deux couleurs; April 1993 Aerospatiale, Centre National d'Etudes Spatiales, OCA-CERGA.

Measuring Atmospheric Dispersion Using A Synchro Scan Streak Camera

Ulrich Schreiber and Stefan Riepl

Forschungseinrichtung Satellitengeodäsie
Fundamentalstation Wettzell
D - 93444 Kötzting
Germany

Abstract

In today's laser ranging technology the influence of the atmosphere belongs to the dominating contributions to the error budget of measurements. In this paper a detection technique for atmospheric dispersion measurement is described. The measurements are carried out using the Wettzell Laser Ranging System WLRS [1], which is designed for satellite – and lunar laser ranging. The dispersion is determined by simultaneous ranging, using laser pulses of the fundamental and second harmonic frequency of a Nd:YAG laser. While propagating through the atmosphere, the frequency dependent refractive index of atmospheric gases causes a different path delay to laser pulses of both wavelengths. As the effect is very weak and the jitter of semiconductor devices is quite high, the calculated atmospheric corrections from the data, obtained with conventional techniques, need independent proof. So a streak camera with high temporal resolution with respect to the differential path delay between both echo pulses is adopted for this purpose. Dispersion measurements to a local ground target ($2.4km$ of optical path) have been carried out. The received signal was observed as a double peak, one corresponding to the infrared, the other to the green laser pulse. In these experiments a RMS of $10ps$ for the path delay between the received pulses was obtained.

1. INTRODUCTION

Streak cameras are, by now, known as the best devices in time resolved spectroscopy. The high time resolution is basically achieved by transforming temporal observation to spatial information. There have been several approaches to use streak cameras for atmospheric dispersion measurements [2], [3]. These efforts make use of it's single scan mode only, i.e. the electron beam is swept across the screen only once, when a laser pulse hits the photocathode. Although this technique offers the highest achievable time resolution, the available time window is very short and has to be known accurately. Therefore this technique still suffers heavily from trigger jitter problems.

Our design follows a proposal done by Abshire [4]. The streak camera is continuously operated in circular scan mode and the gating is only applied to the photocathode and microchannel plate. So the operation is compatible to conventional photon detection devices

and the gate width can be extended to more than $1\mu s$. The circular sweep frequency is set to $120Mhz$, so one scan takes roughly $8.3ns$. Together with the CCD sensor consisting out of 720 Diodes, a temporal resolution of 11.6 ps per channel is obtained, if other effects like local unsharpness of photoelectron creation at the cathode are neglected.

2. CALIBRATION

The necessity of calibration arises from an effect known as streak sweep nonlinearity, which is caused by nonuniform deflecting voltages and the slight misfit of the optical axes of the electron beam and the optical readout system. These circumstances lead to a time varying speed of the electron beam within one sweep along the CCD array. For calibration purposes, the streak camera has been exposed to a number of pulses equally spaced in time from a precise picosecond pulse source. Figure 1 shows an image of 11 recorded laserpulses. The abscissa shows the channels of the CCD readout from 0 to 719, the ordinate the intensity in arbitrary units. In order to perform a calibration, the recorded spacing between every two neighboring peaks p_i and p_{i+1} was measured. These distances show a dependency on the channel area, where they are located. Figure 2 shows a plot of the measured peakdistances Δp versus the location of detection, defined as $l = \frac{p_i + p_{i+1}}{2}$ given in channel numbers. As one can see, the effect of streak sweep nonlinearity is roughly 20%. Normalizing the channel locations to radians, one can express this nonlinearity in terms of an angle dependent sweep frequency $\omega(\varphi)$, which is related to the mean sweep frequency $\bar{\omega}$ by

$$\omega(\varphi) = \bar{\omega} E(\varphi), \tag{1}$$

where $E(\varphi)$ is a normalized function of the channel, expressed in radians. $E(\varphi)$ is determined by fitting the inverse peakdistances to

$$[\Delta p(\varphi)]^{-1} = \sum_{j=0}^{n} a_j \sin^j(\varphi) + b_j \cos^j(\varphi). \tag{2}$$

The result for $E(\varphi)$ can now be written as

$$E(\varphi) = \frac{1}{N}[\Delta p(\varphi)]^{-1}, \tag{3}$$

where N is a normalization constant defined by

$$N = \int_0^{2\pi} [\Delta p(\varphi)]^{-1} d\varphi. \tag{4}$$

Figure 3 shows a corrected data set of measured peakdistances. The overall jitter of the datapoints is about $30ps$ whereas the standard deviation is only $10ps$. This means, that the error in the timescale is reduced from 20% to 1.5%.

3. RANGING TO A GROUND TARGET

The dispersion measurements to a local ground target, were carried out using the Wettzell Laser Ranging System, which is designed for satellite and lunar ranging. It uses a Nd:YAG laser oscillator, which generates pulses with $200ps$ FWHM at a wavelength of $1.06\mu m$. The oscillator is actively and passively modelocked by a dye cell and an acousto optic loss modulator. After passing the pulse selector, the pulses are amplified and frequency doubled to $0.53\mu m$ by a KD^*P crystal. As the conversion rate is about 50%, both signals are beam expanded and transmitted by a $75cm$ aperture telescope. The laser pulses are reflected by a corner cube at a horizontal distance of $1.2km$ and then received by the same telescope. In order to keep the image on the photo cathode of the streak camera as small as possible, spatial filtering has been performed, before exposing the camera to the received doublepulses. By the use of suitable spectral filters either one of the two frequencies could be blocked when necessary. In this way target returns have been recorded at $0.53\mu m$ and $1.06\mu m$ equally good. The advantage of the readout system is, that no complicated image processing procedures are required, because only one line of CCD elements need evaluation. Figure 4 shows a portion of such a data set. The timescale is plotted horizontally, calculated from the position of the CCD element and the correction function. Vertically the intensity of the detected single frequency pulse is shown in arbitrary units. The laser pulse could be reproduced quite well. The received signal of a dualcolor pulse travelling horizontally through $2.4km$ of atmosphere is shown in figure 5. It can be clearly seen, how the two frequency components are split by the dispersive atmosphere.

4. DATA TREATMENT AND RESULTS

From the difference in the time of flight between the two frequency components, the influence of the atmosphere can be calculated. Therefore a precise estimate between the centers of the two peaks is required. This was achieved by fitting a superposition of two gaussians to the streak video signal as given by:

$$F(t) = \sum_{i=1}^{2} A_i exp(\frac{1}{2}(\frac{t - B_i}{C_i})^2) \tag{5}$$

The six coefficients A_i, B_i and C_i $(i = 1, 2)$ were obtained using a simplified Newton algorithm. So the positions of the peaks B_1 and B_2 as well as their difference ΔB can be computed. This was done repeatedly for a large number of dual color echoes. Figure 6 shows a histogram of the measured peakdistances. The maximum for the separation of the peaks is at $130ps$ and the standard deviation was calculated to be $9ps$. There are also lenses to consider, which are part of the ranging system. Taking the group refractive index of BK7 for those, a contribution of $30ps$ was calculated. For the given meteorological data follows a theoretical value [5] of $99ps$. This is in very good agreement with the measurement.

5. SATELLITE AND MODULO RANGING

In order to cover the infrared frequency domain around the wavelength of $1\mu m$, the streak camera is equipped with a S_1 cathode. This has the drawback, that the quantum efficiency is below 0.1%. So a satellite target with a very high reflectivity is required, which excludes most of the geodetic satellites. For this experiment the satellite AJISAI was chosen. The streak camera was hooked up to one of the detector ports of the WLRS in a temporary fashion. It was expected, that the intensity of the satellite echoes would not be far above the noise level. Another problem was, that at that time the ranging system did not have achromatic optics all along the receive path. So this experiment was limited to the use of one frequency only. The infrared echopulse was extracted by a dichroic mirror and focused onto an avalanche photo diode for detection. The displayed satellite returns were used as an indication for the possibility of echoes on the streak camera, throughout the experiment. This made sure, that the pointing of the telescope was right. To distinguish satellite returns from noise events, the laser was run in semitrain mode. This means, that the system was emitting a half pulsetrain, starting with the one having the highest amplitude, thus giving a definitive start event for the ranging timer. As the sweep time on the streak camera is $8.3ns$ and the spacing in time between two consecutive pulses of the semitrain is $7ns$, a distance of $1.3ns$ between two peaks on the recorded readout were expected. Figure 7 shows one of the video signals obtained in this way. One can see, that two pulses of the semitrain have been captured. This shows that the design of the whole experiment works in principle.

During the setup of this experiment, it became obvious, that for the full integration of the streak camera into the routinely used ranging system, the optical arrangement of the receiver section needed to be reconstructed. This work is completed by now. Furthermore it is currently attempted to synchronize the sweep frequency with the driving frequency of the acousto optic loss modulator of the laser oscillator. This gives the advantage, that neighboring pulses of a pulsetrain or semitrain are imaged onto the same area of the CCD-readout, integrating the intensity. This will increase the signal to noise ratio a lot. In the experiment described above, it is only possible to measure the differences in the time of flight of the two laser pulses used. When streak camera and modelocker are synchronized, the complete range information can be obtained as well. To achieve this, the streak camera is exposed to a calibration signal additionally. By counting the number of sweeps between the calibration- and the satellite echo, the range information can be derived, when the difference in the position of the calibration and the returns are considered. This kind of "modulo ranging" can be done at an accuracy well above that of standard photon detection devices such as photomultipliers and avalanche photo diodes. The coming ADEOS satellite mission (launch scheduled for February 1996), carrying the "Reflector In Space" (RIS) will make a good target for this dual color streak camera ranging experiment.

References

[1] W. Schlueter, R. Dassing, P. Sperber, R. Kilger and U. Schreiber, "The Role of the Fundamental Station Illustrated by the Example Wettzell", *Contributions of Space Geodesy to Geodynamics: Technology*, Vol. 25, 125 - 131, AGU, Washington (DC), 1993

[2] H. Hamal and I. Prochatzka", "Modular Streak Camera for Laser Ranging",*SPIE 1358,55*

[3] Th. Varghese, Chr. Clarke, Th. Oldham, M. Selden "Streak Camera Based SLR Receiver For Two Color Athmospheric Measurements", *Proceedings Of 8th International Workshop on Laser Ranging Instrumentation*, (1992)

[4] C. B. Johnson, S. Nevin, J. Bebris, J. B. Abshire, "Circular- scan streak tube with solid- state readout", *Applied Optics 19, 3491-3495*, (15. Oct. 1980)

[5] James C. Owens, "Optical refractive index of air: Dependence on Pressure, Temperature and Composition",*Appl. Opt. 6,51-59*, (1967)

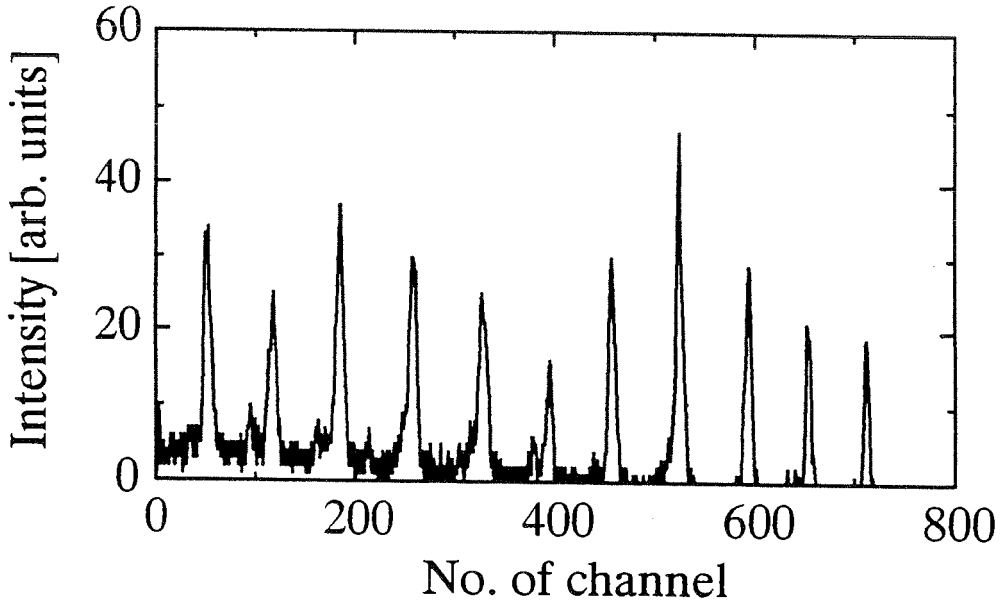

Figure 1: Image from the streak camera readout system, showing 11 equally spaced peaks in time. The ordinate corresponds to the 720 channels of the CCD sensor

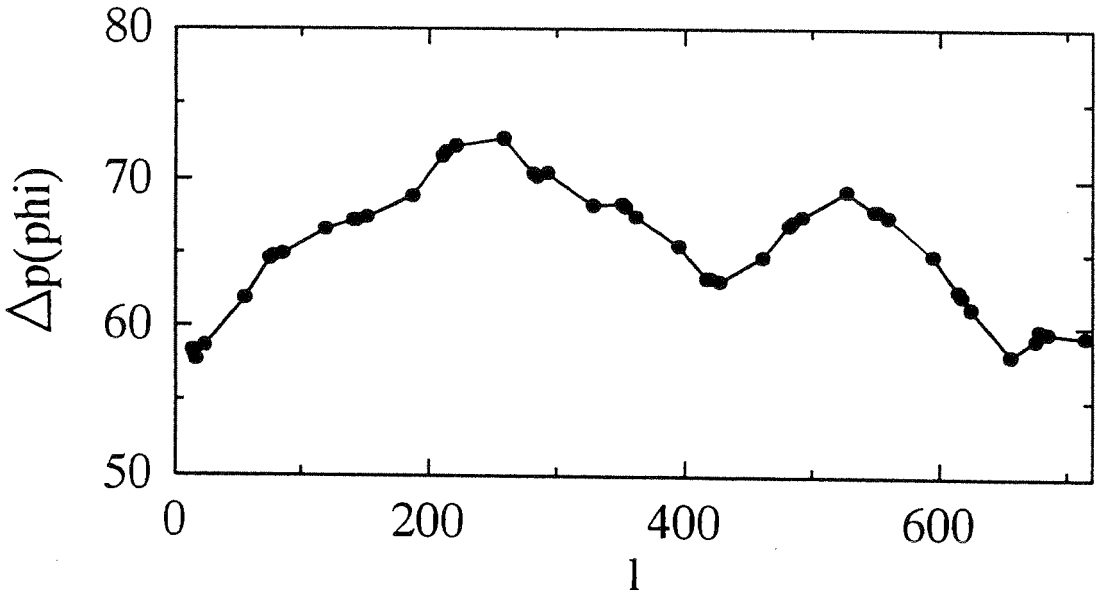

Figure 2: Peakdistances $\Delta p(\varphi)$ vs. location of detection l in units of channels

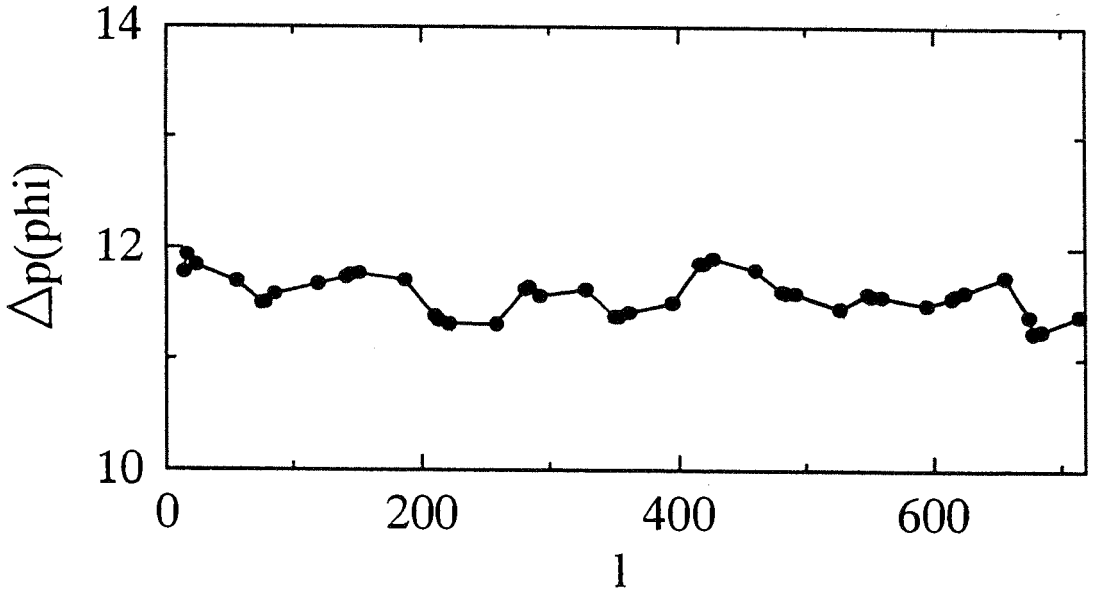

Figure 3: Corrected peakdistances $\Delta p(\varphi)$ vs. location of detection l. The calibration linearizes the data with deviations of only 1.5%

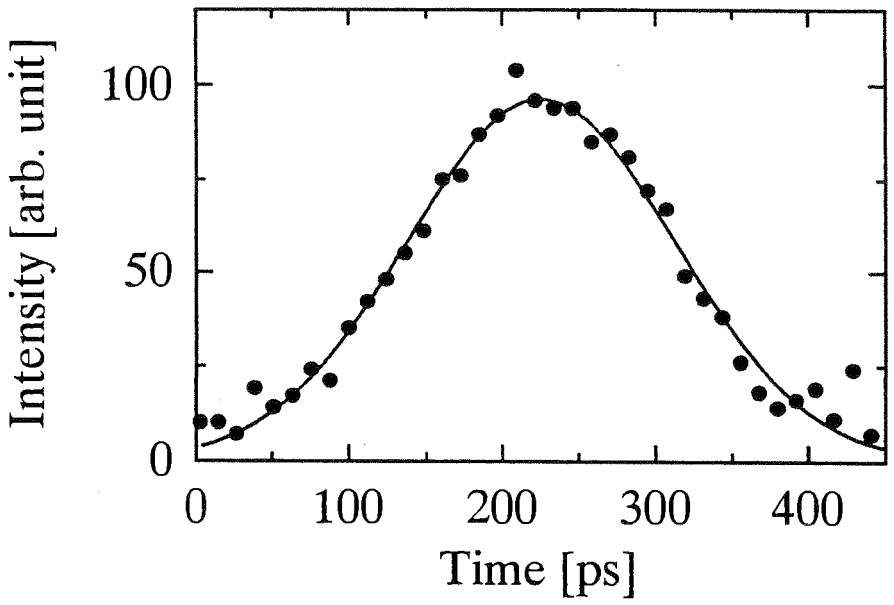

Figure 4: Target echo with single wavelength detection

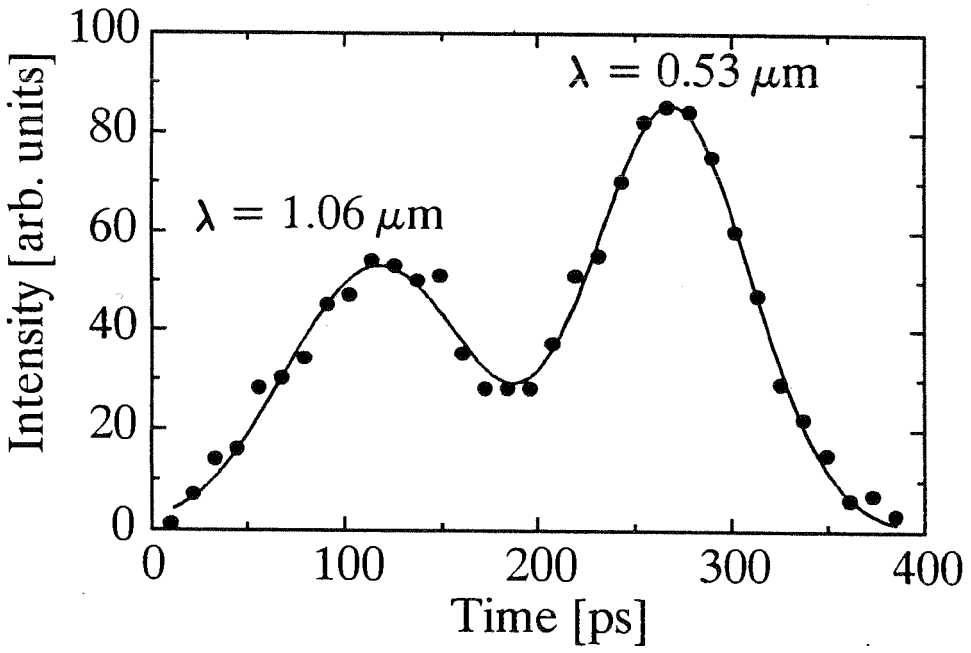

Figure 5: Target echo with dual wavelength detection

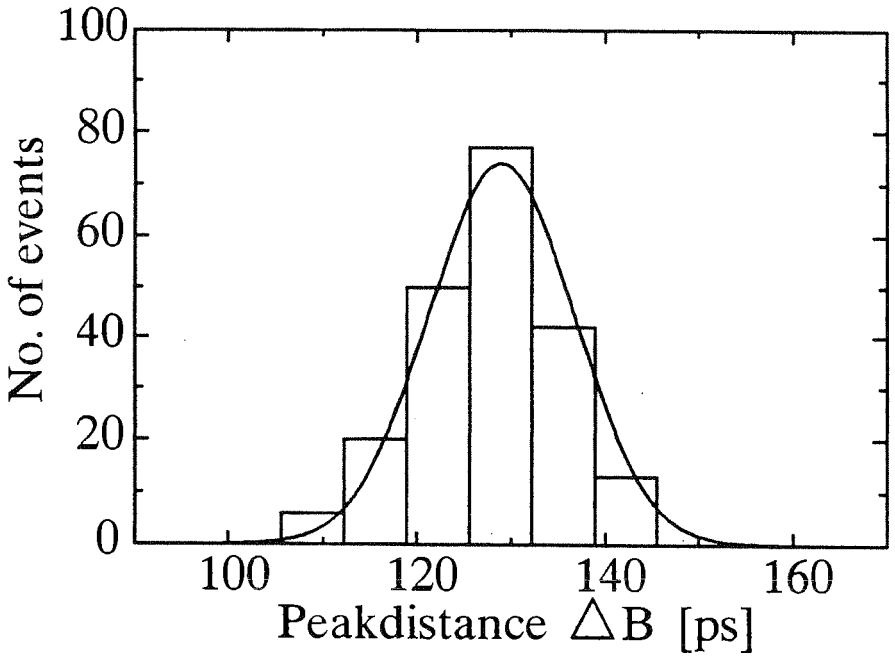

Figure 6: Histogram of calculated peakdistances ΔB out of dual wavelength experiment data

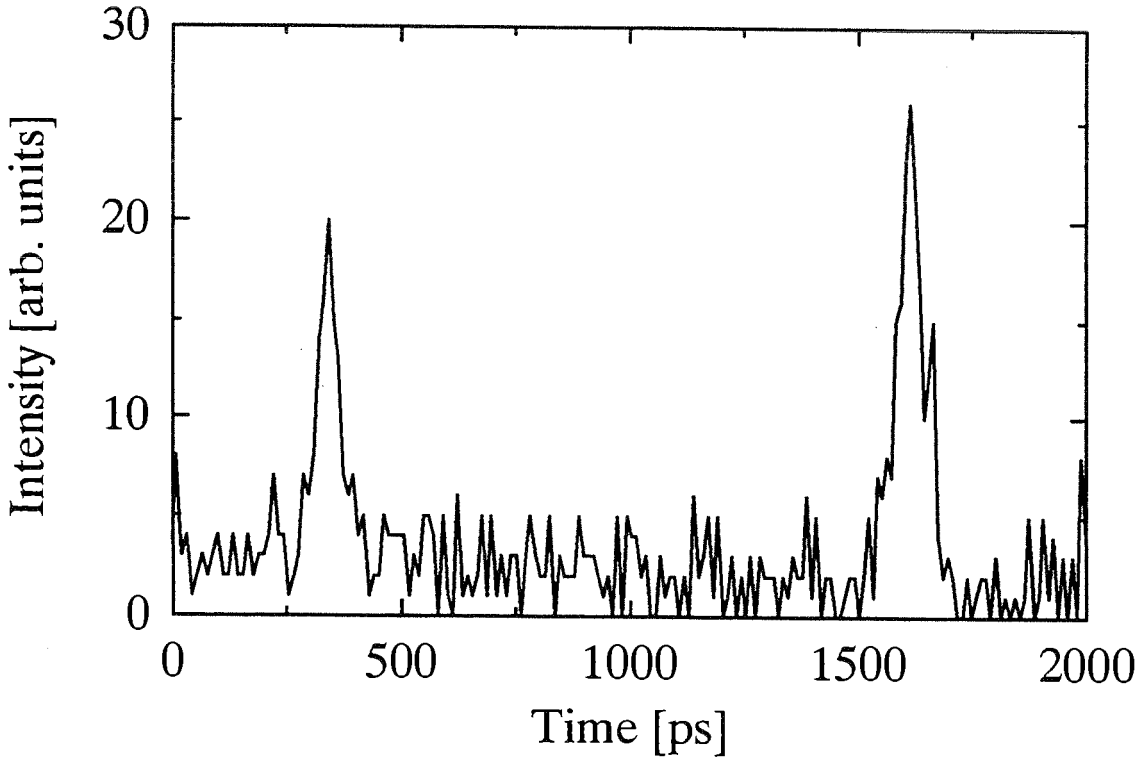

Figure 7: Image of two pulses from a semipulse train, reflected from the satellite AJISAI

ATMOSPHERIC SENSING AND MODELS

Chairperson : Georg Kirchner

System Design Study for an Airborne Laser Radar and a Ground Pulsed Laser Radar at 1.06μm (Nd:Yag) and 10.6μm (CO_2)

Richard J. Becherer (Delta Sciences)
1040 Waltam Street, Lexington, MA 02173-8027, USA
Manuscript Presentators
Dominique Souilhac and Dominique Billerey
Laboratoire d'Electromécanique Théorique et Appliqué
2 Avenue de la Forêt de Haye,54500 Vandoeuvre-lès-Nancy,France

ABSTRACT

In this paper, we describe a system design study of a near-all-weather infrared airborne laser radar and a pulsed Nd:Yag (1.06μm) and CO_2 (10.6 μm) gound based laser radar against cluttered terrain, sky and cloud backgrounds.

System parameters for an airborne CO_2 laser radar are calculated and compare with a microwave and forward looking infrared sensor. For the Nd:Yag and CO_2 pulsed ground based laser radar, system parameters are also calculated for direct and heterodyne detection and are representative of what can be expected in the field.

1. INTODUCTION.

Section 2 of this paper describes a system design study of a near-all-weather infrared airborne laser radar (IRAR) to perform:

(1) Wide field search and detection of moving ground vehicles against a cluttered terrain background.

(2) Narrow field high resolution imagery for object recognition and identification.

We also discuss the impact of weather statistics on IRAR performance.

In section 3, we describe the design of a pulsed ground-based laser radar at 1.06 (Nd:Yag) and 10.6μm (CO_2) , to measure range of a small (unresolved) target just above horizon, against cluttered terrain, sky and cloud backgrounds.

Section 4 is a conclusion.

2.SYSTEM DESIGN STUDY FOR AN AIRBORNE LASER RADAR.[1 9]

2.1. Wide Field Search and Detection.

Fig.1 is a schematic of an airborne laser radar.

Wide field search requires the knowledge of the system field of view (FOV), the azimuth scan rate and the detector bandwidth.

In Fig.2 we calculate the bandwidth required per detector and azimuth scan rate versus slant range, in wide field search mode.

Table 1 gives the theoretical expressions for the projected beam width at ground, the number of beam widths in azimuth scan, the dwell time of the laser radar on each resolution element, the sensor bandwidth and the angular rate of the optical scanner.

If we use a linear array of n detectors, the angular rate of the azimuth optical scanner is reduced by a factor n, the dwell time on each resolution element is increased by a factor n and the transmit beam is fanned out to cover n resolution elements. So in laser radar the use of a detector array can reduce the scanner requirements but does not improve the SNR. (Indeed, in Fig.2, for n=16, the bandwidth per detector is reduced but the fanning beam reduces the laser power pae detector by the same factor).

2.2. Narrow Field High Resolution Imaging.

In Fig.3, we calculate the required sensor aperture diameter for target recognition and identification, versus slant range and Fig.4 gives the corresponding calculated FOV requirement, in narrow field imaging, for identification versus slant range.

Fig.5 is a plot of the calculated narrow field imaging bandwidth which shows the dependance on the FOV and the number of detectors n.

Different types of image processing for high resolution imaging in reflectance, range and doppler, are used: Spectral analysis in CW, pulsed, frequency modulation or in compressed pulsed laser modulation modes. (See Ref.[11] for a detailed experimental analysis).

2.3. Technology Options.

For a laser radar with an angular resolution of 1.5×10^{-4} rad, we need a 20cm aperture. This ensures furthermore, compactness and lightweight. A Cassegrain reflecting telescope with low F/number will be chosen (Fig.6). The different arrangement of surfaces in candidate telescope designs is shown in Fig.7 for the Schmidt, Maksutov and Maksutov-Cassegrain telescopes.

Table 2 give the characteristics of these most famous candidate reflecting telescope configurations and Ref.[12] a detailed analysis of the optical system configuations.

Calculations of the angular blur diameter for these famous candidate optical

systems are based on geometrical optics formulas . In Fig. 6 the dashed line shows the diffraction limited angular blur diameter, for D=20cm, calculated from the following formula:

$$\text{Angular blur diameter (Diffraction limited)} = \frac{2\lambda}{D}$$

where D is the aperture diameter.

2.4. Heterodyne Detector Array.

The heterodyne detection systems exhibit antenna properties (see Ref.[10]). The antenna theorem requires the following condition for optimum sensitivity:

$$\text{Angle between signal and local oscillator} = \phi \approx \frac{\lambda}{D}$$

The effect on detector array and local oscillator beam design is shown in Fig.8,9. In addition, Ref.[11] treats in detail the influence of beam geometry on one detector and the heterodyne efficiency with the presence of speckles.

To meet the antenna theorem requirement for an outside detector, we must satisfy the following condition:

$$\phi \approx \frac{ns}{l}$$

Hence:

$$n < \frac{2\lambda l}{sd}$$

where: l is the distance exit aperture to the image plane, d the detector linear size and s the center to center detector separation.

A concept design which can overcome the above limitation is shown in Fig.10.

2.5. Required SNR_p per pulse:

Two potential laser advantages versus microwave are:
(1) Signal processing gain, (2) Low ground clutter.

In order to determine the required SNR_p per pulse, we use the following procedure:
(1) We use Fig.2.7 of Skolnik (see Ref.[13]) to determine the required SNR in dB for a specified P_D and FAR for a single pulse and a nonfluctuating target.
(2) We use Fig.2.23 of Skolnik to determine the additional required SNR in dB due to the target power fluctuations as compared with a nonfluctuating target, again for a

a single pulse.

(3) We make use of Fig.2.24 of Ref.[13] to determine the integration improvement factor to be realized by integrating n pulses. For P_D=0.99, FAR=4x10^{-4} , case 2 target statistics and n=15 to 30, this procedure gives the following results:

Initial SNR requirement	15dB
Pulse fluctuating target requirement	+17dB
Minus Pulse Integration Improvement	-26 to 28dB
Net Single Pulse SNR Requirement	5 dB

The signal processing gain realized through the integration improvement factor is approximately 27dB.

We notice that the microwave radar case which would correspond to case 1 statistics where the pulses are correlated, the comparable result would be:

Initial SNR requirement	15dB
Fluctuating Target Requirement	+17dB
Minus Pulse Integration Improvement	-10dB
Net Pulse SNR Requirement	22dB

Therefore, by comparison, the high spatial resolution of the 10.6 μm radar provides 17dB additional signal processing gain which is not available with the wide beam width microwave system.

2.5. Minimum Radial Velocity of Ground Target.

Typical frequency spread is as follows:

(1) Laser frequency stability (short term)	$\sigma_p \approx$30KHz
(2) Ground clutter (20Knots wind)	$\sigma_c \approx$ 42KHz
(3) Scan dwell time (30° FOV at 2.5Km)	$\sigma_d \approx$ 17-106KHz

The 30KHz laser stability is available with an inexpensive commercial CO_2 laser (PZT tuning). The ground clutter parameter is obtained from velocity data (Ref.[10]), using:

$$\Delta f = \frac{2}{\lambda} \Delta v \qquad (1)$$

where Δf if the frequency shift, Δv is the velocity change and is the wavelength. For wooded hills, a 20 knots wind (10.2m/s) will cause a standard deviation in velocity of 0.22m/sec for blowing vegetation within the beam. This value of Δv corresponds to Δf = 42KHz. The scan dwell time varies with range according to the following formula:

$$\Delta f = \frac{vh(FOV)}{n\theta^2 R^2} \qquad (2)$$

We assume: v= Aircraft velocity = 165m/s
h= Aircraft altitude = 200m
FOV = Field of View = 30° or 60°
n = Number of detectors = 16
θ= Angular resolution = 0.05mr
R = Range to target = 2-5Km

These parameters lead to the 11-106KHz standard deviation indicated above. The lower frequency spread corresponds to the lower range.

The previously calculated 5dB required SNR_p per pulse yields to a Signal/Noise=3.2, at the output of the notch filter when it is set at 1σ of the frequency distribution. (Fig.11).

The results for the detected minimum target velocity versus range are shown in Fig. 12.

We conclude this section by saying that CO_2 laser radar can measure a 1MPH target velocity at a range of 5Km. Performance is reduced at shorter range as seen in Fig.12 due to wide field search FOV and a resulting bandwidth increase.

2.6. Comparison of Infrared Airborne (IRAR) and Forward Looking Infrared System (FLIR) Performances.

For IRAR, we calculate a system SNR_p:

$$SNR_p = \frac{P_R}{h\nu\, B/\eta} \quad \text{(heterodyne)} \qquad (3)$$

Where P_R = received power = $P\rho e^{-2\alpha R} A\varepsilon\eta / \pi R^2$
$h\nu$ = photon energy
B = IF bandwidth
P = Average laser transmitter power
ρ= Directional reflectance of rough target
α= Atmospheric attenuation coefficient
R= Range from entrance aperture to target
A = entrance aperture area
ε= Optical and electronic efficiency factor

$h\nu$ = Local oscillator photon energy

B = IF amplifier bandwidth

For comparison, the performance of a passive FLIR system is:

$$SNR_V = \left(\frac{P_R}{NEP}\right)^{1/2} \quad \text{(Voltage SNR)} \tag{4}$$

$$NEP = \frac{\sqrt{aB}}{D^*}$$

where a = detector surface area (cm^2)

B = Bandwidth (Hz)

D* = Detectivity ($cm\text{-}Hz^{1/2}\text{-}W^{-1}$)

$$SNR_V = \frac{A\Theta^2 \varepsilon e^{-\alpha R}(\partial M/\partial T)\Delta T}{\pi NEP} \qquad (SNR_V)^2 = SNR_p \tag{5}$$

where A = entrance aperture area

Θ = IFOV

ε = Efficiency of the optics

α = Atmospheric attenuation

R = Range from entrance aperture to the target

ΔT = Effective temperature difference between target and background including emissivity effects

$\frac{\partial M}{\partial T}\Delta T$ = Change of emittance (W/cm^{-2}) in scene per ΔT temperature change

The systems parameters are calculated in Table 3, for the FLIR and IRAR systems and are compared.

2.7. Weather Statistics.

Weather statistics impact CO_2 laser radar performance. A key parameter is the atmospheric transmission coefficient $\alpha(km^{-1}) = (dB/Km)/4.3$. Lowtran 7 is the accurate computer program for the determination of range at which laser radar design provides a SNR_p=64 (18dB) for example. Atmospheric turbulence and system parameters are combined in the computer program in order to calculate the required laser power to acheive a range measurement.

The atmospheric transmittance is given by: $\tau = \exp(-\alpha L)$. α has also contributions from molecular scattering aerosol scattering, molecular absorption and aerosol

absorption.

$$\alpha = \sigma_m + \sigma_a + k_m + k_a \qquad (6)$$

For molecular scattering, σ_m is proportional to λ^{-4} (blue sky). Molecular absorption (k_m) can be avoided by choosing the laser wavelength outside of the specific absorption bands. The transmittance can be expressed as: attenuation=4.34α dB/km. At 1.06 and 10.6μm, the atmospheric attenuation varies respectively from 0.384 to 1.72 in clear summer season, to 1.86 and 0.627 (dB/km) in winter hazy conditions. (Table 4).

Atmospheric scintillation is caused by the variations of the index of refraction which create multipath summation of signals at the receiver, each with different phase (and arrival angles). Optical intensity fluctuates around the zero mean without reducing the average intensity. The atmospheric structure function (Cn^2) characterizes the strength of the turbulence as a function of the altitude (Hufnagel-Valley model). For a weak turbulence, the intensity fluctuations are described by a lognormal intensity statistics and the log intensity variance is given by:[14]

$$\sigma^2_{lnI} = 2.24k^{7/6}\int_0^L C_n^2(x)\left(\frac{x}{L}\right)^{5/6}(L-x)^{5/6}dx \quad , \quad \sigma^2_{lnI} < 1 \quad ; k=2\pi/\lambda \qquad (7)$$

In order to calculate the fade margin necessary to compute a probability thatthe signal will not fade below the minimum level necessary for the receiver , the cumulative density function of the log-normal distribution is given by:

$$P(I) = \frac{1}{2} + \frac{1}{2}\Phi\{(\ln(I/\bar{I}) + \frac{1}{2}\sigma^2_{lnI})/(\sqrt{2}\sigma_{lnI})\} \text{ where } \Phi(x)=(2/\sqrt{\pi})\int_0^x e^{-t^2}dt \qquad (8)$$

As an example of fade margin calculation,we assume that saturated scintillation requires 95% ofthe time that received intensity is greater than or equal to the signal level required by the receiver. In this case $\sigma^2_{lnI} > 1$ and:

$P(I) = 1-\exp(-I/\bar{I})$ and $0.05 = 1-\exp(-I/\bar{I})$, hence $I/\bar{I} = 0.05 = 13$dB

Hence, 13 dB of additional signal power (fade margin) is needed to ensure that95% of the time there is adequate signal to be detected by the receiver.

Aperture averaging can mitigate the effects of scintillation and occurs when the receiver diameter is greater than the average size of a "turble". This can sometimes occur even for modest apertures of a few inches.

See Figures 13,14,15,16,17,18 and Table 5.

Another laser beam turbulence is the case of beam spreading which occurs when transmitting through an aircraft boundary layer which causes a random phase screen in front of a transmitter located on the aircraft. Beam spreading can be described by the

the Strehl ratio of the on-axis intensity without aberration:

$$I/I_o = \exp(-\sigma_\phi^2 k^2) \tag{9}$$

where I_o = on-axis intensity without aberration

k = optical wavenumber = $2\pi/\lambda$

σ_ϕ = variance of optical path length

For example, an aircraft at Mach 0.6 at 8-10km altitude has σ_ϕ=0.08 waves at .89μm Strehl=0.79. Another case where beam spreading can be significant is for uplinks from ground to aircraft or satellite.

3. Pulsed Laser Ranger Design at 1.06μm (Nd:YAG) and 10.6μm (CO_2).

We design now a ground based laser radar in order to measure range of small (unresolved) target just above the horizon against sky and cloud backgrounds(see Fig. 19). $R=ct_R/2$. Where c is the speed of light and t_R the travel time of the laserpulse

The performance of this system is determined by the SNR:

$$SNR_p = \frac{i_s}{\bar{i}_N^2} \quad \text{(Direct Detection)} \tag{10}$$

Where $\bar{i}_N^2$ is the mean square noise current (shot noise+background+shot noise+thermal+ amplifier noise). (See Table 7).

The range loss factor is:

$$L_R = \frac{P_R}{P_T} = \frac{\sigma e^{-2\alpha R} A\ \varepsilon}{\Theta^2 R^2 \pi R^2} \tag{11}$$

where:

P_R = Received optical signal power

P_T = Transmitted optical signal power

σ = Target cross section

Θ = Angular size of transmitted beam

R = Range

α = Atmospheric attenuation coefficient

A = Area of received aperture

ε = Optical efficiency

The received optical background power exclusive of optical system transmission effects is:

$$P_B' = N_\lambda A\ \Theta^2 \Delta\lambda \tag{12}$$

where: N_λ = Spectral radiance

A = Receiver aperture area

Θ = Angular size of transmitted beam

$\Delta\lambda$ = Wavelength interval

The background spectral radiance N_λ is given in Table 8. Fig.20shows the background power collected by the receiver (D=10cm, $\Delta\lambda=\lambda/100$).(D=diameter of receiver). Candidate optical systems are described in Ref. [11] .

The system parameters for direct and heterodyne systems at 1.06 and 10.6μm is shown in Tab..9,10.In order to determine P_T it is now necessary to determine NEP/$Hz^{1/2}$ and $h\nu/\eta$ As stated in section 2.1, the NEP/$Hz^{1/2}$ for direct detection has contributions from:

-Signal shot noise

-Background shot noise

-Dark current shot noise

-Johnson noise

-Amplifier noise

The SNR_p equation for direct detection assumes that the signal shot noise is negligible if the NEP is to be independant of the signal level.

The following equation for the direct detection assumes a silicon avalanche photodiode for 1.06 direct and a HgCdTe photodiode at 10.6μm for both heterodyne and direct detection. Photovoltaic operation for 10.6μm direct detection is required to provide adequate bandwidth for the ranging pulses. For 10.6μm, $h\nu\ \eta = 3.74\times10^{-20}$J for $\eta = 0.5$.

Table 10 shows the NEP/$Hz^{1/2}$ calculations for the following parameters: At 1.06μm G=125, $F'=G^{1/2}=11.2$, $R=\eta q/h\nu=0.13$, $q=1.6\times10^{-19}$C ,η=0.15. $I_D=10^{-7}$, T=300°K,R=50Ω ,F=2, T=0.15. At 10.6 μm these parameters are F'=1, G=1, $I_D=10^{-8}$,R=4.28,η =0.5,T=300°K, R=50Ω,F=2, T=0.15. The background power levels are taken from Fig. 20, the dark current, quantum efficiency and amplifier noise factors are taken from the current representative manufacturer's product literature. The calculations show that for the narrow transmit and receive beam divergences used, the direct detection systems are not background limited. the NEP/$Hz^{1/2}$ for the two wavelengths are approximately equal since the higher responsivity at 10.6μm approximately offsets the lack of a gain mechanism. Fig.21 shows the required laser power P_T to achieve a SNR_p=50 at 1.06 and 10.6 μm (direct and heterodyne).

4. FIELD RESULTS AND CONCLUSION.

In this paper we have presented the calculated characteristics of a design of a

near-all-weather airborne and ground laser radar. This system is currently in the research-development and application phase at the Ministry of Defense in France. The calculated characteristics of IRAR are representative of what can be expected in the field. (See Figure 22).

5. ACKNOWLEDGMENTS:

We acknowledge the theoretical support of Dr Richard J.Becherer (Delta Sciences) and Dr G.Stephen Mecherle (TRW, Inc.) in the field of aerospace applications of laser radar and fundamentals of free-space laser communication, respectively.

6. REFERENCES.

1-R.M.Measures, "Laser Remote Sensing:Fundamentals and Applications)" Ed. J.Wiley and Sons,New York, 1984.

2-D.K.Killinger and A.Mooradian,"Optical and Laser Remote Sensing", Eds.,Springer-Verlag (Optical Sciences, Vol.39) 1983.

3-J.W.Stohbehn,"Laser Beam Propagation in the Atmosphere", Springer-Verlag (Topics in Applied Physics, Vol.25), 1978.

4-R.J.Keyes, "Optical and Infrared Detectors", Ed. Springer-Verlag (Topics in Applied Physics, Vol.19) 1977.

5-Richard J.Becherer, "Introduction to Laser Radar and Lidar", SPIE OE/Aerospace Sensing, Orlando 1992, Course Notes.

6-Richard J.Becherer,"Aerospace Applications of Laser Radar", SPIE OE/Aerospace Sensing, Orlando 1992, Course Notes.

7-G.Stephen Mecherle,"Fundamentals of Free-Space Laser Communication", SPIE OE/LASE Los Angeles 1993, Course Notes.

8-Adam D.Devir,"Remote Sensing and Object Plane Radiometry", SPIE OE/Aerospace Sensing, Orlando 1993, Course Notes.

9-Larry K.Stockum and Michael K.Kasten, "Precision Stabilization, Tracking and Laser Pointing Systems Design and Development", SPIE OE/Aerospace Sensing, Orlando 1993. Course Notes.

10-"The Infrared Handbook, rev. edition, W.L.Wolfe and G.J.Zissis, eds. Environmental Research Institute of Michigan, 1985.

11-Bertrand Rémy, "Imaging CO_2 Laser Radar with Chirp Pulse Compression", Thèse de Doctorat, Université Paris XI, Orsay, 1984.

12-William L.Wolfe,"Infrared System Design", SPIE OE/LASE 1993, Course Notes.

13-M.Skolnik, "Introduction to Radar Systems, McGraw-Hill, New York, 1962.

14-R.E.Hufnagel,"Propagation Through Atmospheric Turbulence", The Infrared Handbook, Editors Wolfe and Zissis, 1989. Chapter 6.

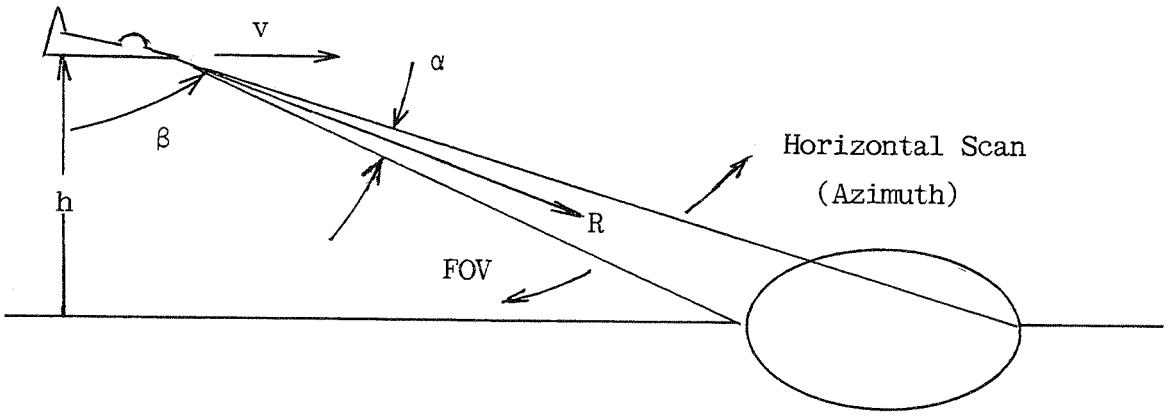

Figure 1

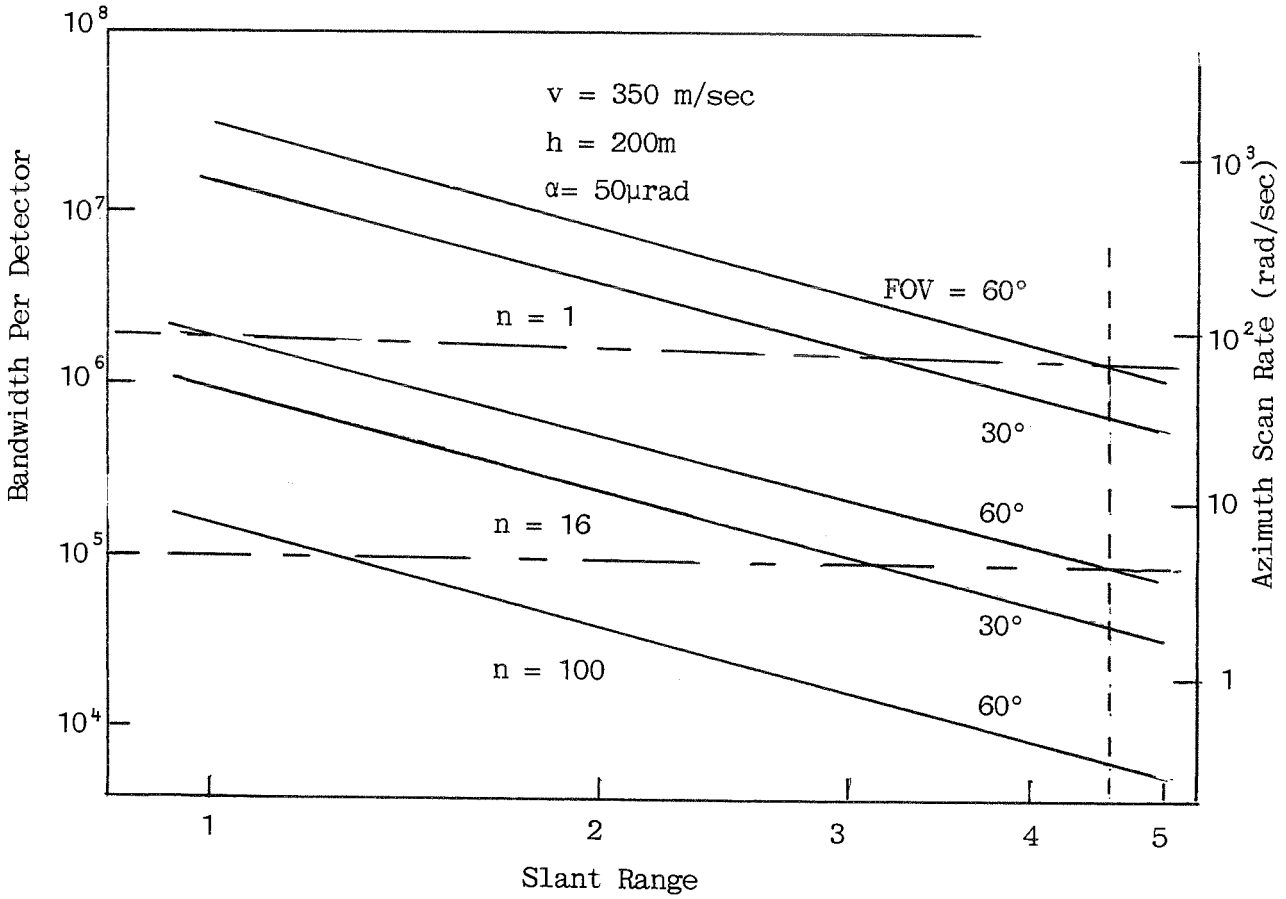

Figure 2. Bandwidth and azimuth scan rate requirements in wide field search mode.

Table 1:

Projected Beam Width at Ground = $\frac{\alpha h}{\cos^2\beta}$

Time to Move Beam Width Forward $= t_A = \frac{\alpha h}{v\cos^2\beta}$

Number of Beam Widths in Azimuth Scan $= \frac{FOV}{\alpha}$

Dwell Time of Laser Radar on Each Resolution Element $t_D = \frac{t_A}{N} = \frac{\alpha^2 R^2}{vh(FOV)}$

Sensor Bandwidth $B = 1/t_D = \dot{F}.\ (FOV)^2/n\Theta^2$

Angular Rate of Azimuth Optical Scanner is: $\dot{\phi} = \frac{FOV}{t_A} = \frac{vh(FOV)}{\alpha R^2}$

(Θ is the instantaneous field of view (IFOV)= angular resolution)
(n is the number of detectors and $\dot{F}$ the frame rate)

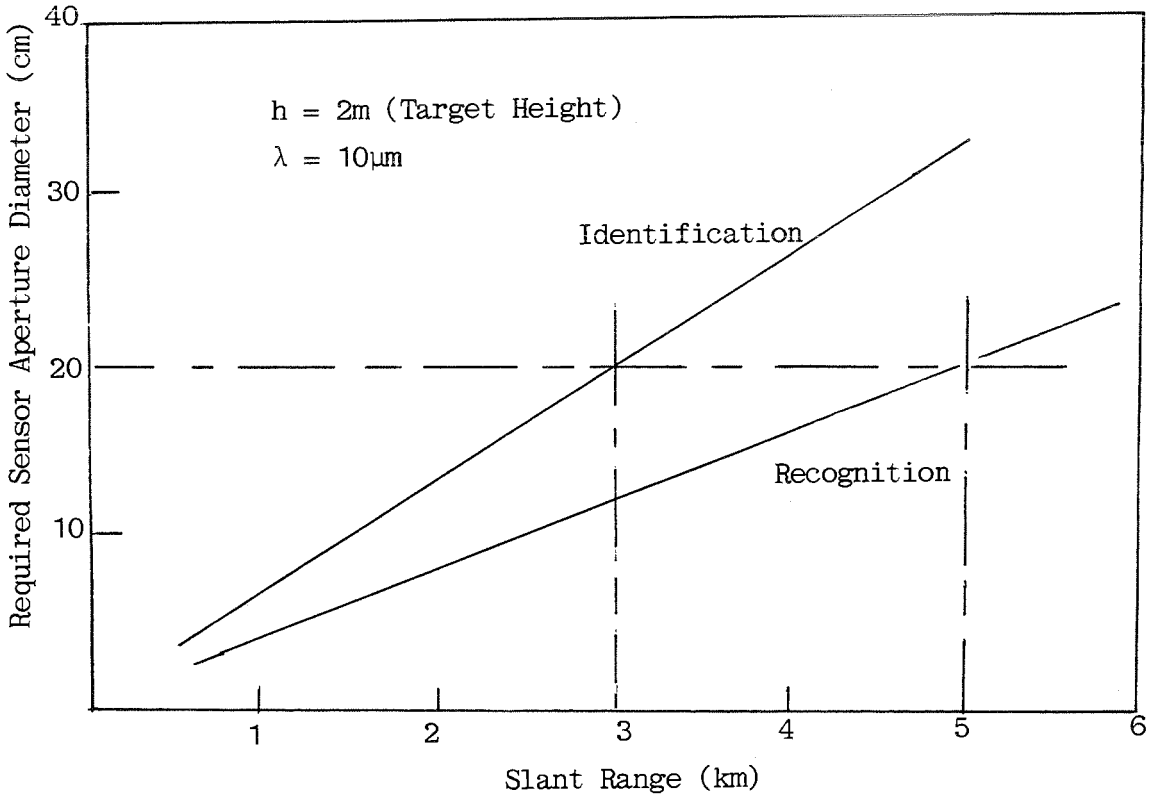

Figure 3: Sensor aperture diameter required for target recognition and identification

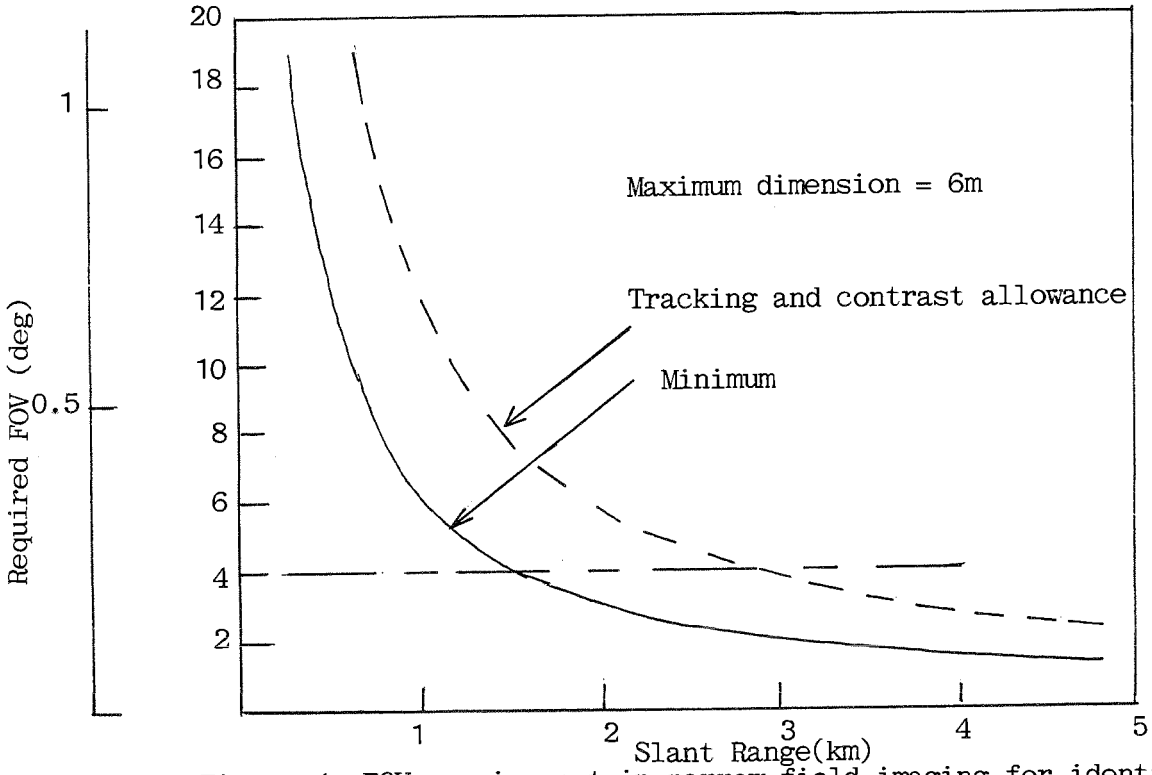

Figure 4: FOV requirement in narrow field imaging for identification

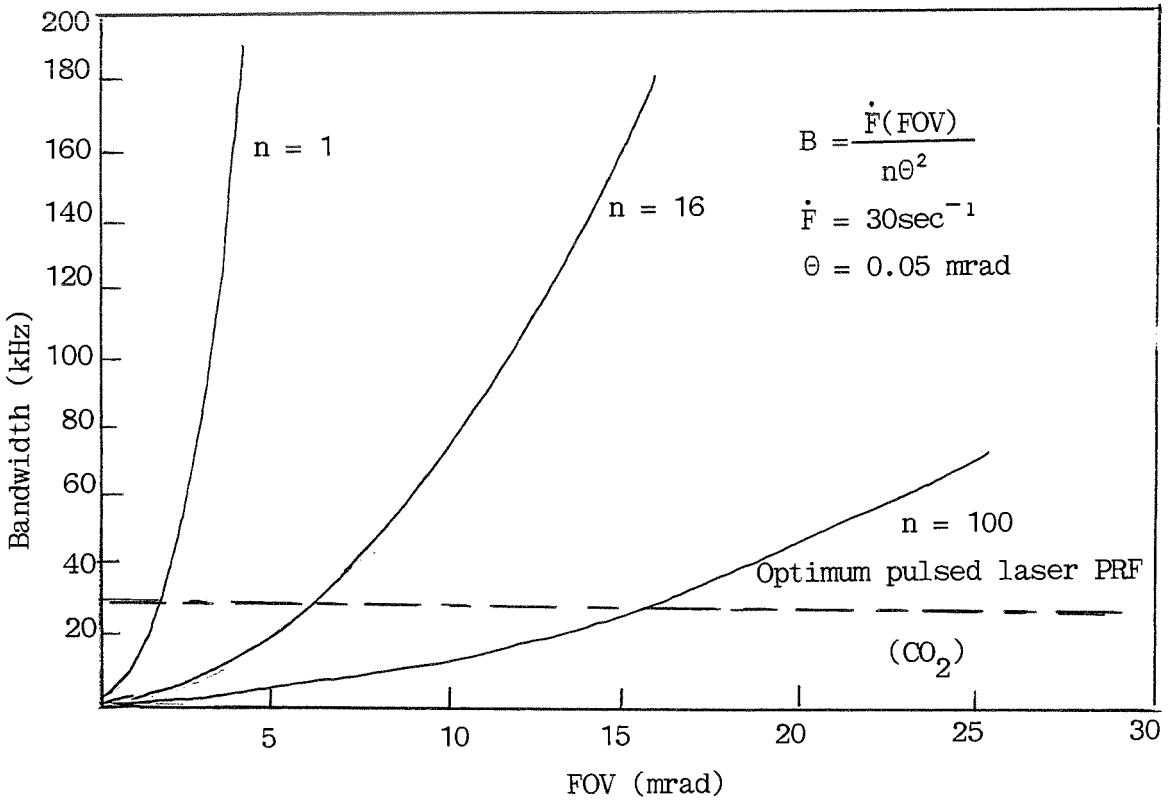

Figure 5: Narrow field imaging bandwidth showing dependence on FOV and on number of detectors n.

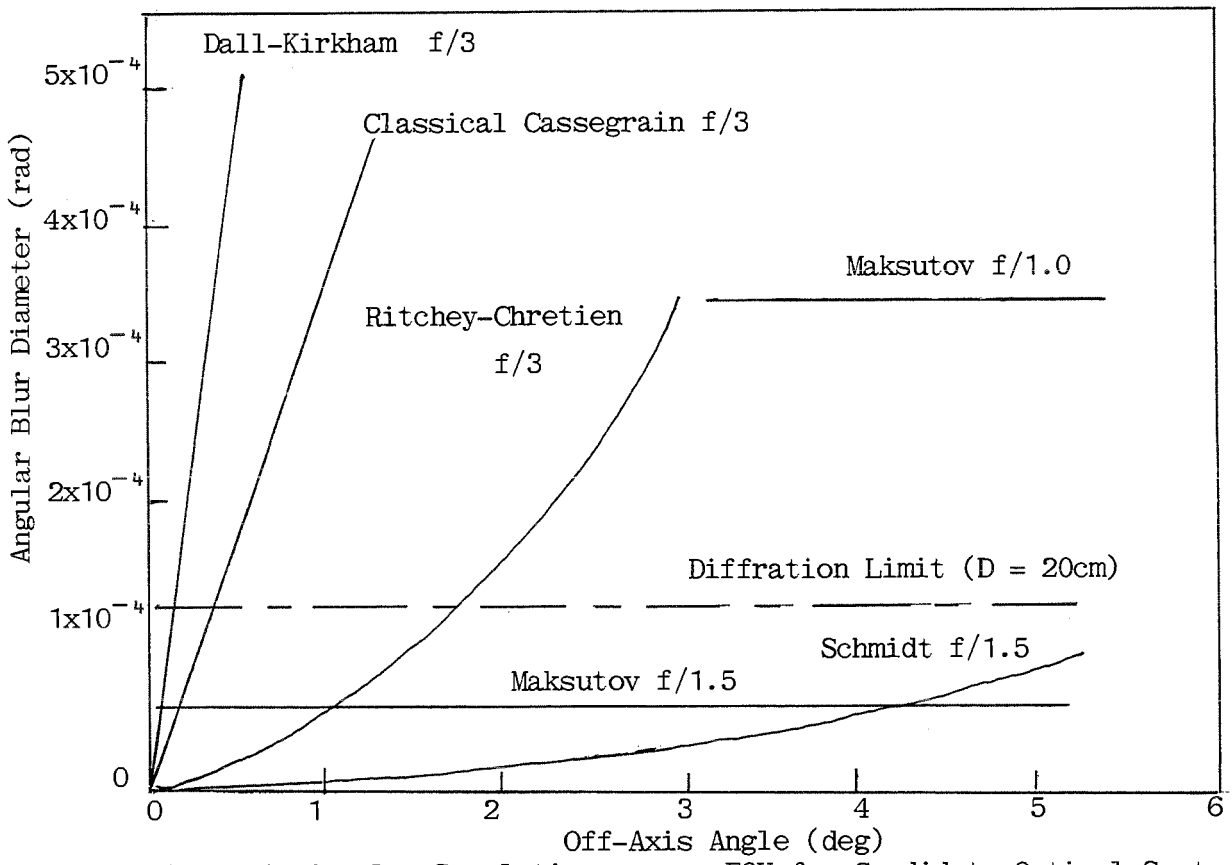

Figure 6. Angular Resolution versus FOV for Candidate Optical Systems.

Table 2. CANDIDATE OPTICAL SYSTEM CONFIGURATIONS

CANDIDATE REFLECTING TELESCOPE CONFIGURATIONS	PRIMARY AND SECONDARY SURFACE SHAPE	UNIQUE FEATURES	DOMINANT RESIDUAL ABERRATION
Dall-Kirkham	Primary-Ellipsoidal* Secondary-Spherical	Secondary Fabrication Simple	Coma
Classical Cassegrain	Primary-Paraboloid Secondary-Hyperboloid	Secondary Fabrication Expensive	Coma
Ritchey-Chretien	Primary-Hyperboloid Secondary-Hyperboloid	Secondary Fabrication Expensive	Astigmatism and Petzval Field Curvature
Schmidt	Primary-Spherical Secondary-None	Aspheric Corrector Plate-Expensive	Curved Focal Plane
Maksutov	Primary-Spherical Secondary-None	Spherical Meniscus Corrector Plate	Curved Focal Plane, Small Residual Spherical
Maksutov-Cassegrain	Primary-Spherical Secondary-None	All Spherical Surfaces, Compact	Curved Focal Plane, Small Residual Spherical

*(Under-Corrected Paraboloid)

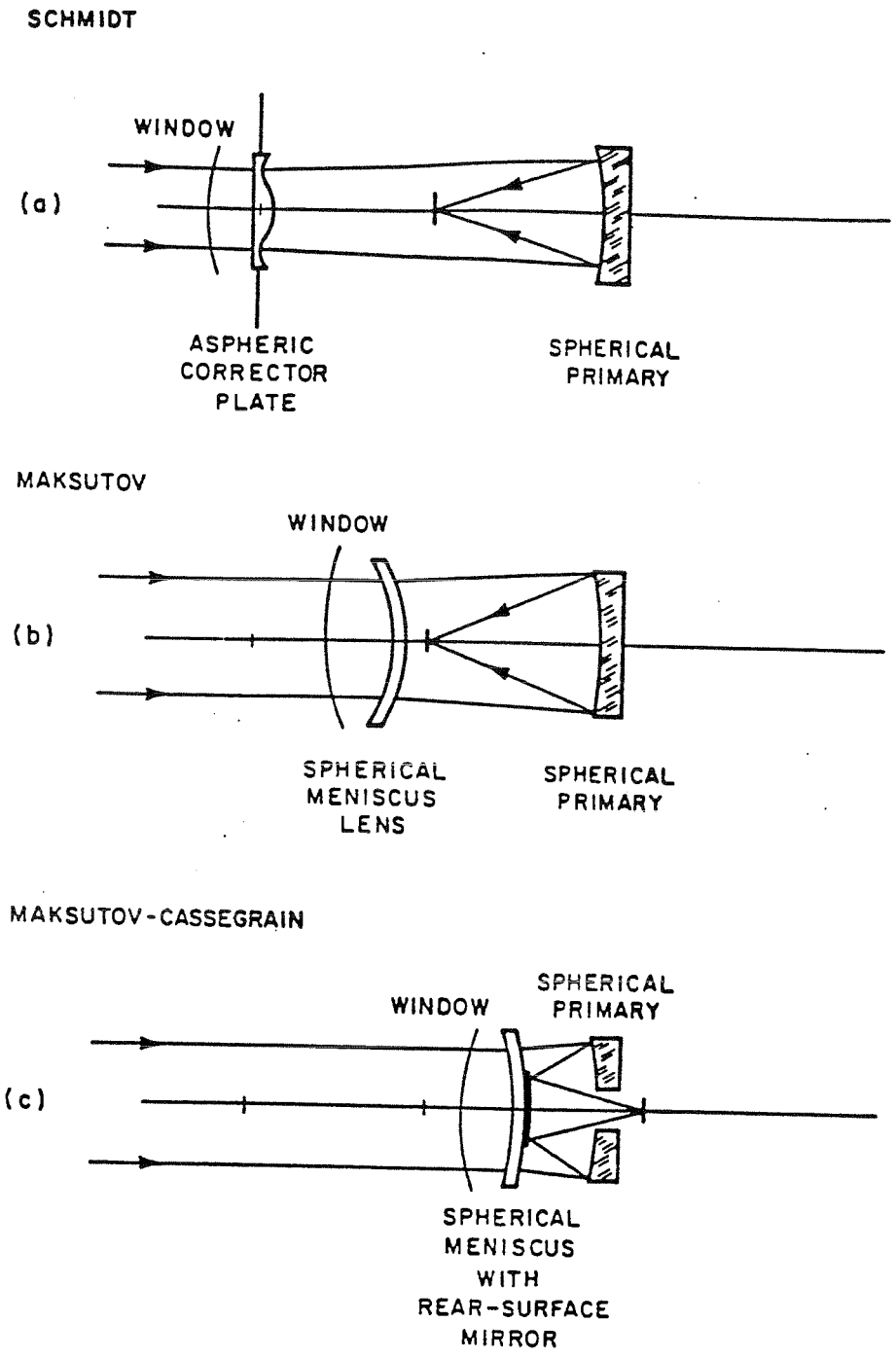

Figure 7. Arrangement of Surfaces in Candidate Telescope Designs.

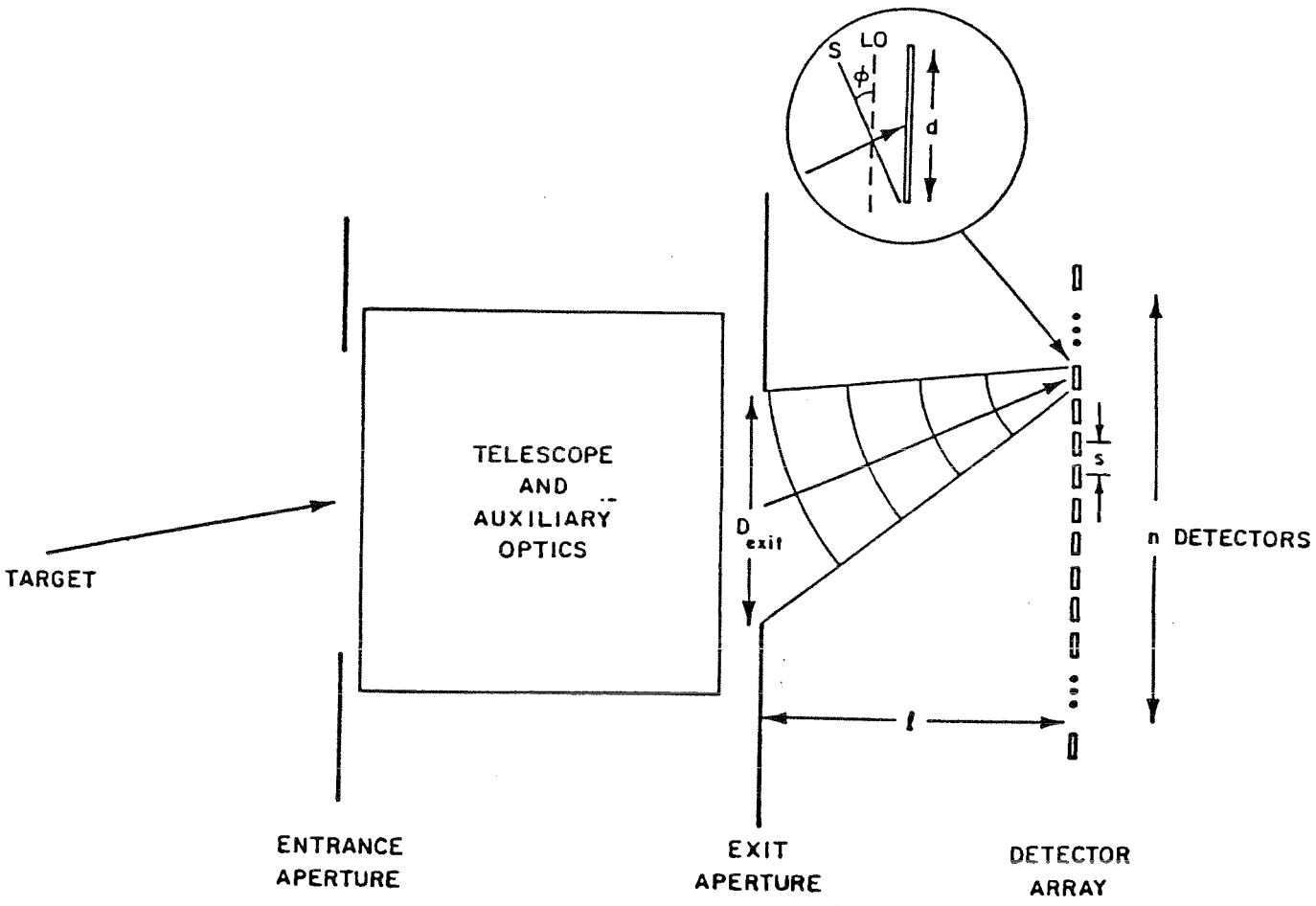

Figure 8. Local Oscillator Phase and Amplitude Matching Conditions for n Element Detector Array.

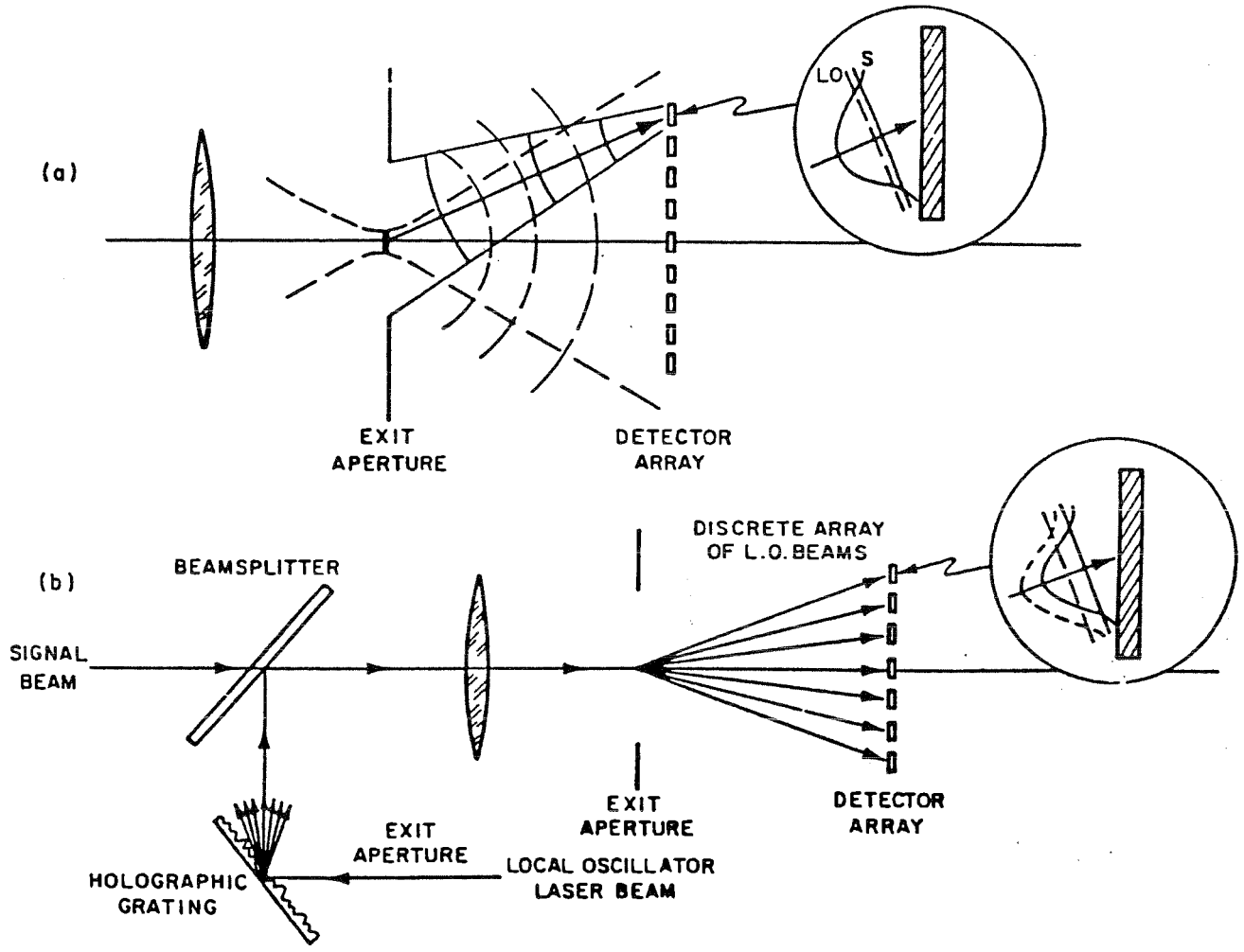

Figure 9. Cylindrical Wave and Holographic Grating Heterodyne Mixing Concepts.

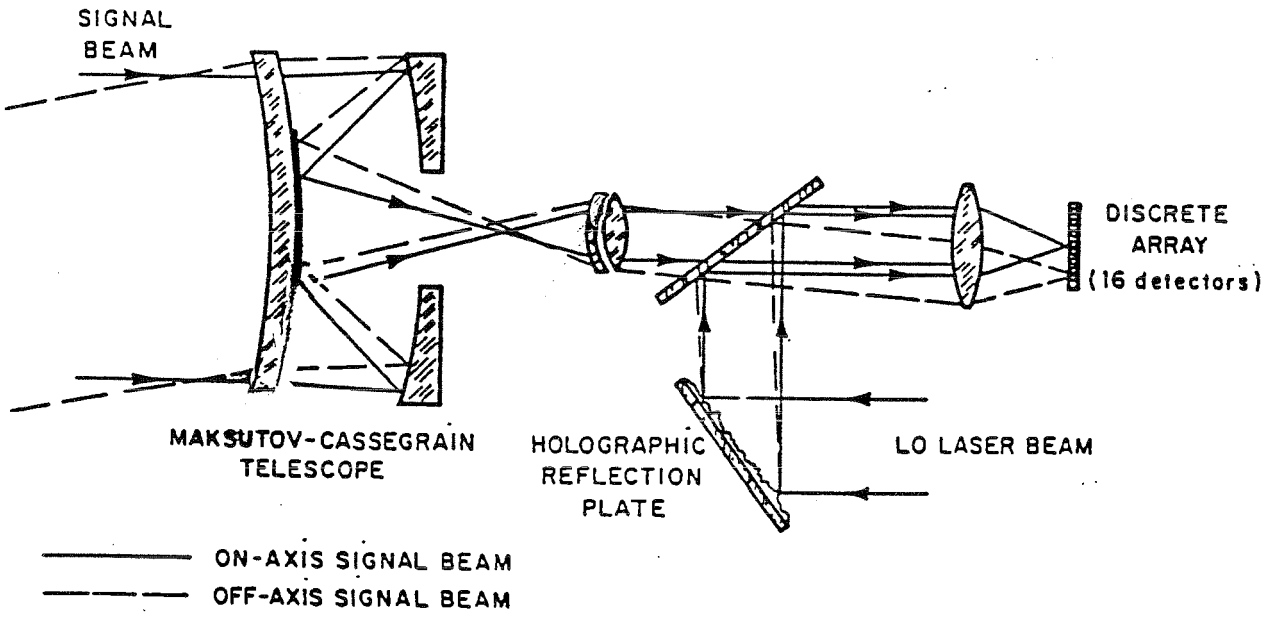

Figure 10. Heterodyne Array Antenna/Receiver.

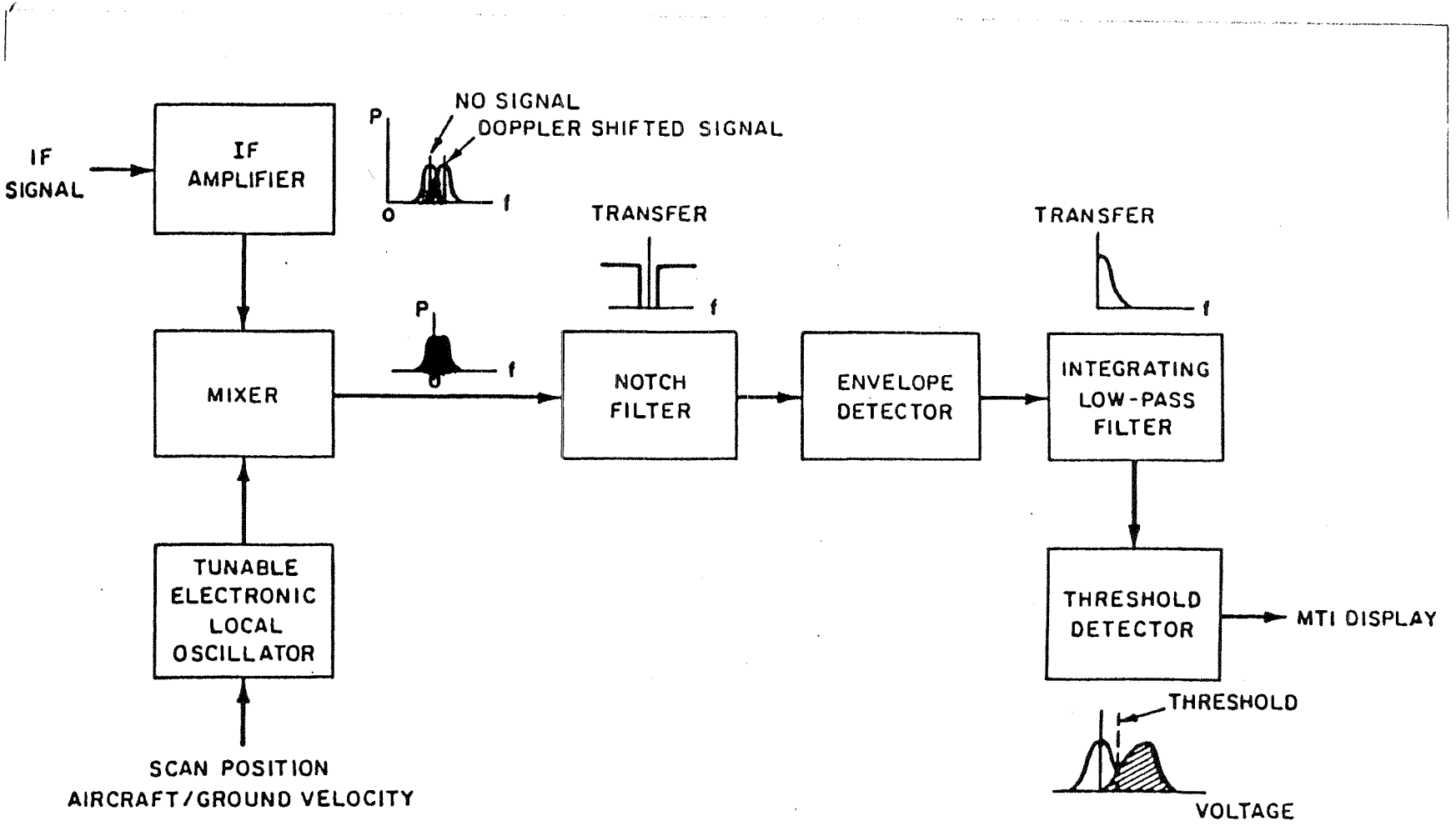

Figure 11. Microwave and Infrared Minimum Target Radial Velocity Signal Processing Block Diagram.

TABLE 3. SYSTEM PARAMETERS.

Parameter	IRAR	State of the Art FLIR	Advanced FLIR Design
Aperture Diameter	20cm	20	20
Angular Resolution	0.05 mr	0.10 mr	0.05 mr
Field of View	9 mr	4°	9 mr
Frame Rate	30	30	30
Laser Power	50 W		
Number of Detectors	16	180	10^4
Detectivity D*		$4x10^{10}cm.Hz^{1/2}Watt$	$4x10^{10}cm.Hz^{1/2}Watt$
Detector Radius		25μm	25μm
Target Signature ΔT		2.5K	2.5K
Δρ	0.05		
Efficiencies Optical	0.32	0.60	0.60
Scan	0.75	0.75	0.75
Quantum	0.70		
Cold Shield		1.00	0.18

TABLE 4. ATMOSPHERIC ATTENUATION VALUES FROM McCLATCHEY ET AL.[6] *

Condition	Total Attenuation = 1.06μm	10.6μm
Midlatitude Summer, Clear	0.384	1.72
Midlatitude Winter, Clear	0.385	0.459
Midlatitude Summer, Hazy	1.86	1.88
Midlatitude Winter, Hazy	1.85	0.627

*Note: These parameters must be combined with:

(1) Atmospheric Turbulence Effects

(2) System Parameters

in order to find the required laser power to acheive the range measurement with the laser radar.

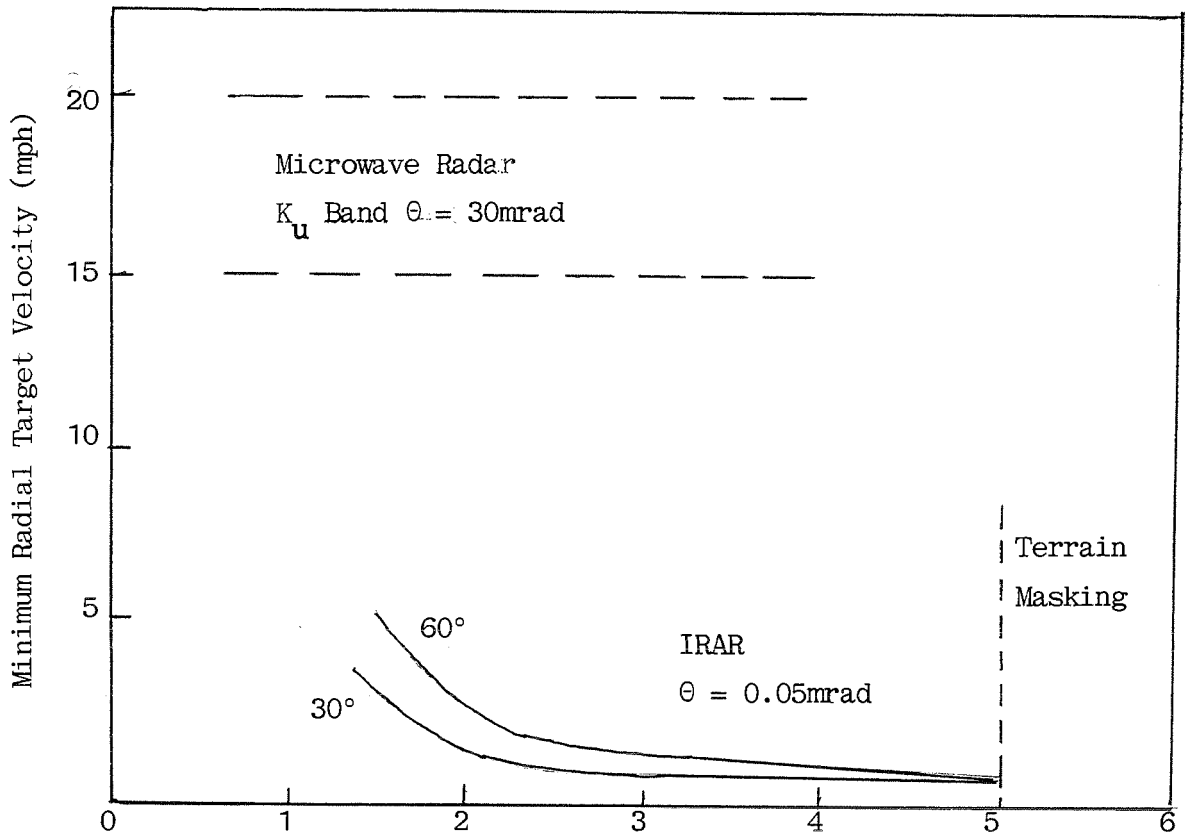

Figure 12: Microwave and Laser Radar Target Search: Minimum Radial Target Velocity versus Range.

Table 5. Normalized Variance of Signal after Aperture Averaging.

Range, km	$D/(\lambda R)^{1/2}$	θ	$\sigma_s^2/\bar{s}^2$ (Direct Detection, λ = 1.06μm) $C_N^2 = 10^{-13} m^{-2/3}$	$C_N^2 = 10^{-14}$	$C_N^2 = 10^{-15}$
10^{-1}	9.7	4×10^{-3}	$(0.01)^2$	$(0.004)^2$	$(0.001)^2$
1	3.1	3×10^{-2}	$(0.58)^2$	$(0.10)^2$	$(0.03)^2$
5	1.4	10^{-1}	$(1.06)^2$	$(1.06)^2$	$(0.29)^2$
10	0.97	3×10^{-1}	$(1.83)^2$	$(1.83)^2$	$(1.48)^2$
10^2	0.31	8×10^{-1}	$(2.99)^2$	$(2.99)^2$	$(2.99)^2$

Table 6. Normalized Variance of Signal (Direct Detection, λ=10.6μm, θ =0).

Range	$C_N^2 = 10^{-13} m^{-2/3}$	$C_N^2 = 10^{-14}$	$C_N^2 = 10^{-15}$
10^{-1}	$(0.06)^2$	$(0.02)^2$	$(0.006)^2$
1	$(0.49)^2$	$(0.15)^2$	$(0.05)^2$
5	$(3.34)^2$	$(0.71)^2$	$(0.20)^2$
10	$(3.34)^2$	$(1.79)^2$	$(0.39)^2$
10^2	$(3.34)^2$	$(3.34)^2$	$(3.34)^2$

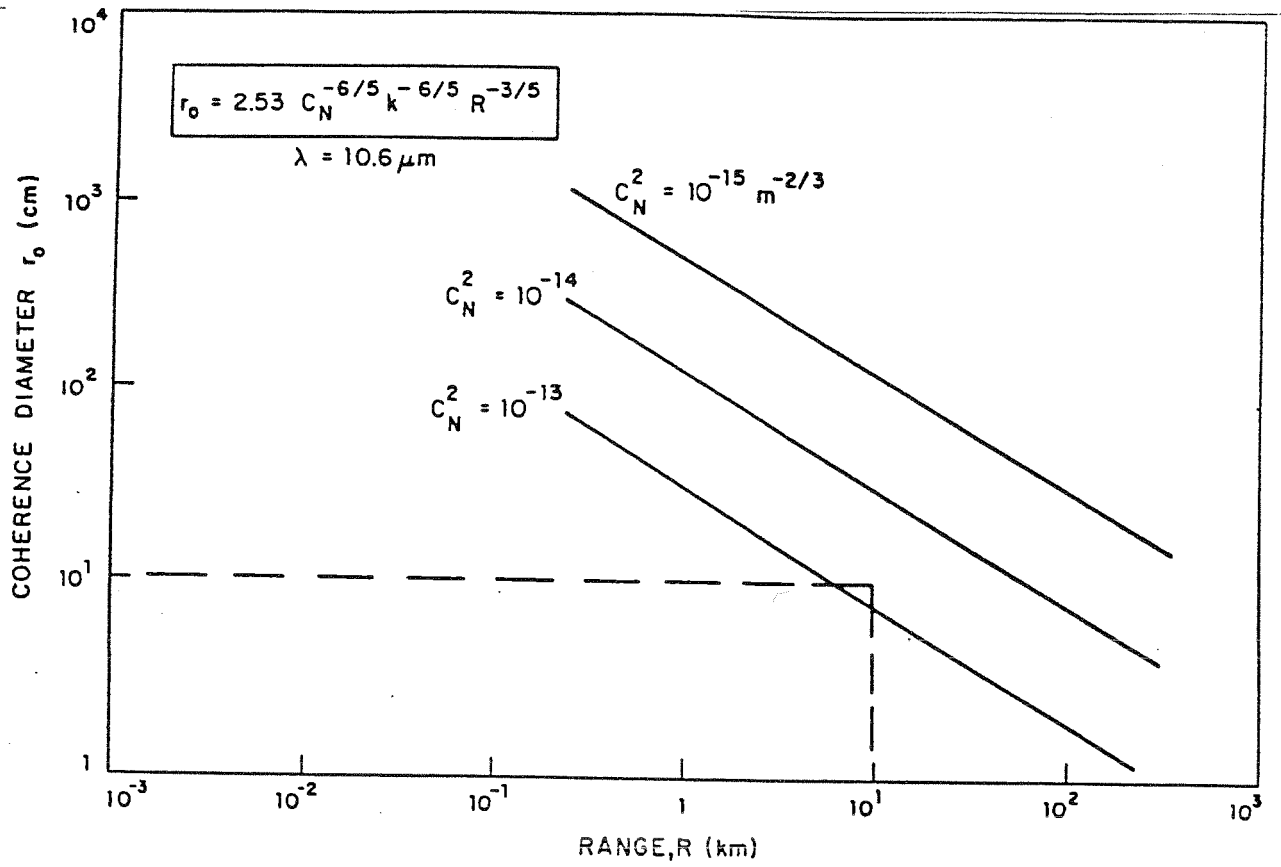

Figure 13. Coherence Diameter for Heterodyne Receiver.

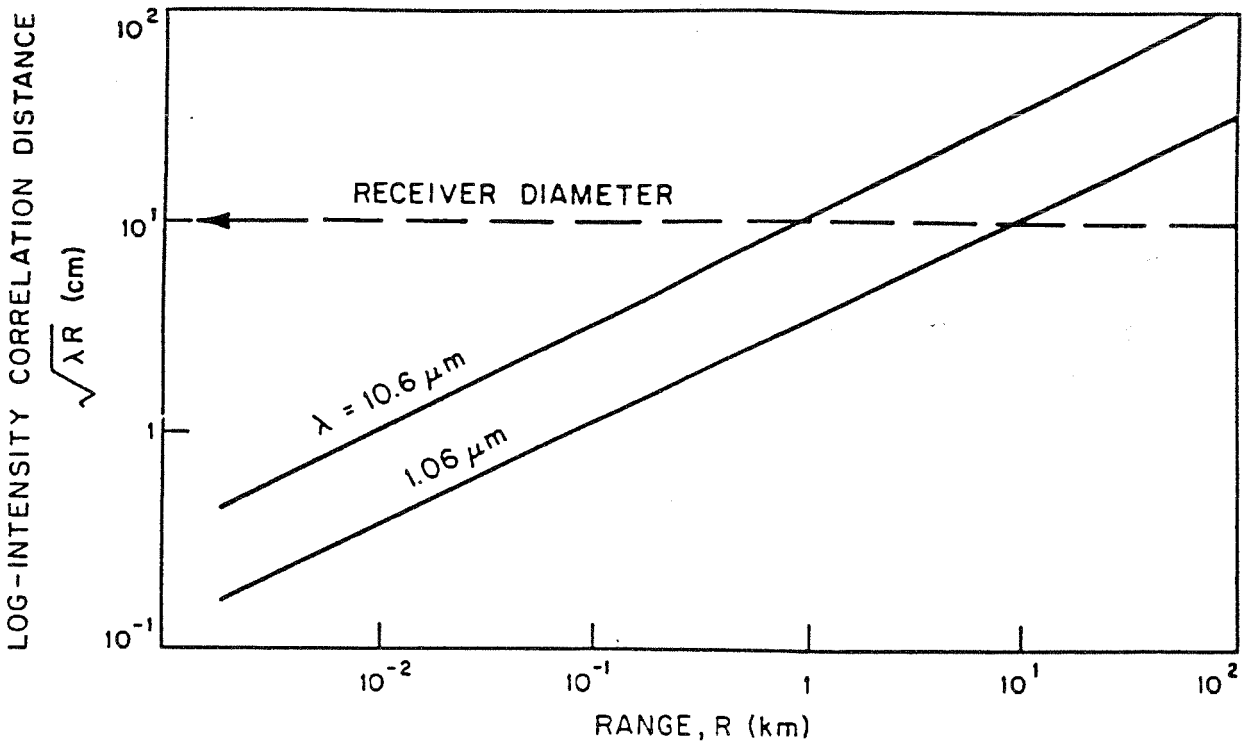

Figure 14. Log-Intensity Correlation Distance.

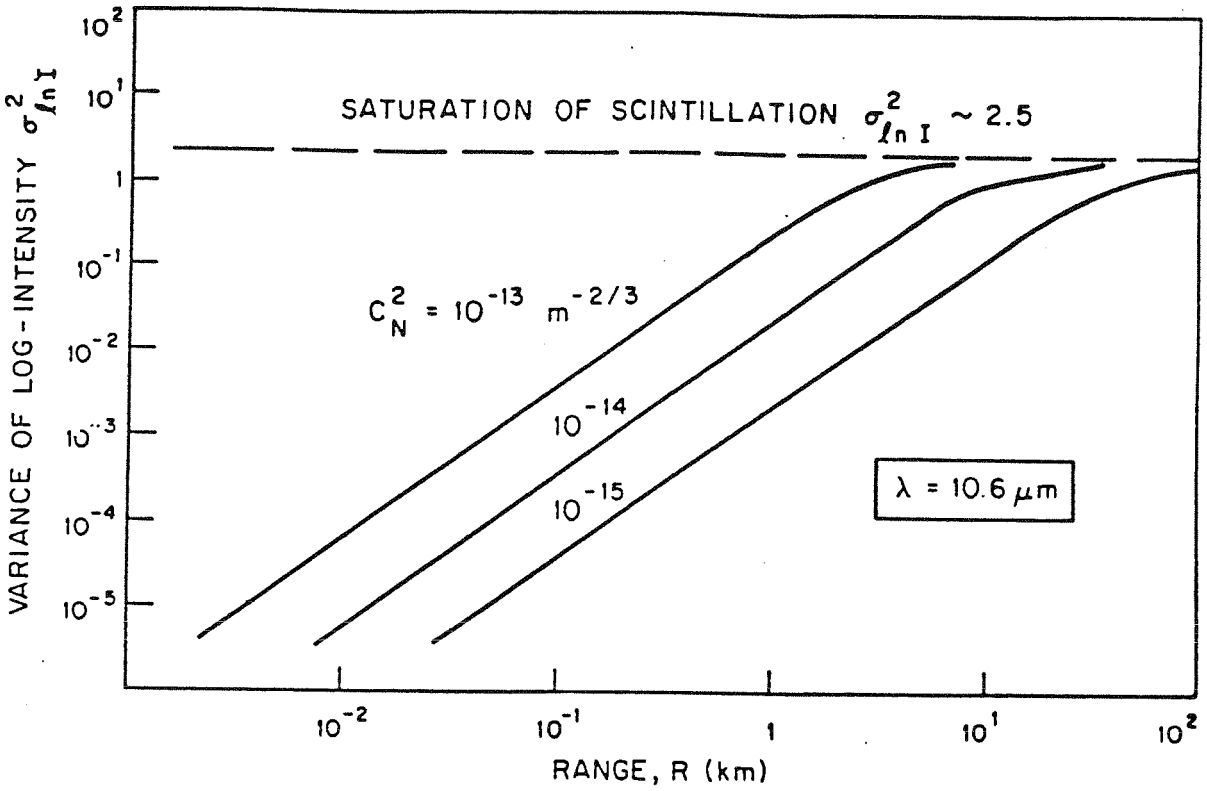

Figure 15. Variance of Log-Intensity versus Range.

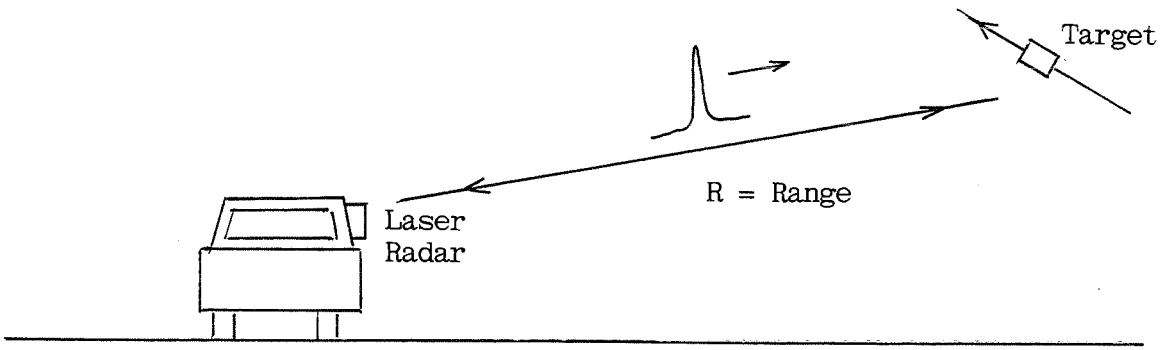

Figure 19. Pulsed Ground Laser Ranger.

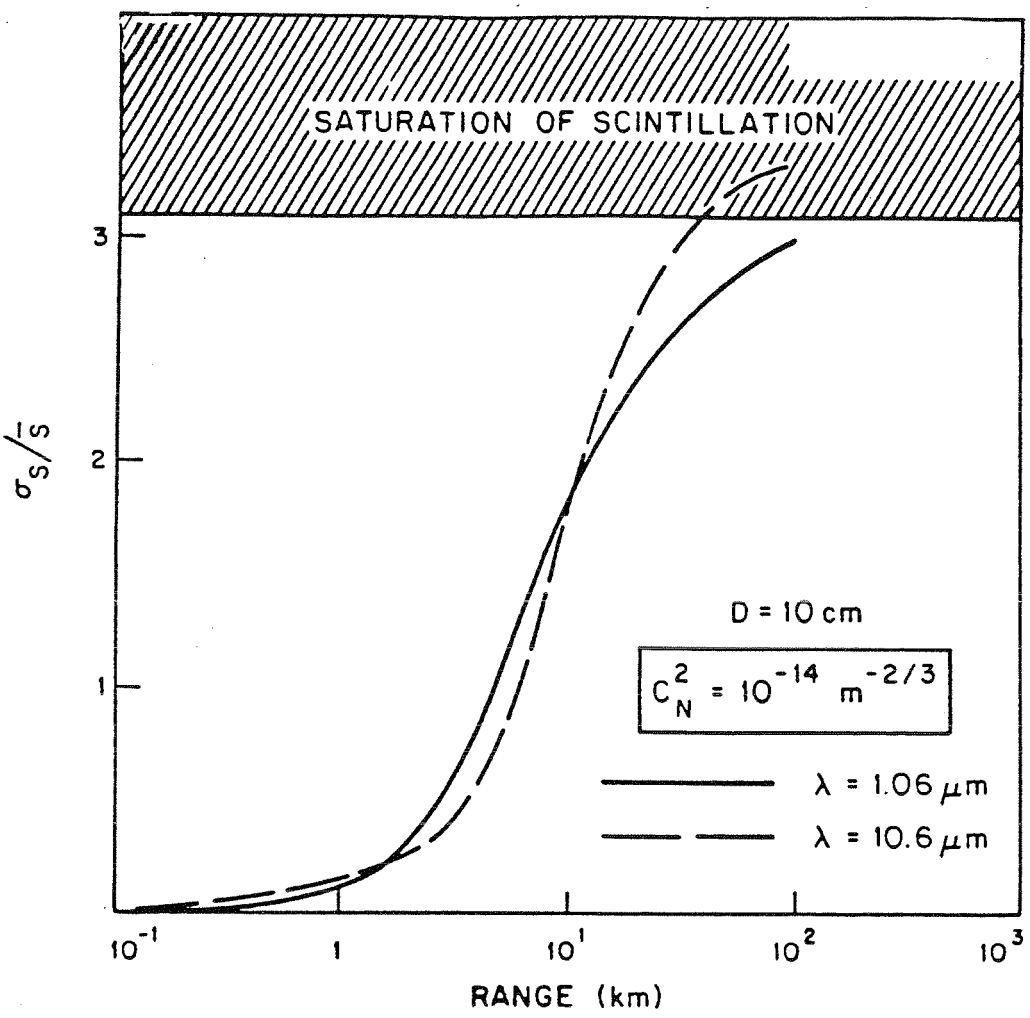

Figure 16. Normalized Standard Deviation of Signal Due to Atmospheric Scintillation.

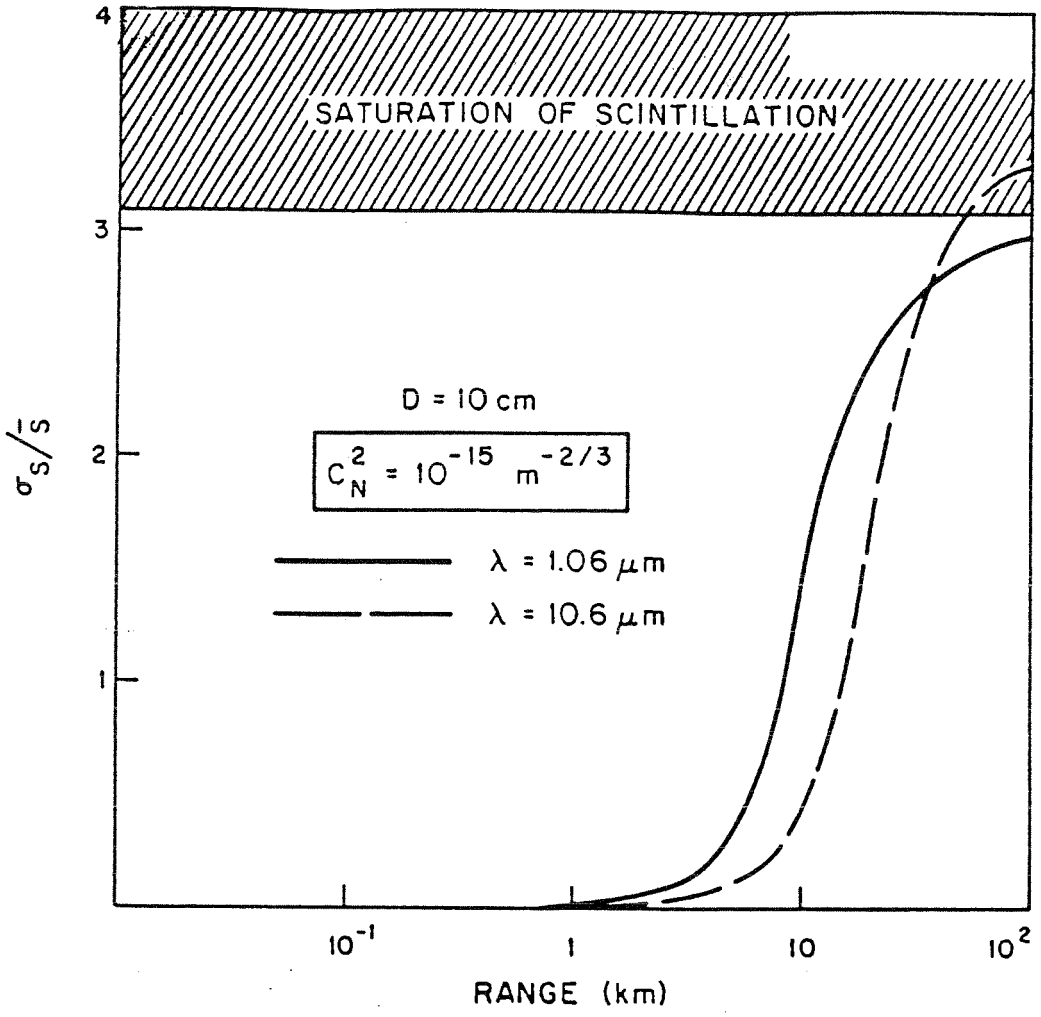

Figure 17. Normalized Standard Deviation of Signal Due to Atmospheric Scintillation.

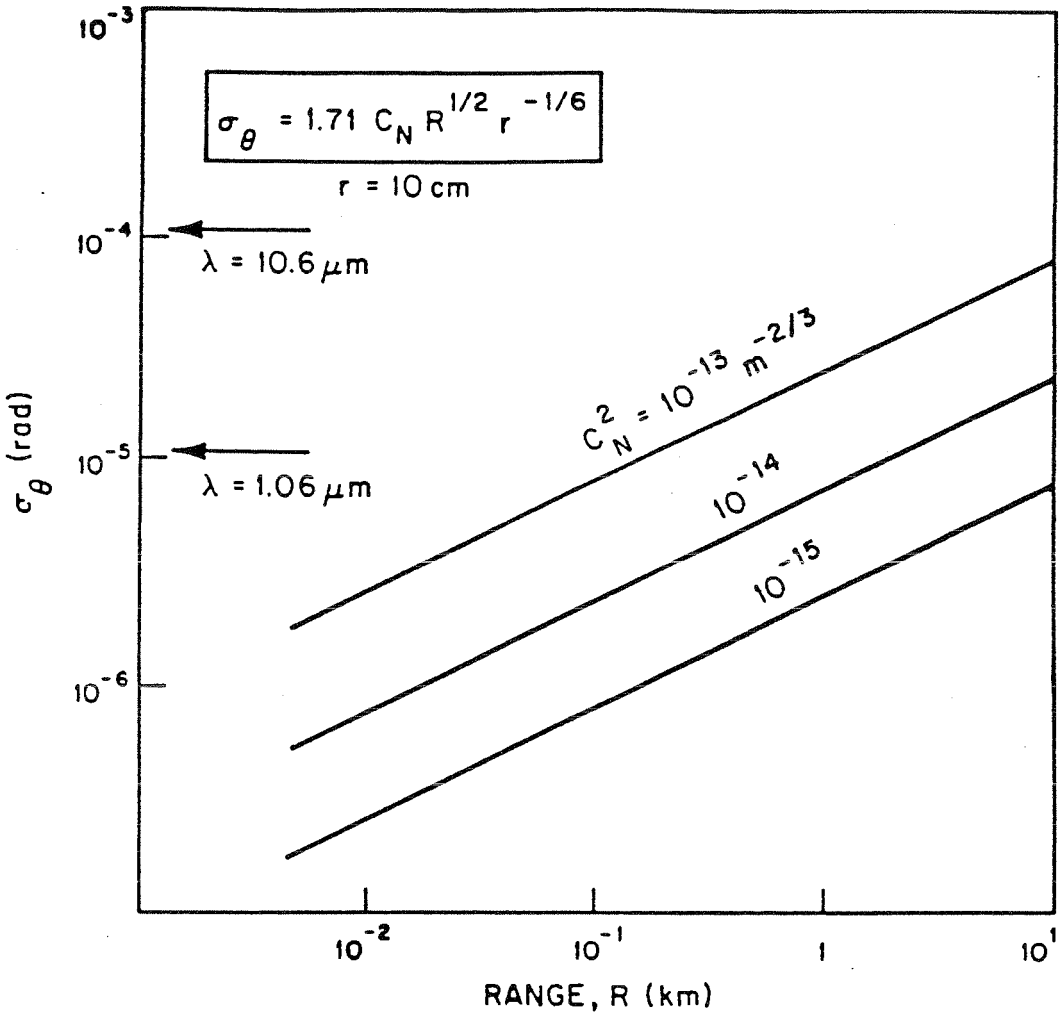

Figure 18. Root Mean Square Angular Beam Spread Due to Turbulence.

Table 7. Noise Sources.

1- Signal Shot Noise.

$$\bar{i}^2_{SN} = 2qG^2F'RP_RB \qquad (P_R \text{ is the received signal power})$$

2- Background Shot Noise.

$$\bar{i}^2_{BN} = 2qG^2F'RP_RB \qquad (P_B \text{ is the background power})$$

3- Dark Current Shot Noise.

$$\bar{i}^2_{DN} = 2qG^2F'I_DB \qquad (I_D \text{ is the dark current})$$

4- Thermal (Johnson) Noise.

$$\bar{i}^2_{TN} = \frac{4kTB}{R_L} \qquad (T \text{ Noise Temperature})$$

5- Amplifier Noise.

$$\bar{i}^2_{AN} = \frac{4(F-1)kT_{290}B}{R_L} \qquad (F \text{ is the Noise Figure})$$

Where:

R = Current responsivity of detector

G = Gain of detector

q = Electronic charge

F' = Detector gain mechanism noise factor

B = Noise bandwidth

k = Boltzmann constant

T = Temperature of load resistor

R = Load resistance

T_{290} = 290K reference temperature

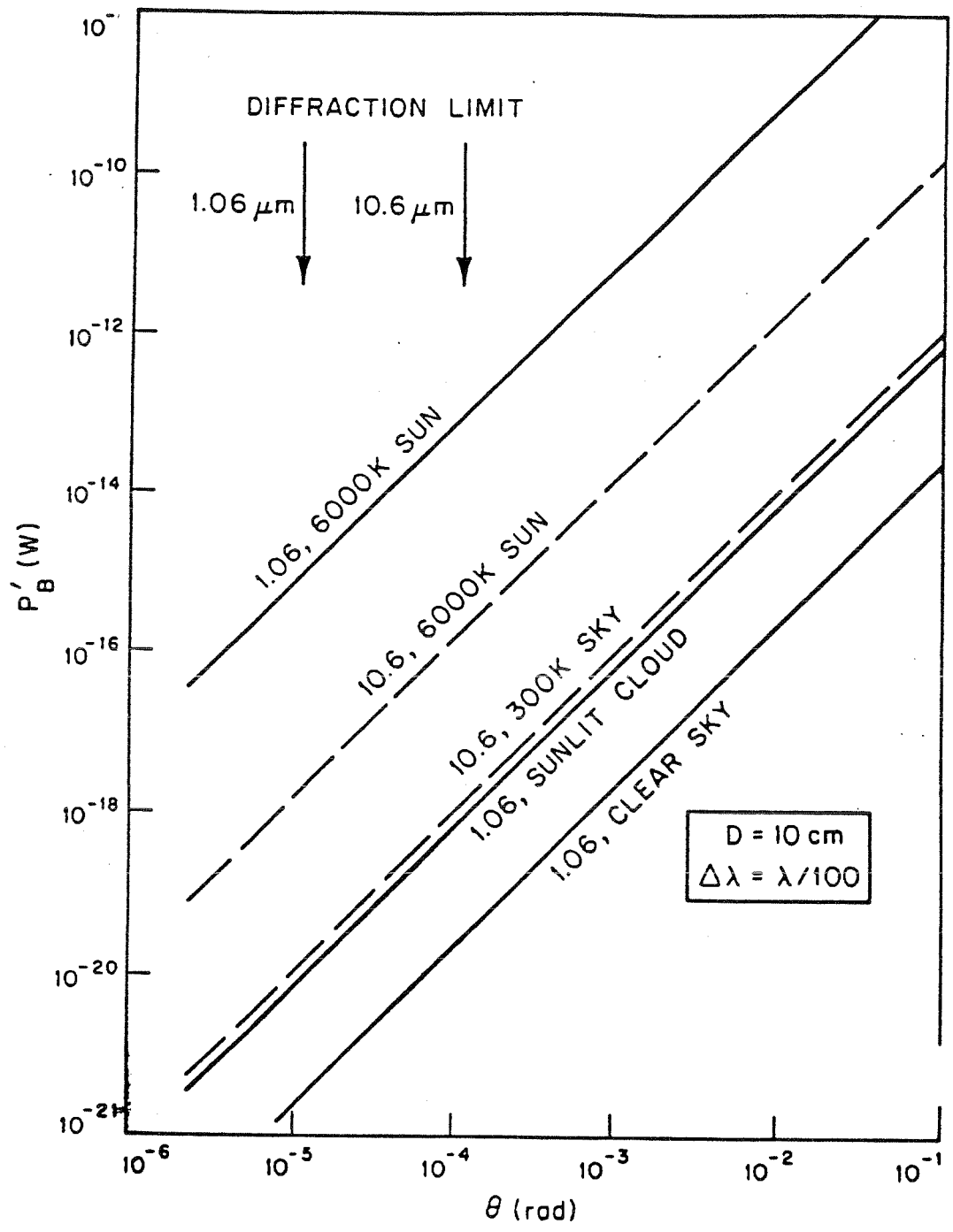

Figure 20. Background Power Collected by the Receiver.

Table 8. Background Spectral Radiance N_λ.

Wavelength	Scattering (Clear Sky)	Sunlit Cloud	6000K Sun	300K Sky
1.06μm	2.5×10^{-8} $W.m^{-2}.sr^{-1}.\mu m^{-1}$	7×10^{-7}	8×10^{-2}	-----
10.6μm	--------	-------	2×10^{-5}	10^{-7}

Table 9. SYSTEM PARAMETERS FOR DIRECT AND HETERODYNE SYSTEMS AT 1.06 AND 10.6μm.

Parameter	1.06 Direct	10.6 Direct	10.6 Heterodyne
σ	10 cm	10 cm	10 cm
Θ	10^{-4}rad	10^{-4}rad	10^{-4}rad
α	$0.610\ km^{-1}$ (2.65 dB/km)	$0.357\ km^{-1}$ (1.55 dB/km)	$0.357\ km^{-1}$ (1.55 dB/km)
A	$\pi(10\ cm)^2/4$	$\pi(10\ cm)^2/4$	$\pi(10\ cm)^2/4$
ε	0.15	0.15	0.15

Table 10 DIRECT DETECTION NEP/$Hz^{1/2}$ AT 1.06 AND 10.6μm

Noise	NEP/$Hz^{1/2}$	1.06μm	10.6μm
Background	$(2qF'P_B'T/R)^{1/2}$	1.5×10^{-18} W/Hz (Sunlit Cloud)	1.0×10^{-19} (300K)
Dark Current	$(2qF'I_D/R^2)^{1/2}$	4.6×10^{-12}	1.32×10^{-12}
Johnson	$(4kT/RG^2R^2)^{1/2}$	1.1×10^{-12}	4.2×10^{-12}
Amplifier	$(4(F-1)kT_{290}/RG^2R^2)$	1.1×10^{-12}	4.2×10^{-12}
Total	$(\sum_i^4 (NEP/Hz^{1/2})^2)^{1/2}$	4.9×10^{-12}	5.9×10^{-12}

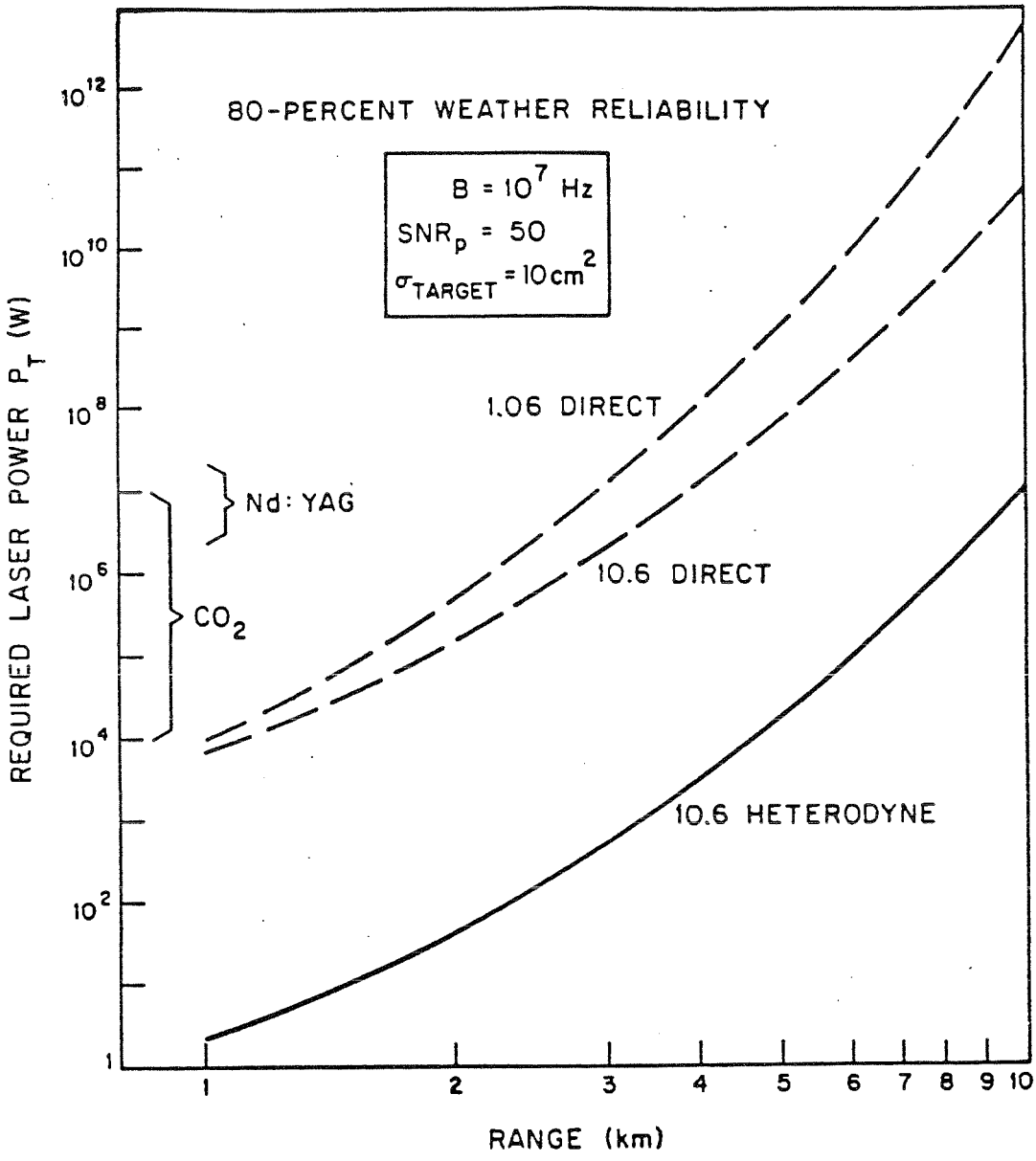

Figure 21. Required Laser Power P_T (W) versus Range.

IMAGING LASER RADARS

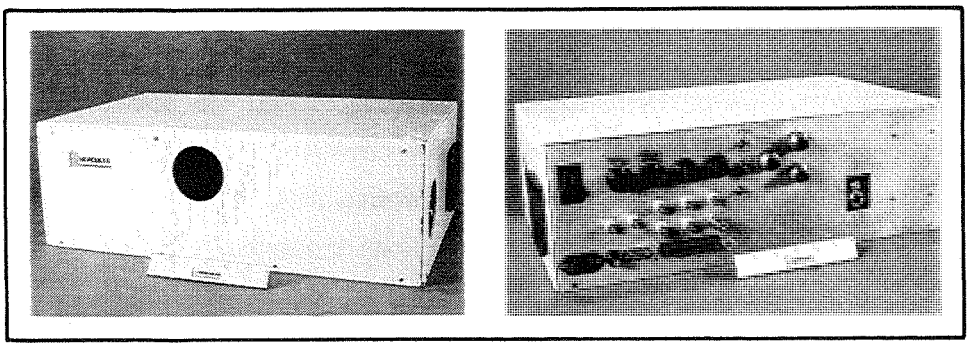

High Performance, Solid State Diode-Pumped Lasers

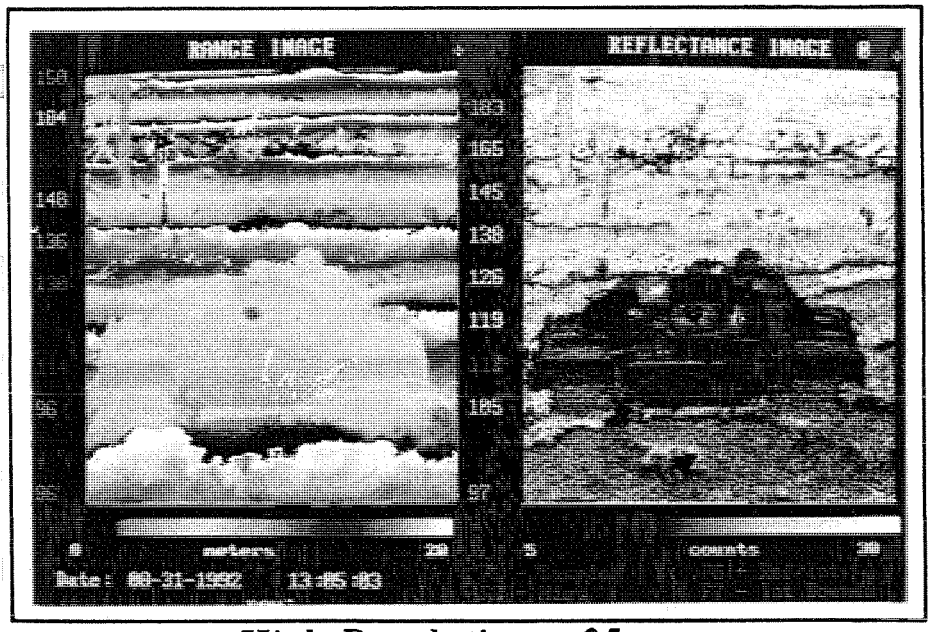

High Resolution .25 mr

BENEFITS

- ★ High Resolution-Reflectance Images
- ★ No Diurnal Image Shifts as in Passive IIR
- ★ Day/Night Operation
- ★ Fully Complements MMW Radar
- ★ Designed to be Low Cost
- ★ Countermeasure-Robust

APPLICATIONS

- ★ Missile Seekers
- ★ Seekers for Recon/BDA/ Lethal UAVs
- ★ Environmental Monitoring
- ★ Drug Interdiction
- ★ Power Line Avoidance

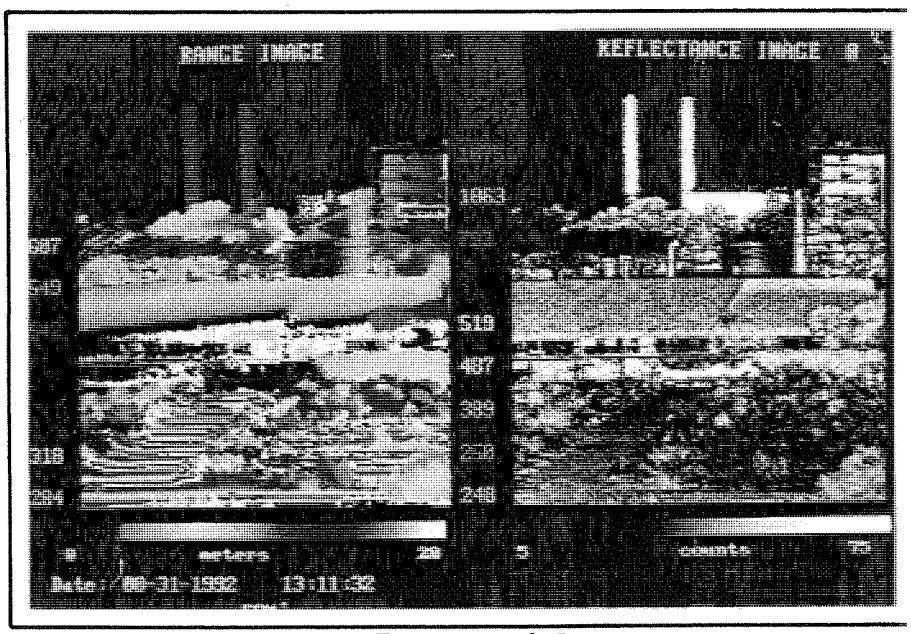

Long Range >2 km

For Further Information, contact:
Smart Weapons Marketing

Phone 813-572-3259

HERCULES

Hercules Defense Electronics Systems, In

13133 34 Street North
Clearwater, FL 3462

Design Study of an Helicopter Mounted Electrooptic Target Acquisition and Laser Designation and Ranging System (HEODS)

Larry A.Stockum, Rockwell International Corporation
Michael K.Masten, Texas Instruments Incorporated
Manuscript Presentators
Dominique Souilhac and Dominique Billerey
Laboratoire d'Electricité et de Mécanique
2 Avenue de la Forêt de Haye,54500 Vandoeuvre-lès-Nancy,France

ABSTRACT

In this paper, we describe a Helicopter mounted Electrooptic target acquisition and laser designation and ranging system (HEODS) using a Nd:Yag laser at 1.06µm and a solar illuminated sensor for acquisition and pointing. System configuration, interface, performance and environmental requirements are defined and a HEODS system design example with its track loop design approach is described which is representative of what can be expected in the field.

1. INTRODUCTION.

A stabilization and tracking system is an electromechanical assembly designated to maintain the orientation of an electronic or optical sensor "payload", so that it is pointed in a preselected or scenario dependent direction (toward the target) and hold steady in inertial space along the selected orientation.

Such system is designed to precision control the angular position of the line-of-sight of a sensor so that it is isolated from the base (airframe of the vehicle) dynamics and accurately pointed toward the target.

Ref.[1-25] list the recent work reported in the field of stabilization,tracking and laser pointing systems.

Section 2 of this paper describes a HEODS system design example using a Nd:Yag laser at 1.06µm and a solar illuminated sensor for acquisition and pointing. The parameters of the laser pointing system are defined, a sensor system baseline design is described and the Nd:Yag laser range receiver signal to noise ratio is calculated.

Section 3 describes the track loop design example of HEODS.

Section 4 is a discussion and conclusion.

2. HEODS STABILIZATION AND LASER POINTING SYSTEM EXAMPLE USING A ND:YAG LASER AND A SOLAR ILLUMINATED SENSOR.

2.1. Mission.

An helicopter mounted electrooptic target acquisition and laser designation and ranging system (HEODS), shall provide target detection-recognition and precision laser designation for an airborne target under daytime conditions.

2.2. Threat.

The target is another helicopter with a cross-section of 4 meters by 3 meters, a reflectivity of 0.5 and an acceleration capability of $5m/s^2$. The target minimum contrast relative to the sky background is 0.25.

2.3. System Configuration.

A two axis platform with a CCD TV sensor and laser mounted on the gimbal is shown in Fig1. The sensor has 400 pixels (horizontally)x300 pixels (vertically) with 20 μm square pixels. The sensor has a responsivity of 50Volts/Watt/m^2 and a noise level of 5 milliwatts RMS. The laser is a Nd:Yag with an output energy of 100 millijoules/pul-se and a raw beam divergence of 1mrad. The range receiver has a noise equivalent power of $30x10^{-9}$ Watts and utilizes a TV sensor optics as the receiving aperture. The system will use an optimum brightness monitor with a magnification of 25.

2.4. Interface Requirements.

The HEODS shall mount over the rotor of the Helicopter and be cued to the target by the operator helmet mounted sight. The maximum weight of the system shall be 75 pounds.

2.5. Performance Requirements.

The performance requirements are:

-Recognition of a target at 10km with 6 cycles resolution on the target.

-Range a target up to a distance of 10km.

-50 millijoules minimum energy on the target per pulse, 90% of the time. The beam centroid is 1.0 meter from the target, 63% of the time.

2.6. Environment.

The translation acceleration is 1G peak at 8 hertz each axis. The angular acceleration is 10 radians/second^2 at 8 Hertz each axis. The atmospheric conditions produce an exponential attenuation coefficient of 0.05/km in the 1.06 μm band. The target is solar illuminated with a minimum illumination of 1000 lumens/m^2.

2.7. HEODS System Design Example.

2.7.1. Selection of the Design Parameters.

We calculate the system cutoff frequency:

$$f_{cs} = \frac{N}{\frac{\text{Tot Size}}{\text{Range}}} = \frac{6}{\frac{3}{10\text{km}}} = 20 \frac{\text{Cycles}}{\text{Milliradian}}$$

We calculate the optics Modulation Transfer Function (MTF) at the cutoff spatial frequency:

$$MTF_{optics}\ (f_x=20) = \frac{2}{\pi}[\cos^{-1}(A) - A(1-A^2)^{1/2}]\ ;\ A = \frac{f_x}{f_c}\ ;\ f_c = \frac{D}{\lambda} \qquad (1)$$

$$f_c = \frac{0.1\ \text{m}}{0.5\mu\text{m}} = 200 \text{ cycles/Milliradians ; hence: MTF } (f_x=20) = 0.81 \text{ (acceptable)}$$

We calculate the Range Receiver Signal-to-Noise Ratio for the Nd:Yag laser:

For a minimum energy on the target of 50mJ/pulse, the energy received by the range receiver is:

$$E_{RR} = \frac{E_{TJ} \cdot \rho_T \cdot e^{-\alpha R} \pi (\frac{D^2}{4}) \cdot \tau_o}{\pi R^2} = \frac{(50\text{x}10^{-3}) \cdot .5 \cdot e^{-.04(10)} (\frac{.1)^2}{4} \cdot .5}{(10^4)^2} \qquad (2)$$

$$E_{RR} = 2.09\text{x}10^{-13} \text{ Joules}$$

The laser pulse width = $20\text{x}10^{-9}$ seconds

$$P_{RCVR} = \text{Power at Range Receiver} = \frac{E_{RR}}{LPW} = \frac{2.09/10^{-13}}{20\text{x}10^{-9}} = 1.04\text{x}10^{-5} \text{ Watts}$$

$$SNR = \frac{P_{RCVR}}{NEP} = \frac{1.04\text{x}10^{-5}}{100\text{x}10^{-9}} = 104 \qquad (3)$$

Hence, a 0.1m aperture is excellent for ranging to 10km.

The Sensor Signal-to-Noise Ratio is calculated as follows:

First, we calculate the solar irradiance corresponding to 1000 Lumens/meter^2

$$E_V = \text{Lumens} = 673 \int_{.38}^{.76} E_e(\lambda) V(\lambda) d\lambda \quad \text{(see Fig.2)} \qquad (4)$$

1000 Lumens requires PEAK on E_e curve of Fig 3 = 17.6 Watt/m^2.µm

Second, we calculate the irradiance on the sensor image plane:

$$E_D(\lambda) = \frac{\pi \tau_o L_t(\lambda) \tau_A}{4F^2_{\ddagger}} \qquad (5)$$

Where τ_o = Transmission of optics = 0.5 (given)

τ_A = Atmospheric Transmission = $e^{-\alpha R} = e^{-(.05)(10)} = 0.606$

$L_t(\lambda)$ = Target Radiance = $E_e(\lambda) \cdot \rho/\pi$ W.cm^{-2}.sr^{-1}

ρ = Target Reflectivity

$F_{\ddagger}$ = Optics Focal Length/Optics Diameter =1.0/0.1 = 10 (See below)

What focal length is required to obtain 20 pixels on the target?

The target minimum angular size is:

$$\theta_{min} = \frac{\text{minimum dimension}}{\text{maximum range}} = \frac{3 \text{ meters}}{10000 \text{ meters}} = 300 \text{ microradians}$$

Instantaneous Field of View = IFOV = Pixel Angular Size = Pixel Linear Size/f_L

Where f_L = Focal Length = $\frac{220 \text{ microns}}{15 \text{ microradians}} \approx 1.33$ m (since 20 pixels on target requires 15 microradians pixels)

The detector resolution is 15 microradians and the system resolution will be larger than 15 microradians and will depend on the optics and the stabilization MTF curve , (Fig.3).

The Field of View = FOV = 400x15μrad by 300x15μrad= 6.0milliradian by 4.5 milliradian = 0.25°x0.34°.

Third, we calculate the detector target signal V_T:

$$V_T = \int_{\lambda_1}^{\lambda_2} E_D(\lambda)R(\lambda)\Delta T d\lambda + \int_0^{\infty} V_{N\lambda} d\lambda = 0.12 \text{ (Fig.2,3)} \quad (6)$$

The background Voltage = $V_B = V_{Background} = \int_{\lambda_1}^{\lambda_2} L_B(\lambda)R(\lambda)\Delta T d\lambda$

The specifications state that the minimum contrast is 0.25.

Therefore: $$\frac{V_T - V_B}{V_T + V_B} = 0.25, \quad \text{hence } V_B = \frac{0.75V_T}{1.25} + 0.6V_T \quad (7)$$

$$V_{SNR} = \frac{V_T - V_B}{V_N} = \frac{0.4V_T}{5mV} = 9.42 \quad (8)$$

Table 1 lists the sensor system baseline calculated characteristics.

2.7.2. Laser Pointing System Design.

The specifications requirements are the following:

(1) 50 mJ/Pulse on the target 90% of the time.

(2) 1 meter, 1σ error.

The design approach is the following:

(1)We calculate the allowable pointing error as a function of the beam divergence and the range.

(2) We select the beam divergence.

(3) We define the pointing error budget

(4) We design the boresight system to meet the boresight pointing error requirement

(5) We design the track loop to meet the dynamic tracking error requirement.

Table 2 and Appendix A calculate the pointing accuracies and the energy of the laser beam energy on the target

2.7.3. Track Loop Design Approach: [15] [16]

We develop a preliminary electro-mechanical configuration based on the sensor package, available volume, gimbal freedom, cost and schedule. We configure a design to maximize the structural modes and minimize friction.

We develop a stabilization design based on the structural modes estimates.

We calculate the expected jitter for the specified environment.

We define the allowable error for each error source and we define the corresponding design requirement. Finally we iterate the design.

Table 3,4 and Fig.6- 18 summarize our trackloop design investigation for HEODS.

3. DISCUSSION AND CONCLUSION.

We have investigated in detail an helicopter mounted electrooptic target acquisition and laser designation and ranging system (HEODS), using a Nd:Yag laser, a solar illuminated sensor and a track loop system for acquisition and tracking of a moving target.

Factors that produce stabilization errors are (1) Friction, (2) Mass unbalance (for high G environment),(3) Geometric coupling and (4) Kinematic coupling.

Laser beam size was selected to maximize the energy on the target for the acheivable pointing error and the target size. A target angular size of 300 microradians by 400 microradians indicates that a beam divergence less than 200 microradians is required to permit 50 microradians pointing errors. Physical packaging constraints and laser beam wavefront characteristics usually limit the minimum beam diameter for an airborne tactical application. 200 microradians is a good first choice for the beam divergence.

The allowable pointing error is determined by the target size, the required energy on the target, the beam divergence and the beam centroid relative to the target centroid requirement requirement. For a 0.4 mR (H)x0.3 mR (V) target, a 0.2 mR beam divergence and a 1 meter at 10000 meters (100 mrad) pointing requirement, an allowable horizontal pointing error is 100 mrad, since this horizontal error will keep the entire beam on the target. An allowable vertical pointing error is 50 microradians to keep the entire beam on the target. Pointing accuracy required to meet 50 millijoules requirement and range receiver requirement have been calculated. The optical aperture significantly affects

the sensor resolution, sensor sensitivity and the receiver signal to noise ratio. Each of these performance parameters requires an analysis which includes the aperture. Additionally, the physical package constraints often limit the aperture size.

Approximate amplitude and phase at 8 hertz of the transfer function of the track loop are caculated from the Bode plots representative of the HEODS system.

All the calculated characteristics of the HEODS system are representative of what can be expected in the field.

4. ACKNOWLEDGEMENTS.

We are grateful to Larry A.Stocckum, Rockwell International Corporation and Michael K.Masten, Texas Instruments Incorporated, for fruitful theoretical support in the field of Stabilization, Tracking and Laser Pointing Systems Design and Development.

5. REFERENCES.

1.Laskin,R.A. and S.W.Sirlin,"Future payload isolation and pointing system technology", Journal of Guidance, control and dynamics, Vol.9(4), 1986, pp.469-477.

2.Stockum,L.A. and C.R.Carroll,"Precision stabilized platforms for shipboard electrooptical systems",Proceedings of the Society of Photo-Optical Instrumentation Engineers,Vol.493, 1984.

3.Forys,E.L.,"Internal bearing stabilized sighting units (IBSSU)-A new concept in stabilization",Proceedings of the Society of Photo-Optical Instrumentation Engineers, Vol.242,1980, pp.159-162.

4."Adaptive Optics Systems and Technology",Proceedings of the Society of Photo-Optical Instrumentation Enginers, Vol.365,August 1982.

5."Adaptive Optics",Proceedings of the Society of Photo-Optical Instrumentation Engineers, Vol.551, 1985.

6.Rue,A.K.,"Stabilization of precision electro-optical pointing and tracking systems",IEEE Transactions on Aerospace and Electronic Systems, Vol.AES-5 (5), 1969, pp.895-819 (Correction:November 1970,pp.855-857).

7."Acquisition, Tracking and Pointing",Proceedings of the Society of Photo-Optical Instrumentation Engineers", vol.641, 1986.

8.Masten,M.K. and J.M.Hilkert,"Impact of Optics Design Decisions Upon Line-of-Sight Stabiliztion",Proceedings of the Society of Photo-Optical Instrumentation Engineers, Vol.389, 1983, pp.107-120.

9.Ellison,Burce and James Richi,"Inertial Stabilization of Periscopic Sights Band Driven Three Axis Gimbal",Proceedings of the Society of Photo-Optical Instrumentation Engineers, Vol.389, 1983, pp.107-120.

10.Gerson,G. and Rue,A.K.,"Chapter 22-Tracking Systems,"The Infrared Handbook, Department of the Navy, Washington,D.C., 1978.

11.Durante,D.D. and C.G.Hunter, "Beam Jitter Transmission and Correction","Proceedings of the Society of Photo-Optical Instrumentation Engineers, Vol.450, 1983.

12.Distefano,III,J.J.,A.R.Stubberud and I.J.Williams, Theory and Problems of Feedback and Control Systems, SDRAUM'S Outline Series, McGraw-Hill, 1967.

13.Research and Development Technical Report ECOM-7043 'Night Visionlaboratory Static Performance Model for Thermal Viewing Systems" April 1975.

14.Masten,M.K. and J.M.Hilkert,"Electromechanical System Configurations for Pointing, Tracking and Stabilization Applications", Proceedings of the Society of Photo-Optical Instrumentation Engineers.Vol.779, 1987, pp.75-87.

15.Guy Bogdadi,"Contrôle I", Course Notes, Ecole de Technologie Supérieure de Montreal 1977.

16.Larry A.Stockum and Michael K.Masten, "Precision Stabilization, Tracking and Laser Pointing Systems Design and Development", SPIE Course Notes,O/E Aerospace Sensing, Orlando 1993.

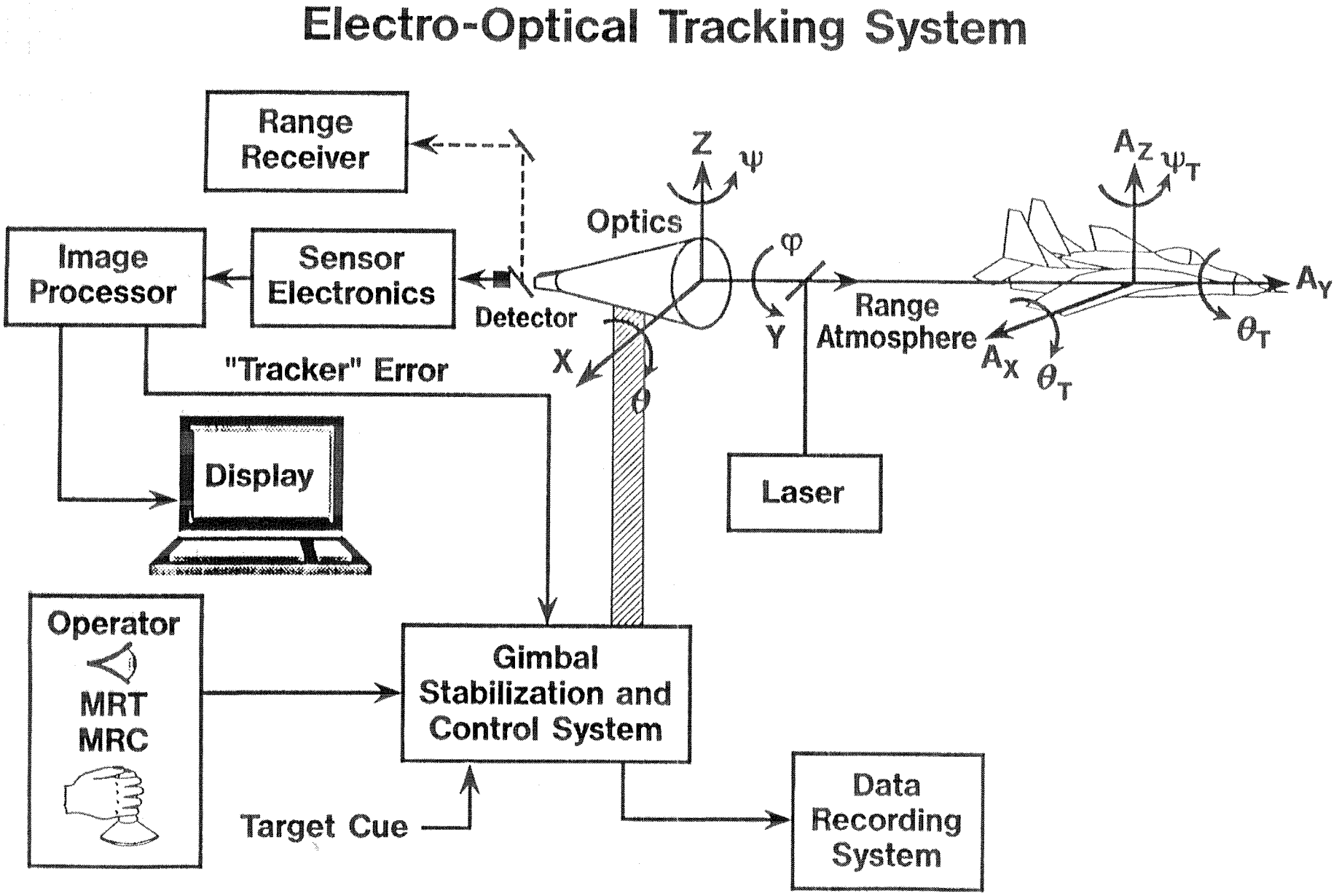

Figure 1: Electro-Optical Tracking System

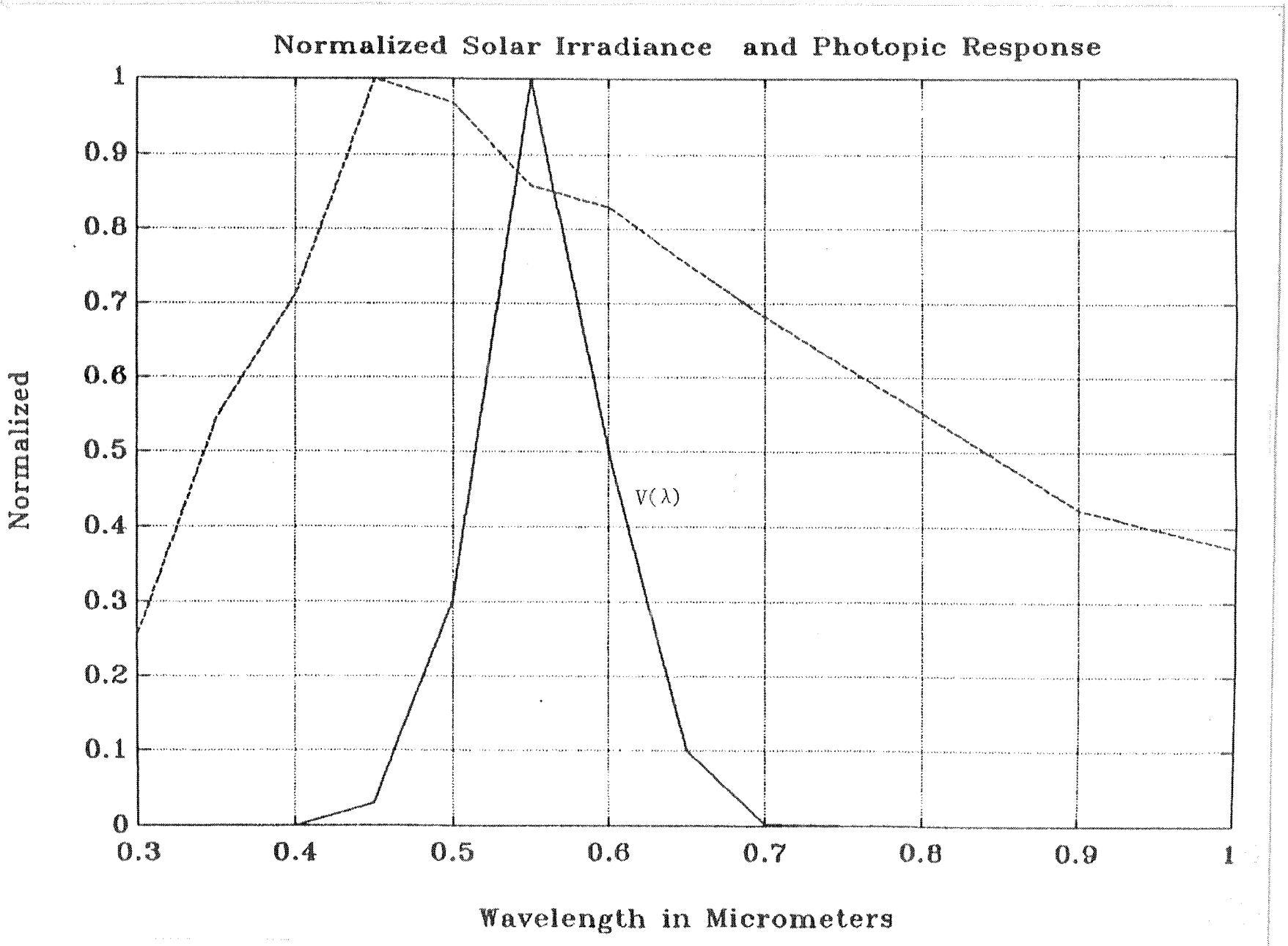

Figure 2. Normalized Solar Irradiance and Photopic Response.

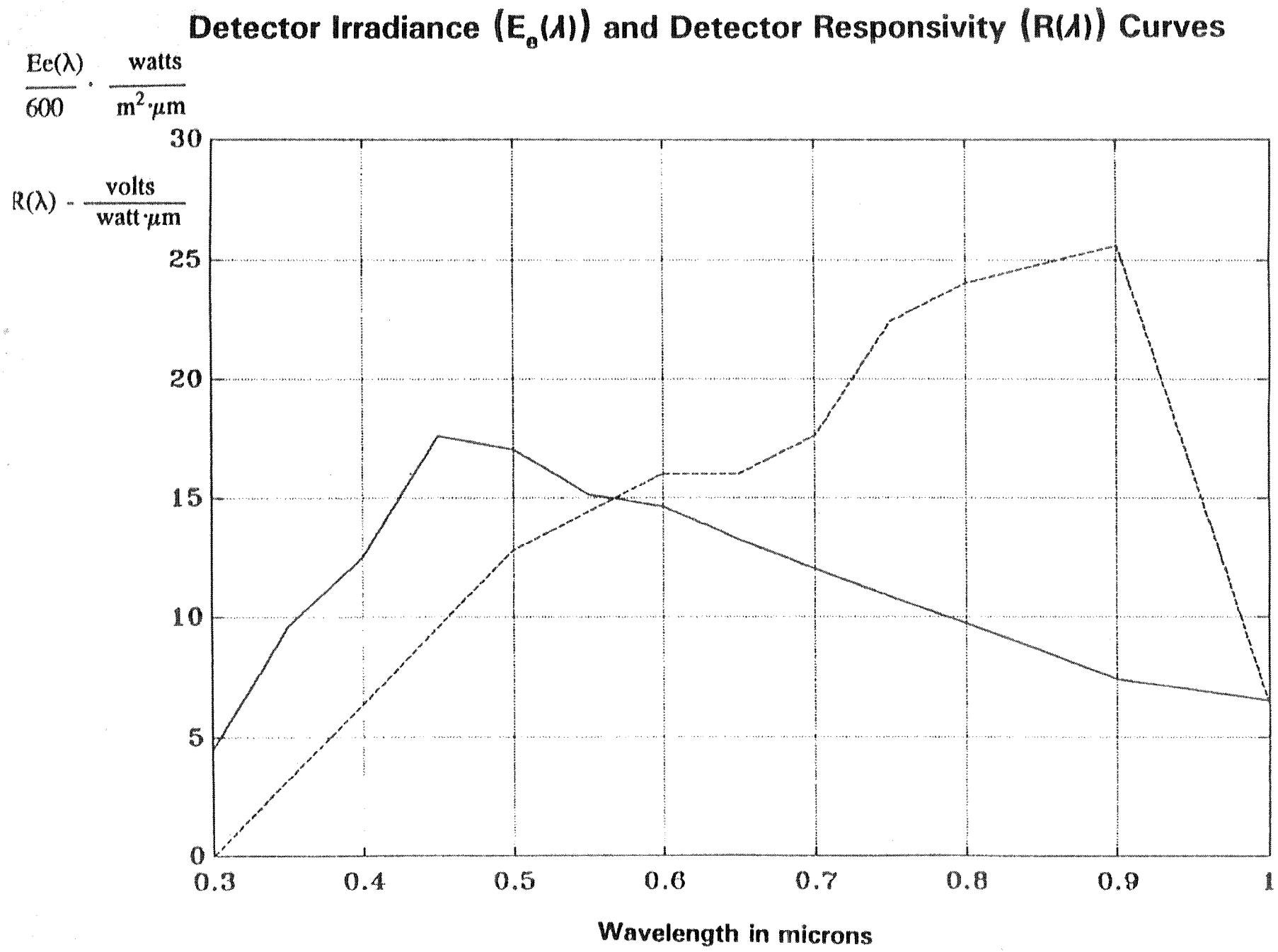

Figure 3. Detector Irradiance ($E_e(\lambda)$) and Detector Responsivity ($R(\lambda)$) Curves.

Table 1. Sensor System Baseline Design.

Aperture: 0.1 meter

Focal Length: 1.0 meter

Detector IFOV: 0.020 milliradian

ΔJ = 0.010 milliradian

Display: Magnification 25, Γ = brightness = 1.0

Optics MTF = $\frac{2}{\pi}[\cos^{-1}(A)-A(1-A^2)^{1/2}]$ $A = \frac{f_x}{f_c}$, $f_c = \frac{D}{\lambda} = \frac{0.1}{0.5}$ = 200Cycles/mR

MTF(f_x=20) = 0.81 (See Fig.4)

Detector MTF = $\frac{\sin(\pi.IFOV.f_x)}{\pi.IFOV.f_x}$ (See Fig.4)

Display MTF = $\frac{\sin(\pi.\Delta J.f_x)}{\pi.IFOV.f_x}$ (See Fig.4)

Display MTF = $e^{-\Gamma f_x/m}$ (See Fig.4)

System MTF = OPticsxDetectorxJitterxDisplay (See Fig.4)

Sensor System Recognition Range Capability (See Fig.4)

Sensor Contrast Performance

$$MRC(f_x) = \frac{2}{1 + \frac{f_{cs}.MTF}{0.03f_x}}$$ (See Fig.5)

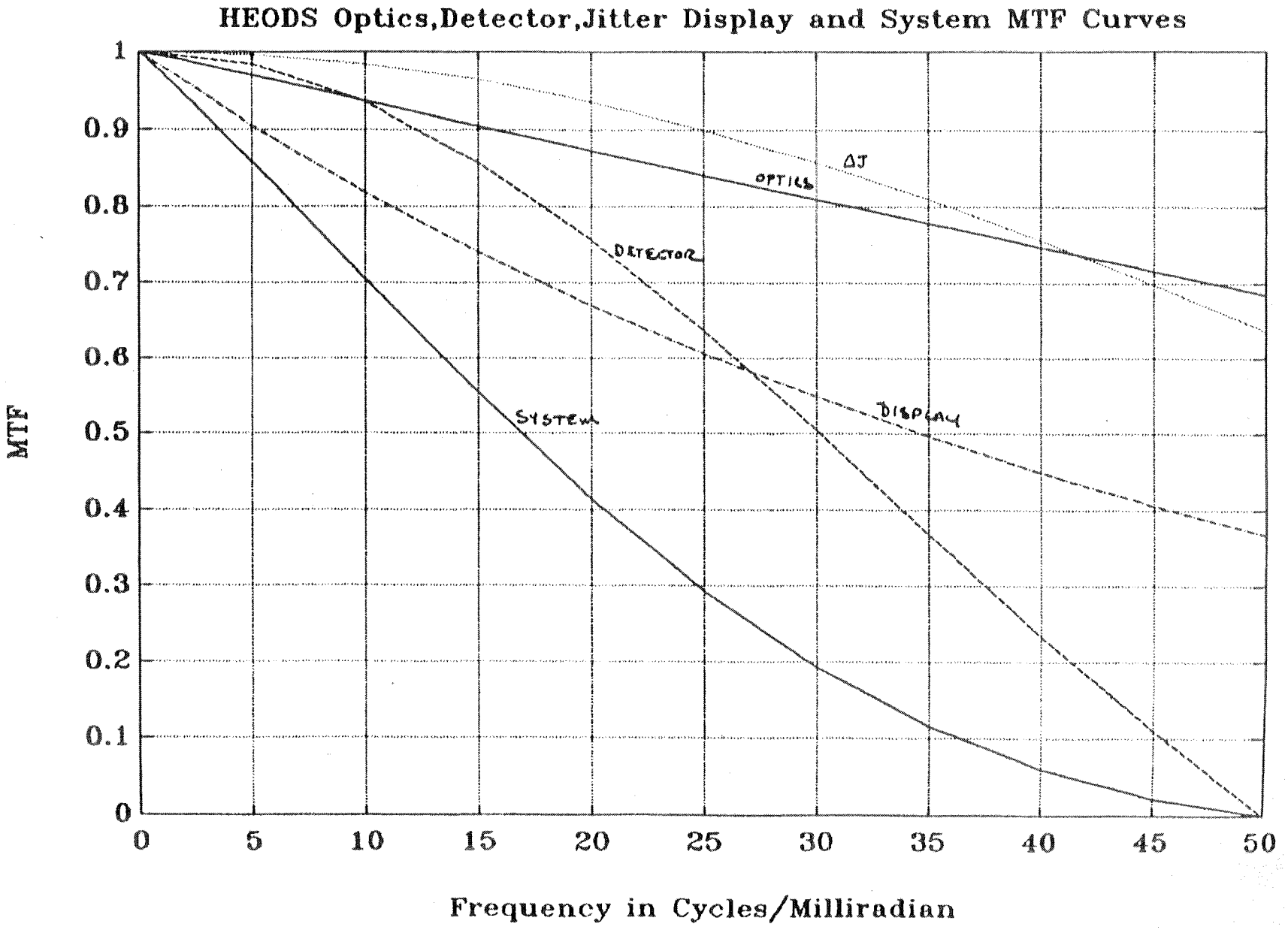

Figure 4. HEODS Optics, Detector, Jitter Display and System MTF Curves.

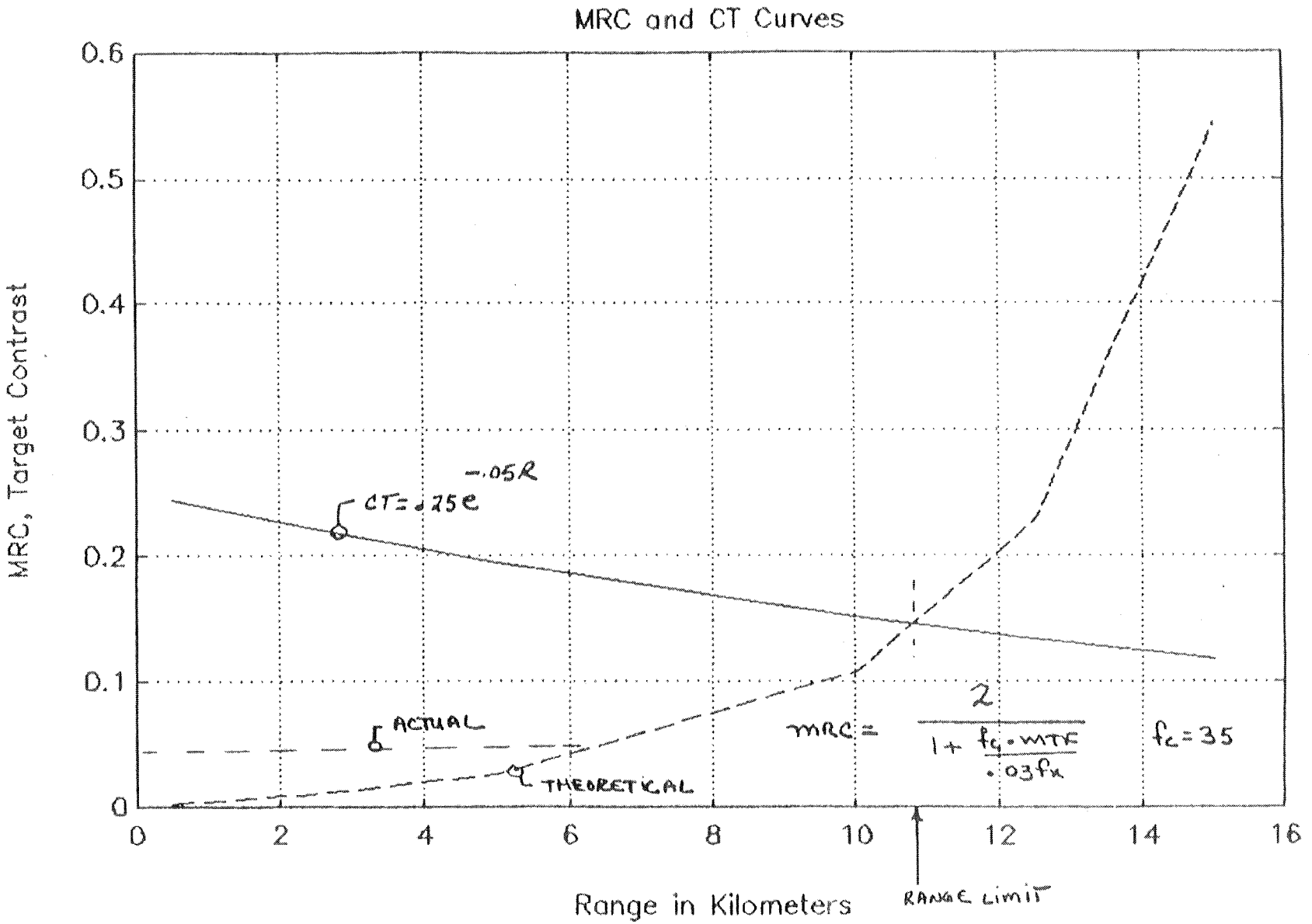

Figure 5. Sensor Contrast Performance

Table 2:

Energy on target calculations show that for a 200 urad beam, the following pointing accuracies are required 90% of the time:

R	$\psi\epsilon$		$\Theta\epsilon$	
	Angular	Linear	Angular	Linear
10 km	100 urad	1.0 M	100 urad	1.0 meter
5 km	300 urad	1.5 M	250 urad	1.24 meter
1 km	1900 urad	1.9 M	1400 urad	1.40 meter

The centroid pointing requirement is 1 meter error 63% of the time, which is equal to the following angular errors versus range:

R	$\psi\epsilon$	$\Theta\epsilon$
10 km	100 urad	100 urad
5 km	200 urad	200 urad
1 km	1000 urad	1000 urad

What is the beam pointing requirement?

90% requirement dominates
Pointing error = mean + dynamic error
Mean errors constant ψ_o, Θ_o

Pointing error requirement
Θ_o = 40 urad, ψ_o = 40 urad (2 pixels)

Range	$\Theta_{1\sigma}$	$\psi_{1\sigma}$
10 km	30 urad	30 urad
5 km	105 urad	130 urad
1 km	680 urad	930 urad

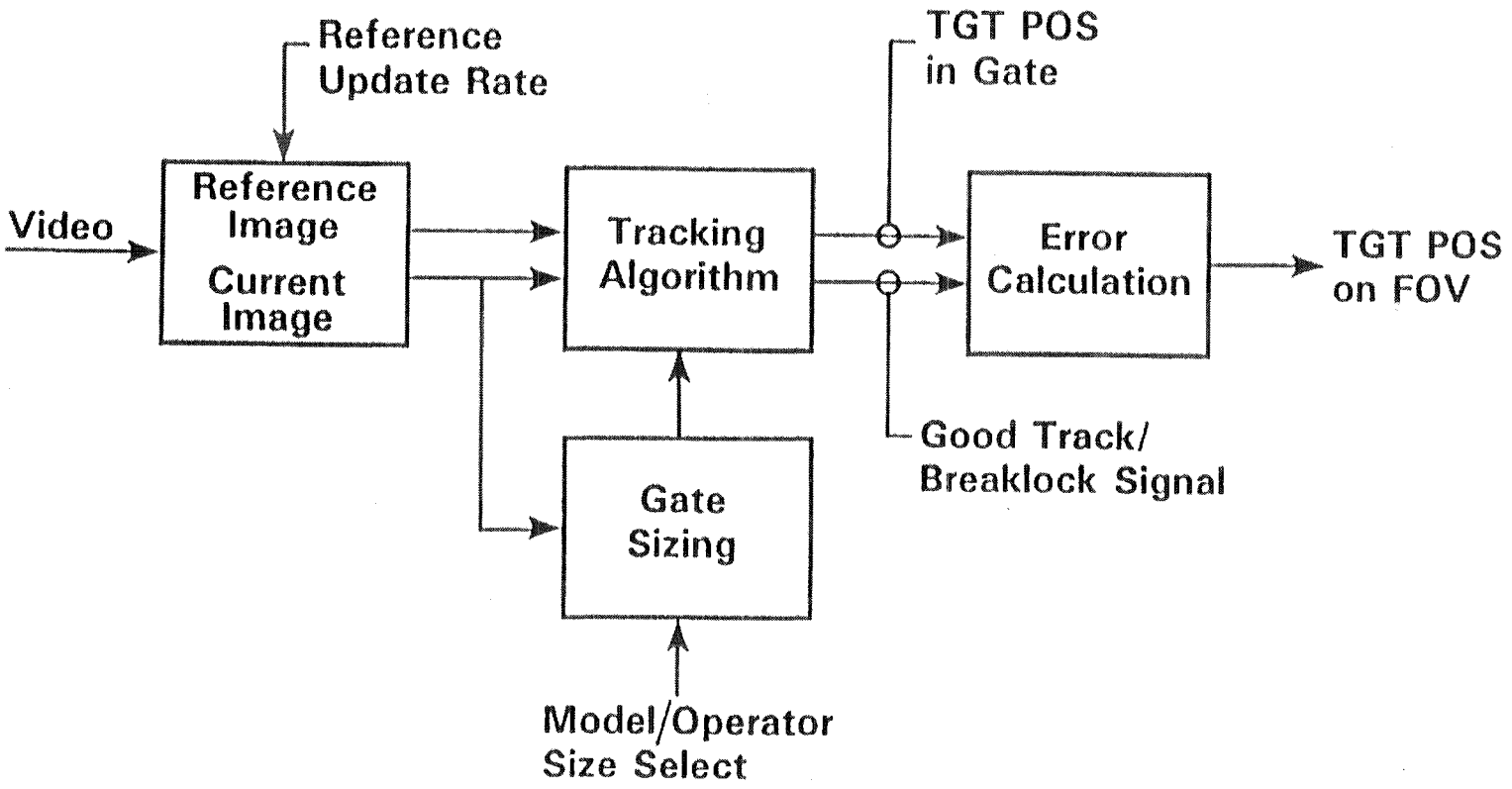

Figure 6 Video Tracker Processing Tasks

Figure 7. IMAGE AND TRACKER GATE COORDINATES
LASER BEAM BORESIGHT CURSOR

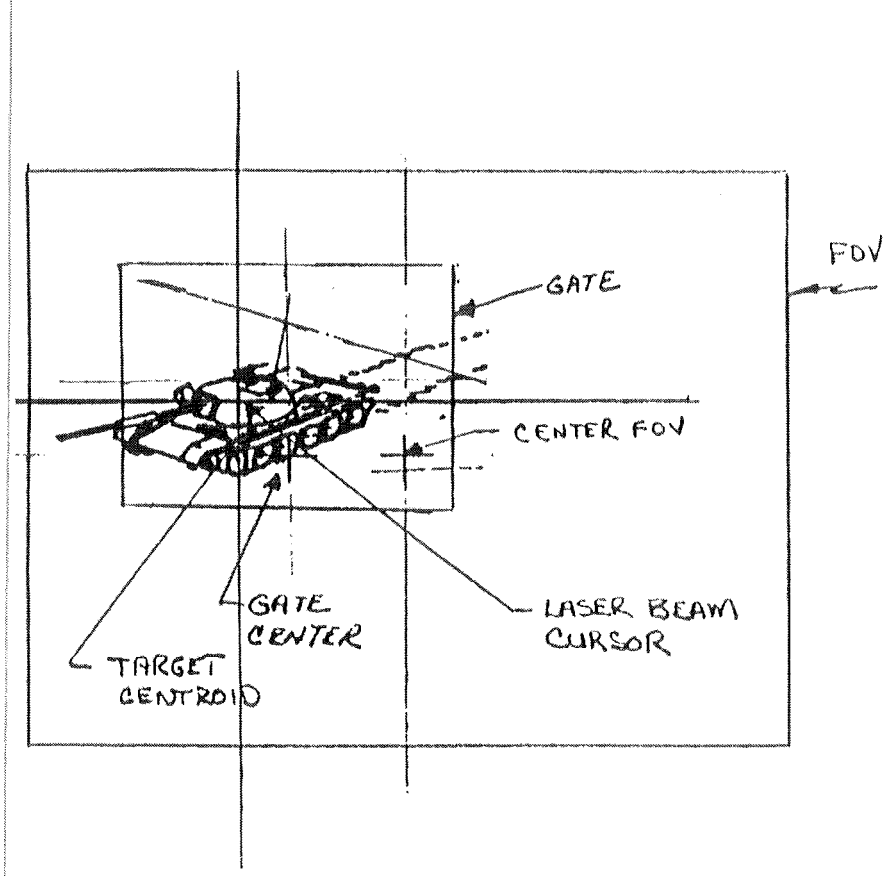

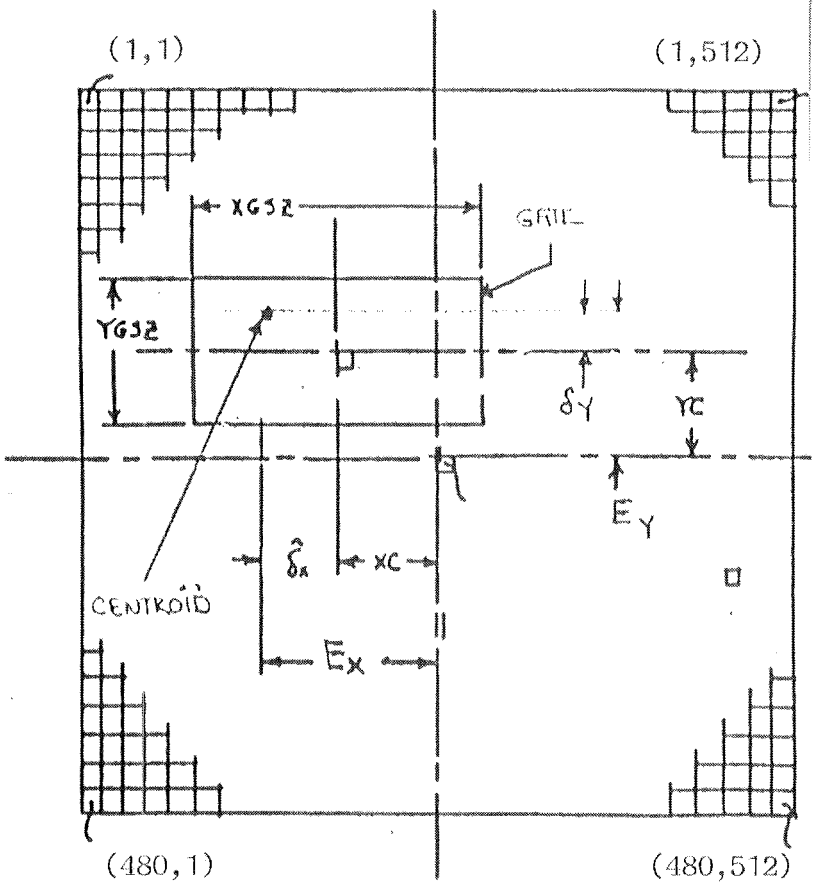

XC, YC = Gate center shift in x,y direction from FOV center
δ_x, δ_y, = Tracker computed target shift from gate center
E_x, E_y = XC + δ_x, YC + δ_y = error signals to stabilized platform

Table 3.

Correlation Algorithm

$$\hat{\delta}_x(k),\hat{\delta}_y(k) = \text{Peak location} = i,j \text{ of } \min \sum_{i'=1}^{8}\sum_{j'=1}^{8} |G'_{kR}(i'-i,j'-j)-G'_k(i',j')$$

$G'_{kR}(i,j)$ = Stored reference image for gate

$G'_k(i,j)$ = Present gate subimage in frame k

$-a<i<b \quad -c<j<d$

Reference
1 1 0 0 0
1 1 0 0 0
1 1 1 0 0
0 0 0 1 1

0	1 1 0 0 0	0
0	1 1 0 0 0	0
0	1 1 0 0 0	0
0	0 0 0 1 1	0
0	0 0 0 1 1	1
1	1 1 1 0 0	0

Best Match

Live

$\hat{\delta}_x=0, \quad \hat{\delta}_y = +1$

Centroid Algorithm

General Form:

$$\hat{\delta}_x(k) = \frac{1}{G'_{ko}} \sum_{i=1}^{M_g}\sum_{j=1}^{N_g} x_j G'_k(i,j)$$

$$\hat{\delta}_y(k) = \frac{1}{G'_{ko}} \sum_{i=1}^{M_g}\sum_{j=1}^{N_g} y_i G'_k(i,j)$$

$$G'_{ko} = \sum_{i=1}^{M_g}\sum_{j=1}^{N_g} G'_k(i,j)$$

$G'_k(i,j)$=Threshold gate subimage array of frame.

M_g,N_g = Number of rows, columns in the gate

Example:

0	0	0	0	0	0	0	0	1	1	
0	0	0	0	0	0	0	0	1	1	
0	0	0	0	0	0	0	0	0	1	
1	0	1	1	1	1	0	0	0	0	
1	1	1	1	1	1	0	0	0	0	
1	1	1	1	1	0	0	0	0	0	
1	1	1	1	0	0	0	0	0	0	
1	1	1	1	1	0	0	0	0	0	
1	1	1	0	0	0	0	0	0	0	
0	1	1	0	0	0	0	0	0	0	
			-3	-2	-1	+1	+2	+3		

$$\hat{\delta}_x = \frac{-3-2-1+1-3-2-1+1+1-3-2-1-3-2-3-2-1}{16}$$

$\hat{\delta}_x = -27/16 = -1.68 \rightarrow -2$

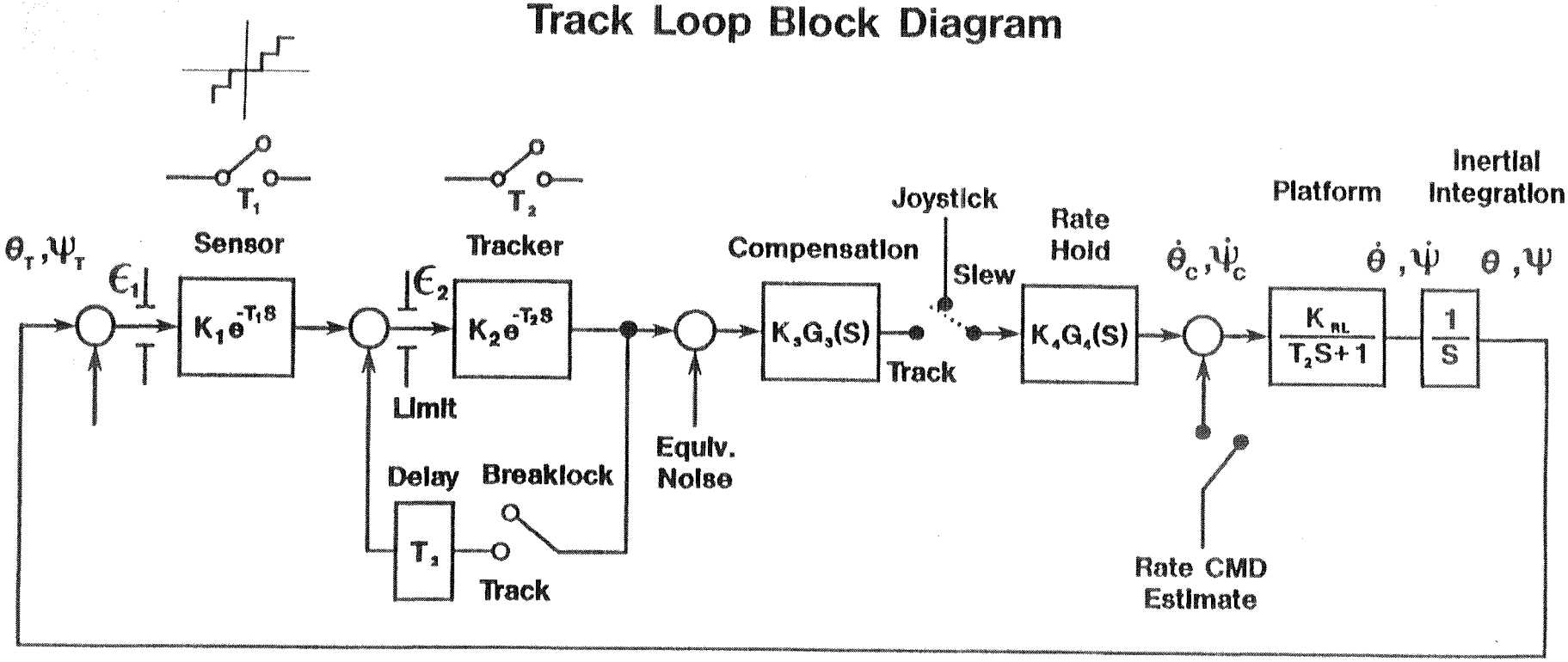

θ_T, ψ_T = Target position in inertial coordinates

$\epsilon_{1\theta}, \epsilon_{1\psi}$ = Target position in FOV

K_1, T_1 = Sensor scale factor (rasters/radian) and time constant (sec)

$\epsilon_{2\theta}, \epsilon_{2\psi}$ = Target position in gate

K_2, T_2 = Tracker scale factor (volts/raster) and time constant (sec)

$K_3G_3(S)$ = Compensation gain and transfer function (volts/volt)

$K_4G_4(S)$ = Rate hold gain and transfer function (volts/volt)

K_{RL}, T_4 = Platform scale factor (rad/sec/volt) and time constant (sec)

Figure 8. Track Loop Block Diagram

Table 4.

Track Loop Bandwidth and Phase Margin-Typical Values.

$$\text{Open Loop Transfer Function} = \frac{K_1K_2e^{-(T_1+T_2)s}K_3G_3(s)K_4G_4(s)KR_L}{s(T_4s+1)}$$

Typical Values:

Type I- $T_1=T_2=0.016$second, $G_3(s)=1$, $G_4(s)=1$, $T_4=0.005$sec, $K_{\text{Bode }1}=10$ to 20

$$\text{OLTF} = \frac{20e^{-0.032s}}{s(0.005s+1)}\Big|_{s=j20} = \frac{20e^{-(0.032)(j20)}}{(20j)(0.1j+1)} \approx 1\angle -132.2 \text{ or } \phi=48^\circ \text{ Great}$$

Type II: $T_1= T_2= 0.016$second, $G_3(s)= 0.2s+1/s$, $G_4(s)=1$, $T_4=0.005$sec, $K_{\text{Bode }2} = 40$

$$\text{OLTF}= \frac{40(0.2s+1)e^{-0.032s}}{s^2(0.005s+1)}\Big|_{s=j10} = 0.89\angle 137.5 \text{ or } \phi=42.\hat{3} \text{ Good}$$

Track Loop Problem Areas

Excessive Time Delay in Loop: $T_1= T_2 = 0.032$sec

Type I System:

$$\text{OLTF}\Big|_{j=20} = \frac{20e^{-(0.064)(j20)}}{20j(0.1j+1)} = 1.0\angle -169 \quad \text{or } \phi=11^\circ \text{ Problem}$$

Type II System:

$$\text{OLTF}\Big|_{j=10} = 0.89\angle -156 \quad \text{or } \phi=24^\circ \quad \text{Minimal}$$

Incorrect Threshold Setting yield loose of target

Lock-on Transients cause SNR reduction or exceed tracker rates.

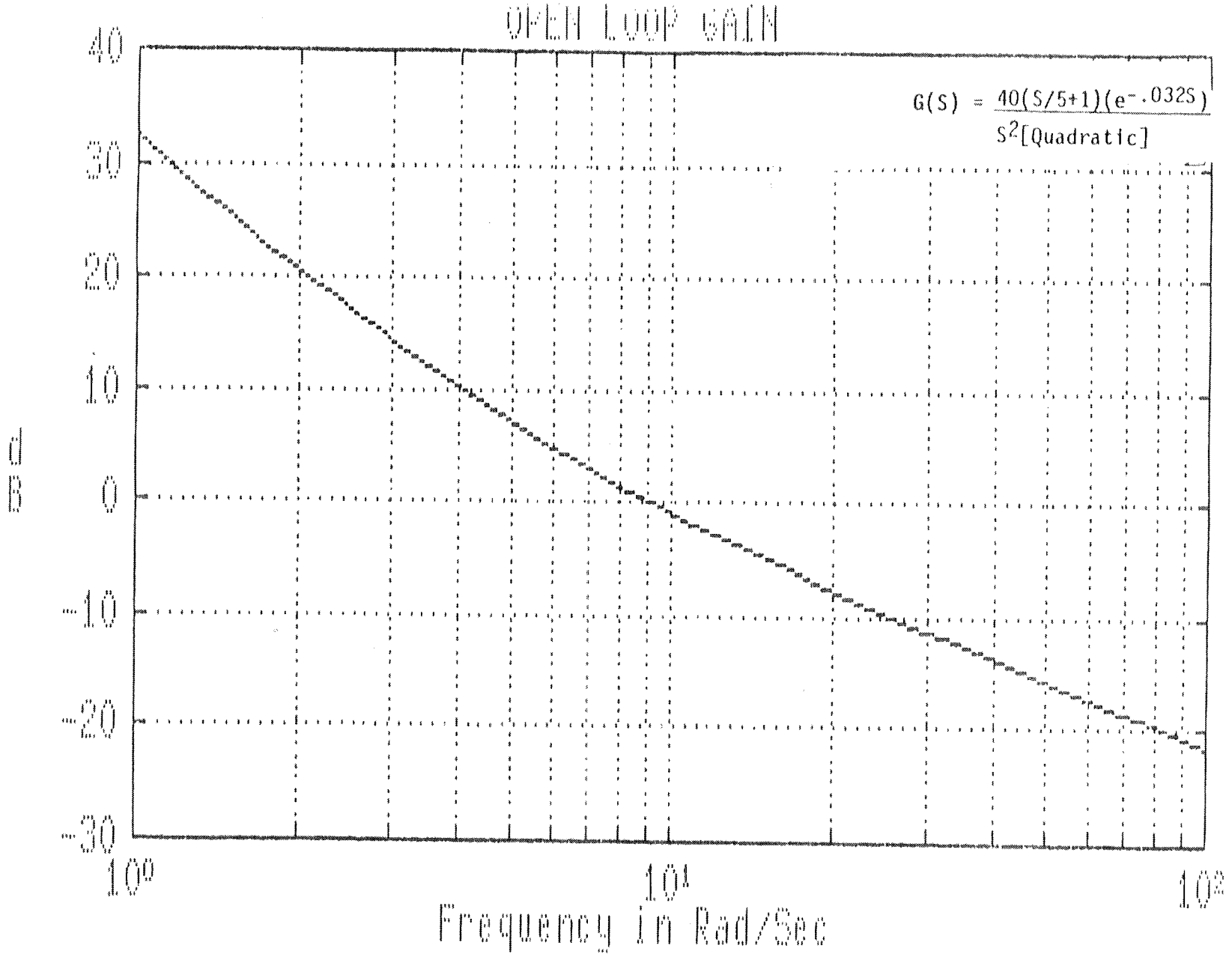

Figure 9: Open Loop Gain

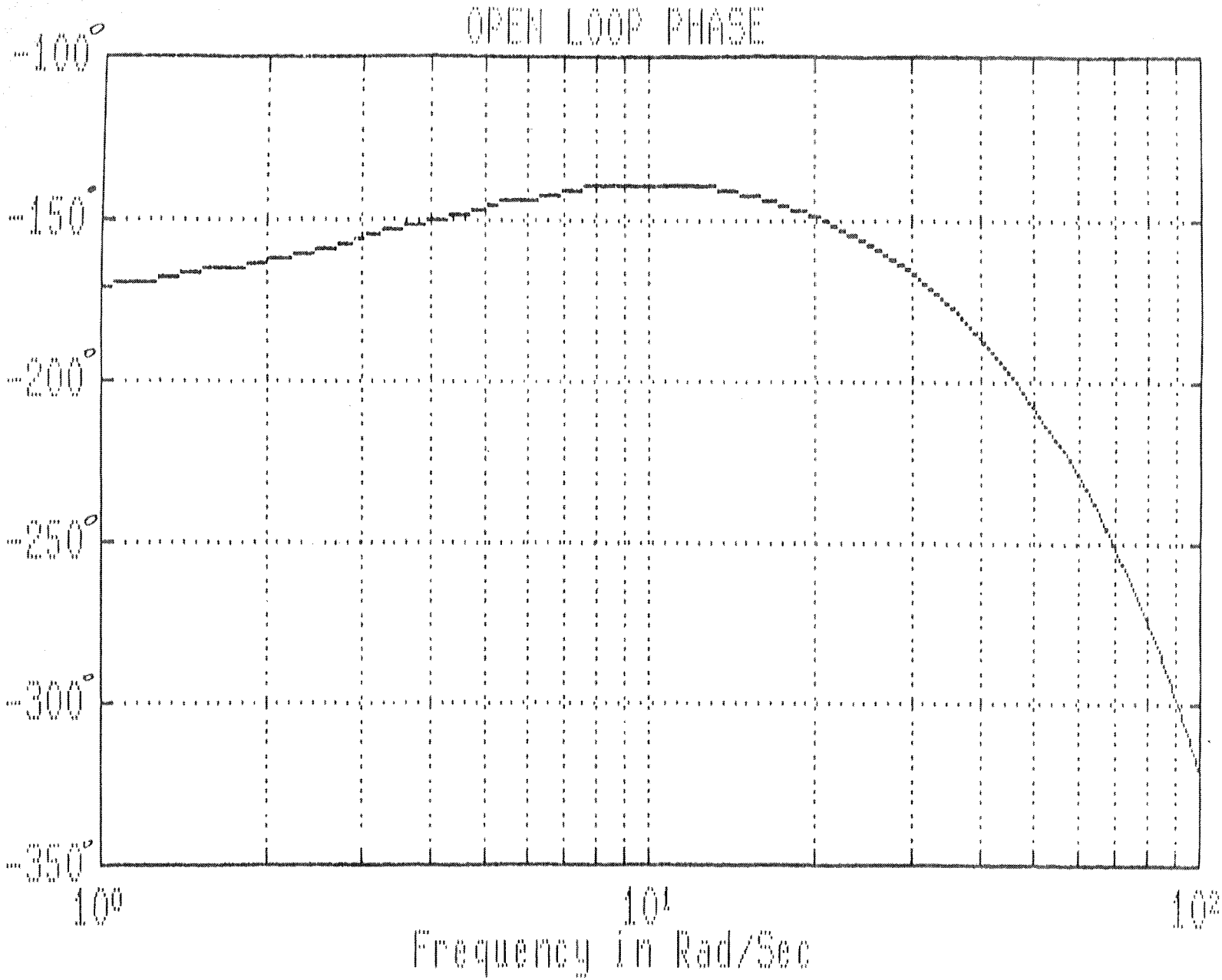

Figure 10: Open Loop Phase

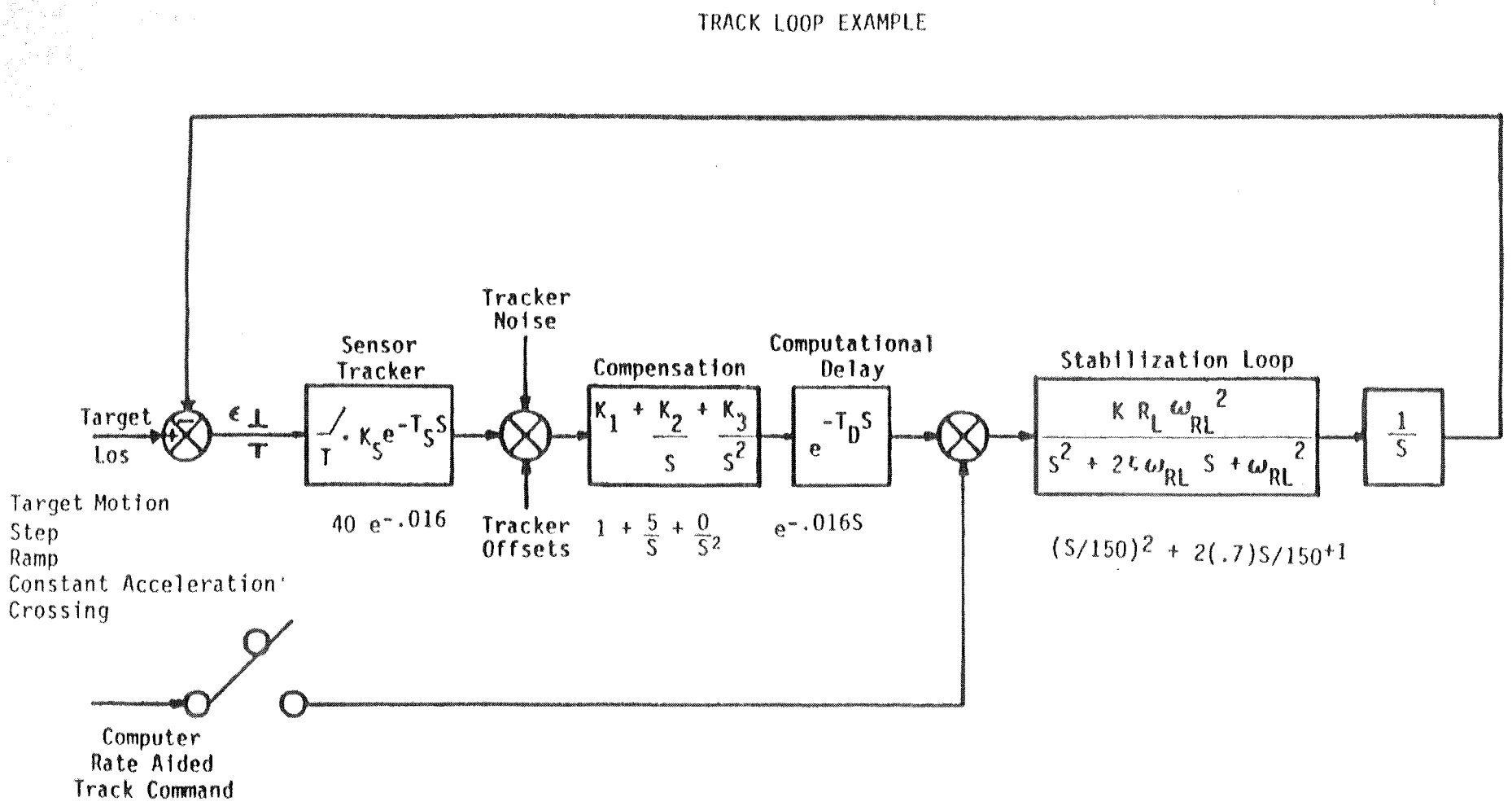

Figure 11: Track Loop Example.

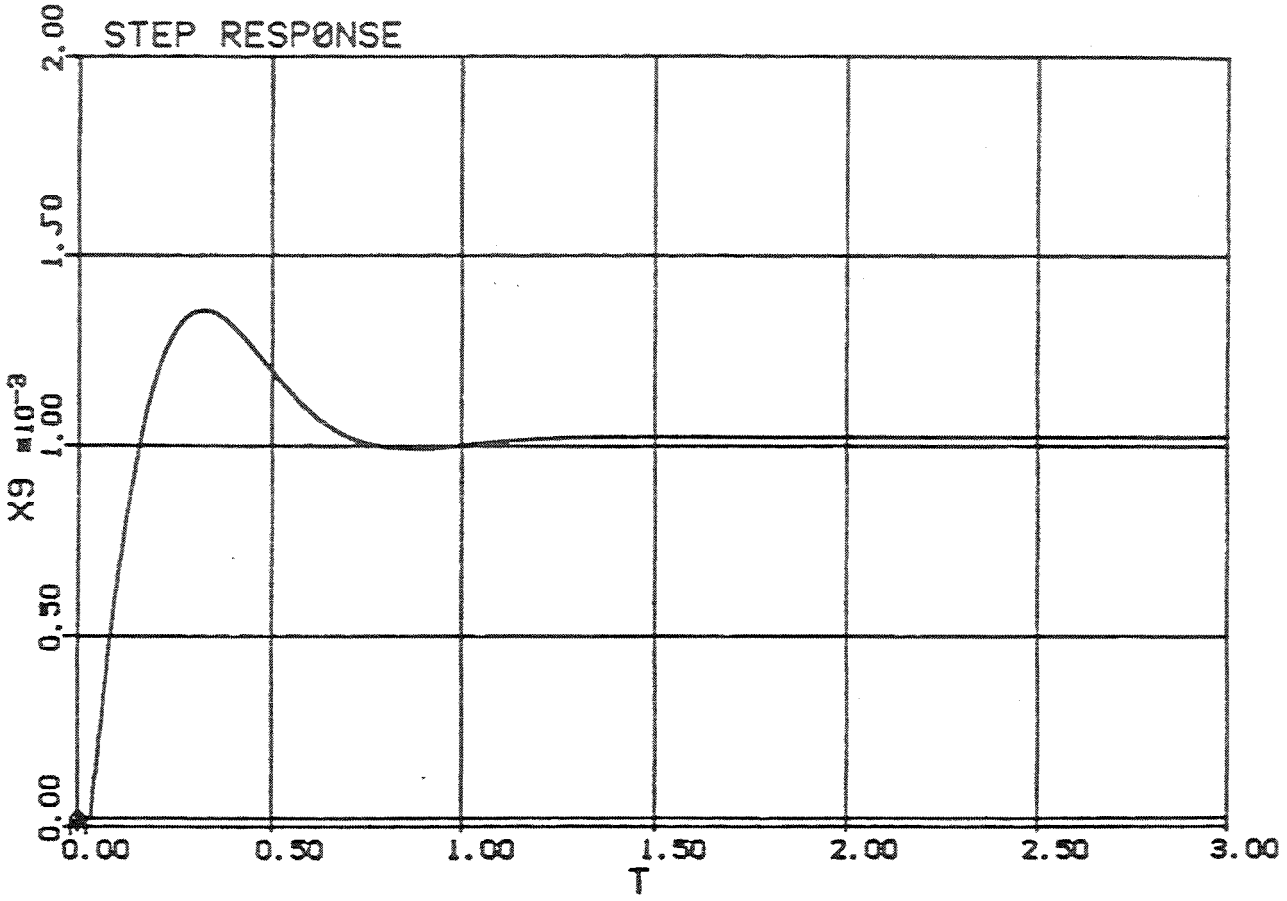

Figure 12: Loop Step Response

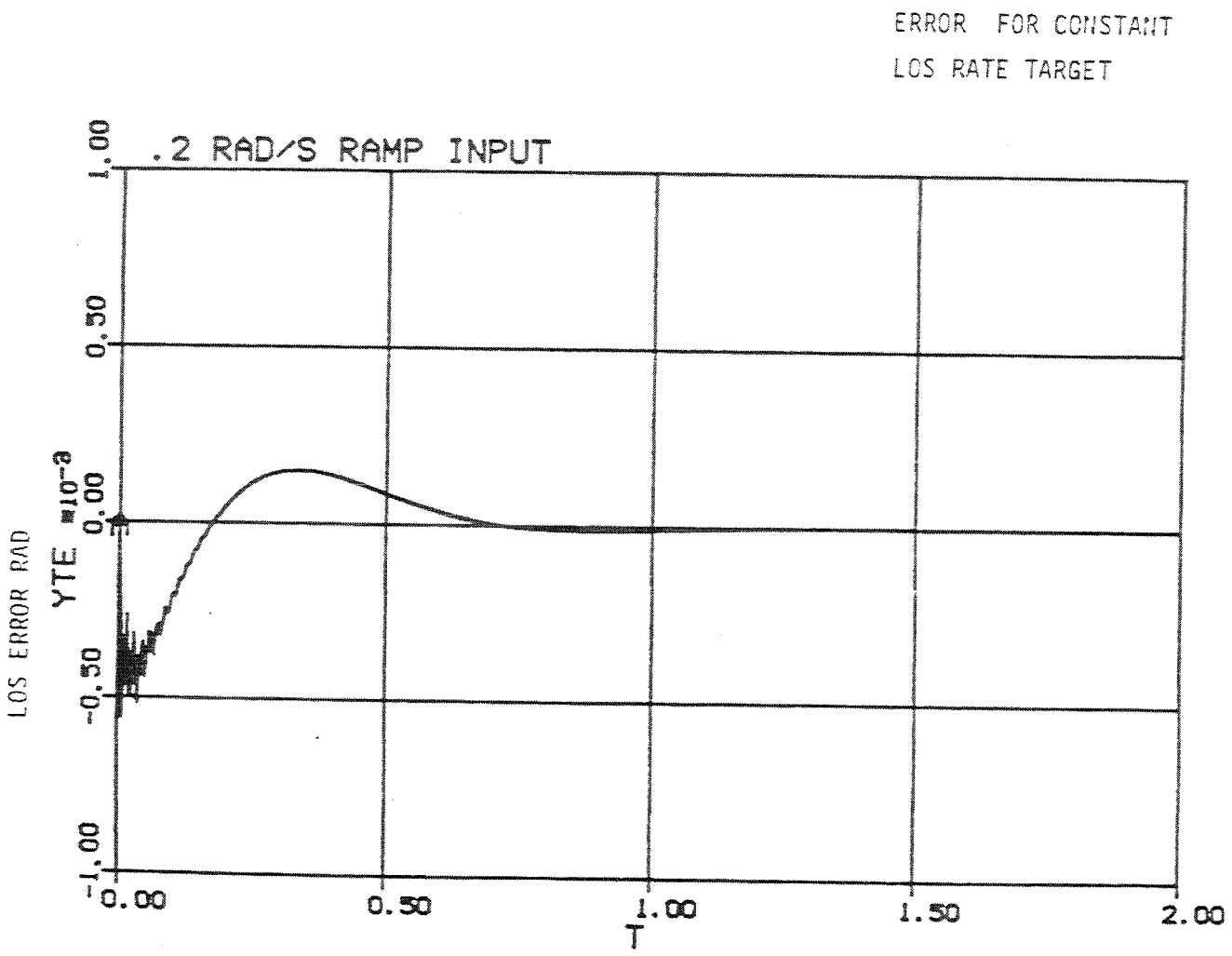

Figure 13: Error For Constant LOS Rate Target.

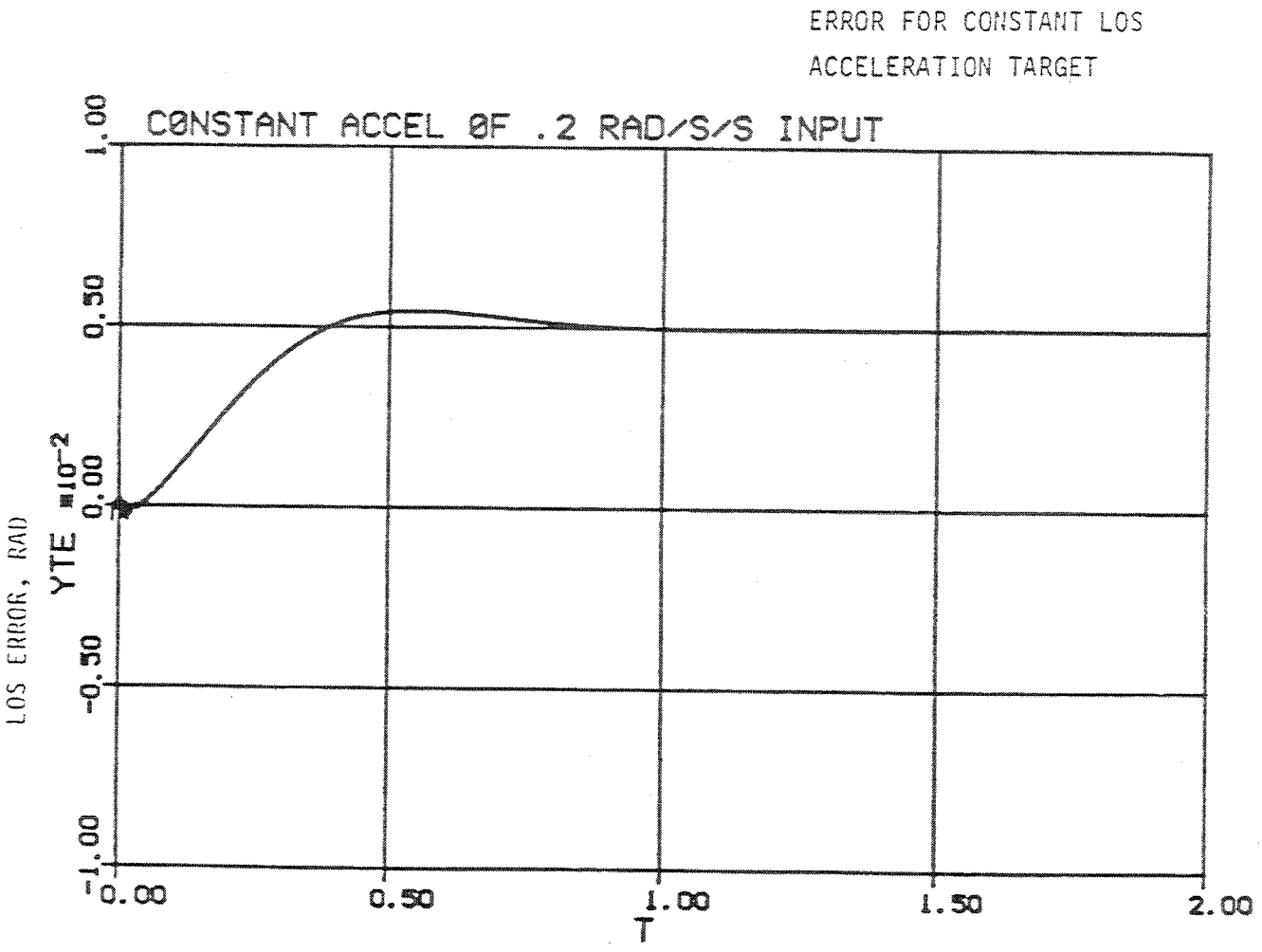

Figure 14: Error For Constant LOS Acceleration Target.

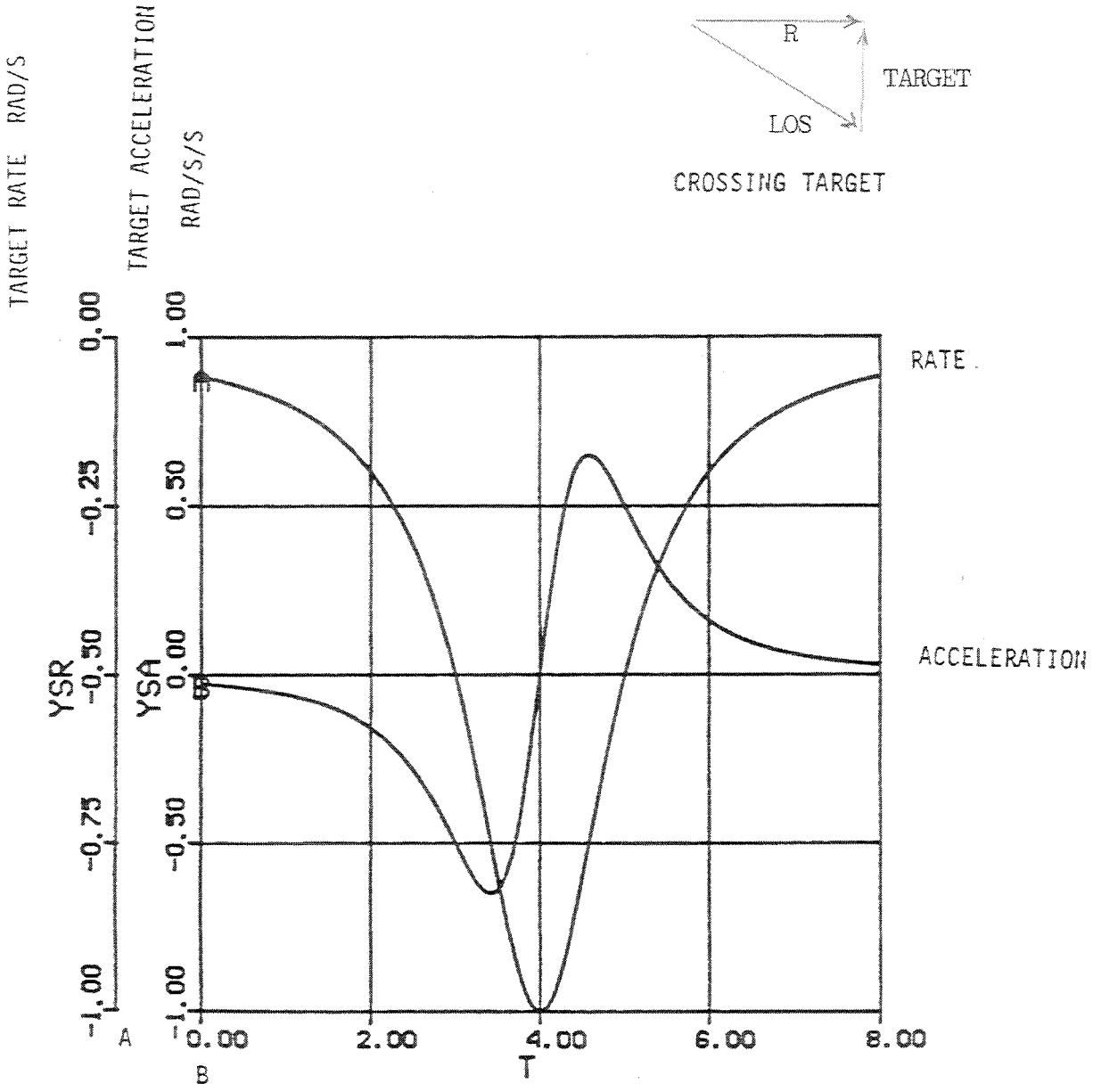

Figure 15: Target Rate and Target Acceleration.

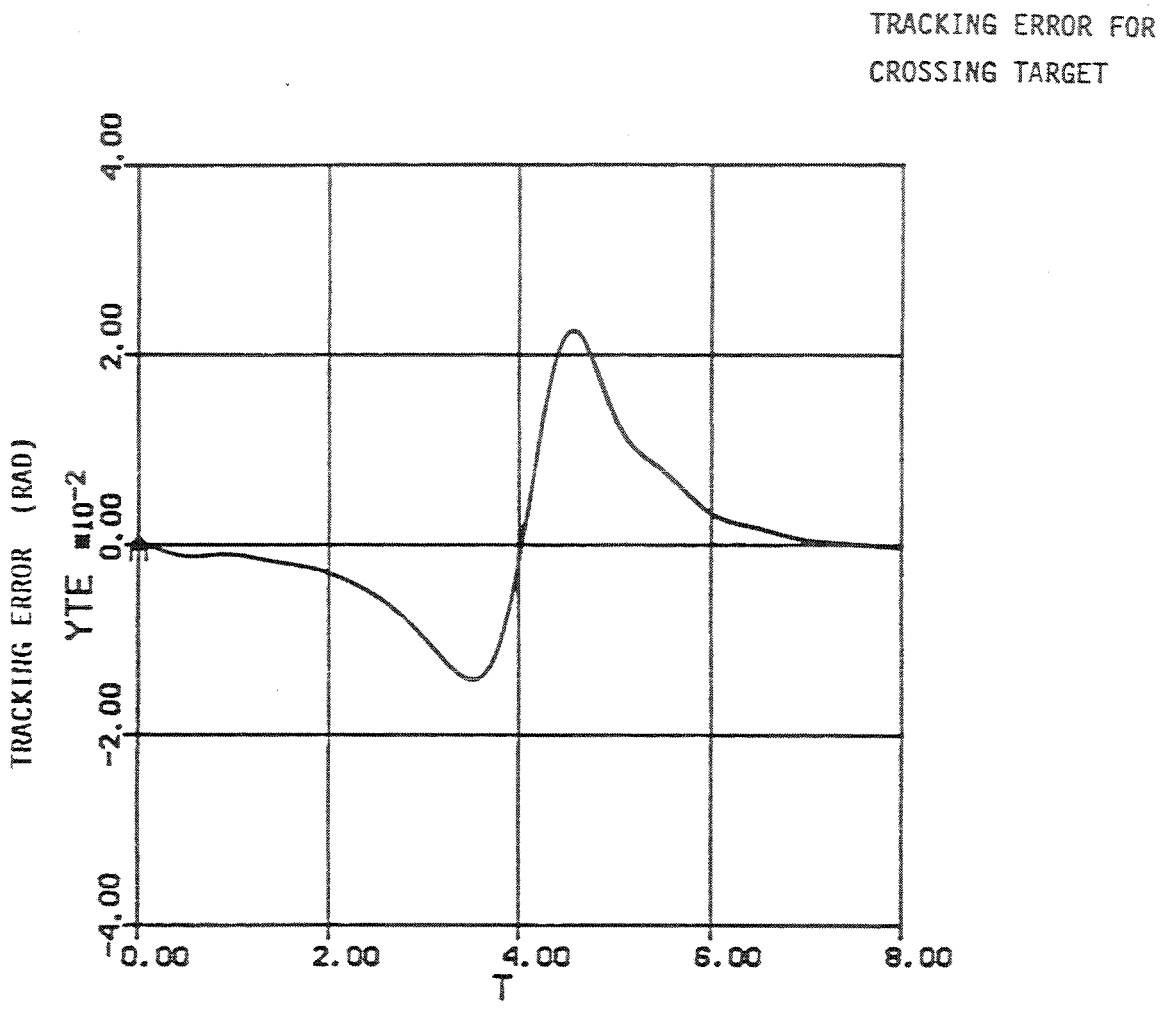

Figure 16: Tracking Error for Crossing Target.

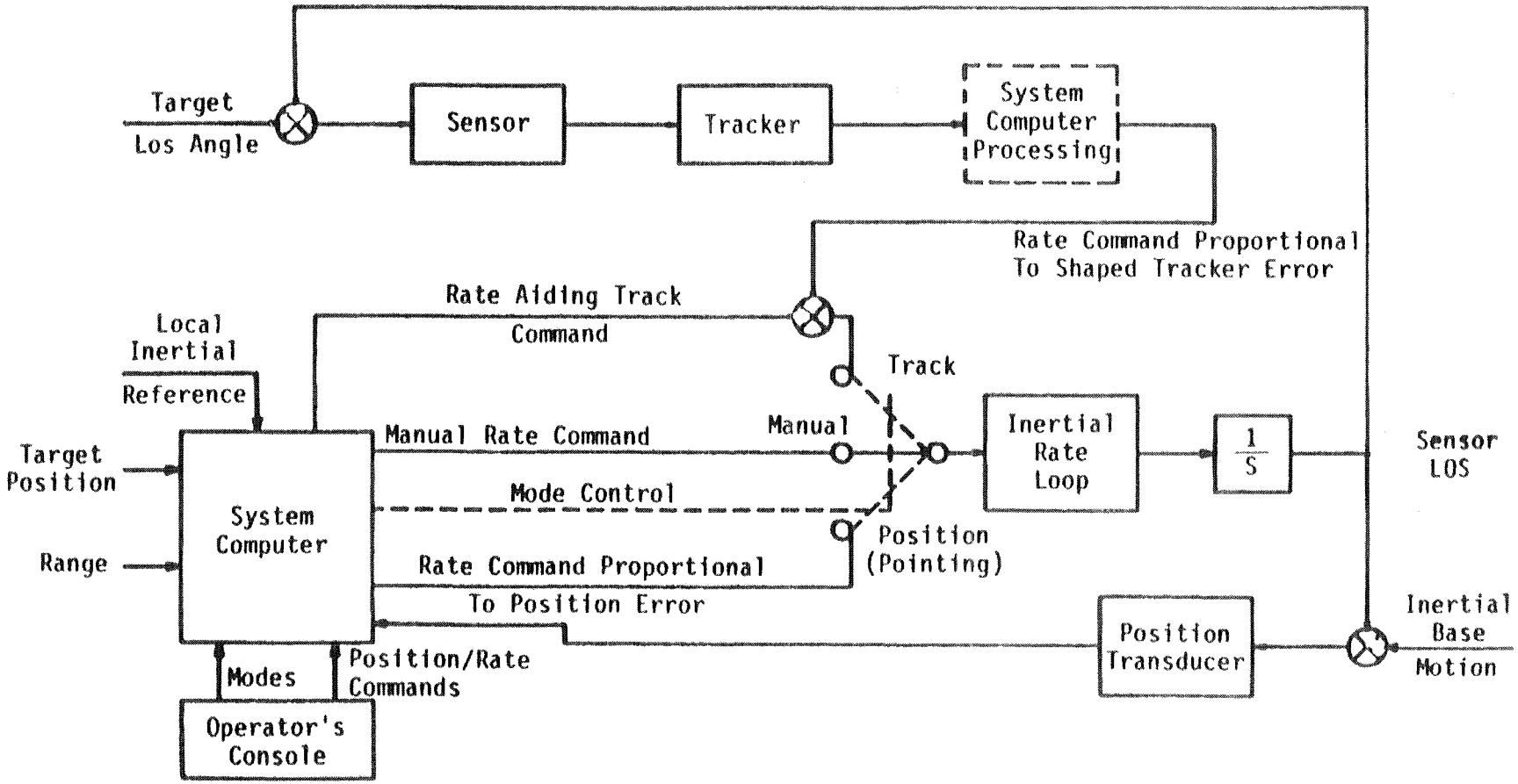

Figure 17: GENERAL POINTING/TRACKING SYSTEM/STABILIZATION BLOCK DIAGRAM

Appendix A:

Laser Rangefinder System Perfrormance Model: Large Target.

Parameters

P_T = Transmitted Power
Θ_B = Beam Divergence
D_o = Receiver Aperture
τ_A = Atmospheric Transmission
R = Range to Target
A_T= Atmospheric Transmission
ξ_T= Target Reflectivity
P_R= Received Power
RNEP = Receiver Noise Equivalent Power
RSNR = Receiver SNR

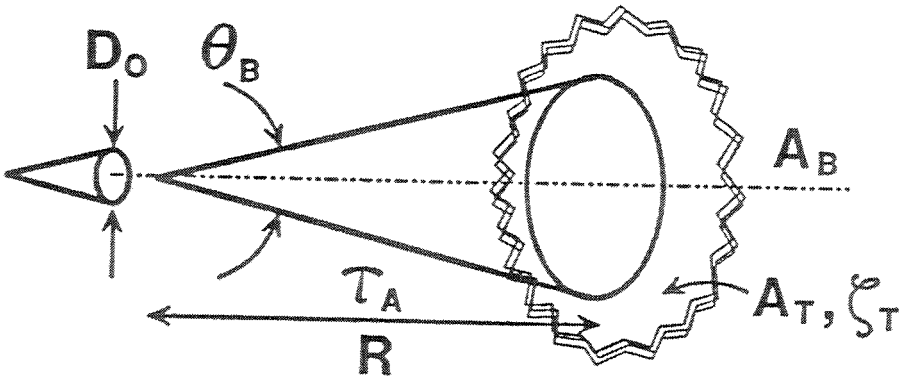

Range Equation-Uniform Beam:

$$PR = \frac{P_T \cdot \tau_A^2 \cdot D_o^2 \cdot A_T \cdot \xi_T}{\pi \cdot \Theta_B^2 \cdot R^4} = \frac{P_T \cdot \tau^2 \cdot D_o^2 \cdot \xi_T}{R^2} \qquad (A_1)$$

RSNR = PR/RNEP

Laser Rangefinder System Performance Model: Small Target.

Parameters

Same as above

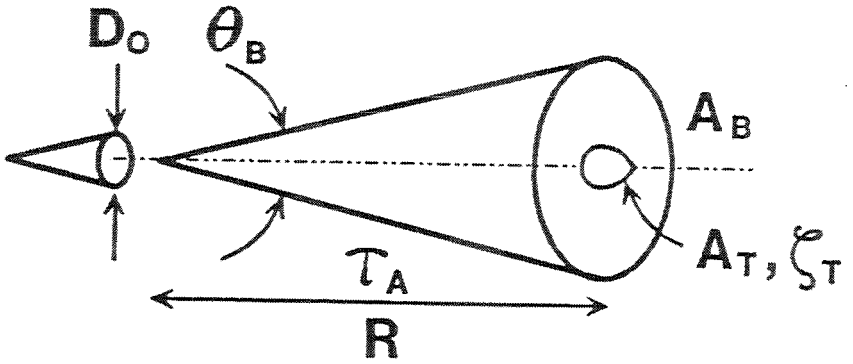

Range Equation-Uniform Beam:

$$PR = \frac{P_T \cdot \tau_A^2 \cdot D_o^2 \cdot A_T \cdot \xi_T}{\pi \cdot \Theta_B^2 \cdot R^4} \qquad \text{and RSNR} = PR/RNEP \qquad (A_2)$$

Laser Beam Characteristics and Error Definitions:

(See Fig.A_1)

Calculation of Energy on Target as a Function of Θ_B, Θ_E, ψ_E.

(See Fig.A_2,A_3,A_4,A_5).

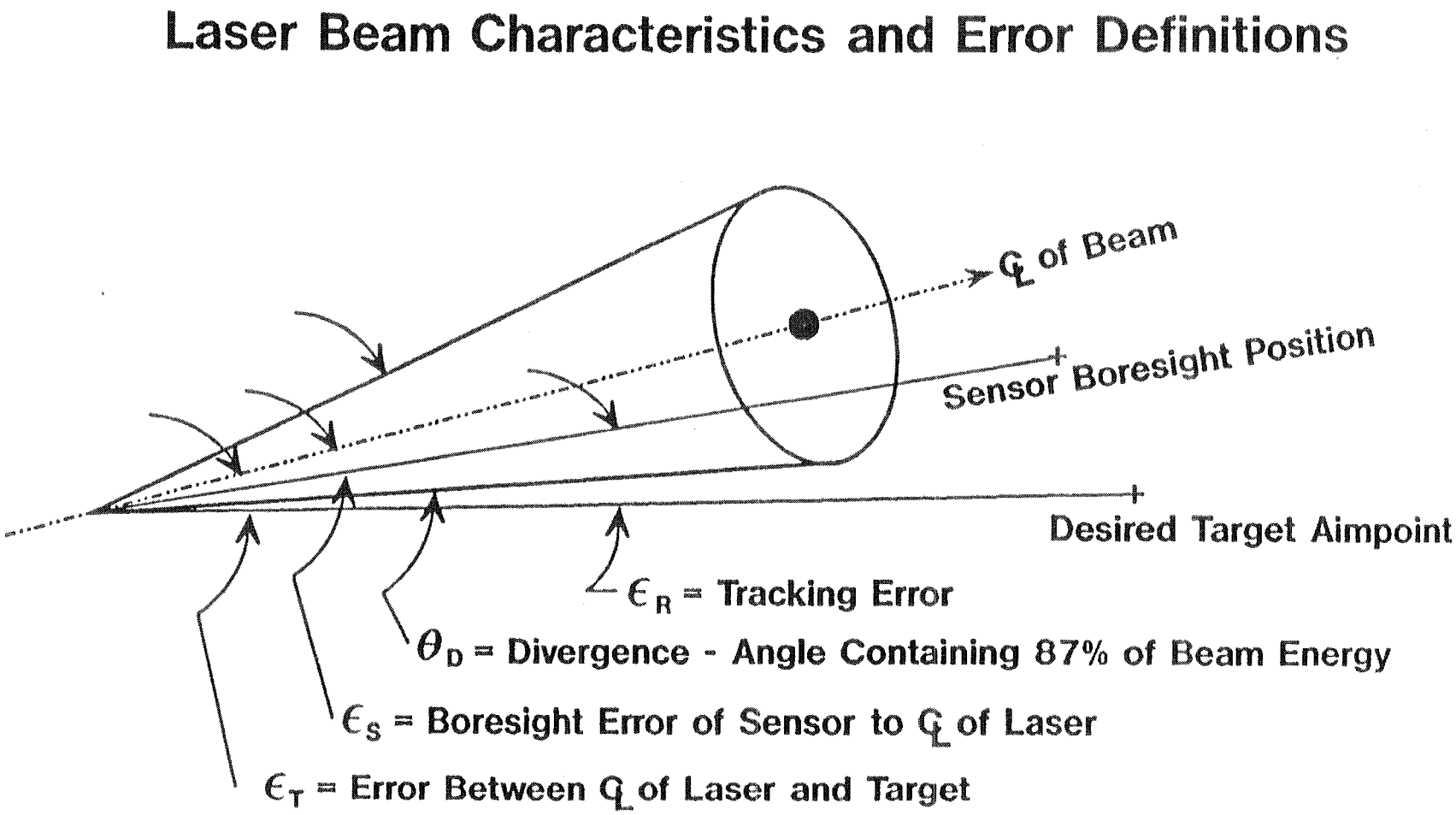

Figure A_1: Laser Beam Characteristics and Error Definitions.

Calculation of Energy on Target as a Function of $\theta_B, \theta_E, \Psi_E$

$$E_{TGT} = E_{SOURCE} \cdot e^{-\alpha R} \cdot \int_{YB}^{YT} \int_{XL}^{XR} \text{Beam}\,(X, Y, R, \theta_E, \Psi_E)\,\text{TGT}\,(X, Y)\,dx\,dy$$

θ_B = beam divergence = angular size containing 87% of laser energy

Beam (X, Y, θ_E, Ψ_E, R) = energy density of beam on target as a function of range, elevation pointing error, and azimuth pointing error

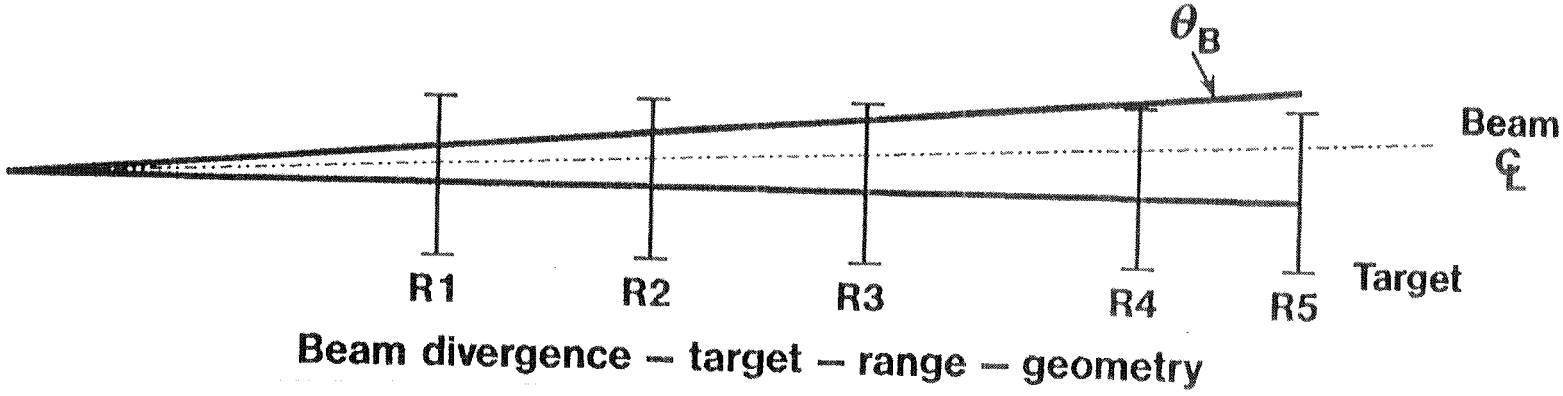

Figure A_2: Calculation of Laser Beam Energy on the Target.

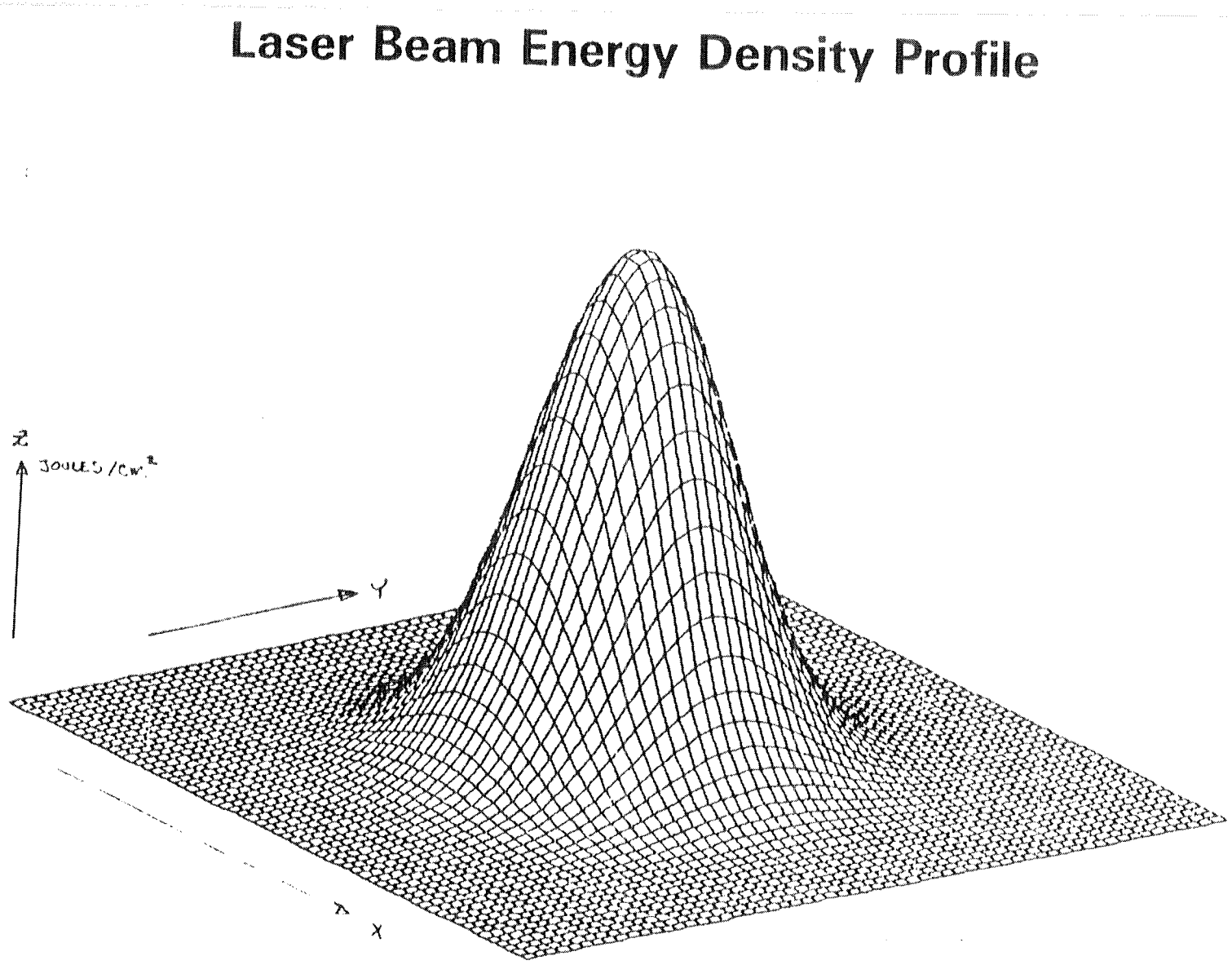

Figure A_3: Laser Beam Energy Density Profile.

Thunderstorm locating and laser triggered lightning of electrical discharge

S. Uchida, Y. Shimada, H. Yasuda, C. Yamanaka
Institute for Laser Technology,
Nakoji 3-11-20, Amagasaki, Hyogo, 661 Japan
Tel 81-6-492-7613
Fax 81-6-492-5641
Y. Ishikubo, N. Shimokura
Kansai Electric Power Co,
Nakoji 3-11-20, Amagasaki, Hyogo, 661 Japan
Tel 81-6-494-9731
Fax 81-6-498-7662
K. Matsu-ura, Z-I. Kawasaki, D-H. Wang
Faculty of Engineering, Osaka University,
Yamada-oka 2-6, Suita, Osaka, 565 Japan
Tel 81-6-878-7134
Fax 81-6-878-7134
S. Nakai, T. Yamanaka, Y. Izawa, H. Fujita
Institute of Laser Engineering, Osaka University,
Yamada-oka 2-6, Suita, Osaka, 565 Japan
Tel 81-6-876-3000
Fax 81-6-877-4799

Introduction

When an intense laser light is focused in air and the intensity is beyond the threshold of the air breakdown, laser plasmas are formed. Using the conductivity of plasmas, induced electrical discharges of thunder clouds can be triggered. It was experimentally shown that a long plasma channel has a guiding effect on electrical discharges [1]. In our experiments, up to 8.5 m of guided discharges were induced at 1 MV applied voltage in laboratory. A US research group made an attempt to trigger lightning using a laser in mid 70's[2]. However, the experiment was unsuccessful due to the shortage of the laser power. Recently Japanese research groups found that the thunder storms in the Hokuriku region seem to be suitable for laser triggered lightning (LTL) experiment because the height of the clouds is relatively low which leads to the high electric fields to the ground. The high electric fields can easily initiate a leader propagation in plasma channels.

Approximately two-thirds of the power electric line accidents are caused by thunderbolts. Thus active methods to prevent the thunder faults are expected. The study of rocket triggered lightning started 10 years ago and has been successfully operated more than one hundred lightning strikes. The method utilizes a grounded wire launched into air by a small rocket and initiate electric leader propagation from the top of the wire to trigger lightning. The LTL scheme has certain advantage over the rocket method in terms of response time and residual debris such as rocket itself and grounded wire. These factors become important when the method is applied to protect live power facilities.

For successful LTL experiments, it is very important to locate the position of thunder clouds. In general, the right timing for the laser irradiation is when the electric field is strong enough for the leader propagation. The electric field of thunder can be very localized and a monitoring system might mislead the laser timing decision. Therefore, the extended diagnostics system is one of the key issues for LTL experiments.

This paper reports the present status of the field experiment for LTL. The field experiment consist of two systems, laser-plasma forming system and thunderstorm diagnosing system. The characteristics of laser propagation in atmosphere is also a important factor since it determines the amount of energies producing the plasma channel.

Laboratory experiments for laser induced long gap discharges

Figure 1 shows the 8.5 m long gap discharge induced by a 7.5 m plasma channel. The laser energy was 100 J and was focused by a multiple focusing optics called "MACH (Multi-

Active CHannel)" mirror [3]. 1-MV impulse was applied to the upper rod electrode. This result shows that approximately 13 J/m laser energy density can guide the electrical discharge.

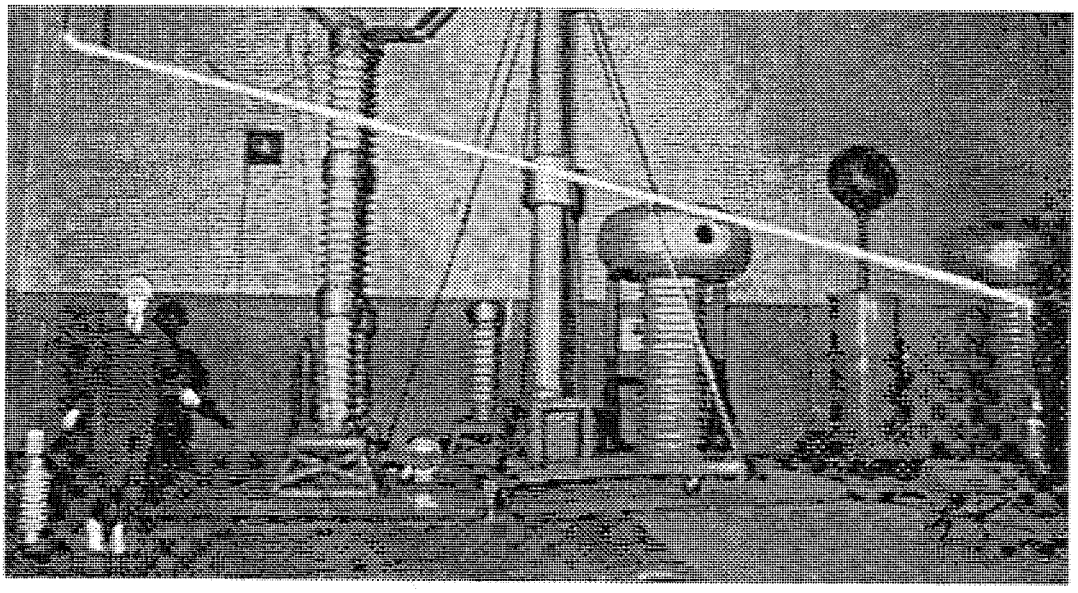

Figure 1 An 8.5-m-long gap discharge induced and guided by a laser produced plasma channel.

Plasma channel forming system

The laser-plasma forming system of the LTL experimental site is depicted in Fig. 2.

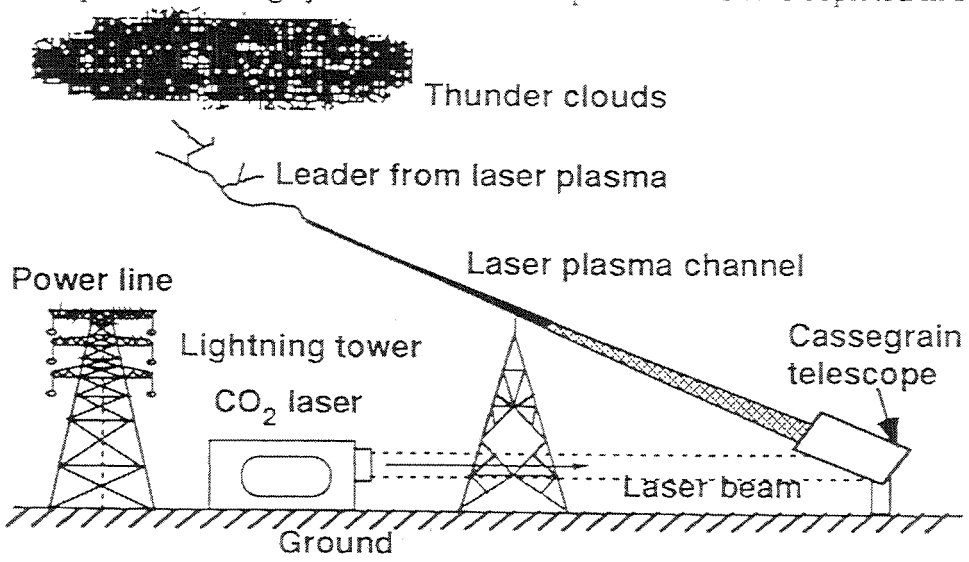

Figure 2 Schematic of the laser triggered lightning (LTL) experimental site.

The system consists of a laser system, a focusing optics, and a lightning tower. We use a high power CO_2 laser system to produce a plasma channel at the top of the lightning tower. The laser is an electron beam controlled CO_2 laser, Lekko II, and delivers approximately 1 kJ in 40 ns. The laser cavity is an unstable resonator and the beam pattern has a concentric shape (inner and outer diameters are 40 and 220 mm respectively).

The height of the tower is 50 m to enhance the ambient electric field under thunder clouds. The enhanced electric fields assist the plasma channel to initiate a leader propagation. The height of the tower is based on the results of laboratory experiments and calculations. It is important to keep high intensity and long focusing of the laser beam simultaneously to produce a long plasma channel at the focus. Laboratory experiments have been carried out successfully to determine the adequate parameters for the plasma channel formation and to induce electrical discharge using a CO_2 laser of 150 J output. A large-aperture (50 cm in diameter) Cassegrain telescope has been prepared. The MACH mirror was used for the secondary mirror to produce a multi-focused long plasma channel.

Thunderstorm locating system

As is described earlier, LTL requires a precise prediction of the right timing for laser irradiation. The prediction is possible with extended knowledge of the thunderstorm activities such as the distribution of space charge and cloud particle, and the size of cloud itself. Although, the field strength at the lightning tower is determined by a local distribution of space charge and charges in thunder clouds, the development of thunderstorm activity must be monitored with an extended time and space range to predict if the storm becomes significant at the experimental site. The thunder storm monitoring system includes SAFIR system, wide-band slow antennas, and field mills. In addition to it, radar data of the thunder storm activities are available from Kansai electric power Co. and the group of Hokkaido University.

The thunder storm monitoring with the longest range is the SAFIR. The system works as an EM wave interferometer to detect the direction of the VHF waves originating from the leader propagation of lightning and determines the location of the lightning activities. The current system consists of three antenna sites each separated by 100 km. The system detects only lightning strikes and not the development of thunder storms.

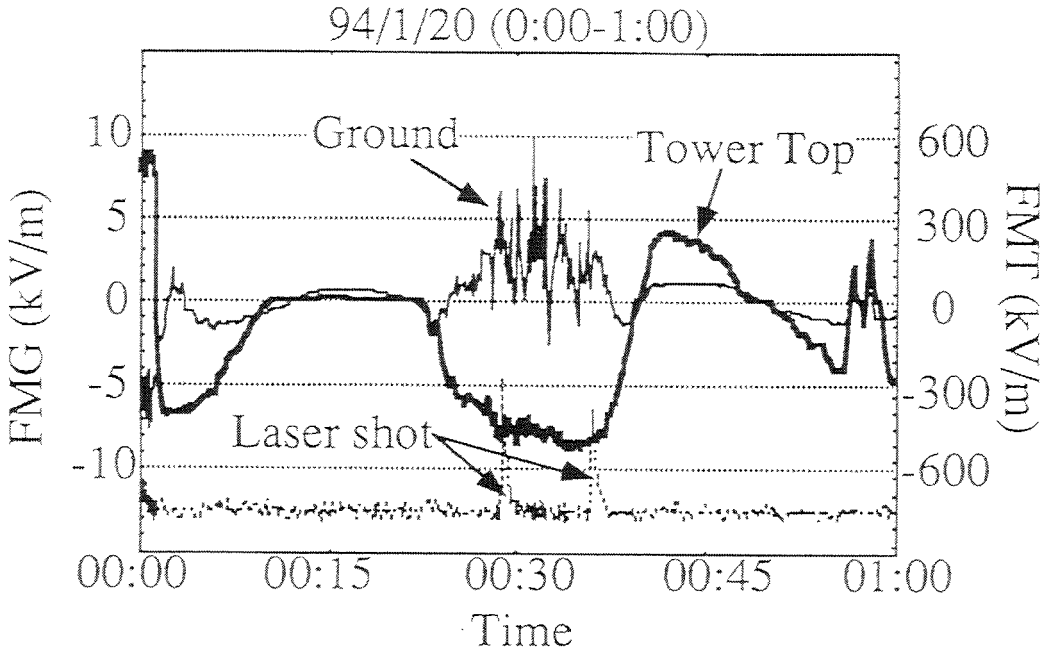

Figure 3 Time elapse of the electric fields at the top of the tower (thick line) and on the ground (thin line).

The wide-band slow antenna system covers the electric field variation due to the lightning activities within the range of 10 km. The current system consists of three antennas separated by 5 km and responds up to kHz field variation. The measurements requires 1-μs synchronization between the antennas which is provided by monitoring the GPS (Global Positioning System) signal. The system provided the lightning path with the accuracy of a few hundreds meters.

The local monitoring system is field mills. The field mill detects ambient DC-field which was considered to directly determine the laser irradiation timing. Two detectors were located at the top of the lightning tower and on the ground, 80 m away from the tower top. However, the measurements occasionally seem to be mislead by locally concentrated space charges. Figure 3 shows the time elapse of the field mill measurements .

In general, the tower-top and on-the-ground field mills indicate the similar field trends. However, in this particular measurement, polarity of the field mills reversed between the tower top and on the ground, phenomenon observed many times during the experiments. This polarity-reverse phenomenon can be due to a space charge distribution of small scale structure of the order of a few tens of meters. When such a space charge structure exists, the electric field of the thunder cloud will be shielded or even the polarity reverse takes place. In other incidence when several lightning strikes took place near the site (the closest one was 350 m away), the field mills observed the polarity reverse. In this particular case, the tower top field was over 500 kV while the on-the-ground field was near zero. These observations indicate that the determination of the laser irradiation timing cannot depend on the field mill measurement alone.

Radar data of the thunder cloud are provided by courtesy of the group from Hokkaido University (Prof. Ueda's group). Their dual-polarization Doppler radar is capable of distinguishing between rain, snow, and hail particles in clouds and measuring their velocity. This radar was located approximately 10 km away from the LTL site. In addition, data from Kusuya radar site will also be available from this winter experiment. The radar data clearly show the growth of the thunder clouds and a strong reflection of a bunch of hail over the LTL site at the time of the lightning strikes.

The right timing of the laser irradiation shall be determined both by the local field measurements, i. e. field mills, and the mid-range radar measurement. Especially the radar measurement can provide the strength and the size of the thunder storm and can be very important to determine if the laser should be irradiated. The radar data was not available on real time basis and should be monitored by the LTL site all the time.

The authors' group is preparing a radar data monitoring system which transfers radar data from Kusuya radar site (about 15 km away) to the LTL site. Using this system, the real time thunderstorm condition will be available at the site and the laser timing will be more accurate.

Laser propagation experiments

The laser propagation was characterized by measuring the transmission of laser energy through various atmospheric conditions in LTL field site. The measurements were performed under fine, rain, snow and hail conditions. The laser light propagated 50 m horizontally to an energy meter in the experiments. The experimental results show that the rain fall does not affect the transmission very much (more than 95 % at 0.7 mm/hour, typical precipitation for the site) while snow does affect the propagation as much as 50 % at 1 mm/s snow fall. Hail has similar effects as snow fall. Therefore, 1 kJ laser energy is sufficient for producing a few tens meters of plasma channel.

Summery

An LTL field experimental site has been assembled to test the laser and focusing system as well as the laser induced thunder lightning system. We have developed the Cassegrain telescope for laser plasma channel production at the top of the lightning tower and verified that the system is capable of producing a few tens meters of plasma channel with 1-kJ CO_2 laser energy. The thunder storm locating system has been provided to get the data of thunderstorms. The laboratory experiments have already performed successfully to prove that an 8 m electrical discharge can be induced by a laser plasma channel. Field experiments are now in preparation.

References

1) E. Fujiwara, Y. Izawa, Z. Kawasaki, K. Matsu-ura and C. Yamanaka, Rev. of Laser Eng. **19**, 528 (1991).
2) C. W. Schubert and J. R. Lippert, IEEE Int. Pulse Power Conf., (1979).
3) S. Uchida, *et al.*, Conference on Lasers and Electro-Optics, (1993).

LIDAR IMPLEMENTATION FOR SLR STATIONS

Peter Pendlebury and Randall Carman

British Aerospace Australia
NASA Moblas 5 Tracking Station
Yarragadee
Western Australia 6525

ABSTRACT.

Utilising the existing laser and tracking mount, a lidar facility may be added to the basic SLR station to produce atmospheric aerosol data. This data is useful for evaluation of atmospheric attenuation during SLR operations and may provide additional financial support. This paper descibes the implementation and early results of lidar at the NASA Moblas 5 station.

1.INTRODUCTION.

During July 1991 a significant reduction in range data quantity from distant satellites was noted. This effect was particularly noticeable when ranging to the two Etalon spacecraft where return rates dropped from 45% to less than 20%. A thorough evaluation of equipment performance showed no deficiencies. The reason for reduced data yields was finally aattributed to atmospheric contamination by ash and dust from the Mt. Pinatubo volcanic eruption.

Substantial savings in manpower and effort could have been effected had facilities been available on site to monitor the range path characteristics. With this in mind and with the possibility of providing more and varied data to the scientific community from the system at Yarragadee, the development of a lidar system has been undertaken.

Taking about 18 months to develop and construct, the low cost TTL/PC based lidar has recently been installed and the first data obtained in October.

Lidar data can be taken at any elevation angle, enabling the SLR operator to obtain a real time display of range path characteristics. The system shows distance along the range path versus noise level from Rayleigh scattering. Currently, to obtain valid data for altitude versus noise level, the telescope must be pointing to zenith. A faster controlling computer will enable the system to show true altitude versus signal level for any elevation angle by application of a correcting algorithm.

2.EQUIPMENT and RESULTS.

The system has been designed to be as stand alone as possible to ensure that no interruption or degradation occurs to scheduled SLR activities. The only existing moblas 5 equipment used on the lidar are the Nd/YAG laser and associated transmit electronics and optics, the 75cm telescope mount to piggyback the lidar receive telescope and the timing subsystem to provide a 5 MHZ clock.

A block diagram of the system (Fig. 1), illustrates the usage of existing and new equipment. The transmit side of the system is the standard Moblas configuration (Table 1),but the receive side is completely new.

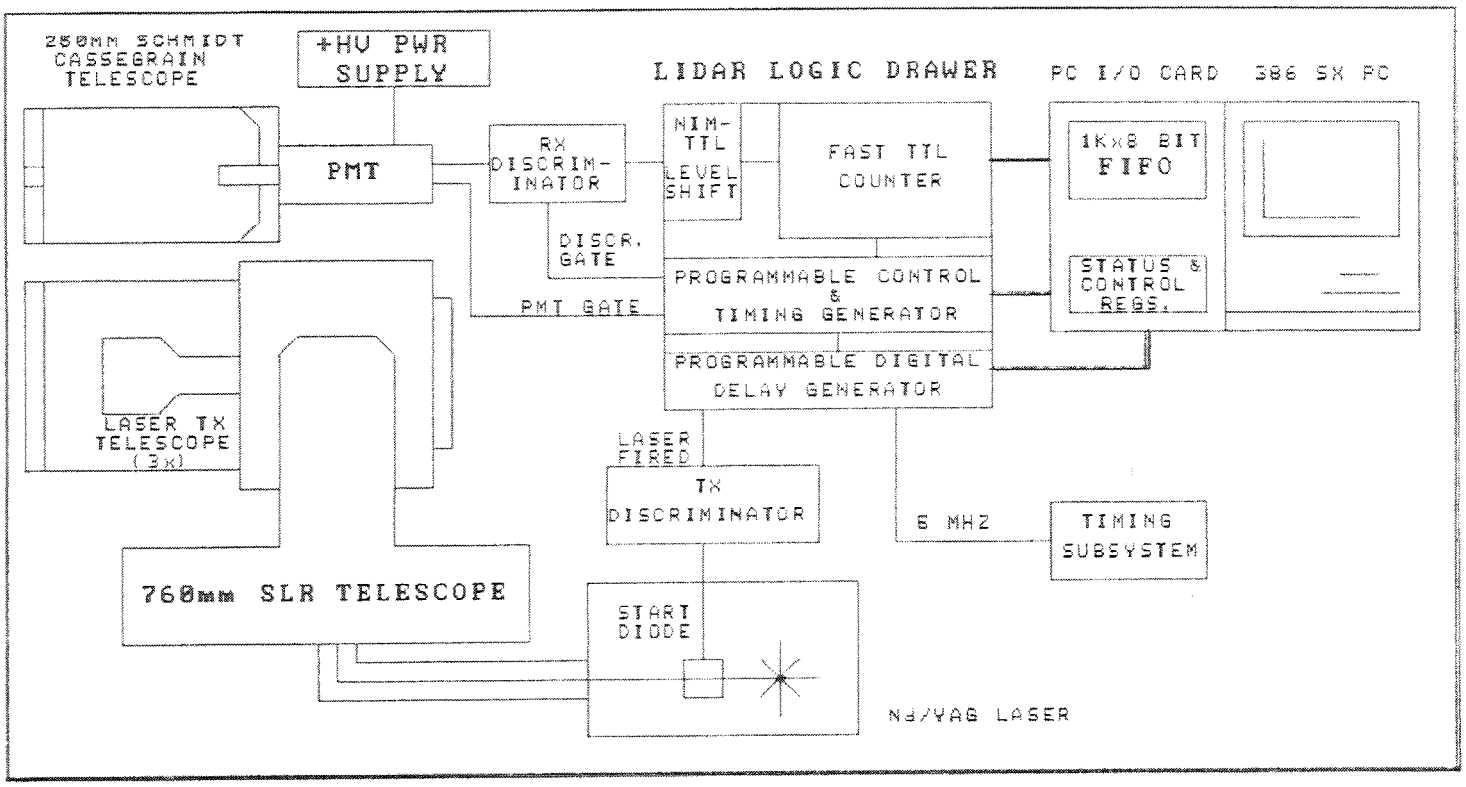

FIGURE 1.
LIDAR SYSTEM CONFIGURATION

Some early tests were performed using the 75cm main SLR telescope and associated MCP but the latter could only be gated on for 13us at the most giving a maximum lidar range depth of 2km. While some interesting data returns were obtained (mainly from significant cloud layers) using that setup, it was obvious that a greater range depth would need to be observed to yield any useful data. Instead of modifying the MCP range gate generator (with possible degradation of SLR sensitivity) it was decided to implement a seperate receiver subsystem.

A 25cm Celestron Schmidt Cassegrain telecope has been piggybacked on the 75cm main telescope. The focal point of the 25cm telescope is 24cm behind the rear exit port which gave plenty of room to install a sun shutter and iris assembly before the PMT.

The PMT used during the feasability stage is an Amperex 56TVP and this supplies the receive signal to a spare Tennelec 454 discriminator channel.

To control the timing of the system and to acquire the data from the discriminator, a pc programmable lidar logic drawer was designed and constructed utilising TTL IC's. The logic drawer provides gating signals to the PMT and receive discriminator and a programmable bin clock to the data acquisition circuitry.

A spare output from the SLR transmit discriminator is used to provide a laser fired pulse to the lidar logic drawer. This pulse is delayed by a programmable digital delay generator to provide a delayed laser fired pulse which is used to initiate data aquisition at a variable lower range.

TRANSMIT PARAMETERS		
LASER	TYPE	QUANTEL Nd:YAG 1064/532nm
	PRF	4 OR 8 HZ
	DIVERGENCE	100 uradians
	PULSE ENERGY	100mJ AT 532nm
RECEIVE PARAMETERS		
TELESCOPE	APERTURE	250mm
	FOV	2200 uradians (max.)
	OPTIC AXIS OFFSET	970mm (from tx telescope axis)
OPTICAL BANDWIDTH		1 nm
DETECTOR		AMPEREX 56TVP PMT
DISCRIMINATOR		TENNELEC TC454 QUAD FRACTION
DATA ACQUISITION		CUSTOM DIGITAL I/P CARD IN 386SX PC
BIN SIZE		200ns(30m)-10us(1.5km) in 200ns steps
COLUMN BASE		1.5km to 1900km in 1km steps

TABLE 1
SYSTEM PARAMETERS

A FAST TTL 8 bit counter is used to count pulses from the receive discriminator and the count for each range bin is latched through synchronously by the bin clock to a 1k x 8 bit FIFO register. The system therefore has 1024 range bins making up the range column.The bin size is adjustable in 200ns(30 metre) steps from 200ns(30 m) up to tens of microseconds(several kilometres) and the base of the column (and subsequently the top) can be adjusted from 30m up to several hundred kilometres.

A 386sx AT programmed in TURBO C, is used to log and display real time data(from the FIFO) as well as perform post-aquisition data processing, display and storage. The 386 is also used to set the programmable features (bin size and column base altitude) and monitor the status of the lidar logic drawer.

Two versions of operating software are currently being used whilst the system is being evaluated.

One program is used for collecting and displaying real time single shot data and is primarily intended as an SLR tracking aid (Fig. 2.). The system parameters are shown down the left hand side whilst the data is displayed for every shot, on the graph on the right. As well as showing range versus counts/bin, a bar extending along the x axis from the origin shows the total returns counted for the path sampled.

The second program is used for collecting and summing data for each bin and displaying the summed data every shot (Fig. 3.). The summing can take place for as many shots as the operator requires.

Once data has been collected and sampling stopped, the data can be averaged over the shots collected and corrections applied for atmospheric attenuation (Fig.4).

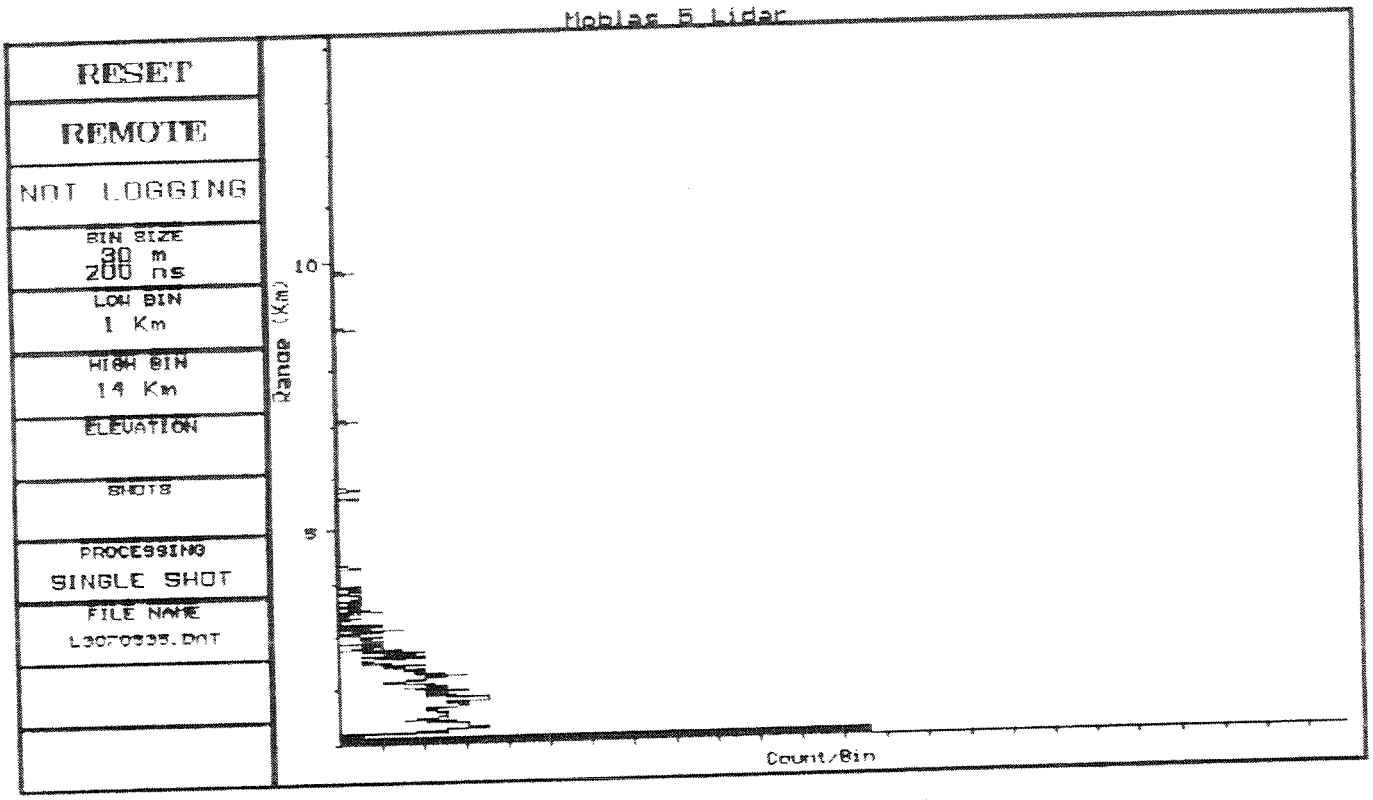

FIG 2.

NOISE COUNTS FROM A SINGLE SHOT,X AXIS SCALING IS 20 COUNTS/DIV.FOR THE BAR,2COUNTS/DIV.FOR THE GRAPH.

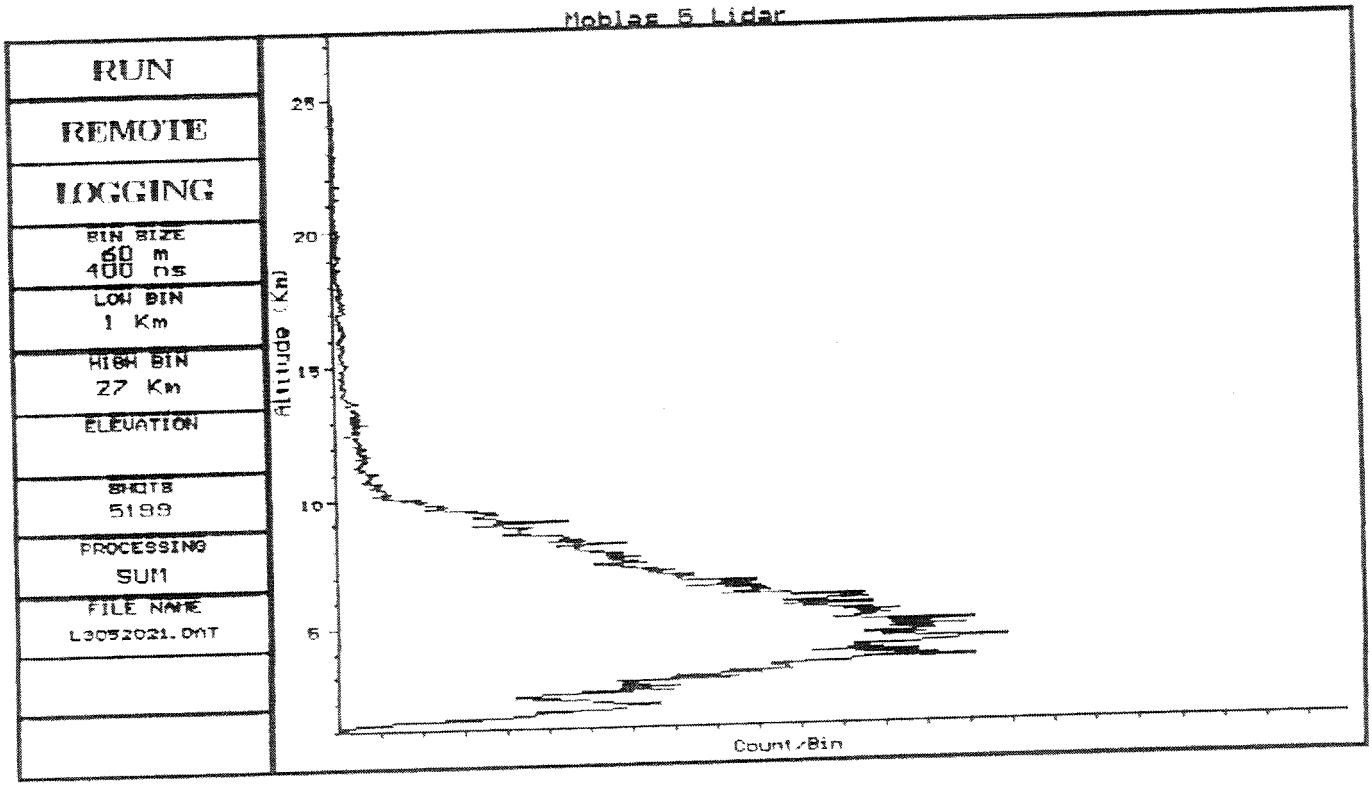

FIG 3.

DATA SUMMED OVER 5199 SHOTS.

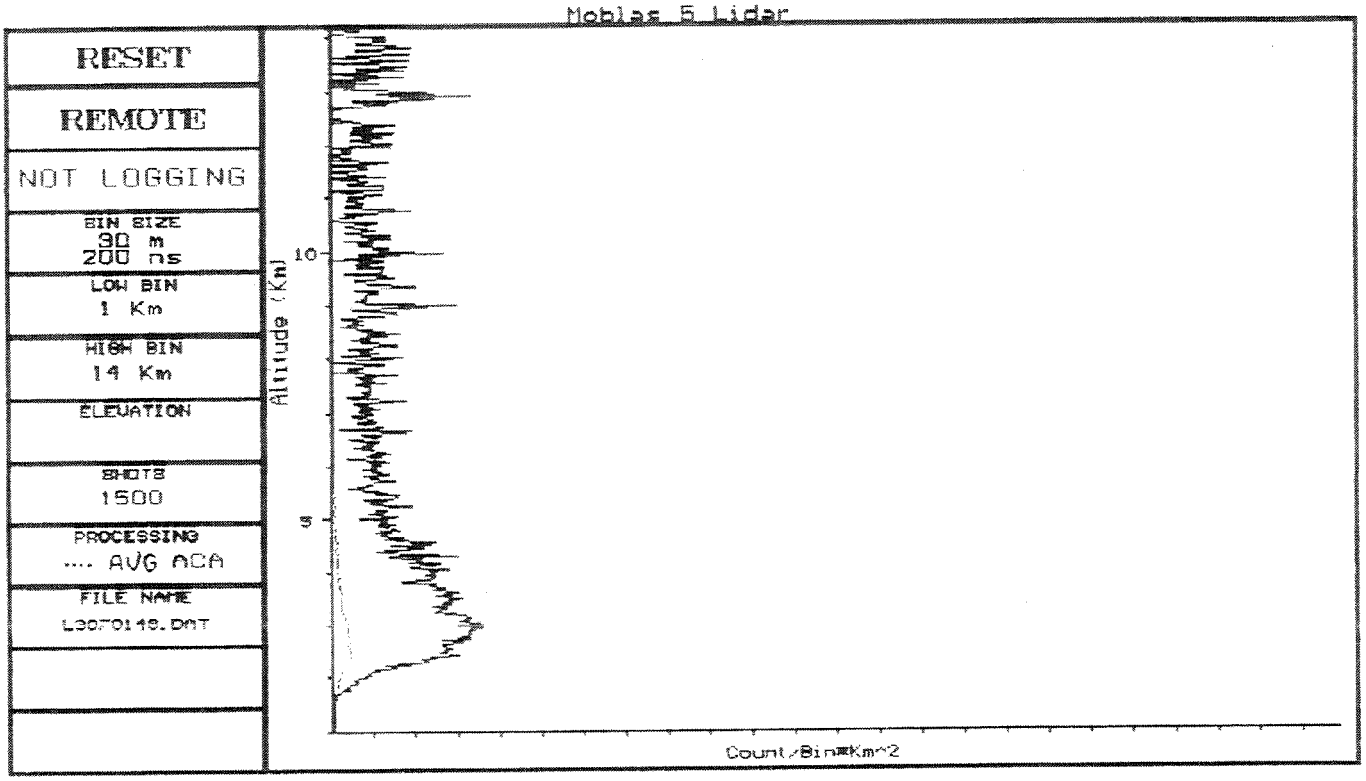

FIG 4.

AVERAGED DATA (AVG) .....
DATA CORRECTED FOR ATMOSPHERIC ATTENUATION (ACA) ———
X-AXIS:0.2 COUNTS/BIN x KM^2 (ACA).PER DIV.
0.2 COUNTS/BIN (AVG). PER DIV.

3. CONCLUSION.

A basic Lidar has been implemented at Moblas 5 without compromising SLR capability. Operations to date have proven that the Lidar can provide real time assesment of SLR path attenuation due to aerosols and cloud. While more work needs to be done to obtain valid scientific data, other organisations with an interest in atmospheric science have expressed a desire to asses our data product. With their help and given the early promising results, there seems to be no reason why Moblas 5 will not be able to increase data yields with a possible increase in client base by utilising the Lidar system. This can only help to justify future funding for the station.

Multiple Wavelengths Ranging in Graz

G. Kirchner, F. Koidl

Institute for Space Research
Observatory Lustbühel
Lustbühelstrasse 46
A-8042 GRAZ / AUSTRIA

K. Hamal, I. Prochazka

Faculty of Nuclear Science
Czech Technical University
Brehova 7, 115 19 Prague 1
CZECH Republique

Abstract

In addition to standard ranging activities with 532 nm, some tests with other wavelengths have been performed successfully in Graz:

- 683 nm: Ranging to satellites up to LAGEOS;
- 435 nm: Ranging to satellites up to LAGEOS;
- 1540 nm: Ranging to calibration targets [1];
- 355 nm: Ranging to calibration targets.

Most of the experiments are done for atmospheric parameter checks; only the 1540 nm target ranging was an initial eyesafe ranging test [1].

The H_2-Raman-Shifting of the 532 nm proved to be quite successful and promising, with good first results in 3 colors from targets and from most satellites.

1.0 Standard Ranging

Usually, all routine passes in Graz are measured with 532 nm; in this standard configuration, we measured 1994 almost 1500 passes, with RMS of 7 to 8 mm (ERS1) and 10 to 12 mm (LAGEOS).

For all satellites, we tried to maximize the return rate by

- using 10 Hz for all satellites up to LAGEOS [2];
- increasing SPAD sensitivity due to higher voltage above break;
- optimizing SPAD optics and alignment;
- using SemiTrain techniques, etc.

We get now - in good conditions - between 10.000 and 20.000 returns for LAGEOS passes, and about 3000 returns for ERS1 passes (inspite of using only a few mJ per pulse).

These high return rates are necessary to use Normal Point statistics, to get the required NP accuracy to check atmospheric corrections with Multi-Color measurements.

1.1 Multi-Color Ranging

When starting Multi-Color (MC) ranging tests with our standard system, we tried to include the following ideas:

- Use the available Nd:YAG laser;
- The SLR system had to remain operational between all MC-tests;
- Switching between standard and MC ranging should be easy and fast;
- Use a single receiver channel (SPAD, Time-of-flight counter) for all colors to minimize or eliminate problems of drifts, calibrations etc. of different receiver channels at the few ps level;
- Instead, use time multiplexing of colors by switching between colors;
- Select suitable colors to maximize atmospheric dispersion.

We selected Raman shifting of the original 532 nm to 683 nm, with the additional option of using the first Antistokes line at 435 nm, although the expected energy budget here was rather limited; but the pair 435/683 nm should give an acceptable figure of merit [3] for MC ranging.

1.2 Raman Conversion

Fig. 1 shows the laser setup for Raman shifting; during standard ranging both removable mirrors are in the shown positions; in Raman mode, these two mirrors are simply removed, and the 532 nm are entering now the Raman tube.

The 1.2-m-Raman tube was built in Graz; the windows on both ends are AR-coated mirror substrates, producing a focus in the middle of the tube. The tube itself is pressurized with Hydrogen (usually 30 Bar). We tried to optimize the Raman conversion efficiency by

- making the tube long enough: The 1.2 m proved to be a good compromise;
- optimizing the H_2 - pressure (Fig. 2); our usual operating values are:
  - 8.0 mJ at 683 nm (SemiTrain energy; ≈ 1.0 mJ for the first pulse);
  - 9.0 mJ at 532 nm (SemiTrain energy; ≈ 1.1 mJ for the first pulse);
  - 1.8 mJ at 435 nm (SemiTrain energy; ≈ 0.2 mJ for the first pulse);

We tested also other methods given in literature (e.g. [4]), which looked promising for higher conversion efficiencies (also for the first Antistokes line), but these could not be verified in Graz (possibly due to our not very Gaussian beam intensity profile).

The first dispersion prism separates the 3 beams and directs each of them into its own telescope, while the second dispersion prism recombines the 3 beams again; this scheme allows for

- independent divergence pre-adjustment of each beam, pre-compensating the non-achromatic transmit telescope on the mount;

- simple switching between colors by blocking 2 colors out of 3, which gives also simple and reliable return color identification in our Single-Photon / Single Receiver Channel MC system.

The non-achromatic transmit telescope still allows full divergence adjustment for all three colors during actual ranging.

2.0 First Results from Satellites

After first successful tests to the targets, we started ranging tests to most satellites; up to now we have tracked in all three colors about 50 passes, including LAGEOS.

Fig. 3 shows an ERS-1 pass, with all SemiTrain returns, and with switching between all 3 colors in more or less regular intervals ; in Fig. 4 the SemiTrain returns are folded on the first track, showing now clearly the switching between the colors. While tracking with the red and the green colors could be achieved easily down to 10°, the quite low energy (≈0.2 mJ/pulse of SemiTrain) and low atmospheric transmission of the blue color makes it difficult to range below elevations of ≈25°.

In Fig. 3 and Fig. 4 all color returns are corrected for 532 nm, and are showing therefore dispersion; applying the theoretical Marini-Murray correction and the measured calibration values for each color, all returns are folded on a straight line (Fig. 5). Preliminary comparisons with the Marini-Murray model show no significant deviations up to now, but this has to be verified by applying NP statistics, better orbital fitting (instead of the presently used polynomials) and more passes in different atmospheric conditions. With this higher accuracy, it should be possible at least to detect - and possibly correct - any atmospheric anomalies (or deviations from the standard models).

Fig. 6 shows a similar pass to LAGEOS-1, with missing returns short after the closest approach (due to laser beam alignment problems); nevertheless it demonstrates MC returns from LAGEOS, with single Laser pulse energies down to about 200 μJ (at 435 nm).

3.0 Future Plans

To bring the MC ranging system in a more operational status, we need

- better alignment of the 3 beams; we are testing different methods;
- more computer power (our HP1000/A400 is limiting at the moment any further developments); we are switching to a PC/486 controlled system in the next few months;
- automatic switching between colors under full computer control.

The postprocessing software already allows for handling the somewhat complex conglomerat of SemiTrain- and MultiColor-Returns, high SPAD noise etc., and applying different atmospheric correction and calibration values; still some effort is required to get final results concerning atmoshperic correction data.

References:

[1] Satellite Laser Ranging at Eyesafe Wavelengths. B. Greene, K. Hamal, I. Prochazka, H. Kunimori, G. Kirchner; these proceedings.

[2] Improving an HP5370A Counter. G. Kirchner, F. Koidl; these proceedings.

[3] Optimum wavelengths for two color ranging. J. Degnan; NASA GSFC, Greenbelt, MD 20771

[4] Stimulated Raman scattering in H_2-AR mixtures. A. Luches, V. Nassisi, M.R. Perrone. Optics Letters, Jan. 1987; Vol 12. No. 1

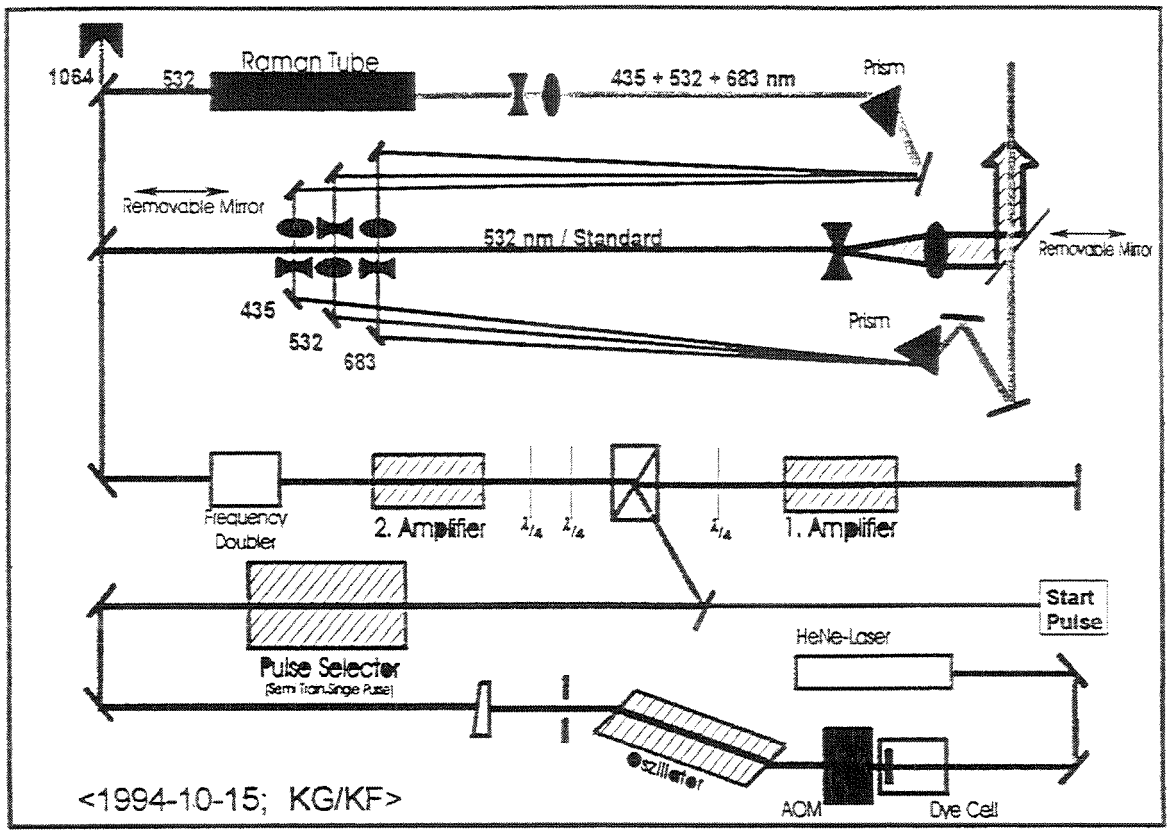

Fig. 1: Graz Nd:YAG-Laser, Multi-Color Configuration

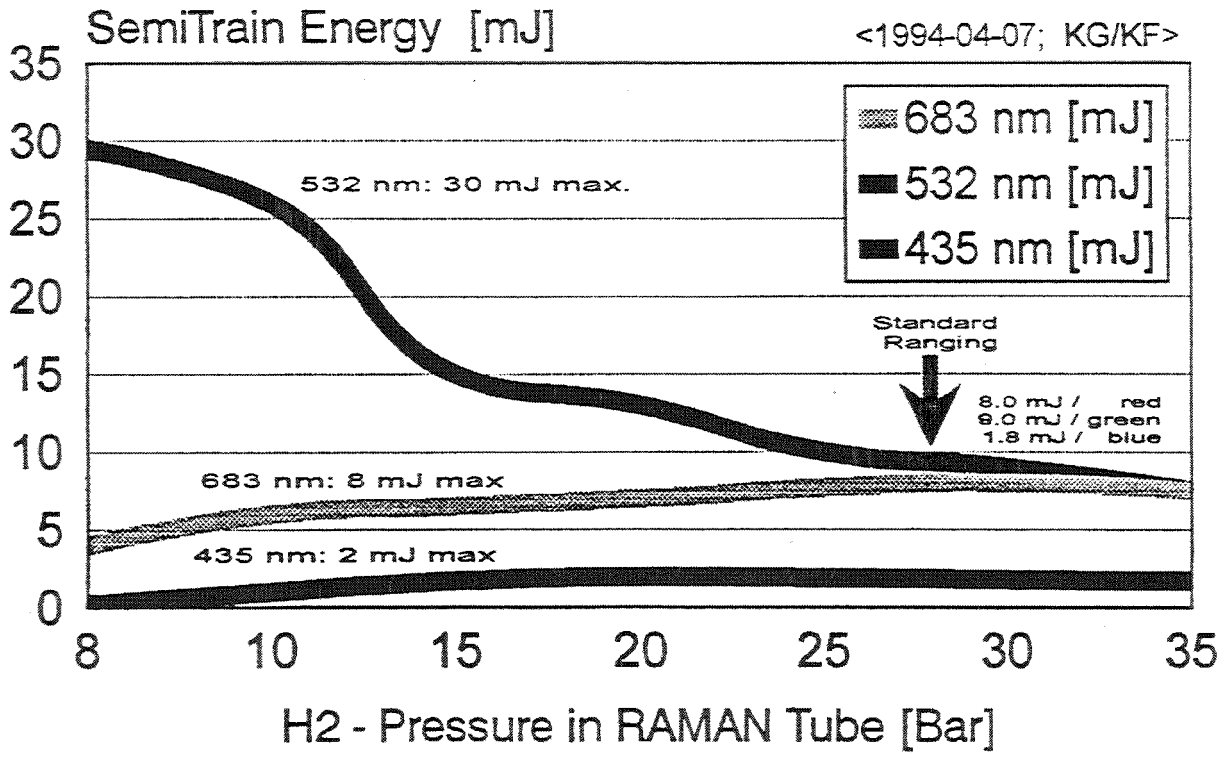

Fig. 2: H2 - Raman Conversion Efficiency; SemiTrain Energies

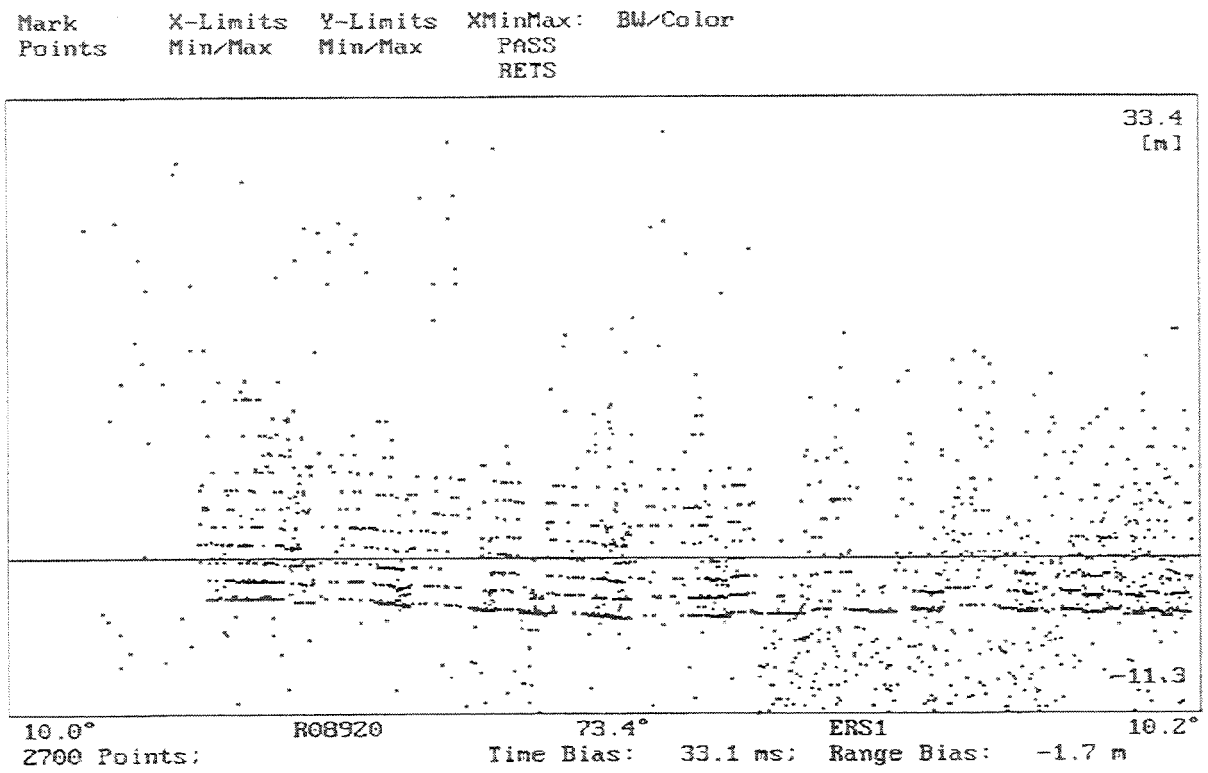

Fig. 3: ERS-1 Pass, with SemiTrain, MultiColor (Blue, Green, Red); and noise ...

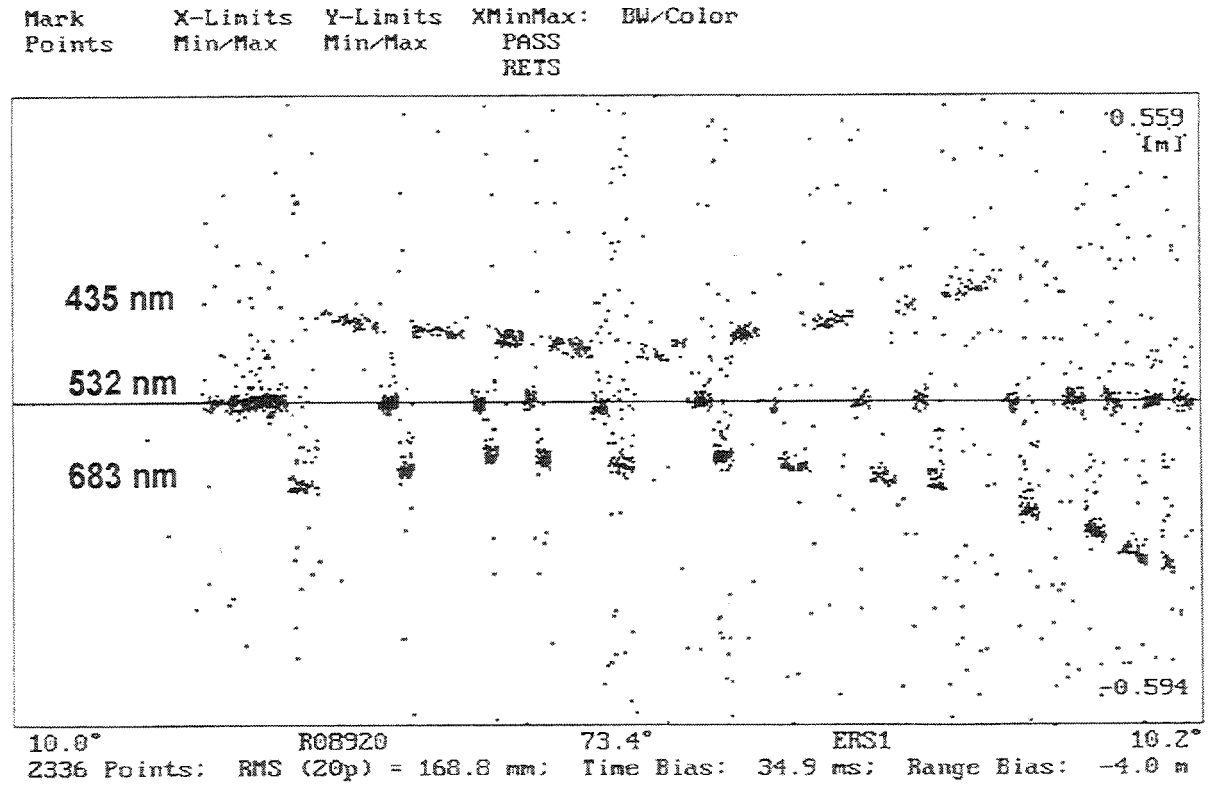

Fig. 4: Same ERS1-Pass; SemiTrain folded: 3 Colors (435, 532, 683 nm)

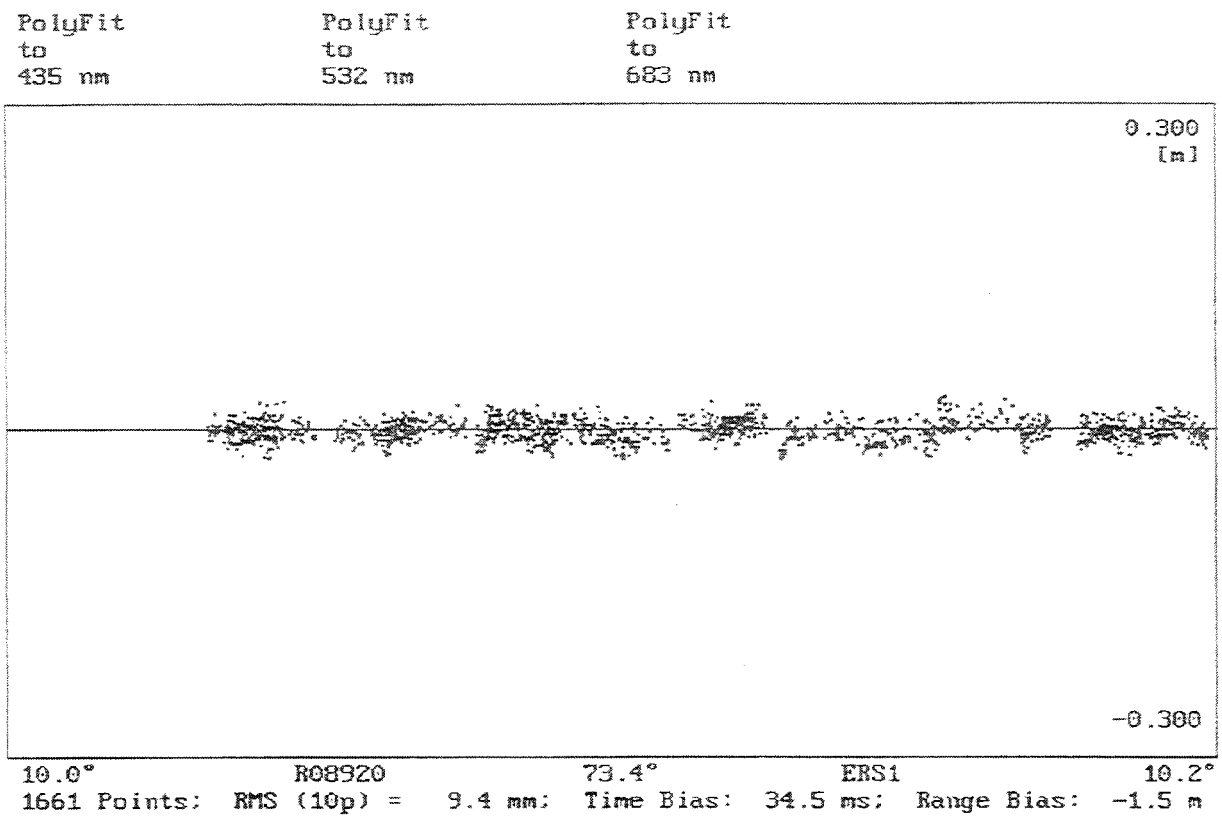

Fig. 5: Same ERS1-Pass; all atmosph. corrections and calibrations added.

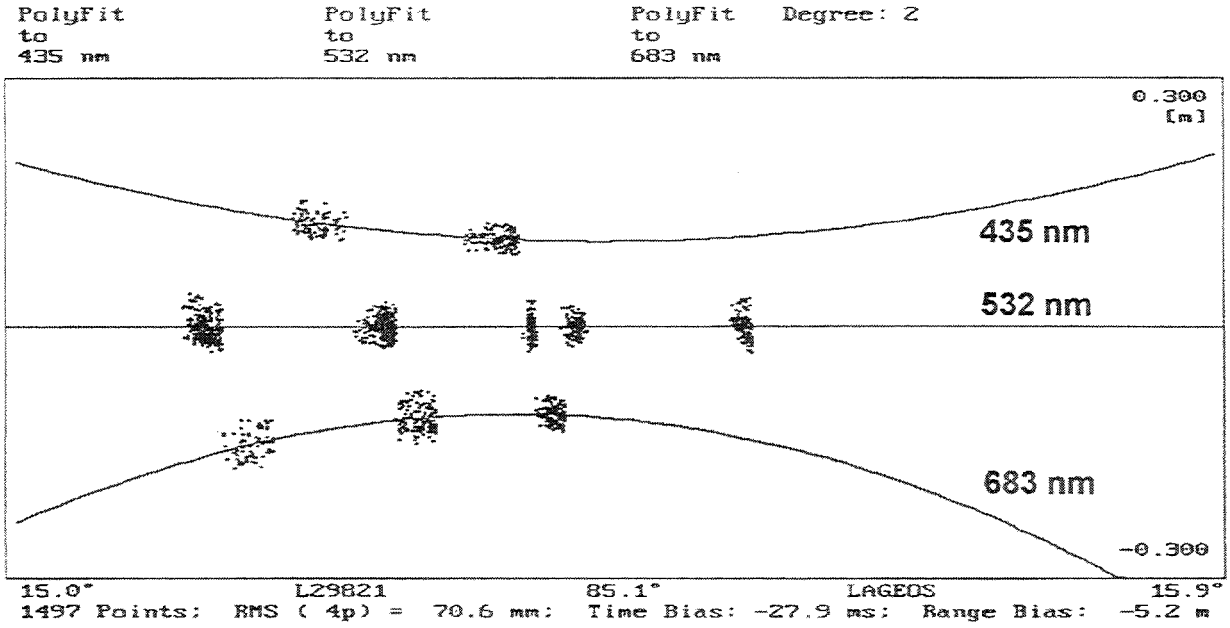

Fig. 6: LAGEOS1-Pass; SemiTrain folded: 3 Colors (435, 532, 683 nm)

Measuring atmospheric dispersion employing avalanche photo diodes

Ulrich Schreiber, Wolfgang Maier and Stefan Riepl
Forschungseinrichtung Satellitengeodäsie
Fundamentalstation Wettzell
D-93444 Kötzting
Germany

Karl Heinz Haufe
Institut fuer Angewandte Geodäsie
Aussenstelle Wettzell
D-93444 Kötzting
Germany

Abstract

The accuracy of today's satellite laser ranging systems (SLR) is limited to a few cm. A significant part of this range error is due to the limitations of the atmospheric correction model. A dual color ranging experiment has been designed to investigate this source of error. When ranging to satellites at the fundamental and second harmonic frequency of a Nd:YAG laser, two different pulse round trip times are obtained simultaneously. The infrared pulse is detected by an avalanche photodiode, operated in the "Geiger mode", while the green pulse is recorded by a microchannel plate photomultiplier (MCP). For a given satellite pass, the jitter in recording the time of flight of the pulse is too high to calculate an atmospheric correction from individual measurements. Due to the many shots per satellite pass, the scatter can be significantly reduced by applying a nonlinear least squares fitting procedure to the data. The results of a large number of satellite passes are compared with the predictions of the Marini- Murray model.

1. INTRODUCTION

The varying index of refraction of the atmosphere can be considered as one of the most important contributions to the error sources for satellite ranging [3]. Following a model of Marini and Murray [1], the additional time for the laser pulse passing through the atmosphere at an elevation angle of 90 degrees, is as much as $8ns$. This model assumes rotational symmetric atmospheric layers with respect to the geocenter and has been established with the help of balloon experiments. Input to this model are atmospheric pressure, temperature and humidity, which are measured around the ranging station. In general it can be said, that this model is very good, so that the requirements for obtaining an experimental improvement are high [2]. By ranging at two or more frequencies simultaneously, the refractive index is measured instead of being calculated on predicted profiles for the input parameters.

2. THE EXPERIMENT

When ranging to satellites at two different wavelengths simultaneously, two different round trip times are obtained. This difference is caused by the wavelength dependence of the refractive index $n(\lambda)$ of the atmosphere. As n is only little different from 1, the entire effect is very small. When calculating a range correction from the differential ranges of a two color measurement, a high precision of $0.24cm$ (i.e. $8ps$) in timing the difference between the detection of the two colors is required. This is because only a $\frac{1}{21}$ of the full range correction is visible in the differential ranges [4]. This requirement is not met by any photomultiplier or avalanche photodiode for an individual measurement. However, applying statistical means to a large number of range measurements, gives the required resolution. This limits the interpretation of the data to effects which are present over the full time of an experiment. Contributions, such as variations in the correction model's input parameters due to horizontal gradients of temperature, humidity and air pressure at some distance from the ranging station can not be analyzed. There are indications from an aeroplane mission, where a retroreflector was carried around the ranging site at roughly $30km$ distance, that these effects are a lot smaller than the ones analyzed here [6].

The wavelength pair used here, is given by the employed Nd:YAG laser. There is the fundamental frequency having a wavelength of $\lambda_1 = 1.06\mu m$ and the second harmonic with $\lambda_2 = 0.53\mu m$. The transmission of the atmosphere is suitable for both frequencies. As conventional photodetectors such as PMTs and microchannel plates (MCP) are not sensitive in infrared, a silicon avalanche photodiode (APD) [5] placed in "Geiger mode" was employed to detect the laser's fundamental frequency, while the MCP was used for the other signal.

When comparing the measured differential ranges with those calculated from the atmospheric model, a good agreement is found in most cases. However, there are also a number of passes, which do not agree. By rescaling the elevation dependence of the atmospheric model (i.e. pathlength through the dispersive media), sufficient agreement could be established in all cases. The measured range differences Δt_{ex} can be expressed by the model Δt_{mod} through

$$\Delta t_{ex}(\Psi) = \alpha \Delta t_{mod}(\Psi) + \beta \tag{1}$$

where Ψ is the pointing elevation angle of the telescope in the local horizontal system, which corresponds to the pathlength through the atmosphere. The parameter α rescales the pathlength dependent part of the predicted atmospheric model, while β expresses a constant offset between the two signals, which is introduced by the ranging system. α and β are evaluated by a nonlinear least squares fitting procedure from the observed data.

A large number of measurements have been carried out over the period of roughly one year, using various geodetic satellites as targets. Only passes to LAGEOS with a high number of returns in both spectral ranges were used for the analysis, while the other passes served as crosschecks. Figure 1 shows a plot of a typical measurement. The echoes of the green color were taken as a reference and after fitting an orbit to this data, the lower part of the diagram is obtained as range residuals over the elevation angle of the telescope. The

upper curved band of residuals is representing the measured difference in time of flight of the infrared pulse with respect to the same orbit. The dashed line is showing the predicted contribution of the atmospheric model, while the solid line gives the rescaled model from the fitting procedure.

3. DATA HANDLING

Figure 2 shows the values of α obtained for a number of LAGEOS passes. In many cases the predictions of the atmospheric model are verified, as $\alpha \approx 1$ is obtained within the error bars of the fits. However a number of passes deviate significantly from 1. At the present time there is no model available, which would allow to compute a correction to the ranges from these dual color measurements. The variable α, which may represent something like a modified optical density of the atmosphere, seems to be very sensitive to the dual color measurements. On the other hand this value cannot be used directly for a range correction, because errors of the order of 15% are definitely not realistic for the model. To get access to the data a simple way of looking at the measurements was found to be quite helpful. At first the constant offset between the range measurements of the two frequencies has been evaluated. Then the data were corrected for the atmospheric contribution to the range by fitting equation 1 to the data. As a result a different value for the offset was obtained. The difference between these two offset values was interpreted as a mean range correction for the satellite pass. This was done for the available passes and the result is plotted in figure 3. The range corrections obtained are all well below $5cm$. This is in accordance with the expectations to the dual color measurement technique. But it must be clearly stated, that a proper method of analysis still needs to be developed.

4. DISCUSSION

4.1. Atmospheric model versus raytracing

After seeing differences between the modeled atmospheric correction and the measurements, it was thought, that this was caused by deviations of the modeled profiles for pressure, temperature and humidity from the real profiles of these parameters. For the analysis of the quality of the model predictions a raytracing program based on [7], [8] and [9] was written. It uses the profiles of the above mentioned atmospheric parameters as obtained from radiosonde launches from a site of the "Deutsche Wetterdienst" roughly 100 km away from the ranging station. Over the period, where this comparison was carried out, dual color ranging was done successfully too, showing significant contributions to α in some of the passes. As a result it was found that even at very low elevations (i.e. 20°), where the effects of the refractive index are maximal, the agreement between the correction model and the raytracing approach was well within $2mm$. As this did not change with different data sets, even this offset is most likely due to some systematic artifact. Because the atmospheric model and the raytracing algorithm are based on some identical assumptions, it was concluded, that the measured effects are not caused by inadequately modeled profiles of pressure, temperature and humidity around the tracking station.

	required change	H_2O Absorption-line (infrared)	CO_2 Variation of concentration	O_3 Variation of Concentration
Deviation from ΔN_{group}	0.1	0.01	0.01	$< 10^{-5}$

4.2. The influence of other constituents

In the next step, it was tested, if variations of the concentration of other prominent atmospheric constituents such as CO_2 and O_3 could be of importance. Ozone is not explicitly contained in the correction model, while for CO_2 it was suspected that excessive variations in the concentration beyond the assumptions of the model may require consideration. The dependence of the refractive index of CO_2 is not very different from that of air. So the variation of the concentration of CO_2 between a standard situation of 0.032 Vol.% and an extreme case of 0.15 Vol.% causes a change of 0.1% in the refractive index. This is at least one order of magnitude below the measured effects. O_3 could be ruled out as well. It is strongly absorbing in the ultraviolet. Its contribution to the dispersion is 10^{-11} under normal conditions. So even extreme variations in the concentration of O_3 do not contribute.

4.3. Absorption lines of water vapor in the infrared

The validity of the dispersion formulas of Owens [10], which are basic elements of the used atmospheric model, are limited to the visible part of the spectrum, at least within the given precision of 10^{-9}. The massive presence of absorption lines of water vapor and CO_2 in the domain above $0.8\mu m$ make an extrapolation into the infrared doubtful. Due to anomal dispersion, the influence of these gases could lead to a higher velocity of infrared light than accounted for by the model. This has been tested, using a theoretical approach proposed by Hill et al. [11] calculating the refractive index out of absorption lines, supplied by the HITRAN database. It was found, that the anomalous group refractive index is increasing between the visible and the infrared. At $\lambda = 1.064\mu m$ a value of about 0.01 is reached. The influence of CO_2 can be neglected, because its absorption lines are far away from the used laser frequencies. The following table, showing the explainable and the requested changes in the difference of the group refractive index summarizes [1] the results so far.

4.4. The obtained corrections compared to model parameters

Looking at pressure, temperature and humidity measured at the ranging station along with the satellite echoes, it was examined, how they correlate to the derived range corrections. In all cases the correlation was not very high. For pressure and temperature a correlation factor of 0.3 was obtained. This was expected, as the raytracing did not give an indication for incorrectly used atmospheric parameters. However it turned out, that for the humidity a correlation factor of 0.5 was calculated. Considering, that variations of the humidity only cause minor changes in the corrections of the atmospheric model, this effect is quite remarkable. This could mean, that the role of the water vapor has not been sufficiently modeled.

[1] $N = (n-1) * 10^6$

5. CONCLUSION

Looking at figure 2 again, one can see, that α may change a lot between satellite passes. This led to the question of what the agility of α is with respect to time. It was attempted to make dual color measurements to passes of various satellites, following as close as possible to an observed LAGEOS pass. It was always found, that passes taken right one after the other, within the error limits obtain almost the same values for α . As the timespan increases, the differences may become larger. Figure 4 shows a plot of $\mid \Delta\alpha \mid$ over the time between passes. The line could then be an indication of what the observed agility of the atmosphere is, with respect to changes of the experienced refractive index over time.

Summarizing, it can be said, that the dual color ranging experiment showed some deviations between measurements and the atmospheric correction model. A raytrace analysis proofed, that this difference was not due to false assumptions on the meteorological input parameters: pressure, temperature and humidity. The influence of other atmospheric constituents, such as CO_2 and O_3 seems negligible, but the analysis could not be done on all species. However, there are some indications, that the water vapor needs further attention. For example, a precise experimental proof regarding the contributions of water vapor in the infrared is still lacking. It also could mean, that the atmospheric correction model must be extended, to cover recent developments in that field. As proposed by Hill et al.[12], the formation of water vapor clusters, caused by the permanent dipole moment of the molecule, could lead to an intrinsic temperature dependence of it's refractive index.

In order to measure the water vapor content along the optical path, attempts for a Raman scattering experiment have been undertaken. The intensity of the frequency shifted pulses is very low. For the detection of water contents of air in the vicinity of the ranging system (ie. a $60m$ bin $1km$ away, assuming a partial pressure of water vapor of $10mbar$) the amount of roughly 5 photons can be expected for a wavelength of $660nm$. Therefore a statistical approach was chosen for the measurement. Another SSO AD-220 avalanche diode, operated in the Geiger mode was placed at the guiding station of the WLRS telescope, which has a reasonable transmission for the Raman shifted echo. The gating of the Geiger pulse was set, so that echos between $20m$ and $1km$ in range could be recorded on a timeinterval counter, which was started by the detecting the outgoing laser pulse. To distinguish between the "Raman-" echo and the elastic backscatter from the laser several different spectral filters were used. The total amount of blocking of the $532nm$ signal was estimated to be higher than 9 orders of magnitude, compared to the desired wavelength. Figure 5 shows one of the test runs. The telescope was pointed to a cloud layer, which was approximately 240 m away, according to the readout of the security radar ($f = 9.5GHz$) of the WLRS. To eliminate the considerable noise recordings from the avalanche diode, the data was corrected by subtracting a pure noise histogram from the measurement. The fitted line through the data indicates an exponential dependence of the intensity with the distance from the tracking station. This was to be expected. At a range of $180m$ the cloud layer becomes visible. However, these experiments are right at the beginning of a closer investigation of water vapor in the "ranging atmosphere". They are not yet suitable for a quantitative analysis. More work needs to be done on that field.

Looking at the measurements done so far, one can say, that it seems feasible to obtain information about the water vapor content of the atmosphere, at least when a Lunar ranging system is used.

6. ACKNOWLEDGMENTS

The authors would like to thank the WLRS team for assisting in the work presented here. Our special thanks are given to W. Schlüter for his support in the project.

References

[1] J. W. Marini and C. W. Murray Jr., "Correction of satellite tracking data for atmospheric refraction at elevations above 10 degrees",*NASA-TM-X-70555*,(1973)

[2] J. B. Abshire, "Pulsed multiwavelength laser ranging system for measuring atmospheric delay", *Applied Optics Vol. 19, No. 20*, (15. Oct. 1980)

[3] J. J. Degnan, "Millimeter Accuracy Satellite Laser Ranging: A Review", *Contributions of Space Geodesy to Geodynamics, Geodynamics Series Vol. 25*, AGU, (1993)

[4] M. Schneider and D. Egger, "Messverfahren der Satellitengeodaesie - Grundlagen 2", *Techn. University Munich, Internal Report*, (1978)

[5] U. Schreiber, K. H. Haufe and R. Dassing, "Measuring Atmospheric Dispersion With WLRS In Multiple Wavelength Mode", *Proceedings Of 8th International Workshop on Laser Ranging Instrumentation* , (1992)

[6] J. B. Abshire, *Private Communication*, at 17. ILRC: Sendai, Japan (1994)

[7] H. S. Hopfield, "Tropospheric effects on signals at very low elevation angles", *Applied Physics Laboratory Maryland, Report No. TG 1291*, (1976)

[8] J. W. Marini, "Correction of satellite tracking data for an arbitrary tropospheric profile", *Radio Science 7, 223 - 231*, (1972)

[9] G. Thayer, "A rapid and accurate ray tracing algorithm for a horizontally stratified atmosphere", *Radio Science 1, 249 - 252*, (1967)

[10] J. C. Owens, "Optical refractive index of air: Dependence on Pressure, Temperature, and Composition", *Appl. Opt. 6, 51 - 59*, (1967)

[11] R. J. Hill, S. F. Clifford and R. S. Lawrence, "Refractive- index and absorption fluctuations in the infrared caused by temperature, humidity and pressure fluctuations", *J. Opt. Soc. Am. 70, 1192 - 1205*, (1980)

[12] R. J. Hill, R. S. Lawrence and J. T. Priestley, "Theoretical and calculational aspects of the radio refractive index of water vapor",*Radio Science 17, 1251 - 1257*, (1982)

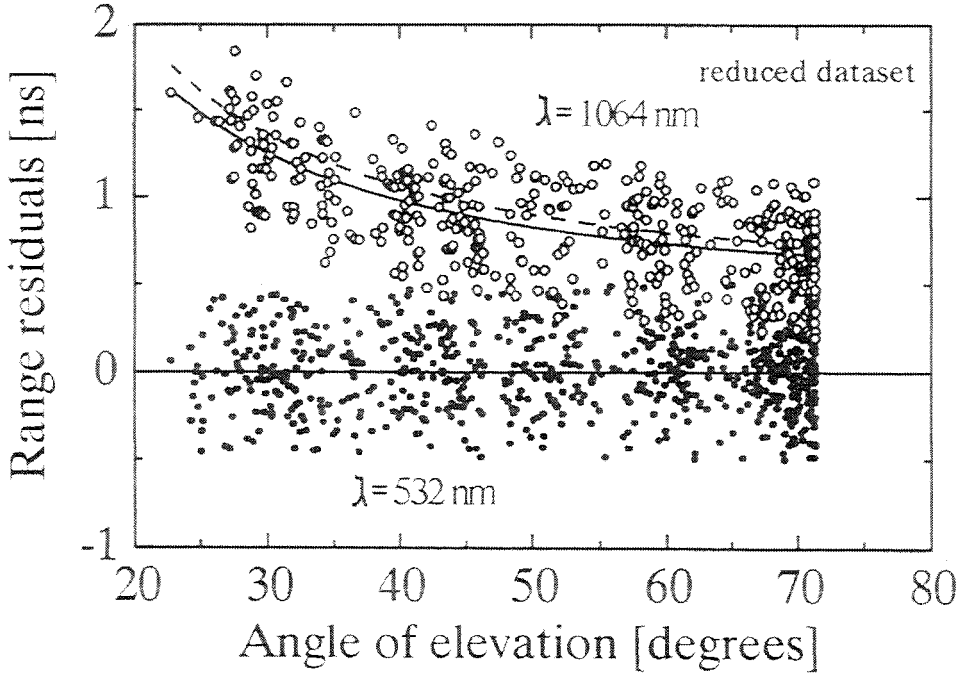

Figure 1: The variation of the difference in time of flight between $\lambda_1 = 1.06\mu m$ and $\lambda_1 = 0.53\mu m$ depending on the elevation angle of an laser ranging system tracking a satellite through the dispersive atmosphere

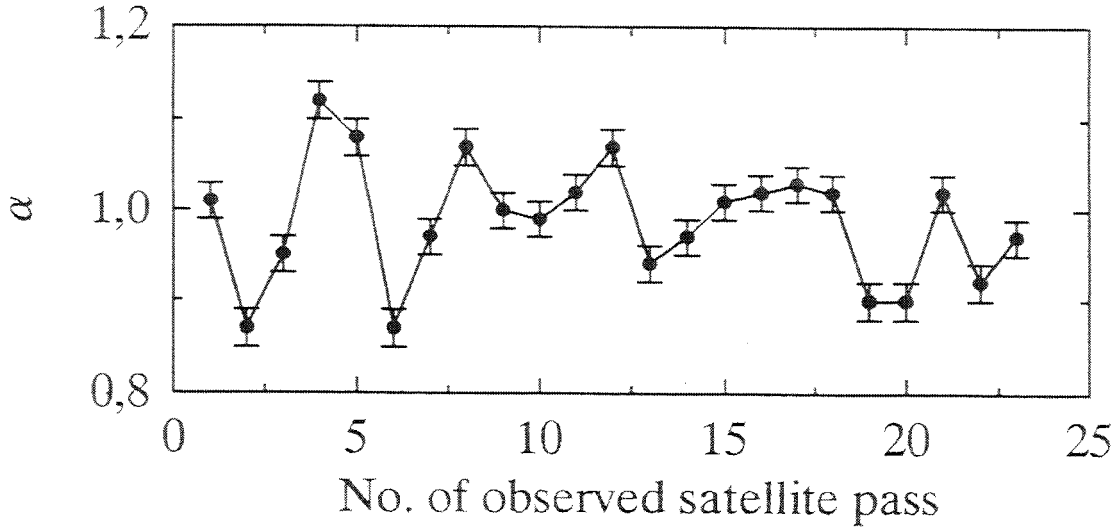

Figure 2: The values obtained for α from the analysis of dualcolor range measurements. All 23 passes were taken from the satellite LAGEOS over a period of roughly one year

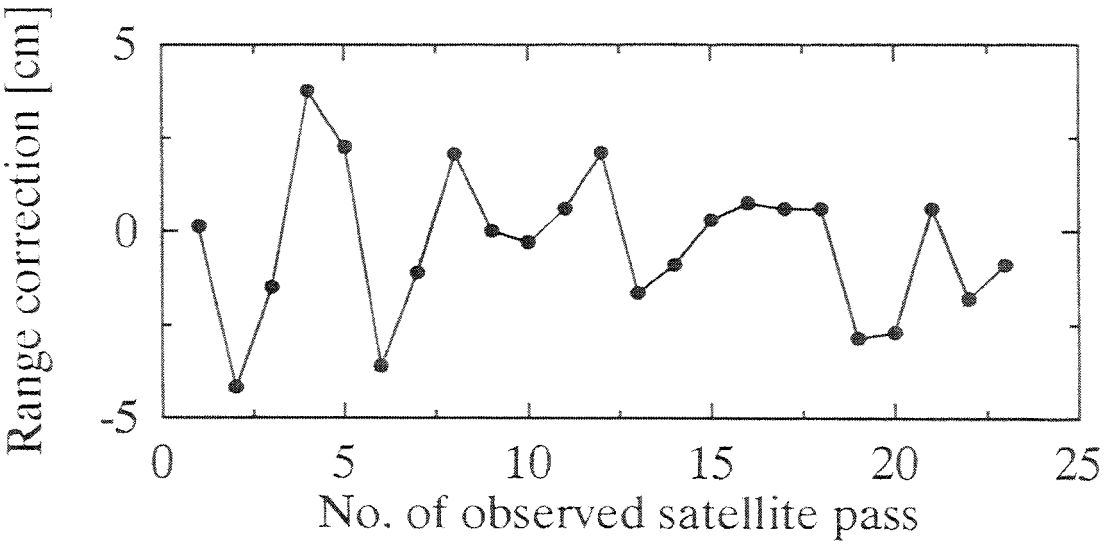

Figure 3: The range corrections from the analysis of dualcolor range measurements as obtained from an empirical comparison procedure

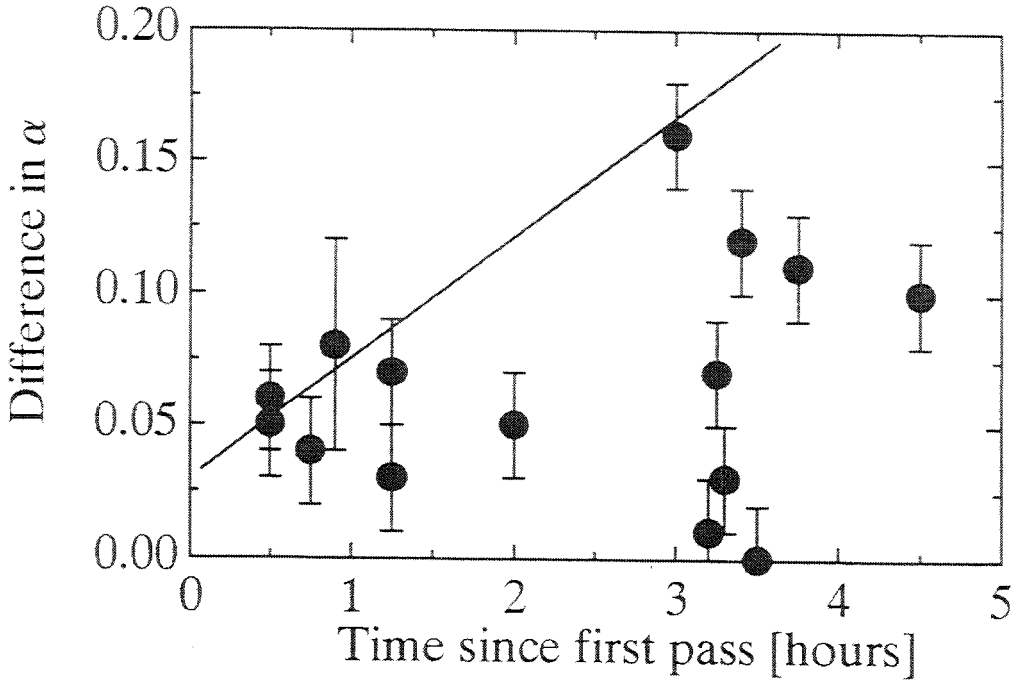

Figure 4: The differences of α in absolute values of two measured satellite passes over the time between crossovers

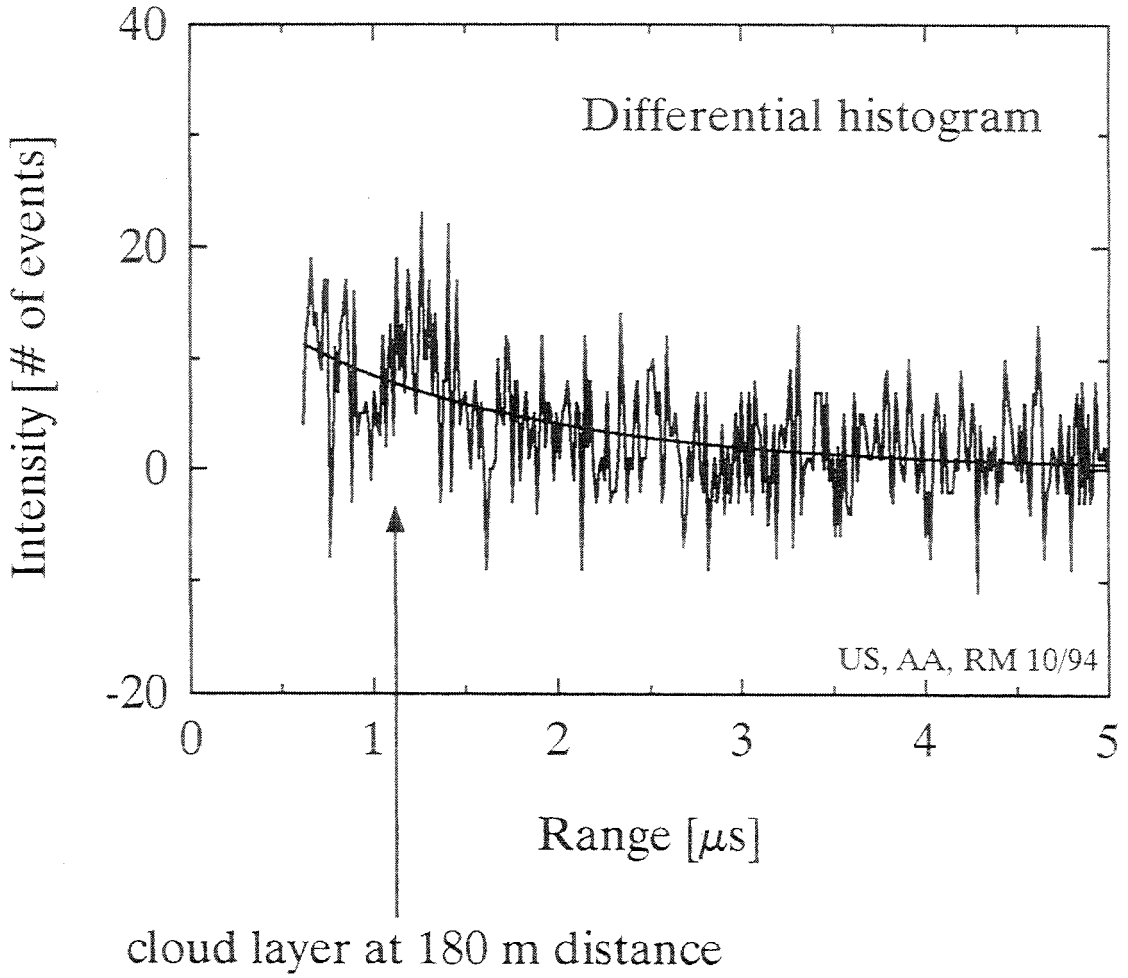

Figure 5: A histogram of raman shifted ($\lambda = 0.66\mu m$) laser pulses scattered back from a cloud layer $180m$ away from the ranging station

Measuring Atmospheric Dispersion Using The Reflector in Space (RIS)

Ulrich Schreiber, Stefan Riepl
Wolfgang Schlueter, Manfred Schneider

Forschungsgruppe Satellitengeodaesie
Fundamentalstation Wettzell
D- 93444 Koetzting, Germany
Phone: (49)9941 603 0
Fax: (49)9941 603 222
Email: SCHREIBER@WETTZELL.IFAG.DE

I. Introduction

The reduction of measured laser pulse roundtrip times between a geodetic tracking station and an appropriate satellite to meaningfull ranges, requires the use of a suitable model to account for the experienced refraction. The presently used model [1] provides an accurracy of better than a few cm and is the major remaining error source in the ranging experiment. Therefore the shot by shot determination of the dispersion of the atmosphere by using two different laser colors simultaneously has been proposed [2,3].

II. Ranging With Solid State Detectors

In recent years, silicon avalanche photodiodes (APD), operated in the Geiger mode, have been employed in various satellite ranging stations. They have the advantage of a still considerable sensitivity (QE~4%) at a wavelength of 1.06 μ m, which is the fundamental frequency of the Nd:YAG pulse laser, operated at most stations. After frequency doubling with a non linear element (KD^*P), two simultaneous pulses (λ_1=0.532 μ m and λ_2=1.06 μ m) are available with sufficient energy. After taking a large number of passes to the satellite LAGEOS in this dualcolor mode and comparing the measured differences in range to the predictions of the refraction model, some disagreement has been found. However the residual scatter of these measurements is still quite high. Although a large number of individual range measurements of each wavelength were obtained by each pass, a higher resolving measurement technique had been looked for.

III. Recording Differential Ranges Using a Streak Camera

Streak cameras in general have a very high resolution in time. This makes them suitable for this application. But there are also a few drawbacks. First of all, the low quantum efficiency of at least one

order of magnitude below conventional detectors for the here selected wavelength pair, must be mentioned. Then there is the need for a precise linearisation of the camera's sweep time. The focussing onto the photocathode is also critical. One of the big experimental problems is the triggering of the sweep a few nanoseconds ahead from the incoming satellite echo. In the construction of the streak camera detection experiment at Wettzell, unlike the approach of [4], the following design goals have been followed.

Usage of the fundamental and second harmonic frequency of the Nd:YAG laser, because they are readily available on the system.

A circular sweep is used, thus allowing more freedom in triggering the datacollection (multiple revolutions).

A circular one dimensional CCD- array is used in order to have a fast readout and a minimum of storage requirements.

The system is capable of taking a measurement every 100 ms. Only differential ranges between the two signals are timed with maximum precision.

The two pulses are emitted simultaneously by the telescope pointing to the satellite, which is carrying the retroreflector. The streak camera itself is a single photon detection device (Hamamatsu; C 1587-01), having a two stage MCP- amplifier. When the echo returns, the synchroscan streak camera is triggered to record the infrared signal first and the green pulse next. To accomplish a complete sweep circle, the camera takes approximately 8.3 ns. The spacing between the two echo pulses due to the atmospheric dispersion is around 1 ns. The window for data recording may be as wide as 60 or 100 ns, corresponding to 10 - 15 successive sweeps. However this leads to the integration of noise, thus bringing down the signal to noise ratio (SNR). Therefore a short window is desirable, but it is no requirement. After exposing the CCD- array, the 720 elements are red into the computer, additional information like pointing angle of the telescope and the epoch of the measurement is added and all information is stored in a datafile for post ranging analysis.

The construction of the streak camera experiment has been started in early 1993. Ranging to a local ground target 1.2 km away from the WLRS was carried out, after the timescale (sweep) was sufficiently linearized. The echo pulses could be clearly separated and the calculated atmospheric dispersion was obtained, after subtracting the ranging system's own constant contribution to the dispersion.

It is to be expected, that the link budget is too marginal to support tracking to most of the geodetic satellites in the desired way. In order to be sensitive in the infrared domain, the streak camera is equiped with a S1 cathode, which has a quantum efficiency of less than 1% on both, the fundamental and second harmonic frequency of the employed laser. Another problem is, that geodetic satellites have more than one reflector contributing to the echo, which causes a degradation of the signal shape, due to superposition of echos from several retroreflectors. Because of the highly increased effective radar crosssection of the target over all other available satellites and the clear pulse shape of the echo, the use of the REFLECTOR IN SPACE of the Japanese ADEOS mission is in preparation.

References:

[1] J. W. Marini, C. W. Murray Jr.;
Correction of satellite tracking data for atmospheric refraction at elevations above 10 degrees;
NASA - TM - X - 70555, (1973)

[2] J. B. Abshire;
Pulsed multiwavelength laser ranging system for measuring atmospheric delay;
Applied Optics Vol. 19, No. 20, (15. Oct. 1980)

[3] C. B. Johnson, S. Nevin, J. Bebris, J. B. Abshire;
Circular- scan streak tube with solid- state readout;
Applied Optics Vol. 19, No. 20, (15. Oct. 1980)

[4] Th. Varghese, Chr. Clarke, Th. Oldham, M. Selden;
Streak Camera Based SLR Receiver For Two Color Atmospheric Measurements;
Proceedings Of 8th International Workshop on Laser Ranging Instrumentation, (1992)

Dualcolor Streakcamera Targetranging (d=2.4 km)

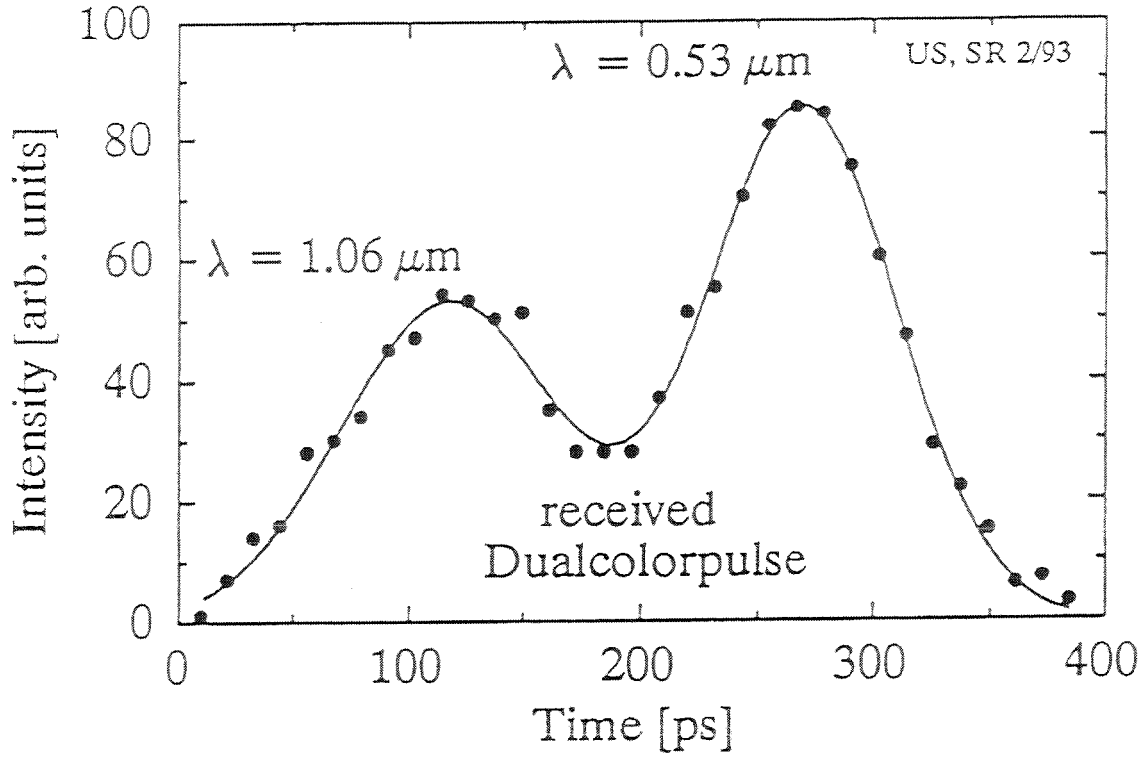

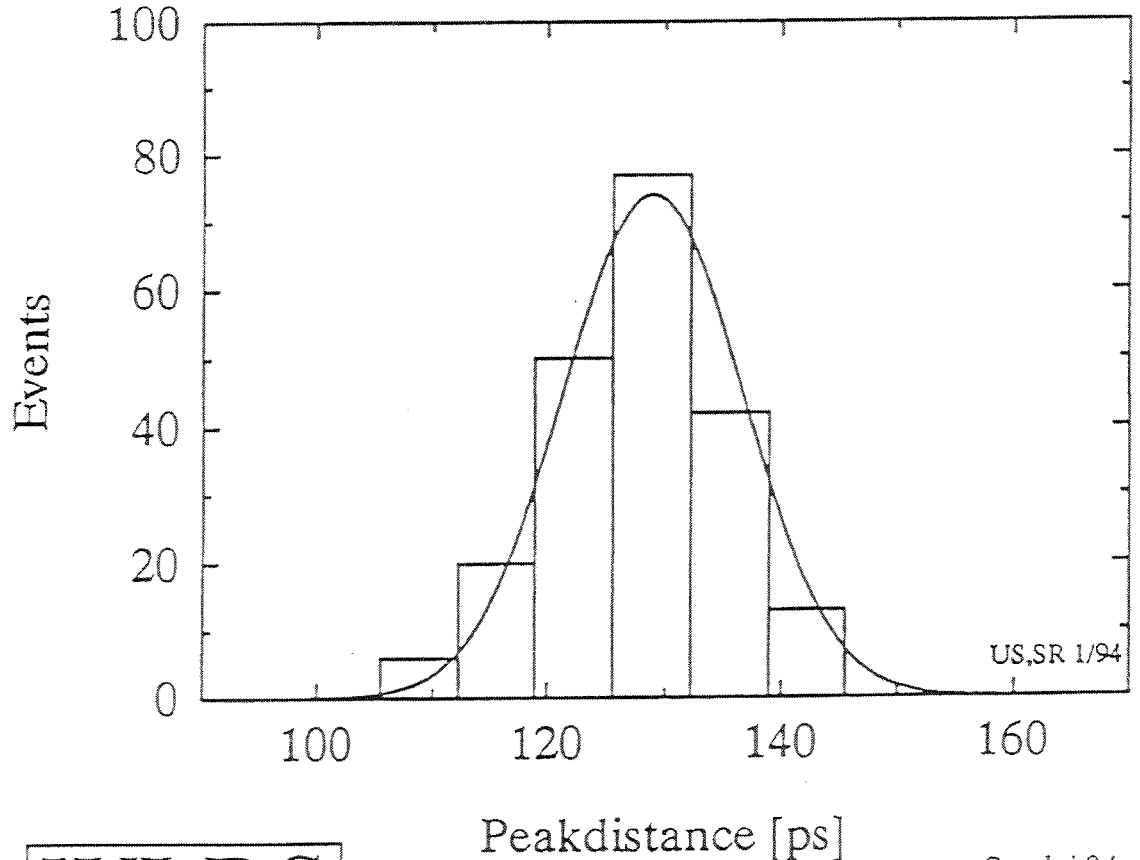

WLRS

Sendai 94 US 7/94

VALIDATION OF TWO COLOR LASER RANGING

comparison between : index integrated on the trajectory and index at the station

C. Lucchini, J. Gaignebet, J.L. Hatat
Equipe de Recherches Electro-optiques OCA-CERGA
Av. Copernic 06130 Grasse France
tel. : (33) 93.40.53.53, fax : (33) 93.40.53.33

In this paper, we try to verify that in using two color laser ranging systems at zenith angle, the knowledge of the atmospheric parameters is not necessary along the trajectory (but only at the laser site in order to reach the best accuracy).

1. Classic Laser Ranging Principle :

fig. 1 :

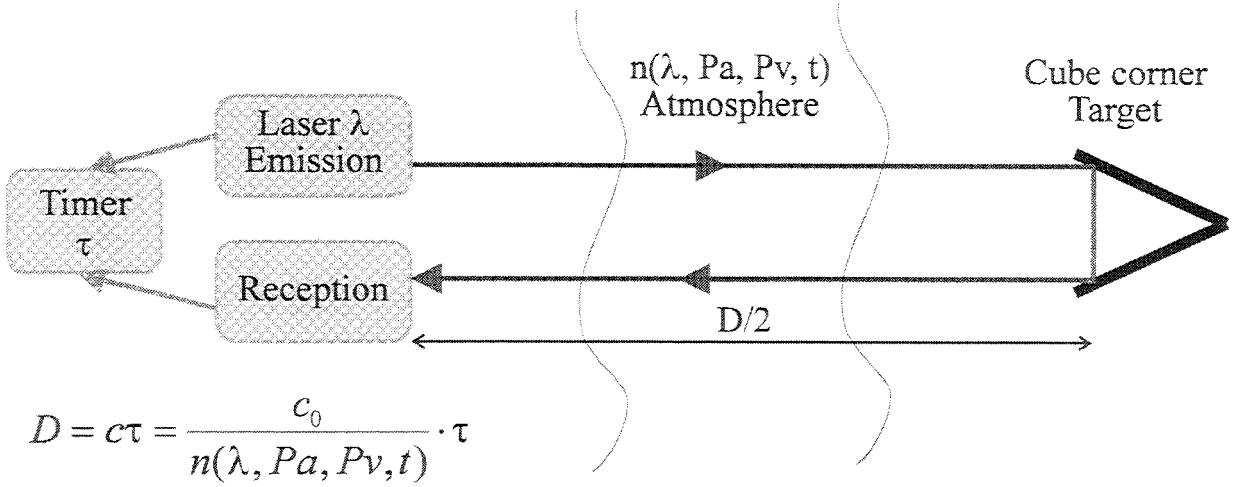

$$D = c\tau = \frac{c_0}{n(\lambda, Pa, Pv, t)} \cdot \tau$$

with : c_0: light velocity in vacuum
c : light velocity in an index n element
D: round trip distance
τ : delay for the light to cover the round trip
λ : light wave-length
Pa, Pv : atmospheric and water vapor pressures
t : air temperature

The figure 1 shows that one knows everything except atmospheric index n(z) that depends of meteorological parameters in each point of the distance covered by the light, where z is the altitude.

2. Three solutions to solve the undetermination on the index n(z) along the way.

2.1. Index models n (λ, Pa, Pv, t.)

The literature provides different index models like Edlen, Marini-Murray and Owens, but their use implies the knowledge of the atmospheric parameters in each point of the way: Pa (z), Pv (z) and t(z) respectively atmospheric pressure, water vapor pressure and temperature at the altitude z.

Marini and Murray index formula :

$$N_g = 80.343 f(\lambda)\cdot\left(\frac{P_a}{T}\right) - 11.3\cdot\left(\frac{P_v}{T}\right) \qquad f(\lambda) = 0.9650 + \frac{0.0164}{\lambda^2} + \frac{0.000228}{\lambda^4}$$

with

Pa : atmospheric pressure (mb)
T : temperature (Kelvin degrees)
Ng : group refractivity of air

co-index : $N_g = (n-1).10^6$

Pv : water vapor pressure (mb)
λ : wavelength (μm)
$f(\lambda)$: dispersion factor

Edlen index formula :

for λ in μm, t = 15 °C,
Pa = 760 mm Hg and Pv = 0 mm Hg.

$$N\varphi_{15} = 83.4213 + \frac{24060.3}{130 - \frac{1}{\lambda^2}} + \frac{159.97}{38.9 - \frac{1}{\lambda^2}}$$

phase co-index at t = 15°C

$$Ng_{15} = N\varphi_{15} + \frac{2}{\lambda^2}\left[\frac{24060.3}{\left(130 - \frac{1}{\lambda^2}\right)^2} + \frac{159.97}{\left(38.9 - \frac{1}{\lambda^2}\right)^2}\right]$$

group co-index at t = 15°C

Generalized expression :

$$N\varphi = N\varphi_{15}\cdot 0.378967084\cdot\frac{Pa}{T}\left[1 + 10^{-6}\,Pa(0.817 - 0.0133t)\right] - \frac{Pv}{T}\left(16.775 - \frac{0.134}{\lambda^2}\right)$$

$$Ng = Ng_{15}\cdot 0.378967084\cdot\frac{Pa}{T}\left[1 + 10^{-6}\,Pa(0.817 - 0.0133t)\right] - \frac{Pv}{T}\left(16.775 - \frac{0.402}{\lambda^2}\right)$$

Owens index formula :

$$N_g = R_d \cdot D_d + R_w \cdot D_w$$

Sum of specifics co-index to dry air and water vapor

$$R_d = 23.7134 + 6839.397 \cdot \frac{\left(130+\sigma^2\right)}{\left(130-\sigma^2\right)^2} + 45.473 \cdot \frac{\left(38.9+\sigma^2\right)}{\left(38.9-\sigma^2\right)^2} \quad \text{and} \quad \sigma = \frac{1}{\lambda}$$

$$R_w = 64.8731 + 1.74174\sigma^2 - 3.55750 \cdot 10^{-2}\sigma^4 + 6.1957 \cdot 10^{-3}\sigma^6$$

$$D_d = \frac{P_d}{T} \cdot \left[1 + P_d\left(57.90 \cdot 10^{-8} - \frac{9.3250 \cdot 10^{-4}}{T} + \frac{0.25844}{T^2}\right)\right]$$

$$D_w = \frac{P_v}{T} \cdot \left[1 + P_v\left(1 + 3.7 \cdot 10^{-4} P_v\right) \cdot \left(-2.37321 \cdot 10^{-3} + \frac{2.23366}{T} - \frac{710.792}{T^2} + \frac{7.75141 \cdot 10^4}{T^3}\right)\right]$$

2.2. Range corrections models

When the atmospheric parameters are not known along the travel of the beam some hypotheses are necessary. Many authors have developed a lot of models to correct the range measurement like Hopfield, Marini-Murray, Herring and Abshire and Gardner.

All these models present themselves on the form :

$$D = C_o.\tau \text{ - } correction$$

For that, it is necessary to suppose ideal symmetrical repartition of atmosphere on our earth (based on the local meteorological parameters) or to have a lot a lot of meteorological stations around the laser site to evaluate horizontal atmospheric gradients.

2.3. Multicolor laser ranging

With this method, only one meteorological station at the laser site is necessary and there is no need to make hypothesis on the atmosphere upside.

3. Multicolor Laser ranging

The laser emits multi-wavelength shots : (λ_1, λ_2, λ_3) at the same time. So, for these wavelengths the different corresponding index of refraction are n_1, n_2, n_3.

At the end of the way, one measures the flight time of one wavelength and the differential flight time between the wavelengths.

Two cases exist :

a) two colors :

many authors describe this process, you have the equation :

$$D = c\tau_1 - Ac \cdot (\tau_2 - \tau_1) \qquad \text{with} \qquad A = \frac{n_1 - 1}{n_2 - n_1}$$

Where : D is the distance that you try to evaluate :
τ_1 : the time flight for the wavelength λ_1 measured by a photodiode
c : the light velocity
A : the sensibility factor that depends of indexes of the air (n_1, n_2) for the two wavelengths
(τ_1 - τ_2) is the differential time flight between the two wavelengths (λ_1, λ_2) measured by a streak camera.

b) Three colors (two colors and a half exactly)

$$D = c\tau_3 - Bc \cdot (\tau_2 - \tau_1) \qquad \text{with} \qquad B = \frac{n_3 - 1}{n_2 - n_1}$$

Where : τ_3 = is the time flight of λ_3 measured by a photodiode
B = is the sensibility factor that depends of the indexes of the air (n_1, n_2, n_3) for the three wavelengths (λ_1, λ_2, λ_3)

In this expression one knows or can measure everything except $n_1(z)$, $n_2(z)$, $n_3(z)$, only known at the laser site (z=0).

So, now, we can show that only the meteorological parameters at the laser site are necessary.

4. Precision of the determination of the sensibility factors A and B

We made a comparison between :

- the actual A and B evaluated by integration of the index of the atmosphere along the path

- the local A' and B' evaluated by measurement of meteorological parameters at the laser site : Pa, Pv, and t at z = 0.

Models used for the Comparison

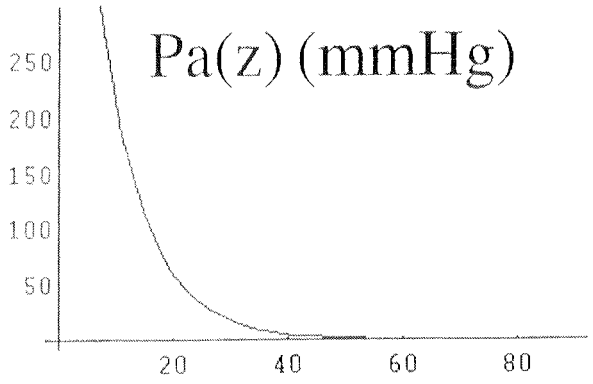

Atmospheric Pressure

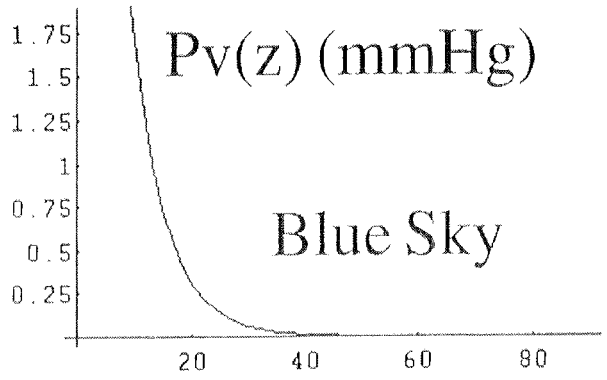

Water Vapor Pressure

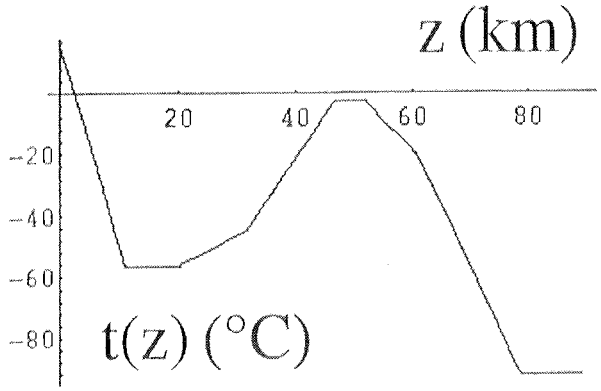

Temperature

Atmospheric Profiles from US Standard Atmosphere and Astrophysical Quantities

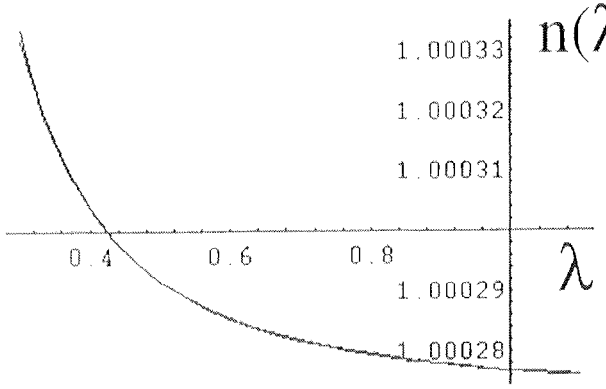

$n(\lambda, Pa(0), Pv(0), t(0))$

Index Models

Marini and Murray 63
Elden 66
Owens 67

Fig. 3

So we have these equations :

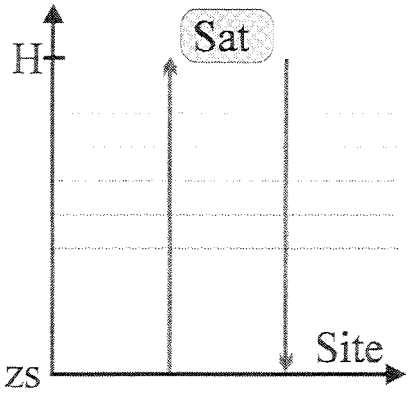

$$A' = \frac{n_{1s} - 1}{n_{2s} - n_{1s}}$$ Actual value

$$A = \frac{\frac{1}{H - zs}\left[\int_{zs}^{H} n'_1(z)dz - (H - zs)\right]}{\frac{1}{H - zs}\left[\int_{zs}^{H} n'_2(z)dz - \int_{zs}^{H} n'_1(z)dz\right]}$$ Local value

With $n_i = \frac{1}{(H - zs)}\int_{zs}^{H} n_i'(z)dz$ Integrated index

Fig. 2.

Where Z_s : laser site altitude
H : satellite altitude
$n'_i(z)$: local value of the index at the altitude z for the wavelength i
n_i : index integrated value

The meteorological parameters Pa (z), Pv (z) and t (z) are functions of the altitude z, consequently the index n (λ, Pa, Pv, t) also.

For the comparison we needed :

- index models, we used Marini-Murray, Edlen and Owens forms.
- atmospheric profiles we used US Standard Atmosphere and Astrophysical Quantities

See next page (fig. 3) for details

5. Conclusion of the comparison

Sensibility / Models	Marini-Murray	Edlen	Owens
A	-42.3509	-42.2792	-42.2299
A'	-42.3822	-42.2322	-42.2425
B	-40.4986	-40.4301	-40.3824
B'	-40.5279	-40.383	-40.393

These values have been evaluated for Pa = 760 mmHg, Pv = 9 mmHg, t = 15°C at the laser site and λ_1 = 0.5398 µm, λ_2 = 0.6958 µm, λ_3 = 1.0795 µm for the wavelengths.

One can see in this chart , the actual A and B determined by integrating the index of refraction along the trajectory (from 0 to 90 km) are not very different from the local A and B.

Taking only atmospheric parameters at the laser site the **error** is less than **0.1 %** that represents at zenith less than **2 mm** (the range correction at zenith is less than 2 meters).

References. :

- J. Gaignebet : Etude sur l'extension des utilisations de la station mobile de calibration laser; ESA INAG contract # 5757/83/F/CG GRGS-CERGA
- J. J. Degnan : Millimeter Accuracy Satellite Laser Ranging :A Review; Contributions of Space Geodesy to Geodynamics : Technology; Geodynamics Series Volume 25 1993.
- J. B. Abshire and C. S. Gardner : Atmospheric Refractivity Corrections in Satellite Laser Ranging; IEEE transactions on Geoscience and Remote Sensing, Vol. GE-23, No. 4, July 1985.
- T. A. Herring : Marini and Murray Atmospheric range correction formula; Report to the CSTG SLR Subcommission meeting held in Munich, FRG, October 18-20, 1988.
- IERS Technical Note 13, July 1992, chap. 11 : Tropospheric model, Satellite Laser Ranging
- C. W. Allen : Astrophysical quantities 1983; Chap. earth atmosphere section 52.
- P. Lena : Astrophysique, méthodes physiques de l'observation 1986; Inter-Editions chap. 2 : L'atmosphère terrestre.
- US Standard atmosphere 1962; NASA, USAF, US Weather Bureau.
- M. L. Baratin and J. J. Walch : La télémétrie laser 2 couleurs (sol/sol) et les corrections de réfraction atmosphérique; stage report July 1990 CERGA-OCA.

SYSTEM AUTOMATION AND OPERATIONAL SOFTWARE

Chairperson : Jan McGarry

Evolution/Automation of NASA HP Data System

Brion Conklin, Win Decker, David Edge, Mike Heinick, Tony Mann, Paul Seery, Michelle Veasey
Allied-Signal Technical Services Corporation

Randy Ricklefs
University of Texas

Jan McGarry
NASA Goddard Space Flight Center

Abstract
Continuing evolution of the NASA HP Data System is planned to support fully automated on site and headquarters data operations. Key objectives are to directly produce all laser data products on site, perform automated data quality control, provide timely data quality feedback, support ongoing station automation projects, support remote software configuration management, deliver all laser data products via Internet, and prepare for unmanned station operations in the SLR2000 era. Recent HP Data System performance, plans to redesign the system in 1995, and plans for future HP data system upgrades will be discussed.

Background/Introduction
The successful deployment of the HP Data System in the NASA Satellite Laser Ranging Network and ongoing improvements to the data system have significantly improved network operational efficiency. These improvements have enabled the NASA SLR network to support continuously increasing tracking requirements which now include more than a dozen operational satellites. These improvements are the first steps in developing fully automated data system operations both at the site and at NASA SLR headquarters. This paper provides a brief overview of recent progress in automating the HP Data System, operational performance of the HP Data System, and future plans to upgrade the data system to support unmanned station operations in the SLR2000 era.

The HP Upgrade Project was initiated in 1987 to prepare the Crustal Dynamics Project SLR Network to meet the operational challenges presented by multi-satellite tracking operations in the 1990's. The technical approach for the HP Upgrade Project was based on the recommendations of the CDP Computer Panel, which recognized that new station requirements to support up to ten operational satellites, and requirements to produce on site normal points could not be supported by existing station computer resources. The basic HP Upgrade Project strategy was to integrate a second computer system into the existing station configuration to provide the required computer resources[Edge, Seery, Ricklefs, et al 1992].

Prototype HP Data Systems were developed at Moblas 7 and MLRS; and, after successful testing, were operationally deployed in 1991. Since 1991, an ambitious plan to improve the HP Data System and to deploy the data system to all operational NASA SLR stations has produced significant improvements in the NASA SLR network capability. Currently in addition to Moblas 7 and MLRS, the HP Data System is operational in Moblas 4, Moblas 5, Moblas 8, TLRS 3, TLRS 4, and Hollas. The availability of Internet resources at selected sites has lead to the automation of data management functions using network communication. In addition, more ambitious software modifications to fully automate data processing operations on site have been recently implemented at Moblas 4 and Moblas 8. Figure 1 presents the current status of ongoing and planned improvements to the NASA SLR HP Data System.

Station automation is the primary NASA strategy to control costs and continue to meet increasingly complex operational tracking requirements. The key data system automation objectives are to directly produce all laser data products on site, perform automated data quality control, provide timely data quality feedback, support ongoing station automation projects, support remote software configuration management, and if possible deliver all laser data products via Internet. Figure 2 presents laser satellite visibility at Moblas 7 during a 24 hour period, illustrating multi-satellite scheduling conflicts and the problem of nearly continuos tracking operations. These operational problems of prioritizing satellite tracking, integrating system calibration, and concurrently performing data processing functions require a fully automated data system.

HP Data System Configuration and Performance

The increase in the number of globally tracked laser satellites, the addition of a second operational shift at some NASA SLR stations and the improved capability of the HP Data System to support multi-satellite operations has resulted in a significant improvement in the global laser data set. Since late 1992, stations equipped with the HP Data System have accounted for approximately 50% of global laser data production and have contributed to both the quality and diversity of the global laser data set. Figure 3 illustrates the increasing HP Data System contribution to the global data set since 1991.

The HP Data System computer system, presented in Figure 4, has successfully handled the increase in data volume with only minor modifications [Edge, Seery, Ricklefs, et al 1992].. Prolific tracking at some of the HP Data System stations, exceeding the computer storage specifications, required an upgrade to the hard disks from 332MB to 660MB. Internet communications has been added to a number HP Data System stations and is playing a key role in automating the data system and other operational station functions. SLR Internet communications have significantly improved in the past two years and are in a state of continuous change providing ongoing opportunities for data system improvement. Figure 5 presents the current status of NASA SLR network communications supporting data system operations.

The major modification to the HP Data System computer involves real time communications to the controller computer in support of the controller project. This upgrade is described in "Deploying the new Graphical User Interface Control Software on the NASA SLR Systems" [McGarry, et al] in these proceedings.

The HP Data System software has undergone continuous refinements since its operational deployment in 1991. A number of HP Data System software modifications were made to support automated data management functions using internet communications at Moblas 4, Moblas 8, Hollas, and Moblas 7 beginning in 1993. A major modification (Version M) of the HP Data System software was completed at Moblas 4 and Moblas 8 in September 1995. Version M automated and migrated all operational processing functions to the field HP Data System software. The Version M upgrade included improvements to the field normal point processing algorithms, automated laser data quality control, production of Merit II full rate data, production of data processing capture files for quality control, support for fully automated internet communications, support for the new Internet data posting system and the addition of quality control flags for normal points. The automated data quality control functions are described in "NASA Automated Quality Control" [Husson, et al] in these proceedings. The new NASA data posting system is described in "Management of Laser Data via the Internet" [Noll, et al].

Version M of the HP Data System software performs fully automated on site data processing and quality control. The system produces all operational laser data products and supporting data quality control statistics 5 to 10 minutes after the completion of the data set. The operator can control the status of the data set for processing and may choose to delay processing to include more data in the satellite pass or to include post pass calibration information. HP Data System stations with at least 56KB of Internet bandwidth automatically transmit all data products and supporting statistics to NASA SLR headquarters hourly via Internet. Basic HP Data System functions and the HP Data System product cycle are presented in Figure 6.

Future HP Data System Upgrades

A major redesign of the HP Data System is planned to better support automated distributed data processing over Internet and to reduce the maintenance overhead required to support changes in software requirements. The redesign introduces object oriented programming (C++) as a more efficient means of translating requirements into code, but is primarily a restructuring of the current HP Data System to better support emerging multi-satellite data processing requirements. The Modularized Integrated Processing System (MIPS) is structured to simplify information sharing between processing modules and to take advantage of processing module independence. Satellite and Calibration processing functions are divided into separate processing systems to more accurately reflect multi-satellite tracking and calibration operations. Satellite and calibration processing run concurrently sharing information as it is produced during tracking operation. The general layout of MIPS is presented in Figure 7.

MIPS will also provide the framework for future software development as the era of SLR2000 approaches. MIPS will use the same computational algorithms, and, where ever possible, the identical code used in the current processing system. MIPS will run in the field on the HP380, and at headquarters on the VAX. It will automatically receive 88 byte raw SLR data from the tracking system, process that data, and deliver the required data products such as Normal Points and sampled data in the CSTG format, Full Rate in the Merit II format, and various database updates.

System Layout and Operation

In MIPS, the data set is at the center of all processing activity as its contents are accessed and operated on by several programs, called process modules. The data set provides input and accepts output, and eventually contains all the information necessary to easily construct all required data products. The format of the file containing the data set is called the consolidated format. Generally, raw values are stored uncorrected, and the corrections are also stored elsewhere in the format. The record lengths are fixed for direct access during I/O operations.

The master file is a catalog of all data sets within the processing system. Master file records contain flags indicating the condition of each data set, as well as audit information and selected analysis information.

Process modules are the tools of the processing system, each performing a single major task and operating independently of other modules. Each module checks the master file for the condition of the data set, reads the data set, performs its task, updates the data set, and, finally, updates the flags in the master file to reflect the new condition of the data set.

Supporting databases link the processing system to the outside world. They are sources of externally produced information and repositories of information produced by the processing system. Eventually, databases will become the primary link between the processing system and user interfaces.

This first version of MIPS will receive data from the tracking system in the current 88-byte format which contains both satellite and calibration data. Pre calibration data, satellite data, and post calibration data will be split into three separate data sets, still in the 88-byte format, and moved to either a satellite data directory or a calibration data directory. The new data sets will be read for identification and audit information. Once a data set identifier has been assigned, a new master file record will be created for each data set. If a data set is to be processed using the presequenced mode, the applicable list of data sets to be processed is updated.

MIPS offers two processing modes, presequenced and scanning. In presequenced mode the system controls the processing of listed data sets. The system determines which modules to run and how certain data set conditions are handled. In scanning mode, each

module scans the master file searching for data sets on which to operate, basing their decision to run on the flags contained in the master file record. Initially, the system will attempt to complete all processing operations on arriving data sets while operating in presequenced mode. Scanning mode will be used primarily to complete operations on data sets abandoned in the presequenced mode. As experience is gained with the system in operation, the use of presequenced and scanning modes will be adjusted to maximize overall performance.

Data products will be delivered to a data transmission staging area on a routine basis. The CSTG normal points and sampled data, Merit II full rate, and database capture records will be deposited in specified directories as soon as they have been generated.

The supporting databases will be the primary source of processing results for operators and analysts. Software accessing these databases will carry the burden of generating ouput in various formats for various devices.

Component Details

The Satellite Data Processing System

Data sources for the satellite data processing system are the 88-byte format and 8 supporting databases. These databases are Station Information, Station Position, Satellite, System Delay, Timing, Tuned IRV, Gravity Model, and Polar Coefficients (Headquarters only).

Data products produced by the satellite data processing system will include Normal Points and sampled data in the CSTG format, Full Rate in the Merit 2 format, and updates to the Summary database. Also, a new Errors database will be updated whenever the processing system encounters certain processing difficulties.

There are eight process modules in the satellite data processing system. They are Conversion, Timing Correction, System Delay, Polynomial Fit, IRV Fit, Normal Point Generation, Sampled Data Generation, and Full Rate Generation. The Conversion module creates the file in the consolidated format, moves information from the 88-byte format to the consolidated format, and gathers readily accessible information from the supporting databases. It also computes or supplies readily accessible corrections such as geometric corrections, satellite center of mass and array corrections, and refraction corrections. An initial shot by shot QC screening will be performed to flag clearly flawed observations. The Timing Correction module will access the Timing Database and update the applicable fields of the consolidated format. The System Delay module will operate in much the same way, accessing the System Delay Database and updating the consolidated format. It will also have to retrieve or produce satellite data set correlated calibration PEB information. The Polynomial Fit module performs a task which is rarely used in routine processing since the implementation of IRV fitting techniques. It is really not necessary for data processing and will be developed last if required. The IRV Fitting

module is the analysis work horse of the processing system. It will perform an IRV fit on the data set, compute range residuals, angle residuals, and refraction corrections based on the computed elevation, and will produce analysis results required for the PEB. After the IRV Fitting module has run, normal Points in the CSTG format will be generated by the Normal Point Generation module and sampled data in the CSTG format will be generated by the Sampled Data Generation module. The Full Rate Generation module will produce the Merit II format. The database interfaces for seven of the MIPS satellite modules are presented in Figure 8.

The Satellite Master File Format includes a system header record, containing file zone boundaries, followed by 107 byte master file records. Each record contains a data set identifier, data set status flags, module control flags, module condition flags, full rate and normal point audit information, a full rate RMS value, and a normal point RMS value. Data set status flags provide a general classification for the data set while a more detailed description of the data set is found in the 256 single bit module condition flags. Module condition flags indicate the condition of the data set as various process modules operate on the data set. The primary purpose of the module condition flags is to trigger and guide further operations on the data set. The system will set flags when modules are running and when they finish. Flags will also be set by the system for any condition determined by a process module which will require follow up actions by other process modules or analysts. The module control flags, consisting of 1 or 2 bits per module indicating on, off, or maybe, force modules to run, prevent them from running, or leave the run / no run decision up to the processing system.

The Calibration Data Processing System

Data sources for the calibration data processing system are the 88-byte format and 3 supporting databases which include Station Information, Target, and System Delay.

The primary products of the calibration data processing system are updates to the System Delay database which is accessed by the satellite data processing system. In addition, the Calibration Summary database will be updated with various results, and the Errors databases will be updated if computing difficulties occur.

For this first version of MIPS only two process modules will be implemented in the calibration data processing system, the Conversion module and the System Delay Database Update module. The Conversion module functions a lot like the Conversion module of the satellite data processing system. It creates the file in the consolidated format, moves information from the 88 byte format, and fills the data set with all readily accessible information. The Conversion module will also compute the shot by shot system delays. As the name suggests, the System Delay Database Update module will update the System Delay Database with new values generated from the calibration data set and information previously stored in the System Delay Database. Calibration data sets will be handled individually and will not be correlated with particular satellite data sets,

so combined system delay and calibration RMS, and pre to post calibration shifts, will be replaced with individual calibration values and slopes between the data sets.

The calibration master file serves the same function in the calibration data processing system as the satellite master file does in the satellite data processing system. The record length is fixed at 86 bytes.

Summary/Future HP Data System Upgrade Activity

MIPS provides the framework which will support future developments in processing and analysis techniques, such as better ways of applying calibration information to satellite data and improvements in data screening and fitting. The structure of MIPS will result in faster, cleaner implementation of upgrades to the system. MIPS is the framework which will support software development for the automated environment of SLR2000. SLR2000 data processing will require sophisticated very low signal to noise data processing to identify satellite ranging observations. The data system will have support unmanned station operations, unattended data processing and communications, and automated scheduling and satellite tracking ["SLR2000: An Automated, Eyesafe System for the Future", Degnan J and "Tracking Satellites with Totally Automated SLR2000 System", McGarry J].

The Moblas controller upgrade project ["Deploying the New Graphical User Interface Control System Software on the NASA SLR Systems", McGarry, et al] is nearing completion at the Goddard Geophysical Astronomical Observatory. The controller project adds HP Data System capability to Moblas 6. Moblas 6, with the prototype controller is scheduled to begin collocation with Moblas 7 in the next few months. The controller upgrade is scheduled to be installed in Moblas 7 in early 1995 and is scheduled to in Moblas 4, Moblas 8, and Moblas 5 later in 1995. Development of a similar controller upgrade for TLRS 3 and 4 is expected to begin in 1995. Also in early 1995, an HP Playback Upgrade is planned for TLRS 2. The Playback upgrade will add basic post tracking HP Data System processing capability to TLRS 2. The TLRS 2 Playback upgrade adds HP Data System (Version M) capability, which migrates all operational processing to the station.

Finally, in 1995 ongoing HP Data System modifications are planned to support the new NASA data posting system [Noll, et al] and to take advantage of improving Internet communications to the NASA SLR network and the global SLR community as soon as possible.

References

Degnan J "SLR2000: An Automated, Eyesafe System for the Future" Proceedings of the Ninth International Workshop on Laser Ranging Instrumentation, Canberra, Australia, Nov 7-11, 1994.

Edge D, Seery P, Ricklefs R, et al "HP Upgrade Operational Streamlining" Proceedings of the Eighth International Workshop on Laser Ranging Instrumentation, Annapolis, Md, May 18-22, 1992.

Husson V, Horvath J, Su G, "NASA Automated Quality Control" Proceedings of the Ninth International Workshop on Laser Ranging Instrumentation, Canberra, Australia, Nov 7-11, 1994.

Noll C, Edge D, Husson V, Stevens, J "Management of Laser Data via the Internet" Proceedings of the Ninth International Workshop on Laser Ranging Instrumentation, Canberra, Australia, Nov 7-11, 1994.

McGarry J, Cheek J, Emenheiser K, Ricklefs R, Seery P "Deploying the new Graphical User Interface Control Software on the NASA SLR Systems" Proceedings of the Ninth International Workshop on Laser Ranging Instrumentation, Canberra, Australia, Nov 7-11, 1994.

McGarry J, Bane B, Conklin B, Dunn P, Eichinger R, Ricklefs R, Seery P "Tracking Satellites with Totally Automated SLR2000 System" Proceedings of the Ninth International Workshop on Laser Ranging Instrumentation, Canberra, Australia, Nov 7-11, 1994.

HP Data System Evolution

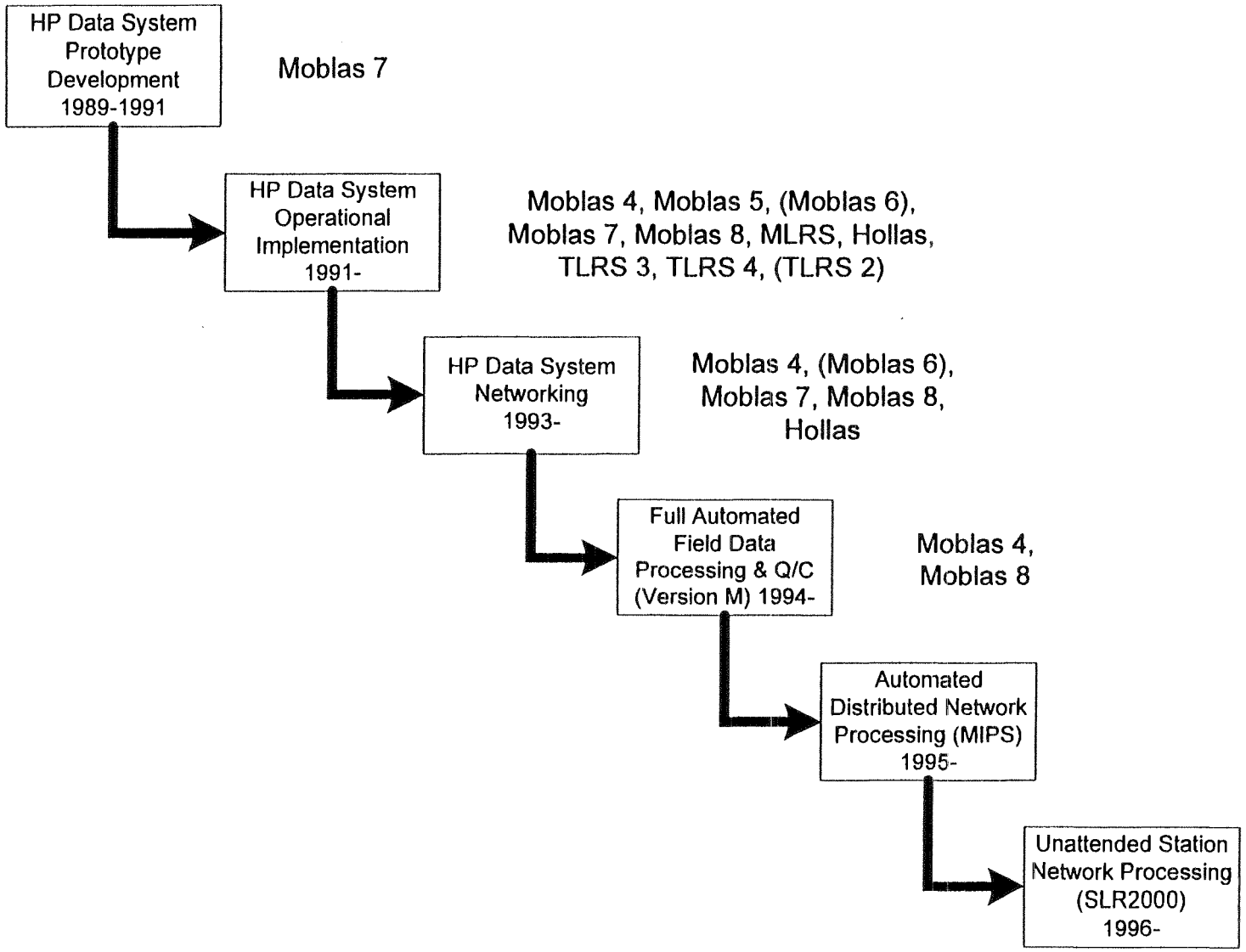

Figure 1

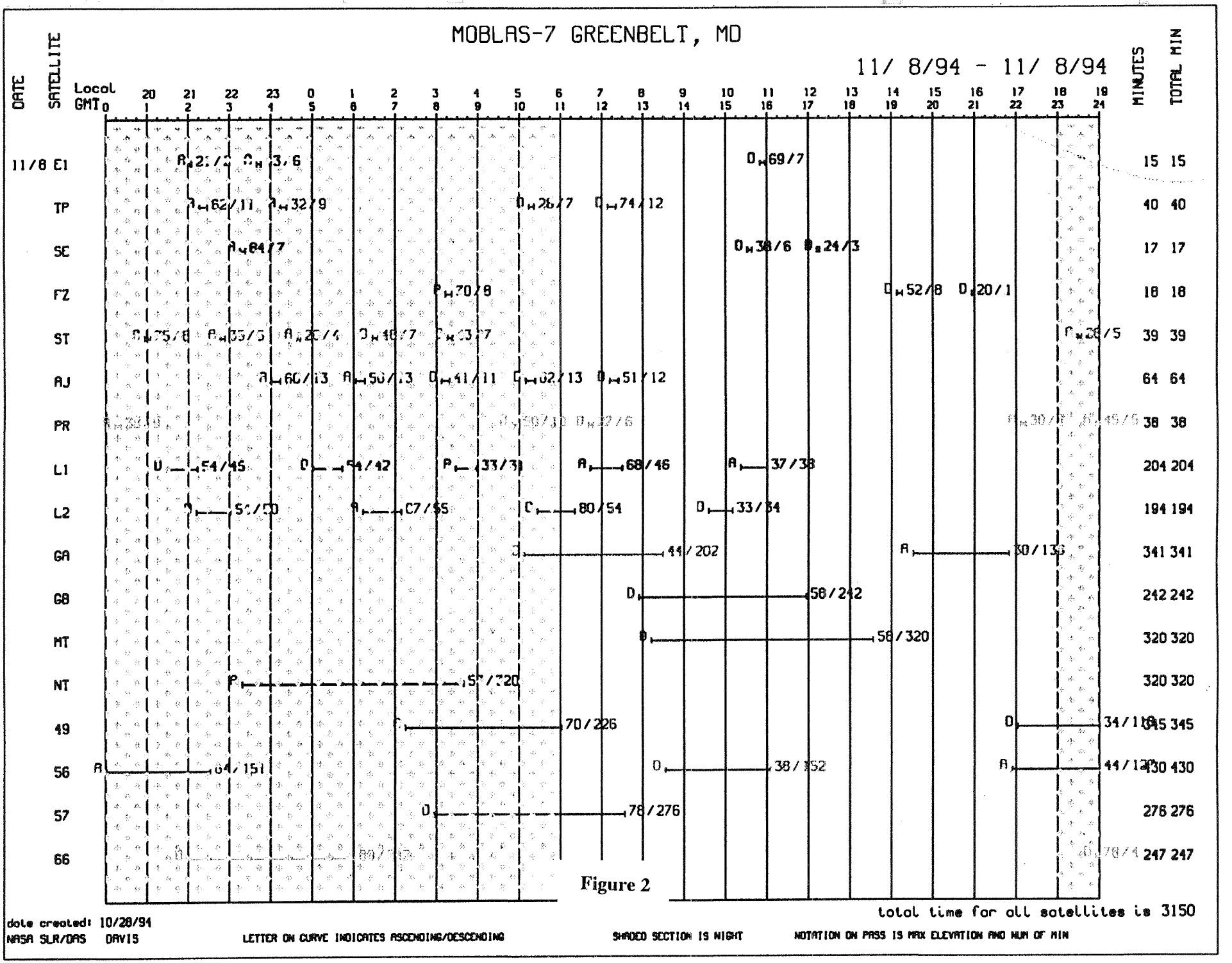
MOBLAS-7 GREENBELT, MD
11/ 8/94 - 11/ 8/94
DATE
SATELLITE
Local GMT
MINUTES
TOTAL MIN
11/8 E1
TP
SC
FZ
ST
AJ
PR
L1
L2
GA
GB
MT
NT
49
56
57
66
total time for all satellites is 3150
date created: 10/20/94
NASA SLR/DAS DAVIS
LETTER ON CURVE INDICATES ASCENDING/DESCENDING
SHADED SECTION IS NIGHT
NOTATION ON PASS IS MAX ELEVATION AND NUM OF MIN

Figure 2

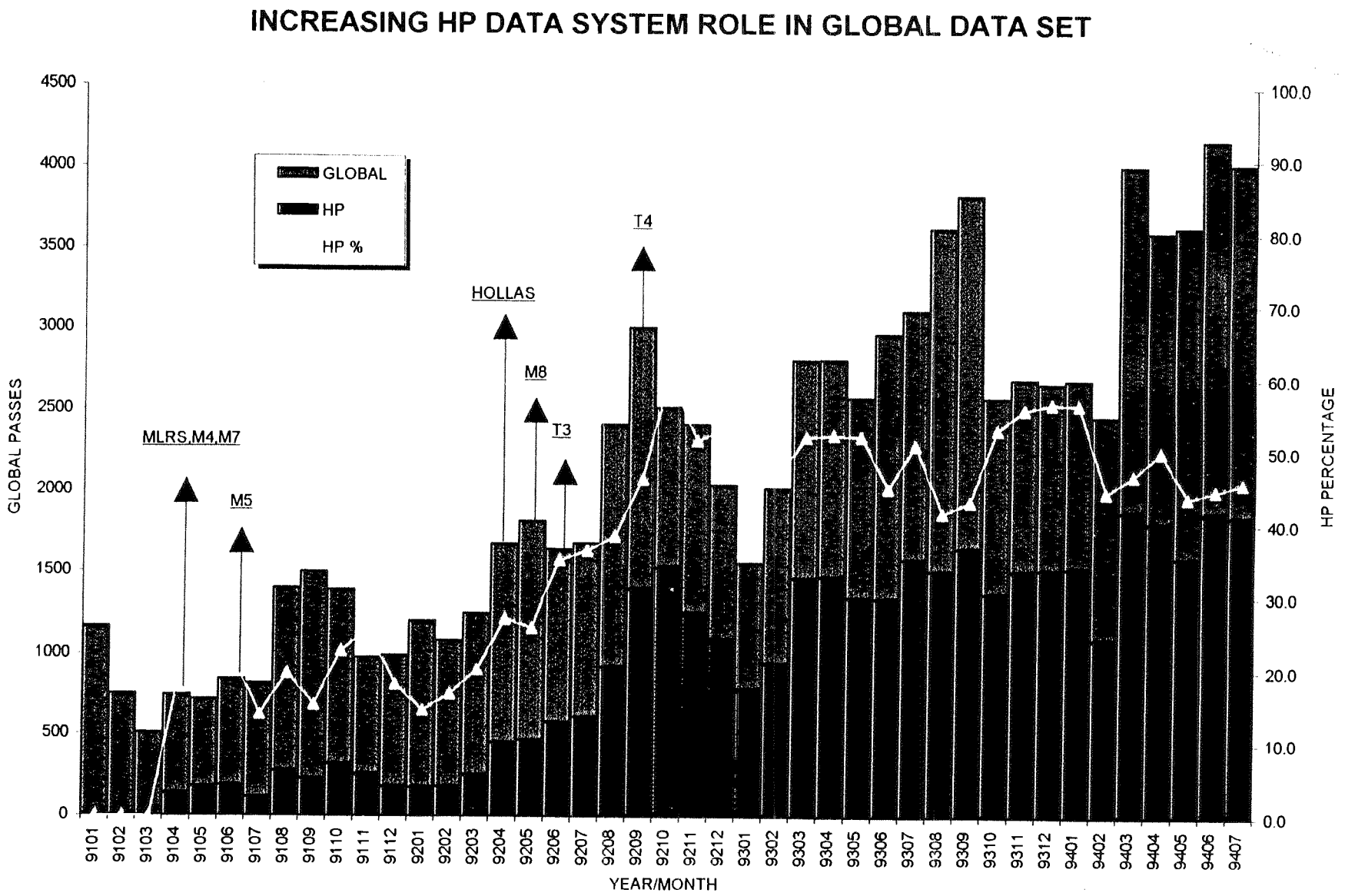
INCREASING HP DATA SYSTEM ROLE IN GLOBAL DATA SET
GLOBAL
HP
HP %
MLRS,M4,M7
M5
HOLLAS
M8
T3
T4
GLOBAL PASSES
HP PERCENTAGE
YEAR/MONTH
4500
4000
3500
3000
2500
2000
1500
1000
500
0
100.0
90.0
80.0
70.0
60.0
50.0
40.0
30.0
20.0
10.0
0.0
9101 9102 9103 9104 9105 9106 9107 9108 9109 9110 9111 9112 9201 9202 9203 9204 9205 9206 9207 9208 9209 9210 9211 9212 9301 9302 9303 9304 9305 9306 9307 9308 9309 9310 9311 9312 9401 9402 9403 9404 9405 9406 9407

Figure 3

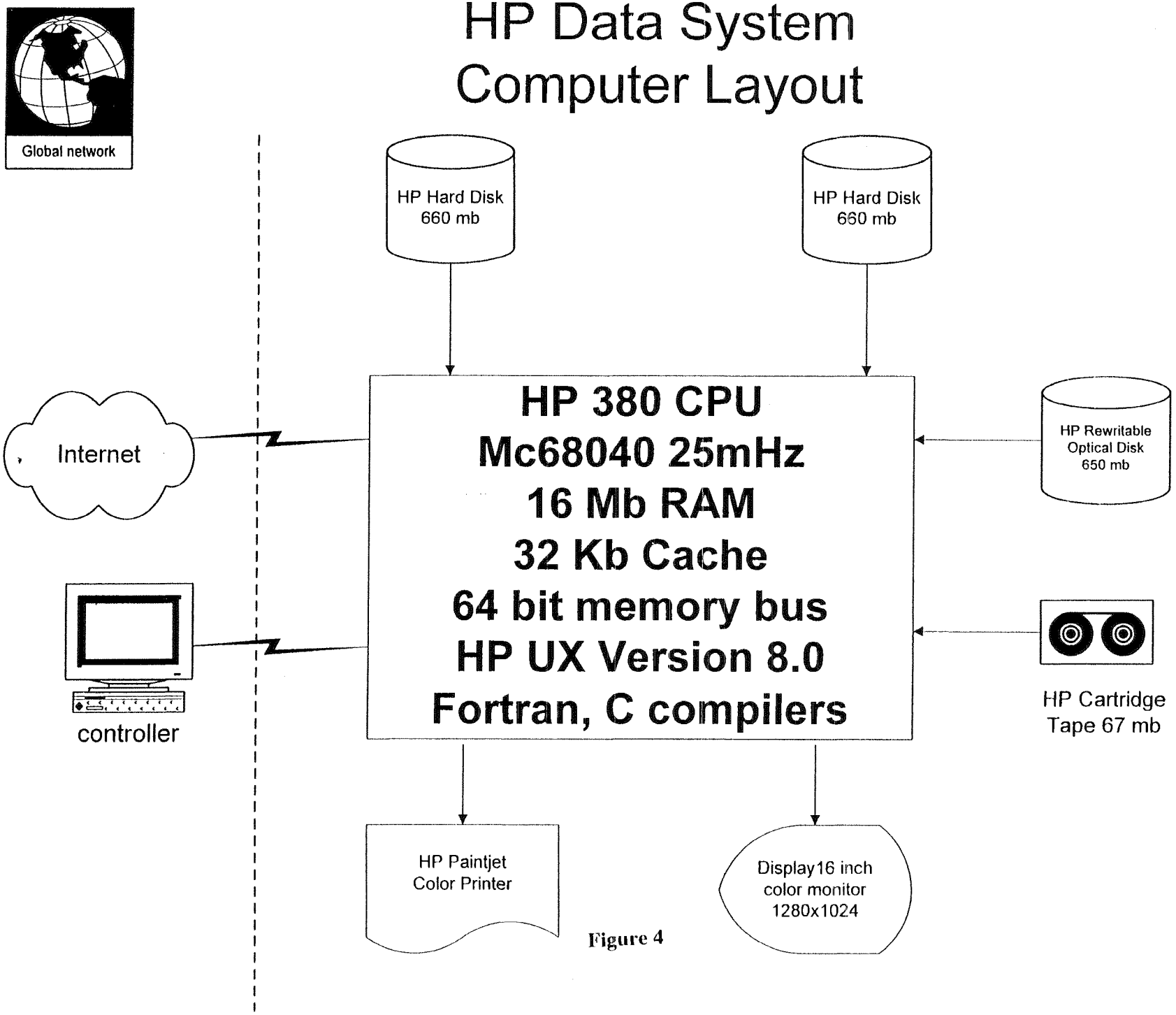
HP Data System
Computer Layout
Global network
HP Hard Disk
660 mb
HP Hard Disk
660 mb
Internet
HP 380 CPU
Mc68040 25mHz
16 Mb RAM
32 Kb Cache
64 bit memory bus
HP UX Version 8.0
Fortran, C compilers
HP Rewritable
Optical Disk
650 mb
controller
HP Cartridge
Tape 67 mb
HP Paintjet
Color Printer
Display16 inch
color monitor
1280x1024

Figure 4

HP Data Systems Communications

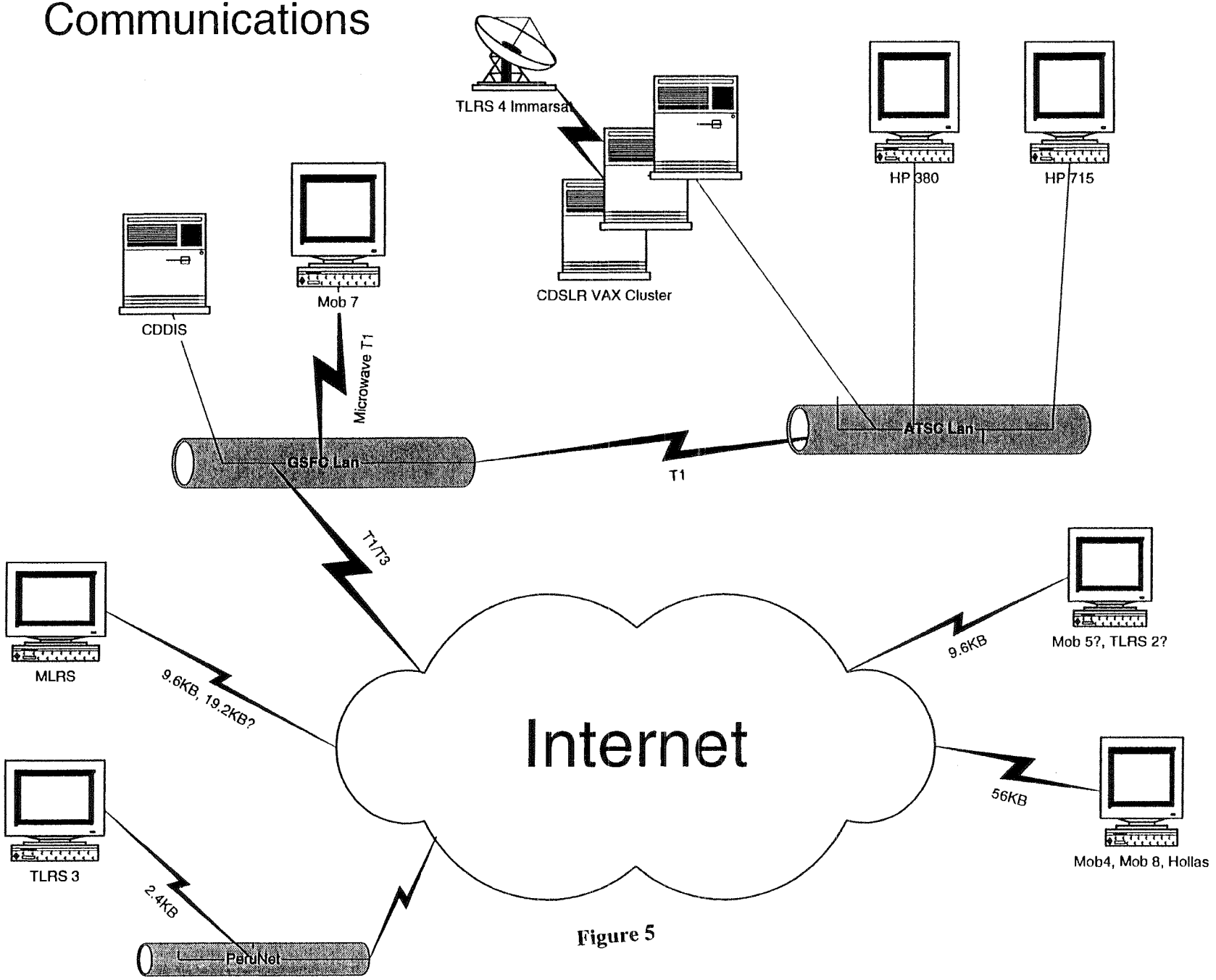

Figure 5

HP Data System Product Cycle

Pre-Pass Operations

Software Configuration Management

System Backups

Data Processing Specifications

Supporting Information Management

Schedule/Acquisiiton Message Communications

Real Time Operations

Real Time Data Communications (Controller)

Data Verification

Data Reformatting

Multi-pass/Calibration Data Staging

Operational Data Products are produced in 5 to 10 minutes after completion of data set

Operational Data Products are automatically transmitted to headquarters hourly

Post Pass Operations

Operator Control/Release

Data Processing/Normal point Computations/Quality Control (1-5 min)

Hourly Automated Network Communications (1-2 min with 56KB Internet))

Automated On-Site Data Archiving (3-5 days)

Data Review (as required)

Figure 6

MIPS General Layout

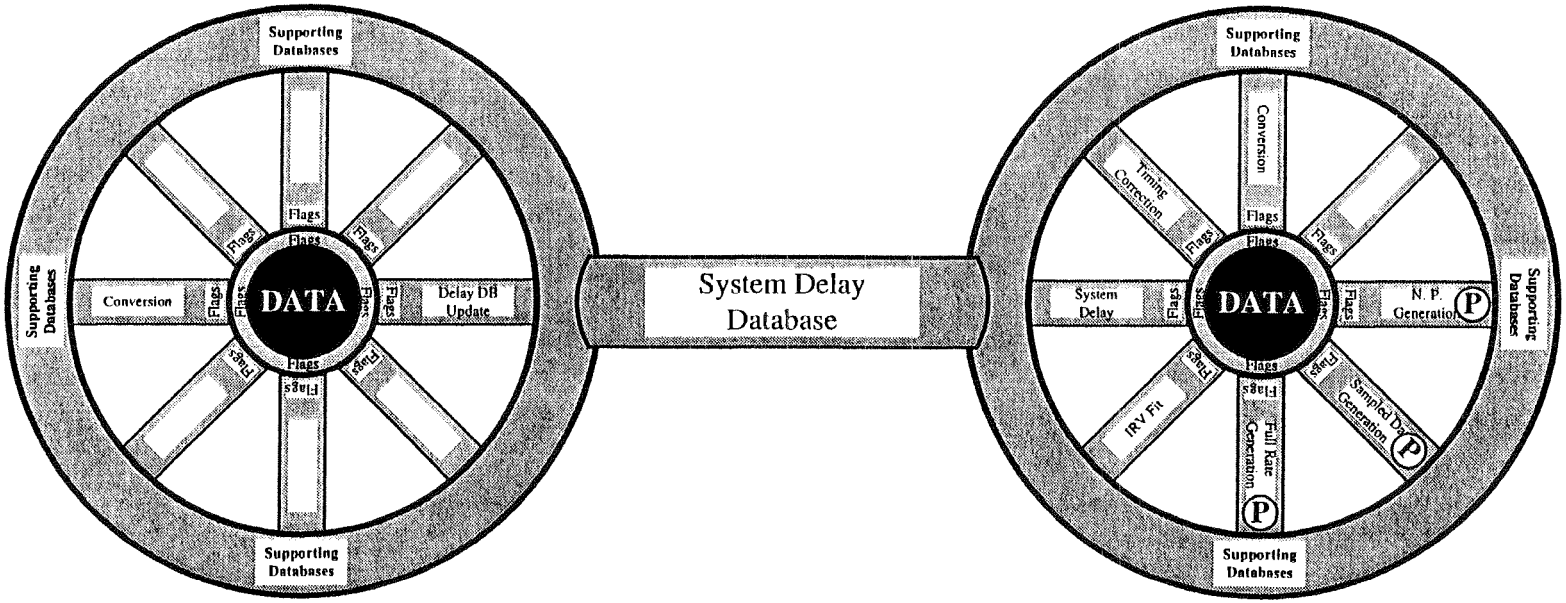

Calibration Data Processor

Satellite Data Processor

Figure 7

(P) = Data Product

MIPS Satellite Modules

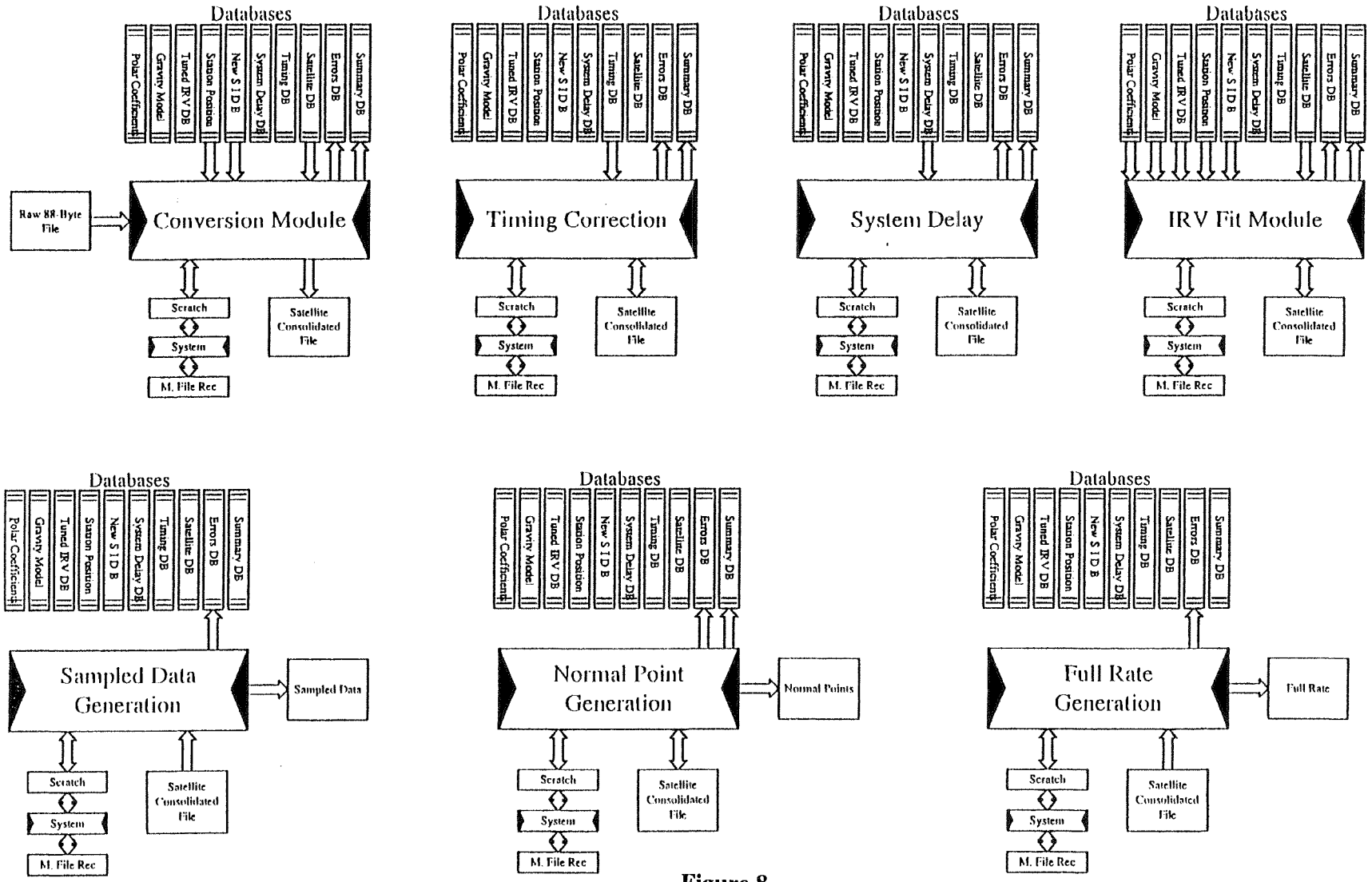

Figure 8

Management of Laser Data via the Internet

Carey E. Noll†
David R. Edge, Van S. Husson, Paul Stevens*

NASA is planning ambitious improvements in the global management and distribution of laser data products using Internet and other global computer network resources. The challenge is to manage normal point data and up to six months of full-rate laser data in on-line data files that can be directly updated by data producers and directly accessed by data users as soon as the data is available. The strategy also includes the use of Gopher and World Wide Web Internet capabilities to capture and maintain all critical supporting information, including station engineering characteristics, required to understand and use laser data products.

INTRODUCTION

The Crustal Dynamics Data Information System[1] (CDDIS) contains a rich historical archive of SLR data, from over 100 sites (over 140 distinct monuments) in over 35 countries and dating back to 1975; the map in Figure 1 illustrates the global coverage of SLR tracking. NASA plans to continue to add to this archive and to make both full-rate and quick-look data available to the global user community as has been the request, while decreasing the cost associated with handling these data. To this end, NASA is striving to streamline the processing of these valuable data sets. With a redesign of the data flow, NASA hopes to simplify and automate data processing and at the same time provide more rapidly-available products to the user community. This paper addresses the current and future accessibility of the SLR full-rate data product as well as the on-site data products (both normal points and engineering quick-look data).

CURRENT SLR DATA PRODUCTS

The global network currently tracks thirteen or more satellites on a routine basis and provides quick-look and full-rate data directly to NASA's SLR contractor, AlliedSignal Technical Services Corporation (ATSC), or to the CDDIS, through the EuroLAS Data Center (EDC) located at the Deutsches Geodätisches Forschungsinstitut (DGFI) in Munich Germany or from SLR operating organizations in China and Japan.

For full-rate data, the entire global data set is merged into monthly increments by satellite; data are interleaved by time and provided in MERIT-II (Monitoring of Earth Rotation and Intercomparison of Techniques) format. The CDDIS then distributes these data sets to users via 9-track tape, 4 mm tape, or electronically. The CDDIS distributes the A (or initial) release of the full-rate data sixty days after the end of the observation month. The B (or second) release, containing additional or updated passes, is typically available six months after the end of the observation month. Subsequent releases, containing any outstanding passes, are

† Computing Systems Office, NASA/Goddard Space Flight Center, Code 920.2, Greenbelt, MD 20771.
* AlliedSignal Technical Services Corporation, Goddard Corporate Park, 7515 Mission Drive, Lanham, MD 20706.

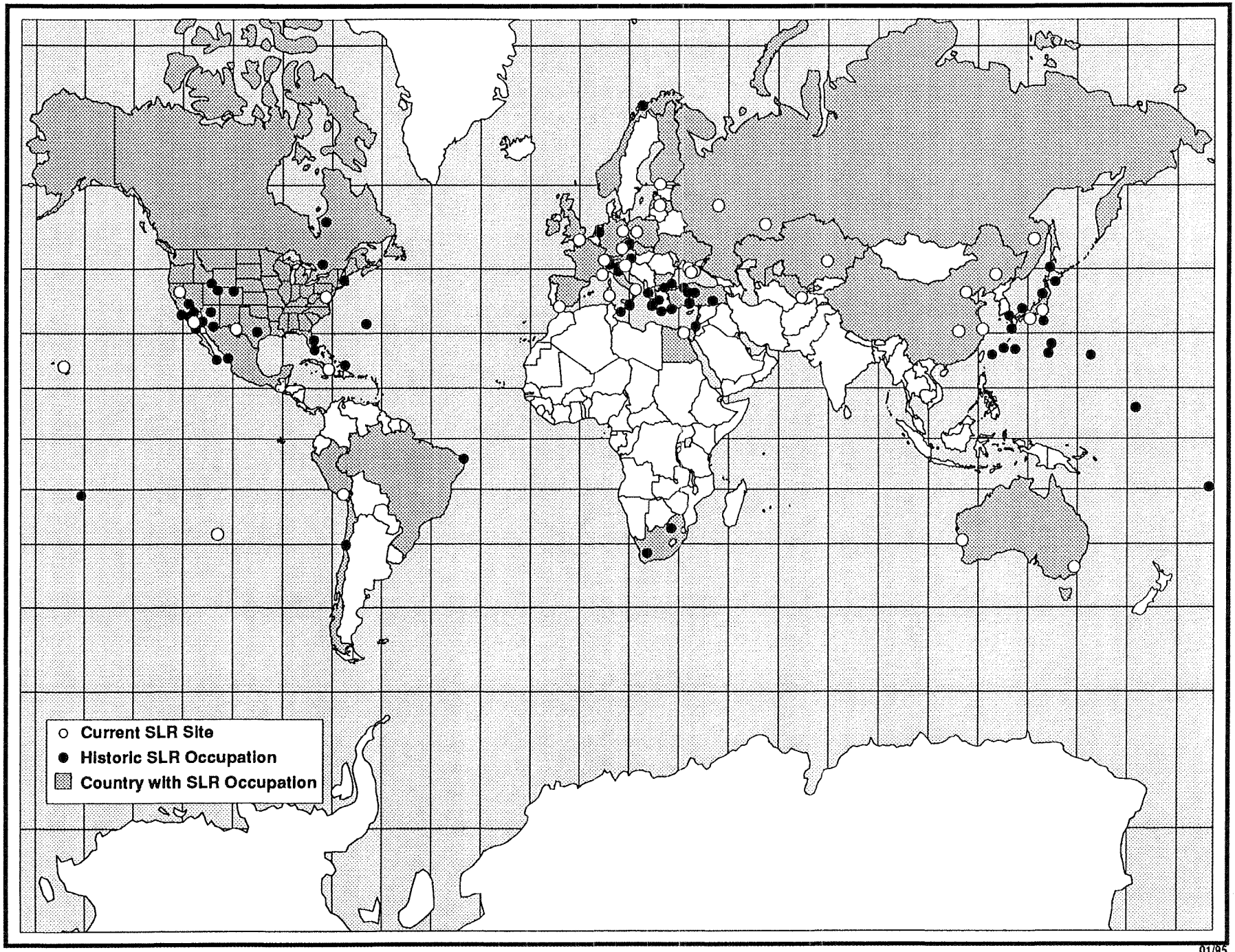

Figure 1. Current and Historic SLR Occupations

generated on an as-needed basis. Typically, the size of the merged, time-sorted, monthly full-rate SLR releases are 400 to 500 Mbytes, the equivalent of four to five 9-track tapes (6250 bpi).

At this time, normal points are generated from full-rate data; these data are available from the CDDIS electronically or via tape, also in monthly increments and in MERIT II format.

SLR data generated on-site has been available on-line from the CDDIS since late 1991. Currently, the CDDIS supplies these data to users electronically, in daily files, each file containing all data received during the last 24 hours. Therefore, the file may contain data from several days. Sometime after the end of the month, the CDDIS creates a monthly, time-sorted file from these individual daily files. A typical day's worth of on-site SLR data is approximately 25 Kbytes. The format of the data is CSTG (International Coordination of Space Techniques for Geodesy and Geodynamics) normal point format. The CSTG format is designed to accommodate both normal points and sampled data points for engineering purposes. Currently, SLR systems which do not at this time produce normal points are converted to CSTG format; the normal point indicator is set to 0 for all data converted from other formats (e.g., CSTG sampled, STDN, or SAO formats). As of late 1994, any sampled (engineering) data forwarded by the global SLR network is also available from the CDDIS.

RATIONALE FOR CHANGE

Over the past twenty years, the volume of SLR full-rate data has increased exponentially, as illustrated in Figures 2, 3, and 4. Thus, the monthly merging, sorting, and compilation required for these data sets has become increasingly expensive and time consuming. These costs increase further when issuing updates to previously released data to include late-arriving or modified data. Full-rate data are a valuable resource for engineers and data producers for diagnosing system problems. Furthermore, full-rate data would be required if normal point algorithms are updated or modified; historic normal points would thus need to be recomputed. NASA realizes the importance of the full-rate data set and has initiated changes in the data handling to ensure the continued availability of the data. The electronic connectivity of the global user community is now available, making on-line posting of SLR data, both on-site and full-rate, a viable solution to the expensive, monthly data processing scenario now employed.

PROPOSED SLR DATA PRODUCTS

Table 1 below shows the current and planned directory structure for the quick-look, full-rate, and full-rate normal point data sets available on-line via the CDDIS.

Table 1.
Current and Planned Disk and Directory Locations for On-Line SLR Data

Type of SLR Data	Former Disk Location and Root Directory	New Disk Location and Root Directory
Full-rate data (monthly merged)	DIS_DATA:[SLRDATA.FR]	SLR_DATA:[SLRFR.MONTHLY]
Full-rate data (daily passes)	SLR_DATA:[SLRFR.satname]	No change
Normal points from full-rate data	DIS_DATA:[SLRDATA]	SLR_DATA:[SLRNPT.satname]
Quick-look data	DIS_DATA:[satnameDATA]	SLR_DATA:[SLRQL.satname]

Notes: *satname* is AJISAI, ERS1, ETALON1, ETALON2, FIZEAU, GLONASS##, GPS35, GPS36, LAGEOS1, LAGEOS2, METEOR3, MSTI2, STARLETTE, STELLA, or TOPEX.

Full-Rate Data

The diagram shown in Figure 5 illustrates the proposed flow of SLR full-rate data. Where possible, full-rate data will be sent electronically from the site, nominally on a daily basis, to be processed by ATSC (and, perhaps, by EDC). These data will be stored in compressed files on

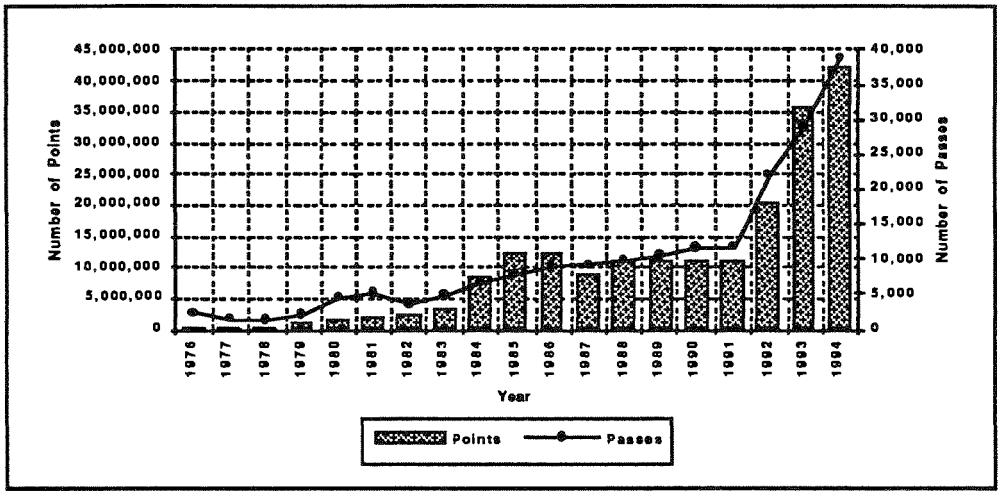

Figure 2. Yearly SLR Full-Rate Pass and Point Totals

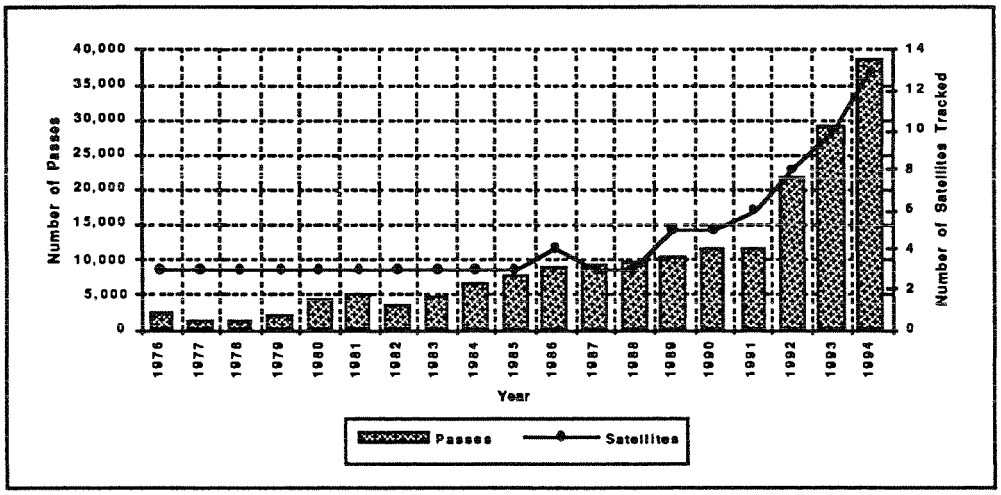

Figure 3. Yearly SLR Full-Rate Pass Totals vs. Number of Satellites Tracked

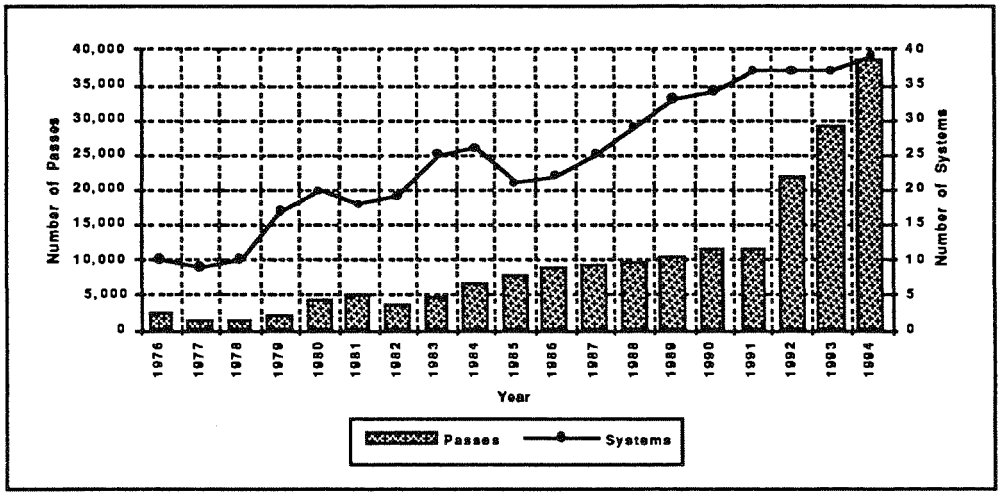

Figure 4. Yearly SLR Full-Rate Pass Totals vs. Number of Operational Systems

the CDDIS by satellite, by station, and by day. Figure 6 shows the proposed top level directory structure for all SLR data on the CDDIS; Figure 7 shows the proposed directory structure for the on-line SLR full-rate data files. Filenames will have the form: *stat_yymmdd_v.satname_Z* where *stat* is the four-digit station number, *yy* is the two-digit year, *mm* is the two-digit month, *dd* is the two-digit day of the first observation of the pass, *v* is the one-character version of the data, *satname* is the satellite name, and *_Z* indicates a compressed file. As an example:

7105_950101_A.LAGEOS1_Z contains LAGEOS-I data from MOBLAS-7 at station 7105 where the first observation of all passes were taken on January 01, 1995 (compressed format)

7105_950101_B.LAGEOS1_Z contains any late arriving or updated LAGEOS-I data from MOBLAS-7 at station 7105 where the first observation of all passes were taken on January 01, 1995 (compressed format)

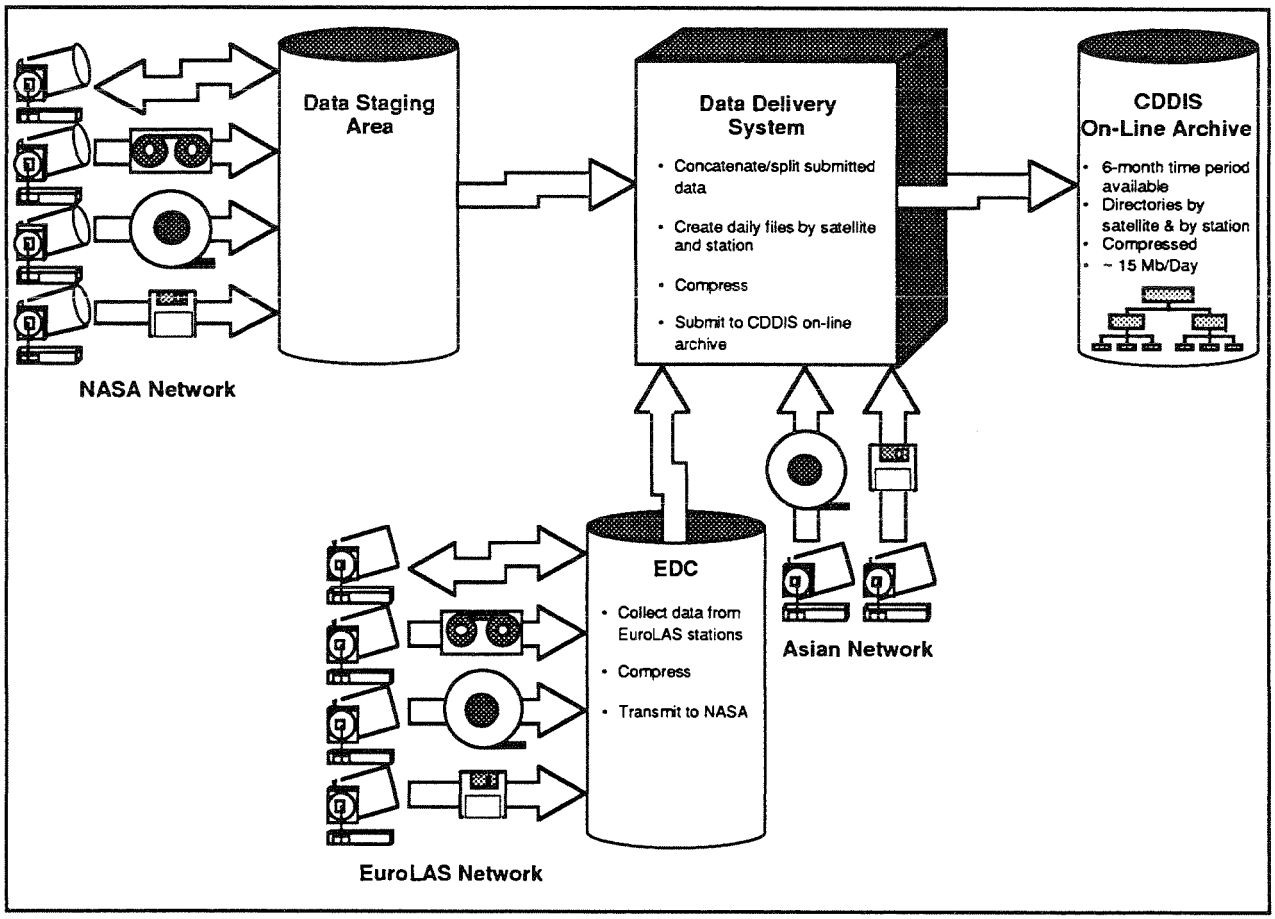

Figure 5. Proposed SLR Full-Rate Data Flow

Automated procedures will ship these full-rate files to the CDDIS with a three day delay. For any data still delivered via magnetic tape, procedures will be executed on the data sets to create these daily satellite/station files in the appropriate formats. Data will be retained on-line on the CDDIS for at least six months. Data more than six months old will be made available to users from the CDDIS via special request. Data arriving at the CDDIS later than six months after the observation day will be retained on-line for a sufficient period of time to allow user access. Notices will appear in an on-line information file to alert the user community of late arriving data, problem data, and other special information.

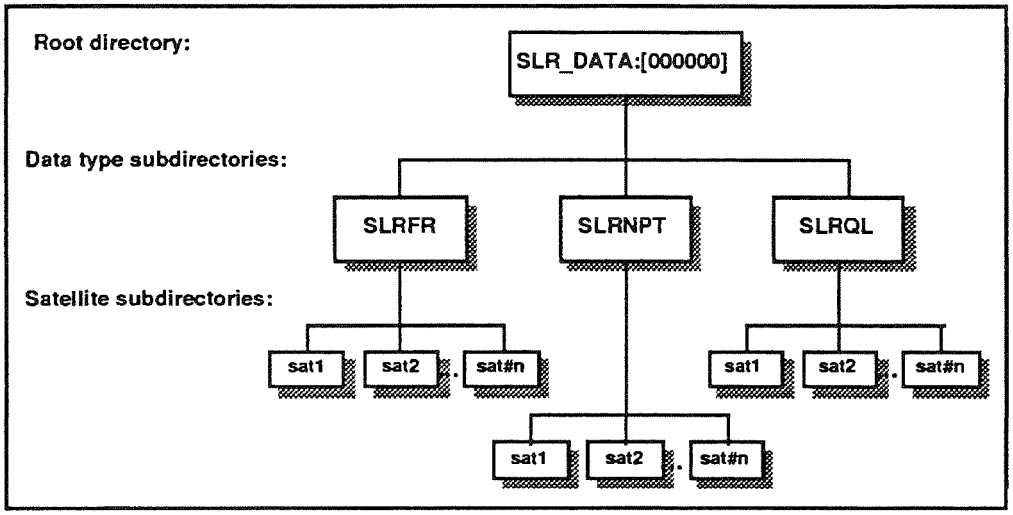

Figure 6. Main Directory Structure for On-Line SLR Data

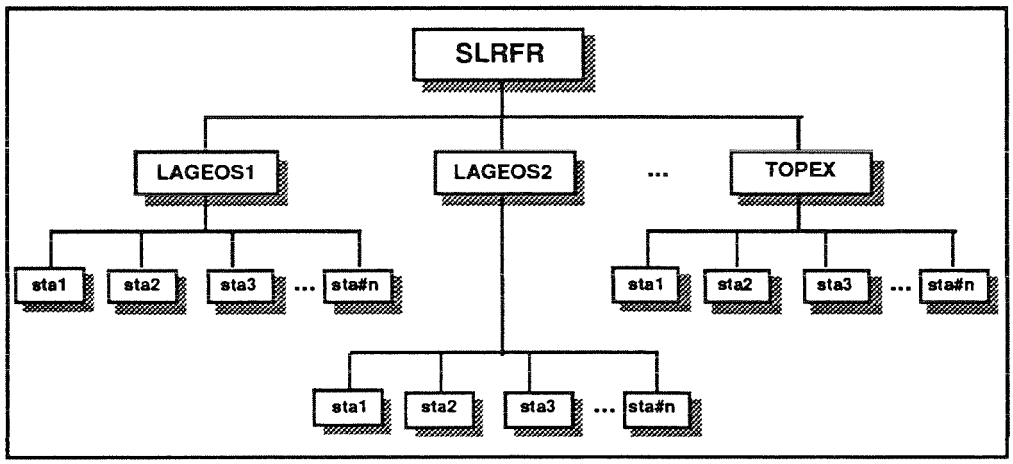

Figure 7. Proposed Directory Structure for On-Line SLR Full-Rate Data

Replacement of full-rate SLR data will be kept at a minimum. However, late-arriving or seriously flawed data will be made available in the day/station/satellite file format and noted by an increment in the version label in the filename. Thus, users of a particular day's worth of data for a station must apply any files labeled with version B or higher to the original A version of the file. Version A of files will not be modified; any additional or replacement data will be placed in a new file with an incremented version code (e.g., B, C, etc.).

The data will be stored in compressed form using the UNIX compression algorithms; software for IBM PC and VAX systems to decompress the files. are available on the CDDIS via anonymous ftp Studies have shown that this method of compression reduces the size of the files by a factor of five. Table 2 shows statistics for an example set of full-rate data implemented on the CDDIS for testing purposes in 1994.

Figure 8 illustrates an ftp session for listing and downloading an SLR full-rate data file in the proposed format. Users should note that since these files are in compressed form, they must be downloaded in binary or image mode via ftp.

```
Note:   User entries shown in bold; descriptive text shown in bold italics

$ ftp cddis.gsfc.nasa.gov                                   FTP to CDDIS computer
CDDIS.GSFC.NASA.GOV MultiNet FTP user process 3.2(106)
Connection opened (Assuming 8-bit connections)
<CDDIS.GSFC.NASA.GOV MultiNet FTP Server Process 3.2(14) at Fri 28-Oct-94 11:03AM-EDT
CDDIS.GSFC.NASA.GOV>user dis                                Login as CDDIS user DIS
<User name (dis) ok. Password, please.
Password: ***                                               Enter password (not echoed)
< ********************************************************************************
<     Welcome to the Crustal Dynamics Data Information System
<                              C D D I S
<                  A data center for the space geodesy data
< The following files are available to help in accessing on-line data:
<   README.* -- General info about the CDDIS and available data
<   TREE.*   -- Directory tree structure for the available data
< Contact noll@cddis.gsfc.nasa.gov for additional access information.
< ********************************************************************************
<User DIS logged into MANAGE:[DIS] at Fri 28-Oct-94 11:03, job a987.
CDDIS.GSFC.NASA.GOV>cd sir_data:[sirfr]     Change directory to SLR full-rate root directory
<Connected to SLR_DATA:[SLRFR].
CDDIS.GSFC.NASA.GOV>ls                                      List contents (satellite directories)
<List started.
ajisai.dir
ers1.dir
etalon1.dir
.
.
topex.dir
<Transfer completed.
CDDIS.GSFC.NASA.GOV>cd [.lageos1]           Change directory to LAGEOS1 full-rate directory
<Connected to SLR_DATA:[SLRFR.LAGEOS1].
CDDIS.GSFC.NASA.GOV>ls                                      List contents (station directories)
<List started.
1181.dir
1863.dir
.
.
8834.dir
<Transfer completed.
CDDIS.GSFC.NASA.GOV>cd [.7105]              Change directory to MOBLAS-7 station directory
<Connected to SLR_DATA:[SLRFR.LAGEOS1.7105].
CDDIS.GSFC.NASA.GOV>ls                                      List contents (daily files)
<List started.
7105_930801_a.lageos1_z
7105_930810_a.lageos1_z
.
.
7105_930831_a.lageos1_z
<Transfer completed.
CDDIS.GSFC.NASA.GOV>bin                                     Change to binary mode
Type: Image, Structure: VMS, Mode: Stream
CDDIS.GSFC.NASA.GOV>get 7105_930831_a.lageos1_z     Get data file for August 31, 1993
 To local file: 7105_930831_a.lageos1_z                     Specify local file
<VMS retrieve of SLR_DATA:[SLRFR.LAGEOS1.7105]7105_930831_A.LAGEOS1_Z;1 started.
<Transfer completed.  240927 (8) bytes transferred.
CDDIS.GSFC.NASA.GOV>quit                                    End FTP session
<QUIT command received. Goodbye.
```

Figure 8. Sample Script Listing and Retrieving SLR Full-Rate Data on the CDDIS

Table 2.
Sample Full-Rate Data Set (August 1993, Release B)

August 1993 Version B data set consists of:		
Number of satellites		8
Number of stations		33
Number of passes		3,362
Number of observations		4,461,273
On-line version of the data (in daily files) consists of:		
Number of files	2,389	
Total size* of all files (Mbytes)	225.0	(1,125)
Average file size* (Mbytes)	0.1	(0.5)
Merged, time sorted version (in monthly files) consists of:		
Number of files	8	
Total size* of all files (Mbytes)	550.0	(100.0)
Average file size (Mbytes)	68.5	(12.5)

* represents compressed size; non-compresses size shown in ()

Studies by ATSC have shown that the quality of normal points generated on-site are equal to that of the normal points derived from full-rate data. Therefore, NASA has decided to discontinue generating normal points from full-rate data for any data acquired after January 1, 1995.

Quick-Look Data

As stated above, for several months, the CDDIS has provided access to both normal points and sampled engineering data produced on-site at the SLR station. These data have been stored in separate files by data type. Thus far, data has been converted into normal points for those SLR stations only capable of producing SAO, STDN, or CSTG sampled data. However, as of February 1, 1995, these conversions will no longer be performed. All SLR quick-look data will thus be provided to the users in their original formats. Figure 9 shows the directory structure for the on-line SLR quick-look data files. Figure 10 illustrates an ftp session for listing and downloading an SLR quick-look data file in the proposed format. The quick-look files are stored uncompressed; therefore, retrieval of files in ASCII or text mode is appropriate.

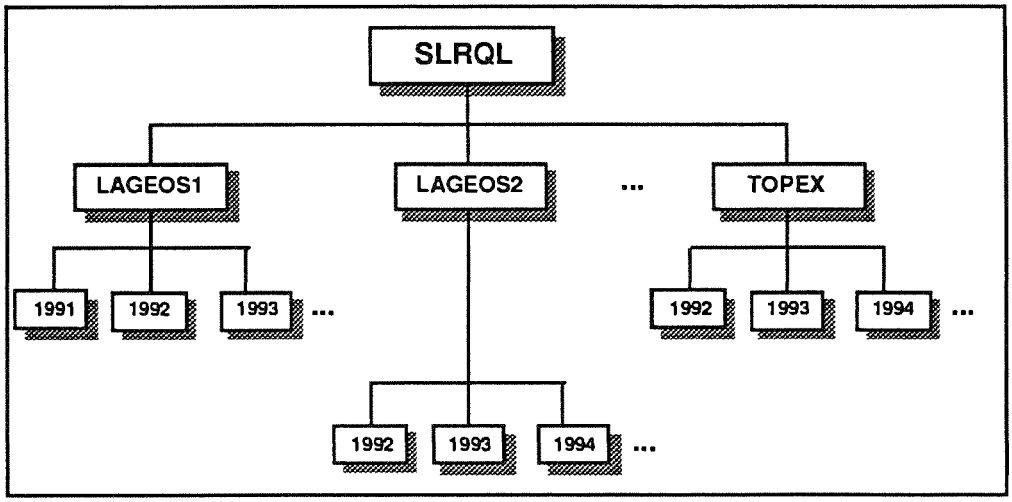

Figure 9. Proposed Directory Structure for On-Line SLR Quick-Look Data

```
Note:   User entries shown in bold; descriptive text shown in bold italics

$ ftp cddis.gsfc.nasa.gov                                   FTP to CDDIS computer
CDDIS.GSFC.NASA.GOV MultiNet FTP user process 3.2(106)
Connection opened (Assuming 8-bit connections)
<CDDIS.GSFC.NASA.GOV MultiNet FTP Server Process 3.2(14) at Fri 28-Oct-94 11:09AM-EDT
CDDIS.GSFC.NASA.GOV>user dis                                Login as CDDIS user DIS
<User name (dis) ok. Password, please.
Password: ***                                               Enter password (not echoed)
< ********************************************************************************
<     Welcome to the Crustal Dynamics Data Information System
<                              C D D I S
<                  A data center for the space geodesy data
< The following files are available to help in accessing on-line data:
<   README.* -- General info about the CDDIS and available data
<   TREE.*   -- Directory tree structure for the available data
< Contact noll@cddis.gsfc.nasa.gov for additional access information.
< ********************************************************************************
<User DIS logged into MANAGE:[DIS] at Fri 28-Oct-94 11:09, job a987.
CDDIS.GSFC.NASA.GOV>cd slr_data:[slrql]          Change directory to SLR QL root directory
<Connected to SLR_DATA:[SLRQL].
CDDIS.GSFC.NASA.GOV>ls                                      List contents (satellite directories)
<List started.
ajisai.dir
ers1.dir
etalon.dir
.
.
.
topex.dir
<Transfer completed.
CDDIS.GSFC.NASA.GOV>cd [.lageos1]      Change directory to LAGEOS1 quick-look directory
<Connected to SLR_DATA:[SLRQL.LAGEOS1].
CDDIS.GSFC.NASA.GOV>ls                                      List contents (yearly directories)
<List started.
1992.dir
1993.dir
1994.dir
<Transfer completed.
CDDIS.GSFC.NASA.GOV>cd [.1994]                   Change directory to 1994 yearly directory
<Connected to SLR_DATA:[SLRQL.LAGEOS1.1994].
CDDIS.GSFC.NASA.GOV>ls                          List (monthly and daily sampled and npt files)
<List started.
new_en9409.lag
new_en940919.lag
.
.
.
new_ql9409.lag
new_ql940901.lag
.
.
.
new_ql941028.lag
<Transfer completed.
CDDIS.GSFC.NASA.GOV>get new_ql941028.lag  Get normal point data file for October 28, 1994
  To local file: new_ql941028.lag                           Specify local file
<VMS retrieve of SLR_DATA:[SLRQL.LAGEOS1.1994]NEW_QL941028.LAG;1 started.
<Transfer completed.  25036 (8) bytes transferred.
CDDIS.GSFC.NASA.GOV>quit                                    End FTP session
<QUIT command received. Goodbye.
```

Figure 10. Sample Script Listing and Retrieving SLR Quick-Look Data on the CDDIS

TIMELINE FOR IMPLEMENTATION OF CHANGES

The posting of SLR full-rate data using this new, on-line procedure will begin with data observed after January 1, 1995 (inclusive). Data observed prior to this date, however, will continue to be released in monthly increments (versions A, B, etc.). Normal points generated from full-rate data will be discontinued with data observed after January 1, 1995. Monthly distribution of SLR data via magnetic tapes will be phased out during 1995, as users become familiar with the on-line distribution service. However, special arrangements can be made for those users requiring full-rate data but not having reliable, adequate access to electronic networks.

FUTURE PLANS

Quick-Look Data Products

During 1995, NASA and ATSC plan to study the SLR quick-look data product. We hope to apply lessons learned in the full-rate data posting effort to the flow and organization of SLR quick-look data.

World Wide Web (WWW)

A recent development gaining popularity in the scientific community is electronic data publishing via the World Wide Web (WWW). The WWW[2] is a method for exploring resources available over the INTERnet. The WWW is a distributed, hypertext-based information system and publishing tool developed at the Center for European Laboratory for Particle Physics, CERN, in Geneva Switzerland. The WWW allows users to navigate through hypertext links to obtain information. Users specify a link to be followed and a new data object is retrieved and presented to the user through client software running on their local computer (e.g., personal computer, workstation, etc.). This link can be as simple as clicking highlighted text or can be specified by entering a Uniform Resource Locator (URL). Text, graphics, images, and sound can be displayed (and heard) through the WWW, providing the user's client software supports these.

A CDDIS home page on the WWW has recently been implemented and is shown in Figure 11; the URL to view this page is: *http://cddis.gsfc.nasa.gov/cddis.html.* This page provides information about the CDDIS and its data holdings, the Space Geodesy Program (SGP), the Dynamics of the Solid Earth (DOSE) investigation, and current space geodesy techniques (SLR, GPS, and VLBI). Furthermore, the CDDIS home page provides links to other areas of interest at NASA and internationally. Various documents sponsored by the SGP can also be browsed through the WWW.

During 1995, the CDDIS plans to provide access, through the WWW, to SLR ancillary information, such as data holding summaries, system occupation histories, monument coordinate and eccentricity data, and system configuration data. It is hoped to further enhance this information with pictures and/or diagrams of SLR systems and sites.

CONCLUDING REMARKS

Only full-rate SLR data (MERIT-II format) and on-site normal point and sampled engineering data (CSTG format) will be available as data products to the user community. The CDDIS will study the need to create monthly merged full-rate data sets, allowing for a sufficient time delay to capture as much late-arriving data as possible. Therefore, users should be aware that the monthly full-rate data tapes will no longer be available from the CDDIS under the current two-month (A release) and six-month (B release) delay schedule.

CDDIS

CRUSTAL DYNAMICS DATA INFORMATION SYSTEM

Crustal Dynamics Data Information System, NASA/GSFC, Greenbelt, MD 20771

The Crustal Dynamics Data Information System (CDDIS) supports data archiving and distribution activities for the space geodesy and geodynamics community. The main objectives of the system are to store space geodesy and geodynamics related data products in a central data bank, to maintain information about the archival of these data, and to disseminate these data and information in a timely manner to NASA investigators and cooperating institutions. The CDDIS is operational on a dedicated Digital Equipment Corporation (DEC) VAX 4000 Model 200 located at NASA's Goddard Space Flight Center in Greenbelt, MD.

Current Programs and Activities:

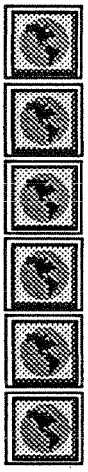

NASA's Space Geodesy Program (SGP)

NASA's Dynamics of the Solid Earth (DOSE) Investigation

SGP Catalogue of Site Information

CDDIS Bulletin (past issues available)

SGP Personnel and Networking Directory

CDDIS Anonymous FTP

Related NASA Resources and Programs:

NASA Home Page

Goddard Space Flight Center (GSFC)

Laboratory for Terrestrial Physics (LTP)

Related International Resources and Programs:

International GPS Service for Geodynamics (IGS)

Scripps Orbit and Permanent Array Center (SOPAC)

University NAVSTAR Consortium (UNAVCO)

Southern California Integrated GPS Network (SCIGN)

DGFI's Geodetic Information System (GeodIS)

For further information contact Carey Noll, noll@cddis.gsfc.nasa.gov
Code 920.1, NASA Goddard Space Flight Center
Greenbelt, MD 20771, USA
(301) 286-9283

Figure 11. CDDIS Home Page on the WWW (as of January 1995)

This new data flow has been implemented on the CDDIS with all full-rate data received since January 1, 1995. The NASA SLR management believes that this new system will meet the requirements of the global SLR community. Users requiring further information about the proposals in this paper should contact the CDDIS staff.

REFERENCES

[1] Noll, C. E., "Data Archiving and Distribution for the Crustal Dynamics Project: The CDDIS", Contributions of Space Geodesy to Geodynamics: Technology. AGU Geodynamics Series, Vol. 25. 1993.

[2] Berners-Lee, T.J., and R. Cailliau. 1990. World Wide Web: Proposal for a Hypertext Project. Available as: http://info.cern.ch/hypertext/WWW/Proposal.html.

Internet Facilities and SLR Sites[1]

A. Novotný
Faculty of Nuclear Sciences and Physical Engineering
Czech Technical University, Prague
The Czech Republic
E-MAIL: NOVOTNY@TROJA.FJFI.CVUT.CZ

Abstract

The situation in worldwide networking has completely changed since the last workshop. The SLR community does not seem to notice the fact, though. The data centers do provide the stations with an incomplete information database (or no database at all), some stations do not communicate with the center via E-mail, the stations do not communicate among themselves. The state of the communication froze at the level of E-mail and file transfer; no HTML or gopher services are available.

The author makes some suggestions on connecting all the stations to Internet, on building a spare connection channel and on new possible Internet services.

Preface

Only two years passed since the last IWLRI in Annapolis, MD, but the situation of worldwide networks has completely changed. E-mail became excessively used; it's only a fragment of networks' potential though. Webs of Internet are spread to the most countries. Internet protocol reached all of the commercial networks so important. I think the time has come for all the SLR sites to be connected to Internet and to start using its capabilities and resources. Any SLR site may have Internet connection, assuming that every SLR site has got a telephone access. To fulfill all the demands of present and future scientific projects concerning data availability and immediate data delivery, the SLR site of the near future has to have a worldwide network access anyway, and Internet is perhaps the best option.

---

[1]Presented at the 9th International Workshop on Laser Ranging Instrumentation, Canberra, Australia, November 1994

Internet Connectivity

Connecting to a computer network, there are two important factors determining completely the availability and usefulness of the connection: data line (modem) speed and price (charges, hardware, software). Today we may - unfortunately - see a paradox: more developed (in the sense of telecommunications) countries enable free Internet access to all academical sites with E-mail as well as HTTP, WAIS, gopher, remote login, file transfer etc. capabilities; on the other hand, fewer developed countries do have only Internet on commercial basis, i.e., expensive and not so fast, or no Internet nodes at all. (But it does not mean that user cannot create the first Internet node there.)

There are two possible types of connection between a computer and Internet:

1. The computer is an Internet node, i.e., it is a part of a network with unique Internet identification. All Internet resources are available to the user, if software is present.
2. The computer is connected as a terminal to an Internet node. The user does not have to care for the software (except modem software). The number of available resources is limited by the node software.

In both cases, the computer may be connected permanently (i.e., by leased phone line, Ethernet line etc.) or on irregular basis (dial-up lines). The user would face some problems connecting a network node to a network on irregular basis.

Dial-up lines

Generally, it is better for a computer to be an Internet node, not only a terminal, but sometimes it is not possible. In such cases, the services are available via dial-up lines (not only lines to other Internet nodes, but also lines to other networks that have Internet connection, for example CompuServe, America On Line, SprintNet, BITNET etc.; but, generally, the non-Internet nodes enable only some Internet services).

Naturally, the dial-up line quality is the most acute problem, especially in those countries with analogous telephone networks.

The technical speed limits on ordinary dial-up lines are 28.8 kbps but such modems are not very common (yet). Most of the networks nowadays announce 14.4 kbps V.32 bis protocol dial-up modems. (The protocol is used to keep communication error-free.) On the other hand, on Helwan SLR station we make a connection to a DEC terminal server at Cairo University (40 km far from Helwan); the Egyptian telephone network is analogous. The phone line does not allow more than 2.4 kbps V.32 bis connection. (SprintNet in Ukraine, Russia, Kazakhstan etc. offers only 2.4 kbps dial-up modems.)

SLR Data Centers

Both centers in USA and Europe are connected to Internet. The EDC (Eurolas Data Center) in Munich provides anonymous FTP; the structure of the data depository was described in EDC Information Bulletin, No. 5. , July 1994. NASA built a large NSSDC Online Data and Information Service (NODIS) providing HTTP, gopher, FTP, remote login, unfortunately, according to NASA Science Information Systems Newsletter, Iss. 31, February 1994, there are no SLR information/data there. (Why?) The information (ephemerides, times biases, QL analysis) are distributed by E-mail to all interested SLR sites.

SLR Stations

The stations in North America, Australia, Europe (excl. former USSR), Japan are (or may easily be) connected to Internet. (I recommend the stations with only SPAN access to upgrade their connection to Internet as well.)

In Africa, Helwan station is connected to Internet via dial-up line (as a terminal), next year it will be hopefully connected by a leased line (as Internet node). The station in South Africa could be easily connected to Internet. There are Internet nodes in Tunisia.

In Asia, there are regions with good Internet accessibility (for example Israeli, Saudi Arabia, South Korea, Japan, East China, Malaysia, Singapore, Thailand etc.). There are regions with SprintNet accessibility at least (former USSR).

To be more specific about the former USSR countries: some countries have at least one Internet node (the European countries of former USSR and Russia). Russia builds also another commercial network (GlassNet) with Internet connectivity. According to the CompuServe information database, about 50 cities in the former USSR has dial-up SprintNet connection to CompuServe (CompuServe is establishing the full Internet connectivity).

Internet boom in South America has started just recently, but some countries have great Internet accessibility. SprintNet, TymNet and other commercial networks are spread there already for a long time and they allow Internet connectivity.

About 95% of all the countries have PDN (public data network) services with nodes at PTT (post, telegraph & telephone) that enable access to Internet, CompuServe etc. An agreement with local PTT is obligatory for obtaining an account.

Generally, the user has to gain some access rights to connect to Internet. If the user is connecting as a terminal, the user has to obtain username (with the password) and the mailbox at every node user is connecting to.
Of course the user may connect to any of your Internet nodes via long-distance call. However, the user should obtain an account nearer because of the line reliability.

On the other hand, on the CompuServe the users have only one (and unique) username, no matter where is the user connected from. The user may even connect via SprintNet, TymNet and thirteen other networks without having an account on those networks Inbound Internet connection allows remote login into CompuServe. Therefore, I recommend CompuServe for mobile SLR stations. It may be used also by other SLR stations as a spare communication channel.

Notes on Information Management

The information management at the SLR sites is not still the topic of the day. The SLR station may have perfect hardware (laser, mount, detectors, epoch timing etc.) but still, if your data is not delivered to the center quickly enough, your effort was in vain. And vice versa, if the center does not provide completely reliable (and quick) source of information (ephemerides, time biases, results analysis etc.), it cannot expect good data from the stations. There is no direct communication between the stations. There is no information database (with exception of EDC in Munich providing only file transfer access).

➲ I think that the SLR International Scientific Community should apply for cooperation with NASA Science Internet (NSI) and NASA Network Applications and Information Center (NASA NAIC).

➲ I recommend running somewhere a distribution list (on some listserv software) for a communication between SLR sites and both centers (questions, answers, recommendations, information about useful Internet resources etc.).

➲ The data centers should provide a user-friendly data access for SLR stations. They should support HTML (HyperText Markup Language) - a client/server system used in systems like WWW (World Wide Web) or NASA NODIS. The client systems today use Lynx (line mode) or Mosaic (graphical mode) computer programs; those programs are available on all computer platforms including MS-Windows, X-Windows and VT100 terminals.

➲ The Internet communication software should become a part of the SLR Operational Software kit. SLR operators should be skilled in using Internet. These software packages are available from Internet as a freeware or shareware.

➲ The ranging results (including FR) should be sent directly from the SLR site on the same day, just after the on-site analysis. (EDC is still receiving FR data of the ERS-1 satellite from some stations - even those with an Internet address - with a delay of three or four months.)

➲ I suggest that SGAPO Global Configuration Survey of SLR Stations inspired by Tom Varghese carried out at May 1994, would be followed by the third part - Internet and Communication Facilities on SLR Stations.

References

[1] Novotný, A.: Computer Networking at SLR Stations. In: Proceedings of the Eighth Int. Workshop on Laser Ranging Instrumentation. Annapolis, MD USA, 1992.

[2] EDC Information Bulletin, EUROLAS Data Center at GFZ/DGFI Munich (1991 -1994)

[3] ERS-1 FR Laser Tracking Data Preprocessing, GFZ/D-PAF , Monthly Reports

[4] NASA Science Information Systems Newsletter, Issue 30 (Nov. 93), Issue 31 (Feb.94).

[5] Internet Network Information Service (HTML, gopher, ftp)

[6] CompuServe Information Service (online)

[7] The SHAREWARE book in Electronics form:

* THE ONLINE WORLD *
Version 1.7 - August 1994
(Version 1.0 was released in Aug. 93)

By Odd de Presno
4815 Saltrod, Norway (Europe)
Voice (registrations only): +47 370 31204
Internet mail: opresno@extern.uio.no
Data/BBS: +47 370 31204
FAX: +47 370 27111

The book describes the breadth of the offerings by focusing on selected applications on major global networks and services including Internet, CompuServe, Fidonet, Usenet, and BITNET. Perspective is global. It is an ASCII text file that is suitable for sending to a printer.

Deploying the New Graphical User Interface Control Software on the NASA Satellite Laser Ranging Systems

Jan F. McGarry
NASA Goddard Space Flight Center

Paul J. Seery, Kenneth S. Emenheiser
AlliedSignal Technical Services

John W. Cheek
Hughes/STX

Randall L. Ricklefs
McDonald Observatory, University of Texas

In 1991 NASA embarked on upgrading the control computers and associated software for their Satellite Laser Ranging Systems. The impetus for this was the need to replace aging and obsolete onsite equipment, and to replace software that was difficult to operate, to maintain, and to upgrade. The computer chosen was a 486PC using the realtime UNIX operating system LynxOS. The software was designed to be user friendly, with mouse driven menu selections, interactive graphical windows, and realtime plots. The first operational version of this software was installed on the MOBLAS-6 and University of Texas MLRS systems this year. Preliminary tracking at both systems showed good results. MOBLAS-6 with this new software is scheduled for collocation with MOBLAS-7 early in 1995. MLRS is expected to be fully operational using the new system by the spring of 1995. MOBLAS-7 and the rest of the MOBLAS systems will be upgraded in the coming months, and other systems, including NASA's 1.2m Telescope and the University of Hawaii LURE, are currently in progress.

Intro and Background

The upgrade of the NASA Satellite Laser Ranging (SLR) system control computers was begun in 1991 in an effort to replace the almost 20 year old SLR system electronics [Ricklefs]. The function of the control computer is to drive the telescope, control the laser ranging system, and record the tracking and ranging information. The existing computers were vintage 1970 systems installed during the initial development of the SLR systems and were not only obsolete, but were becoming difficult to maintain and almost impossible to upgrade. Much of the existing software was written in assembly language, with in-house developed operating systems. Software and hardware expertise on these systems was a shrinking resource.

In addition there were many different system configurations across the Network involving many different brands of computers, operating systems, and programming languages. Our goals for this upgrade were to (1) standardize the computers, operating systems,

languages, and user interfaces as much as possible, (2) make the software portable (attempting to minimize later computer upgrades), (3) make the software and systems more user friendly to operate, (4) provide the framework for automation, and (5) lay the foundation for remote monitoring and remote control.

For the computer we chose a 486-DX2/50Mhz PC with standard interfaces, including RS232, CAMAC, Ethernet, IEEE and SCSI. For timing we used an internal PC board to provide the 20pps interrupts and to synchronize the timing to the start of the 1 second. We decided from the beginning to minimize other hardware changes, except for the computer and its interfaces, in order to keep the scope of the upgrade within attainable limits [Wetzel]. We also chose to keep the current onsite CPU configuration and replace only the control computer functions. In this configuration there are two onsite computers: the control computer and the analysis computer. The analysis computer, an HP9000/380, performs realtime formatting and analysis of the data, determines system performance, communicates with the central computer facility, and provides onsite archiving of the data [Emenheiser, Edge].

UNIX was the Operating System (OS) of choice due to its good programming environment, X-windows support, support for FORTRAN and C, portability to other platforms, and compatibility with the existing onsite HP computer. The operating system, however, had to have realtime performance, and we wanted a POSIX compliant OS, developed by a thriving company. Lynx Realtime Systems was chosen since it satisfied all of our requirements.

Software Design Overview

The servo and ranging software was designed to reside in two layers above the operating system:

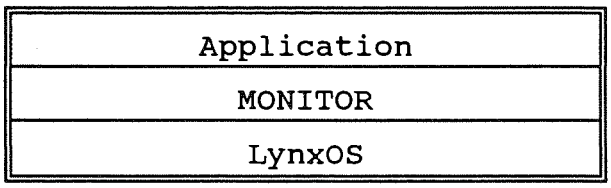

The MONITOR program is the primary layer and was designed to be running at all times during normal operations. The applications software (ie star or satellite tracking) resides on top of MONITOR. MONITOR serves three purposes. First, MONITOR provides a display for the operators to see the date/time, the mount pointing angles, the weather, and various other telescope related parameters. Second, MONITOR also gives the operator rudimentary control of the telescope via bias pointing. Third, MONITOR provides the interface to the hardware and operating system for the operational applications software. In this design the applications programs are responsible for predictions, operator

interface and data recording, and are shielded from all servo and ranging system I/O and most OS interfaces by MONITOR.

For non-operational diagnostic applications, MAINT replaces MONITOR as the primary layer above the OS. This is because MONITOR forces telescope and ranging I/O at set rates and in a set order. Certain subsystem diagnostics may require outputs at other rates, or asynchronously, or may require some subsystems to be shut down entirely. MONITOR does not allow that flexibility due to its very operational design. MAINT, however, does not interact with the hardware unless directed to by the applications software, thus providing a very flexible system for diagnostics.

Applications Programs

The two major operational applications are the Star Calibration Program (STARCAL) and the Satellite Tracking Program (SATTRK). Diagnostic software was also developed which includes full-system servo test programs, subsystem diagnostics for the ranging, servo, and timing subsystems, and diagnostics for the CAMAC, Paroscientific pressure unit, and serial interfaces. Optical Attenuation Mechanism (OAM) and IEEE interface diagnostics are under development.

STARCAL is used to calibrate the telescope pointing errors by pointing to known star positions. Biases, input to the system to center the star image in the telescope field of view, are used to develop a model of the pointing errors. The STARCAL program can produce a post-processed least squares fit of the mount model to the data, or can, as an operator option, update the mount model on a star by star basis using a Kalman Filter update process. Stars are selected from the FK5 catalog (reference J2000.0), their positions are updated to the current time and converted from mean to apparent. Stars to be used in the modelling can be selected to fit a grid pattern in the sky or to fit along a satellite arc (for a quick update of the mount model prior to a pass).

Various plots are available in the STARCAL program for operator reference. A polar sky map graphically displays the stars chosen and indicates by color which stars have been recorded. Other plots include a polar plot of the mount model values at each star location, and post fit residual plots in either polar or rectangular coordinates.

The operator can input angular biases via hardware switches (if available on the system), or using a graphical interactive bias window which allows input from the mouse (see Figure 3). The later proves to be a very convenient method when the operator has a camera display of the telescope field of view.

The STARCAL program records its data to the hard disk and produces its own solution of the mount model. No interaction

with the HP is required for STARCAL solutions, however, the HP380 periodically updates the UT1 file on the PC, and this file is required for STARCAL pointing.

The satellite tracking program (SATTRK) is the main operational application and, as such, is expected to be running (with MONITOR) most of the time. This program computes the telescope pointing and generates the laser ranging system designate to track satellites using predictions supplied from a central facility. At MLRS SATTRK also includes lunar ranging capability. The satellite predictions are obtained from the central facility by the onsite HP analysis computer which converts the incoming Tuned IRVs (TIVs) to one set of polynomials per pass. A set of polynomials consists of three sets of coefficients (x,y,z) with time as the independent variable, and are in an earth centered rectangular inertial reference frame. The polynomials are written to the PC's hard disk by the HP nominally once per week. The operator can select a satellite pass from a window that shows all passes occurring within the next 1.5 hours. The software will eventually select the passes to track from a pre-loaded satellite priority schedule. Currently, however, the operator reads the satellite priority schedule and selects the passes manually.

All of the currently existing satellite program functions are available in the new software. These include the start, suspend and end scenario functions which permit the operator to take calibration data at various times and associate that calibration data with satellite passes occurring at other times. The operator controls the range window, range bias, and IRIS from the computer. Angular biases or time/crosstrack biases can also be entered via an interactive graphical widget. A realtime plot of the returns in the range window (O-C plot), along with an associated histogram of the ranging data, for both satellite and calibration, is available in the MLRS software and will soon be available for all systems.

The operator has various logging options, including recording all shots, or recording only returns (the operational default). Data is written directly to the PC's hard disk. The HP remotely mounts the PC's hard disk over the Ethernet and reads the data from it in realtime or in a non-realtime playback mode.

Internal Design Details

Each program (MONITOR, STARCAL, SATTRK, etc) is a separate process written as a set of threads. Threads are paths of execution which all share the same virtual address space. Using threads allows the tasks within a program (process) to easily share memory and other resources.

MONITOR's execution is started by the operator. When requested

by the operator, MONITOR then starts an application by forking; this creates a child process which has the same file descriptor tables, shared memory segments and signal handling arrangements. Files, shared memory and signals are used by MONITOR and the applications to pass information back and forth. For example, each application passes the predicted servo information to MONITOR via shared memory. MONITOR performs the necessary I/O at the required times and passes back the ensuing system information. Signals are software interrupts used to synchronize tasks between various processes. For example, the MONITOR 50msec servo thread signals the application's 50msec thread to execute (see Figure 1). This ensures that the servo prediction computations and the servo drive output always occur in the same sequence. Binary Semaphores (Bsem) are used in a similar fashion to synchronize events between threads within a process.

The timing board is a board in the PC's backplane which synchronizes the computer tasks with the external clock. 20pps and 1pps are input to the board from the Time Code Generator (TCG). The 20pps interrupt generates a signal which drives the MONITOR servo task; the 1pps is used to synchronize the time of day with the actual start of the second. The time of day is kept internally and updated at 20Hz. The TCG is interrogated once every 10 seconds and a comparison is made between the internal time and the TCG time. An alarm message is issued to the operator if they differ and the system is resynchronized to the external clock.

MONITOR, STARCAL and SATTRK each contain approximately 5 tasks or threads. Each of the three programs contains a servo thread which runs at 20Hz. In MONITOR this task's major function is to read the encoders, difference this with the commanded angles from the application, perform any servo compensation required, and output the drive values to the analog motors. In both STARCAL and SATTRK the servo task is used to compute the commanded servo angles for the next 50msec interval.

MONITOR and SATTRK each have a laser ranging task which runs at the laser fire rate (1,2,4,5, or 10Hz). In MONITOR this task outputs the range gate values and reads the data from the return time interval unit (TIU). In SATTRK the laser ranging task produces the range gate value for a future laser fire.

All three programs contain a GUI or display thread. This thread occurs asynchronously upon operator menu selection or interactive widget action.

Data recording threads in both STARCAL and SATTRK handle writing the data to disk. This task is initiated in STARCAL by the operator selecting the record button, and in SATTRK by a binary semaphore from the 50msec thread after selection is made via the GUI display.

Menu and Graphics

The display software is written using X-windows/MOTIF. Each program has an associated screen display (see Figures 2 - 4). The displays include telescope, ranging (except STARCAL), weather and other pertinent information. The top level menu is displayed in the upper bar. The menus are pulldown and can be accessed in the standard manner using the mouse/trackball or the keyboard. Tables 1 through 3 show the menu system for MONITOR, STARCAL and SATTRK. Here "-->" implies a submenu, and "..." implies a keyboard pop-up entry box will appear.

In the screen display, the area below the top-level menu is the alarm or error message area. Error messages appear as boxes or buttons in this area. Some error buttons can be cleared by clicking on them, some display a submenu or a keyboard type-in box when clicked. A reoccurring error will cause the alarm message to reappear. Colors for these buttons have meaning. Red implies error, yellow is warning, green is normal, blue is not nominal but nevertheless OK, and white is for information only. Plots and interactive graphical windows can be resized and moved anywhere on the screen.

The following are the available graphical plots and interactive graphical widgets for the two major applications programs:

SATTRK	STARCAL
AZ/EL bias	AZ/EL bias
XT/Time	Polar plots: Sky Map, Model Map, Error Map
IRIS	IRIS
O-C & hist	Rectangular model error plots
Range bias	

Backups and software updates

All control computer systems will have a 525 Mbyte cartridge tape, a 1.44 Mbyte floppy, and an Ethernet connection to the HP with its 650 Mbyte rewriteable optical disk. As long as the backup or restoration of software does not involve the OS, any backup or software update can occur to any of the above.

Normal backups are performed in two parts: backup of specific and dynamic site information to floppy, followed by system backup to tape. Restoration occurs in the reverse order. Software updates can be delivered to the site via the Network (where available and if not an OS update), via floppy (if small enough), via 525 Mbyte tape, or via the HP optical disk (if the update is not to the OS itself).

OS and FORTRAN Compiler Problems Encountered

We encountered several problems with both LynxOS and the FORTRAN

compiler during the course of our software development. We found the set of device drivers available to us very limited and had to resort to writing our own. We developed the timer card and the CAMAC drivers in-house and contracted out to a Lynx suggested source for the serial mux and the IEEE drivers.

Other problems included an X-windows release developed by Lynx that was not complete. This was corrected however when Lynx switched to the Metro-X implementation of X-windows. The C language function "sprintf" did not work properly until the latest release; printing out floating point numbers with it would occasionally cause the system to crash. Lynx switched FORTRAN compiler support from Liant to EPC half way through our development requiring purchase and familiarization with the new compiler. EPC FORTRAN came with its own set of problems. The library is not thread safe. This remains an unsolved EPC problem, forcing us to write a work around. We can not call FORTRAN subroutines from multiple threads, but must duplicate subroutines so that each is called only from a single thread.

Improvements in User Friendliness

The new controller software not only facilitates hardware upgrades to the SLR system (since we now support standard interfaces) and improves ease of software maintenance and upgrade, but also gives the operator an improved environment to work in. In the MOBLAS system this includes having all of the electronics in a single trailer (down from two), giving the operator greater visualization via graphs and plots, and allowing the operator greater control over the system from the computer console.

Current status

The following is our best estimate of the schedule for controller computer upgrades at the NASA SLR systems:

System	*Status - Expected completion of upgrade*
MOBLAS-6	Has successfully tracked satellites. In collocation with MOBLAS-7 by February 1995. Fully operational by March 1995.
MLRS (Texas)	Has successfully tracked satellites. Fully operational by Spring 1995.
1.2m Telescope	Star calibrations successfully demonstrated. Complete switch to new system by Spring 1995.
MOBLAS-7	Hardware upgrade expected March 1995. Collocation with new MOBLAS-6 expected May 1995. Upgrade complete by Summer 1995.
MOBLAS-4,5,8	Upgrade during 1995.
LURE (Hawaii)	Upgrade just starting; completion during 1995.
TLRS-3/4	Hardware/software design completed Fall 1995. Upgrade completed in early 1996.
TLRS-2	Will follow TLRS-3/4 design.

Future work

Our goal is to continue to work toward making the systems easier to operate. This will involve automating as much of the operation as possible, including having the computer select and set up for the passes, adding auto star calibrations to those systems that can support it, and working on satellite autotracking in conjunction with SLR2000.

We also plan to add planetary tracking to the Starcal program, and include O-C and histogram plots in SATTRK on all systems by early 1995.

Acknowledgements

The software team would like to thank John Bosworth and John Degnan for their support of and patience with this project, and would also like to thank the hardware efforts of Herb Hopke, Bill Bane, Jim Bouras, Jerry Wiant and the many more ATSC and MLRS team members too numerous to name.

References

Edge, D., M. Heinick, et al, "Evolution/Automation of the NASA HP Data System," in this Proceedings.

Emenheiser, Ken, "Hewlett Packard 380 Users Guide," CDSLR-04-0009, Bendix Field Engineering Corporation, May 1992.

Ricklefs, Randall L., Jack W. Cheek, et al, "Upgrading NASA/DOSE Laser Ranging System Control Computers," Proceedings of the Eighth International Workshop on Laser Ranging Instrumentation, NASA Conference Publication 3214, May 1992.

Wetzel, S., W.Bane, et al, "MOBLAS Controller Upgrade Status," in this Proceedings.

Table 1
MONITOR MENU

File-->
- Delete-->
  - Site Files...
  - Target Files...
  - Log Files...
  - History Files...
  - OAM Files...
  - Mask Files...
  - Raw Files...
  - Poly Files-->
    - Selected Files...
    - All Files
  - Star Files-->
    - Star Data...
    - Coefficients...
    - Co-Variances...
    - Analysis...
- View/Print-->
  - Site Files...
  - Target Files...
  - Log Files...
  - History Files...
  - Raw Files...
  - Slew Files...
  - Servo Files...
  - Star Files-->
    - Star Data...
    - Coefficients...
    - Co-Variances...
    - Analysis...
    - Star_Default.dat
    - IERS-Bulletin-A
- Shutdown Computer
- Reboot System
- Fix disk system
- Format floppy disk
- Backup/Restore Operating System
- Backup/Restore Operating System to HP Optical
- Exit

Edit-->
- Site Database...
- Target File...
- OAM Satellite File...
- Masks-->
  - Pre-limits
  - Stop-limits
  - Laser limits

Tracking-->
- Satellite/Target

```
        Star Calibration
        Servo Program
        Slew Program
Misc-->
        Select (TCG) Time
        Select (CPU) Time
        Enter Simulation Time...
        Enter Clock Offset...
Help
```

Table 2
STARCAL MENU

```
File-->
     Select coeff set-->
                          Def. Global
                          Def. Kalman
                          Other...
     Open data set...
     Save data set
     Save data set as...
     Discard data set
     Exit
Edit-->
     Zero coefficients
     Set scale covariances flag...
     Set initialize covariances flag...
     Set solution criteria-->
                          Global
                          Kalman
                          Rejection criteria...
     Reject stars-->
                          Reject last star
                          Reject other star...
     Change mag limits-->
                          Change/view limits...
                          Reset limits to default
     Select catalog-->
                          FK5 extension
                          MESSIER
                          FK5 catalog (default)
Mode-->
     Select/load objects to track-->
                          Select from Catalog-->
                                    Grid
                                    Satellite Arc...
                                    Selected Grid...
                                    Keyboard Table...
                                    Automated
                                    Bright
                                    By Catalog Number...
```

```
                              Keyboard RA/DEC-->
                                        Apparent...
                                        Mean Epoch...
                                        Mean J2000.0...
     Generate final solution and summary
     Accept starcal
     View summary-->
                              View current
                              View other...
     View coefficients-->
                              View current
                              View other...
Star-->
     View / choose from table...
     Alignment Star
     Automatic
Biases-->
     Interactive Graphical AZ-EL bias
     Iris control
Displays-->
     Turn off all window displays
     Display Sky Map
     Display Mount Model Map
     Mount Sky Error Map
     Display deltas-->
                              Delta AZ versus Delta EL-->
                              AZ versus Delta AZ-->
                              EL versus Delta AZ-->
                              AZ versus Delta EL-->
                              EL versus Delta EL-->
                                             current
                                             file...
                                             current vs file...
```

Table 3
SATTRK MENU

```
File-->
     Select Target to Track-->
               Poly-->
                    Directory Scan...
                    Pass Schedule...
               IRV...
     Select Mount Model Coeff-->
               Global
               Kalman
               Coefficient File...
     Delog...
     Exit
Edit-->
     Edit IRV...
```

Operation-->
- Begin Real Time
- Suspend Tracking Scenario
- Clear Tracking Scenario
- End of Tracking Scenario
- Re-open Tracking Scenario

Control-->
- Range Gate Source-->
  - Computer
  - Delay Generator
- Scope sync-->
  - Range Window
  - Start Diode
- System Mode
  - Operate
  - Test
- Override to Beam Divergence
- Simulation Range...
- Select TCG Time
- Select CPU Time
- Enter Simulation Time...
- Enter IRIS...
- Enter Slew Granularity...

Biases-->
- Pointing Biases/Selection-->
  - Satellite Rectangular Scan...
  - Corner Cube Scan...
  - AZ/EL (Biases)
  - Time/Xtrack (Biases)
- Range Bias
- Time Bias Offset...

Display-->
- O-C Plot
- Satellite Histogram
- Calibration Histogram
- CAMAC display

Help

Figure 1 TELESCOPE CONTROL SYSTEM

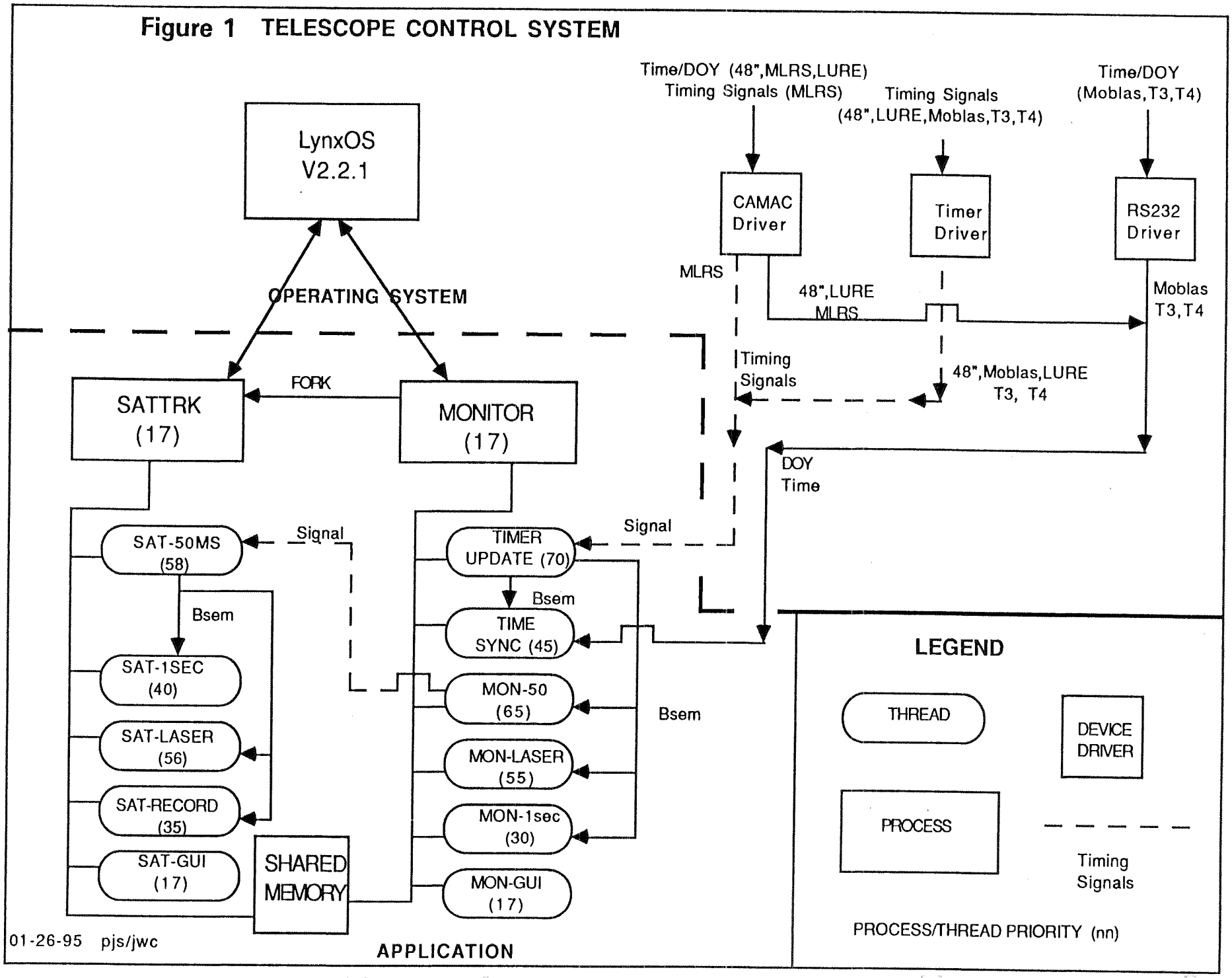

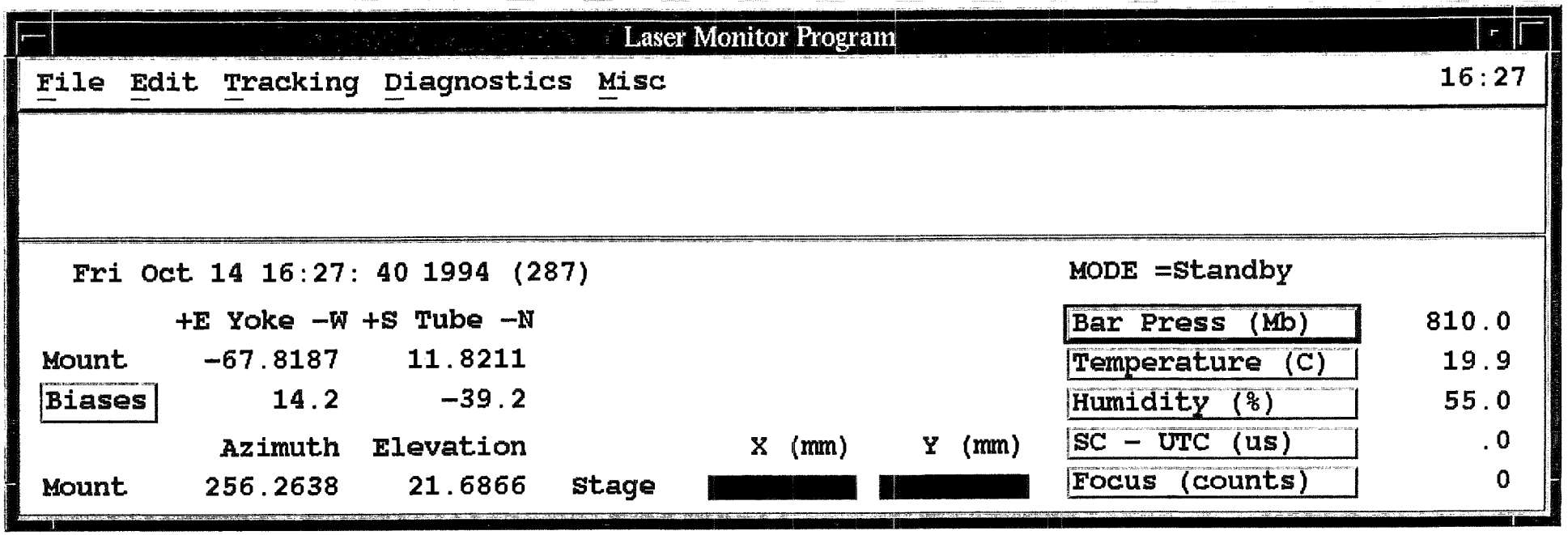
Laser Monitor Program
File Edit Tracking Diagnostics Misc
16:27
Fri Oct 14 16:27: 40 1994 (287)
MODE =Standby
+E Yoke -W +S Tube -N
Mount -67.8187 11.8211
Biases 14.2 -39.2
Azimuth Elevation
Mount 256.2638 21.6866
Stage
X (mm)
Y (mm)
Bar Press (Mb) 810.0
Temperature (C) 19.9
Humidity (%) 55.0
SC - UTC (us) .0
Focus (counts) 0

Figure 2

Figure 3

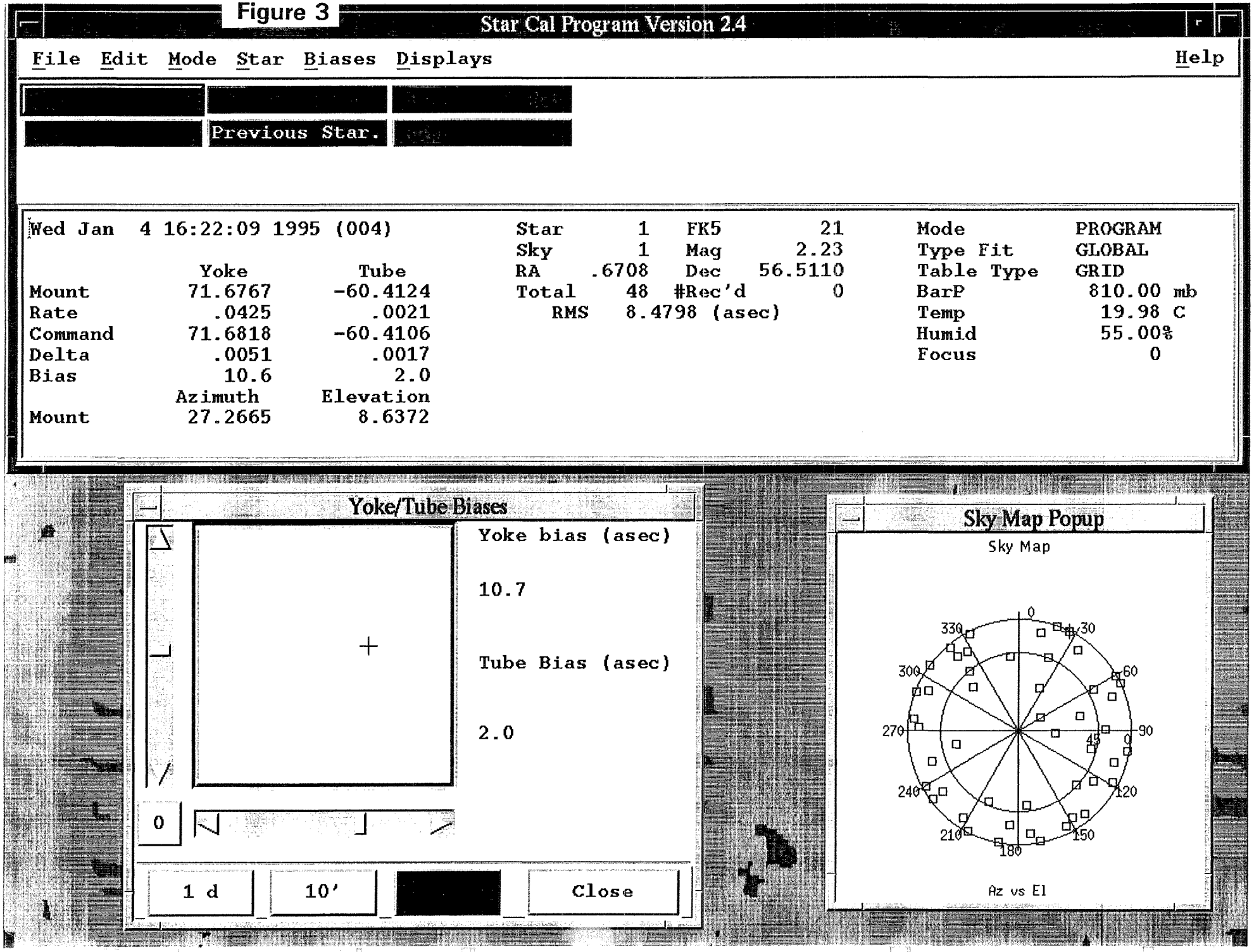
Star Cal Program Version 2.4
File Edit Mode Star Biases Displays Help
Previous Star.
Wed Jan 4 16:22:09 1995 (004)
Yoke Tube
Mount 71.6767 -60.4124
Rate .0425 .0021
Command 71.6818 -60.4106
Delta .0051 .0017
Bias 10.6 2.0
Azimuth Elevation
Mount 27.2665 8.6372
Star 1 FK5 21
Sky 1 Mag 2.23
RA .6708 Dec 56.5110
Total 48 #Rec'd 0
RMS 8.4798 (asec)
Mode PROGRAM
Type Fit GLOBAL
Table Type GRID
BarP 810.00 mb
Temp 19.98 C
Humid 55.00%
Focus 0
Yoke/Tube Biases
Yoke bias (asec)
10.7
Tube Bias (asec)
2.0
0
1 d
10'
Close
Sky Map Popup
Sky Map
0
30
60
90
120
150
180
210
240
270
300
330
45
Az vs El

Figure 4

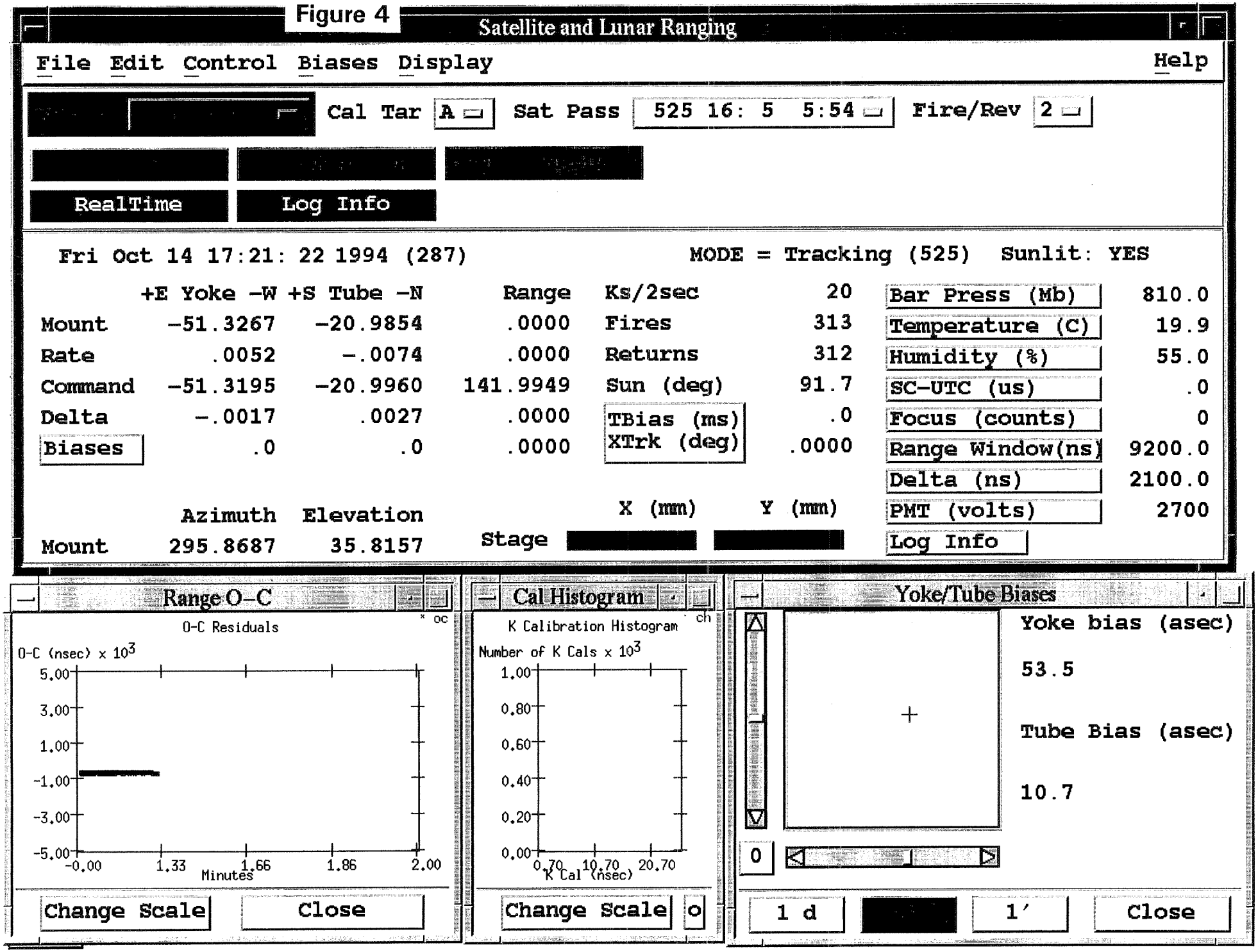
Satellite and Lunar Ranging
File Edit Control Biases Display Help
Cal Tar A
Sat Pass 525 16: 5 5:54
Fire/Rev 2
RealTime
Log Info
Fri Oct 14 17:21: 22 1994 (287)
MODE = Tracking (525) Sunlit: YES
+E Yoke -W +S Tube -N Range
Mount -51.3267 -20.9854 .0000
Rate .0052 -.0074 .0000
Command -51.3195 -20.9960 141.9949
Delta -.0017 .0027 .0000
Biases .0 .0 .0000
Ks/2sec 20
Fires 313
Returns 312
Sun (deg) 91.7
TBias (ms) .0
XTrk (deg) .0000
Bar Press (Mb) 810.0
Temperature (C) 19.9
Humidity (%) 55.0
SC-UTC (us) .0
Focus (counts) 0
Range Window(ns) 9200.0
Delta (ns) 2100.0
PMT (volts) 2700
Log Info
Azimuth Elevation
Mount 295.8687 35.8157
X (mm) Y (mm)
Stage
Range O-C
O-C Residuals
O-C (nsec) x 10^3
5.00
3.00
1.00
-1.00
-3.00
-5.00
-0.00 1.33 1.66 1.86 2.00
Minutes
Change Scale
Close
Cal Histogram
K Calibration Histogram
Number of K Cals x 10^3
1.00
0.80
0.60
0.40
0.20
0.00
0.70 10.70 20.70
K Cal (nsec)
Change Scale
Yoke/Tube Biases
Yoke bias (asec)
53.5
Tube Bias (asec)
10.7
0
1 d
1'
Close

685

Parallel aspects of Laser Ranging Control

J.W. Offierski

Kootwijk Observatory for Satellite Geodesy
P.O. Box 5030
2600 GA Delft
The Netherlands

Until recently, software for SLR control systems was designed mostly for linear programming. For given tasks, some programming routines check the epoch and dependent of it, dedicated action was taken (e.g. new position, read counter, etc.). These routines consist of many 'if' statements and in addition the execution time could easily become critical. Especially difficult is real time position approximation in this way.
An alternative method is to generate time and event interrupts (e.g., counter ready for reading etc.). Inside these routines, the programmer must also watch the execution time, but in the intermediate time it is possible to prepare some data for the next action. Usually these routines are written in assembler.

Two other problems are present in control systems which use linear programming:

1 controlling telescope movement
If the telescope has its own controller (e.g. the Contraves system) then the control task can be simplified to sending commands. If not, then this function requires second processors [], which take care of PID (Proportional, Integral, Derivative filter), positioning, speed and acceleration. An alternative solution is to build very extensive electronics. A combination of both solutions is also

feasible.

2 data storage
in relatively slow mass storage memories this frequently causes time critical problems.

The presented software for a SLR control system is designed for a four-processor network, and runs in parallel tasks, both inside one processor and externally in different processors.

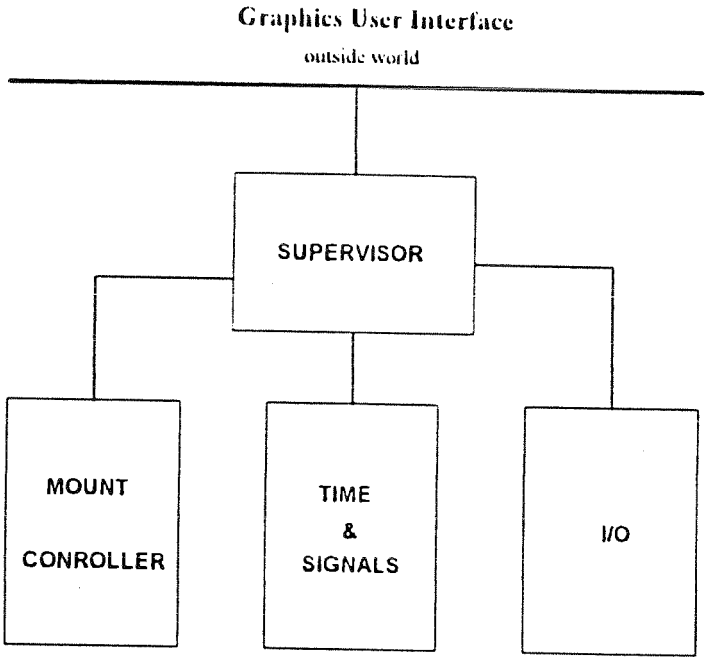

The structure of the control system design logically distributes tasks over the different processors.

1 the supervisor processor
for communication with outside world, internal network and distribution of tasks between processes.
2 the mount controller
for telescope movements.
3 time registration and signal generation.
4 input/output

to and from standard units (e.g. meteorologic, counters etc.).

All software is written in ANSI-C and is deeply structured into levels, which give the possibility to logically divide tasks between processors and easily exchange objects. The programs are not yet Object Oriented but they are bound to this structure.
There are three levels[]:
a) task level (fully parallel),
b) unit level (dependent of type of connected instruments and configuration),
c) protocol level (dependent of type of interface and unit).

The b) and c) levels are not fully parallel but sometimes behave like it when two parallel processes use an identical interface or an identical unit. In linear programs the same routine could be called from difference places but couldn't work in the same time (being called from two different processes). In any type of program it is clear that the same unit cannot be used more than once in the same time.

All software is divided into processes which are working in parallel. At start-up programs are loaded to the processor network. The next step (linear) is to initialize and check the system hardware. After this, communication with the outside world is established. Control system communication is based on command exchange (with or without parameters) or data request, via fast serial connection. If any hardware unit does not respond or reports an error, the unit will be simulated automatically and a message is sent to the operator. When this task is ready, the parallel processes will start running. There are various types of processes defined in the software, processes which:
- are always running,
- run on request,
- wake up periodically,
- run when an event occurs,
-are activated temporarily,
- are scheduled for a task.

General processes.

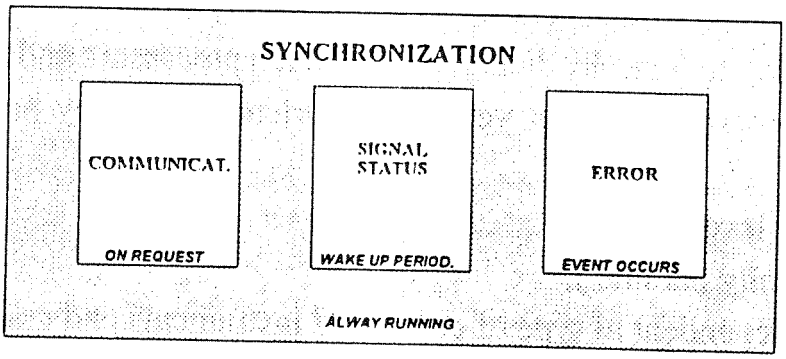

The most imported task is to synchronize (*always running*) all processors and all processes to UTC scale. At start-up and when synchronization is lost, the hightail priority synchronization process is scheduled. For this process the 1 pps signal from an accurate source (GPS, Cesium) is used. All processors and processes are synchronized within 1 μs, but the time and mount processor have their own 1 pps connection for more accurate definition of the epoch.

The communication process (*on request*) interprets a command from the outside world. Dependent on the command, a process is activated or data is distributed to object (prediction) or a built-in action is started (if no other hardware available, a full simulation process (*on request*) will be started, in which even observation data will be simulated).

The system signal status process (*periodically wake up*) checks all signals from systems which are connected to the control system. Dependent on the situation only information is sent to the user or an additional routine is called. These signals (end switches, on/off status from instruments, etc.) can, in severe cases, determine that the whole system must stop. The wake up period is a system parameter and can be changed.

The error handling process (*when event*) controls mathematical and electronic errors. It can be activated from the mathematical co-processor (built-in processor) or from the signal status process or from an interrupt (alarm button, encoder index pulse etc.). If a mathematical error occurs, it is ignored the first three times followed by a request for new data (prediction parameters). An index pulse interrupt will only check the precision of the actual telescope position. If it is correct there is no reaction. In all other cases the simulation of broken unit process (*when request*) is started and the user is informed.

All these processes are always active but sometimes can be in wait or in sleep mode.

Processes which are only *temporarily activated.*

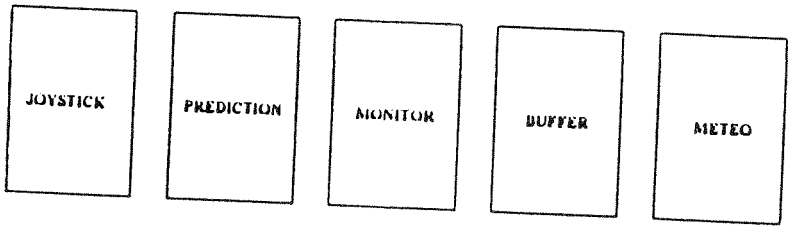

The joystick handling process reads the status from the joystick buttons. With the joystick, various parameters in the system can be changed during tracking:

- Azimuth, Elevation correction,
- Time Bias, Across track correction,
- Range Gate, Window size correction.

The correction mode can be changed by the operator as well as the step size. In all other cases the joystick gives the possibility to move the telescope to any position.

When prediction parameters arrive the system will prepare for observations (clear buffers, synchronize shutter, define beginning position, etc.). Predictions are calculated in every process which need, in real time. Predictions are calculated from a polynomial approximation to the track with an order which depends on the target.

The process for Monitoring position, velocity and system status can be activated on request from the user or from the internal tracking routine. Position is defined at the epoch of the request or laser fire start epoch.

The buffer process collects observation data from any other process which generates it and prepares the data for transmission at any time. There are two data buffers in the system to store 64 k data records (epoch, range, position) each.

In a defined period the meteorological data reading process is activated. These data are used for calculating the refraction correction and can be collected at any time by

the user to combine it with the observation data. This process can also obtain meteorological data from operator manual input if the instruments are not available. In that case external data are used for calculating the refraction correction.

Processes which are only *scheduled for* a dedicated *task*.

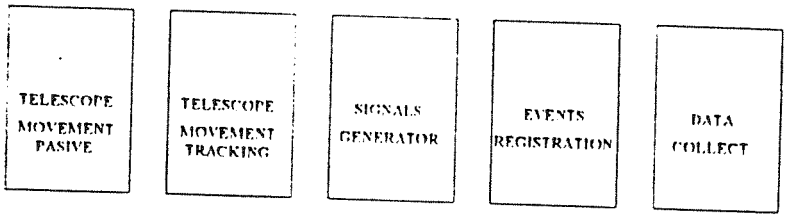

Telescope movement to desired position. This process can be scheduled from the joystick or by user command.

Telescope movement for tracking. In base on before prepare data on given time telescope will start tracking the object. Dynamically during tracking, corrections for Azimuth, Elevation, Along- and Across-track can be changed from the joystick or from the outside world program. Position data is also recorded.

Signal engender process generates electronic signals for Range Gate, Shutter and Laser Trigger. These signals are events in UTC time scale referred to the laser fire epoch. These events are measured inside the system with 500 ps accuracy and within this accuracy, the Range Gate is created. Therefore the length of Range Gate and Window is unlimited and independent from the next start pulse.

The event registration process is started on the START signal from the start detector or the STOP signal from the stop detector. The time elapsed between this event and the next 10 MHz clock pulse is measured on an external counter (HP5370 or SR620) and on an internal 100 ns resolution UTC epoch event counter.

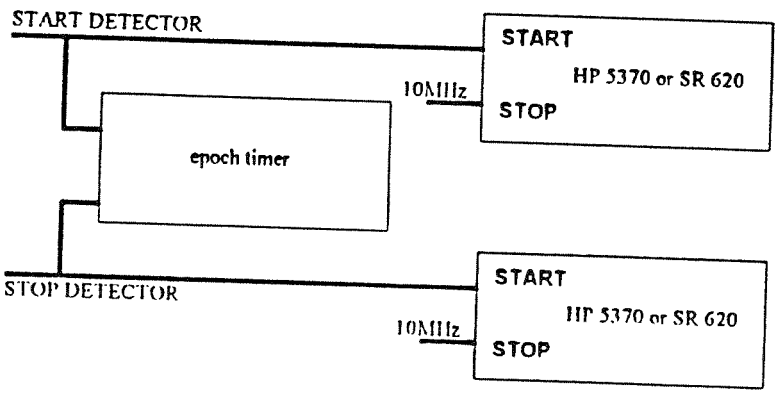

The accuracy of the counter is not reduced, because the 10 MHz pulses are synchronized to the internal time expander in the SR620 or to the coincidence interpolator in the HP5370. Therefore the jitter from this channels are constant and can thus be excluded during calibration. This configuration gives also the possibility to handle more laser pulses in flight.

The data collection process calculates the range from observed data, and formats and stores them in the buffer.

All processes are running in parallel. There are several techniques for data exchange. In order to adhere to the standard only global and local structure are used. Activating a process at the right moment is realized with the technique of semaphores, witch are know from POSIX standard.
It is important to know that these processes are running in one or in several processors. Some parts of a process might at some time be waiting for data from another part, but from the programmer point of view this is not visible.

Designing a control system program in this way facilitates future extension, and replacing elements is relatively easy. The hardware structure gives the opportunity to add one or more processors, if the required computing power becomes insufficient.
The only disadvantage of this design is that debugging becomes quite difficult.

Compact Laser Radar Control System with Auto-tracking Capability

Miroslav Čech

Czech Technical University in Prague
Faculty of Nuclear Sciences and Physical Engineering
Department of Physical Engineering
Brehova 7, 115 19 Prague 1
The Czech Republic
phone: +42-2-85762248
fax: +42-2-85762252
E-mail: mcech@troja.fjfi.cvut.cz

Abstract:

Very compact laser radar control system (LRCS) based on microprocessors is described. A laser radar electronics system with all important functions for satellite ranging and calibration (mount control, range and epoch counter, laser trigger, counter arming, HP5370B interface, PMT or SPAD gate control, etc.) consists of an IBM/PC as master computer, HP5370B as a range counter and the LRCS. Connecting CCD camera ST-4 to the system, a small position corrections during satellite tracking can be done automatically (auto-tracking capability).

The system has been installed and tested on Helwan SLR, Egypt at this year.

The computer controlled laser radar system in Helwan, Egypt has been operating since 1981. In 1989 the HP1000 computer was replaced by IBM/PC clone computer [1],[2]. In this year SLR Helwan II is being upgraded.
An optical receiving system and motor drives are being changed [3]. DC servo motors are used in the system. Fig. 1. shows the block scheme of the new system.

A new compact control system was developed. The control system is multiprocessor system slaved to a main station computer - IBM/PC - via serial line. The system provides all important tasks for satellite ranging. A fully 10 Hz Lageos ranging is implemented by switching HP5370B counter to binary mode of operation and by special HP-IB interface and timing (with no changes inside HP5370B).

Fig 2. shows the block scheme of the control system. The system consists of two printed board built-in to CAMAC unit with a size 14x22x30 cm. A microprocessor Zilog Z-80 is used as CPU in all subsystems. The main microprocessor provides a time synchronization of a whole

system (including time synchronization of the IBM/PC). The second board consists of two parts - special HP-IB interface for HP5370B counter and a mount controller based on a special microchip. Main system characteristics are described on Fig.3.

The electronic system can drive stepper motors (open or close loop) or DC servo motors with close loop feedback. A special microchip Hewlett-Packard HCTL-1100 is used for close loop feedback. HCTL-1100 is a high performance, general purpose motion control IC [4]. It frees the host processor for other tasks by performing all the time-intensive functions of digital motion control. The programmability of all control parameters provides maximum flexibility. The HCTL receives its input commands from a host processor and position feedback from incremental encoders with quadrature output. The HP HEDS-5540 optical encoders [5] are used in the system. The HCTL compares the desired position (or velocity) to the actual position (or velocity) to compute compensated motor commands using a programmable digital filter D(z). HCTL has the capability of providing electronic commutation for DC brushless and stepper motors. The motor command is also externally available as an 8-bit byte for D/A convertor and at the PWM port as Pulse With Modulated signal. Mount control system parameters are:

- close loop with digital filter, 2 msec control period
- incremental encoders HP HEDS-5645-I13
  resolution. 512 counts/rev = 32768 counts/deg = 9.1counts/arcsec
- 2 deg/sec max. velocity (AZ+EL)
- 0.5 deg/sec^2
- 140 W DC servo motors

Electrical accuracy one arcsec is being achieved with this system. Electrical accuracy one arcsec means that difference between required position and position determinated by encoders is one arcsec. Because the encoders are mounted on the shaft of the motors, a mechanical accuracy is worse, approx. 1 arcmin.

To improve a tracking accuracy of the system, CCD camera ST-4 was implemented to the laser radar system. The ST-4 Star Tracker/Imaging Camera is a multipurpose instrument [6]. It can be used as an automatic star (satellite) tracker or, with personal computer, as a highly sensitive imaging camera. The camera has these functions in our system:
a) we can see satellites now. With our configuration (Celestron C11 telescope + ST-4 camera, exposure time 3 seconds), Lageos (magnitude approx. 13) is observed very well.
b) interfacing the camera as an optical position detector to the system, we can improve tracking accuracy of the mount.

The principal scheme of the auto-tracking system is on Fig.4. When the TRACK button is first pressed, the ST-4 takes initial image and finds and records the X and Y position of the brightest object in the field of view. It uses that initial position as the track-to or zero-error position. The ST-4 then cycles repeatedly, taking images, measuring the brightest object's position, calculating a tracking error, which is the satellite's current position minus the track-to position, and making corrections to drive the satellite back to the track-to position. At each pass through the tracking loop, the Average tracking error is shown on the display. All errors are in term of 0.2 pixels error units, meaning an error display of 1 corresponds to a tracking error of 0.2 pixels. One pixel corresponds to 1 arcsec in our configuration. The LRCS receives the error signal from ST-4 and controls the motors to eliminate tracking error.

We obtained the average tracking error 1 arcsec from satellites Lageos, Etalon-1 and Topex. Of course, the auto-tracking system has one drawback - it can be used for visible satellites only.

Conclusion:

The system was successfully tested on June 1994. We recognized the system fulfill all requirements for satellite laser tracking.
Goals of the control system:

- very small size
- high reliability
- high tracking accuracy
- low cost
- single person operating staff

A high performance and reliability of the control system (configuration- stepper motors and no auto-tracking) can be demonstrated on Station Helwan II monthly report September 1994: 204 passes were measured (blind tracking, night passes only).

References:

[1] K.Hamal,H.Jelinkova,A.Novotny,I.Prochazka,M.Cech
Interkosmos Second Generation Laser Radar
Proceedings of the Fourth International Workshop on Laser Radar Rangin Instrumentation, Austin, USA, 1982

[2] M.Cech,A.Novotny
Satellite Laser Radar Electronics Based on IBM PC Computer
Proceedings of the Seventh International Workshop on Laser Radar Rangin Instrumentation, Matera, Italy, 1989

[3] K.Hamal,I.Prochazka,M.J.Tawadrows,J.S.Mikhail
Helwan II Satellite Laser Ranging Station
In this proceedings

[4] General Purpose Motion Control IC HCTL-1100 Series, Technical Data, Hewlett-Packard

[5] Two and Three Channel Optical Encoders HEDS-5540, Technical Data, Hewlett-Packard

[6] Model ST-4 Star Tracker- Imaging Camera, Operating Manual, Santa Barbara Instrument Group, Santa Barbara, CA 93108

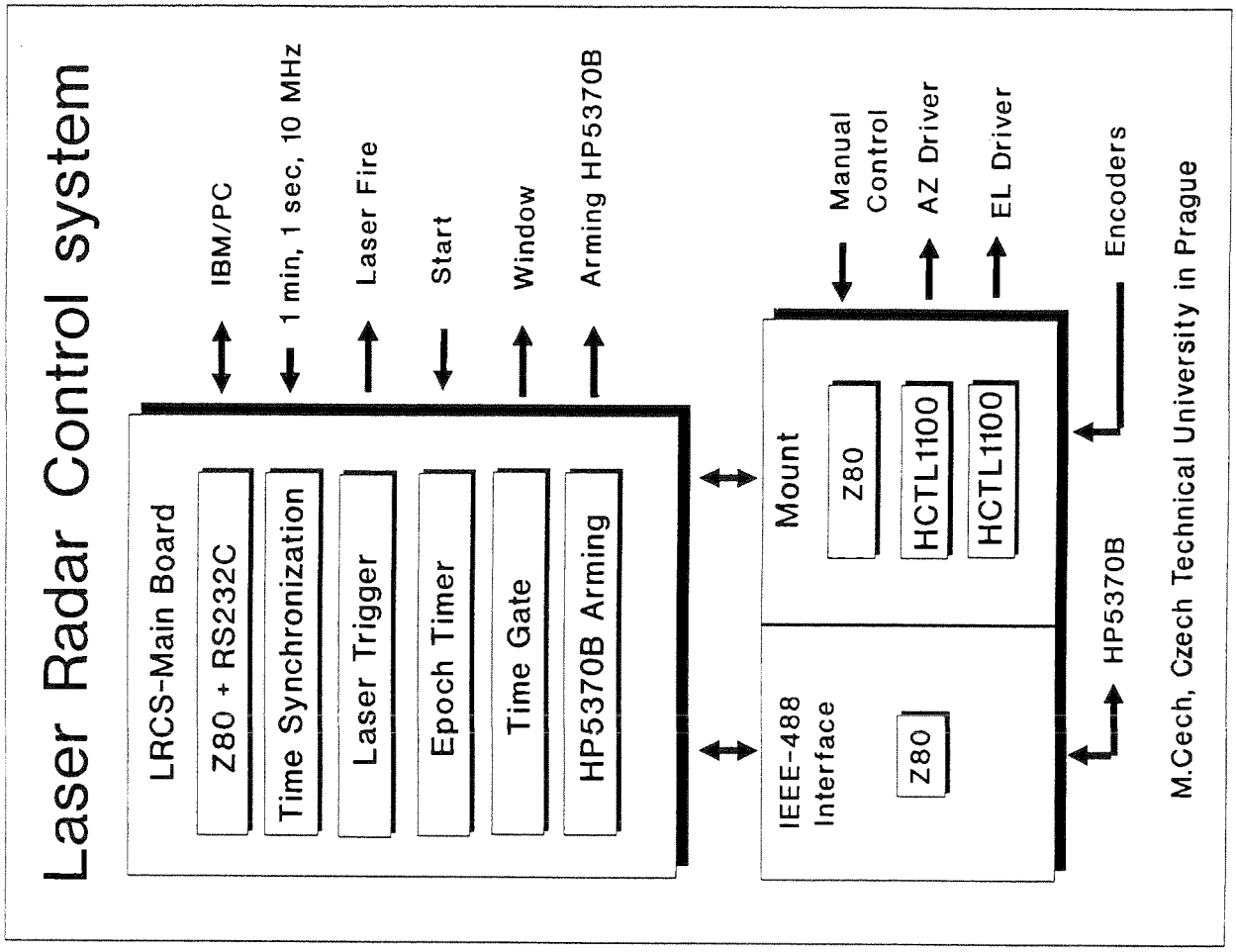
Laser Radar Control system
IBM/PC
1 min, 1 sec, 10 MHz
Laser Fire
Start
Window
Arming HP5370B
Manual Control
AZ Driver
EL Driver
Encoders
LRCS-Main Board
Z80 + RS232C
Time Synchronization
Laser Trigger
Epoch Timer
Time Gate
HP5370B Arming
Mount
Z80
HCTL1100
HCTL1100
IEEE-488 Interface
Z80
HP5370B
M.Cech, Czech Technical University in Prague

Fig. 2.

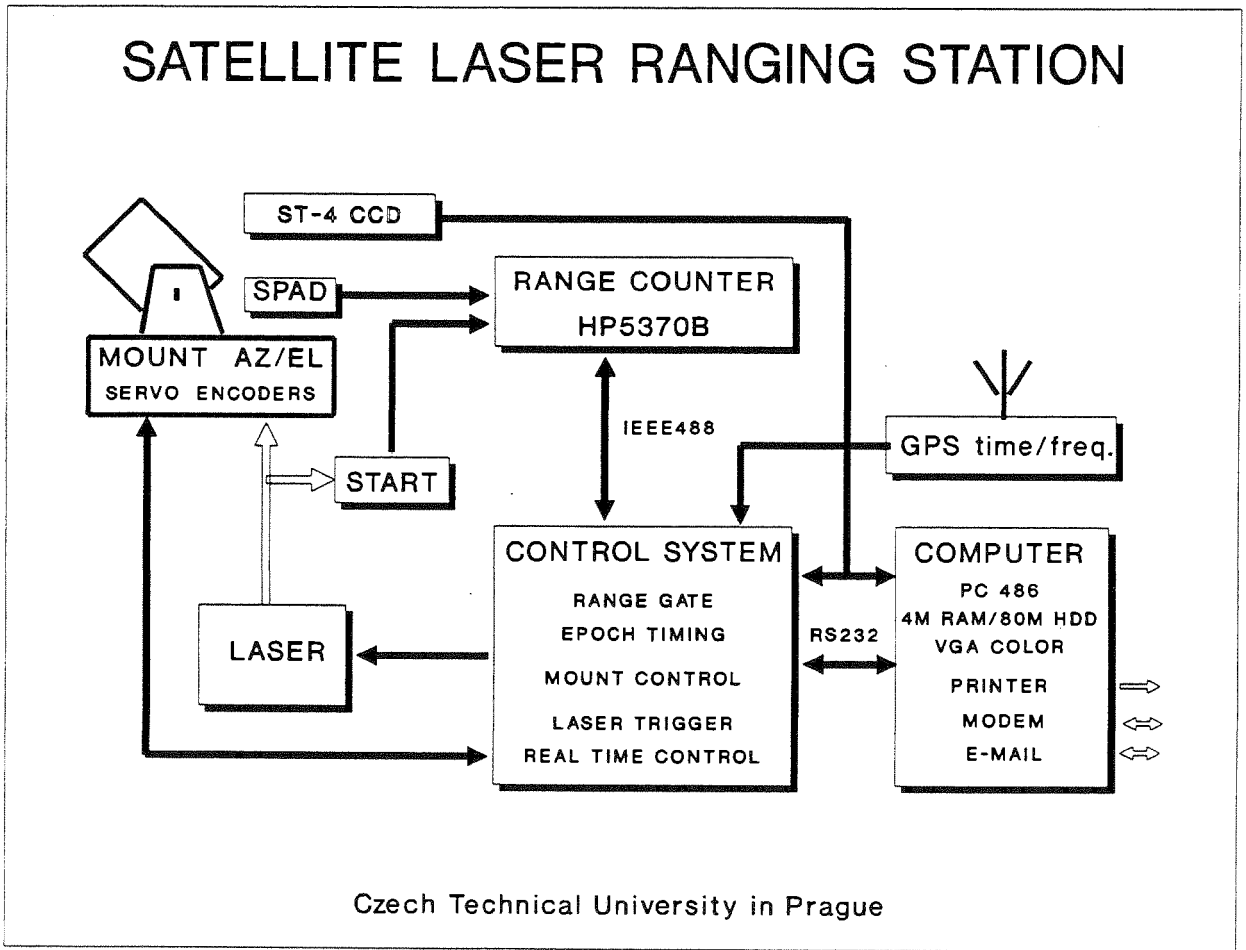
SATELLITE LASER RANGING STATION
ST-4 CCD
SPAD
RANGE COUNTER
HP5370B
MOUNT AZ/EL
SERVO ENCODERS
IEEE488
GPS time/freq.
START
CONTROL SYSTEM
RANGE GATE
EPOCH TIMING
MOUNT CONTROL
LASER TRIGGER
REAL TIME CONTROL
RS232
COMPUTER
PC 486
4M RAM/80M HDD
VGA COLOR
PRINTER
MODEM
E-MAIL
LASER
Czech Technical University in Prague

Fig. 1.

Laser Radar Control System

General	Laser radar control system-LRCS for full 10 Hz Lageos ranging with on-line graphics display
Configuration	• Time epoch counter • Time gate generator • Time synchronization with GPS • Laser trigger generator • HP5370B arming • IEEE-488 interface for HP5370B counter • Motors controller (DC servo or stepper motors) - incremental encoders
Parameters	
Laser trigger	0.1 - 1 sec, res. 100 msec
Time gate	100 nsec - 1 sec, res. 50 nsec
Time epoch	res. 100 nsec
Main computer	IBM PC/486 33 MHz EGA or VGA card Hard disk, Microsoft mouse RS232C port for LRCS comm.

M.Cech,Czech Technical University, Prague

Fig. 3.

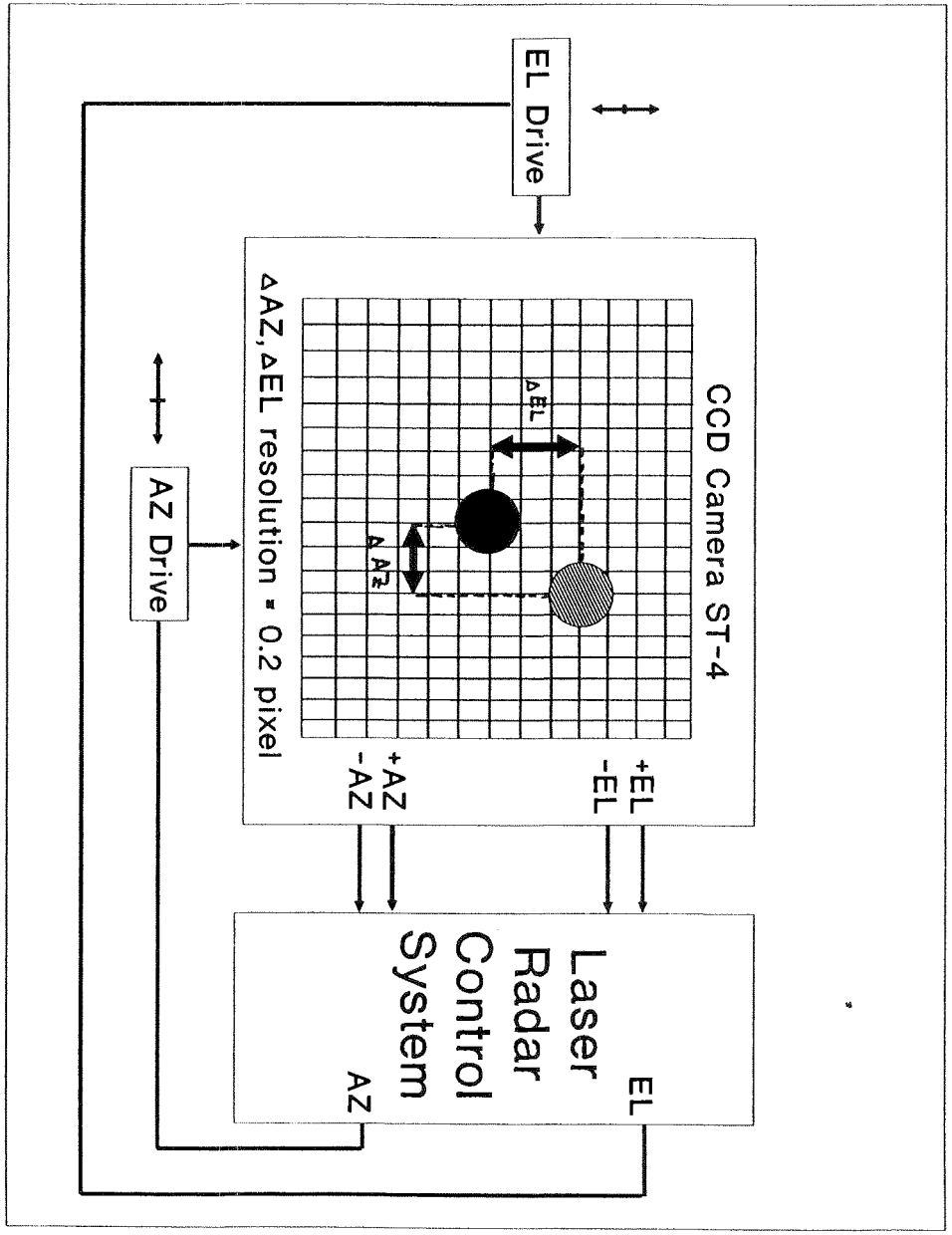

Fig. 4.

NASA Automated Quality Control

Van Husson, Julie Horvath, Grace Su
AlliedSignal Aerospace
AlliedSignal Technical Services Corporation
NASA SLR
7515 Mission Drive
Lanham, Maryland 20706 USA

Abstract - A feasibility study was conducted to determine what percentage of NASA Satellite Laser Ranging (SLR) data quality problems could be identified by an automated quality control algorithm in near real time. Quick identification of system performance problems is one requirement for SLR system automation. The results of this investigation show that at least 99% of the NASA SLR data problems can be identified by the field automated quality control algorithm in combination with following standard operating procedures. The results of our analysis and the current implementation status of this model are discussed in more detail in the remainder of this paper.

1. INTRODUCTION

AlliedSignal Technical Services (ATSC), formerly Bendix Field Engineering Corporation, has been responsible for NASA SLR Network data processing, analysis, quality control, and data management since the late 1970's. In the early and mid 1980's the NASA SLR network hardware was upgraded with 200 picosecond pulsed non-mode locked Quantel lasers, Micro-Channel Plate Photo-Multiplier Tubes (MCPPMT), cascaded Tennelec discriminators, and stable short range calibration targets [*Husson*, 1992]. These hardware upgrades coupled with improvements in ATSC data analysis techniques have improved the NASA SLR data accuracy from the 10cm level in 1980 to the sub-cm level in 1990.

The NASA SLR Data volume has increased 4-5 fold since 1991 (see Figure 1), and at the

Figure 1. NASA SLR Data Volume by Quarter

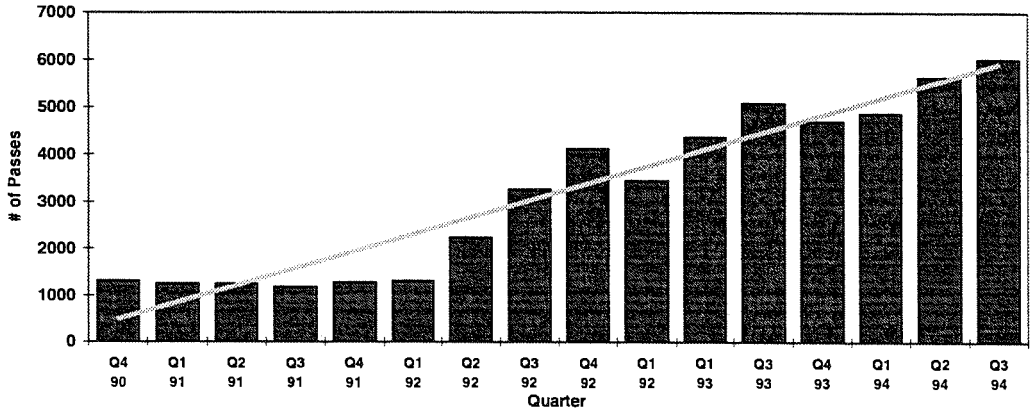

same time the NASA SLR budget has been steadily declining with possibly dramatic cuts planned in the mid to late 1990's. For these 2 reasons, ATSC performed a study to determine if an automated algorithm could be created to identify data problems in near real time at the field stations.

This model had to be designed so that approximately 95% of problem data could be identified in near real time, so that field personnel could take corrective action if required. At the same time the model had to be designed to minimize the flagging of non-problem data so that the field crews were not wasting manpower investigating non-problems. Problem data is defined as any data having a known systematic error or bias greater than 1cm. Over 50 years of ATSC data analysis experience was used to develop the first quality control (QC) model based on LAGEOS, and later other satellites were added.

Due to standardization of the NASA systems, the exact same algorithm can be used for each system. All of the NASA systems used in this study (MOBLAS-4, MOBLAS-5, MOBLAS-6, MOBLAS-7, MOBLAS-8, TLRS-3, TLRS-4, and HOLLAS) contain similar hardware and software configurations. These include the MCPPMT receive package, Tennelec discriminators, the HP5370 Time Interval Unit, external calibration, HP data processing computer, HP data processing algorithms, and data products. The on-site data products include CSTG normal points, CSTG sampled data, and Laser Mailing Tape (LMT) 88 byte raw data. Five years of NASA SLR LAGEOS-1 and LAGEOS-2 (1988 - 1993) data, consisting of a total of 11,167 passes, were used to benchmark this model (see Figure 2).

Figure 2. Benchmark Data Set

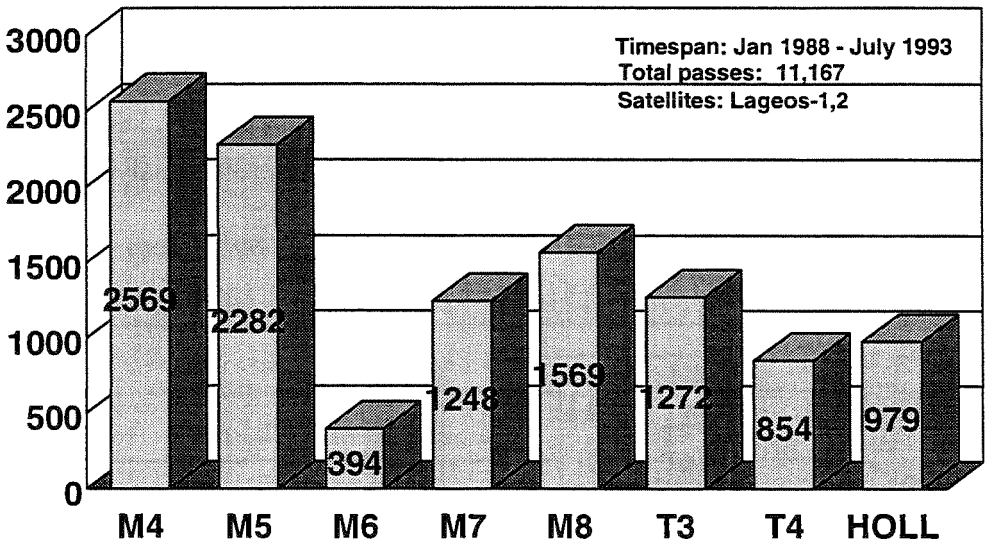

2. ALGORITHM

Below is the current algorithm that we have developed:

If satellite RMS > 150% of expected RMS or
if calibration shift > 10 mm or
if calibration RMS > 10 mm then

flag the data as being potentially bad

All three of these parameters (Satellite RMS, calibration shift, calibration RMS) are by-products of the field data processing system produced within minutes after the post-calibration is taken. Satellite RMS and calibration RMS are indicators of data precision not data accuracy. However, our experience has shown that when these values exceed these limits that accuracy of the data is severely degraded. Calibration shift is a direct measure of data accuracy and system stability. There are routine NASA SLR standard field operating procedures [*Gardner*, 1993] that also ensure data accuracy. These procedures include daily barometric comparisons, daily monitoring of station time via GPS, periodic multi-target stability tests, and daily reference frequency checks.

3. RESULTS

First we will discuss the data that did not pass the QC filter and determine what percentage of this data was actually problematic. Then we will discuss problematic data that would have not been flagged by this filter.

3.1 Potential Problem Data

Nine percent of the 11,167 passes did not pass the QC filter (see Figure 3). Not all passes flagged contained a serious data problem. Using results from orbital analysis, collocation

Figure 3. Potential Problem Pass Analysis by System

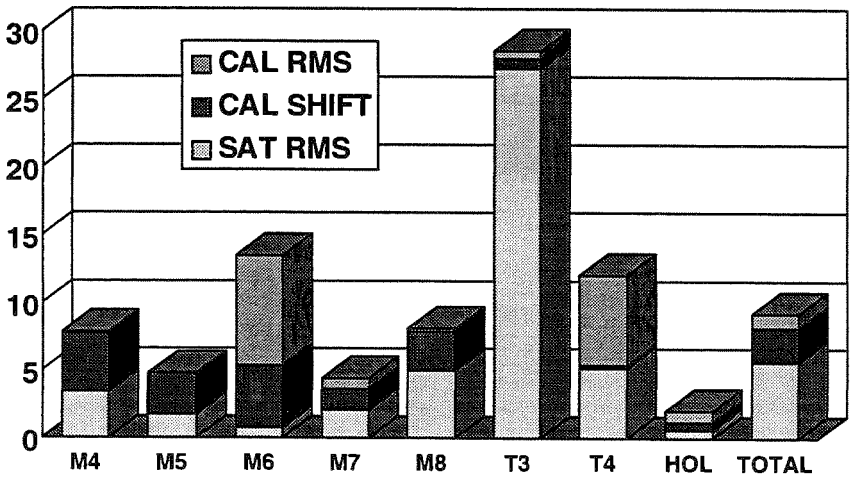

analysis, and specialized analysis, we could actually determine which passes from the benchmark data set were bad. This in-depth investigation revealed that 5% of the total data set had systematic biases and in addition flunked the QC filter (see Figure 4). However, the QC algorithm did not identify all the problematic data.

Figure 4. Real Problem Pass Analysis by System

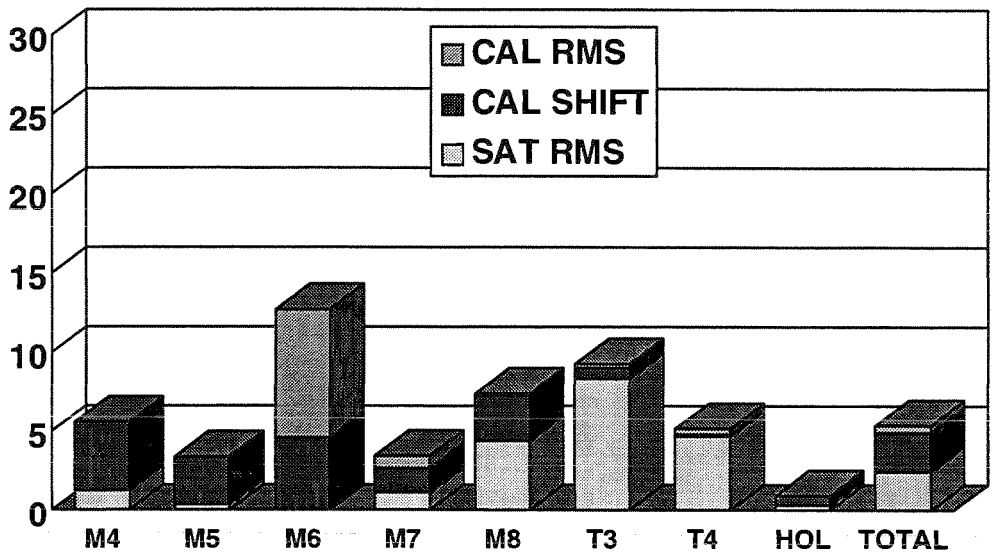

3.2 Real Problem Data

Fifteen percent of the total benchmark data set had significant errors, of which five percent were detected by the filter. The remaining ten percent of the data, had errors that would not manifest itself in either an abnormal satellite RMS, calibration shift, or calibration RMS. However, these problems, which affect accuracy but not data precision, are detectable through other routine operational procedures and ground tests. These procedures were mentioned previously in Section 2. For instance, reference frequency errors, changes in system eccentricities, timing errors, and barometric problems, in most instances do not degrade data precision but do impact it's accuracy.

4. CONCLUSIONS

Initially, the goal for the Quality Control model was to flag 95% of problem data and minimize the flagging of non-problem data. Actually, the filter flagged 85% of real problem data and only filtered 4% of total passes where the data was actually good. We discovered that data problems are system dependent, and most data quality problems occur in consecutive passes. With the combination of the automated QC algorithm and following standard operational procedures, NASA SLR data can be quality controlled at

the 1cm level with 99% confidence. Using this model instead of relying on headquarters analysis feedback, problems can be identified quickly by field personnel who then can take corrective action resulting in significantly less bad data. Figure 5 is a QC process map.

Figure 5. QC Process Map

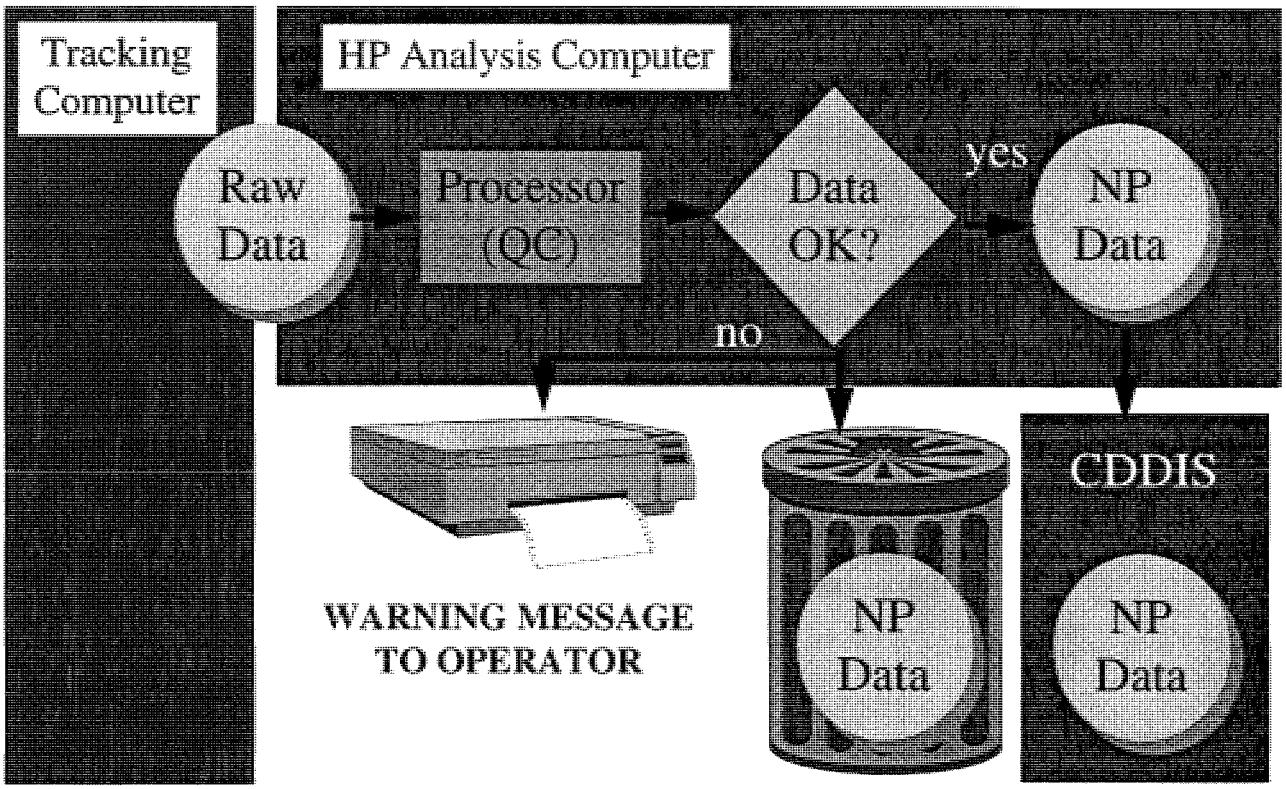

5. CURRENT STATUS

The QC Model is currently in place in MOBLAS 4, MOBLAS 7, MOBLAS 8, and HOLLAS. By April 1995, these model will be in place in all of the NASA SLR systems. This model will be enhanced as our knowledge grows and will be incorporated in SLR 2000.

6. REFERENCES

Husson V, "Historical MOBLAS System Characterization", Proceedings of the Eighth International Workshop on Laser Ranging Instrumentation, Annapolis, Md, May 18-22, 1992.

Gardner V, Murdoch A, "NASA Satellite Laser Ranging Network Operating Procedures", Revision 7, Dec 1993.

Automated Direct Detection Ranging Measurements for the US Naval Research Laboratory System

D. Roberts, A.R.Peltzer, A.T.Olson, G.C. Gilbreath, and R.A. McKnight Jr.

Abstract:

The US Naval Research Laboratory's satellite laser ranging system is being integrated at Phillips Laboratory's Starfire Optical Range in Albuquerque, New Mexico. The core design is based on NASA's direct detection system, with additional computerized automation and a new approach to time/frequency standards. Round-trip time delays for the gated photomultiplier tube are generated by a FORTRAN-based propagation program. Data acquisition and control of the round-trip delays, timing, and related instrumentation is conducted over an IEEE-488 interface bus using the C programming language on a 486PC. Other enhancements to the system include the incorporation of a GPS refreshed Rubidium time/frequency standard and a high speed waveform digitizer for detailed analysis of the returning optical pulse.

I. Introduction:

The US Naval Research Laboratory (NRL) is installing and integrating a laser ranging system at the USAF Phillips Laboratory's Starfire Optical Range (SOR) in Albuquerque, New Mexico. The overall design is based on NASA's direct detection system but features several enhancements. These include: automation of a significant portion of the system; a GPS refreshed time/frequency standard; and a high speed pulse digitizer for detailed analysis of returned optical pulses. The measurement sequence will be summarized first, followed by a detailed discussion of the automation scheme and timing standard.

II. Transceiver Operation:

A detailed block diagram of the transceiver is shown in Figures One and Two. The electronics associated with the transmit pulses and gate delays are summarized in the block diagram shown in Figure One. Receive pulse electronics are similarly summarized in

Figure Two. Descriptions of the two halves of the system are given in the following sections.

A. Transmitter Electronics

The measurement sequence begins when scattered 1.06 um light is detected from the laser cavity using a PIN diode, which is place in the laser enclosure near the source. The pulse width detected is on the order of 250 ps. The detected pulse is inverted and directed to the constant fraction discriminator (CFD) which corrects for potential timing ambiguities from varying pulse intensities. The CFD start channel provides three outputs: one to the SR620 Universal Time Interval Counter (UTIC) which starts the round trip time delay measurement, and the second and third to delay generators that trigger other events within the receiver.

The first delay component in the chain is the Berkeley Nucleonics (BNC) 7085. This unit provides the gating function for the return pulse detection. The BNC 7085 is automatically provided a delay value, from an IBM compatible 486 computer (PC486), based on predicted range from the target. The BNC7085 in turn triggers the Hewlett-Packard (HP)8082 delay width generator which provides a manually adjusted vernier delay for the purpose of fine tuning the total delay to an optimum value. (The vernier delay is digitally displayed by the second SR620 as an aid in setting the value.) The 8082 then triggers the BNC 6040 delay generator and the Avtech Pulse Transformer. This unit provides the high voltage pulse necessary to gate the photo-multiplier tube (PMT) used to detect the returning optical pulse. The BNC6040 provides a secondary delay that gates the stop channel of the CFD and provides the trigger for the display oscilloscope.

The second delay generator triggered by the start CFD is the Stanford Research DG535. The DG535 performs three functions upon receipt of the start pulse. It provides a pulse to the IRIG box to cue the time tag for the start pulse, it provides a default stop pulse to the stop channel of the round trip time delay UTIC in the event a return pulse is not detected, and finally, it triggers a second DG535 which is used to trigger the shutter for an intensified CCD camera that monitors the optical alignment of the receive train.

B. Receiver Electronics

The return sequence is initiated by returned optical pulses detected by an ITT F4129f MCP enhanced PMT. The PMT is gated by

the delay generators triggered on the transmit side. The PMT output is fed to a wideband amplifier that is required for very low level return pulse intensities. The amplifier output can be split between the stop channel input of the CFD and a high speed digitizing scope. The stop CFD is also gated by the BNC6040 as mentioned above in the transmit side. This gate is delayed by 2 us from the PMT gate to avoid triggering the CFD on PMT noise near the beginning of the gate. The stop channel CFD then triggers the stop channel of the SR620 UTIC, completing the measurement of the round trip time delay. A Tektronix 1 GHz analog oscilloscope is used as a visual aid in centering the return pulse in the gated window.

C. Timing Sequence

Because of emission limitations at the SOR site, it was not possible to perform calibration runs on ground based targets placed a distance away from the telescope. Therefore, calibration of the system is accomplished by making round trip time delay measurements to a retro-reflector mounted on the spider of the telescope. Since the distance from the retro to the geometric center of the telescope is known very accurately, the time delay between these two points can be calculated and subtracted from the total calibration round trip delay. The remainder of the delay is then attributed to the propagation delays in the measurement system and is applied as a correction factor to actual ranging measurements.

Since the calibration target is only meters away from the source, the round trip calibration delay is approximately 100 ns. This creates a problem in gating the receive electronics because the inherent propagation delays in the gating electronics exceed 300 ns. The equipment configuration to perform both calibration and SLR measurements is illustrated in Figure three.

The problem was solved by having start pulse N initiate the gating delay that will cause the PMT to be gated and ready for return pulse N+1. The laser pulse repetition interval is 100 ms (10 Hz). By adding 100 ms to the expected round trip delay, whether the measurement is for calibration or for an actual satellite target range, the PMT will be enabled by transmitted pulse N when returned pulse N+1 arrives. In this way, only the very first return pulse is lost and the entire laser/transceiver system configuration will be identical for calibration and actual ranging measurements.

III. Transceiver Automation

Transceiver operation is controlled by two separate controllers with different functions: a PC486 and a Macintosh IIfx.

The PC486 is the host computer for two functions. The first function is the computation of delay values from one or two line element sets for the targets of interest. From these sets, a FORTRAN based program is used to calculate the estimated round trip time delay to the target from the ground site as a function of time. This calculation is done prior to a pass and stored in a file. The second function of the PC486 is to provide control of the instrumentation for the transceiver and automated acquisition of round trip delay values. The data acquisition portion of the PC486 tasking is written in "C". Once the receiver registers a start pulse, an IRIG time code generator (TCG) gives the pulse a time tag. The PC486 is then flagged that an event has occurred. The PC486 then reads the time tag and polls the UTIC. Once the return pulse is detected, the PC486 reads the round trip delay measurement from the UTIC and correlates it to the IRIG time tag. Finally the PC486 sends the next predicted delay value to the BNC7085 to properly gate the PMT for the next return pulse.

Data acquisition and control of the digitizing oscilloscope is performed by the Macintosh using Labview software. The oscilloscope is used to record the return pulse waveform for further analysis. The scope is also capable of time tagging the recorded pulses so that they may be correlated to target position and orientation at a given time during the pass.

IV. GPS Time/Frequency Standard

The time/frequency reference chosen for this receiver is a Ball/Efratom GPS-RR receiver with integral Rubidium standard. In addition to the usual GPS functions of providing accurate time and position, the unit has an integral Rubidium atomic standard that is "steered" by the GPS receiver. Based on information the GPS receiver provides, the Rubidium oscillator is automatically adjusted every four hours for absolute time accuracy and every 24 hours for frequency accuracy. Using these techniques, the unit provides an absolute time accuracy to within 100 ns of universal time code (UTC) as generated by the GPS system and a 1E-12 short term frequency stability (100 s time average). The unit also provides the IRIG-B time code to the IRIG time code generator and the external 10 MHz reference to the round trip delay UTIC for accurate delay measurements. An additional component has been designed by NRL

to interface with the unit's 10 MHz output to provide stable 1000 Hz and 1 pps signals to be used by the telescope control electronics.

Summary

The Naval Research Laboratory is installing a high power, high precision SLR system at the Starfire Optical Range in Albuquerque, New Mexico. The transceiver incorporates some of the elements common to the NASA MOBLAS transceivers as well as a different approach to transceiver automation. This hybrid approach provides control of the transceiver functions throughout the measurement pass, recording of all pertinent data that includes high resolution waveform recording of returned optical pulses. The transceiver also includes a new and cost effective approach to maintaining accurate time and frequency references used by the receiver.

Future enhancements may include real time data transfer between the SLR transceiver and telescope control.

References:

[1] A.E.Clement, G.C.Gilbreath, R.Q.Fugate, J.M. Spinhirne, and J.J.Degnan, "Naval Research Laboratory's Satellite Laser Ranging Capability at The Phillips Laboratory Starfire Optical Range", Proceedings of the 9th International Workshop on Laser Ranging Instrumentation, Canberra, Australia, November, 1994.

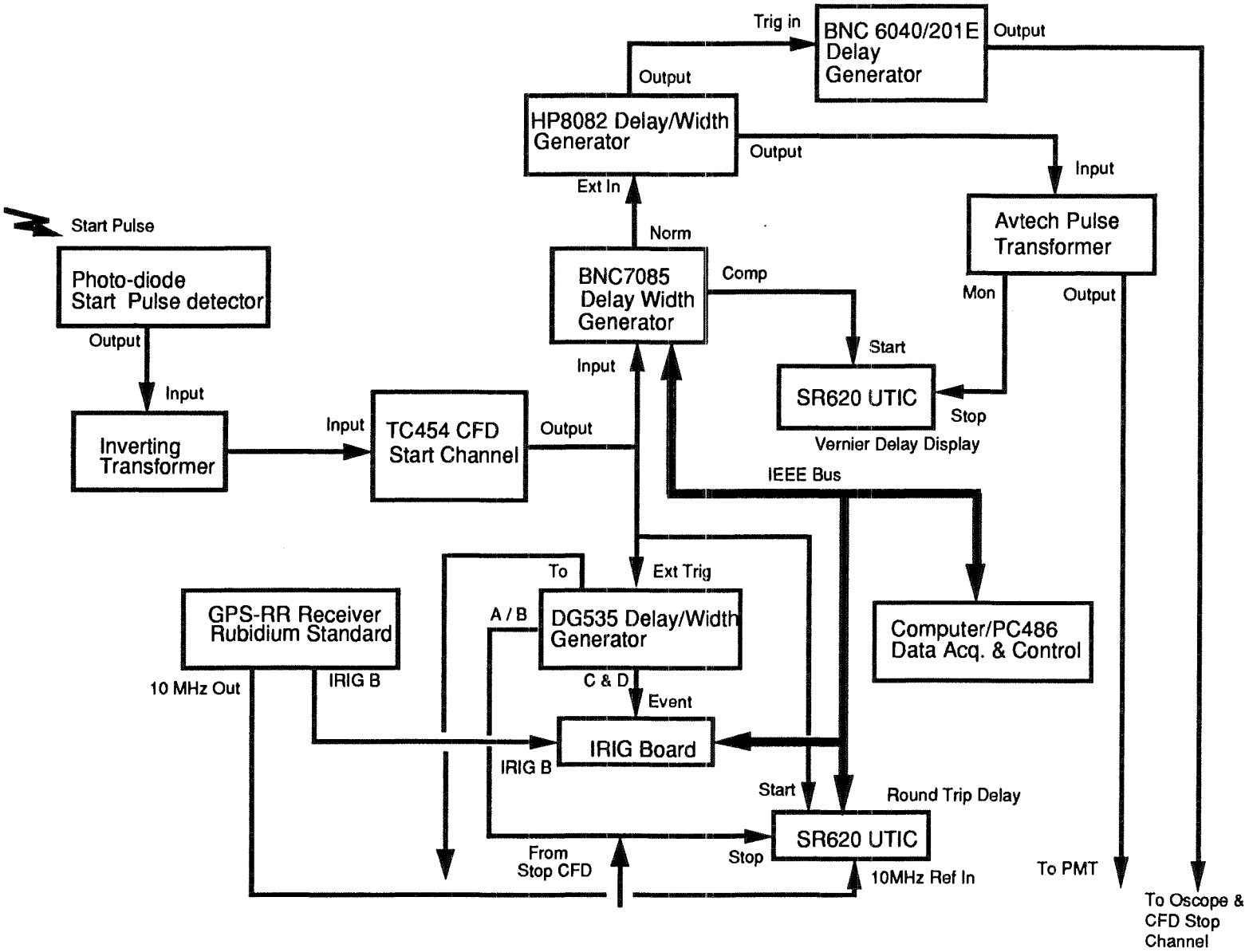

Figure 1. Electronics associated with transmitting optical pulses and generation of gate delays. Details provided in text.

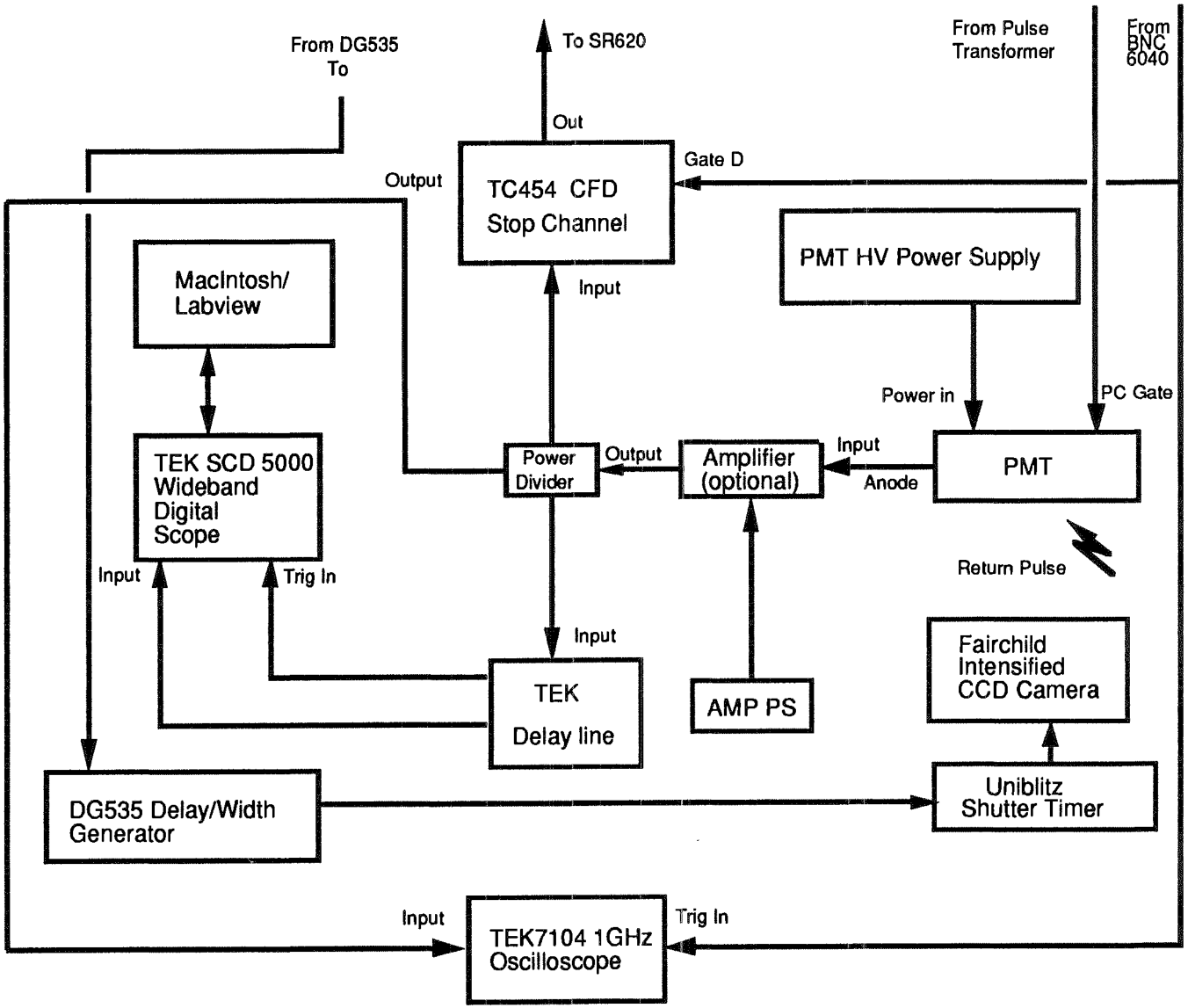

Figure 2. Electronics Associated with receiving and recording returned optical pulses for NRL system.

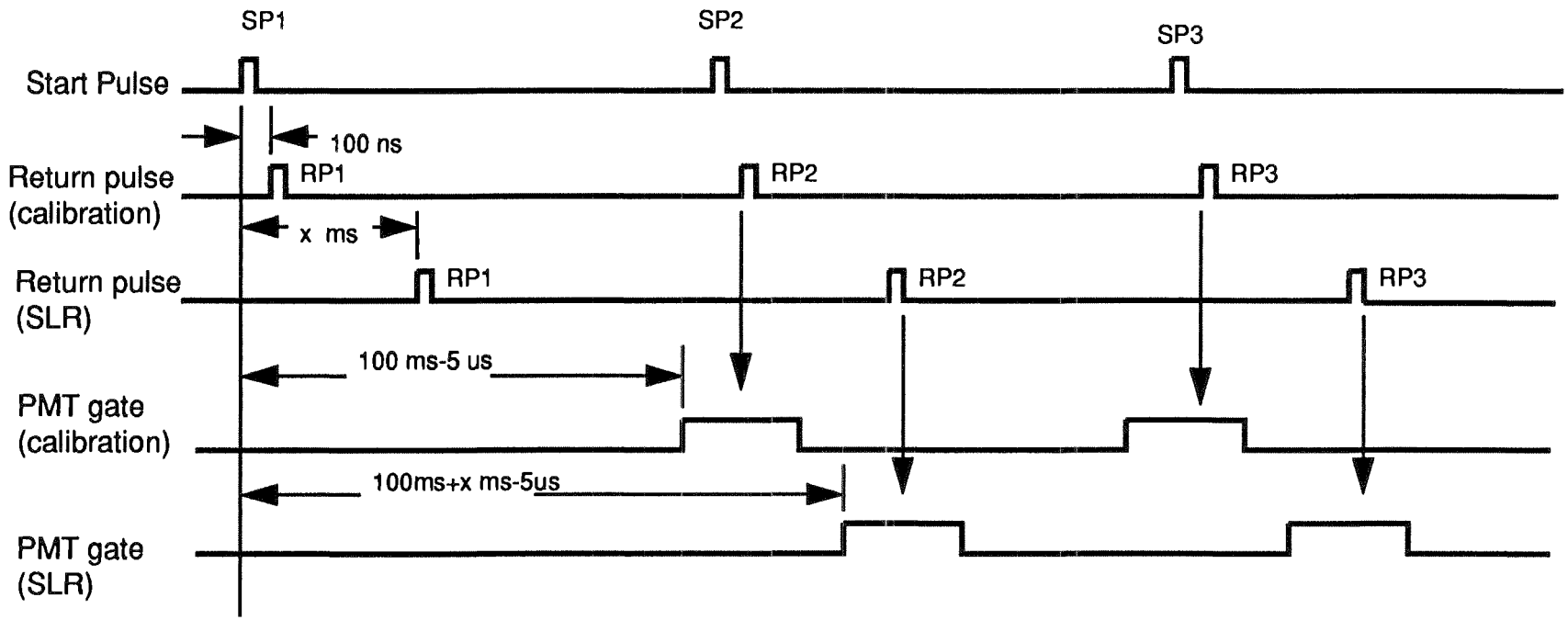

Figure 3. The timing scheme for the gating electronics is shown above. The goal was to keep the transceiver configuration identical for both calibration and SLR measurement runs. Since the round trip delays for calibration runs were too short for the transceiver electronics to handle, the solution to the problem was to have start pulse N provide the gate for return pulse N+1. Further details are provided in the text.

Automatic Pre-processing Method for Laser Ranging Data Using an Image-processing Algorithm

Toshimichi Otsubo* **(otsubo@crl.go.jp)**
Communications Research Laboratory (Headquarters)
4-2-1 Nukui-kita, Koganei, Tokyo 184 JAPAN

Tadahiro Gotoh
Kashima Space Research Center, Communications Research Laboratory
893-1 Hirai, Kashima, Ibaraki 314 JAPAN

1. Introduction

The raw data set of the laser ranging includes not only the signal (echo) returning from satellites or from the Moon but also the noises coming from sunlight, starlight or ground light. The noise elimination process, therefore, is necessary to produce the signal data set like the full-rate format, and the process is called "pre-processing," as one of the tasks in the laser ranging data flow. It has been performed by a computer, but usually with the help of men.

The noise will appear in spite of the narrow wavelength filter, the narrow telescope's reception angle and within the narrow gate width of the detection system. However, it is impossible to select the signal data from the noise data only by the least squares filtering, if the data set has many noises in such cases as the daytime ranging. In order to make the laser ranging system automatic, the noise elimination process should be performed without the manual editing.

In this study, let us define the x-axis as the observation time whose full scale is usually one satellite pass, and the y-axis as the residual range (= [observed range] - [predicted range]) whose full scale is the gate width applied for the detecting system. The noise points will scatter in the plane at random if the observation condition keeps unchanged for the period. On the other hand, the signal points will line up on a certain curve whose shape we cannot predict at the time of observation or pre-processing. The objective of this study is to establish a new automatic method to select the signal points and to reject the noise points.

2. Problems in Polynomial Least Squares Filtering

The CRL (Communications Research Laboratory) already has software for pre-processing called "*xmopp*" on UNIX X-window system, which has had the modules for the polynomial (0 to 25 degree) fit and the manual noise elimination. The procedure used to require the help of a man such as a mouse operation, always for the daytime ranging, and sometimes for the nighttime ranging. To reduce the noise, the gate width should be shortened, or the spectral filter of a narrow bandwidth should be used. However, there is a possibility to miss the signal itself.

Figure 1 shows the raw data of Etalon 1 pass on October 23, 1990, from the CRL Tokyo station. Including many noises, it is a typical data set for the daytime laser ranging. In this case, the signal to noise ratio approximates 1:2. From now the noise elimination procedure is discussed using this example.

Without the manual filtering, the noise data could not be rejected at all as shown in Figure 2 in which only one noise was rejected. The 16th-degree polynomial curve was drawn in the figure because the RMS (root mean squares) of the post-fit residuals was the "best" in the polynomial fitting from 0th to 25th degree.

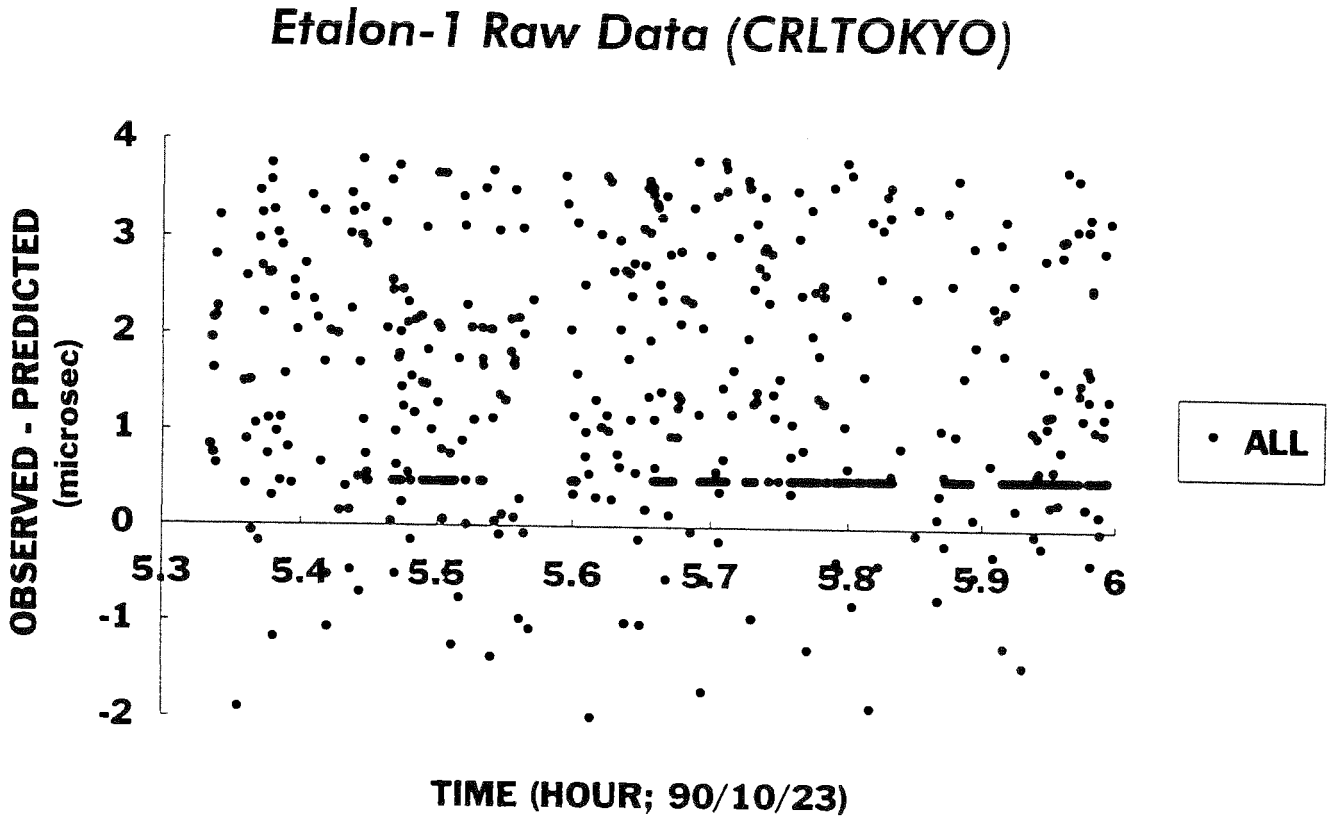

Figure 1: Raw range data of Etalon 1 from CRL Tokyo station around 6:00 UT, October 23, 1990.

In this way, the polynomial rejection cannot work in this case. However, a man can detect the curve. Why can he?

3. "BROOM" Method

Now, let us change the point of view from rejecting the noise to selecting the signal. We contrived a new algorithm (*"broom"*) to detect the curve in the scattered noises using a fundamental technique of the image processing.

3.1. Algorithm

First, the x-y plane should be divided into many square partitions which are defined as the equivalence of the *"pixel"* in the image processing technique. The size of each partition should be determined from the return signal rate in time and from the precision of the predicted orbit. In our operation, the size is usually set to 10 seconds in time axis and 50 nanoseconds in O-C axis.

Second, the number of points in each partition should be counted. If there are only the noise and the observation condition does not change in time, the points will be scattered in the x-y plane

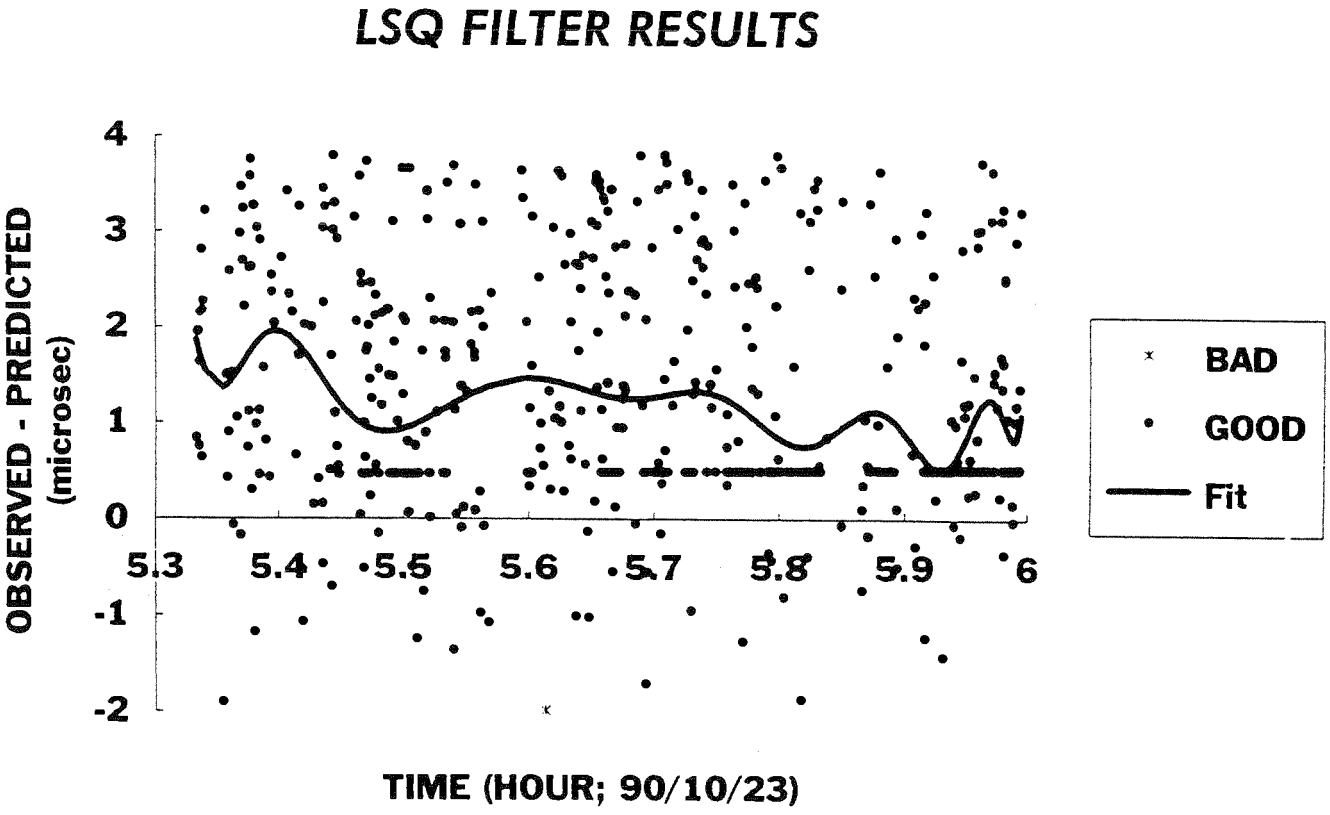

Figure 2: Fitted 16th-degree polynomial curve for the Etalon 1 data and the results of noise rejection by the three-sigma criterion.

at random. The probability (b) containing k points in each partition follows the binomial distribution and is written as:

$$b(k;n,p) = \binom{n}{k} p^k (1-p)^{n-k} \tag{1}$$

where

n : total number of points

p : probability for a points to come in a certain partition
= reciprocal of the number of total partitions

On the other hand, the signal will be unusually concentrated on a certain curve and will not follow the binomial distribution. In other words, the signal data will make high density partitions, and the high density partitions is expected to include the signal data. In the selection of dense

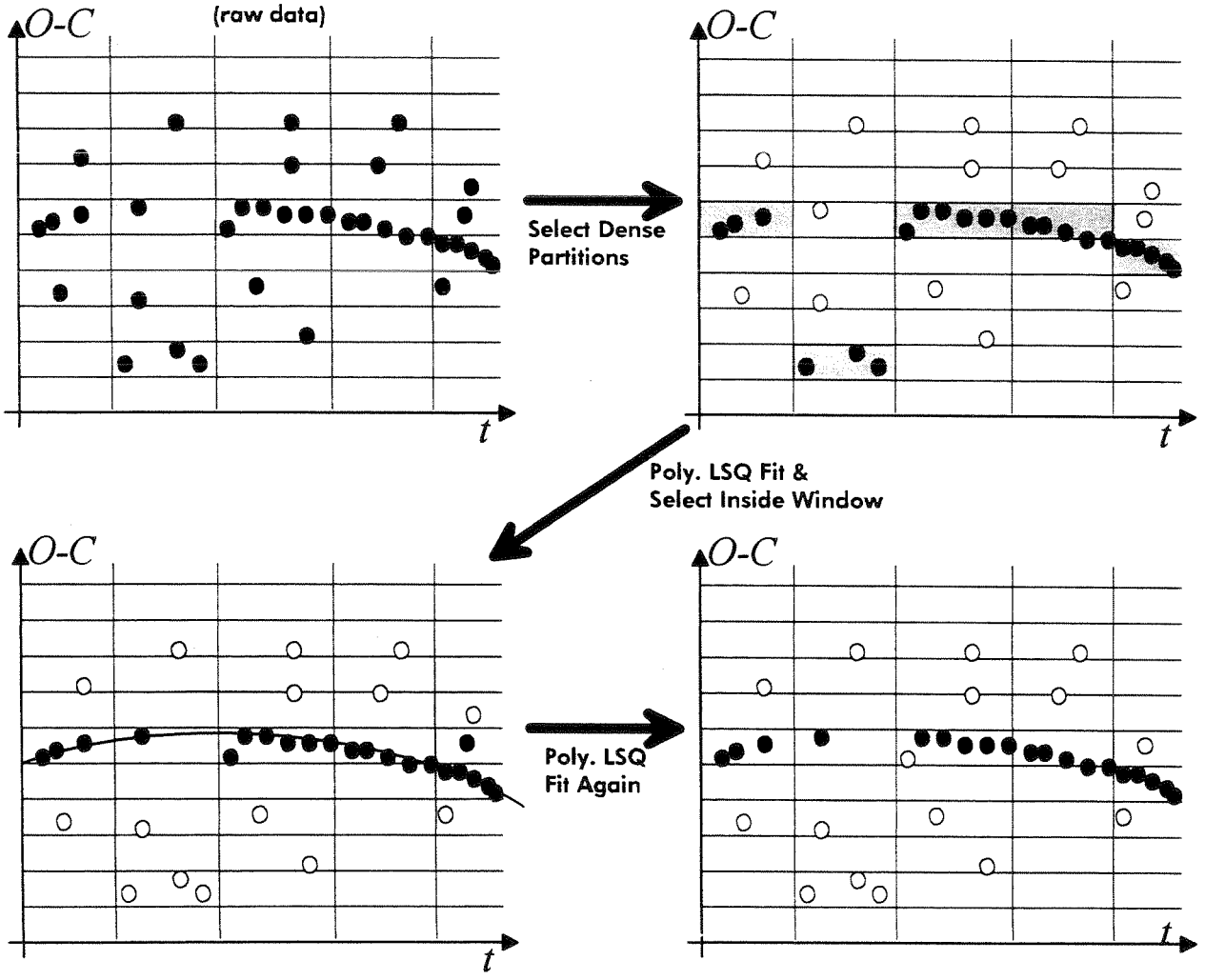

Figure 3: Broom algorithm.

partition, the equation (1) was applied to determine the threshold level of the number in a partition. The maximum probability is set to 0.1 % in our operation, which means the noise-only partition will be selected only once in one thousand. The threshold number $k_{threshold}$ of the density is hence determined by the equation (1).

Third, a best-fit polynomial function for the selected signal data in dense partitions should be estimated by the least squares method. Then, the selected noise at this stage will be rejected by three-sigma criterion. Because some signal data in sparse partitions may be rejected here, the points around the best-fit curve should be revived.

Lastly, the least squares estimation should be done again in order to reject the noise data that exist close to the best-fit curve determined in the previous phase.

Figure 3 shows the total flow of the broom algorithm.

3.2. Results

Figure 4 is the result of the broom filtering applied to the Etalon 1 pass. The signal and the noise were completely classified as well as the manual filtering, except for some selected noise data

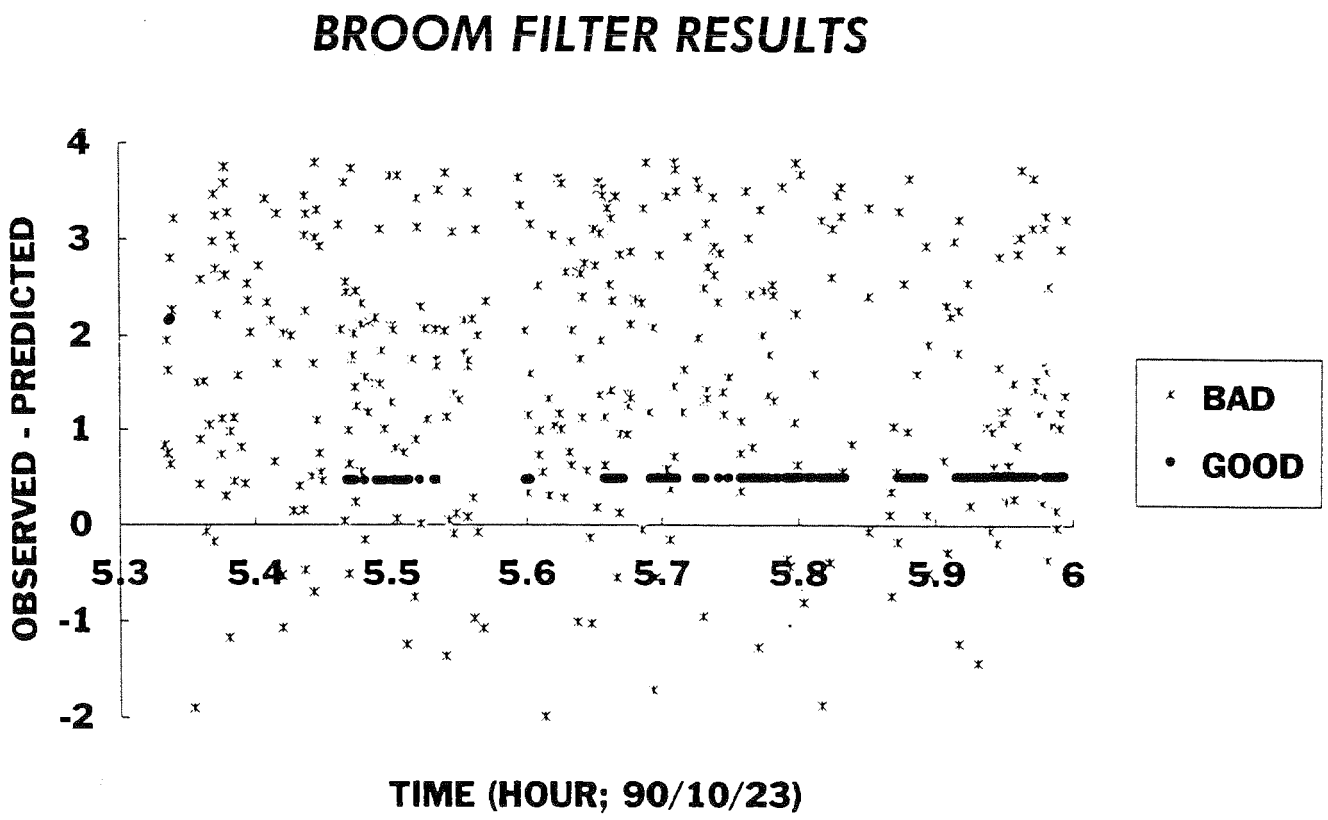

Figure 4: The results of noise rejection for the Etalon 1 data by the broom algorithm.

at the beginning. The selected noises at the beginning or at the end are not serious, since such a small number of noise data can be easily rejected by the orbital analysis software.

4. Conclusion and Future Plan

We discussed the effectiveness of the broom filter using one sample of the Etalon 1 pass, and the method was proved to be powerful for the noise elimination of laser ranging data.

A simulation test was also performed as a feasibility study. It showed that the method can be applicable even in such a bad condition as the number of signal/noise = 100/2000, if the noise points are scattered at random in the x-y plane.

This method is already used to process our ranging data, and it was proved to be applied to more than 90 % of ranging passes. For some data sets which include only a small number of signal data less than one hundred, it sometimes does not work. To make the filter fully automatic, this problem should be solved in the future.

We also have a plan to modify this method for the real-time signal/noise classification. For the automatic tracking system this kind of filtering method is promising.

References

Tan Detong, et al.: "Application of the Robust Estimate in SLR Data Preprocessing," *Proceedings of 8th International Workshop of Laser Ranging Instrumentation*, May 1992.

Tracking Satellites with the Totally Automated SLR2000 System

Jan F. McGarry
NASA Goddard Space Flight Center

Brion Conklin, William Bane, Richard Eichinger, Paul Seery
AlliedSignal Technical Services

Randall L. Ricklefs
McDonald Observatory, University of Texas

Peter J. Dunn
Hughes/STX

NASA is developing a totally automated system, called SLR2000, which is designed to operate for months without human intervention. This system must automatically choose a satellite to track, control the tracking and ranging to the satellite, determine if the system is getting satellite returns, and close the tracking loop to acquire and then optimize the satellite returns. Because SLR2000 must be eye safe, all of this must be done in a low probability of detection and potentially high noise environment. To permit SLR2000 to accomplish these autotracking tasks, our team has been looking into (1) improving the predictions to remove as much error in the pointing and ranging as possible, (2) using lunar ranging techniques to determine returns from noise, and (3) developing scanning techniques to automatically acquire the satellite. We are also developing a Monte Carlo simulator to allow testing of the SLR2000 autotracking techniques by simulating the relevant system errors and then checking the performance of the autotracking algorithms against the system truth.

Background/Introduction

SLR2000 is NASA's concept for a totally automated Satellite Laser Ranging (SLR) system [Degnan 1994], designed to track satellites up to LAGEOS altitude. The system is expected to operate around the clock for months without human intervention, communicating electronically with a central facility, receiving schedules and predicts and sending back satellite ranging data. The system will be eye-safe, transmitting around 100 microjoules per pulse at 2kHz with a laser divergence of a few arcseconds. The desired return rate is at least five returns per second. Due to the low energy level, the system must operate at a low receiver threshold level which will result in a potentially high noise environment during daylight operations.

Tracking satellites with this totally automated system will involve several issues. The system must be able to search for and acquire satellites from predicts that may not be exact. To acquire and track, the system must be able to determine signal from noise in the range window, and must be able to follow the signal by modifying the predicts as needed in realtime. The system must also

be able to determine (1) when operations should not occur (such as due to precipitation or system health), and (2) when a satellite search would be futile due to clouds or heavy haze. These last two are issues that must be addressed, but will not be discussed here.

This paper discusses our preliminary development work in automating the processes of determining signal from noise, and of acquiring and tracking satellites. Our work involved the development of a Monte Carlo satellite laser ranging system simulator, whose design, development, and use in testing autotracking algorithms is also presented.

Determining Signal from Noise

SLR2000's potentially high false alarm rate and relatively low probability of detection make the determination of signal from noise similar to the lunar case. One of the algorithms under investigation makes use of the lunar Poisson Filtering technique [Abbot 1973]. This technique assumes the noise follows a Poisson distribution. The range returns are binned into a histogram in the O-C (observed minus calculated) space. Each bin in the histogram is then tested against the probability that it is noise. Any bin whose probability of being noise is less than 50% is considered signal. The signal bin with the most number of data points is the actual bin chosen. This technique works well in the lunar environment and has worked well so far in the simulated SLR2000 environment. There is, however, one problem in the use of this technique which must be overcome: satellite range data does not have always have a zero slope in O-C space, making it difficult to histogram. The magnitude of the slope is a function of the timebias error and the error in the knowledge of the station location. Some work has already been done on using this technique in the nonzero slope satellite environment [Ricklefs 1992], but a final resolution of the problem remains to be found.

Figure 3 shows simulator results of an autotracking algorithm which determines the signal from the noise using the lunar Poisson Filtering technique. In these plots the dots represent returns in the range window (both noise and satellite), the boxes mark the actual satellite returns (which the simulator knows, but which the autotracking algorithm has no knowledge of), and the "X"s mark the returns that the autotracking algorithm has determined are actual satellite returns. The top plot shows the Poisson Filtering algorithm working in a low probability of false alarm and low probability of detection environment ($p_{fa}<0.001$, $p_{det}<0.001$). The algorithm has correctly picked four out of the five actual satellite returns, and identified the one noise return correctly. After determining the signal from the noise, at shot 4000, the autotracking algorithm corrected the predicts and centered the data.

The center plot of Figure 3 shows the Poisson Filtering algorithm working in a high probability of false alarm environment. Boxes

and "X"s have been left out of this plot due to the large amount of data. The satellite returns, however, can be identified as the line in the otherwise random data. As the algorithm finds the actual satellite returns, it corrects the predicts to center the data and closes down the range window to reduce the noise. The windows shown are 1 microsecond (shots 0 to 2000), 100 nanoseconds (shots 2000 to 4000), and finally 10 nanoseconds (shot 4000 on). As the window closes at shot 2000, the probability of detection increases from 0.04 to 0.13, and the probability of false alarm decreases from 0.91 to 0.23. The bottom plot of Figure 3 is a section of the this middle plot enlarged to show detail. The boxes and "X"s displayed here have the same meaning as in the top plot.

Other methods of determining signal from noise have been proposed and will be investigated in the coming months with the use of the simulator.

Acquisition

Members of the NASA SLR2000 team have been investigating updating the satellite ephemeris on a daily basis to minimize the time spent in acquisition. For those satellites whose orbits are well known, updating the orbits and transmitting the predicts to the site daily should allow the system to open loop track. Tests run on STARLETTE and LAGEOS are encouraging, showing range prediction errors of less than 20 nanoseconds and angular pointing errors of only a few arcseconds.

But open loop pointing cannot be achieved for all satellites, especially for those satellites just launched. We anticipate that for new satellites, where the predicts are very bad, SLR2000 will have to wait for sunlit passes at night, where a CCD camera or other optical aid will be used to correct the angular pointing.

Even for well known orbits, an acquisition sequence will certainly be required at times, including initial site setup when the station location may not be well known. Acquisition will involve a search pattern in the sky in three dimensions: time, crosstrack, and range. The range window will be opened to the maximum (1 microsecond) and will be moved around the nominal predicted location, in a coordinated search along with changing the timebias and crosstrack bias. The beam divergence can also be increased to help in the search for low earth orbiting satellites. In this search, the signal detection algorithm continues to run, determining which returns are noise and which are actual satellite returns.

Tracking

Once the system has determined that it has actual satellite returns in the range window, the system will switch from acquisition to tracking mode. Here the time and range biases are calculated from

the range data, and are then applied to the predicts to center the range returns in the window. The range window is then closed down to reduce background noise. The signal to noise determination continues throughout tracking. In tracking mode, the window will eventually be closed to its minimum value (nominally 10 nsec) and the software will continue to refine the time and range biases and apply them to the predictions. Actual orbital update with tracking information will take place onsite between passes (ie non-realtime).

SLR Simulator

The SLR simulator was developed to checkout candidate autotracking algorithms prior to hardware development (see Figure 1). The simulator can be used to test algorithms for: (1) determining signal from noise, (2) automated acquisition and tracking, (3) realtime prediction update, and more. The program models the tracking subsystem, the receiver subsystem, the laser, the satellite, the environment, and their associated errors. Only those parts of these subsystems that affect the autotracking are modelled; there is no attempt to make a complete system model and only as much detail is added as is required. The functions/errors modelled in the simulator are shown in Table 1. The models were obtained from John Degnan [Degnan 1993] and Jim Abshire [Abshire 1994]. Table 2 lists the nominal SLR2000 parameters used in the attached test results.

The following are the current outputs from the simulator:

For information:
(1) Summary of information for each shot indicating hardware inputs and outputs, algorithm decisions, and actual satellite location.
(2) Calculation of probability of detection, probability of false alarm, and average return signal strength.

For plotting:
(1) All returns in the range window.
(2) Actual satellite returns in the range window.
(3) Autotracking algorithm's selection of satellite returns.
(4) Satellite truth vs actual mount pointing.

Figure 2 contains three plots of simulator output showing SLR2000's expected signal and noise within a 100 nanosecond range window. The top plot is STARLETTE as seen by the station at 20 degrees elevation. The roundtrip time to the satellite was 13.7 milliseconds. This data was simulated with a threshold of 1 photoelectron (pe), and shows STARLETTE to be a relatively easy target for SLR2000. In this run there was no noise in the window. The probability of detection was 80%.

The middle plot is LAGEOS as seen from the station at 60 degrees elevation, using a threshold of 1 photoelectron. The roundtrip

time to the satellite was 42.2 milliseconds. While the signal was sparse (p_{det}=0.02), there were enough returns available for the Poisson Filtering algorithm to correctly find the satellite. The algorithm response, however, is not shown in this plot.

An alternative configuration for LAGEOS is shown on the bottom plot. Here the same pass is taken, but with a threshold of zero. This results in more signal (p_{det}=0.3), but also more noise (p_{fa}=0.2). Since the Poisson Filtering algorithm can correctly find the satellite in either case, it would be advantageous to use the zero threshold if data quantity is an issue.

Status/Future Work

Work on the SLR2000 design is still in a very early phase. The SLR simulator has been developed and initial testing has been completed. This simulator has already become a very useful tool in the autotracking algorithm development. In the coming year an APD receiver model will be added, and further testing of the autotracking algorithms will occur. Work will also continue on the analysis of updating the ephemeris daily in order to minimize the time spent in acquisition. As the autotracking algorithm develops, sections of this algorithm will be ported to NASA's 1.2m telescope for field testing. Final testing must await the design and development of a Prototype SLR2000 system, whose concept is actively being pursued by a small group at NASA.

References

Abbot, Richard I., Peter J. Shelus, et al, "Laser Observations of the Moon: Identification and construction of normal points for 1969-1971," The Astronomical Journal, Vol 78, No.8, October 1973.

Abshire, James B., Jan F. McGarry, et al, "Laser Altimetry Simulator, Version 3.0," NASA Technical Memorandum 104588, January 1994.

Degnan, John J., "Millimeter Accuracy Satellite Laser Ranging: A Review," Contributions of Space Geodesy to Geodynamics: Technology, Geodynamics 24, American Geophysical Union, 1993.

Degnan, John J., "SLR2000: An Automated, Eyesafe System for the Future," in this Proceedings.

Ricklefs, R.L., P.J.Shelus, "Poisson Filtering of Laser Ranging Data," Proceedings of the Eighth International Workshop on Laser Ranging Instrumentation, NASA Conference Publication 3214, May 1992.

Table I
Functions/Errors currently modelled in the Simulator

- Pointing System
  - Bias of mount system (error in mount model)
  - Random repeatability error

- Receiver Timing
  - Model receiver (PMT currently; APD later)
  - TIU error modelled as random Gaussian noise
  - Assume no gating error or start time error
  - Compute background noise above threshold
  - System delay bias can be applied

- Receiver Energy
  - Assume fixed transmitter energy
  - Assume Gaussian pulse
  - Compute transmitter gain as function of laser divergence
  - Attenuate with system and atmospheric transmission
  - Attenuate as function of pointing error
  - Treat satellite as single cube with given cross-section

Table II
Hardware Parameters for SLR2000 Test Runs

Shotrate	2000 Hz
Wavelength	532 nanometers
Spectral filter	10 Angstroms
Laser divergence	4.0 arcseconds (full angle)
Transmit energy	75 microjoules
Mount repeatability	1 arcseconds (1-sigma)
Mount model error	1 arcseconds (1-sigma)
System delay	20 nanoseconds
Tiu error	100 picoseconds (1-sigma)
Receiver area	0.071 meters**2
Receiver FOV (solid angle)	9.6D-10 sterradians
System transmission	0.54
Detector quantum efficiency	0.20
System impulse response	200 picoseconds
PMT dark current	2.0D-13 amps
PMT gain	200.
PMT load resistance	50. ohms
Atmospheric transmission	0.92 (at zenith)
Solar irradiance (day)	0.014 Watts/Ang-ster-meters**2
LAGEOS lidar cross-section	7.0D6 meters**2
STARLETTE lidar cross-section	0.8D6 meters**2

SLR2000 SIMULATOR

Tool for use in algorithm development and checkout

Use to examine algorithms for:
(1) Determining signal from noise, (2) Auto Acquisition/Tracking, (3) Realtime prediction update

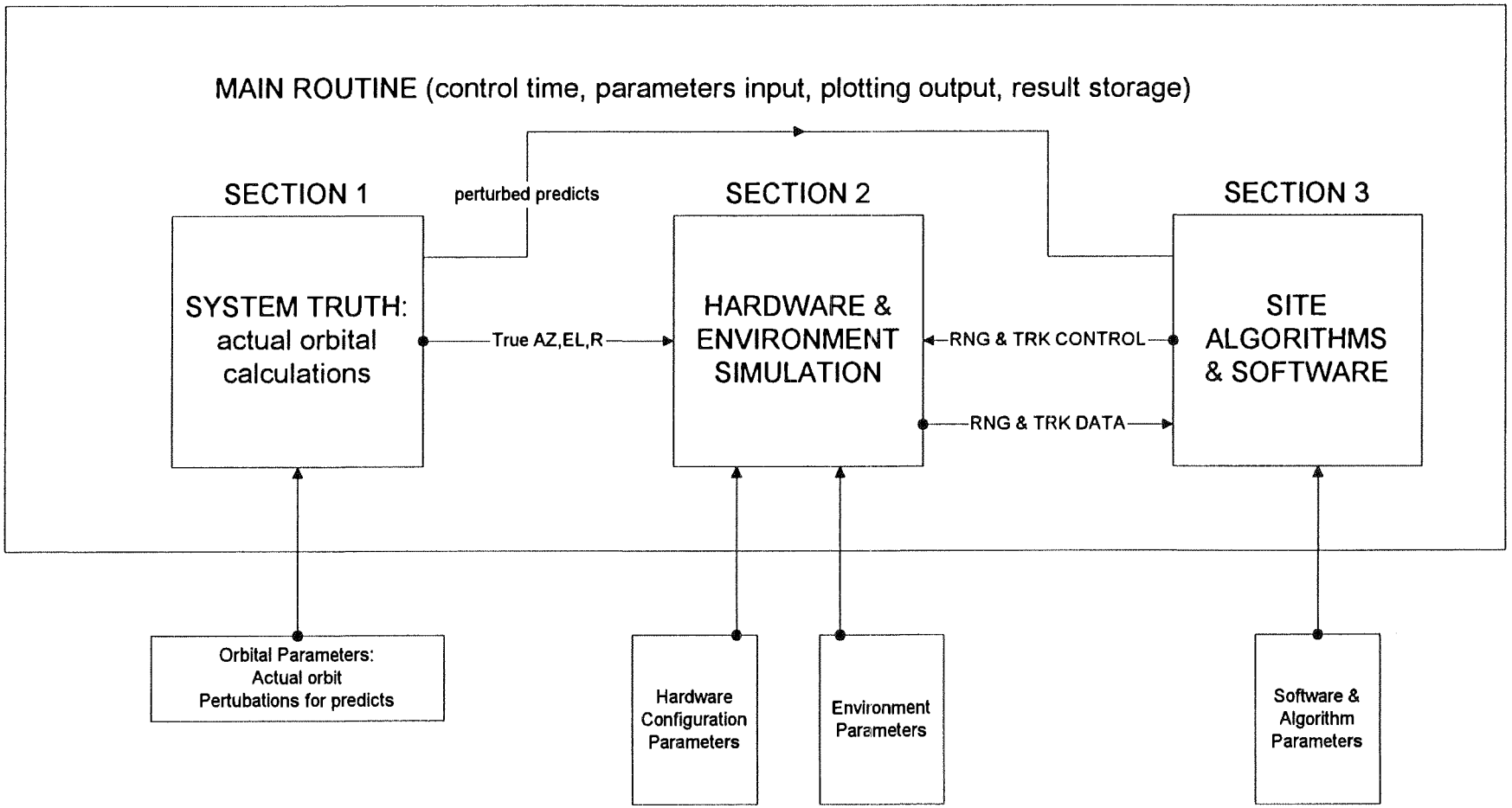

Figure 1

Figure 2: Simulated Satellite Data

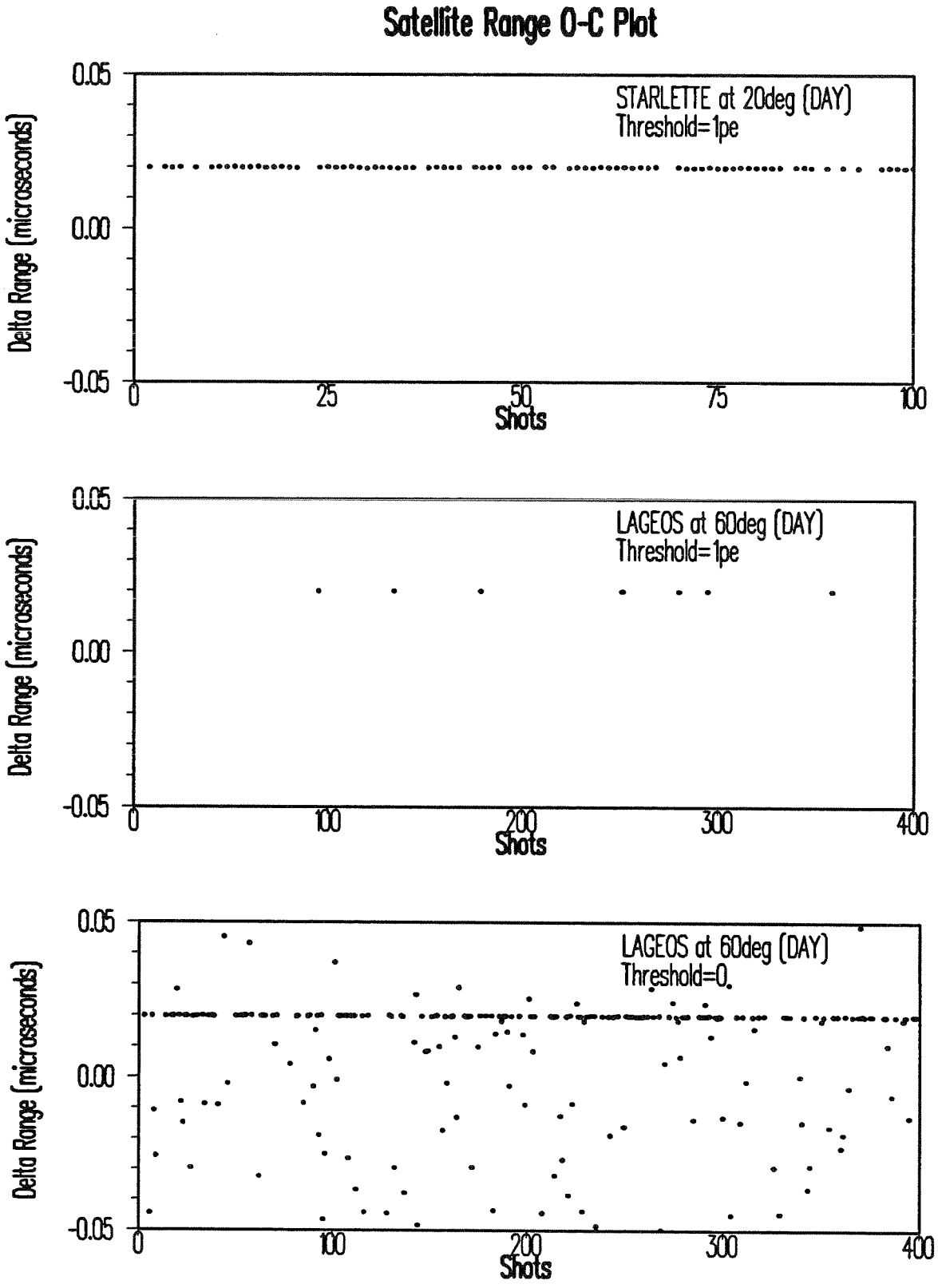

Figure 3: Autotracking Algorithm Response
to Simulated Satellite Data

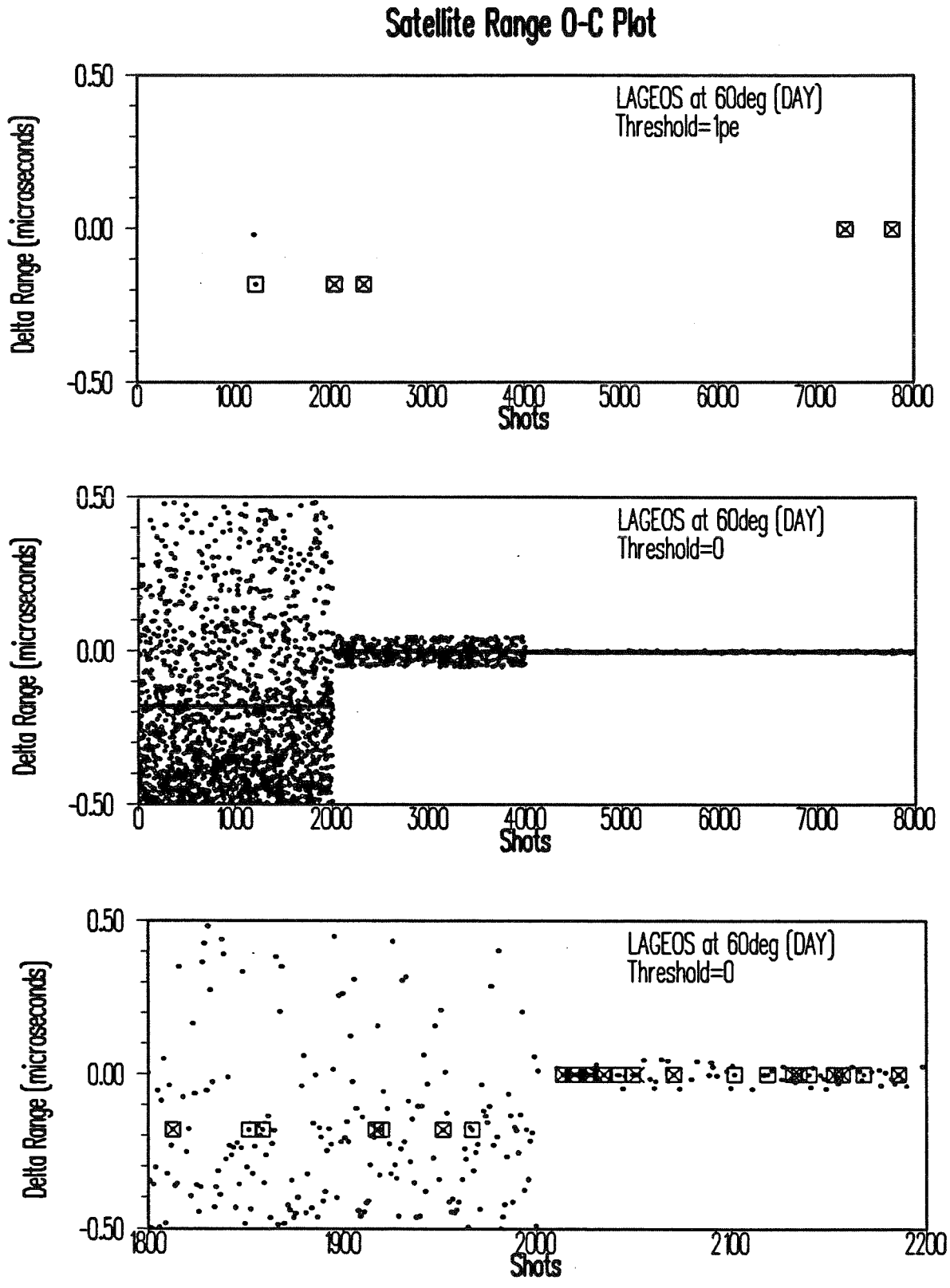

An Optimizing Satellite Tracking Shift Scheduler

presented at
9th International Workshop on Laser Ranging Instrumentation
Canberra, Australia
November 6-11, 1994
Session:
System Automation
and
Operational Software

by
Daniel J. O'Gara, Michael T. Maberry
University of Hawai`i
LURE Observatory
Institute for Astronomy
Mt.Haleakala, Maui, Hawai`i

Summary

In the last two years, the number of artificial earth satellites being tracked at LURE have increased from 6 to 13. It became increasingly difficult to schedule the two shifts operating at LURE so that the optimum number of satellites were attempted.

The programs RESOLVE and SCHED are used in concert to help schedule optimum operations shifts given the complete list of visible passes for a given time period. The program RESOLVE is run first to resolve the pass time conflicts based on the selected priority for each target. The program SCHED is then run on the output of RESOLVE. The program SCHED would usually be run multiple times, using different input parameters, until the desired schedule is produced. These programs have significantly reduced the time needed to produce the weekly tracking schedules.

RESOLVE and SCHED were written in F77 and currently run on the DEC PDP-11/73 under the RSX-11/M operating system. Minor modifications would be needed to port these programs the the HP360 and HP-UX environment.

1.RESOLVE

The program RESOLVE will read a list of passes (with their start, stop times and PCA elevation) visible at LURE and produce an output file that is to be used as input to the SCHED program. RESOLVE will look for passes that overlap in time, and will dispose of pass times of lower priority targets that are overlapped in time by higher priority targets. If there are targets to be tracked only at night, day light pass time will be removed from consideration. (Night is defined in the program to be any time the sun is < -5° in elevation.) If targets of equal priority overlap, the time is divided amongst the two based on the amount of time that each is visible. The pass that is visible for the shorter period of time is allocated a larger proportion of the overlap time using the formula:

$$A = \frac{O * P}{2}$$

where:
A is Allocated time
O is Overlap Time
P is Proportionality Factor

The Proportionality Factor is calculated as: $\frac{LOP(n)}{LOP(m)}$

where:
LOP is Length of Pass function
n is the shorter pass
m is the longer pass

The longer pass would get the resulting Allocated Time portion of the overlapping time, while the shorter pass would get what remains. (Overlap Time - Allocated Time)

2.SCHED

This program will look for the best schedule based on an assigned score. The user tells SCHED how long a shift is to be "on site", and at what times of the day that the shift is to start. With this information, SCHED will score all possible shifts within the limits of the input parameters. SCHED uses a time "window" of plus/minus "on site" length centered on the highest priority target within the window. The score is computed for each pass as :

$$\text{Score} = 1/\text{Priority} + \text{PCA elevation}/180$$

The highest priority target is assigned a priority of "1", the second highest priority target is assigned a priority of "2", and so on. The maximum value would be 1/1 = 1, the minimum value is 1/n (n=minimum priority).

The PCA (Point of Closest Approach) elevation is an indication of how long this pass is visible (relative to other passes of the same target ID). The maximum value would be 90/180 = 0.50, the minimum value would be 20/180 = 0.11. Therefore, a "higher" pass of any given target is given added value over a "lower" pass of the same target. If a pass is fragmented because of a priority conflict, each fragment will have the PCA elevation scaled by the time allocated for that fragment. The scale used is the ratio of the pass time for the fragment to the pass time of the unfragmented pass.

$$\text{PCA} = \text{PCA} * \frac{\text{LOP(fragment)}}{\text{LOP(pass)}}$$

For a shift with "m" scheduled passes, the total score will be: $\sum_{n=1}^{m} \text{score}(n)$

3.SCHED Method

The program focuses on Priority 1 satellites. If your list of targets has no #1 priority target, the program will consider priority 2 as the highest priority target, and so on to priority #n.

The program will search for the highest priority passes. Each of the highest priority passes is then used as a center for a window of time that is initially set to twice the length of the "on site" time. All possible "sub-windows" of "on site" length are then assigned a score. The choice of which window to be published is up to the user and is determined by the selected start time. This start time can be given a time window to allow flexibility in choosing the highest scoring window over a range of start times. To find the optimum schedule for any 24 hour period, the user could select a start time in the middle of the 24 hour period, with a starting time range of +/- 12 hours. This is a good choice of input parameters for the initial run of the program.

The program SCHED will also schedule calibrations. An attempt is made to schedule both a pre and post calibration for each pass. If this cannot be done, the pass is flagged "Uncalibrated" on the output. If only a pre or post calibration can be scheduled this fact is also noted. These situations occur only if pass time must be sacrificed in order to get a calibration. Resolution of this problem is left up to the user. Calibrations are scheduled at a maximum time apart so that all intervening passes can use the calibrations.

The time needed to take a calibration is a modifiable parameter, as is the "turnover" time. (The turnover time is defined to be the amount of time needed to come up on a target.) The maximum time between calibrations is also set by the user.

4. EXAMPLE

4.1 ATSC Visibility chart for LURE Observatory

The table below was generated by ATSC (AlliedSignal Technical Services Corp), and lists all passes available for tracking at LURE on days 185-186, 1994. This is the general schedule used at LURE. The following listing is the optimal shifts available from these total passes, and was produced by RESOLVE/SCHED.

Station - XWW Shift - 1 Week of 07/04

Sat	DOY	Date	Aos	Los	AOS_AZ	LOS_AZ	EL	Concurrent Stations
G1155MS	185	940704	00:14	01:02	153	333	87	
G1500MS	185	940704	03:09	03:20	344	92	38	
G5986MS	185	940704	03:47	04:27	321	63	33	
G4146MS	185	940704	04:40	06:25	318	259	27	
G9009MS	185	940704	05:02	05:06	10	192	88	
G0307MS	185	940704	05:08	05:12	53	97	22	
G1500MS	185	940704	05:10	05:23	303	168	52	
G0307MS	185	940704	06:55	07:05	334	211	43	
G1134MS	185	940704	07:30	07:39	333	116	56	
G5986MS	185	940704	07:53	08:46	321	153	83	
G6177MS	185	940704	07:56	08:00	117	46	28	
G0643MS	185	940704	08:51	08:59	174	340	70	
G4377MS	185	940704	08:56	09:08	192	30	74	
G1134MS	185	940704	09:21	09:26	268	208	24	
G6177MS	185	940704	09:36	09:38	238	269	20	
G4146MS	185	940704	11:29	14:22	132	31	43	
G1155MS	185	940704	12:57	13:45	27	205	85	
G3535MS	185	940704	15:24	22:29	240	125	47	
G1155MS	185	940704	16:37	16:56	353	301	24	
G9009MS	185	940704	16:52	16:56	189	329	52	
G1500MS	185	940704	17:55	18:08	195	61	50	
G3636MS	185	940704	18:00	00:47	220	96	55	
G0307MS	185	940704	18:59	19:09	202	347	58	
G4377MS	185	940704	19:00	19:11	2	122	43	
G0525MS	185	940704	19:48	23:06	144	28	51	
G1500MS	185	940704	19:58	20:09	261	11	39	
G6177MS	185	940704	20:17	20:21	62	127	24	
G4377MS	185	940704	20:57	21:05	295	217	29	
G0643MS	185	940704	21:17	21:24	6	202	73	
G5986MS	185	940704	21:21	22:16	206	40	81	
G6177MS	185	940704	21:56	21:59	323	273	24	
G1134MS	185	940704	22:34	22:42	232	29	63	
G1155MS	185	940704	22:55	23:39	125	348	59	
G5986MS	186	940705	01:40	02:21	290	32	34	
G1500MS	186	940705	02:16	02:24	357	66	25	
G1155MS	186	940705	02:32	03:04	204	294	32	
G4146MS	186	940705	02:38	05:52	332	218	50	
G1500MS	186	940705	04:16	04:29	317	145	84	
G5986MS	186	940705	05:59	06:50	328	119	59	
G0307MS	186	940705	06:38	06:48	338	200	54	
G1134MS	186	940705	07:49	07:59	315	146	78	
G0643MS	186	940705	08:25	08:32	151	8	56	
G6177MS	186	940705	08:59	09:06	188	328	51	
G4377MS	186	940705	09:19	09:31	217	11	65	
G5986MS	186	940705	10:07	10:45	295	200	35	
G4146MS	186	940705	11:23	12:02	78	55	21	
G0525MS	186	940705	11:23	14:12	328	231	41	
G1155MS	186	940705	11:37	12:20	43	176	50	
G1155MS	186	940705	15:09	15:48	9	257	43	
G3535MS	186	940705	15:20	22:25	241	127	47	
G9009MS	186	940705	16:11	16:13	107	49	24	
G1500MS	186	940705	17:03	17:12	170	87	30	

```
G3636MS   186   940705 17:56 00:43  219     96  55
G0307MS   186   940705 18:41 18:52  193    356  73
G1500MS   186   940705 19:03 19:16  240     28  60
G0525MS   186   940705 19:13 21:06  105     41  29
G4377MS   186   940705 19:22 19:34  344    149  75
G5986MS   186   940705 19:33 20:18  174     59  43
G0643MS   186   940705 20:51 20:58   29    172  54
G1134MS   186   940705 21:06 21:11  176     92  31
G6177MS   186   940705 21:20 21:27  359    210  57
G1155MS   186   940705 21:41 22:14   92    360  34
G1134MS   186   940705 22:55 23:00  268    354  32
G5986MS   186   940705 23:33 00:24  247     29  53
-------------------------------------------------------------------
```

4.2 RESOLVE/SCHED Output

The following is the output of the SCHED program, using input from RESOLVE with the listed parameters, operating on the above ATSC schedule. These listings could be edited by the user to produce a final form that is used by the observers during the shift. All information for the production of the LASER OPERATIONS REPORT (LOR) is contained on this list that is kept at the operators console. The COMMENT field is filled in by the operator after a pass is taken so that the LOR can be completed later. The NOTES column tells the operator the resolution of the pass. This column can have one of the following NOTES.

1. FULL PASS - There are no modifications to the start and/or stop times of this pass.

2. START LATE - A higher or equal priority pass has preempted a part of this pass or part of the pass is nighttime only, and you will start tracking after the 20 degree rise time.

3. STOP EARLY - A higher or equal priority pass has preempted a part of this pass or part of the pass is nighttime only, and you will stop tracking prior to the 20 degree set time.

4. START LATE/STOP EARLY - One or more higher priority passes have preempted parts of this pass at rise time and at set time or there has been day light interference. You will be tracking some middle portion of this pass.

5. CONTINUATION OF PASS - A higher or equal priority pass overlaps some time at the beginning of this pass, but a fragment of this pass has been previously scheduled. You will start tracking this target some time after the 20 degree rise time. You will track down to the 20 degree set time.

6. NIGHT TIME ONLY - This pass will not be attempted because the entire pass occurs in day light and you have selected this target at a nighttime only target.

7. PRIORITY CONFLICT - This pass will not be attempted because the entire pass has been preempted by a higher priority pass.

8. CALIBRATION - A calibration is scheduled for this time slot.

```
LURE Scheduler for file GWW0704.OUT
 Shift On Site  = 7.75 Hrs
 Start/End Dates= 7/ 4/94 -  7/11/94 UT
 Starting Times =12:00 +/- 12.00 Hours
 Display Times as GMT +  0.00 Hrs. 24hr: T
          Targets/Priorities
  6177/ 1  4377/ 2  9009/ 3  0643/ 4  1134/ 5
  0307/ 6  1500/ 7  1155/ 8  5986/ 8  3636/ 9
  3535/ 9  4146/10  0525/10  0000/ 0  0000/ 0
  0000/ 0  0000/ 0  0000/ 0  0000/ 0  0000/ 0

 Score=  783.1 Number of Passes= 14
 Number of Passes By Priority
 2, 1, 1, 1, 2, 2, 2, 0, 2, 0, 0, 1, 0, 0, 0, 0, 0, 0, 0, 0
 First Pass Starts..> 94/07/04 03:09  Mon DOY=185
 Last  Pass  Ends...> 94/07/04 09:38  Mon DOY=185
 NOTE:This is the optimum sub-window of the main window
 #     ID  Start  End   PCA       Notes              Cals      Comments
           03:01  03:07     5Hz CALIBRATION #A
 #002 1500 03:09  03:20  38 Full Pass           A/C_____________________
 #003 5986 03:47  04:27  33 Full Pass           A/C_____________________
           04:47  04:53     4Hz CALIBRATION #B
           04:54  05:00     5Hz CALIBRATION #C
 #005 9009 05:02  05:06  88 Full Pass           C/E_____________________
 #006 0307 05:08  05:12  22 Full Pass           C/E_____________________
 #007 1500 05:14  05:23  52 Continuation of Pass  C/E_____________________
 #004 4146 05:30  06:25  27 Start Late          B/D_____________________
           06:27  06:33     4Hz CALIBRATION #D
           06:47  06:53     5Hz CALIBRATION #E
 #008 0307 06:55  07:05  43 Full Pass           E/F_____________________
 #009 1134 07:30  07:39  56 Full Pass           E/F_____________________
           07:45  07:51     5Hz CALIBRATION #F
 #010 5986 07:53  07:54  83 Stop Early          F/G_____________________
 #011 6177 07:56  08:00  28 Full Pass           F/G_____________________
 #010 5986 08:02  08:46  83 Continuation of Pass  F/G_____________________
 #012 0643 08:51  08:54  70 Stop Early          F/G_____________________
 #013 4377 08:56  09:08  74 Full Pass           F/G_____________________
 #014 1134 09:21  09:26  24 Full Pass           F/G_____________________
 #015 6177 09:36  09:38  20 Full Pass           F/G_____________________
           09:40  09:46     5Hz CALIBRATION #G
-------------------------------------------------------------------------
Score=  791.8 Number of Passes= 13
 Number of Passes By Priority
 2, 2, 1, 1, 1, 0, 2, 2, 1, 0, 1, 0, 0, 0, 0, 0, 0, 0, 0, 0
 First Pass Starts..> 94/07/04 15:24  Mon DOY=185
 Last  Pass  Ends...> 94/07/04 23:09  Mon DOY=185
 NOTE:This is the optimum sub-window of the main window
 #     ID  Start  End   PCA       Notes              Cals      Comments
           15:16  15:22     4Hz CALIBRATION #A
 #018 3535 15:24  15:29  47 Stop Early          A/B_____________________
           15:31  15:37     4Hz CALIBRATION #B
           16:29  16:35     5Hz CALIBRATION #C
 #019 1155 16:37  16:50  24 Stop Early          C/D_____________________
 #020 9009 16:52  16:56  52 Full Pass           C/D_____________________
 #021 1500 17:55  18:08  50 Full Pass           C/D_____________________
 #022 3636 18:00  00:47  55 (7) Nighttime ONLY
           18:30  18:36     5Hz CALIBRATION #D
 #024 4377 19:00  19:11  43 Full Pass           D/E_____________________
 #023 0307 19:00  19:09  58 (7) Priority Conflict
 #025 0525 19:48  23:06  51 (7) Nighttime ONLY
 #026 1500 19:58  20:09  39 Full Pass           D/E_____________________
 #027 6177 20:17  20:21  24 Full Pass           D/E_____________________
           20:31  20:37     5Hz CALIBRATION #E
 #028 4377 20:57  21:05  29 Full Pass           E/F_____________________
 #029 0643 21:17  21:24  73 Full Pass           E/F_____________________
```

```
#030 5986 21:26  21:54  81 Start late/Stop Early E/F_____________________
#031 6177 21:56  21:59  24 Full Pass           E/F_____________________
#030 5986 22:01  22:16  81 Continuation of Pass E/F_____________________
          22:26  22:32     5Hz CALIBRATION #F
#032 1134 22:34  22:42  63 Full Pass           F/G_____________________
#033 1155 22:55  23:09  59 Stop Early          F/G_____________________
          23:11  23:17     5Hz CALIBRATION #G
-------------------------------------------------------------------------
 Score=  623.1 Number of Passes= 12
 Number of Passes By Priority
 1, 1, 0, 1, 1, 1, 1, 1, 2, 0, 0, 2, 1, 0, 0, 0, 0, 0, 0, 0
 First Pass Starts..> 94/07/05 04:16  Tue DOY=186
 Last  Pass  Ends...> 94/07/05 12:01  Tue DOY=186
 NOTE:This is the optimum sub-window of the main window
 #     ID  Start  End   PCA       Notes              Cals      Comments
          04:08  04:14     5Hz CALIBRATION #A
 #038 1500 04:16  04:29  84 Full Pass           A/C_____________________
          05:23  05:29     4Hz CALIBRATION #B
          05:30  05:36     5Hz CALIBRATION #C
 #037 4146 05:38  05:52  50 Start Late          B/D_____________________
 #039 5986 05:59  06:36  59 Stop Early          C/E_____________________
 #040 0307 06:38  06:48  54 Full Pass           C/E_____________________
 #039 5986 06:50  06:50  59 Continuation of Pass C/E_____________________
          06:52  06:58     4Hz CALIBRATION #D
          07:31  07:37     5Hz CALIBRATION #E
 #041 1134 07:49  07:59  78 Full Pass           E/F_____________________
 #042 0643 08:25  08:32  56 Full Pass           E/F_____________________
 #043 6177 08:59  09:06  51 Full Pass           E/F_____________________
 #044 4377 09:19  09:31  65 Full Pass           E/F_____________________
          09:33  09:39     5Hz CALIBRATION #F
 #045 5986 10:07  10:45  35 Full Pass           F/H_____________________
          10:47  10:53     4Hz CALIBRATION #G
          11:15  11:21     5Hz CALIBRATION #H
 #047 0525 11:23  11:24  41 Stop Early          G/J_____________________
 #046 4146 11:26  11:35  21 Start late/Stop Early G/J_____________________
 #048 1155 11:37  12:01  50 Stop Early          H/I_____________________
          12:03  12:09     5Hz CALIBRATION #I
          12:11  12:17     4Hz CALIBRATION #J
-------------------------------------------------------------------------
Score=  643.9 Number of Passes= 12
 Number of Passes By Priority
 1, 1, 1, 1, 2, 1, 2, 1, 2, 0, 0, 0, 0, 0, 0, 0, 0, 0, 0, 0
 First Pass Starts..> 94/07/05 16:11  Tue DOY=186
 Last  Pass  Ends...> 94/07/05 23:56  Tue DOY=186
 NOTE:This is the optimum sub-window of the main window
 #     ID  Start  End   PCA       Notes              Cals      Comments
          16:03  16:09     5Hz CALIBRATION #A
 #051 9009 16:11  16:13  24 Full Pass           A/B_____________________
 #052 1500 17:03  17:12  30 Full Pass           A/B_____________________
 #053 3636 17:56  00:43  55 (7) Nighttime ONLY
          18:03  18:09     5Hz CALIBRATION #B
 #054 0307 18:41  18:52  73 Full Pass           B/C_____________________
 #055 1500 19:03  19:16  60 Full Pass           B/C_____________________
 #056 0525 19:13  21:06  29 (7) Nighttime ONLY
 #057 4377 19:22  19:34  75 Full Pass           B/C_____________________
 #058 5986 19:36  20:18  43 Continuation of Pass B/C_____________________
          20:20  20:26     5Hz CALIBRATION #C
 #059 0643 20:51  20:58  54 Full Pass           C/D_____________________
 #060 1134 21:06  21:11  31 Full Pass           C/D_____________________
 #061 6177 21:20  21:27  57 Full Pass           C/D_____________________
 #062 1155 21:41  22:14  34 Full Pass           C/D_____________________
          22:20  22:26     5Hz CALIBRATION #D
 #063 1134 22:55  23:00  32 Full Pass           D/E_____________________
 #064 5986 23:33  23:56  53 Stop Early          D/E_____________________
          23:58  00:04     5Hz CALIBRATION #E
```

FUTURE ROLES FOR LASER RANGING INSTRUMENTATION

Chairperson : Kurt Lambeck

FUTURE ROLE FOR LASER RANGING INSTRUMENTATION: A PERSONAL VIEW

Kurt Lambeck

Research School of Earth Sciences, The Australian National University, Canberra, ACT 0200, Australia

In order to say something about future roles we need to have a good understanding of what the past and present roles have been. What have we learnt about the physics of the Earth or about physical principles and processes that we would not have learnt had there been no laser ranging to satellites. Only when this is answered can we ask the next question: What do we want to learn about the Earth that requires on-going and improved laser ranging to satellites or the Moon.

In attempting some answers I will give my own views : in the spirit of getting the debate going rather than trying to be correct. I doubt that there is a correct answer in any case, the nature of scientific investigation being what it is .

Scientific uses of satellite laser ranging (SLR) fall into at least two categories: geophysical applications (including the dynamics of the Moon), and fundamental physics (aspects of relativity theory, high-precision time transfer). I will comment briefly on the first and others hopefully can comment later on the second area.

In making these comments it is important to understand my strong conviction that the geodetic satellite observations are of little value unless they are considered in a broad geophysical and geological context. This comes about in two ways: The inversion of geodetic data for geophysical parameters is seldom unique, and geodetic estimates of rates invariably give snapshots of processes that occur over much longer time scales. Hence they need to be taken together with other geophysical or geological evidence in their interpretation.

The use of the laser ranging data in studies of the Earth can be illustrated by Figure 1. Here an Earth, with a response function R, is acted on by forces F, and in consequence is subject to deformation D. This last is the quantity inferred from the laser range data. Sought is either F or R, or both. In some cases F can be assumed known and the sought function is R. One example is the lunar and solar tidal deformation of the Earth. In other cases R is assumed known and F is inferred. One example of this is the Earth's rotation where the inference may be the zonal wind patterns. In most cases both F and R are unknown or at best only partially known. Examples here include the Earth's gravity field. In this case the "deformation" is the geoid or gravity anomaly map and the unknowns are the forces acting within the mantle and the internal response of the mantle to these forces.

Figure 2 illustrates a range of processes that act on the Earth from periods of seconds to hundreds of millions of years. One of the objectives of geophysics is to understand the response of the Earth, its rheology, over this large range, from 10^0 to 10^{17} seconds, using a wide range of observational evidence. Geodetic measurements, particularly laser ranging to satellites, can contribute significantly to this problem.

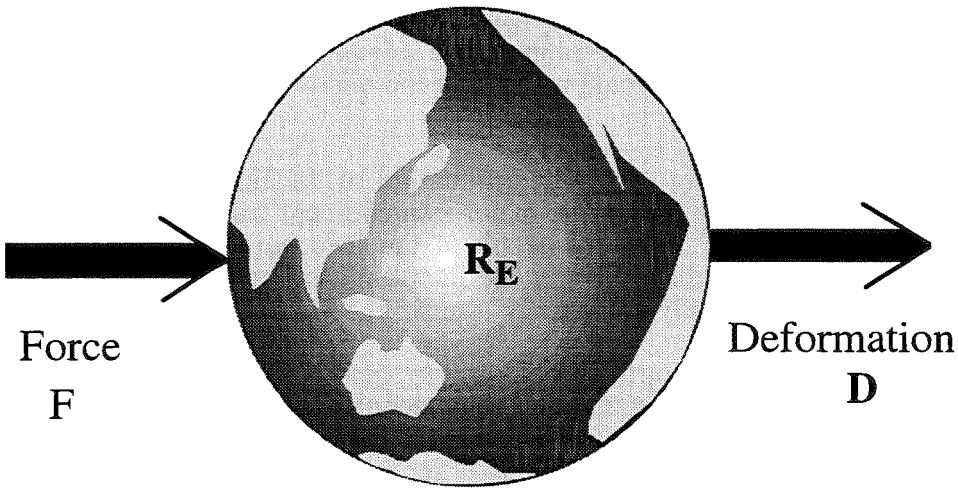

Figure 1. Schematic illustration of the relation between force F and the resulting deformation for a planet with a response function R.

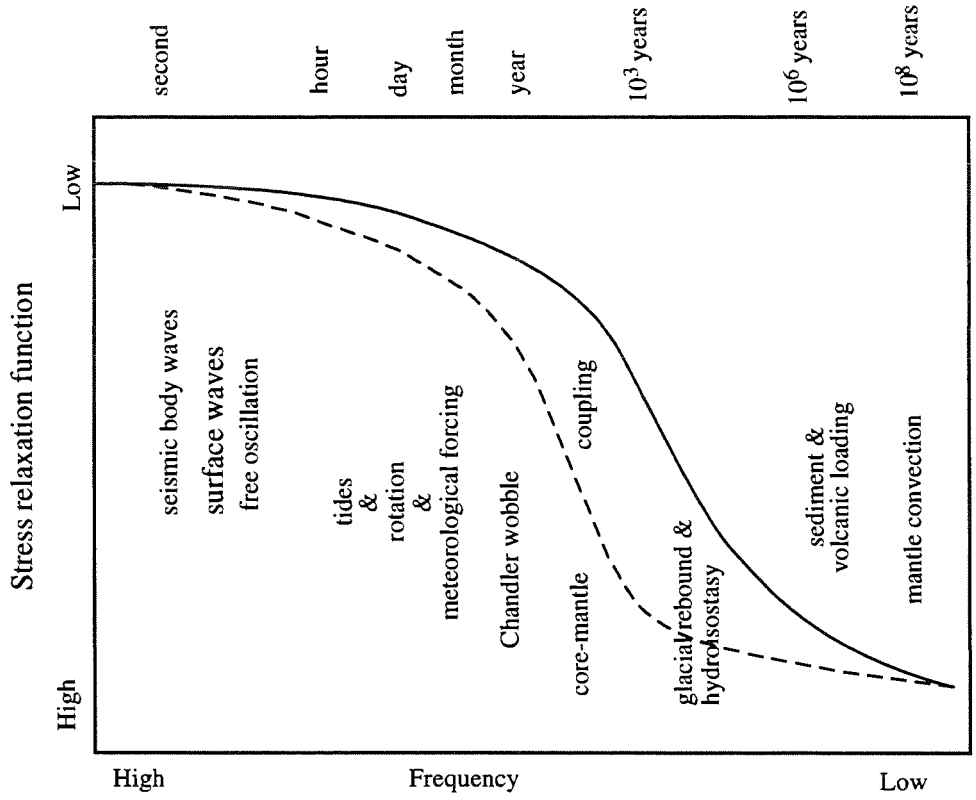

Figure 2. Schematic spectrum of time-dependant processes deforming the Earth. One objective of the studies of the Earth is to define the response function between the elastic response at very high frequencies and essentially fluid response at very low frequencies.

The SLR applications to geophysics can be divided into two categories: one where the satellite laser ranging is used to examine dynamic aspects of the Earth; mainly its gravity field, the other where the measurements contribute to the setting up of a global reference frame with respect to which the planet's rotational motion, or the relative crustal motions of parts of the Earth can be examined.

The impact of laser ranging on the determination of the Earth's gravity field has been important, as is shown in Figure 3. The major improvement from the SE 1966 to SE 1969 models, for example, were largely the result of the incorporation of the first laser data. Subsequent improvements follow closely the increasing accuracy of ranging data and the increasing amount of data actually available.

The overall result is that the Earth's global gravity field is known with better precision and resolution than, with one exception, any other geophysical data set. (The exception is topography and even this would not be one if I included gravity field models incorporating satellite altimetry data.) The inversion of gravity for Earth structure is non-unique and unique solutions are possible only by incorporating other data or model assumptions. But if the other geophysical data bases are limited then I do not think that we will learn much more about the Earth by pushing for higher resolution, higher precision models.

Having said this, I immediately insist on two caveats. One important contribution to the gravity field studies is the measurement of the time dependence of some of the very long wavelength components in the field. Observations of such change constrain the Earth's rheology at intermediate periods and I think still have an important contribution to make to understanding the physical properties of the Earth. A difficulty here, and one to which I return later, is that a major contribution to these time dependencies comes from the hydrosphere-atmosphere and the fluid domains of the Earth will have to be better understood. In several instances one can point to such improved understanding having been driven by satellite laser ranging results, and an immediate example is the improvement in ocean tide modelling that was motivated largely by new results for the tidal perturbations in satellite orbits.

The second caveat concerns the use of the geoid as a reference surface for measuring long-period fluctuations in the sea surface topography (SST). Many of the important climatic fluctuations occur on time scales of years to decades and they exhibit considerable ocean-atmosphere interaction. The time scales of some of the SST changes are longer than the typical lifetimes of satellite instrumentation and there is a need to have a high accuracy geoid so as to be able to link altimeter results from successive satellite missions. Accuracy requirements for these geoids are of the order of a few centimeters or better and SLR data remains the best tracking information to achieve this.

For these dynamical applications it is well recognized that SLR provides the best tracking method for obtaining high accuracy orbits. Electronic tracking will generally be less satisfactory on two counts: additional atmospheric propagation problems, including the ionosphere, and satellites not configured to reduce the surface area to mass ratios. These limitations are to a great extent overcome by the much higher tracking density that is usually achieved with electronic methods. This nearly tempts me to suggest that improved tracking coverage should be a higher priority than improved tracking accuracy for certain classes of geophysical applications.

In the second category of geophysical applications, laser ranging has made a significant contribution to the study of the Earth's rotation although here the method does not reign supreme. VLBI is my preferred method here because of its ability to give both long-term stability to the reference frame (something that SLR by the nature of satellite orbital motion cannot provide) and high resolution observations of very short (diurnal and less) duration irregularities in rotation.

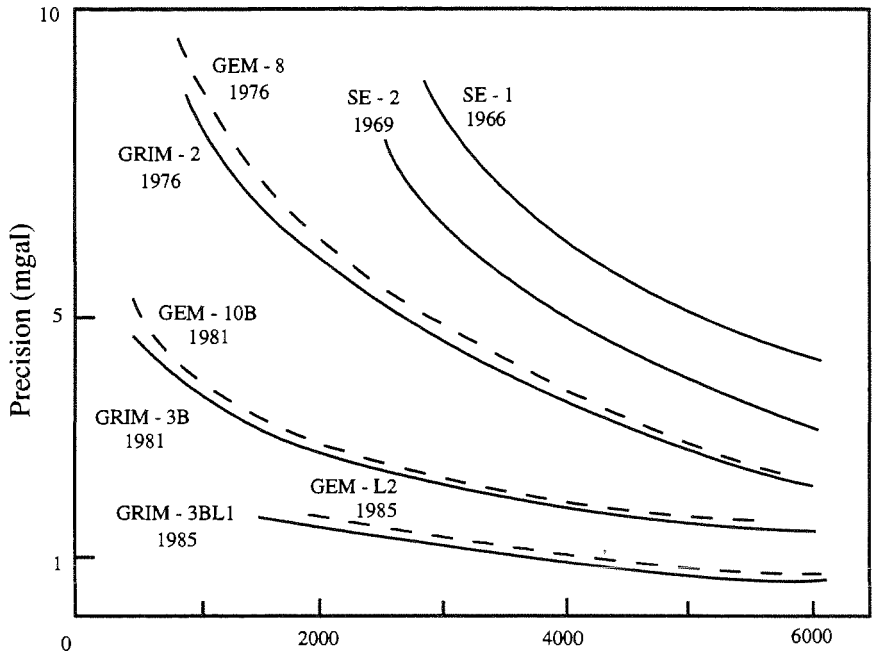

(a)

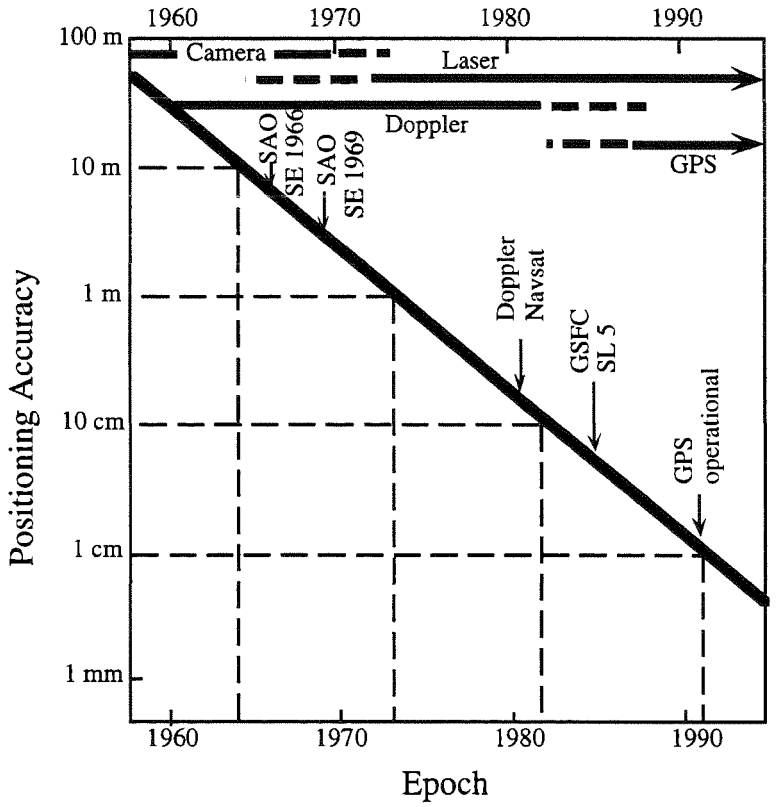

(b)

Figure 3. (**a**) Error spectra of gravity field models as a function of spatial resolution for models published between 1966 and 1985. (**b**) Spectrum of geodetic positioning accuracies as a function of time.

Certainly the laser ranging results present a very major improvement over previously existing methods and has caused us to reconsider questions about the excitation and dissipation of the Chandler wobble, albeit it without resolution. What is required is a long series of high accuracy rotation data (length-of-day and polar motion) to enable questions about the multitude of forcing functions (Figure 4) to be answered. These include the already mentioned questions about the excitation and dissipation mechanisms of the Chandler wobble; the amplitude and phase of the tidal signals in the Earth's rotation from 12 hour to 19 year periods; the nature of the core-mantle coupling and its relation to "decade" scale changes in length-of-day; the secular and, 'decadel' oscillations in the pole path. Here one also runs into the hydro-atmosphere barrier, where "fluid" signals mask the solid-Earth signals. That this occurs over a broad spectrum has been known for several decades but unless the quality of the global meteorological, oceanographic and groundwater data bases improves little new physical information about the Earth will be obtained.

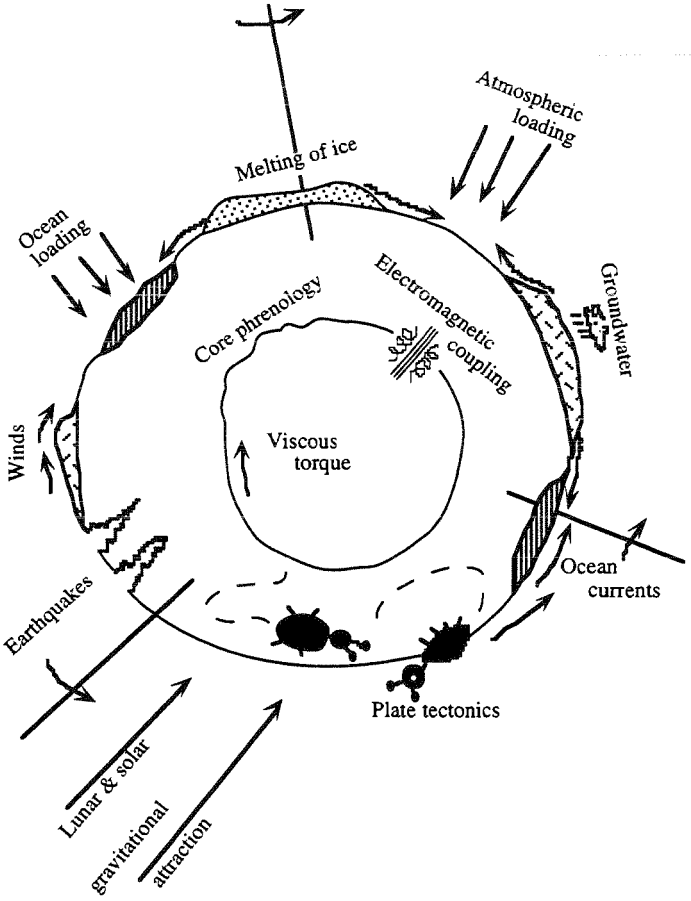

Figure 4. Schematic representation of excitation mechanisms driving the Earth's variable rotation.

Where SLR has made an important impact is in measuring crustal displacements, in particular the confirmation of the main aspects of plate tectonic motions and rates and the observation that average rates for the past few million years are essentially the same as decadel and shorter averages. But plate tectonics has gone much beyond the first-order theories of relative motions of a few major plates whose boundaries appear as simple lines on maps and the really important work will be the examination of the spatial and temporal strain distribution across the boundary

zone. Figure 5 illustrates a complex but not unusual boundary zone between the Pacific and Australian plates where motions occur in orthogonal directions at rates from less than 1 cm/year to up to 15 cm/year. Up to 8 plates have been defined in this area and to determine their relative motions would require a minimum of 24 sites. But this would not give a complete picture of the deformation process because it would not establish the nature of the deformation across the broader deforming zones such as across the Papua New Guinea Highlands, between the eastern end of New Britain and New Zealand, or across the Woodlark Spreading Zone within the d'Entrecasteaux group of islands. The requirements here are to be able to measure positions at the cm or better level such that rates of displacement can be measured with very high accuracies even for short repeat times as is required for examining the strain cycles associated with large earthquakes. In many instances stations will lie within a few tens of kilometers, or less, of each other. In terms of accuracies SLR is clearly the most appropriate technique but in terms of cost and practicality GPS wins hands down. What I think the role of SLR is here is the provision of a regional 1000 km scale network of reference sites within which the GPS positions are fixed. In this context, the laser tracking of GPS satellites is most important and I would hope that this community can exert some influence to get more GPS satellites equipped with retro-reflectors.

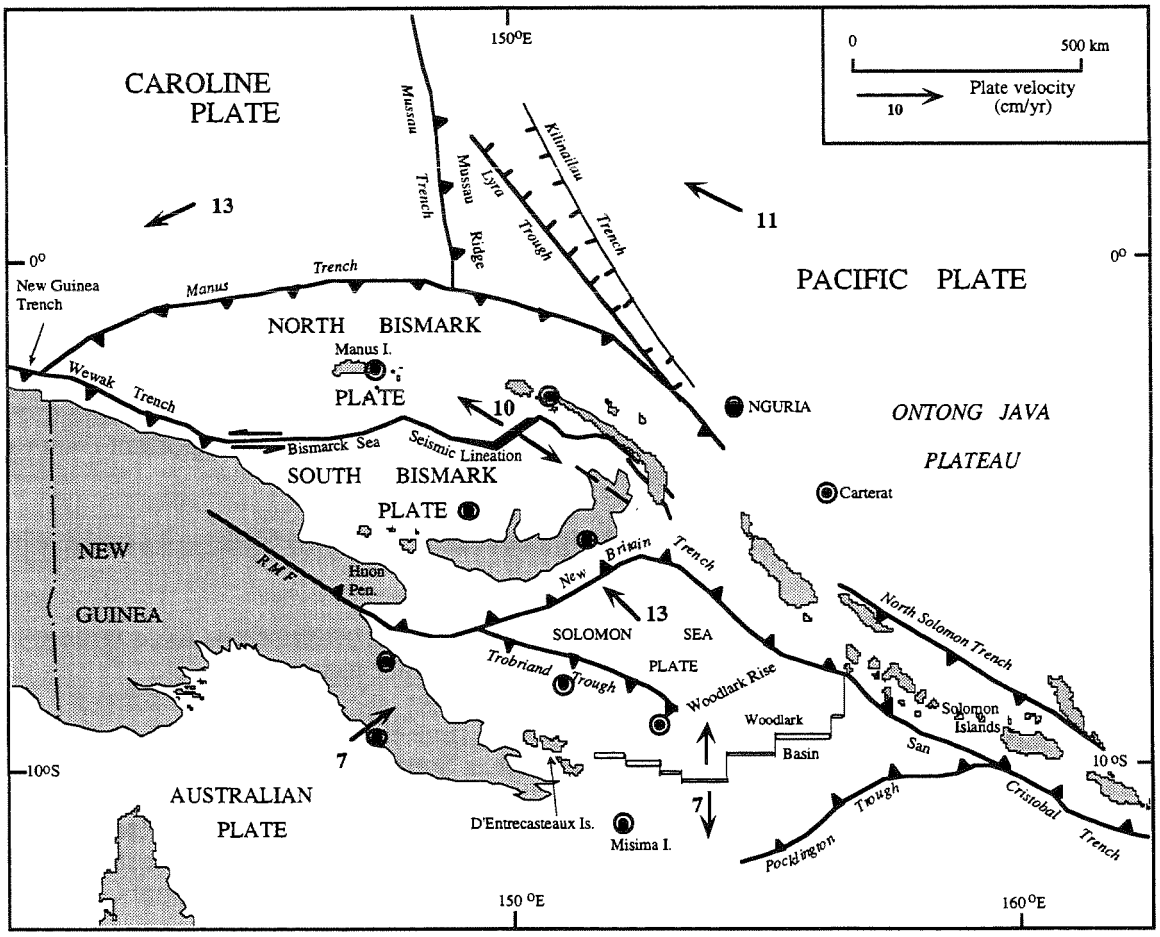

Figure 5. The complex zone of deformation between the Pacific and Australian plates. Arrows indicate directions of relative movements, and rates are in cm/year. The region includes a number of subduction zones, a spreading ridge in the Woodlark basin, transform faults and a fold belt in the New Guinea Highlands. Circles indicate the location of GPS sites.

With the conventional views of plate tectonics, most emphasis is placed on the horizontal displacements. But vertical motions are often more indicative of physical processes than are horizontal motions and high-accuracy vertical positioning is essential. Vertical motions are usually an order of magnitude or more smaller than horizontal motions and this is perhaps where the SLR community's biggest challenge lies. The vertical rates are particularly important because it is sometimes possible to obtain good long-term (10^3 - 10^5 year) estimates of uplift or subsidence using geological or archaeological observations so that it becomes possible to compare "instantaneous" and long-term rates. Rates of uplift along the Antarctic margin, for example, provide good scientific targets but the rates are small, of the order of 1 mm/year and less. Such measurements would contribute to understanding earlier ice volumes over the polar continent.

The vertical motion determination also is most important in the context of trying to measure secular changes in ocean volumes. Tide gauges measure changes in sea level with respect to the rock or pillar upon which the gauge is mounted and will experience its own movements relative to the Earth's centre of mass. To interpret the tide gauge record in terms of changes in ocean volume, caused for example by anthropogenic factors, requires that both components of the motion are known at the mm/year level. This is probably the most exacting requirement from SLR or any other form of tracking because what is sought is long-term accuracy, not just precision. Also, it will not be adequate to have this measurement from a single site because there is no such physical quantity as a globally uniform sea-level rise or fall. Because of mutual gravitational self attraction of land ocean and ice sheets and because of the Earth's response to changing water loads, even in the absence of tectonic factors sea-level change will not be uniform.

I haven't discussed laser ranging to the Moon (LLR) at this point. I believe that this should not be ignored because ultimately one may learn more about solid planet behaviour by studying the Moon than by studying the Earth because of this satellite's freedom from the hydro-atmospheric disturbances. I think that studies of the Earth's rotation are better done with VLBI and the sole rationale for LLR is to examine the rotational dynamics of the Moon and fundamental physics experiments, much as was argued when the method was first proposed. The rotational deformations of the Moon are at least an order of magnitude smaller than those of the Earth and the requirement for the highest accuracy is clear. But more important than this is to get data on a regular basis from a southern latitude site.

To summarize: for geophysical purposes high accuracy (sub-cm) SLR will continue to be important for:

(i) Providing the critical tracking system of satellite altimetry missions to provide a long-term stable surface for measuring changes in sea-surface topography.

(ii) Provide the essential data base for measuring time-dependent changes in the Earth's gravity field by tracking passive satellites such as Starlette and Lageos.

(iii) Provision and maintenance of a global reference frame for measuring tectonic motions and for providing the standards (calibration) for GPS work over much shorter distances. These stations would provide the reference frame for high-density regional GPS surveys rather than be used as mobile stations for the latter surveys.

(iv) Providing ultra-high accuracy for vertical crustal motions and for calibrating GPS determinations of changes in height.

(v) Providing information on the rotational and orbital dynamics of the Moon (including tidal deformations).

Two more general comments are also appropriate.

(vi) With the increasing measurement accuracies one hits the hydro-atmosphere noise barrier and improvements in the knowledge of the Earth-ocean-atmosphere system will be essential if the improved data is to provide new insights into the workings of the Earth.

(vii) The geodetic measurements provide new insights into the workings of the Earth only if they are accompanied by other geophysical and geological data sets, new scientific concepts and numerical modelling schemes.

FUTURE TECHNOLOGIES AND MISSIONS

Chairperson : Michael Pearlman

Session 15: Future Technologies and Missions

Chairperson: Michael Pearlman

This session was originally to a panel discussion on Future Technologies and Missions. Members of the Panel included: John Degnan (NASA), Tom Varghese (ATSC), Ivan Prochazka (TUP), Ulrich Schreiber (Wettzell), Jean Gaigneget (CERGA), and Ben Greene (EOS). Instead of the advertised topic, we focussed more on the future direction of laser ranging: Where are we going? and What will we look like when we get there?

The Panel members were asked to comment on an issue that they wanted to stress or one that they thought needed strong consideration in the planning of our future evolution (or survival, depending upon your view).

Degnan argued that we needed to move to a regime of automated, inexpensive, easily replicated SLR systems that would significantly reduce the cost of operations. Cost has become such a driving factor in today's world that groups will eventually be put out of business unless significant changes are made. NASA is embarking on the design and development of the SLR 2000 to address this need and to eventually replace its current network of various vintage instruments. Although two wavelength capability is essential to achieving the highest capability from SLR either through field deployment or model development, NASA plans to begin the SLR 2000 program with single wavelength operation, but provide a platform where additional wavelength can be added later. Initially, they expect sub-cm. performance which should reach the mm. level as the systems evolve. Degnan also pointed out that along with reduction in instrument and field operation costs, NASA is also working to reduce headquarters infrastructure cost. In this connection, it is essential that we strive toward more standardization of performance and data product.

Varghese argued that economic forces are indeed strong, but even with cost reduction, SLR had to be responsive to strong scientific requirements, and that scientific requirements must drive the data acquisition program (data quality, data quantity, site distribution, etc.). In addition, the technique must respond to evolving technologies and technological philosophies; otherwise we will get caught in dead end, non-competitive situations. Varghese discussed the natural split in SLR applications between those requiring a modest number of fixed systems and those requiring either a large numbers of systems, or systems with high mobility that can occupy many sites rapidly. Although most applications are at the moment adequately serviced by consistent 1 cm. ranging accuracy, projected needs for most are in the mm region, with the most stringent requirement being measurements in the vertical for post glacial uplift, subsidence, etc. Varghese stressed the need to strive for a baselined global network with similar hardware, software, procedures, and validated ranging capabilty. A few systems should also be actively pursuing fifth generation technology with 1 mm. capability.

Prochazka outlined conceptual proposals for two laser ranging related systems that might have general interest. The first is a two color laser ranging system for air or spaceborne applications. The transmitter is a diode pumped YAG operating at 5 kHz with an output of 0.1 mJ at both the fundamental and second harmonic. The detector is a SPAD with single photon capability. Data points are averages over 0.1 - 0.3 sec. The timing system has a resolution of 20 psec. The goals of the design are ranging precision of 5 - 8 mm, two color differential range measurements of 3 - 5 psec, and an overall range accuracy of 1 cm. The system would be rugged, all solid state, self calibrating, and eye safe. The second is a SPAD detector package for a hydrogen maser timing package in space.

Schreiber reviewed the unique capabilites of SLR/LLR: high resolution, simple optical measurement, reduced suceptibility to degradation from refraction, small ground system, cheap satellite segment, etc. He stressed the need to optimize the current network resources: moving stations to achieve better global distribution (both geographically and in terms of distribution of global tracking workload), associating different functions with different stations (fundamental, low orbit POD, etc.) and job and site sharing with other applications. We need to stress our flexibility: near real-time provision of data, continuous (24 hour) tracking, resolution of high frequency (sub-diurnal) phenomena, and a provider of mission support for a broad base of potential users. The laser ranging technique will continue to evolve and must be open to new related applications (lidar, timing ,etc.). The evolving capabilty, however, will place new demands in metrology, gravimetry, monumentation, etc. at the site that we must accommodate.

Gaignebet stressed the importance of the time transfer capability of laser ranging and the need to exploit this to the level of the technology. He reviewed the current double pass strategies for cancelling error sources and discussed some of the Lasso experiences which are now working toward 100 ps. time transfers.

Greene placed great importance on moving to eyesafe ranging for implementation of automated systems and for reasons of public relations. Several groups including EOS are working toward both eyesafe and automated designs.

There was general concensus that we are placing too much reliance on solid Earth sciences, and that we needed to seek our position in a much broader range of applications. Precision orbit determination, time transfer, measurement of the vertical, etc. require consistent, unambiguous, high accuracy data. We need to significantly increase cost effectiveness through automation at the stations and smarter strategies in data processing and performance evaluation. Global resources must be used more efficiently. The global distribution of the SLR stations and the distribution of tracking workload among stations at different locations and of different performance characteristics must be improved to better support the growing complex of retroreflector satellites. SLR must continue to strive for increased performance (accuracy, data yield, coverage, etc.) making use of newer technologies and concepts to meet the needs of the scientific community. If we allow ourselves to stagnate technologically, we will fall by the wayside.

We should consider carefully our strengths and weaknesses and try to position ourselves where

our capabilities are unique, and where we can provide a strong synergistic component to the space geodesy measurement complex.

WORKSHOP SUMMARY AND RESOLUTIONS

Chairperson : Ben Greene

Ninth International Workshop on
LASER RANGING INSTRUMENTATION

SUMMARY SESSION REVIEWS

Chairperson: Michael Pearlman

Each session chairperson gave a brief summary of his or her session. Each provided a brief writeup which is attached.

Session 1: Future Science and Applications
Chairperson: Christian Veillet

During the Workshop, we very often heard the word "survive". The past is full of dead techniques which proved to be very efficient at one time, but are no longer used. Should we really worry about the survival of laser ranging, or should we think to the interest of the science we can contribute to? Laser ranging is not just Satellite Laser Ranging. It includes also Lunar Laser Ranging, which addresses many scientific goals. Ranging itself is in fact a time measurement, and applications of the technique are not only for "ranging", but can be used for transferring time, which opens a wide area of applications.

Many of us mentioned a "unique" contribution of laser ranging. We should focus more on the interest of the contribution rather than on its uniqueness! You can be alone doing something which is not of interest to anybody.

Relativity is everywhere. It is true in the equations we use for modelling the measurements. It is also true in the quality of the arguments we use for defending laser ranging. We should not forget that arguments, which seem very strong for us in our small community, are very weak when considered from further away, especially with respect to other science or other techniques.

Many scientific applications require long term continuity (long series) of measurements. These include: precession/nutation (18.6yr), changes with time in station positions or gravity field, and long term maintenance of the reference frames.

High accuracy metrology techniques do not thrive individually. Other techniques must be available to verify performance and help isolate sources of systematic errors. This is true for the accurate positioning provided by laser ranging on the ground or in space. It is true also for the time transfer possibilities of laser techniques and for calibration of altimetric measurements.

Metrology does not like haste. As new techniques emerge, the old techniques should be maintained and upgraded, if possible, to provide a comprehensive means of performance evaluation. A long overlap will be very important for providing continuity.

Six scientific or technical domains of applications of laser ranging can be listed in conclusion of these comments :

- Earth Sciences (Belmont...)

  - Improve the present results (especially through a better accuracy of the measurements)
  - Look into the changes with time (gravity field, station positions, ...)
  - Contribute to technique combinations (IERS)

- Reference Frames

  - Terrestrial (center of mass of the Earth)
  - Solar System linked to Extragalactic frame through LLR
  - Obliquity and Right Ascension origin detemination

- Lunar Physics and Orbit

  - Liquid or solid core?
  - Earth-Moon system evolution ...

- Fundamental Physics

  - General Relativity is a basic tool for modelling laser ranging measurements
  - LLR is the best test of the Equivalence Principle

- Light Pulse Travelling in Space

  - Physics very clean, and interaction with environment minimal
  - To be used for space/time metrology, time transfer (if stations accurate) and light/gravitation interactions.

- Telescope and Laser

  - Adapatative optics tests
  - Space communication tests
  - Technical support (as positioning of TV satellites)

Session 2: Target Signatures and Biases
Chairperson: A.T. Sinclair

Papers were presented by J. Degnan and by R. Neubert giving theoretical calculations of the position of the mean reflection point of sphericalsatellites, and the position of the detection point for such a satellite using a single photon detection device, and the variation of the position of this detection point with receive energy. They give numerical examples for Lageos. Their results for the variation of the detection point agree well, but their values for the position of the mean reflection point differ by about 8 mm. This needs to be resolved.

The paper by G.M. Appleby and P. Gibbs gave observational results that demonstrated the shift of the detection point of a satellite, using ranging data from a SPAD system to various satellites with a varying return level.They also showed from ranging results to a calibration target that variations with receive energy occur due to the pulse width of the laser and to the internal properties of a SPAD. These variations are repeatable and can be calibrated, or can be avoided by using only low return rates.

I. Prochazka and J. Blazej presented results from indoor testing of an array of corner cube reflectors using a short pulse laser and SPAD detector and could resolve the returns from individual corner cubes separated in range by only 4 mm.

G Kirchner and F. Koidl reported on investigations at Graz that demonstrated the variation of detection point with receive energy for various satellites, both by ranging with different energies and by using the different return rates that are obtained routinely from the semi-train of laser pulses used at Graz.

U. Schreiber, W. Maier, K. Haufe and B. Kriegel described the results of an investigation of timewalk effects of avalance photo diode detectors caused by varying the receive energy, and also the effects of varying the laser pulse width. V. Husson, J. Horvath and G. Su have carried out a detailed characterisation of the NASA SLR stations by examining engineering and other records, and have located a number of possible causes of biases in the data, which have a high correlation with the biases actually determined from analysis of Lageos data. Their paper provides a reference document for these engineering
biases.

P. Dunn and M. Torrence are concerned with trying to extract very fine geophysical signal from the analysis of SLR data, particulary that arising from real height variation of the stations, but find that this can be hidden by instrument errors causing range and time biases. They demonstrate that the signatures of range bias and genuine height variation can beseparated using range data from Lageos I and Lageos II over a sufficiently large range of elevation.

R.J. Eanes, S.V. Bettadpur and J.C. Ries show that by using SLR data from several satellites (they used Lageos I and II, Ajisai, Stella and Topex) it is possible to resolve the range bias, time bias and frequency bias of a station from the height determination. They find that it is important to have a combination of high and low targets.

Session 3: New Mobile Stations
Chairperson: Erik Vermaat

A range of new transportable Satellite Laser Ranging systems is presently under development, spanning the entire spectrum of mobility:

Portable (in cases < 50 kg)	FTLRS	France
	PSLR	Australia
Van type (TLRS class)	TSLRS	Japan
	CTLRS	PRC
Container type (MTLRS-class)	TIGO-SLR	Germany

Such variety triggers the question of how mobility relates to the mission objectives for those systems and which other requirements are of importance for mobile system design.

The "traditional" role for transportable SLR systems of regional network densification, in which they were deployed for durations of four to eight weeks on one site, with site spacing less than 1000 km, has in general been taken over by GPS and other radio techniques. A prime contemporary application of transportable SLR systems is to help improve the geographic distribution of the global SLR network by (semi-) permanent deployment at fiducial sites, preferably collocated with other space- and terrestrial techniques. This does not require a high level of mobility, although smaller systems have the advantage of more easy access to remote (e.g. island) sites. Highly mobile systems can play an important role in collocation experiments with stationary systems. In their design characteristics smaller systems should not bargain on the capability to observe all geodetic SLR satellites, but they should at least access satellites up to and including the LAGEOS satellites, in order to play a role in high precision global geodesy.

Session 4: New Fixed Stations
Chairperson: Yang Fu Min

The oral presentations and poster papers, provided the following information on new fixed stations:

Six new fixed stations have been set up and put into operation since last Workshop:

* Postdam (Germany, 1 meter telescope, operation in 1992);
* Changchun (China, 60 cm telescope, 1992);
* Beijing (China, 60 cm telescope, 1994);
* Borowiec-2 (Poland, 65 cm telescope, 1994 and will be moved to Tunisia);
* Mendeleevo (Russia, 1994);
* Sarapul (Russia, 1994).

Seven new stations will be completed in the next two years:

* Helwan 2 (Egypt, 28 cm telescope, 1995);
* SALRO (Sandi Arabia, 75 cm telescope, 1995);
* ZIMLAT (Switzerland, 1 m telescope, 1995);
* Metsahovi (Finland, 63 cm telescope, 1995)
* Kunming (China, 1.2 m telescope, 1996)
* MLRO (ITALY, 1.5 m telescope, 1996).
* Altair (Russia, 1996)

Updating reports were provided by:

* Wettzell (WLRS, Germany, 75cm telescope)
* CRL (Japan, 1.5 m telescope)
* Simosato (Japan, 60 cm telescope)

Dr. A. Clement of NRL and Dr. R. Fugate of USAF Phillips Laboratory discussed the performance of their satellite laser ranging station at the Phillips Laboratory Starfire Optical Range and the facilities and results using adaptive optics with laser guide star techniques.

Session 5: Timing Devices and Calibration
Chairperson: Hiroo Kunimori

Presentations were given on the capability and/or upgrade of the HP5370A and Stanford SR620 time interval counters. Talks were also given on the status of the GPS steered rubidium frequency standard being developed by NASA, on a high precision event timer being developed by EOS, and on the overall status of Moblas-7. There was also a presentation on the time synchronization between stations using Ajisai.

Session 6: Lunar Laser Ranging
Chairperson: Peter Shelus

The science that the Lunar Laser Ranging (LLR) technique addresses is highly multi-disciplinary and includes, among others, astronomy, celestial mechanics, gravitational theory, relativity, and Earth physics. Even after more than 25 years of continuous activity, the technique remains a significant observational challenge. However, with care, attention and dedicated effort, as evidenced by past and present operations at the Observatoire de Cote d'Azur in France (CERGA/OCA), the LURE Observatory on the island of Maui and the McDonald Observatory in Texas (MLRS), it has been shown that LLR observations can be regularly and routinely carried out. The German station at Wettzell is nearing routine LLR capability. As evidenced by the three papers presented at this workshop, the LLR community continues to "push the envelop" to improve the precision, accuracy and volume of this important data type.

CERGA/OCA, already a very high volume station for LLR data, is striving with a new detector and multi-color and timing technology to reach millimeter precision and accuracy levels. MLRS/UTx, with a significant number of hardware and software upgrades, has increased its LLR data volume by a factor of 3-5 in the past 18 months. The MLRS is also beginning to use Avalanche Photo Diode (APD) detectors and modern auto-guiding technologies to not only further increase data volume, but to increase it's accuracy and precision levels as well. Efforts by personnel at Wettzell in Germany and Orroral Valley in Australia continue to establish LLR as a viable observational technique at those stations. A new laser ranging station with LLR capability is currently being constructed to replace the present Matera artificial satellite station. Other groups around the world were encouraged to investigate whether LLR can be established at their laser ranging stations.

Session 7: Eyesafe Systems
Chairperson: John Luck

NASA presented its plans for the SLR2000 and EOS presented some discussion on low power systems for eyesafe operation. Presentations were also given by EOS on selection of eyesafe wavelengths for operational systems and by ATSC on an aircraft surveillance radar for monitoring air traffic above the station. The radars, coupled with other personnel safety features, will reduce the manpower required to operate the SLR systems.

Session 8: Data Analysis and Models
Chairperson: Guiseppe Bianco

- Data taken by state-of-the-art SLR systems have demonstrated a precision of 3-5 mm. This precision is less than the intrinsic limits of the ranging systems (2-3 mm) as observed on ground target calibrations; this is probably due to satellite signatures, errors in modelling, etc.

- Analysis of high precision SLR data has shown the evolution of station heights over a few years to precision levels of 2-3 mm. This clearly sets SLR as the best available technique for monitoring vertical motion (e.g. post glacial rebound) and also for the precise calibration of satellite-borne altimeters.

- Evolution of SLR baselines can be routinely recovered at a level of a few mm/yr. (1 mm/yr for fixed SLR stations) . Velocity fields recovered from the analysis of SLR data are generally in good agreement with current models (such as NUVEL-1A), but several important differences are evident which need to be explored.

- SLR routinely provides earth orientation parameters with a precision of 0.3 mas.

- SLR is the only techniques to demonstrate the determination of the geocenter to a few mm. This is crucial for a number of global change related investigations (ocean circulation, mass redistribution, atmospheric circulation, etc.).

- SLR, with its capability to generate precision orbits (2 - 3 cm) for GPS satellites, will allow us to resolve the anomalies in the orbits computed directly from GPS data and to isolate timing and orbital errors. However, this will require good quality data, global coverage, and appropriate geometry.

Session 9: Spectral Filters and Detectors
Chairperson: Ulrich Schreiber

More and more systems are using avalanche photo diodes. New devices are showing a high sensitivity and rugged construction. Drawbacks are high thermal noise rate and intensity dependencies which effect range measurements and cannot be corrected by constant fraction discriminators or similar units. However, the understanding of these effects is now quite good. The avalanche photo diodes can be characterized as:.

1. Satellite Signature Effects are usually small (in the order of a few millimeter) and caused by the shape and optical depth of the target satellite and can be modeled quite well.

2. Timewalk effects are caused by excessive intensity at the detector, which is easily achieved by returns from low altitude satellites. This can contribute range bias as much as 20 cm (laboratory measurements). There is no timewalk present in the low intensity domain. The timewalk is caused by light induced variations in the multiplication process during avalanche build up. It can be avoided in practical ranging by keeping the return energy low.

3. In recent years, great progress has been made in silicon diode devices. Work continues on Germanium- and InGaAS- diodes which had posed greatly difficulty because of their high noise rate. However, with cryogenic instrumentation these units are beginning to look promising. This is important because of the current trend towards eye safe ranging.

In the field of spectral filters, it now seems feasible to build filters with a bandwidth of less than 0.2 nm and a total transmission of well above 70%. By using an acousto-optic crystal, a frequency agile spectral filter seems to be feasible. This would allow frequency-tagged multicolor ranging and computer controlled signal level adjustments.

Session 10: Laser Technology Development Session Summary
Chairperson: Karel Hamal

The contributions to the session were focussed on new lasers and the eye safety.

The Ti:Sapphire based laser developed for the new Wettzell SLR station TIGO (A.Ferario, P.Sperber) delivers 0.5 Watt average power at each wavelength in 25 picoseconds. The pair 0.84 um and 0.42 um is well matched for two color ranging with the existing receivers based either on photomultipliers or Silicon detectors.

The Raman commercial laser (K.Hamal) exploits the Brillouin and Raman backscattered stimulated emission. The compact laser delivers 20 mW average power in the visible range.

To fulfill the eyesafety requirements, two approaches were discussed: keeping the energy/power below the eye safe limit (J.Degnan) or using a laser wavelength within the so called the eye safe window (K.Hamal). The NASA SLR2000 project operating below the eye safety limit is based on the diode pumped Q-switched microlaser delivering 1 milliWatt average power in 200 to 50 picoseconds long pulses.

A laser operating in the eye safety window can be based on Optical Parametric Oscillator or the Raman scheme. The Raman laser based transmitter (K.Hamal) can exploit either backward (40 milliWatts average power) or forward (no information on the average power yet) stimulated Raman in methane pumped by 1.064 um with both generating outputs at 1.54 um.

J.Gaignebet presented a laser for two color long distance ground and satellite laser ranging optimized for the streak camera based receiver package.

Session 11: Streak Camera Systems Session Summary
Chairperson: Ivan Prochazka

Only four papers were submitted; the number being rather low in comparison to other sessions, perhaps indicating the decrease of priority which the scientific groups are giving to the streak camera based systems.

The main outputs of the presented contributions :

Satellite signature measurements and analysis are underway at NASA using a streak camera at the 1.2 meter telescope tracking facility at GSFC. The system permits the measurement and analysis of satellite signatures and far field diffraction behavior of retroreflectror equipped satellites in orbit and comparison to known models and prelaunch test data. The satellite signature effects and their proper understanding is one of the key issues to achieving millimeter precision ranging.

Schreiber discussed the use of a synchroscan streak camera for dual color laser ranging; This is one of the attempts to apply the existing SLR hardware to LIDAR remote sensing.

The new approach to the long horizontal baseline laser ranging was presented by Suzuki. Measurements with a single wavelength, together with an improved atmospheric model developed for optical paths over the sea surface, has been underway over three long baselines for several years.

A new approach to the two color ranging exploiting the laser pulse stretching and compression technique was discussed by Gaignebet.

Persisting problems in the application of the streak camera technology include:

- Energy budget link,
- Timing resolution of the two wavelength delay in two wavelength ranging,
- Timing biases caused by input light direction fluctuations,
- Overall system complexity,
- System hardware/operation costs.

Session 12: Atmospheric Sensing and Models
Chairperson: Georg Kirchner

"Some developments take a while to put into operation"
Mike Pearlman (11.11.1994)

although mentioned in another connection, seems to describe nicely the problems faced in dual/multicolor ranging. Multiwavelength ranging was first discussed at the workshop about ten years ago. By the Annapolis Workshop in 1992, a few talks addressed the subject. In Annapolis (1992), a few talks were given about dual color ranging, including:

- Reports of plans how to implement it;
- First results on satellites available;
- No routine dual color operation.

At this session reports were given on stations that were ranging at different wavelengths to both ground targets and satellites:

Satellites: 355 / 435 / 683 / 1064 nm
Targets: 355 / 435 / 683 / 1064 / 1540 nm

but there are still no routine operations. We are still facing major problems at some wavelenths; and only now are we getting our first checks of available data against models.

We are now collecting much more multicolor data, undertaking detailed analysis of multicolor data, and addressing the technical issues required to make this technique operational.

We should not forget about the LIDAR possibilities.

Session 13: System Automation and Operational Software
Chairperson: Jan McGarry

There were 16 presentations in the System Automation and Operational Software Session covering the topics of satellitepredictions, Internet data transfer and posting, parallel processing, new operational software, and automation.

Rolf Koenig and Andrew Sinclair showed how the current method of producing and using predictions onsite would not be accurate enough for low earth orbiting satellites. This will be particularly true for GFZ-1, which is scheduled to be launched March 1995. Sinclair suggested that the SLR Network produce four Tuned IRVs per day instead of the current one per day to solve the problem. Koenig said that in order to maintain a good orbit, data was needed from the global network on a daily basis.

The use of the Internet by the laser ranging community was a theme running through many of the presentations, but especially those of Dave Edge, Carey Noll, and Antonin Novotny. The Internet is an important tool for reliable, fast data transfer and posting. Novotny showed how the Internet should and could be so much more than just e-mail (such as World-Wide-Web), and indicated that it was important for all laser ranging stations to connect to Internet. His presentation suggested options for connecting remote stations. Dave Edge showed how the NASA network is currently using the Internet for hourly data transmission. Carey Noll's paper presented how NASA will begin posting the SLR data at the start of 1995, and also how the CDDIS will be using World-Wide-Web for data dissemination.

Parallel processing was also a common theme in the presentations. This ranged from as simple as two computers onsite (Veillet and Edge), to the more complicated multiple CPU scenario (Offierski). Parallel processing can increase both I/O and processing speed. Synchronization is the main issue here, but is often not much more complicated than the synchronization of tasks in the single CPU environment.

Descriptions of new operational software were given for the NASA SLR systems (McGarry and Edge), Grasse's LLR (Veillet), Helwan's Compact Laser Radar (Cech), and the US Naval Research Lab's system at the Starfire Optical Research Facility (Peltzer). Brion Conklin presented a standardized Normal Point and Acquisition software package that is available to the global community via Internet.

The next generation of SLR and LLR systems will be much more automated than those currently operational. Almost every talk in this session made reference in some way to automation. Dave Edge showed that automation is occurring at the central facilities as well as onsite. The onsite automation issues specifically addressed in this session were: (i) data assessment and quality control (Husson), (ii) data processing and transfer (Edge and Novotny), (iii) closed loop tracking (Cech), and (iv) data filtering (Otsubo and McGarry). It was clear from the presentations that automated SLR system will be operational before the decade is out.

Ninth International Workshop on
LASER RANGING INSTRUMENTATION

DISCUSSION AND RESOLUTIONS

Chairperson: Michael Pearlman

DISCUSSION

The participants were asked to comment on the format of the Workshop and make suggestions on how it might be improved in the future. The following points were made:

1. The topics for the sessions were appropriate and timely.

2. There were too many talks and/or they were too long. We should use more poster sessions and provide 2-3 minute introductory presentations for the poster presenters.

3. The lunchtime format was good, it provided an easy opportunity to mix and discuss.

4. On a workshop-by-workshop basis we are seeing considerable refinement of the SLR technique, but we are not seeing as much new technology and new concepts as we should. We need to continue reaching out to bring in additional technologies and new people.

5. With a narrow focus of satellite and lunar laser ranging we suffer from the vagaries program evolution and changing priorities. We need to expand our view and look for broader applications that may be related by technique such as LIDAR, timing, and propagation measuring activites.

RESOLUTIONS

1. Whereas the Proceedings of the Workshops on Laser Ranging Instrumentation receive very limited distribution and are not a recognized reference for workers in allied fields of research, we strongly recommend that the laser ranging community establish an improved means of publishing novel work in laser ranging technology.

2. Recognizing that the exchange of information that occurs at the Workshop sessions is a prime stimulant for workers in the field of laser ranging, and that as the list of attendees increases, scheduling becomes more and more difficult, we recommend that the Workshop be held every two years and that the timing be announced shortly after the previous Workshop.

3. Recognizing the importance of global distribution to SLR, and in particular, the close proximity of SLR sites in the western regions of Russia and the Ukraine, we strongly encourage (1) the relocation of the "Crimea 5" SLR station from Pulkova (after it is established and working satisfactorily) to the Far East (Blagoveshchenk), and (2) the relocation of either the Simeiz or Katzively station to a site in the central or Far East region.

4. Recognizing (1) the importance of improving effective cross-section of satellite retroreflectors especially on high satellites at Lageos altitudes and above, so that more compact ground systems can be implemented, and (2) the need to keep spacecraft retroreflector arrays very compact so that center-of-mass correction and targets for multi-wavelength ranging are compatible with future mm ranging requirements, the Workshop participants (1) greatly appreciate the work done by the Russian Space Agency on the development of the Fizeau retroreflectors and the installation of the retroreflectors of this type on Meteor-2 and (2) recommend the continued testing and implementation of this concept.

5. The participants of the Workshop recognize the progress and the importance of the Chinese Satellite Laser Ranging activities within the global SLR network, and encourage the Chinese Stations to continue and expand their SLR operations and system development.

6. Recognizing the importance of regional integrated space geodesy programs in general, and the particular interest in the geology and geodynamics of the Western Pacific region, the participants strongly support the establishment of the Western Pacific Satellite Laser Ranging Program and its role within the broader space geodesy programs.

7. The participants of the Ninth International Workshop on Laser Ranging Instrumentation express their sincere appreciation to the Australian Land Information Group (AUSLIG) and Electro Optic Systems Pty. Ltd. (EOS) for their organization and hosting of this very successful Workshop, and recognized the substantial efforts of Dr. John Luck and Dr. Ben Greene in making this event possible.

BUSINESS MEETING

Chairperson : Peter Dunn

SELECTION OF THE LOCATION FOR THE NEXT WORKSHOP

Chairperson: Peter Dunn

There were three proposals to host the next Workshop. The proposers were Dr. Stanislaw Schillak of Poland for Posnan, Dr. Yang Fu Min of China for Shanghai, and Dr. Wolfgang Schleuter of Germany for Wettzell. The participants felt that all of the offers represented excellent places to hold the meeting, but this was the second time the Chinese had offered and a meeting had never been held in Asia before. The vote was strongly in favor of Shanghai in the October-November, 1996 timeframe.

Dr. Yang Fu Min will firm up the arrangements and inform the community.

ORGANIZING COMMITTEE FOR THE TENTH WORKSHOP

The Organizing Committee for the next workshop was selected. It will include:

Dr. John Luck and Dr. Ben Greene (present workshop hosts)
Dr. Yang Fu Min (Host for the next workshop),
Dr. Giuseppe Bianco
Dr. Peter Shelus